ISSW 2019

Proceedings of the 17th

International Ship Stability Workshop

10-12 June 2019, Helsinki, Finland

Proceedings

Pekka Ruponen (editor)

ISSW 2019

Proceedings of the 17th

International Ship Stability Workshop

10-12 June 2019, Helsinki, Finland

Arranged and hosted by NAPA and Aalto University

Aalto University
School of Engineering

Supported by:

ELOMATIC CONSULTING & ENGINEERING

FORESHIP

MEYER TURKU SHIPYARD 1737

Cover photo: © Helsinki Marketing / Suomen Ilmakuva

Proceedings of the 17th International Ship Stability Workshop (ISSW 2019)

Helsinki, Finland, 10-12 June, 2019
Editor: Pekka Ruponen
ISBN: 978-952-60-3767-7
ISBN(PDF): 978-952-60-3768-4

ABOUT INTERNATIONAL SHIP STABILITY WORKSHOP

International Ship Stability Workshop (ISSW) is a part of a longstanding series of international technical meetings in the field of ship stability, dynamics and safety, consisting of the STAB conferences, which are held every third year, and the ISSW workshops, which are held in the years between the conferences. These conferences and workshops are initiated and supervised by an International Standing Committee (ISC) and arranged and hosted by a Local Organizing Committee, each time in different corners of the world. General information about ISSW, STAB, ISC, SRDC (Stability Research and Development Committee), proceedings from past events, and other information concerning ship stability, dynamics and safety, can be found at www.shipstab.org.

PREVIOUS INTERNATIONAL SHIP STABILITY WORKSHOPS

1995, Glasgow, UK
1996, Osaka, Japan
1997, Hersonissos, Crete, Greece
1998, St. John's, Newfoundland, Canada
2001, Trieste, Italy
2002, New York, USA
2004, Shanghai, China
2005, Istanbul, Turkey
2007, Hamburg, Germany
2008, Daejeon, Korea
2010, Wageningen, the Netherlands
2011, Washington, USA
2013, Brest, Brittany, France
2014, Kuala Lumpur, Malaysia
2016, Stockholm, Sweden
2017, Belgrade, Serbia

ARRANGEMENT OF TECHNICAL SESSIONS

The topics and chairmen for the technical sessions were decided by the STAB International Standing Committee in autumn 2018, accounting for initial input from the local organizers. The chairmen were responsible for planning and organizing of the sessions, including invitation, review and acceptance of the papers.

ACKNOWLEDGEMENTS

Pirjo Anttonen and Minna Ranta are thanked for the help in the practical arrangement of the workshop. The assistance from the finance & administration team of NAPA is also gratefully acknowledged.

DISCLAIMER

The opinions expressed in the papers are those of the authors and not necessarily those of any organization with which the authors have been associated.

CONTENTS

Session 1: Introduction & 80 years of Rahola criterion

Chaired by Alberto Francescutto & Pekka Ruponen

Session 2: Stochastic rolling and big data

Chaired by Vadim Belenky & Alexander Degtyarev

Session 3: Intact stability and operational matters

Chaired by Naoya Umeda & Teemu Manderbacka

Session 4: Direct assessment methods

Chaired by William Peters & Dimitris Konovessis, co-organized by Jan Otto de Kat

Session 5: Small craft and wave impact loads

Chaired by Frans van Walree & Jerzy Matusiak

Session 6: Damage stability

Chaired by Hendrik Bruhns & Jakub Cichowicz

Session 7: Outcomes from eSAFE (enhanced Stability After a Flooding Event – A joint industry project on damage stability for cruise ships)

Chaired by Dracos Vassalos & Gabriele Bulian

Session 8: Roll damping

Chaired by Luis Pérez-Rojas & Toru Katayama

Session 9: The future of stability assessment

Chaired by Konstantinos Spyrou

Documentary analysis of STAB and ISSW proceedings

Hélène Dartois, *Stagiaire de l'École nationale des Chartes*, helene.dartois@chartes.psl.eu
Paul Creismeas, *DGA Hydrodynamics 27105 Val de Reuil, France*, paul.creismeas@intradef.gouv.fr
Jean-François Leguen, *DGA Hydrodynamics 27105 Val de Reuil, France*, jean.françois.leguen@intradef.gouv.fr

ABSTRACT

From the beginning, the Stability R&D Committee (SRDC) made a huge effort to collect and dematerialize all the proceedings of the STAB and ISSW congresses since the first editions. All these dematerialized documents have been uploaded on the website www.shipstab.org. Search is now possible directly on the website. It is proposed to present work on the use of these data. The documentary tools presented will allow better search and an optimized classification of articles. Roadmap is suggested, such as the harmonization of keywords, providing recommendations to future conference STAB and ISSW authors and organisers.

Keywords: *stability, congress, documentation*

1. INTRODUCTION

The work presented in this paper was initiate by SRDC (Stability Research & Development Committee), with its help and under its control, in order to promote and disseminate the work presented during STAB and ISSW congresses which is a part of the SRDC mandate.

2. PREVIOUS WORK DONE

SRDC efforts

Since the beginning of SRDC (first meeting in Washington DC in 2011 during ISSW 2011), efforts were done to work on papers from STAB and ISSW congresses. Because it seemed that nobody has the complete set of proceedings, the first step was to centralise proceedings of all conferences from the first STAB conference in 1975 and the first ISSW in 1995, both in Glasgow. With help of all, it was possible with reasonable efforts to find a version, at least a paper version for oldest years, of all congresses and workshops. The second steps was the OCR process of every proceedings. This task was shared in many places. It was chosen to separate papers in several independent "pdf" format files. In parallel of this process, tentative to fill metadata of the files to facilitate research was performed but this task was never fully ended because it is a very time consuming task if it is handmade.

At the end of those first steps, it was possible to upload about a thousand independent "pdf" files of all STAB and ISSW papers on STAB/ISSW website, www.shipstab.org. Many files contains metadata (as date and place of the conference, session name, authors and including keywords) and have standardized names (made from author names to facilitate researches). An index was also written in an MS Excel file with usual information in order to facilitate the searching process outside of internet and to propose a standalone CD-ROM, which is useful or mandatory in some situations.

Now the website is up-to-date at the end of every congress and contain a search engine. In order to improve searching process and output information from this huge database it was decided at DGA Hydrodynamics to try some new tools and new methodologies.

The initial corpus

At DGA Hydrodynamics a documentation about ship stability expertise field is needed and expected in order to be able to produce very significant researches and tests. The SRDC helps the creation of a specific corpus for this test center since its creation in 2011. One of its objectives was to centralize every article about ship stability for tests centers around the world. The corpus presented at DGA Hydrodynamics is made of more than 1400 PDF files of nearly all the STAB conferences and ISSW workshops. This corpus is increased every

year with new documents from ISSW or STAB which proves the daily effectiveness and usefulness of those documents in this test center.

As previously mentioned, every congress and workshop books were split into smaller chunks in order to obtain a single PDF file for each article. This way, the indexation in an MS Excel file was easier and more relevant. Plus it helps the creation of more complete metadata for each article.

Through the year, DGA Hydrodynamics has obtained a nearly complete set of articles which is an advantage when it comes to make precise analysis on vocabulary or on the different point of interests about ship stability through the year.

3. NEW OBJECTIVES

The website: www.shipstab.org gives access to every STAB and ISSW articles plus thesis but there is some limits that need to be improved. The search engine doesn't allow the researcher to do a precise research on metadata, it only allows us to search in a full-text mode. The result page is also quite limited: every result for a research gives an access to a more specific result page where we can download the full proceeding book and not the article that we are interested in. The results do not specify on which article the keyword was found, which means we have to search within the PDF of all articles before actually finding the result announced on the search engine.

The work beginning at DGA Hydrodynamics intend to overcome those limits. The tools we propose will not only allow advanced research on the content of the article but also on the metadata fields of each article in order to study the evolution of stability work over the year. This paper also submits recommendations to authors and organisers to obtain a standardization of the outputs of congresses, a bibliographic structure easy to extract and a more precise research engine.

4. DOCUMENTATION TOOLS

The ISSW and STAB corpus collected by SRDC are made of PDF, some of them are quite old which means the OCR is not perfect. As most PDF, they are readable with any PDF viewer but they are not easily modified which is a problem when it comes to make those corpus more usable and searchable for the engineers. For instance, it's nearly impossible to add rich metadata to a PDF file and this can be a challenging point when it comes to give access to technical and scientific information. A corpus of technical documents is interesting only if we can search precisely on it and structured metadata are key to search and to use effectively any kind of corpus.

In order to help engineers getting a privileged access to this scientific and specific ship stability documentation, different tools were created to search onto those documents. Since the beginning of the project an emphasis was made on the use of freeware and license free software. The aim is to propose a re-usable and easy system to access the different corpus and to search them at DGA or in other institutions. The accessibility can only be guaranteed by freeware and license free programs. Most of the tools were coded in python language and required a python 3 version to run. At the moment, all the tools are available only on one computer, but if the solutions created are good enough, the different codes could be combined into the shipstab website and thus becoming accessible for everyone without the obligation to install python on a computer.

The OCR process

For older articles, a primary step is necessary before using the GROBID API to get the TEI : the articles need to be pass on a OCR software.

Sometimes, the OCR is quite difficult to produce because of the low quality of the original document (archives can be nearly unreadable or an old printed version of an article can be of low quality which induce many errors during the OCR process). To reduce the number of errors or to increase the effectiveness of the OCR process an simple image treating process can be made. At DGA-Hydrodynamics, M. Paul CREISMEAS uses the Omnipage Ultimate software, which is not a license free software but it allows us to treat the quality of the image by adjusting the contrast and luminosity, the orientation of the page, selecting the content zone, etc.

Those image treatments are essentials to produce a good quality TEI document and to use it effectively without spending hours on corrections over the original document. This all process is just an

example of what is possible to do with old article that still have a scientific interest.

GROBID

First and foremost, it was necessary to convert the PDF files into a format that allows us to add metadata and/or to specify the existing metadata.

To do so, the GROBID API[1] was used: "GROBID" is a machine learning library for extracting, parsing and re-structuring raw documents such as PDF into structured TEI[2] -encoded documents"[3]. This new format allows us to create more accurate metadata or to increase the already existing metadata. To do so, we use the XML Copy Editor program which is, like GROBID, a license free program.

XML Copy Editor

This software is design to write XML type document. It provides a validation tool to verify the validity of the document towards TEI guidelines. This way, we make sure the document can be used by another XML program and can be exchange without damages. We are only modifying or creating metadata for each document, we will never modify the content of the document in itself.

Before adding anything to the document we create a list of essential metadata. This list contains every field that will be searchable on the application:

- author (forename, surname),
- affiliation (organization name and type (research, certification, industrial, test center), address (country, settlement),
- title,
- keywords,
- abstract.

We tried to create the smallest list possible because adding too much metadata will be time consuming and it will be in contradiction to our main objective: creating a simple application to search the collection of articles.

The TEI format is made to structure a document and add some metadata in order to explore a text document in different aspects such as metadata, specific formulas or bibliographic references. But like every markup language it is quite a heavy format to use to exchange data or documents. We choose to convert the new TEI document, once the metadata were added, to another web oriented format called JSON[4] (pronounced « Jason »). This format preserved all the information added with XML modifications but it simplifies the document structure and it work as an array in JavaScript. The conversion was made with a python scripts which parsed XML files and convert them into JSON files. All those files contain the necessary metadata to search precisely onto the documents.

Elasticsearch

Once the JSON files are ready we add them to a search engine program. Searching in full-text was one of the main requirement for the application besides the possibility to use structured metadata and to do so, we decide to use Elasticsearch[5], a JSON document oriented search engine compatible with Python, JavaScript, PHP etc. The JSON documents are indexed into Elasticsearch clusters according to their structure. This way, it will be possible, with a web application, to do full-text search and very specific and precise researches in the corpus such as a research by organization type or by bibliographic reference. The application will be coded to search on multiple fields of metadata in the documents such as authors, institution, date, keywords, abstract, and to search on plain-text, bibliographic references etc. On the frontend, the user deals with a search page and the application will return the PDF file for each response. That way, we made sure that none of the document could be modified or deleted by the user, the application only gave access to the non-changeable document, the PDF file.

5. PROCESS

The mind-map (Figure 1), represents the process to create the research application with all the tools

[1] API is an application programming interface.
[2] Text Encoding Initiative P5, the last version was launched in 2007 by Lou Burnard and Syd Bauman with the TEI Consortium.
[3] Grobid documentation can be found at : https//grobid.readthedocs.io/en/latest/

[4] Java Script Object Notation is a web exchange format created by JavaScript, during the 2000's, to simplify the data communication on the web.
[5] Elasticsearch is an API that allows to index document in a JSON format and to search upon the documents with a REST API compatible with many other langages such as PHP or Python.

that will be deployed at DGA Hydrodynamics. This process is already an ambitious one because it requires multiple actions to obtain the structured document in a good format before the indexation on a search engine. But this is also a starting point for a more precise analysis of this important documentation and it will give a privilege access to the content in a very simple way.

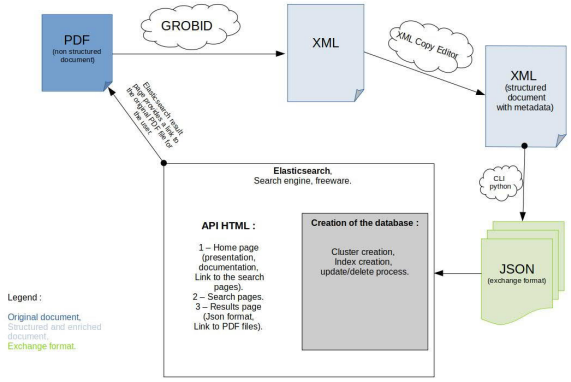

Figure 1: STAB and ISSW treatment process

In this mind map we assume the document is already in a good quality and in a PDF format. If the document needs to be dematerialized, an OCR process can be useful. Once this step is done, we first transform our PDF file into an XML document with the web API GROBID. Once we have obtained this new document we enrich the metadata with the XML Copy Editor software. Then, we transform the XML into a JSON format that simplify data exchange on the web and on the application. This conversion is made with a python script. Finally we add the JSON file to our Elasticsearch cluster so that we can interrogate it with all our other articles.

After all those steps, the documents and their metadata and content are searchable and ready for a more complete analysis.

6. EXAMPLE

In this part, we introduce examples to demonstrate what it is possible to obtain through the analysis of documents metadata. To do so, we extract from the whole initial corpus a subcorpus on which the work can be realizable by hand, the tools described upper in the text are under construction. This subcorpus is comprised of the communications from ISSW 2013, 2014, 2016 and 2017 and from STAB 2015 and 2018, totalling approximately 260 documents to be further analysed.

The set of metadata connected to each of these documents are keywords in relation with the activities in stability domain. To identify telling keywords, we are guided by a map depicting the main activities of the domain and the relations among them, Figure 2.

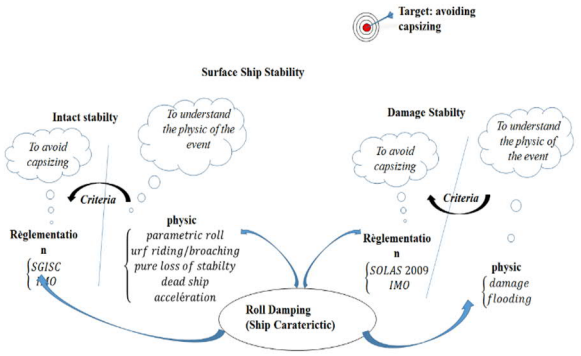

Figure 2: Map of the activities connected to the stability domain and the relations among them.

The list of the chosen keywords is given below:

- Roll
- Seakeeping
- Manoeuvrability
- Offshore
- Experimental technics
- Probability
- Intact Stability
- Damaged Stability

At each keyword, we associate a measure of the importance of the keyword in the documentation related to an element of the subcorpus. Such a measure is performed by computing the *density*, also called:

Term Frequency-Inverse Document Frequency, "Tf-Idf" (Leydesdor, 2011), (Thijs, 2011), which is a weighted counting of the keyword among the documentation. For example, we assess the importance of the activity *Roll* in the congress STAB 2015, $d_{Roll,STAB2015}$ through the following formulae:

$$d_{Roll,STAB2015} = \frac{N_{Roll,STAB2015}}{N_{STAB2015}} . log \frac{N_{subcorpus}}{N_{STAB2015}} \quad (1)$$

With:

- $N_{Roll,STAB2015}$ is the number of communications from the congress STAB 2015 concerned with rolling phenomena,

- $N_{STAB2015}$ is the total number of the documents from the congress STAB 2015,
- $N_{subcorpus}$ is the number of the considered documents in the subcorpus,
- *log* is the decimal logarithm function

In Figure 3 and Figure 4, the evolution of all the keywords is depicted versus ISSW workshops and STAB congress, in a chronological order. We must be careful before drawing out definitive conclusions, but it is very interesting to notice the importance of both *Roll* and *Seakeeping* activities during the period over six years from 2013, figure 3. But the other figure, figure, show us straightforwardly that the main point of concern over this period of six years is the *intact stability*.

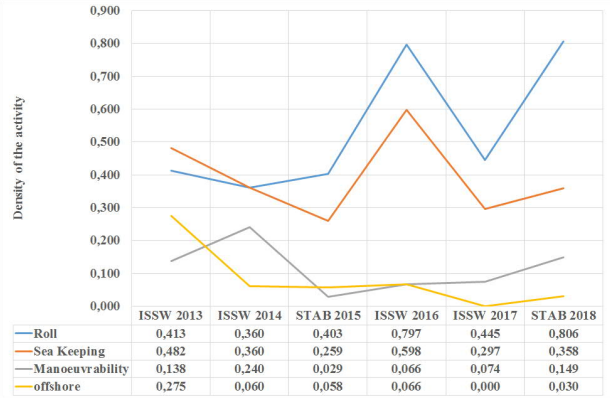

	ISSW 2013	ISSW 2014	STAB 2015	ISSW 2016	ISSW 2017	STAB 2018
Roll	0,413	0,360	0,403	0,797	0,445	0,806
Sea Keeping	0,482	0,360	0,259	0,598	0,297	0,358
Manoeuvrability	0,138	0,240	0,029	0,066	0,074	0,149
offshore	0,275	0,060	0,058	0,066	0,000	0,030

Figure 3: Evolution on the importance of some keywords related to intact stability versus the workshops ISSW and congress STAB, chronological order over a range of six years

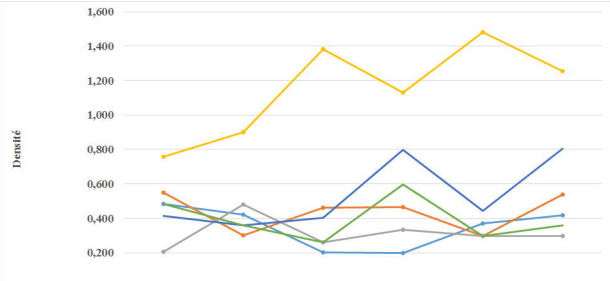

	ISSW 2013	ISSW 2014	STAB 2015	ISSW 2016	ISSW 2017	STAB 2018
Experience	0,482	0,420	0,201	0,199	0,371	0,418
probabilite	0,551	0,300	0,461	0,465	0,297	0,537
damaged Stability	0,206	0,480	0,259	0,332	0,297	0,299
Intact Stability	0,757	0,901	1,382	1,129	1,483	1,254
Roll	0,413	0,360	0,403	0,797	0,445	0,806
Sea Keeping	0,482	0,360	0,259	0,598	0,297	0,358

Figure 4: Evolution on the importance of some keywords versus the workshops ISSW and congress STAB, over a range of six years.

7. RECOMMENDATIONS

Because it was an objective of this study, preliminary version of recommendations are suggested below.

Recommendations to authors

Those analysis and uses of the corpus are only possible if a few recommendations are filled. Those recommendations do not requires a great amount of time for the authors but it determines the success of the future researches and investigations.

First, we must underline the importance of creating a structured article. This can be easily achieved with the article guide given by the organisers of each congress. The article guide is conform to GROBID training data so the result are accurate and quick. Moreover, this guide presents example for bibliographic references and figure model.

Another point of interest is on formulas. GROBID was not trained to achieve good results while recognizing mathematical formulas. But one of the possible evolution of the project could be to make research over specific formulas. In order to try to achieve this objective, authors could, when possible, name the formulas they used with a specific sentence such as: "GM calculation formula:" followed by the mathematical formula. This would help creating a model to search on all the articles.

Lastly, we recommend that the session name appeared as a keyword in the article whenever it is possible or added by organisers to increase the research possibility. This way, it would be possible to find every article belonging to the same session and to the same theme for a specific congress or workshop.

Recommendations for references

The use of the article guide with a bibliographic standard will give the possibility to generate a stability bibliography from all articles, and thus to have access to a large bibliography about this scientific field that can be increased regularly. We recommend the use of the APA[6] (2009) standard for bibliographic reference because the GROBID API

[6]The American Psychological Association created a bibliographic standard for students and psychologist in 1929.

model data use the APA standard to recognize any bibliographic references present in a document

This standard is well known among researchers and it also a standard that can be used when we want to produce a bibliography with Latex for example.

You can find all the information and examples to use this standard on the official website: http://www.apastyle.org/. This site also contains a tutorial presenting the basic rules for the standard.

Recommendations to organisers

To help the use of the STAB and ISSW corpus, it is important to maintain the habit to create an update of the database for every STAB and ISSW session. This update should present, at least, a few metadata field such as author(s), title, organization name and type, keywords and abstract. This will help adding metadata and update the Elasticsearch cluster regularly.

In the tool presentation section we made a list of the fields we want to be able to search within the python application. But all those fields are not required in an article. The only fields that we recommend to be put in every article are the following:

- title,
- author(s),
- keyword(s), preferably separated with commas,
- name of session,
- abstract.

Those fields represent the core metadata of each article. They will be used to search the document database.

For future congresses, we suggest that every participant has an easy access to a small documentation. This documentation have to work as a reminder of good practise while writing an article. This way it will be easier to have a homogeneous corpus of document that share the same structure.

This can be easily achieved by adding the documentation directly on the www.shipstab.org. This documentation page, on the website, should at least contain a guide for article redaction with the excepted structure. This will encourage author to write in a re-usable format for GROBID for instance. A link to the APA standard for bibliography would also help the redaction of article. Plus, the use of the standard will help for a better indexation on Google Scholar or on a university website. Finally a short documentation about the expected metadata for each article would help reducing the time to treat every article after the conferences.

8. REFERENCES

APA, Publication Manual for American Psychological Association, (6th edition), Washington DC, 2009.

Leydesdor, L. and Welbers, K., "The semantic mapping of words and co-words in context". Journal of Infometrics, 2011.

Thijs, B., "Mapping of science". In www.scientometrics-school.eu, editor, ESSS European Summer School for Scientometrics. 2011. Leuven, Belgium.

Alternative stability criteria for ships

Lech Kobylinski, *Polish Academy of Sciences*, lechk@portilawa.com

ABSTRACT

In the year 2010 Intact Stability Code was included by reference to SOLAS Convention and from this date on part A of the Code became compulsory. However, the work on stability criteria has not been completed, and as stated in Code, some problems of safety of ships from the point of view of stability should be considered further. The paper proposes to include in the SOLAS Convention and in the Code provisions allowing Administrations to apply alternative criteria for novel ships, or ships which present high risk to people or environment. Goal oriented approach to the development of alternative criteria including risk assessment methods is proposed.

Keywords: *Ship stability, stability criteria, risk analysis.*

1. INTRODUCTION

Year 2010 could be assessed as a year when IMO work on adopting international stability norms or standards was completed because the Intact Stability Code was included by reference to SOLAS convention and from this date on Part A of the Code comprises compulsory basic stability criteria for all ships to which SOLAS convention applies. Part B of the Code is still, however, recommended only, but this part covers mainly requirements to some special ship types and other requirements and guidelines. This decision taken after almost fifty years of development is an important step towards assuring safety against loss of stability casualties of ships. Adoption of basic stability criteria fifty years ago followed by adoption of the weather criterion seventeen years later resulted in drastic reduction of casualties related to stability. The requirements, however, were based on the characteristics of standard ships, mainly in operation during the second half of twentieth century.

Looking at the text of the Intact Stability Code we see, however, in the preamble an important statement that reads: "*It is recognized that in view of the wide variety of types, sizes of ships and their operating and environmental conditions, problems of safety against accidents related to stability have generally not yet been solved. In particular, the safety of a ship in a seaway involves complex hydrodynamic phenomena which up to now have not been fully investigated and understood. Motion of ships in a seaway should be treated as a dynamical system and relationships between ship and environmental conditions such as wave and wind excitations are recognized as extremely important elements. Based on hydrodynamic aspects and stability analysis of a ship in a seaway, stability criteria development poses complex problems that require further research.*"

This very important statement clearly says that work on stability criteria is not completed and there is a need to arrange further research programs on ship hydrodynamic aspects of stability criteria. In fact this statement reveals also views quite often expressed by some national delegations to IMO Subcommittee, indirectly indicating that future stability criteria should be performance oriented and prescriptive design criteria, of the type such as are current criteria included in the Code.

Almost ten years ago work on so called Second Generation Stability Criteria was initiated by the IMO SLF Subcommittee. Currently work on those criteria was almost completed and the SDC Subcommittee agreed to recommend them and publish in the form of MSC Circular. Moreover, the subject related to further work on stability criteria was removed from the future programme of the subcommittee.

2. CONCEPT OF ALTERNATIVE CRITERIA AND EQUIVALENT METHODS

The above quoted text of the preamble to the Intact Stability Code clearly indicates that the

present requirements of the Code are not the final word. Further work in the future might be necessary. The problem is, how to approach this important problem with the view that existing criteria might be not fully adequate to modern ships differing in size and design features from ships operating in the past.

In the introduction to the Code in paragraph 1.3, there is another important sentence included, that reads: *"Administrations may impose additional requirements regarding the design aspects of ships of novel design or ships not otherwise covered by the Code".* This sentence opens the possibility to the Administration of a particular country to have some flexibility in application of stability norms with regard, however, design features of the ship.

It seems that the above statements, although properly reflecting current status of stability regulations implicate that additional or alternative requirements should be design oriented.

In its 49th session the SLF Subcommittee discussed possibility to introduce in Part A of the Code the clause allowing Administrations to apply equivalent requirements to those already specified in the Code, similarly as it was done in the section 1.4 of Chemical Carriers Code and Gas Carriers Code and in section 1.11 of the High Speed Code 2000. This was proposed by Norway and was supported by some other delegations. Proposal to introduce to the Intact Stability Code a clause allowing Administrations to apply equivalent methods of assessing safety was widely discussed in the paper by Chantelauve (2005). Other authors also supported this proposal, e.g. Vassalos (2002) and Kobylinski (2006). This clause should apply to nonconventional ships or ships to which application of current requirements to existing ship types because of their dimensions, construction and operating conditions would not be practical.

During the discussion at IMO some delegations were of the opinion, that this clause should be formulated similarly as it is included in the SOLAS Convention in the Regulation II-2/17 in relation to fire protection. Text of this regulation shows, that when applying equivalent requirements it would be necessary to apply engineering analysis according to the guidelines included in the IMO/Circ.1002. After discussion the Subcommittee did not take any decision in this matter, however.

All existing stability requirements, including Second Generation Criteria mentioned are design oriented. However analysis of the stability casualties reveals, that design faults only rarely contribute to casualty. It is true, that it is very difficult in the majority of stability failures to discover a single cause of casualty. Usually accident is a consequence of a chain of events where other factors, including human factor play predominant role. The analysis of 364 stability casualties collated from various sources (Kobylinski 2008) allowed to draw some general conclusions revealing that in the great majority of cases (about 80%) human and organisational errors (HOE) are responsible for the accident, that usually results of a sequence of events that involve other factors as well. Most casualties took place in rough sea, although forces of the sea were not often the primary cause of casualty. Many casualties happened in calm sea. Design features of the ship are responsible for a rather small percentage of casualties.

Human factor is not taken into account in any stability criteria, on the other hand all available sources related to loss of stability casualties show that this factor is the most common cause of casualty. Human and organisation errors (HOE) according to some authors are responsible for about 80% of all accidents at sea (Manum 1990). Other source definitely stated that this percentage is between 75% and 80% (US Coast Guard 1995)

Analysis of the P&I Club (Boniface and Bea, 1996) reveals that HOE are the cause of 62% of all marine claims. It may be concluded therefore that operational aspects are the most important in assuring safety at sea.

Other data on the same subject:

<u>*According to US Transportation Safety Board:*</u>

57% of all accidents at sea are caused by wrong organisation of operation and errors of the crew members
10% technical errors of pilots
33% mechanical problems, weather and other factors

<u>*According to Swedish Marine Administartion:*</u>

71% of accidents are result of errors of crew members and lack of understanding
10% lack of knowledge and training
19% other factors

Bearing in mind that currently used stability criteria, but also Second Generation Stability Criteria under final development, are basically

design oriented, it was suggested that alternative criteria should be holistic, taking into account all elements of the ship stability system.

This system at least should include four basic elements, as shown in the often quoted Venn's diagram reproduced in Figure 1, where all four element are shown: ship, cargo, environment and operation. In the operation element, human factor plays important part.

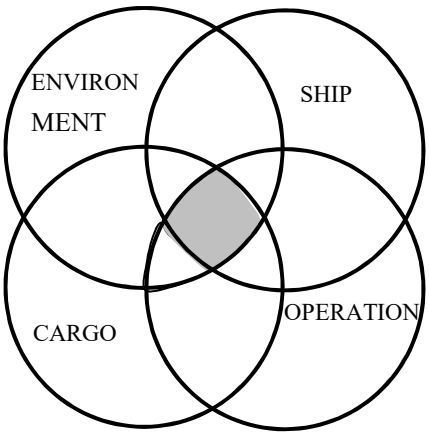

Figure 1. Venn's diagram showing simplified stability system

The essence of the current proposal is to include in the SOLAS Convention, as well as in the Stability Code, a provision allowing national Administrations to use equivalent alternative criteria or methods of assessing safety against stability accident. It should also be recommended, that methods used will be based on holistic approach where all elements of stability system including HOE are taken into consideration. It is obvious that if such provision will be included, there would be necessary to develop suitable detailed guidelines concerning those methods. This clause may be applicable to ships to which present requirements in the view of the Administration are not sufficient to assure safety. Table 1 illustrates this idea:

The schematic presentation of location of the proposed system of stability criteria is shown in Figure 2. In fact Intact Stability Code in few places mentioned alternative or additional requirements. In the introduction (par.1.3) there is included already provision allowing Administrations to impose additional requirements regarding the design aspects of ships of novel design or ships not otherwise covered by the Code. In Part A, second part of paragraph 1.2. says: *"Having regard to the phenomena described in this section, the Administration for a particular ship or group of ship may apply criteria demonstrating that the safety of the ship is sufficient".* In the text of the Code alternative criteria related to wind effect are mentioned, they also mentioned in several other places in Part B of the Code. However in the first quotation application of alternative criteria is limited to design aspects only, in the second place, to the critical phenomena in waves.

Table 1. Method assuring safety against stability accidents

Ship types	Method of assuring safety
Conventional, not sophisticated	Prescriptive criteria included in the Stability Code
Nonconventional or requiring safety analysis because of their dimensions, construction or functional features	Safety analysis under the provision regarding possibility to apply alternative criteria or methods of assuring safety

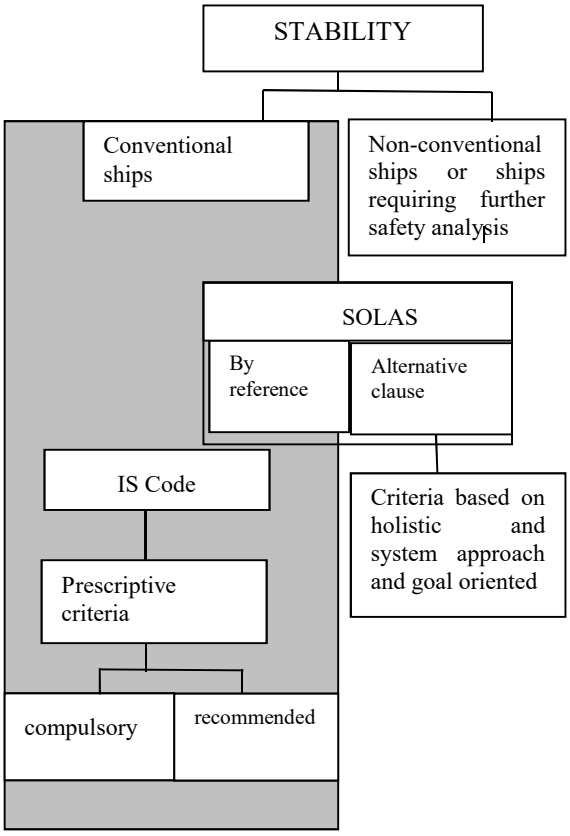

Figure 2. Schematic presentation of location of the proposed alternative clause

In the proposal presented the intention of alternative criteria or methods of assuring safety is to allow Administrations to use entirely different holistic and system approaches. Obviously method or methods used in alternative approach should be

approved by IMO, also important part falls to Classification Societies and to Universities and other scientific organizations. Application of the mentioned provision would solve problem of safety for ships of all types, including those of novel design allowing at the same time further continuation of work on the development of new criteria.

3. SUGGESTED METHODOLOGY OF DEVELOPING ALTERNATIVE STABILITY CRITERIA

The most general concept of advanced method of formulation of safety regulations is goal-based approach. Few years ago the concept of goal based regulations was discussed at IMO. Goal based regulations do not specify means of achieving compliance, but sets goals to allow alternative ways of achieving compliance (Hoppe 2006). Goal based standards were for some time considered at IMO and appraised by some authors (Chantelauve 2005, Vassalos 2002) and they were introduced in some areas, but not in the systematic way. Possibility to use goal based approach for damage stability was considered thoroughly by Papanikolaou et al (2012).

Marine Safety Committee recommended a five tier system for goal based requirements as follows:

Tier 1: Goals
Tier 2: Functional requirement
Tier 3: Verification of compliance
Tier 4: Technical procedures and guidelines, classification rules and industry standards
Tier 5: Codes of practice and safety and quality systems for shipbuilding, ship operations, maintenance, training, etc.

When considering goal oriented approach to safety IMO MSC Committee agreed in principle on the following general goal to be met: "*Ships are to be designed and constructed for a specific design life to be safe and environmentally friendly, when properly operated and manufactured and maintained under specified operating and environmental conditions, in intact and specified damage conditions, throughout their life.*"

The goal oriented approach consists of multitude of means assuring safety that includes compulsory requirements as e.g. included in the SOLAS Convention, recommendations related to operational factors, guidelines related to specific subjects and other instruments as shown in the above list.

The goal oriented approach is probably the most suitable methodology that may be used in the development of alternative requirements because in this methodology multitude of approaches could be used and in which all elements of stability safety system could be included. Risk analysis is included as the main element used to develop and formulate those instruments.

Traditional approach, where stability criteria are of prescriptive nature and design oriented probably will not attract much attention in the future, in particular with regard to alternative criteria. The design oriented criteria do not take into account that stability requirements, similarly to all other safety requirements, should be based on system approach where all elements of the stability safety system should be taken into account

Adoption of the proposed clause allowing Administrations to use alternative methods of assurance safety against stability accident opens the problem of developing appropriate recommendations for Administrations. Without doubts suggested methodology would not be a simple one. Some precedents already do exist, e.g. Interim Guidelines for alternative assessment of the weather criterion in MSC.1/Circ.1200. There is a possibility that Second Generation Stability Criteria, or at least some parts of them and associated methodology may be recommended as alternative in a similar way.

The criteria in the above methodology (apart level III criteria) are performance oriented stability criteria, based on physical models of phenomena. The broader definition says that performance based approach where the behaviour of the vessel is analysed in a set of environmental scenarios taken as realistic as possible on the basis of her performance in terms of safety against capsizing.

Another possible approach that could be used in the future work on the development of the future stability requirements is to base them on probability of capsizing in a seaway. Progress in this direction is already substantial and several papers on this subject were presented to IMO (e.g. IMO 2004, 2006, 2008), also paper by Cramer et al. (2004), containing proposals to use the probability of capsizing in the computer simulated wave train as a safety criterion. The probability of capsizing could be also assessed by model test in the towing tank or

in open waters. However it seems that capsizing in a seaway is not the only hazard for ships and in assessing safety other phenomena and factors should be taken into account, such as water on deck, broaching, etc. and similar effects important from the point of view of overall safety.

4. SHORT REMARKS ON THE RISK ANALYSIS

Goal oriented approach includes risk analysis. Risk based methodology is a procedure widely used in many areas of industry, also in marine technology, supporting decision making process in particular in situations of uncertainty. In off-shore industry it is used as a rule. It involves estimation of the probability of casualty. The first attempt to use probabilistic approach to damage stability requirements was made in the alternative requirements included in the IMO Resolution A.265 (IMO, 1973).

There are, however not many attempts to apply FSA methodology to stability problems. In the book edited by Papanikolaou (2009) methods, tools and applications of risk-based methodology in ship design are thoroughly discussed. However on the subject of intact stability only brief chapter is included covering probabilistic approach to rolling and parametric resonance. Author in several papers advocated application of risk methodology to intact stability requirements discussing difficulties and advantages of the proposed procedure, e.g. Kobylinski (2005). Briefly FSA method was used to investigate casualty of a small Dutch container ship DONGEDIJK (ter Bekke et al 2006). Also risk approach was used in analysing of cargo shift in rough seas (Ericson et al 1977). Papers by McTaggart and de Kat (2000) and also by Schauer et al. (1995), have to be mentioned in this context.

The basic dichotomy in the conception of safety requirements appears between prescriptive criteria and risk analysis. The main shortcomings of prescriptive criteria is that they bounding designers and they do not allow introduction of novel design solutions. They are based on experience gained with existing objects and they are not suitable for novel types. Usually they were amended after serious casualties occur. The risk involved and the level of safety with the application of prescriptive regulations is not known.

At the opposite to the prescriptive regulations there is risk-based approach. In the risk based approach the regulations specify objectives to be reached that is safe performance of an object. Risk based approach could be described as a goal oriented approach utilizing usually probabilistic calculations. It gives free hand to designers to develop new solutions, it actually allows taking optimal solutions from the point of view of economy and risk to the public and to the environment. Risk estimated may be accepted or not, taking into account established criteria.

The essential element of the risk analysis is assessment of risk involved in realization of a particular object with the view to support decision. Risk according to the definition is equal to product of probability of failure (P) and its consequences (C):

$$\mathbf{R = P \times C}$$

IMO recommends to use in the risk assessment the logarithmic scale in the form:

$$\mathbf{\log R = \log (P) + \log (C)}$$

This formulation is more easy to apply and to construct a risk matrix where for probabilities (frequencies) of failure ranking is adopted from FI = 1 (extremely rare) to FI = 7 (frequent) and for consequences ranking is adopted from SI = 1 (negligible) to SI = 4 (catastrophic) with associated probabilities.

Risk analysis includes the following steps:

1. Identification of hazards
2. Risk assessment
3. Risk control options
4. Cost-benefit assessment
5. Recommendations for decision making

Risk analysis is at present a well-established procedure used as a rule, when planning sophisticated systems. IMO recognized the advantages of using risk-based approach as an alternative to the prescriptive criteria in different areas of ship safety and ultimately the Marine Safety Committee of IMO recommended this approach as Formal Safety Assessment (FSA). IMO adopted several recommendations advising application of risk-based approach in the rule – making process. The main steps in promoting application of risk analysis are as follows:

- 1995 UK proposal on application of FSA (Formal Safety Assessment
- 1997 Interim Guidelines on FSA
- 2002 FSA Guidelines, version 1
- 2007 FSA Guidelines, version 2

Risk analysis, is direct methodology, but complex and time consuming. It requires organization of the team of experts that at several sessions will consider all aspects involved, estimate risk and possible consequences and finally will advise decision makers and all stakeholders accordingly.

Obviously this methodology is not suitable to routine cases but in case of planning construction of a large cruise vessel, for example carrying 6000 passengers it would be fully appropriate.

5. CONCLUSIONS

Adoption of recommended international stability criteria by resolutions A.167(ES,IV) and A.168(ES.IV) in the year 1968 and later on weather criterion by resolution A.562(14) in the year 1985 resulted in a drastic reduction of stability casualties. Replacement of these resolutions by the international code on intact stability, the part A of which was made compulsory in the year 2010, should be considered as an important step towards assurance of safety of ships with respect of stability. However existing stability criteria not are not always applicable to certain types of ships, in particular to ships of novel or unusual design features. For those ships alternative methods of assuring sufficient stability are required. To solve this problem, first of all proper clauses should be included in IMO instruments and secondly, suitable methods for the use of alternative criteria should be recommended. Holistic and goal oriented method including risk analysis would possibly be the best methodology for this purpose.

REFERENCES

Chantelauve, G., 2005: "On the use of risk analysis in maritime certification and classification". *Advances in Safety and Reliability ESREL*, *Proceedings,* Vol. I p.329

Vassalos D., 2002: "Total ship safety – a life-cycle risk-based DOR for safety". *The Stability Research Centre, Universities of Glasgow and Strathclyde.*

Kobylinski L., 2006**: "**Alternative stability requirements based on system and risk approach".. *Proceedings of the 9th International Conference on Stability of Ships and Ocean Vehicles, Rio de Janeiro.*

Kobyliński L., 2009: "Remarks on future generation stability norms". *Proceedings of International Workshop on Dynamic Stability Considerations in Ship Design (DSCSD), Iława*,

Manum I.A. 1990: "What have guided international activities on intact stability so far?" *Proceedings of the 4th International Conference on Stability of Ships and Ocean Vehicles, Naples*

U.S. Coast Guard 1995: "Prevention through people". *Quality Action Team Report*

Boniface D.E., Bea R.G. 1996: "Assessing the risk and countermeasures for human and organisation error". *SNAME Transactions, Vol 104 pp.155-177*

Hoppe, H. 2006: "Goal-based standards – a new approach to the international regulations of ship construction". *IMO News, No. 1.*

Papanikolaou A., Hamann R., Byung Lee, Tvedt E., Vassalos D., Zaraphonitis G., Lamoine L., Mains Ch. Olufsen O., "Goal Based Damage Stability of Passenger Ships" *SNAME Annual Meeting 2012*

IMO 2004, 2006, 2008: "Revision of the Intact Stability Code". *Docs. SLF 47/INF.3 (2004); SLF.49/INF.3.(2006); SLF 51/INF.3.(2008) Submitted by Germany.*

Cramer H., Krueger S., Mains C., 2004: "Assessment of intact stability – revision and development of stability standards. Criteria and approaches". *Proceedings, of the 7th Ship Stability Workshop. Shanghai China.*

IMO 1973: "Regulations on Subdivision and Stability of Passenger Ships as an Equivalent to Part B of Chapter II of the International Convention for the Safety of Life st Sea, 1960". *Resolution A.265(VIII)*

Papanikolaou A. (Editor): "Risk-Based Ship Design. Methods, Tools and Applications". *Springer, 2009*

Kobyliński L., 2005: "Appraisal of risk assessment approach to stability of ships". *International Workshop on Ship Stability, Istanbul.*

Bekke, ter E.C.A., van Daalen, E.F.G., Willeboordse, E.J., Boonstra, H., Keizer, E.W.H., Ale, B., (2006): "Integrated safety assessment of small container vessels". *International Conference on Probabilistic Safety Assessment and Management, New Orleans.*

McTaggart K., de Kat J.O., 2000: "Capsize Risk of Intact Frigates in Irregular Seas". *SNAME Annual Meeting 2000*

Ericson, A., Person, J. and Rutgersson O. 1997: "On the use of formal safety assessment when analyzing the risk for cargo shift in rough seas", *Proceedings of RINA International Conference on Design and Operation for Abnormal Conditions, Glasgow.*

Schauer T., Romberg B., Jiang Ch., Troesch A.W., 1995: "Risk assessment of small fishing vessel trap net operations". *Marine Technology, Vol. 32, No 4.*

Rahola criterion revisited: an overview of Jaakko Rahola's research and career

Pekka Ruponen, *Aalto University, School of Engineering, Marine Technology,* pekka.ruponen@aalto.fi

ABSTRACT

Jaakko Rahola's doctoral thesis, entitled "The Judging of the Stability of Ships and the Determination of the Minimum Amount of Stability – Especially Considering the Vessels Navigating Finnish Waters", has had an enormous influence on the development of international regulations for intact stability. This paper presents the background for Rahola's research, along with the key findings of the thesis. Finally, a brief summary of Rahola's career and contribution to education of naval architecture and shipbuilding industry in Finland is provided.

Keywords: *Jaakko Rahola, ship stability criteria, history*

1. INTRODUCTION

Jaakko Rahola's thesis for the degree of Doctor of Technology was accepted on May 26th, 1939, by the Technical University of Finland, later known as Helsinki University of Technology (HUT, or TKK in Finnish), and finally merged to Aalto University, since 2010.

This thesis, entitled "The Judging of the Stability of Ships and the Determination of the Minimum Amount of Stability – Especially Considering the Vessels Navigating Finnish Waters", has had an enormous influence on the development of international regulations for intact stability, and even after 80 years, the "Rahola criterion" it is still often cited in various related literature.

Over the years, Rahola's research has been summarized and discussed, and for example, Herd (1979) has presented an extensive study on the Rahola criterion in respect to previous work on ship stability. In addition, a short biography, Arjava (2015), has recently been published also in English. This book provides a more detailed description of both Rahola's career and his character.

This paper presents a short overview of the key elements of Rahola's thesis, the so-called "Rahola Criterion" that is considered as the foundation for today's intact stability regulations. In addition, the essential parts of his professional career are briefly summarized.

2. BACKGROUND TO RAHOLA'S RESEARCH WORK

Jaakko Rahola was born in Mänttä on June 1st 1902. He graduated as a naval architect in 1925. His Master's thesis was "Designing a Gunboat". After this he was occupied as a shipbuilding engineer at the naval base, and eventually appointed head of the Construction Office at Navy Headquarters in 1933. During those years, he spent a lot of time designing and supervising the construction of submarines and gunboats, Arjava (2015).

During 1920s and early 1930s, several Finnish ships capsized and sank, with notable loss of life, both in the Baltic Sea and in the Finnish lakes. Two of them are briefly described.

One such incident was the capsizing of the Finnish torpedo boat *S2* in heavy weather in the Gulf of Bothnia in 1925. The whole crew of 53 were lost in the disaster. The ship had fairly good stability but apparently there was some leakage. Rahola was working for the Finnish Navy at the time.

Another disaster took place in the Lake Näsijärvi in 1929. The sinking of the steamship *Kuru* led to the loss of 136 lives. According to Arjava (2015), some of the casualties were relatives of Rahola. The deckhouse of the *Kuru* had been extended in 1927, thus raising the centre of gravity. At the same refit, the bulwark in the bow had been closed without scuppers. Accumulation of water on deck in the heavy weather was considered as the primary reason for the accident.

These two disasters, and a couple of smaller accidents, were the primary reason why Rahola became interested in development of a method for judging the stability of ships and determination of the minimum amount of stability, especially for ships navigating in Finnish waters. Rahola had been involved in analysing some of the capsizing accidents. He had managed to gather material on various capsized vessels, and he was planning to write his doctoral dissertation on this subject.

In autumn 1937, the shipbuilding professorship fell vacant at the University of Technology. Rahola applied for this position, and he was given 18 months to qualify for this post. He obtained a grant and leave of absence from the navy for this period.

Rahola managed to finalize his doctoral thesis within the given time frame. A notable contribution was provided by Mr. Tauno Kaartti from Naval Headquarters, who helped Rahola, for example by drawing various figures and graphs, Arjava (2015).

3. RAHOLA'S RESEARCH WORK

Methodology

Rahola started his thesis with an extensive review on methods for judging stability of ships, considering initial metacentric height, main dimensions of the ship and finally the righting lever curve. He noted that: "Only about a hundred years after forming the principles for the theory of stability one began to understand, by reason of a certain accident having occurred, the great importance the stability qualities of a vessel have for its seaworthiness and non-sinking qualities."

Most of these previous studies considered ships operating in high seas. Rahola focused on ships operating in Finnish waters, and he divided these fairways into two separate categories:

- Baltic Sea and Lake Laatokka (part of Finland at the time, now known as Ladoga)
- lakes, rivers and inner waters

The vessels and the operating conditions in these two areas were considered to be very different, and consequently, Rahola decided that different judging methods were needed.

During his studies, Rahola had spent over one month abroad, in Vienna, Berlin, Hamburg and London, Arjava (2015). The main objective of this travel was to gather detailed information on several capsizing accidents.

Rahola noted that for judging stability arm curves, he first needed to examine such cases, where a poor stability has evidently, or very likely, been the reason for the accident. During his travels, he had managed to gather a large number of stability curves for vessels having suffered accidents abroad (outside Finland).

In the appendix, Rahola describes 34 accidents that occurred outside Finland. However, he presents detailed stability analysis only for 13 ships, where reliable righting lever curves from various sources were available. Since the objective of the research was focused on ships operating in Finnish waters, most of these sample ships were quite small, representing typical coastal vessels. Rahola then divided these ships into three categories:

- adequate/sufficient stability
- critical stability
- insufficient stability

For this categorization, he used the available accident investigation reports, and especially comments on the stability characteristics of the ship and their influence on the casualty. Some of these ships were actually included in more than just one category since different loading conditions were considered separately, Table 1. For example, the whaler *Rau III* that capsized during sea trials in 1937 is included in all three groups. The actual loading condition clearly had insufficient stability, but the planned condition was judged as critical, and with full cargo the ship would have had adequate stability.

Table 1: Summary of the sample ships, and number of loading conditions in each category.

Name	Insufficient	Critical	Adequate
Torp. Boat no 10	1		
Margarethe Russ	1		1
Cargo ship	1	1	1
840 t cargo ship	2		
Negros	1	1	1
Flottbek	1		1
Rau III	1	1	1
Monica	1	1	
Kreuzsee	1	1	
Galleon		1	
Elbe I		1	1
Narvik			1
Calder	1		1
Total	**10**	**7**	**8**

It is worth noting that Rahola used symbols from the German Society of Naval Architects, and hence e.g. the initial metacentric height is marked with M_0G instead of the currently preferred GM_0. In this overview paper, all symbols and terminology are the same as in Rahola's thesis.

Stability Arm Characteristics

In 1930s the initial metacentric height was in practice the only measure of stability that was considered in Finland. Rahola noted that stability at large heel angles were more suitable for judging. He selected the following characteristic parameters for detailed comparison:

- righting arm values at 15°, 20°, 30° and 40° heel angles
- heel angle, where the maximum righting arm occurs, denoted as the "critical statical heeling angle", φ_m
- capsizing angle (i.e. vanishing stability), φ_k

The righting arms at the studied heel angles for the sample ships were plotted, based on the categorization for sufficient stability, Figure 1. The righting arms that were judged as sufficient were plotted on the right hand side, whereas the insufficient and critical cases were placed on the left hand side of each respective heel angle. The adopted plotting technique allowed drawing of a demarcation line between sufficient and critical stability.

Rahola also examined the literature and the various previous proposals for the critical capsizing angle φ_k and the heel angle φ_m, where the maximum righting arm is achieved. Based on this review and detailed analysis of the sample ships, he noted that with all probability, sufficient limits for the statical critical heeling angle and capsizing angle of small seagoing vessels are $\varphi_m \geq 35°$ and $\varphi_k \geq 60°$, respectively.

Rahola further noted that determination of the minimum righting arm at 40° heel is futile, because once the conditions of the smaller heel angles are complied with, also the stability at this large heel angle is sufficient.

When considering the capsizing angle, Rahola noted that it is not as important as the statical critical heel angle. Consequently, he concluded that the stability of a seagoing ship can be judged as sufficient if the following is satisfied:

- righting lever for 20° heel, $h_{20°} \geq 0.14\text{m}$
- righting lever for 30° heel, $h_{30°} \geq 0.20\text{m}$
- heeling angle of maximum righting arm $\varphi_m \geq 35°$

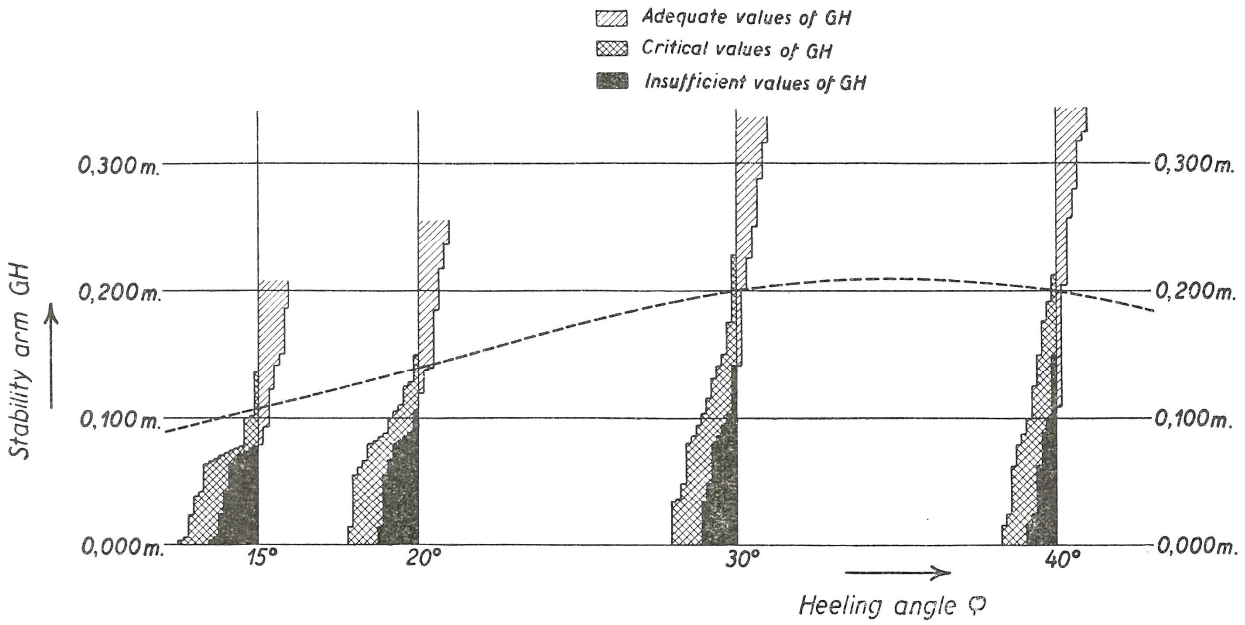

Figure 1: Critical righting arm values based on the sample ship data, adopted from Rahola (1939)

Rahola referred these requirements as the "minimum rule for the statical stability". In the subsequent text, he emphasized that this rule was not intended for general use, because the examined lost ships were mainly small ones, and the applicability of the same standard righting arm curve for ships with different size was considered unsuitable. In addition, he noted that for large ships a small initial stability may be compensated by means of greater righting arm values at large heel angles, mainly due to higher freeboard.

Limit Heel Angle for Dynamical Stability

Rahola noted that the dynamical stability of a vessel has a greater importance than the statical stability. He first raised the question on the limit angle, up to which the dynamical stability arm should be calculated.

For the limit angle of the range of stability φ_r, Rahola suggested the minimum of the following:

- critical statical heeling angle φ_m
- immersion angle of non-watertight hatches (i.e. down-flooding angle)
- estimated dynamical angle of repose of unsecured cargo (based on simplified method accounting for the roll period and the cargo hold)
- absolute maximum of 40°

Since full details of the sample ships were not available, the immersion angle and dynamical angle of repose were not applied by Rahola in the analysis of the sample ships.

It is also noteworthy, that the statical critical heeling angle is not considered as a range limit in the current intact stability regulations.

Minimum Dynamical Stability

After having determined the limit heel angle φ_r for calculation of the dynamic stability arm, i.e. the area under the righting lever curve, Rahola focused on defining the threshold value, using the same set of sample ships and loading conditions.

In order to obtain a precise picture, Rahola plotted the dynamical stability levers at the limit heel angle for the sample ships, Figure 2. He used the same drawing method as for the statical righting arm. Based on this result, he concluded that the dynamical stability is sufficient, if:

$$e_r = \int_0^{\varphi_r} h(\varphi) d\varphi \geq 0.08\text{mrad} \qquad (1)$$

Rahola called this "the new minimum rule for dynamical stability of seagoing vessels".

It is noteworthy that for some sample ships with adequate stability, the dynamical stability was limited to the heeling angle with maximum righting arm φ_m notably smaller than the absolute maximum of 40°.

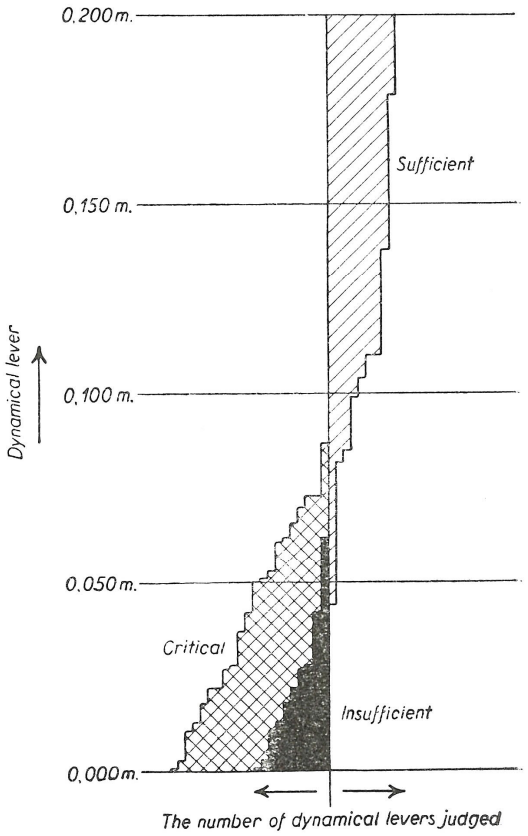

Figure 2: Critical dynamical righting lever value based on the sample ship data, adopted from Rahola (1939)

Rahola Criterion for Seagoing Vessels

The principles for judgment of stability of seagoing vessels are summarized in Figure 3. Although, Rahola considered both statical and dynamical stability, these requirements are usually simply known as the "Rahola criterion".

Rahola also briefly compared the statical and dynamical methods for judging sufficient stability, and concluded that they are in good agreement.

However, he noted that the dynamical one is more favourable to a ship designer, since it does not impose requirements for initial stability (metacentric height), even indirectly.

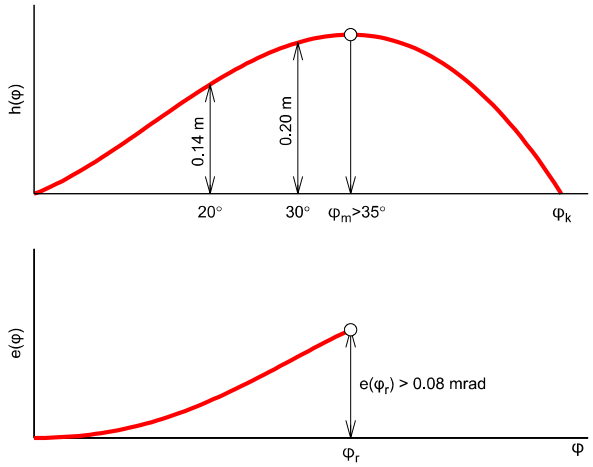

Figure 3: Visualization of the Rahola criterion for seagoing vessels, considering both statical and dynamical stability

Judging Method for Inner Waters

In addition to the well-known judging methods for stability of seagoing vessels, Rahola dedicated a full chapter for consideration of stability of vessels operating on the Finnish lakes.

Rahola considered that a separate judging method should be used for these vessels, mainly because they were not governed by the International Load Line Convention from 1930, and the freeboard varied notably between different vessels.

Consequently, Rahola believed that it was futile to establish requirements for critical statical heeling angle of lake vessels, and an alternative approach was needed. First, Rahola examined heeling in steady turning motion, considering both rudder and centrifugal forces. For this purpose, he had organized manoeuvring tests in calm water for several Finnish lake steamers in the summer of 1938.

Rahola continued with the wind and passenger crowding moments. After a careful literature analysis, he recommended to use 20 m/s for steady wind and 28 m/s for a gust in a gale, as suitable values for Finnish inland waters. Finally, he considered also the effects of waves and water on deck.

The final conclusion was that the determination of the minimum stability of a vessel in inland waters must be based on the most unfavourable situation, where heeling moments of turning motion and wind are combined. For this purpose Rahola presented various pre-calculated tables and diagrams for the evaluation of the sufficient dynamical stability.

Compared to the well-known judging method for seagoing vessels, the presented approach for vessels operating in inner waters is much more complex and immature.

Demonstration of the Judging Methods

The final chapter of the thesis contains calculation results and discussion on the stability of various Finnish ships that had capsized. Among them are the torpedo boat *S2* and the lake passenger steamer *Kuru*, the main motivators for Rahola's research work. The developed criteria, both for seagoing and lake vessels, were used, depending on the location of the accident.

4. LATER CAREER

In 1941 Jaakko Rahola was appointed Professor of shipbuilding. However, during the war, he was also a temporary head of the shipbuilding division at Naval Headquarters.

After the war, Rahola was made responsible for organizing the ships to be delivered to the Soviet Union as war reparations. The administration of this task was entrusted to the War Reparations Commission (Soteva). Later he was appointed Soteva's head of the shipbuilding department, and deeply involved in the development of the Finnish shipyards to undergo the enormous task of building 508 new ships in a short time period. These included sail, steam and motor ships, and they were built by several Finnish shipyards. The effort was ended in 1950, and Rahola could again concentrate on teaching at the university.

According to Arjava (2015), it appears that Rahola had some plans to continue his research on ship stability. However, considering his enormous workload during and immediately after the war, it is quite understandable that these plans never materialized.

In 1955 Rahola was appointed Rector of the university, a position that he held for ten years. During this time, the university moved from central

Helsinki to nearby Otaniemi, where the Aalto University campus is still located.

For the final years of his professional career, Rahola was working as Permanent Secretary at the Ministry of Trade and Industry, where he retired in 1969. Professor Jaakko Rahola died on September 10th 1973.

5. CONCLUSIONS

The criteria for sufficient the stability of seagoing vessels that Jaakko Rahola developed in his doctoral thesis were based on personal judging and categorization of quite limited set of sample ship data, Kobylinski and Kastner (2005). However, this pioneering work paved way for establishment of the first proper international regulations for intact stability at IMCO (Inter-Governmental Maritime Consultative Organization, predecessor of IMO) in 1960s, as discussed by Thomson and Tope (1970). A comprehensive overview of the development of the intact stability regulations is given by Kobylinski and Kastner (2005).

In addition to his significant research work in the late 1930s, Rahola's contribution to the war reparations program and teaching of naval architecture have had a notable effect on the subsequent success of the Finnish shipbuilding industry.

REFERENCES

Arjava, J. 2015. "Rahola Criterion – The life and work of Professor Jaakko Rahola", https://aaltodoc.aalto.fi/handle/123456789/15447

Herd, R.J. 1979. "Rahola Criterion – 40 Years On", *Royal Institution of Naval Architects*, Australian Branch, Sydney 17 August 1979.

Kobylinski, L.K., Kastner, S. 2005. "Stability and Safety of Ships – Volume 1: Regulation and Operation", Elsevier.

Rahola, J. 1939. "The Judging of the Stability of Ships and the Determination of the Minimum Amount of Stability – Especially Considering the Vessels Navigating Finnish Waters", https://aaltodoc.aalto.fi/handle/123456789/15149

Thompson, G., Tope, J.E. 1970. "International Consideration of Intact Stability Standards", *Transactions of the Royal Institution of Naval Architects*, Vol. 112, pp. 43-67.

Rahola criterion and the development of the Intact Stability Code

Alberto Francescutto, *University of Trieste, Italy,* francesc@units.it

ABSTRACT

The Criterion for Intact Ship Stability proposed by Rahola in 1939 spread around different countries and after the war also, due to its simplicity, constituted the basis for the first international provision on intact stability in 1968 in the frame of the recently created International Maritime Organization. This Criterion, although heavily criticized since the beginning for its semi-empirical nature, was included in both the Intact Stability Code, Res. A. 749, and, with some modifications, got mandatory status in the International Intact Stability Code 2008. It is quite easy to foresee that it will survive in the near future too, at least until the Second Generation Intact Stability Criteria, if and when adopted, will undergo thorough testing and tuning.

Keywords: *ship stability, stability criteria, IMCO, IMO, Jaakko Rahola.*

1. INTRODUCTION

Considering the last two millennia, from Archimedes (Francescutto and Papanikolaou, 2011), or more realistically the last two hundred years, from Bouguer (1746), it is clear that Ship Stability is an extremely complex and at the same time controversial subject.

Historical summaries of the developments at scientific, practical and regulatory levels have been provided by several Authors (Rahola, 1939, Bird and Odabashi, 1975, Kuo and Welaya, 1981, Steel, 1956, Herd, 1979, Kobylinski and Kastner, 2003) and, more recently reviewed by Francescutto (2016) in the frame of the development of the Second Generation Intact Stability Criteria in progress at IMO. There is a clear progress in terms of comprehension of the dangerous phenomena; this, however for long time was not accompanied by a parallel progress at regulatory level. This is particularly true for what concerns Intact Stability, the issue discussed in this paper. The different role played by the different parties and the request to be "simple", indeed, delayed the practical application (Francescutto, 1993). If this was justified when calculations were made "by hand", it is becoming less and less justified now, especially if we think that the developed regulations should guarantee the safety of ships carrying the population of a small town or substances able to heavily contaminate the environment. The length of time required to pass from formulation of a stability problem to adoption of a measure to avoid it has been highlighted in (Francescutto 2016). To quote recent developments in progress, it is interesting the history of parametric rolling. The first scientific developments in this field, are typically connected with the names of Kerwin, Paulling, Grim and Wendel, all active on this phenomenon about 60 years ago. Bird and Odabashi (1975), however, remind us that parametric rolling was already mentioned in 1892 (Pollard and Dudebout, 1892), 20 years after Mathieu (1868), studying the vibrations of an elliptic membrane, introduced the well known equation suitable for its description. Partial stability failures have been reported attributable to this phenomenon, and yet in 2019 there is still some doubt concerning the adoption of criteria against parametric rolling!

As known, the development of provisions for Intact Stability at international level was started by IMCO, later IMO, triggered by the conclusions of SOLAS1960, and of SOLAS1974, this latter asking for explicit consideration of the effects of meteo-marine environment. After some post-processing this led to the Code of intact stability for all ships covered by IMO instruments (IMO, 1993).

In the following we will analyze the origins of this document, mainly consisting of two Stability Criteria, applicable to all ship types, which are based in two studies published in the 1930s of past century (Pierrottet, 1935, Rahola, 1939), i.e. around 80 years ago.

There is no doubt that the Code of Intact Stability, although issued as a "recommendation" improved substantially the safety of navigation and the protection of the environment. A number of critical points, however, were raised since the beginning to these Criteria, based on the statistical nature of the first one and on the many empirical data and formulas used in the second one.

Situation changed with the adoption at IMO of the Formal Safety Assessment (IMO, 2002) changing the point of view for the development of regulations from "what went wrong" to "what could go wrong", i.e. from a "reactive" approach to a "proactive" one.

The combination of criticism and FSA led, in recent times, to the revision of the Code of intact stability for all ships covered by IMO instruments, producing the new International Intact Stability Code 2008 (IMO, 2008) which to a large extent consists in a reorganization of the previous Code and is still in force, and to the studies aimed at the development of the Second Generation Intact Stability Criteria, which is still in progress.

In the following of this paper, we will consider in some detail the developments leading to the Code of intact stability for all ships covered by IMO instruments as contained in IMO Res. A.749 (IMO, 1993), to identify the reasons of the fortune of the approaches contained in the two above mentioned papers.

2. THE SITUATION OF INTACT STABILITY PROVISIONS AT THE BEGINNING OF THE 1960s AND THE SOLAS'60 CONFERENCE

The situation of Intact Stability provisions in the period between Great War and WW II, with few exceptions related to individual designers, shipyards or shipping companies, was often more dominated by comfort (Vincent, 1939), i.e. indications of maximum values of metacentric height, than by stability safety, i.e. by minimum values of metacentric height. These latter were quite generic, with some notable exceptions.

After WW II, perhaps along with the needs connected with the large scale reconstruction, requiring new fleets, and the slow restructuration of shipping lines due to the competition with the airplane, a new sensibility concerning stability safety spread-out.

At the beginning of the 1960s, several countries had adopted provisions:

- based on discriminatory analyses on the statical and dynamical elements of righting arm, conducted on databases of accidents of the type of that proposed by Rahola (1939),

and/or

- provisions based on physical modelling of the external forces acting on the ship, based on statical balance or on energy balance. Noteworthy of the first type, was the Russian standard (see IMO, 1988), developed on the basis of the proposal contained in (Blagoveschensky, 1932), while the Japanese standard (Yamagata et al., 1959), based on the proposal contained in (Pierrottet, 1935), is of the second type.

Consideration of the effects of wind was also part of the criteria developed by US Coast Guard and Germany.

The 1960 SOLAS Conference was held in London from 17th May 1960 to 17th June. The Conference was attended by delegates from 55 countries. It was the first Conference to be held by IMCO. During the Conference both Damage and Intact Stability were discussed in detail. Here a short summary of the discussion concerning the Intact Stability is reported following Spinelli (1961). In the meetings of the Subcommittee for the compartmentation and stability studies, the delegate of the URSS stressed the fact that the provisions of the SOLAS Convention relating to stability in the event of damage do not ensure sufficient intact stability of the ship, so it is essential to establish special rules on the intact stability of the ship to be applied to all types of ships, so that it is possible to count on sufficient safety of the ship during normal navigation. These rules should take into account the ability of the ship to resist external forces such as the actions of wind and sea and the agglomeration of passengers on one side of the ship.

Almost all the delegations agreed on the need to study norms regarding intact stability, rules that should be imposed especially for small ships, but at the same time it was pointed out that the problem

was so important and so complex, that an in-depth study of it would have been impossible during the few days available for the work of the Conference. It was therefore unanimously decided to refer the matter to IMCO so that it could organize, with a matter of urgency, the study of intact stability provisions, which was the subject of recommendation n. 7 ("Intact Stability of Passenger Ships. Cargo Ships and Fishing Vessels") to the 1960 Convention (SOLAS, 1960):

"The Conference, having considered proposals made by certain Governments to adopt as part of the present Convention Regulations for intact stability, concluded that further study should be given to these proposals and to any other relevant material which may be submitted by interested Governments."

The Conference therefore recommended that "the Organization should, at a convenient opportunity initiate studies, on the basis of the information referred to above of:

a) intact stability of passenger ships,
b) intact stability of cargo ships,
c) intact stability of fishing vessels, and
d) standards of stability information,

taking into account the decisions of the present Conference on requirements for damage stability and the results of any further studies which may be carried out by the Organization on the subdivision and damage stability of cargo ships in pursuance of Recommendation 8 of the Conference, the object being the formulation of such international standards as may appear necessary."

The Conference further recommended that "in such studies the Organization should take into account studies already undertaken by the Food and Agriculture Organization of the United Nations on the stability of fishing vessels and should co-operate with that Organization on that aspect of the matter."

3. THE STATISTICAL APPROACH AND THE DEVELOPMENT OF THE GENERAL STABILITY CRITERION

As well reported in (Bird and Odabashi, 1975, Herd, 1979) several Authors developed Intact Stability provisions based on empirical formulas, with consideration of samples of ships, by discriminating some parameters, mostly consisting in the initial metacentric height and in characteristics of the statical righting arm. None of these had fortune, i.e. none became at least the basis for a national regulation.

Different consideration had the analysis done by Rahola (1939). While general details about this work are contained in the companion paper by Ruponen (2019), we consider here some strong points. It is a too important contribution to be summarized here, but it is important to consider at least the following couple of sentences from the Introduction: "The object of the present investigation is to find a procedure by means of which it may be possible to judge with adequate certainty the amount of the stability of a certain vessel which may come to navigate under the conditions prevailing on the lakes and the waters adjacent to our country, and to decide whether it is sufficient or not." … "With regard to stability circumstances we must clearly make a distinction between the determining and the judging of stability.". As reported by Kuo and Welaya (1981): "Rahola's thesis raised great interest throughout the world because it was the first comprehensive study of its kind and because the method is fairly simple to apply as it does not require any computations so long as the statical stability curve in still water is known. That is the reason why many national stability regulations or recommendations still rely on this approach in judging the stability of their fleets."

The situation regarding the current status of national stability requirement in various countries was analyzed in 1964 by the IMO Working Group on Intact Stability as a background for the development of international standards.

As reported by Kobylinski (in Kobylinski and Kastner 2003), commencing its work on intact stability criteria the STAB Sub-Committee stated that when developing international criteria, it is necessary to take into account the heeling moments from external forces at sea. It realized, however, that such an approach would not enable the development of stability criteria in a short time. Therefore, the SubCommittee decided to base future criteria, as a first step, on statistics of casualties, and in particular, analyzing stability parameters for ships which capsized and for those which were considered safe in operation. It decided also to analyze the contents of existing national stability requirements. As a result of this decision, the Intact Stability Working Group (IS) as well as the Panel of Experts on

Stability of Fishing Vessels (PFV) began to collect data on ships and fishing vessels that capsized and on ships that were considered safe in operation.

Rahola's work (1939), which at the time was already the base of several national regulations on Intact Stability, was considered the more systematic attempt to develop stability standards by applying an original method of analysis of stability parameters of ships that capsized and of ships considered safe in operation. This method, with modifications, was applied by IMO when developing the stability standards included in Resolutions A.l67 (IMO, 1968a) and A.l68 (IMO, 1968b), hence the nickname of "Rahola Criterion" often used to indicate these regulations.

Details on the development of IMO Res. A.167, regarding the extended sample of ships used in the statistics and the probability methods employed are contained in (Kobylinski and Kastner, 2003 and in Part C of International Intact Stability Code 2008). See also Nadeinski and Jens (1968) and Thompson and Tope (1970).

In their critical analysis, Bird and Odabashi (1975) discuss the cases of two ships in order to show the desirability of improved criteria with respect to Res. A.167 and A.168. Those ships more than fulfilled the minimum stability requirements of IMCO but yet capsized,

They concluded: "These examples show that IMCO recommendations, by themselves, are not sufficient to provide acceptable safety of ships, and as in both the cases the weather conditions were not too severe, we must look for some other basic reasons causing the capsize.". We note that this is presently under discussion at IMO.

4. THE ENERGY BALANCE AND THE DEVELOPMENT OF THE WEATHER CRITERION

Moseley (1850) introduced the concept of "dynamic stability" as the work done in inclining a ship and consequently stored as potential energy. The dynamic stability arm was used since long time to supplement the information contained in the initial metacentric height and in the statical stability arm. This allowed to obtain the series of semi-empirical stability criteria, progressively including analyses of accident at sea, culminating in the Rahola proposal in 1939. We had, however to arrive at 1935 (Pierrottet, 1935) to have the first complete formulation of an "energy balance" criterion. It is interesting to follow the debate following Pierrottet presentation at Royal Institution of Naval Architects; following the Chairman, "I do not wish in the least to detract from the good work that Professor Pierrottet has done. I think the Paper will be very useful to us, but I do hope it will be a long time before it is made the basis for new Board of Trade regulations by the Classification Societies. The number of losses from Capsizing is so exceedingly small, even more tiny than he says, that it would be a very stiff to impose these regulations."

We had to wait 15 years and the tragedy of Toya Maru to have a national regulation based on a weather criterion, and additional 35 years to have an international one.

The discussion above referred is cyclical in this field. The warnings of Reed became clear only after the painful sinking of the monitor Captain 150 years ago; unfortunately, it looks that this spirit was not completely absent in recent discussions at IMO.

As mentioned in § 2 above, at the beginning of the 60's, several countries had developed and adopted Criteria on Intact Stability based on physics, i.e. on the calculation of the heeling effect produced by external factors, like wind and waves, or internal factors, like passenger aggregation on side or manoeuvring. Two of them, although different as far as the "dynamic effects" were considered, i.e. if the maximum heeling was the result of a static balance or of the energy balance, were completely developed as Weather Criteria and applied since several years. In 1962 (Sarchin and Goldberg, 1962), laid the basis for what soon became the US Navy Weather Criterion.

It is interesting to note (as reported, for instance, in Spinelli, 1961) that during the Conference SOLAS'60, there was a wide discussion on Intact Stability, almost entirely based on a document submitted by the Russian delegation describing their intact stability criterion. The ensuing discussion was focused on the effect on stability of external forces. No conclusion could be reached, however, due to the important differences between the different criteria already existing, notably between the Russian and the Japanese criteria. Hence the above mentioned Recommendation n. 7. As we have seen in previous paragraph, the working group at IMO decided

differently, converging on the modification of Rahola's work, which could guarantee an acceptable outcome in the short term available.

The following SOLAS Conference, while acknowledging the progress made, thus recommended that "steps be taken to formulate improved international standards on intact stability of ships taking into account, inter alia, external forces affecting ships in a seaway which may lead to capsizing or to unacceptable angles of heel." (SOLAS, 1974).

The result was the adoption of the "Weather Criterion" in 1985 (IMO, 1985) for passenger and cargo ships, and in 1991 for fishing vessels (IMO, 1991), mainly as effect of merging the Japanese Criterion (Yamagata, 1959) with elements of the Russian Criterion (Blagoveshchensky, 1932, see also IMO, 1988).

Actually, the first proposal of a criterion for "Severe Wind and Rolling" at an International level was done in Regulation 31 in the frame of the Torremolinos International Convention on Safety of Fishing Vessels (IMO, 1977). The original text of the Conference quoted: "Vessels shall be able to withstand, to the satisfaction of the Administration, the effect of severe wind and rolling in associated sea conditions taking account of the seasonal weather conditions, the sea states in which the vessel will operate, the type of vessel and its mode of operation". The Guidance on a Method of Calculation of the Effect of Severe Wind and Rolling in Associated Sea Conditions was contained in Recommendation I of Attachment 3 to the Final Act of the Conference. The Criterion contained in the Guidance was extremely close to what later on became the IMO Weather Criterion for passenger and cargo ships other than fishing vessels. The fast progress leading to this proposal was certainly due to the strict collaboration between IMO, FAO and ILO, in view of the extremely high risk for human life associated with this occupation. Unfortunately, the completion of the Weather Criterion for fishing vessels came only in 1991 (IMO, 1991) and all the matter never became mandatory (see Francescutto, 2013).

5. THE CODE OF INTACT STABILITY FOR ALL SHIPS COVERED BY IMO INSTRUMENTS, THE INTERNATIONAL INTACT STABILITY CODE 2008 AND BEYOND

The provisions contained in the mentioned IMO Resolutions (IMO, 1968a, 1968b, 1985), with the addition of all other provisions developed for other ship types, were finally included in the Resolution A.749 - Code of intact stability for all ships covered by IMO instruments (IMO, 1993). This Code was amended in several points by Res. MSC.75 (IMO, 1998).

In 2001 (IMO, 2001a), following a submission from Italian delegation (IMO, 2001b) criticizing the methodology adopted to calculate several parameters of Weather Criterion, the SLF Sub-Committee was tasked to start the revision of the Intact Stability Code as contained in Res. A.749. At the beginning the activity of the working group operating in the frame of the SLF Sub-Committee was concentrated on the development of "rational" intact stability criteria. Soon, however, priority was given to polishing and restructuring Res. A.749 to make Part A of the Code mandatory, under SOLAS and ILLC Conventions, as requested by German delegation who provided an FSA analysis supporting this decision (IMO, 2003). This part was completed in 2007 with adoption of the new International Intact Stability Code 2008 (IMO, 2008). This transformation, from "recommended" to "mandatory" of both the "General Criterion (ex Res. A.167) and the Weather Criterion (ex Res. A.562), made it necessary to provide alternative ways (IMO, 2006, Part C of ISC2008) to comply with Weather Criterion for ship typologies which previously could be managed at national level.

We note, in particular, that, in view of the difficulty for some ship typologies to fulfill the requirement regarding the position of the maximum of the righting arm curve the Res. A. 167 was modified by setting the angle to 25 deg and allowing to go down to 15 deg with a compensation in dynamic stability (see IMO, 2008, Part C). It is interesting to note that Rahola originally proposed 35 deg. This standard, in fact, was ambiguous since the very beginning, since the regulation stated: "The maximum righting arm should occur at an angle of heel *preferably exceeding* 30 deg *but not less than* 25 deg.".

The working group could at this point restarted the activity on development of "rational" intact stability criteria, finally changing the title in "Second Generation Intact Stability Criteria". The situation up to 2015 was summarized in (Francescutto, 2016); an updating of the progress of this item is contained in (IMO, 2019).

It is noteworthy that the two pillars of the Intact Stability Code, i.e.:

- Criteria regarding righting lever curve properties, present evolution of "Rahola Criterion";
- Severe wind and rolling criterion (weather criterion),

already survived 50 years, with reasonably small changes, and in addition reached the mandatory status. The statement "Criteria included in the Code are based on the best state-of-the-art concepts, available at the time they were developed, taking into account sound design and engineering principles and experience gained from operating ships." was reiterated in the Preamble to ISC 2008.

In this moment it is not completely clear which will be the status of the Second Generation Intact Stability Criteria, if and when finalized. One possibility is that they will supplement the existing Criteria as interim recommendations (possibly on voluntary basis) for the time needed to gain sufficient experience from their application.

6. CONCLUSIONS

The Criterion proposed by Rahola (Rahola, 1939) was the last before WW II; it included an extremely detailed critical analysis of all the research and regulations existing at the time and was the result of an innovative discriminatory analysis conducted on a sample of ships. After the war, it spread around in different countries and, also due to its simplicity, constituted the basis for the first international provision on intact stability in the frame of the recently created International Maritime Organization. This Criterion, although heavily criticized since the beginning for its semi-empirical nature, was included in both the Intact Stability Code, Res. A. 749, and, with some modifications, got mandatory status in the International Intact Stability Code 2008.

It is quite easy to foresee that it will survive in the near future too, at least until the Second Generation Intact Stability Criteria, if and when adopted, will undergo thorough testing and tuning.

REFERENCES

Bird H., Odabasi A. Y., 1975, "State of Art: Past, Present and Future", *Proceedings International Conference on Stability of Ships and Ocean Vehicles*, Glasgow, pp. 312-317.

Blagoveshchensky S. N., 1932, "On a Method of Stability Standardisation", *Transactions of Scientific Research Institute of Shipbuilding USSR* 12.

Bouguer P., 1746, "Traité du Navire, de sa Construction et de ses Mouvements (Treatise of the Ship, its Construction and Movements)", Jombert, Paris.

Francescutto A., 1993, "Is it Really Impossible to Design Safe Ships?", *Transactions of the Royal Institution of Naval Architects* 135, pp. 163-173.

Francescutto A., Papanikolaou A. D., 2011, "Buoyancy, Stability and Subdivision: from Archimedes to SOLAS2009 and the Way Ahead", *International Journal of Engineering for the Maritime Environment (Proceedings of the Institution of Mechanical Engineers PartM)* 225, pp. 17–32.

Francescutto A., 2013, "The Evolution of the Regulatory Stability Regime for Fishing Vessels", Proceedings of the International Conference IDS2013, Iquitos, Perù, 17th – 19th July 2013, Iquitos, Peru, pp. 14.1-14.18.

Francescutto A., 2016, "Intact Stability Criteria of Ships – Past, Present and Future", *Ocean Engineering* 120, pp. 312-317.

Goldberg L. L., Sarchin T.H., 1962, "Stability and Buoyancy Criteria for U.S. Naval Surface Ships", *Transactions of the American Society of Naval Architects and Marine Engineers* 70, pp. 418–458.

Herd R. J. 1979, "Rahola Criterion – 40 Years On", *Royal Institution of Naval Architects*, Australian Branch, Sydney 17 August 1979.

IMO, 1968a, "Resolution A.167 - Recommendation on Intact Stability for Passenger and Cargo Ships Under 100 Metres in Length", 28 November.

IMO, 1968b, "Resolution A.168 - Recommendation on Intact Stability of Fishing Vessels", 28 November.

IMO, 1977, "International Conference on Safety of Fishing Vessels 1977 - Final Act of the Conference, with Attachments, including the Torremolinos International Convention for the Safety of Fishing Vessels, 1977".

IMO, 1985, "Resolution A.562 - Recommendation on a Severe Wind and Rolling Criterion (Weather Criterion) for the

Intact Stability of Passenger and Cargo Ships of 24 Metres in Length and over", 20 November.

IMO, 1988, "SLF 33/INF.4 - Development of intact stability requirements for all types of ships covered by IMO instruments, Submitted by the USSR", 6 May.

IMO, 1991, "Resolution A.685(17) - Weather Criterion for Fishing Vessels of 24 Metres in Length and Over", 6 November.

IMO, 1993, "Resolution A.749 - Code of intact stability for all ships covered by IMO instruments", 4 November.

IMO, 1998, "Resolution MSC.75(69) - Adoption of Amendments to the Code on Intact Stability for all Types of Ships Covered by IMO Instruments (Resolution A. 749(18))", 14 May.

IMO, 2001a, "SLF 44/18 - Report to the Maritime Safety Committee", 18 October.

IMO, 2001b, "SLF 44/INF.6 - Weather Criterion for Large Passenger Ships, Submitted by Italy", 12 July.

IMO, 2002, "MSC/Circ.1023 - MEPC/Circ.392 - Guidelines for Formal Safety Assessment (FSA) for use in the IMO Rule-Making Process", 5 April.

IMO, 2003, "MSC 78/24/1 - Revision of the Code on Intact Stability, Submitted by Germany", 15 December.

IMO, 2006, "MSC.1/Circ.1200 - Interim Guidelines for Alternative Assessment of the Weather Criterion", 24 May.

IMO, 2008, "International Code on Intact Stability".

IMO, 2018, International Intact Stability Code 2008.

IMO, 2019, "SDC 6/WP.6 - Finalization of Second Generation Intact Stability Criteria - Report of the Experts' Group on Intact Stability", 7 February.

Kobylinski, L. K., Kastner, S. 2003, "Stability and Safety of Ships – Volume 1: Regulation and Operation", Elsevier.

Kuo C., Welaya Y., 1981, "A Review of Intact Ship Stability Research and Criteria", *Ocean Engineering* 8, pp. 65-84.

Mathieu E., 1868, "Mémoire sur le Mouvement Vibratoire d'une Membrane de Forme Elliptique", *Journal de Mathématiques Pures et Appliquées* (2) 13, pp. 137-203.

Moseley H., 1850, "On the Dynamical Stability and on the Oscillations of Floating Bodies", *Philosophical Transactions of the Royal Society of London* 140, pp. 609-643.

Nadeinski V. P., Jens, J. E., 1968, "The Stability of Fishing Vessels", *Transactions of the Royal Institution of Naval Architects* 110, pp. 1-27.

Pollard J., Dudebout A., 1892, "Théorie du Navire, Vol. III - Dynamique du Navire: Mouvement de Roulis sur Houle, Mouvement Rectiligne Horizontal Direct (Résistance des Carènes)", Gauthier-Villars, Paris.

Pierrottet E., 1935, "Standards of Stability for Ships", *Transactions of the Royal Institution of Naval Architects* 77, pp. 208–222.

Rahola J. 1939, "The Judging of the Stability of Ships and the Determination of the Minimum Amount of Stability – Especially Considering the Vessels Navigating Finnish Waters", Doctoral Thesis, Helsinki, https://aaltodoc.aalto.fi/handle/123456789/15149

Ruponen P., 2019, "Rahola Criterion Revisited: An Overview of Jaakko Rahola's Research and Career", *Proceedings of the 17th International Ship Stability Workshop ISSW2019, Helsinki, Finland*, pp. 15-20.

SOLAS, 1960, "International Convention for the Safety of Life at Sea, 1960", London.

SOLAS, 1974, "International Conference on Safety of Life at Sea 1974 - Final Act of the Conference, with attachments, including the International Convention for the Safety of Life at Sea, 1974", London.

Spinelli F., 1961, "La Compartimentazione e la Stabilità delle Navi Mercantili dopo la Conferenza di Londra 1960 sulla Salvaguardia della Vita Umana in Mare (Compartmentation and Stability of Merchant Ships after London Conference of 1960 on Safety of Human Life at Sea)", *Tecnica Italiana* 26, pp. 1-17.

Steel H. E., 1956, "The Practical Approach to Stability of Ships", *Transactions of the Royal Institution of Naval Architects* 98, pp. 381-409.

Thompson G., Tope J. E., 1970, "International Consideration of Intact Stability Standards", *Transactions of the Royal Institution of Naval Architects*, Vol. 112, pp. 43-67.

Vincent, S. A., 1939, "Transverse Stability", Principles of Naval Architecture – Written by a Group of Authorities , Rossell, H. E. and Chapman,L. B.(Eds.), Vol. I.,SNAME, New York, pp. 99-137.

Yamagata M., 1959, "The Standard of Stability Adopted in Japan", *Philosophical Transactions of the Royal Society of London* 101, pp. 417-443.

Can the generalized Pareto Distribution be useful towards developing ship stability criteria?

Panayiotis A. Anastopoulos, *Department of Naval Architecture and Marine Engineering, National Technical University of Athens, Greece,* panasto@central.ntua.gr

Kostas J. Spyrou, *Department of Naval Architecture and Marine Engineering, National Technical University of Athens, Greece,* k.spyrou@central.ntua.gr

ABSTRACT

The paper investigates the effectiveness of the generalized Pareto Distribution (GPD) for modelling the tail of the distribution of ship rolling motions and particularly, for calculating the probability of capsize in beam seas. To this end, large-scale Monte Carlo numerical experiments were performed for an ocean surveillance ship assumed to operate in two qualitatively different, in terms of the observed frequency of stability failures, sea states; one where capsizes are realized quite often and another where they are extremely rare. For both sea conditions, GPD models were fitted to datasets containing roll exceedances above a pre-defined threshold and their reliability is tested herein against the rough Monte Carlo estimates, obtained by direct counting. The possibility of approximating the tail through several GPDs is discussed and the idea of associating threshold selection with the shape of the GZ curve is proposed for enhancing the accuracy of the approach. To evaluate the rumored "extrapolation" character of the GPD beyond the largest observation used in the fitting procedure, a comparison with the predictions of the "critical wave groups" method is presented for the second (mild) sea state.

Keywords: *Probability, Capsize, Generalized Pareto Distribution, Statistical extrapolation, Extreme events, Critical wave groups.*

1. INTRODUCTION

Several techniques can be employed for obtaining the distribution of the responses of a dynamical system subjected to random excitation (e.g. Chai et al., 2017). However, their application in the problem of ship capsize is hindered by their large computational requirements and/or deficiencies in dealing with the complexity of ship dynamics at large angles. Brute-force Monte Carlo simulations, despite being very attractive due to their accuracy, can easily turn into a computationally intensive exercise when a large number of extremely rare events, like capsizing, must be produced.

One possibility to alleviate the problem could be the tools provided by Extreme Value Theory (EVT), a branch of statistics focused on making inferences about the extreme values in a random process. Specifically, the second extreme value theorem (Balkema and de Haan, 1974; Pickands, 1975) states that, under certain conditions, the generalized Pareto distribution (GPD) is a limiting distribution for excesses over thresholds. This has motivated the development of a number of threshold-based methods seeking a solution to the problem of rarity of extreme ship responses through fitting the GPD to data obtained from pertinent time-domain simulations (e.g. Belenky et al., 2016; Campbell et al., 2016). Nonetheless, it is the strong data-driven character of such methods that may eventually deteriorate their effectiveness and therefore, their application for direct ship stability assessment remains an open question.

As is well known, the main issue, arising rather naturally in practical implementations of the theorem, is the selection of an appropriate threshold for fitting the GPD. Despite the model being mathematically exact at infinitely high levels, it is believed that it could still be reliable if determined with respect to a sufficiently high threshold. This, runs the danger, on the one hand, of idly expending computational resources if an exceptionally high threshold is set, resulting in datasets with only few (if not any at all) extremes. On the other hand, a lower threshold may not be able to produce reliably the tail. In practical ship stability, normally we do not need very large roll angles for judging safety since, beyond some moderate to high angle, the

flooding of closed spaces is inevitable. Hence, a question is raised whether the GPD could be meaningfully applied towards developing a stability criterion. Much of effort has been put over the last years in efficiently fitting the GPD using reasonably-sized datasets generated by fast, yet qualitatively realistic, hydrodynamic codes (e.g. Weems et al., 2016).

In our current work, the possibility of analyzing the tail structure through successive GPD fits is discussed for the problem of ship rolling in beam seas. At the same time, an attempt is made to associate threshold selection with the shape of the GZ curve of a vessel. The idea is to identify regimes where response exhibits different probabilistic qualities and then, utilize the limits of these regimes for thresholding. The performance of the approach for calculating the probability of capsize in severe sea conditions is tested against the rough Monte Carlo estimates, obtained by direct counting. Finally, to evaluate the reliability of the GPD for "statistical extrapolation" (i.e. for predicting events beyond the largest observation used in the fitting procedure), a comparison with the results of the "critical wave groups" method (Anastopoulos and Spyrou, 2018) is presented for a sea state characterized by very rare extremes.

2. MATHEMATICAL BACKGROUND

In this section, the second extreme value theorem is formulated and the basic properties of the GPD are outlined. The potential of the model for treating the problem of rarity, described in the above, is discussed in the context of a more general framework, commonly known as the "principle of separation" (e.g. Belenky et al., 2012; Mohamad and Sapsis, 2016).

The principle of separation

The term is often utilized to express the idea of decomposing the ship response problem into sub-problems with the aim of analyzing the rare extremes separately from a background state, mostly associated with conventional non-rare outcomes. Thence, the "non-rare" part deals with the distribution of the conditions that can lead to the occurrence of extreme events, while the "rare" one targets the conditional probability of extremes, given that specific conditions are met:

$$Pr(X > x) = \underbrace{Pr(X > x | X > u^*)}_{rare} \times \underbrace{Pr(X > u^*)}_{non-rare} \quad (1)$$

where X is the response process, x is the associated state variable and u^* is a threshold introduced for distinguishing extreme from non-extreme regimes.

As realized, ship motions have, thus far, been classified with respect to their relative frequency of occurrence (rare/non-rare), rather than according to the corresponding level of nonlinearity governing the dynamics of each sub-problem. In the "rare" part, however, one is confronted with phenomena that are not only very unlikely, but also strongly nonlinear. On the contrary, a "non-rare" event is not essentially linear; neither nonlinearity itself is sufficient to infer rarity. To explicitly account for the effect of nonlinearity also on the solution of the "non-rare" part, the last term in Eq. (1) is further decomposed as:

$$Pr(X > u^*) = \underbrace{Pr(X > u^* | X > u_L)}_{nonlinear} \times \underbrace{Pr(X > u_L)}_{linear} \quad (2)$$

where u_L is an intermediate threshold indicating the limit between linear and nonlinear ship responses within the "non-rare" sub-region. Definitely, through this concept, one could go even deeper by disassembling both the "rare" and "non-rare" sub-problems of Eq. (1) in more parts; yet this would require a rational procedure for selecting those additional intermediate thresholds $u_i, i = 1, \dots, n$ that would separate regimes with different levels of nonlinearity.

In this setting, it is straightforward to calculate the last term in Eq. (2) using a Gaussian distribution. Mathematical justification for the solution of the "rare" sub-problem will be provided by the second extreme value theorem, presented in the following section. As for the probability of non-rare and nonlinear events, there are numerous statistical models to try. In this study, however, the GPD is employed once again knowing that it embodies a large class of distribution functions covering a continuous range of possible shapes. This allows for

the data to decide the most suitable amongst the models integrated into the GPD.

The generalized Pareto Distribution (GPD)

Generally, the GPD is specified by three parameters (u, σ, ξ) and below it is expressed in terms of its complementary distribution function $F_X(x) = 1 - \bar{F}_X(x)$:

$$\bar{F}_X(x) = \begin{cases} \left(1 + \frac{\xi(x-u)}{\sigma}\right)^{-1/\xi} & , if\ \xi \neq 0 \\ exp\left(-\frac{x-u}{\sigma}\right) & , if\ \xi = 0 \end{cases} \quad (3)$$

where $x \geq u$, if $\xi \geq 0$ and $u \leq x \leq u - \sigma/\xi$, if $\xi < 0$. In Eq. (3), u is the location parameter of the distribution representing the minimum value that the associated random variable X can attain. Whenever the GPD is employed for modelling the tail of another distribution, u is basically the point where the two distributions merge. The scale parameter σ is the "spread" factor, controlling the dispersion of X above u. Finally, ξ affects the shape of the distribution in a more qualitative way. For distributions with exponentially decreasing tails, such as the Normal, the GPD leads to $\xi = 0$. For heavy-tailed distributions, often encountered in the case of unbounded systems, $\xi > 0$. The opposite ($\xi < 0$) implies a light-tailed distribution and thus, the existence of an upper bound at $x = u - \sigma/\xi$.

The theoretical importance of Eq. (3) was proved by Balkema and de Haan (1974) and Pickands (1975) who showed that the distribution of independent and identically-distributed (i.i.d.) excesses over u asymptotically tends towards the GPD, as $u \to \infty$. The statement holds if and only if the parent distribution belongs to the so called "domain of attraction" of one of the extreme value distributions (i.e. Gumbel, Fréchet and reverse Weibull), all incorporated into a single model, known as the generalized Extreme Value distribution (GEV). Moreover, it can be verified that if times until exceedance constitute a Poisson random process with GPD excesses, then the GEV is obtained as the distribution of the corresponding extremes. Another interesting property of the GPD is "threshold stability", meaning that if X is a GP-distributed random variable for some $u^* > 0$, then it is also generalized Pareto for any $u > u^*$ retaining the same shape parameter. It is worth noting that the GPD is uniquely characterized through the last two properties since no other family of distributions exhibits such qualities (Davison and Smith, 1990).

Threshold selection

On these terms, it is rather natural to assume that local stabilization of the shape parameter could be the key for detecting the minimum threshold value above which the distribution of excesses has practically converged to the GPD. The idea has been discussed in several studies, often in comparison with alternative identification procedures, such as those described in e.g. Campbell et al. (2016). Yet, the threshold stability property itself could be the source of inherent limitations in pinning down the threshold. If a dataset obeys the GPD at one threshold, then, the model, in order to preserve its validity at all higher thresholds, should be free to adapt through its only left unconstrained parameter, i.e. the scale parameter. Equally, restricting the threshold to a fixed value in an attempt to extrapolate a trend into the tail region could entail the possibility of overfitting.

The invariance of the model form at high levels was an additional motivation for investigating the tail structure by employing successive GPDs in Eqs. (1) and (2). Even though consistency with the theorem may not be fulfilled for u_L, being essentially the angle up to where ship motions are relatively small, the GPD, due to its very flexibility, will probably succeed in fitting data within the intermediate range $[u_L, u^*]$. The crucial step, however, is the selection of u^* so as to reflect a lower bound for the occurrence of extremes. From a ship design perspective, the angle φ_{max} corresponding to the maximum of the GZ curve could be tried since rolling beyond this limit is quite likely to result in capsize or, at least, in an extreme dynamic event.

3. RESULTS AND DISCUSSION

Massive Monte Carlo simulations were performed for an ocean surveillance ship, with main parameters listed in Table 1, to evaluate the accuracy of the GPD-based approach presented in the above. The concept of separation, as expressed through Eqs. (1) and (2), is illustrated in Figure 1, where the GZ curve of the vessel is divided into three sub-regions with limits indicated by vertical lines:

I. $\varphi \in [0, u_L]$, with $u_L = 20\text{deg}$
II. $\varphi \in [u_L, u^*]$, with $u^* = 37\text{deg}$
III. $\varphi > u^*$

Table 1: Main parameters of the vessel.

Parameter	Dimensional value	Dimensions
$I + A_{44}$	5.540×10^7	$kg \cdot m^2$
Δ	2.056×10^6	kg
B_1	5.263×10^6	$kg \cdot m^2/s$
B_2	2.875×10^6	$kg \cdot m^2$
C_1	3.167	m
C_3	-2.513	m

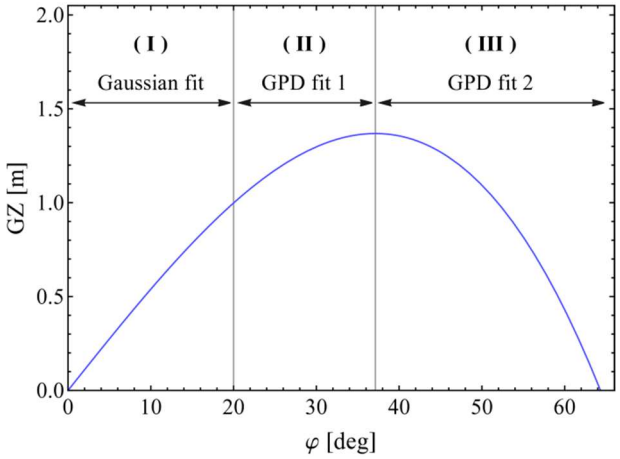

Figure 1: The restoring arm of the vessel divided into sub-regions: (I) non-rare/linear, (II) mildly rare/nonlinear and (III) rare/nonlinear.

The ship is assumed to operate in sea conditions described by the Bretschneider spectrum (Ochi, 1998):

$$S_{\eta\eta}(\omega) = \frac{1.25}{4}\frac{\omega_p^4}{\omega^5}H_s^2 exp\left[-\frac{5}{4}\cdot\left(\frac{\omega_p}{\omega}\right)^4\right] \quad (4)$$

where H_s is the significant wave height and $\omega_p = 2\pi/T_p$ is the modal frequency of the spectrum. Two sea states of slightly different severity were duly selected for demonstrating certain capabilities and limitations of the proposed method. Their characteristics are given in Table 2.

Table 2: Sea state characteristics.

	H_s	T_p
Sea state *A*	4m	11s
Sea state *B*	3m	11s

Time-histories of roll motion $\varphi(t)$ were generated using a simple 1DOF roll equation:

$$(I + A_{44})\ddot{\varphi} + B_1\dot{\varphi} + B_2\dot{\varphi}|\dot{\varphi}| + \\ +g\Delta(C_1\varphi + C_3\varphi^3) \\ = M(t) \quad (5)$$

with $I+A_{44}$ being the total roll moment of inertia (including the added mass effect), g is the gravitational acceleration, Δ is the ship displacement and B_1, B_2 and C_1, C_3 are the damping and restoring coefficients, respectively. The wave-induced moment was modelled using the standard spectral representation method (St. Denis and Pierson, 1953):

$$M(t) = \\ \sum_n \sqrt{2S_{\eta\eta}(\omega_n)F_{roll}(\omega_n)\delta\omega_n}\cos\theta_n(t) \quad (6)$$

where $\theta_n(t) = \omega_n t + \varepsilon_n$. In Eq. (6), ε_n are random variables uniformly distributed over $[0,2\pi)$, $d\omega$ is the frequency resolution, A_n are the amplitudes of the wave components and ω_n are the associated frequencies. Details for the roll moment amplitude operator F_{roll} of the vessel can be found in Su (2012).

Eventually, statistics of roll motion were obtained without assuming the ergodic property for the response. Consequently, the analysis was made on a set of 6,000,000 short-duration realizations, sampled at a fixed time instant $t_s = 150\text{s}$. The great benefit from this approach is that collected roll data are statistically independent, as required by the second extreme value theorem. Roll data were partitioned in 15 datasets and for each dataset, the GPD parameters (shape and scale) were calculated using the Maximum Likelihood Estimation method (MLE). The mean values of the 15 pairs of parameters were selected as the most representative values for fitting the whole dataset (6,000,000 samples).

Sea state scenario A

In this case study the objective is to evaluate the reliability of the GPD for calculating the probability of capsize when data are available in the entire range of stability $[0, \varphi_v]$, where $\varphi_v = 64\text{deg}$ is the angle of vanishing stability of the vessel. The selection of the capsize limit was based on the well-known feature of Eq. (5) concerning the time-depending shifting of the unstable equilibrium in the presence of wave excitation (e.g. Falzarano et al., 1992). In this regard, response trajectories that exceeded (in absolute

sense) the limiting value $1.2\varphi_v$ before reaching $t_s =$ 150s were marked as corresponding to capsize, resulting in a total number of 393 capsizes for the specific sea state. No doubt, considering stability failure at an exceptionally high roll angle is unreasonable since flooding is very likely to occur at lower angles. As a matter of fact, it is sufficient to confirm accuracy in GPD predictions only up to intermediate roll angles representing practical capsize limits (e.g. 40deg-50deg). For scientific curiosity reasons however, and since a similar model could be the subject of investigation in a different (non-marine) context, the tail region $[\varphi_{max}, \varphi_v]$ is examined in its entirety just for highlighting particular features of the ship rolling process that may not be so evident at lower levels.

Next, results are first presented for the case of "bounded" ship motions, meaning that desired statistics were computed after filtering out the 393 capsize cases. As realized, eliminating the possibility of capsize may conceal valuable information for our analysis. It is, nevertheless, interesting to investigate the effectiveness of traditional techniques of EVT, such as the POT/EPOT (peaks or envelope peaks over threshold) methods, which rely solely on the peak excesses of a random process for fitting the GPD. Since a "peak" by definition implies the return of a response trajectory towards the upright state, it is clear that these methods deal with a qualitatively different problem where the underlying system remains always bounded. On the contrary, in our approach the GPD is fitted to all the exceedances recorded at the selected sampling instant t_s, regardless of being peaks.

Figure 2 shows the probability of exceedance P_e of rolling angles $\varphi \in [0, \varphi_v]$ derived from the Monte Carlo (MC) simulations through direct counting (circles) for the bounded system. The solution of the linear "non-rare" sub-problem, being the Gaussian fit curve (solid line), is extended up to region (III) for comparison purposes. Dashed lines indicate the solution of the combined nonlinear sub-problem ("non-rare" + "rare"), obtained by two individual GPD fits; one in region (II) and one in region (III). The shaded area illustrates the corresponding 95% confidence interval (CI). In analogy to Figure 1, vertical lines denoting the limits of regions (I-III) are included. Details for the estimated GPD parameters are provided in Table 3.

Table 3: GPD fitting results (bounded system).

region II: [20deg, φmax]			
scale parameter		shape parameter	
mean value	95% CI	mean value	95% CI
3.471	[3.443, 3.499]	-0.024	[-0.029, -0.018]
region III: [φmax, 64deg]			
scale parameter		shape parameter	
mean value	95% CI	mean value	95% CI
3.550	[3.240, 3.860]	0.071	[-0.019, 0.161]

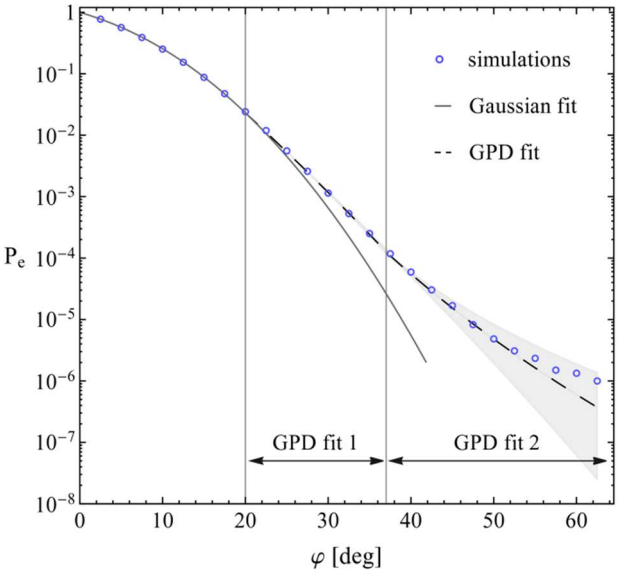

Figure 2: GPD fits (dashed lines) vs. rough Monte Carlo estimates (circles) for the bounded system.

As observed, there is good coincidence between the proposed calculation scheme and the MC results in the entire range of stability of the vessel. Moreover, the negative shape parameter in region (II) confirms the existence of a right boundary, as anticipated. Despite that, a heavy tail is eventually obtained since in region (III) the shape parameter becomes positive, yet with the associated confidence interval containing also negative values. The fact that the method fails to maintain the light tail trend in region (III) is, therefore, explained by the uncertainties arising in the estimation of the shape parameter at higher levels, where data are naturally fewer. Finally, it is remarkable that there is less discrepancy in the computation of the scale parameter, given that its value is practically the same in both regimes.

Below, the assumption of bounded motions is removed to assess the validity of the treatment presented so far. To this end, statistics were derived separately for threshold exceedances that led to capsize ("escapes") and for short-time exceedances that remained bounded in the long run ("returns"). In

Figure 3, P_c is the conditional probability of a return/escape, given that a roll angle threshold φ, displayed on the horizontal axis, has already been exceeded. Since P_c is, in fact, the ratio of observed escapes/returns to the total number of exceedances over a threshold $\varphi \in [0, \varphi_v]$, this plot essentially reflects the contribution of each outcome to the overall probability of exceedance P_e. A circle has been placed on the curve of the escapes at $u^* = \varphi_{max}$ to highlight that in region (III) extremes are, at least, 34% underpredicted with respect to their "true" values that would be obtained if capsizes had been included in the calculations. This demonstrates the necessity of developing methods free of POT/EPOT-like assumptions, often introduced in the light of "strict-sense stationarity" of ship response (Kougioumtzoglou and Spanos, 2014).

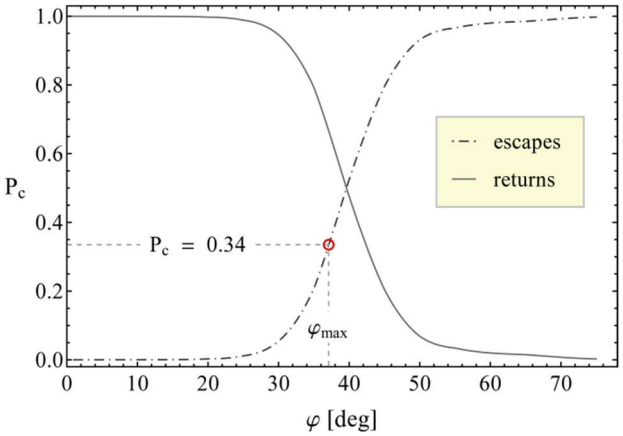

Figure 3: Contribution of escapes and returns to the total probability of a threshold exceedance.

At the same time, Figure 3 reveals new locations for potential thresholding, other than those used in this study. Even more, one may be tempted to analyze individual sub-problems into more parts than those proposed here. For instance, one could perform the decomposition over both/either the point where the two curves intersect (e.g. at 40deg) and/or the angle where the maximum curvature on the escapes curve is observed (e.g. at 50deg). However, proceeding to exhaustive decompositions is not recommended because information could be lost due to the separation principle itself. The concept assumes that threshold exceedances have negligible dependence on the statistics below the threshold. In this sense, it may be more difficult to capture the whole picture when approximating the solution through a large number of conditionals, considering that extremes may not eventually be consistent with the mechanism that generates the main body of the data.

In Figure 4, the probability of exceedance P_e was derived by analyzing the entire sample, including the 393 capsize cases. The notation is the same as in Figure 2. The results of the corresponding GPD fitting procedure are summarized in Table 4. As noticed, the MC trend (circles) implies a heavy tail that in region (III) becomes almost parallel to the φ-axis. However, this cannot be inferred from the GPD model of the current method (dashed lines). Evidence for the tail structure has already been given in Figure 3 where it is shown that above 40deg exceedance probabilities are mostly determined by the escaping trajectories. With returns gradually vanishing in the very extreme region ($\varphi >$ 50deg), the probability of exceedance P_e naturally tends to the probability of capsize (393 capsizes / 6,000,000 samples). In Figure 4, this resulted in almost two orders of magnitude greater probabilities than those presented in Figure 2 for the bounded system.

Table 4: GPD fitting results (unbounded system).

region II: [20deg, φmax]			
scale parameter		shape parameter	
mean value	95% CI	mean value	95% CI
3.221	[3.200, 3.243]	0.085	[0.080, 0.090]
region III: [φmax, 64deg]			
scale parameter		shape parameter	
mean value	95% CI	mean value	95% CI
7.038	[5.526, 8.551]	0.781	[0.657, 0.904]

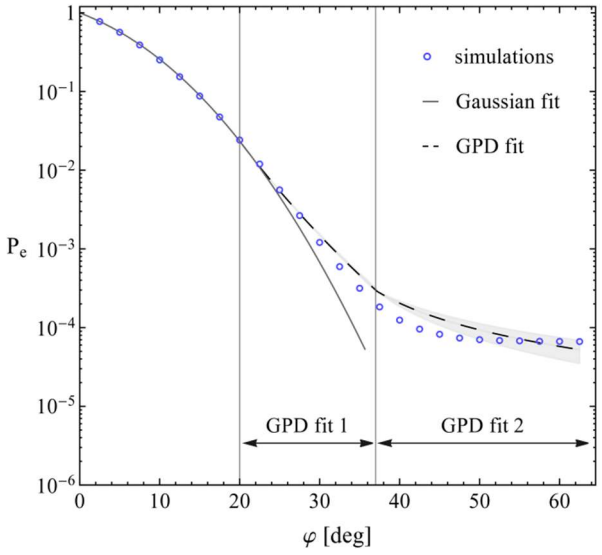

Figure 4: GPD fits (dashed lines) vs. rough Monte Carlo estimates (circles) for the unbounded system.

The poor performance of the method could stem, at least partially, from the very special shape of the roll response distribution, provided that validity of the GPD is asserted only if the underlying distribution belongs to the domain of attraction of the GEV distribution. However, there is no proof on whether ship rolling truly fulfills this requirement. It is remarkable, though, that in region (III) the produced GPD is characterized by a large positive shape parameter, indicating that the model realizes the qualitative changes induced by the now existing possibility of system escape. Again, large uncertainties are observed in region (III), despite the presence of quantitatively more extremes than in the case of bounded motions.

Although having a "rich", in terms of capsize occurrences, sample enhances the reliability of the MC estimates, the coexistence of states with distinct dynamics (escapes-returns) entails technical difficulties in their joint statistical description. Specifically, to calculate exceedance probabilities from a sample containing aggregated data of escapes and returns, one has to define the "capsize state" (here noted as φ_∞). In our MC setup, if a response trajectory exceeded the capsize limit $1.2\varphi_v$ at some time instant $t < t_s$, the integration of Eq. (5) was terminated and a fixed value $\varphi_\infty = 1.2\varphi_v$ was eventually kept for further analysis (e.g. Figure 4). On the other hand, assigning the exact same value φ_∞ to all capsized cases will inevitably result in artificial "mass" concentration in the corresponding probability density function (PDF), as illustrated in Figure 5. Due to the data-driven nature of fitting procedures, the location of this mass is expected to affect the calculation of the GPD parameters.

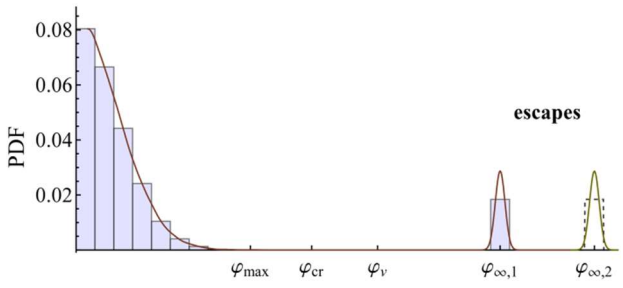

Figure 5: Sensitivity of GPD estimates to the statistical description of escapes.

The sensitivity of the current method to the selection of φ_∞ in calculating the probability of exceeding 50deg was investigated for four φ_∞ scenarios ($1.2\varphi_v$, 80deg, 90deg and 180deg). The results confirmed that by changing the relative distance between φ_∞ and the main probability mass the GPD monotonically overestimates (from 1.2 up to 2.4 times) the corresponding probability obtained from the MC simulations in Figure 4. Hence, in Figure 4, the GPD was shown in its utmost performance since setting $\varphi_\infty > 1.2\varphi_v$ would certainly deteriorate its accuracy. This is because the sample variance in region (III) varies through φ_∞ and thus, the GPD adapts, although not very successfully, to the data. This sensitivity justifies why the scale parameter is larger in Table 4 than in Table 3, where the φ_∞ parameter is not involved.

Sea state scenario B

Lowering H_s by only 1m leads to substantial changes in ship behavior, given that for the specific sea conditions all the collected observations were below φ_{max} (no capsizes recorded). Therefore, the interest here lies in utilizing the GPD for predicting events that are considerably more extreme than those found in the available simulation data. However, evaluating the "extrapolation" quality of the model having only few nonlinear/extreme data is a non-trivial task. One idea could be to compute the percentage of datasets (out of the 15 partitions) with associated GPD estimates containing within their confidence band the "true" probability of stability failure (obtained by analyzing the entire sample). Although straightforward, the approach would still suffer from uncertainty issues due to the calculation of the GPD parameters from essentially small subsets (Weems et al., 2016).

To avoid such problems, in this study the GPD trends are compared with the predictions of the "critical wave groups" method (Themelis and Spyrou, 2007). Unlike the method presented here, the "critical wave groups" scheme does not make any assumptions regarding the shape of the distribution of extreme responses. Instead, it quantifies instability tendency implicitly, through the probability of encountering any wave group that could provoke the instability using distributions describing statistical properties of the wave field. Recently, the potential of the method for handling the rarity of extremes was demonstrated by Anastopoulos and Spyrou (2018).

Considering that the largest (in absolute sense) observed roll angle was only 35deg, the GPD was first fitted to exceedances over $u_L =$ 20deg. Then, it

was extrapolated to region (III). In Figure 6, the results (dashed line) are tested against the MC (circles). As before, the shaded area refers to the 95% confidence intervals (CI) of the associated GPD parameters, given in Table 5. Information for the "critical wave groups" (CWG) probabilities is directly available from the work of Anastopoulos and Spyrou (2018) who applied the method to the vessel examined here and for the same sea conditions. Although their results cover the entire nonlinear part $[u_L, \varphi_v]$, in this investigation, staying below 40deg seems to be sufficient for reaching conclusions since from very early (25-30deg) the GPD and the "critical wave groups" curves exhibit different trends. Besides, due to lack of data in region (III), the GPD confidence band will become excessively large. Finally, in this plot, the Gaussian fit (solid line) is not extended beyond region (I) because it was noticed that the result would be almost identical with the GPD curve. This is explained by the large confidence interval of the shape parameter in Table 5, indicating that nonlinear data are very few (only 2‰ of the sample size) because the ship spends most of the time below u_L. The GPD captures this feature but without further guidance it cannot do more than to extrapolate Gaussianity also in region (II).

Despite the unambiguous linear character of the GPD in Figure 6, the negative shape parameter in Table 5 suggests that the model eventually turns into a light tail. Since the probability of capsize is, in general, non-zero (even for this seemingly innocuous sea state), a heavy tail should be expected. Here, though, it is masked by the problem of rarity, leading the GPD to assume the existence of a physical boundary. This is the reason for the deviation between the GPD and the "critical wave groups" curves. The latter succeeds in tracing the unobserved heavy tail and because of its consistency with the MC values from lower levels (20-25deg) one could argue that it is more appropriate for extrapolation in the specific sea conditions. However, in view of the inherent uncertainties in the interpretation of direct counting estimates when data in the range of interest are very few, comparing results obtained from techniques originating from different principles would, at least, contribute towards their mutual development, if not achieving the ultimate validation goal.

Table 5: GPD fitting results (no escapes observed).

region II: [20deg, φmax]			
scale parameter		shape parameter	
mean value	95% CI	mean value	95% CI
1.893	[1.836, 1.951]	-0.051	[-0.071, -0.032]

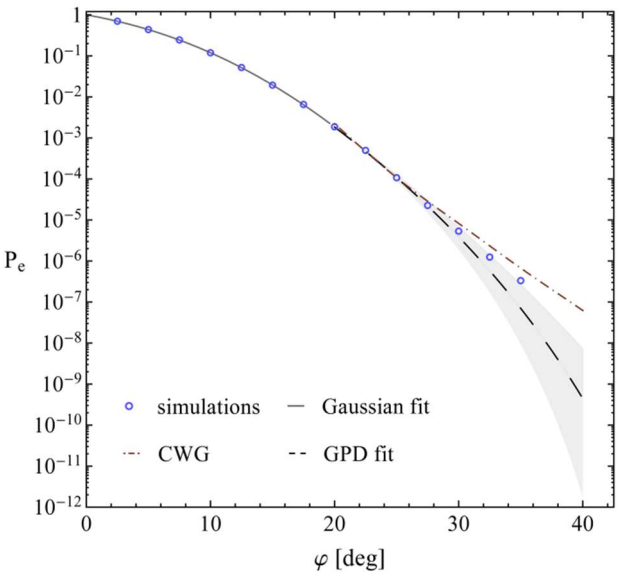

Figure 6: GPD fit (dashed line) vs. rough Monte Carlo estimates (circles) and comparison with the "critical wave groups" (CWG) predictions (dot-dashed line).

4. SUMMARY AND CONCLUSIONS

A method based on Extreme Value Theory (EVT) was proposed for calculating the probability of exceeding exceptionally high roll angles in beam seas. The method analyses the ship response problem into three parts (sub-problems), each associated with a different level of rarity and/or nonlinearity. For the first part, targeting statistical description of small-amplitude motions, a Gaussian distribution was utilized. In the nonlinear part, the solution was composed by fitting the generalized Pareto Distribution (GPD) to roll exceedances over two levels: a) a "non-rare" intermediate threshold and b) a "rare" extreme threshold. The selection of these thresholds was based on the shape of the GZ curve which provides indications for the limits of regimes where the response distribution exhibits qualitatively different probabilistic characteristics.

The performance of the approach was tested against the rough estimates of Monte Carlo simulations, obtained by direct counting. Several aspects regarding the implementation of the approach were discussed and particular attention was given to the problem of capsize. The results reveal that, given "sufficient" data, the method can accurately determine the probability of extreme

dynamic events, yet if the possibility of system escape is practically zero. However, information is essentially lost due to this assumption since escaping induces qualitative changes in the shape of the response distribution. In the case of unbounded motions, though, the GPD-tail produced by our method could not fit the data successfully. In the light of this finding, one could speculate that ship capsize is not within the range of applicability of classical EVT tools.

Finally, the "statistical extrapolation" character of the approach was evaluated through a comparison with the predictions of the "critical wave groups" method. In this context, preliminary evidence suggests that, for the examined sea conditions, the latter may be more suitable for making inferences beyond the largest observation. However, further investigation is definitely needed for reaching more general conclusions. Towards this direction, assessing methods with different backgrounds against each other seems the only option for their mutual validation in regimes where extremes cannot be directly "seen" through straightforward Monte Carlo procedures. It should be noted, though, that the desire of controlling the probability of stability failures directly through the ship design parameters requires, in fact, knowledge of the GPD form at a time when simulation data are often not available. Therefore, even if the effectiveness of the GPD idea is eventually proven, this very desire will presumably remain unsatisfied due to the data-driven nature of the concept itself.

ACKNOWLEDGEMENTS

The work of Mr. Anastopoulos was partly supported by NTUA's Special Account for Research Grants (ELKE). The idea of performing multiple GPD fits came up during a discussion with Dr. Vadim Belenky. Both Dr. Vadim Belenky and Mr. Kenneth Weems (David Taylor Model Basin, NSWCCD) are thanked for providing valuable feedback during this study.

REFERENCES

Anastopoulos, P.A. and Spyrou, K.J., 2018, "Evaluation of an Improved Critical Wave Groups Method for the Prediction of Extreme Roll Motions", Proceedings of the 13th International Conference on the Stability of Ships and Ocean Vehicles (STAB2018), Kobe, Japan, pp. 565-574.

Balkema, A. and de Haan, L., 1974, "Residual Life Time at Great Age", *Annals of Probability* 2, pp. 792-804.

Belenky, V., Weems, K.M., Bassler, C.C., Dipper, M.J., Campbell, B.L. and Spyrou, K.J., 2012, "Approaches to Rare Events in Stochastic Dynamics of Ships", *Probabilistic Engineering Mechanics* 28, pp. 30-38.

Belenky, V., Weems, K. and Lin, W.M., 2016, "Split-Time Method for Estimation of Probability of Capsizing Caused by Pure Loss of Stability", *Ocean Engineering* 122, pp. 333-343.

Campbell, B., Belenky, V. and Pipiras, V., 2016, "Application of the Envelope Peaks Over Threshold (EPOT) Method for Probabilistic Assessment of Dynamic Stability", *Ocean Engineering* 120, pp. 298-304.

Chai, W., Dostal, L., Naess, A. and Leira, B.J., 2017, "Comparative Study of the Path Integration Method and the Stochastic Averaging Method for Nonlinear Roll Motion in Random Beam Seas", *Procedia Engineering* 199, pp. 1110-1121.

Davison, A.C. and Smith, R.L., 1990, "Models for Exceedances over High Thresholds", *Journal of the Royal Statistical Society. Series B (Methodological)* 52, pp. 393-442.

Falzarano, J.M., Shaw, S.W. and Troesch, A.W., 1992, "Application of Global Methods for Analyzing Dynamical Systems to Ship Rolling Motion and Capsizing", *International Journal of Bifurcation and Chaos* 2, pp. 101-115.

Mohamad, M.A. and Sapsis, T.P., 2016, "Probabilistic Response and Rare Events in Mathieu's Equation under Correlated Parametric Excitation", *Ocean Engineering* 120, pp. 289-297.

Ochi, M., 1998, "Ocean Waves: The Stochastic Approach", Cambridge University Press, Cambridge, England, ISBN: 978-0-521-01767-1.

Pickands, J., 1975, "Statistical Inference Using Extreme Order Statistics", *Annals of Statistics* 3, pp. 119-131.

Kougioumtzoglou, I.A. and Spanos, P.D, 2014, "Stochastic Response Analysis of the Softening Duffing Oscillator and Ship Capsizing Probability Determination via a Numerical Path Integral Approach", *Probabilistic Engineering Mechanics* 35, pp. 67-74.

St. Denis, M. and Pierson, W.J., 1953, "On the Motions of Ships in Confused Seas", *SNAME Transactions* 61, pp. 280-332.

Su, Z., 2012, "Nonlinear Response and Stability Analysis of Vessel Rolling Motion in Random Waves Using Stochastic Dynamical Systems", PhD thesis, Texas A&M University, United States.

Themelis, N. and Spyrou, K.J., 2007, "Probabilistic Assessment of Ship Stability", *SNAME Transactions* 115, pp. 181-206.

Weems, K., Belenky, V. and Campbell, B., 2016, "Validation of Split-Time Method with Volume-Based Numerical Simulation", Proceedings of the 15th International Ship Stability Workshop (ISSW2016), Stockholm, Sweeden, pp. 103-108.

A perspective on theoretical estimation of stochastic nonlinear rolling

Atsuo Maki, *Osaka University,* maki@naoe.eng.osaka-u.ac.jp
Yuuki Maruyama, *Osaka University,* yuuki_maruyama@naoe.eng.osaka-u.ac.jp
Naoya Umeda, *Osaka University,* umeda@naoe.eng.osaka-u.ac.jp
Yuu Miino, *Tokyo University of Technology*, miinoy@stf.teu.ac.jp
Toru Katayama, *Osaka Prefecture University*, katayama@marine.osakafu-u.ac.jp
Masahiro Sakai, *Osaka University,* sakai@naoe.eng.osaka-u.ac.jp
Tetsushi Ueta, *Tokushima University*, ueta@tokushima-u.ac.jp

ABSTRACT

Development of the probabilistic assessment method for nonlinear ship motion in irregular seas is essential. Particularly, theoretical based method is useful for practical and wider application such as stability evaluation in preliminary design stage. In this research, the method in which Monte Carlo Simulation and theoretical method were combined is newly proposed. Here, from the limited number of Monte Carlo Simulation (MCS) realizations, the unknown coefficients containing in the theoretically obtained non-Gaussian probability density function (PDF) were successfully determined. In this research, the results on roll motion in beam sea condition and parametric rolling in longitudinal waves were shown. Then, it was found that this approach is capable of determining the PDF, and the tail of the obtained PDF shows good agreement with the theoretical results.

Keywords: *Extreme Roll Motion; Capsizing; Parametric Rolling; Probability Density Function* (*PDF*).

1. INTRODUCTION

A reliable and practical probabilistic assessment method for detecting nonlinear ship motion in irregular seas is essential in preliminary ship design stage. In our research field, the subsequent research from Haddara (1974 and 1975), a considerable amount of research from the viewpoint of the modern probabilistic theory has been carried out by Roberts (1982a), Roberts and Vasta (2000), Francescutto and Naito (2004), Kougioumtzoglou et al. (2014), Maki (2017) and Maki et al. (2018). Some of these papers were reviewed in detail in our previous research (Maki, 2017). Besides, Dostal (2012, 2014) established an energy-based stochastic averaging method to predict the ship motion in beam conditions. Results based on his theory were compared with those of the path integration (PI) method proposed by Naess (2000) in the paper of Chai et al. (2017). Chai et al. showed good agreement of Dostal's theory with the result of PI method and Monte Carlo simulation (MCS) results. This kind of theoretical approach has great advantage for saving computational time. Therefore, it is worthy of further development for practical application to an early design stage.

In our previous researches on roll motion in beam seas (Maki, 2017), the authors have proposed the estimation method of the joint probability density function (PDF) of instantaneous roll and roll rate based on the methodology proposed by Sakata et al. (1979 and 1980) and Kimura et al. (1980, 1995, 1998 and 2000). Furthermore, based upon the split time approach proposed by Belenky (1993 and 1994), the estimation method for the probability of capsizing was proposed (Maki, 2017). In this calculation method, the non-Gaussian PDF of roll response was determined by combining the moment method with equivalent linearization technique. As shown in the previous research, the results obtained from this method showed good agreement with MCS results. In the calculation process, the steady solution of the moment equation was obtained by an iterative calculation method such as the Newton method. However, in the Newton method, the choice of the initial value and step size to perform robust

convergence to the solution was not easy tasks. In each iterative step, time consuming double-integral of the joint PDF for roll and roll rate is required. Considering these issues, the proposed method is not necessarily universal for practical use.

On the other hand, probabilistic assessment of parametric rolling in longitudinal waves is also important. So far, since Price (1970), Haddara (1975), Muhuri (1980)), Roberts (1982b), a considerable number of researches had been carried out. More recently, Mohamad and Sapsis (2016) provided the methodology to estimate probabilistic response for a Mathieu-type equation under parametric excitation. They successfully captured the non-Gaussianity in the PDF. The theoretical approach for parametric excitation system is still considered to be one of the difficult problems in our field, and the robust methodology for identifying the rare event in longitudinal waves should be established for practical uses. Therefore, in this paper, with use of the same approach for roll motion problem in beam seas, the parametric rolling probability is theoretically obtained via the limited number of MCS realizations.

2. MCS-BASED THEORETICAL PDF APPROACH FOR SHIP MOTION IN BEAM SEA

As stated in the introduction, the authors (Maki et al., 2018) have been conducted by using the equivalent linearization method combining with moment equation method utilized by Sakata et al. (1979 and 1980) and Kimura et al. (1980, 1995, 1998 and 2000). In the beginning, this method is briefly reviewed in this paper.

The equation of motion is shown in Eq. (1). Here, t: time, ϕ: ship roll angle, α: linear damping coefficient, β: quadratic damping coefficient, W: ship weight, I_{xx}: moment of inertia in roll (including added moment of inertia), GM: metacentric height, GZ_i: i-th component of GZ polynomial fit, $M_{wave}(t)$: time-dependent roll moment induced by wind (normalized by I_{xx}), and $M_{wind}(t)$: steady roll moment induced by wind (normalized by I_{xx}). In this study, the overdot denotes the differentiation with respect to time t.

$$\begin{aligned}&\ddot{\phi}+\alpha\dot{\phi}+\beta\dot{\phi}\left|\dot{\phi}\right|+\frac{W}{I_{xx}}\left(GM\phi+GZ_2\phi^2\right.\\&\left.+GZ_3\phi^3+GZ_4\phi^4+GZ_5\phi^5\right)\\&=M_{wind}+M_{wave}(t)\end{aligned}\tag{1}$$

In Eq. (1), setting $\omega_0=\sqrt{W\cdot GM/I_{xx}}$, $G_1=\omega_0^2$ and $G_i=\omega_0^2 GZ_i/GM$ ($i=2,3,4,$ and 5) results in the following:

$$\begin{aligned}&\ddot{\phi}+\alpha\dot{\phi}+\beta\dot{\phi}\left|\dot{\phi}\right|\\&+G_1\phi+G_2\phi^2+G_3\phi^3+G_4\phi^4+G_5\phi^5\\&=\sum\nolimits_{N_{wave}}a_n\cos\left(\omega_n t+\varepsilon_n\right)\end{aligned}\tag{2}$$

Here, a_n, ω_n and ε_n describe amplitude, frequency and phase of wave induced roll moment for each discretized wave component.

In our previous research, the authors utilized the following PDF.

$$\begin{aligned}&p_1(\phi,\dot{\phi};d)=C_1\exp\left\{-d_1\left[\alpha H+\frac{8\beta}{9\pi}(2H)^{3/2}\right]\right\}\\&\text{where }\ H=\frac{1}{2}\dot{\phi}^2+\sum_i\int_0^{\phi}G_i\phi^i\,d\phi\end{aligned}\tag{3}$$

Here, C_1 and d_1 included in Eq. (3) were determined by following integral form conditions.

$$\begin{aligned}&\int_{-\infty}^{\infty}d\dot{\phi}\int_{\phi_{VN}}^{\phi_{VP}}p_1(\phi,\dot{\phi};d)\,d\phi=1\\&\int_{-\infty}^{\infty}d\dot{\phi}\int_{\phi_{VN}}^{\phi_{VP}}\phi^2\,p_1(\phi,\dot{\phi};d)\,d\phi=\mathrm{E}\left[\phi^2\right]\end{aligned}\tag{4}$$

The range of these integrations was bounded as $[\phi_{VN},\phi_{VP}]$ where they represent the angles of vanishing stability in negative and positive sides. The upper condition in Eq. (3) is a normalization condition of the PDF. In the lower condition, $\mathrm{E}[\phi^2]$ is the variance of roll motion, and it is iteratively determined from a set of moment equation by the Newton method. In this paper, the detailed explanation is omitted for the sake of brevity.

As introduced in Section 1, the Newton method is not always robust and easy to use. Furthermore, in each iterative step, time consuming double-integral scheme is essential. On the other hand, the equation of motion dealt with in the previous paper (Maki, 2017 and Maki et al., 2018) was 1 DoF one, and the calculation amount is not so large. Therefore, the limited number of MCS realizations can be completed in a short time. If small amount (10 or 20 times) of MCS realizations provided the necessary and sufficient information on the form of the PDF, the Newton iteration to solve the moment equation

could be bypassed. Of course, the limited amount of MCS realizations cannot detect the tail of the PDF and rare event such as capsizing on its own. However, by using the theoretically obtained PDF for this function fit, the tail behavior of the PDF can be approximately detected. Therefore, even probability of capsizing can be calculated from the obtained approximate PDF.

The calculation conditions are summarized in Table 1, and the utilized GZ curve is shown in Figure1. Figure 2 shows the PDF obtained from MCS. Here, this MCS contains 20 realizations in which each duration is one hour. Since the number of realizations is limited, the obtained points of the PDF is only distributed around the origin. Figure 3 shows the fitted PDF from the results in Figure 2. The utilized PDF form is Eq. (3), and unknown parameters were C_1 and d_1. In this paper, these unknowns can be determined by the Covariance Matrix Adaptation-Evolution Strategy (CMA-ES) (Akimoto et al., 2012, Sakamoto and Akimoto, 2017a and Sakamoto and Akimoto, 2017b). On the other hand, Figure 4 shows the theoretically obtained PDF based upon our previous method (Maki et al., 2018). Although the utilized MCS information in PDF fitting is quite limited as shown in Figure 2, the obtained PDF shape well resembles the theoretically obtained PDF. As long as the theoretical based PDF form is utilized, the PDF is likely to be successfully extrapolated even for tail behaviors.

Table 1: Calculation conditions.

Items	*Values*
Ship displacement (W)	1,500 ton
Natural roll period (T_φ)	10.0 s
Effective wave slope coef. (γ)	0.9
Metacentric height (GM)	1.00 m
Roll damping coefficient (α)	0.03
Roll damping coefficient (β)	**0.00**

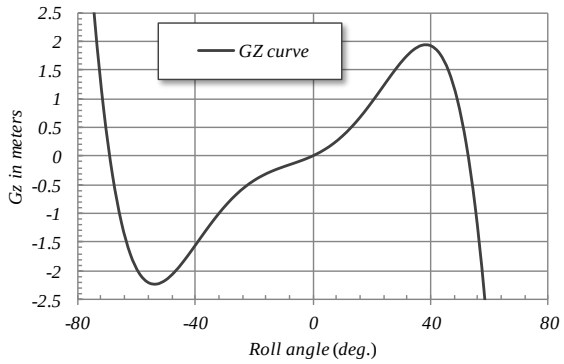

Figure 1: The utilizaed GZ curve.

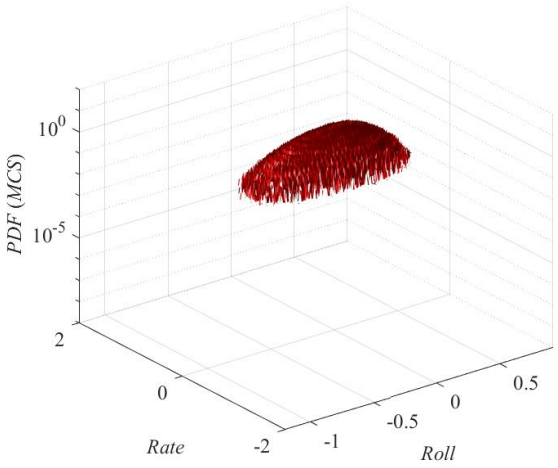

Figure 2: PDF obtained from MCS (3600 s × 20 realizations).

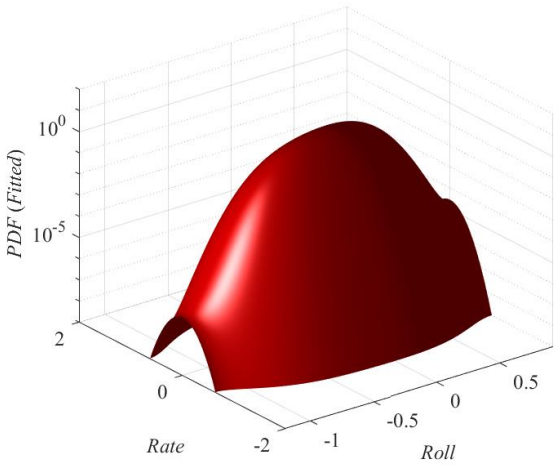

Figure 3: PDF obtained from the present method for MCS.

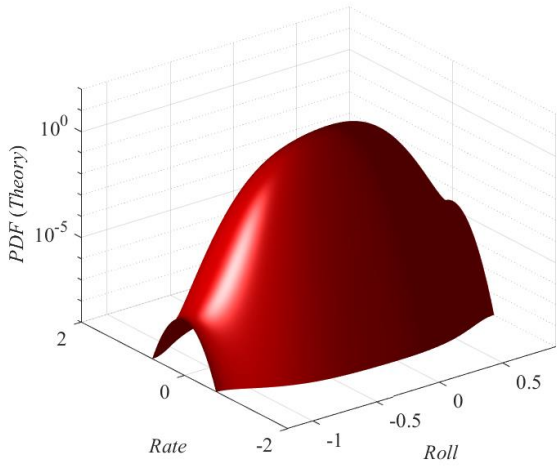

Figure 4: PDF obtained from the theory.

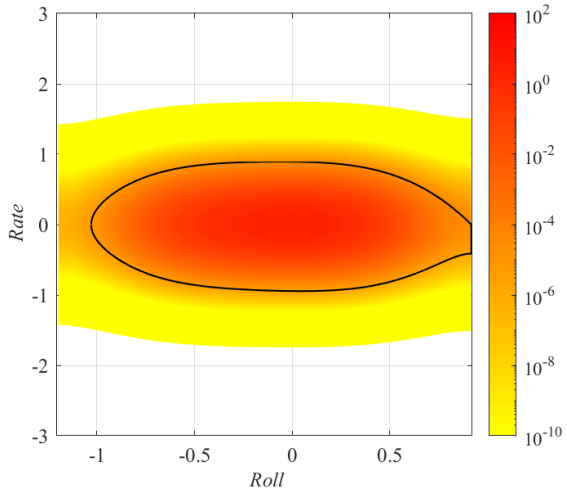

Figure 5: PDF obtained from the theory and safe basin (capsizing boundary in calm water).

Next, let us consider the probability of capsizing. Here, two methodologies for calculating the probability of capsizing are examined. One of them is the method based upon the split time approach proposed by Belenky (1993 and 1994). Belenky divided the restoring range into three ranges. Main range includes a stable upright equilibrium point. Here, this range is called range 0. The other range does unstable saddle type equilibrium point, and these range is called range 1. Range 2 includes another stable equilibrium point, that is capsizing. Since there does not exist the resonance in range 1, the capsizing condition can be approximately determined as a threshold of roll rate. Then, from the up-crossing exceedance probability and roll rate probability at the border between range 0 and 1, the probability of capsizing can be calculated. The previous research (Maki, 2017) illustrated the validity of this split time approach. On the other hand, Umeda et al. (1990 and 1994) proposed the another calculation technique for probability of capsizing due to pure loss of stability in astern waves. In their framework, capsizing probability could be estimated by integrating the joint PDF of roll and roll rate outside the safe basin when a ship meets a wave crest. In the case assumed here, this safe basin is calculated for calm water condition. The example of this safe basin is shown in Figure 5. In this figure, the contour of the joint PDF is also plotted. The final results of capsizing rate are shown in Figure 6. In this figure, "*Method 1*" means the capsizing rates per one second based on the split time approach whereas "*Method 2*" means those based on the double-integral on the phase plane. Blue and red color correspond with the results based upon the MCS-based PDF and the theoretically obtained PDF, respectively. Besides, MCS results of the capsizing rate is also plotted on this figure. This MCS results are obtained from 50,000 realizations of one hour simulation. In this figure, horizontal axis is the threshold (boundary) roll angle of range 0.

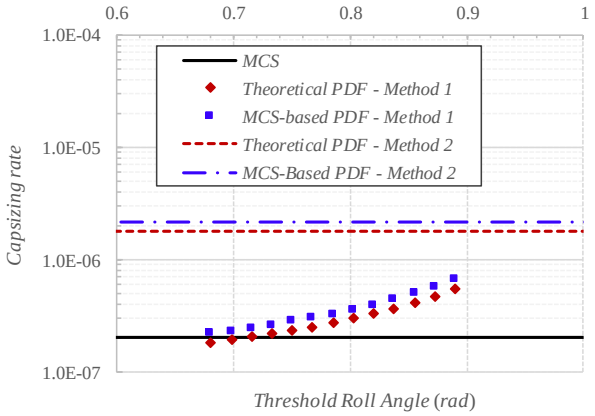

Figure 6: Capsizing rate per one second

First of all, from this figure, only small deference can be found between the theoretical PDF results and the MCS-based PDF results. It demonstrates the validity of the proposed MCS-based theoretical PDF approach. On the other hand, there exists visible discrepancy of capsizing rates between the split time approach and the double-integral method within safe basin on phase plane. The reason of this discrepancy is considered to be came from the complexity of safe basin erosion due to heteroclinic bifurcation. Figure 7 shows the stable and unstable invariant manifolds on the Poincaré map. This is an interesting example of this fractal erosion on the Poincaré map. In this figure, the utilized system is no longer equation (1),

but equation (5) having cubic restoring component with regular external roll moment (Duffing oscillator).

$$\ddot{\phi}+\alpha\dot{\phi}+G_1\phi+G_3\phi^3=B\cos\omega t \qquad (5)$$

The reason why the equation used here is switched to Duffing oscillator is that instability of the saddle-type fixed point of the original system (5) is too strong for numerical computation. Therefore, the use of original system to the analysis is skipped. However, the qualitative characteristic, such as softening characteristics, is considered to be almost same between the two. These manifolds are calculated by the method proposed by Miino et al. (2019). By using this method, the manifolds are accurately obtained for this stiff system. In this figure, heteroclinic points of stable and unstable manifolds can be found. Furthermore, the stable manifolds of ${}_1D_1^1$ and ${}_1D_2^1$ correspond the shape of safe basin erosion. As illustrated in this figure, the shape of the safe basin greatly changes in accordance with the external moment amplitude. Therefore, the method relying on the double-integral within the safe basin for zero external moment could not necessarily evaluate the probability of capsizing in this case once heteroclinic bifurcation occurs. This problem should be further explored in our future work (Maki et al., to be submitted).

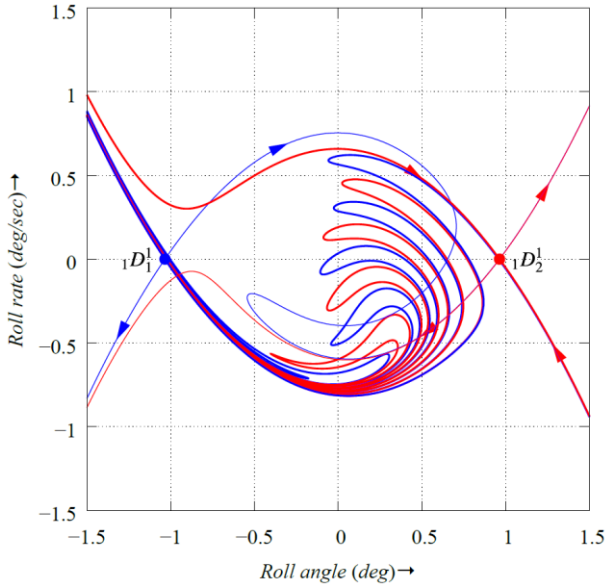

Figure 7: Manifolds of ${}_1D_1^1$ and ${}_1D_2^1$ for Duffing equation on Poincaré map ($\kappa=0.04455$, $G_1=1$ and $G_3=-1$)

As long as surveyed here, the obtained results illustrate that even the limited number of MCS realization provides the sufficient information to determine the unknown parameter included in the theoretically obtained PDF. Furthermore, since the theoretical PDF is utilized, even tail behavior characteristics can be captured within sufficient accuracy. Therefore, as shown in this chapter, the probability of capsizing was successfully calculated. Considered the robustness of the proposed method, this method could be applicable to practical uses such as in the first design stage.

3. MCS-BASED THEORETICAL PDF APPROACH FOR SHIP MOTION IN LONGITUDINAL WAVES

Among many researches on the estimation of parametric rolling probability, the paper written by Roberts (1982b) was the beginning of the research challenge for this topic. Roberts utilized the stochastic averaging technique using the SK limit theorem (Stratonovitch, 1964 and Khasminskii, 1966), then he provided the PDF of parametric rolling. More recently, Dostal showed the extension of the application of the stochastic averaging method (2012).

In this paper, the equation of ship roll motion in longitudinal waves can be represented as Eq. (6). Concerning with the roll damping term, not only linear and quadratic components but also the cubic component is taken into account from the practical viewpoint.

$$\begin{aligned}&\ddot{\phi}+2\zeta\omega_0\dot{\phi}+\beta|\dot{\phi}|\dot{\phi}+\frac{\nu}{\omega_0}\dot{\phi}^3\\&+\omega_0{}^2\left(\phi+k_3\phi^3+k_5\phi^5\right)\\&+\omega_0{}^2\,\phi\,q(t)=m(t)\end{aligned} \qquad (6)$$

Here, ν: cubic damping coefficient, k_3: 3rd order restoring coefficient, k_5: 5th order restoring coefficient. Based on the stochastic averaging technique proposed by Roberts (1982b), the probability of parametric rolling amplitude can be obtained as:

$$p_s(A)=\frac{C}{A^{1+2\lambda}}\exp\left(-\frac{A}{\mu}-\frac{A^2}{\xi}\right) \qquad (7)$$

Here, C is a normalization constant of the PDF, and

$$\lambda=\frac{\zeta\omega_0-S'}{S'},\ \mu=\frac{3\pi S'}{8\beta\omega_0},\ \xi=\frac{8S'}{3\nu\omega_0^2} \qquad (8).$$

As can be seen in Eq. (8), all coefficients include S' as defined in Eq. (9).

$$S' = \frac{\pi S_p(2\omega_0)}{4\omega_0^2} \tag{9}$$

where S_p indicates the spectral density of metacentric height in waves.

Since stochastic averaging method is the approximation technique, there could exists the error in the estimations of the drift and diffusion in FPK equation. Therefore, in this paper, the authors consider S' as unknown parameter, and then S' is determined in the meaning of the least square fit. The obtained results are shown in Figures 8-9. The subject ship is the C11 class containership which is utilized in our previous probabilistic approach (Maki et al., 2011). Figure 8 represents the results with the Froude number (Fn) of 0.000 whereas Figure 9 does those with Fn of 0.207. In these results, "stochastic averaging" represents the results obtained by Roberts's method (1982) whereas "Fitting" does those done by the proposed method in this paper. Besides, MCS results are also plotted.

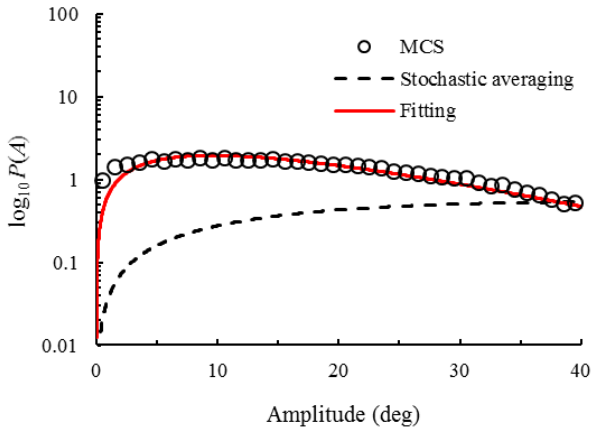

Figure 8: Comparison of roll amplitude PDF between MCS and theory with *Fn* = 0.000 in head seas.

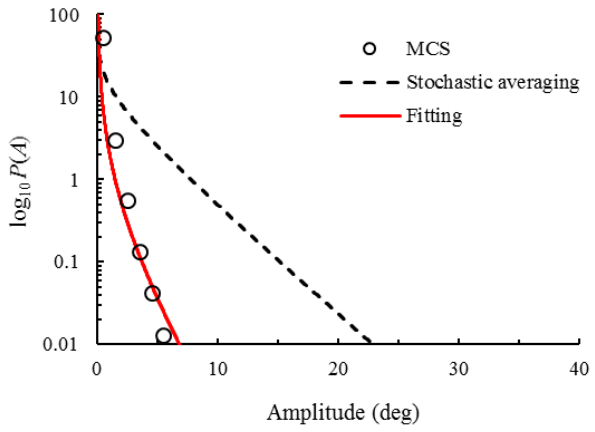

Figure 9: Comparison of the roll amplitude PDF between MCS and theory with *Fn* = 0.207 in head seas.

From these figures, it is found that the results of original averaging method results by Roberts do not show the good agreement with MCS results. These discrepancies are considered to be came from the estimation error of the coefficients in the PDF. On the other hand, the proposed fitting method using non-Gaussian PDF shows satisfactory good agreement with MCS results. This results illustrate the validity of the proposed method, and further exploration could be one of our future tasks.

4. CONCLUDING REMARKS

In this paper, the new methodology to estimate the joint PDF of roll and roll rate from the limited number of MCS realizations was proposed. Here, the unknown coefficients containing in the analytically obtained non-Gaussian PDF were successfully determined. The results obtained for roll motion in beam sea condition and parametric rolling in longitudinal waves show satisfactory agreement with MCS results. This results illustrate the validity of the proposed method. This methodology could be useful for reducing the computation time of level 3 calculation in new generation intact stability criteria.

ACKNOWLEDGEMENTS

This work was supported by a Grant-in-Aid for Scientific Research from the Japan Society for Promotion of Science (JSPS KAKENHI Grant Number 19H02360).

REFERENCES

Akimoto, Y., Nagata, Y., Ono, I. and Kobayashi, S., 2012, Theoretical Foundation for CMA-ES From Information Geometry Perspective, Algorithmica, vol. 64, no. 4, pp. 698-716.

Belenky, V.L., 1993, A Capsizing Probability Comparison Method, Journal of Ship Research, Vol.37, No.3, pp.200-207.

Belenky, V.L., 1994, Piecewise linear method for the probabilistic stability assessment for ship in a seaway, 5th International Conference on Stability of Ship and Ocean Vehicle, Melbourne, Vol.5, No.2, pp.1-18.

Chai, W. and Naess, A., 2015, "Stochastic Dynamic Analysis and Reliability of a vessel rolling in random beam seas", Journal of Ship Research, Vol.59, No.2, pp.113-131.

Chai, W., Dostal, L., Naess, A. and Leira, J.B., 2018, "A Comparative Study of the Stochastic Averaging Method and the Path Integration Method for Nonlinear Ship Roll Motion in Random Beam Seas", Journal of Marine Science and

Technology, Vol.23, No.4, pp.854-865.

Dostal, L., Kreuzer, E. and Namachchivaya N.S., 2012, "Non-Standard Stochastic Averaging of Large-Amplitude Ship Rolling in Random Seas", Proceeding of the Royal Society of London A: Mathematical, Physical and Engineering Sciences, Vol.468, pp.4146-4173.

Dostal, L. and Kreuzer, E., 2014, "Assessment of extreme rolling of ships in random seas", ASME 2014 33rd international conference on ocean, offshore and arctic engineering. American Society of Mechanical Engineers, p. V007T12A-VT12A, 2014.

Francescutto, A. and Naito, S., 2004, "Large Amplitude Rolling in a Realistic Sea", International Shipbuilding Progress, Vol.51, No.2/3, pp.221-235, 2004.

Haddara, M.R., 1974, "A Modified Approach for the Application of Fokker-Plank Equation to the Nonlinear Ship Motion in Random Waves", International Shipbuilding Progress, Vol.21, No.242, pp.283-288.

Haddara, M.R.,1975, "A study of stability of the mean and variance of rolling motion in random waves", Proceedings, International Conference on the Stability of Ships and Ocean Vehicles, University of Strathclyde, Glasgow, U.K.

Khasminskii, R.Z., 1966, "A limit theorem for the solutions of differential equations with random right-hand sides", Theory of Probability and Its Applications, Vol.11, pp.390-405.

Kimura, K. and Sakata, M., 1980, "Non-Stationary Responses of a Non-Symmetric Non-Linear System Subjected to a Wide Class of Random Excitation", Journal of Sound and Vibration, Vol.76, No.2, pp.261-272.

Kimura, K., 1995, "Non-Gaussian Equivalent Linearization for Estimation of Stochastic Response Distribution of Nonlinear Systems (in Japanese)", Transactions of the Japan Society of Mechanical Engineers Series C, Vol.61, No.583, pp.831-835.

Kimura, K. and Morimoto, T., 1998, "Estimation of Non-Gaussian Response Distribution of a Nonlinear System Subjected to Random Excitation (Application to Nonwhite Excitation with Nonrational Spectrum (In Japanese)", Journal of the Japan Society of Mechanical Engineers, Vol.64, No.617, pp.1-6.

Kimura, K., Takahara, K. and Yamamoto, S., 2000, "Estimation of Non-Gaussian Response Distribution of a System with Nonlinear Damping (in Japanese)", Dynamics and Design Conference.

Kougioumtzoglou, L.I. and Spanos, P.D., 2014, "Stochastic Response Analysis of the Softening Duffing Oscillator and Ship Capsizing Probability Determination via a Numerical Path Integral Approach", Probabilistic Engineering Mechanics, Vol.35, pp.67-74.

Maki, A., Umeda, N., Shiotani, S and Kobayashi, E., 2011, "Parametric rolling prediction in irregular seas using combination of deterministic ship dynamics and probabilistic wave theory", Journal of Marine Science and Technology, Vol.16, No.13, pp.294-310.

Maki A, 2017, "Estimation method of the capsizing probability in irregular beam seas using non-Gaussian probability density function". Journal of Marine Science and Technology, Vol. 22, No. 2, pp.351–360.

Maki, A, Sakai, M. and Umeda, N., 2018, "Estimating a non-Gaussian probability density of the rolling motion in irregular beam seas", Journal of Marine Science and Technology, doi.org/10.1007/s00773-018-0606-7 (First Online).

Maki, A, Umeda, N., Miino, Y., Sakai, M. and Ueta, T., 2019, "Estimating a non-Gaussian probability density of the rolling motion in irregular beam seas Part 2", Journal of Marine Science and Technology (to be submitted).

Miino, Y, Ueta, T., Maki, A., Umeda, N and Kawakami, H., A., 2019, Computation method to calculate the stable manifold of a ship dynamical system, NOLTA Society Conference, (in press).

Mohamad, A.A. and Sapsis, T.P., 2016, Probabilistic response and rare events in Mathieu's equation under correlated parametric excitation, Ocean Engineering, Vol.120, pp.289-297.

Muhuri, P.K., 1980, "A study of the stability of the rolling motion of a ship in an irregular seaway", International Shipbuilding Progress, Vol.27, pp.139-142.

Naess, A. and Moe, V., Efficient Path Integration Methods for Nonlinear Dynamic Systems, Probabilistic Engineering Mechanics, Vol.15, No.2, 221-231, 2000.

Price, W.G., 1964, "A stability analysis of the roll motion of a ship in an irregular seaway", International Shipbuilding Progress, Vol.11, p103-112.

Roberts, J.B., 1982a, "A Stochastic Theory for Nonlinear Ship Rolling in Irregular Seas", Journal of Ship Research, Vol.26, No.4, pp.229-245, 1982.

Roberts, J.B., 1982b, "Effect of Parametric Excitation on Ship Rolling Motion in Random Waves", Journal of Ship Research", Vol.26. No. 4, p.246-253.

Roberts, J.B. and Vasta, M., 2000, "Markov modelling and stochastic identification for nonlinear ship rolling in random waves", Philosophical Transaction of Royal Society of London A, Vol.358, pp.1917-1941.

Sakamoto, N. and Akimoto, Y., 2017a, "Improvement to the Box Constraint Handling Method for the CMA-ES and its Generalization to Linear Constraints (In Japanese)", Transaction of the Japanese Society for Evolutionary Computation, Vol. 8, No. 2, pp. 23-35.

Sakamoto, N. and Akimoto, Y., 2017b, "Modified box constraint handling for the covariance matrix adaptation evolution strategy", In Genetic and Evolutionary Computation Conference, Berlin, Germany, July 15-19, 2017, Companion Material Proceedings, pp. 183-184.

Sakata, K. and Kimura, K., 1979, "The Use of Moment Equations for Calculating the Mean Square Response of a Linear System to Non-Stationary Random Excitation", Journal of Sound and Vibration, Vol.67, No.3, pp.383-393.

Sakata, K. and Kimura, K., 1980, "Calculation of the Non-Stationary Mean Square Response of a Non-Linear System Subjected to Non-White Excitation", Journal of Sound and Vibration, Vol.73, No.3, pp.333-343.

Stratonovitch, B.L., 1964, "Topic in the Theory of Random Noise", Gordon and Breach, 1964.

Umeda, N, Yamakoshi, Y. and Tsuchiya, T., 1990, Probabilistic Study on Ship Capsizing due to Pure Loss of Stability in Irregular Quartering Seas, Proceedings of the 4th International Conference on Stability of Ships and Ocean Vehicle, Naples, pp.328-335.

Umeda, N. and Yamakoshi, Y., 1994, Probability of Ship Capsizing due to Pure Loss of Stability in Quartering Seas, Naval Architecture and Ocean Engineering, The Society of Naval Architects of Japan (Tokyo), Vol.30, pp.73-85.

Review of probabilistic methods for dynamic stability of ships in rough seas

Clève Wandji, *Bureau Veritas,* cleve.wandji@bureauveritas.com

ABSTRACT

This paper is focused on reviewing some probabilistic methods to evaluate dynamic stability event (for example large roll angle or large acceleration). In order to analyze the assumptions behind these methods and to identify the link between them, these different statistical methodologies will be tested in two datasets obtained by numerical simulations. The first dataset represents a nonlinear process (parametric roll condition) and the second a linear process. Both processes are obtained from a very long simulation 3000 hours (3h x 1000) in order to insure a better statistical convergence of the sampling. In addition, when possible, a Pearson chi-square test goodness of fit will be performed to determine whether there is a significant difference between the expected data and the observed data.

Keywords: *Probabilistic methods, nonlinear process, direct stability assessment, independence of events, Chi-square test.*

1. INTRODUCTION

Predicting the stability of a ship in waves is quite an important and challenging problem as recognized by the International Maritime Organization (IMO). The generalized problem of stability in waves has been subdivided into five stability failure modes, which are: parametric rolling, pure loss of stability, surf-riding/broaching, loss of stability under dead ship condition and excessive accelerations (Wandji and Corrignan 2012). Note that the Ship Design and Construction IMO Sub-Committee is developing the Second Generation Intact Stability Criteria (SGISC) for these five stability failure modes. These SGISC are based on a multi-tiered assessment approach. The third level also called direct stability assessment used probability for the definition of the criteria and also for the safety level.

Difficulties to evaluate probability of large event (roll angles and accelerations) are related to both the rarity of the event and the nonlinearities of the dynamical system describing ship behavior in rough seas. These nonlinearities are due to stiffness, roll damping, excitation for example, and since they are essential to properly model these phenomena, alternatives for accurate assessment may be limited to numerical simulations (for example using potential code for parametric roll) and model test. These stability failure modes are caused by irregular waves and/or gusty wind, and the inherent randomness of these environmental conditions makes the use of the probability of stability failure a very useful tool for both design and operation.

In order to test and understand the assumptions behind the different methodologies, an example has been generated and used for different probabilistic approaches. These approaches are discussed in this study. The present work is subdivided in the main following parts: first of all, the example case generated to test different methodologies will be presented; secondly, definitions of different statistics used in this work and their application on a linear process and a nonlinear process are presented; and finally the link between these different statistics are discussed.

2. EXAMPLE CASE

The roll motion time series has been obtained by performing time domain simulation on C11 containership. The main characteristics of this vessel are contained in Table 1 and a body plan is shown in Figure 1.

Simulations conditions

Nonlinear time domain computations using HydroStar++ (see Wandji C. (2018) for more details on this tool) have been performed in following, irregular and short crested seas having Hs = 6m and Tp = 12.5s. For this sea state, 1000 realizations have been computed. For each realization a different set of random phases, frequencies of the wave component composing the sea state is used.

Table 1: Main characteristics of C11 containership

Parameter	Value	Unit
Length between perpendiculars	262.0	m
Breath	40.0	m
Speed	0.0	m/s
Natural roll period	25.1	s
Metacentric height	2.75	m
Bilge keel length	76.28	m
Bilge keel breath	0.4	m

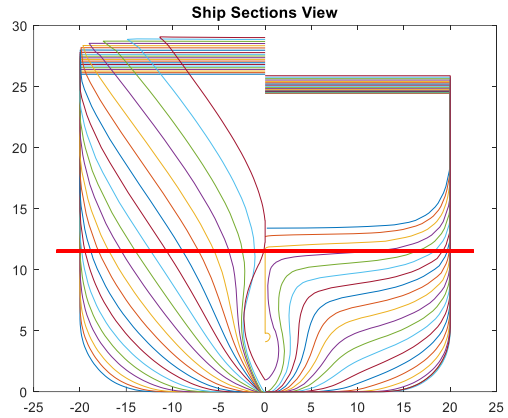

Figure 1: Body plan of C11 containership.

The ship experiences large roll motions in almost all realizations which can be related in this case to parametric rolling, since we are in following waves and the natural roll period is about twice the encounter period. An example of roll motion time series for one realization is shown in Figure 2 (blue line). Note that this signal can be considered as a nonlinear process since parametric rolling is a highly nonlinear phenomenon.

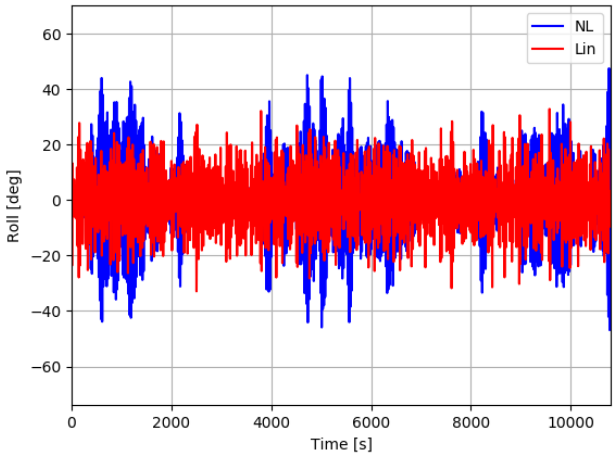

Figure 2: Time series for nonlinear (parametric roll, blue line) and linear processes (red line) for 3h.

Construction of the linear process

Using the 1000 simulations (3000 hours = 3 hours x 1000) for the nonlinear process, a power spectral density has been built, afterward the linear process has been generated. Thus the nonlinear and linear processes have the same energy content. Figure 3 shows the two spectrums derived from the two processes, they are identical. Figure 2 shows an example of time series for one realization of 3 hours for both processes.

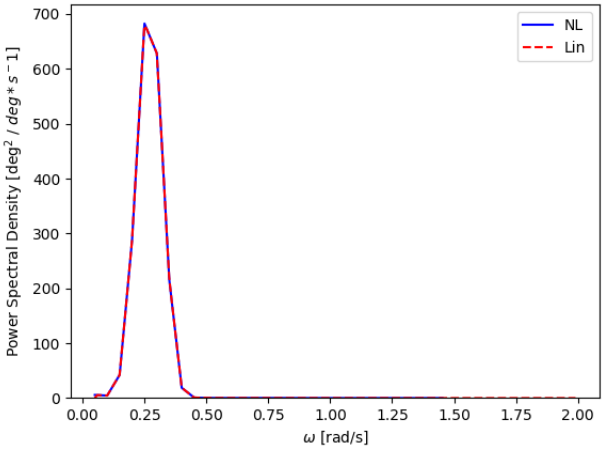

Figure 3: Power spectral density for nonlinear (blue) and linear (red) processes.

Using the two processes (linear and nonlinear) defined above, we will review, define and test some available formulations for connecting the probability of occurrence (large roll angle or accelerations for example) and the time of exposure. In this paper, all results for the linear process will be represented in red and those for the nonlinear process in blue.

3. DISTRIBUTION OF INSTANTANEOUS VALUES

Instantaneous value distribution is the distribution of the process itself at each instant of time, for example for our example case the instantaneous value distribution will be the distribution of roll angle at any instant of time. For a linear process x (for example roll angle), with standard deviation σ_x, it is known that the instantaneous value distribution F_i follows a Gaussian or Normal distribution with zero mean:

$$F_i = \phi\left(\frac{x}{\sigma_x}\right) \quad (1)$$

Note that ϕ is the standard normal distribution (with zero mean and unit variance). Using the linear and nonlinear processes presented in section 2 the instantaneous value distribution have been computed and the results are shown in Figure 4 (probability density function) and Figure 5 (exceedance probability). As expected, the linear

process follows very well the theoretical distribution (named Gauss in Figure 4 and Figure 5), while the nonlinear process has an unknown shape.

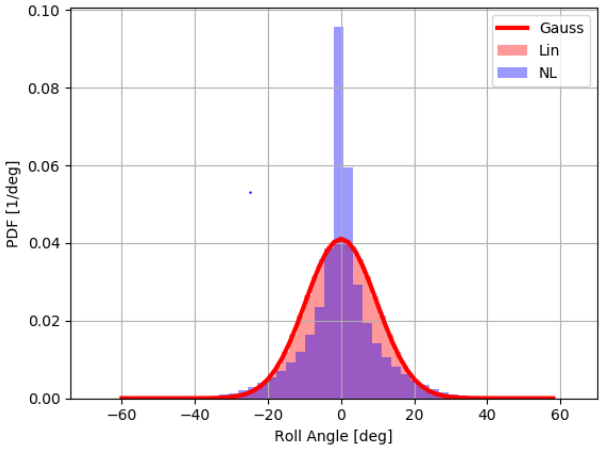

Figure 4: Probability density function of the instantaneous value distribution.

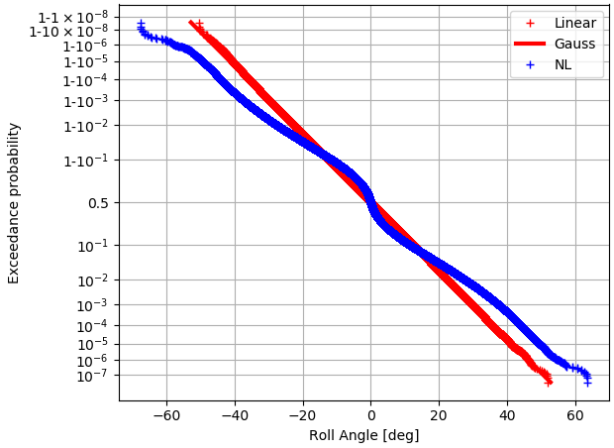

Figure 5: Instantaneous value distribution for linear and nonlinear processes.

4. UPCROSSING RATE DISTRIBUTION

Using the crossing theory, the upcrossing rate ν of a process x can be found using equation (2) under the condition that the process is differentiable with $\dot{x}$ being the time derivative of the process x.

$$\frac{dp}{dt} = \int_0^\infty f(x,\dot{x})\dot{x}d\dot{x} = \nu\big(x(t)\big) \qquad (2)$$

The integral in formula (2) has also the meaning of derivative of the instantaneous probability of event p with respect to time. If in addition the process is stationary, the rate of events is constant and equation (2) can be simplified, since the first derivative of a stationary process is independent of the process itself, and formula (2) becomes:

$$\nu(x) = f(x)\int_0^\infty f(\dot{x})\dot{x}d\dot{x} \qquad (3)$$

For a Normal process, the theoretical rate of events can be found by substitution of the normal distribution into formula (3):

$$\nu(x) = \frac{1}{2\pi}\left(\frac{\sigma_{\dot{x}}}{\sigma_x}\right)\exp\left(-\frac{x^2}{2\sigma_x^2}\right) = \frac{1}{T_Z}\exp\left(-\frac{x^2}{2\sigma_x^2}\right) \qquad (4)$$

In formula (4), $\sigma_{\dot{x}}$ is the standard deviation of the time derivative of the process and T_Z is the upcrossing period of the process. Using the linear and nonlinear processes of the example case, upcrossing rate has been built for different levels by upcrossing counting. Figure 6 shows the results for both processes.

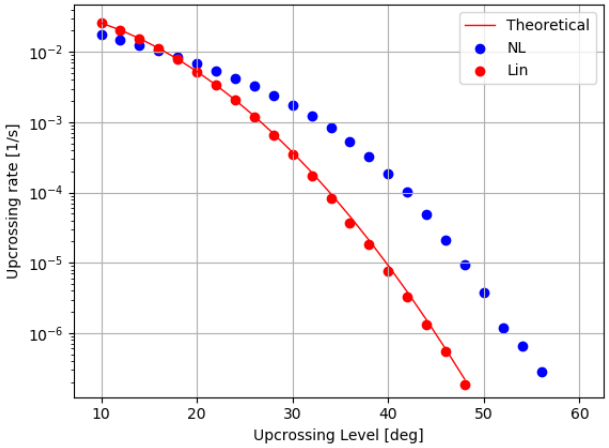

Figure 6: Upcrossing rate for linear and nonlinear processes

The upcrossing rate for the linear process is very close to the theoretical upcrossing rate (equation (4)). This result was expected, since we have seen in section 3 that the linear process follows a Normal distribution and the theoretical rate (equation (4)) was derived under the assumption of Normal distribution.

5. TIME TO FIRST EVENT DISTRIBUTION

The time to first event can be considered as the time to first upcrossing. Since an upcrossing may occur at any instant of time, the time to first event is a random variable. In reliability engineering, time to first event statistics are used, and the exponential distribution is the only distribution used to model this random variable. The exponential distribution is derived under the assumption of the independence of events. The probability density function assuming an

exponential distribution for an exposure time T and failure rate λ_x related to an upcrossing level x is given by equation (5):

$$f_x(T) = \lambda_x \exp(-\lambda_x * T) \quad (5)$$

Using both processes described in section 2, a sample of intervals before the first upcrossing has been populated. To ensure the independence of events, the time to failure was measured from the beginning of the simulation up to the instant when the failure level is passed, afterwards the simulation was stopped and restarted from the beginning for another seed in the same sea conditions.

For a given level, the time to first event (also called time to failure) was determined as the mean of the thousand time to failure obtained from each simulation. Obviously, there are some cases where the time series did not crossed the failure level. If these cases are not taken into account, the mean time to failure will be biased.

To correct such a bias a censoring procedure was used. The censoring procedure used in this work consisted to link the case in which no upcrossing occurs with those where there was an upcrossing. This lead to have in one hand time to failure greater than the length of record in some cases, and on another hand the reduction of the number of the sample. Results for a failure level of 20 degrees are shown in Figure 7 in term of exceedance probability.

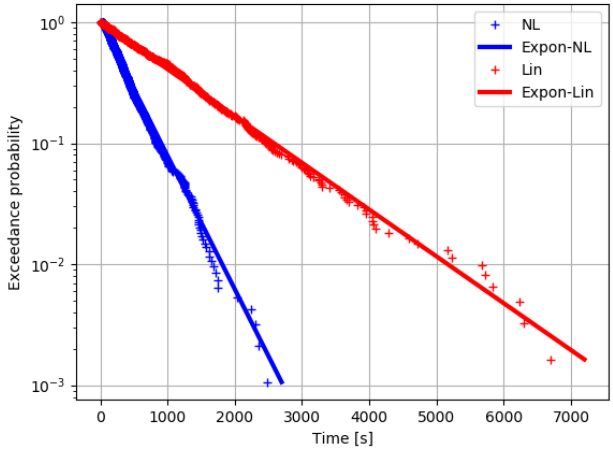

Figure 7: Time before first event distribution for linear and nonlinear processes – 20 degrees failure level.

Both linear and nonlinear processes are very close to the theoretical distribution. In addition, a Pearson chi-square goodness of fit test was performed for both distributions. The results of the tests are 0.93 for the linear process and 0.92 for the nonlinear process. The tests show that the fit are good for both processes since the probability are well above the accepted significance value of 0.05 assuming a confidence level of 95%. Other levels have been tested and the results were very good, and this confirm that the independence between events are respected and the time to first event are distributed following an exponential distribution. Note that in the current stage of development of the SGISC the time to first event is the standard method used in Level 3 (also called direct stability assessment) in full probabilistic assessment and in the probabilistic assessment in design situation as described in SDC 6/WP.6 – Annex 1.

6. TIME BETWEEN EVENTS DISTRIBUTION

An estimate of rate of events can also be evaluated from statistics of time between events. It's assumed that time between failures follows an exponential distribution. Therefore the probability density function of time between events can be described by formula (5) substituting the failure rate of the time before event λ_x by the failure rate of the time between events δ_x.

Using the dataset described in section 2, a sample of time between crossings has been populated for the linear and nonlinear processes. Results for a failure level of 20 degrees are shown in Figure 8.

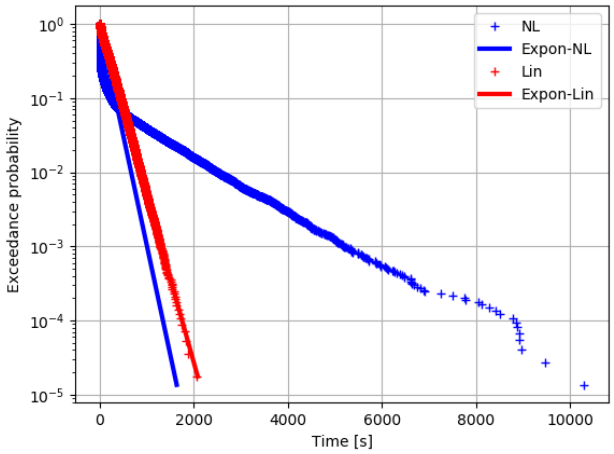

Figure 8: Time between events distribution for linear and nonlinear processes – 20 degrees failure level.

The linear process shows a good agreement with the theoretical distribution and this was confirmed also by a Pearson chi-square goodness of fit test which provided a result of 0.62 > 0.05 (for 95% confidence level). While for the nonlinear process, the computed distribution and the theoretical

distribution are different; in addition the computed distribution failed the Pearson chi-square goodness of fit test, since the probability is below the accepted significant value (0.00156 < 0.05), and therefore the hypothesis of exponential distribution is not supported by observed data. The most important condition is the independence of upcrossing.

Looking into the time series for the crossing level of 20 degrees, using the nonlinear process, most of upcrossings are clustered and there are many cases where neighboring periods have upcrossings.

7. CYCLE AMPLITUDES DISTRIBUTION

The cycle amplitudes distribution is built by determining and counting for example the greatest positive peak in each cycle. Therefore, secondary peaks are not taken into account.

Figure 9 shows an example for the linear process of the peaks taken into account to build the cycle amplitude distribution.

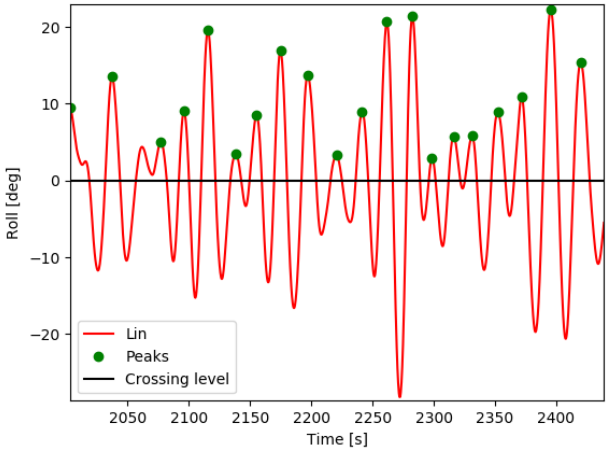

Figure 9: Example of identified peaks to build cycle amplitudes distribution for the linear process.

It's known that for a Normal process (linear process) having a narrow bandwidth spectrum, the distribution of cycle amplitudes is a Rayleigh distribution. The probability density function f_a of a Rayleigh distribution is given by:

$$f_a(x) = \frac{x}{\sigma_x^2} * \exp\left(-\frac{1}{2}\left(\frac{x}{\sigma_x}\right)^2\right) \qquad (6)$$

Using both processes of our example case, an upcrossing analysis has been performed to derive cycle amplitude distribution. The results of these analysis are shown in Figure 10.

As expected, the distribution for the linear process follows very the theoretical distribution, and the result of a Pearson chi-square goodness of fit test (0.94 > 0.05) confirmed also this result. We can also observe that distribution of peaks of the nonlinear process are not Rayleigh distributed. An explanation could be that the peaks determined for each cycle are not always independent.

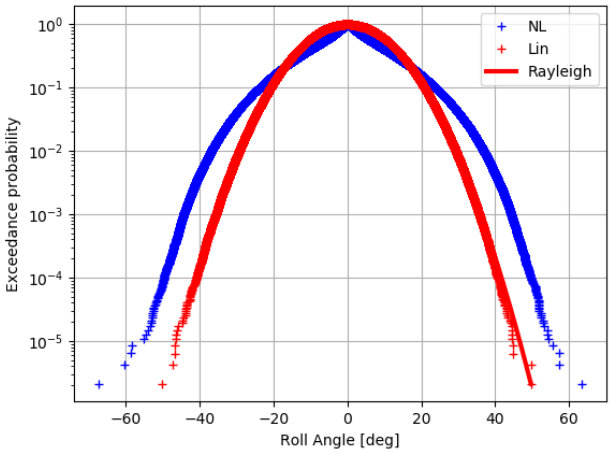

Figure 10: Cycle amplitudes distribution for linear and nonlinear processes.

8. MAXIMUM OVER A DURATION DISTRIBUTION

The maximum over a duration distribution or block maxima method consists of dividing the observation period into none overlapping independent blocks of equal size and restricts the attention to the maximum observation in each block. For a Normal process, the theoretical distribution for the maximum over a duration is given by:

$$F_T(x) = \left[1 - \exp\left(-\frac{1}{2}\left(\frac{x}{\sigma_x}\right)^2\right)\right]^{\frac{T}{T_Z}} \qquad (7)$$

In equation (7), T/T_Z represents the number of upcrossing cycles contained in the period T (block length). When the number of cycles is large enough (that means mathematically tends to infinity) the equation (7) becomes:

$$F_T(x) = \exp\left[-\frac{T}{T_Z} * \exp\left(-\frac{1}{2}\left(\frac{x}{\sigma_x}\right)^2\right)\right] \qquad (8)$$

Using both processes of our example case, for each simulation (with a duration of 3 hours), the maximum value of this 3 hours roll time series has been determined and the exceedance probability based on these 3 hours maxima is built. The results of these calculations are shown in Figure 11.

The results for the linear process are very close to theoretical distribution as expected. A Pearson chi-square goodness of fit test was done and the

results (0.54 > 0.05) confirmed also that the fitted distribution is supported by the data.

The maximum over a duration distribution can be considered as the most comprehensive definition with regards to design criteria. The final aim of short term probabilistic approach is to get this distribution.

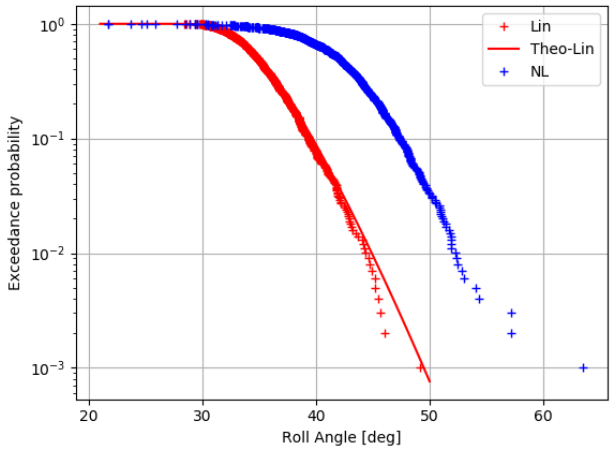

Figure 11: 3h maxima block exceedance probability for linear and nonlinear processes.

9. LINK BETWEEN DISTRIBUTIONS

This section describes the links between the different distributions defined from section 3 to section 8. The derivation of the distributions presented from sections 3 to 8, were not free of assumptions and jumping from one statistic to other might require also some assumptions among those: stationarity of the process (meaning that the conditions during the exposure time under assessment can be considered unchanged), the process is differentiable (meaning that the derivative of the process exists), and the events are independent and identically distributed.

Upcrossing rate vs maximum over a duration

Using the upcrossing rate ν, and assuming independent upcrossings and a Poisson process, the exceedance probability of the maximum over a duration could be computed using the formula (9):

$$F_T(x) = 1 - \exp(-\nu(x) * T) \qquad (9)$$

Using the results obtained in section 4, the exceedance probability over a duration of 3 hours has been computed using upcrossing rate for both processes and the results compared to those of section 8. The results of this comparison are shown in Figure 12.

From Figure 12, one can observe that the linear process results are very close to the reference (Max-Lin in Figure 12) for almost all roll angle. While for the nonlinear process, there are some differences below 44 degrees between the reference case (Max-NL) and the results obtained using upcrossing rate. These differences could be explained by the fact that the assumptions of independence of upcrossings is not verified for the nonlinear process below 44 degrees.

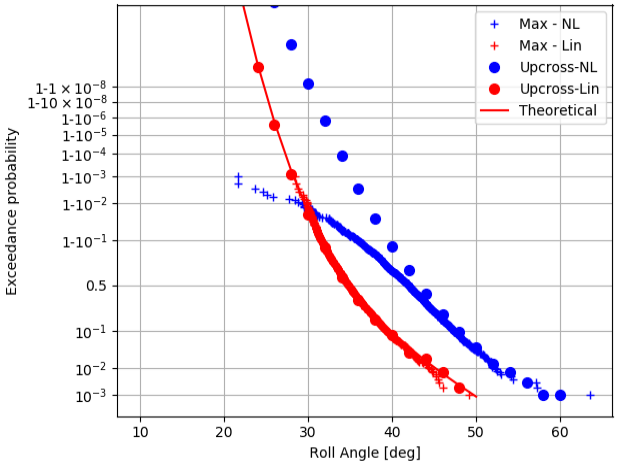

Figure 12: Maximum over a duration (3h) using upcrossing rate for linear and nonlinear processes.

Time to first even vs maximum over a duration

Using the time to first event failure rate λ, and assuming independent upcrossings and a Poisson process, the exceedance probability of the maximum over a duration could be computed using the following formula:

$$F_T(x) = 1 - \exp(-\lambda(x) * T) \qquad (10)$$

Using the results obtained in section 5, the exceedance probability over a duration of 3 hours has been computed using the time to first event failure rate for both processes. The results are shown in Figure 13.

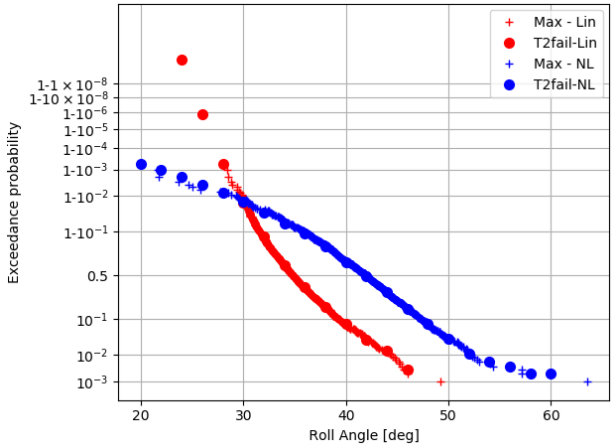

Figure 13: Maximum over a duration (3h) using time to first event for linear and nonlinear processes.

From results in Figure 13, one can observe that the results using time to first event for both linear and nonlinear processes are in agreement with the reference data (Max-Lin and Max-NL). These results are not surprising since independence of events is enforced during the construction of the time to first event for both processes.

Time between events vs upcrossing rate

Upcrossing rate (average number of upcrossings per unit of time) is obtained by counting the number of upcrossings above a given threshold, while time between events failure rate (inverse of the average time between upcrossings) is obtained by counting directly the time between upcrossings. Using the results obtained in section 4 (upcrossing rate distribution) and section 6 (time between events distribution), the rate of events obtained from upcrossing counting and time between events counting are compared and the results are shown in Figure 14.

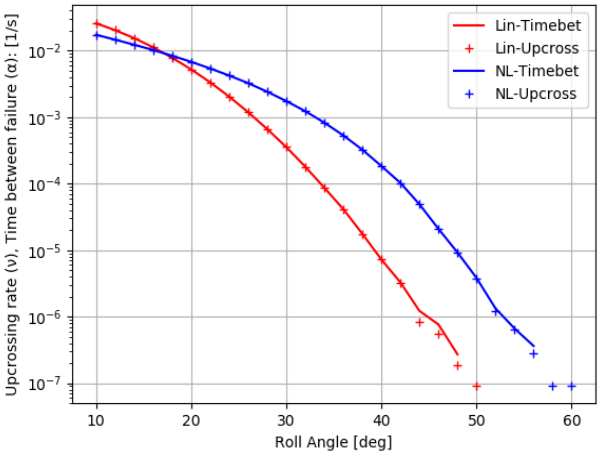

Figure 14: Comparison between upcrossing rate and time between events rate for linear and nonlinear processes.

One can observe that for both processes, the failure rate obtained from upcrossing and time between events are almost identical especially when the number of events are large. Therefore, the comments made on comparison between upcrossing rate and maximum over a duration are also valid for the comparison between time between events and maximum over a duration.

Cycle amplitudes distribution vs maximum over a duration

Using distribution of cycle amplitudes described in section 7, and assuming independent peaks, and a fixed upcrossing period, the probability for the maximum over a duration could be computed using the formula (7). Using the results obtained in section 7, the exceedance probability over a duration of 3h has been computed using the cycle amplitudes distribution for both processes and compared to the results obtained in section 8, the results of these comparisons are shown in Figure 15.

The results presented in Figure 15 show that for the linear process the exceedance probability obtained using cycle amplitudes distribution (Lin in Figure 15) follow very well the reference for linear process (Max-Lin in Figure 15). While for the nonlinear process, there are some discrepancies between the results obtained from cycle amplitudes distribution (NL in Figure 15) and the reference nonlinear case (Max-NL in Figure 15) when the roll angle is smaller than 44 deg.

These discrepancies are due to the independence between events condition which is not fulfilled below 44 degrees for the nonlinear process.

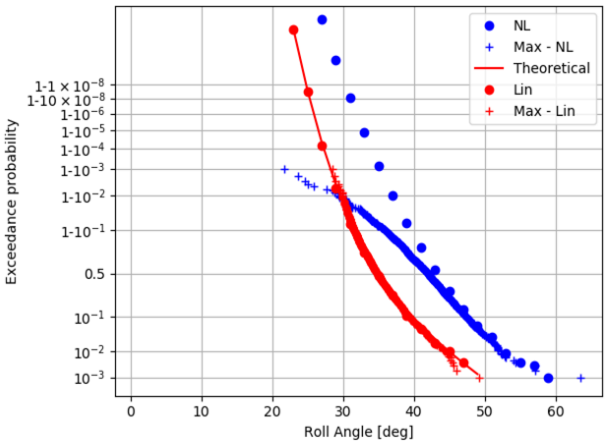

Figure 15: Maximum over a duration (3h) using cycle amplitudes distribution for linear and nonlinear processes.

Instantaneous value distribution vs upcrossing rate

The link between these two distributions is given by First Order Reliability Method (FORM). The statistical distribution of nonlinear ship responses can be estimated using FORM method, well known from structural reliability problems. One of the main result of FORM approach is the mean upcrossing rate of the process (roll motion for example) together with the most probable waves scenarios leading to the specified maximum roll angle for example.

Within FORM approach the mean upcrossing rate can be written according to Jensen and Capul (2006) using the FORM reliability index β_{FORM} as:

$$\nu(x) = \frac{1}{T_Z}\exp\left(-\frac{1}{2}\beta_{FORM}^2\right) \qquad (11)$$

The instantaneous value distribution is related to the FORM reliability index (β_{FORM}) by the following approximated relation:

$$F_i \approx \phi(\beta_{FORM}) \quad (12)$$

Since computing the reliability index (β_{FORM}) is time consuming, values of β_{FORM} have been selected directly from the instantaneous value distribution computed in section 3 for both linear and nonlinear processes as shown in Figure 16.

Having these reliability indexes, the upcrossing rate with FORM approach have been computed and the results are shown in Figure 17. From Figure 17, one can see that the upcrossing rate computed for the linear process using FORM approach are very close to those obtained using the theoretical formula (11).

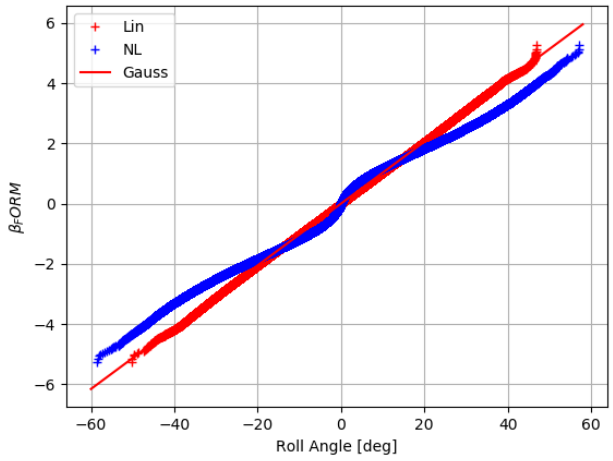

Figure 16: Instantaneous values distribution in FORM approach for linear and nonlinear processes.

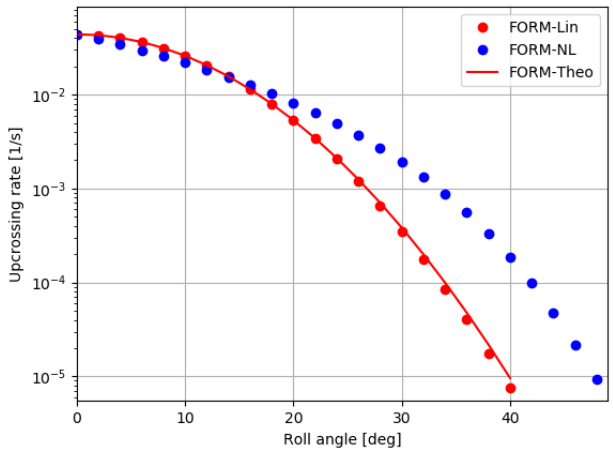

Figure 17: Upcrossing rate distribution using FORM approach for linear and nonlinear processes.

In addition, a comparison between the upcrossing rates obtained using FORM approach and upcrossing rates obtained using upcrossing counting (as described in section 3) has been carried out for both processes.

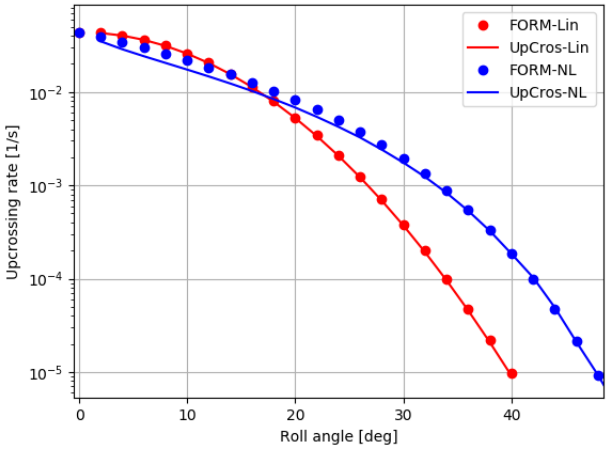

Figure 18: Comparison between upcrossing rates obtained from upcrossing counting and those from FORM approach for linear and nonlinear processes.

The results of this comparison are shown in Figure 18. From Figure 18 we can notice that for the linear process the two results are identical and there are some differences for the nonlinear process especially at lower roll angles.

10. INDEPENDENCE OF EVENTS ASSUMPTION

We have seen that independence of events is one of the most important condition to fulfill when using these different statistics.

Nonlinear process case

For example at 20 degrees roll angle using the nonlinear process, we have seen that most of upcrossings (for example for upcrossings counting, time between events, and cycle amplitudes) are clustered. Consequently there are many cases where neighboring periods have upcrossings as shown in Figure 19.

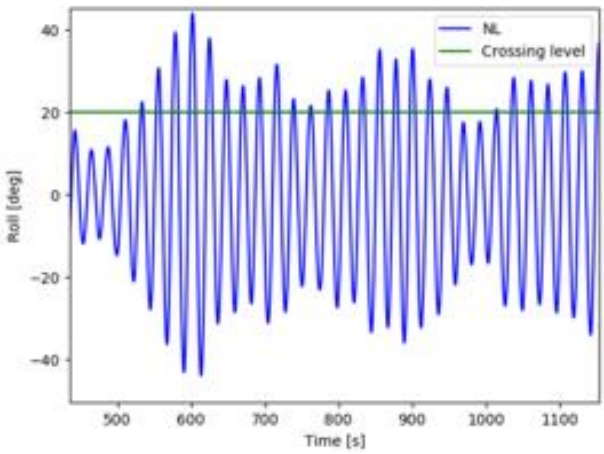

Figure 19: Time series of nonlinear process; 20 degrees upcrossing level.

Declustering the data could be a potential way to overcome this issue and a technique for declustering could be to use the envelope approach as described in Campbell and Belenky (2010).

Linear process case

For linear process i.e. Normal process, the autocorrelation function provides all information about dependence. This dependence has a limited duration, and the time it takes the autocorrelation function to drop below a given level is often used as a measure of this dependence. Using the linear process of the example case, the autocorrelation function has been computed and the result is shown in Figure 20. If the level is set to 0.05, it can be seen from Figure 20 that it takes about 50 seconds for this autocorrelation to die out.

To confirm this result, an assessment of time between events at 5 degrees has been computed and the results are shown in Figure 21.

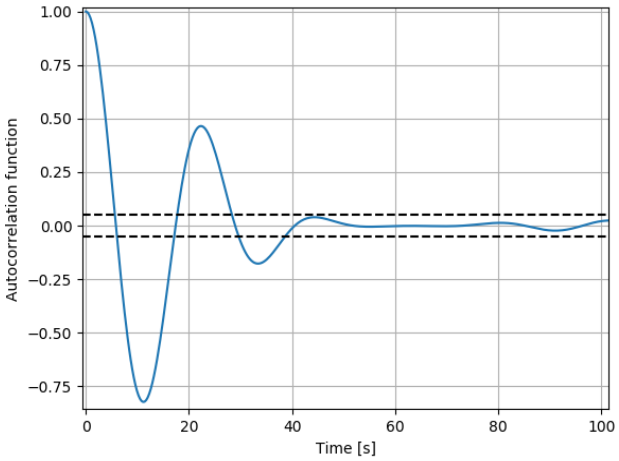

Figure 20: Autocorrelation function for the linear process.

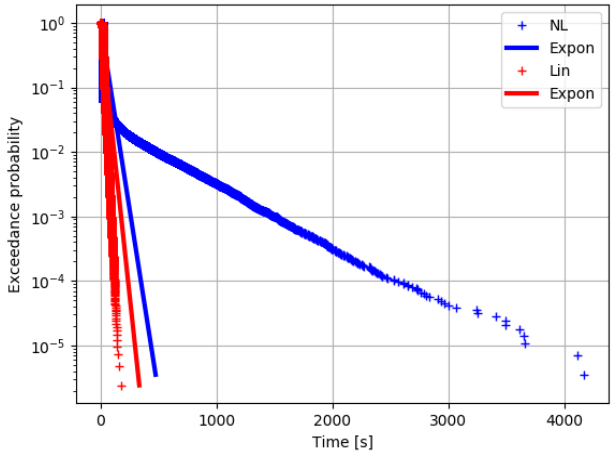

Figure 21: Time between events distribution for 5 degrees failure level for linear and nonlinear processes.

From Figure 21, one can observe that both processes do not show agreement with the theoretical distribution. In fact, a Pearson chi-square goodness of fit test (with the result of 0.0012 for the linear process and 0.00068 for the nonlinear process) rejects the exponential distribution based on time between events for 5 degrees level crossing. The theoretical distribution did not match the observed data for linear process because the observed data are clustered (for the upcrossing level of 5 degrees) and the independence of upcrossings are no longer guaranteed. This information is confirm also using autocorrelation function, since the mean time between events for 5 degrees upcrossing level is 38.6 seconds < 50 seconds (the required time to autocorrelation function to cross 5% level of significance (dashed black line in Figure 20)).

11. CONCLUSIONS

The difficulties to evaluate the probability of large roll angles are related to both the rarity of the event and the nonlinearity of the dynamical system describing the motion of a ship. One solution to overcome this issue is to use probabilistic or statistical techniques.

In summary this work focused on the review of existing probabilistic methods of evaluating dynamic stability using a dataset originated from numerical simulation. The different statistical distributions under these short term methodologies have been revisited and tested on two datasets consisting on a linear process and a nonlinear process. We have seen that these distributions under some assumptions are connected. Figure 22 presents the link between these different distributions.

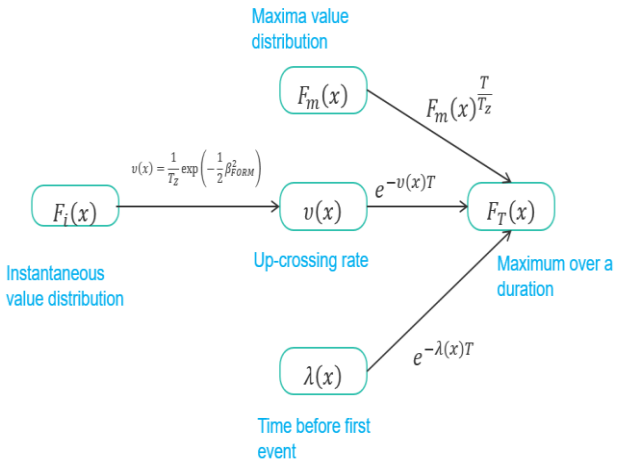

Figure 22: Overview of statistical distributions and their different links.

In Figure 22 the middle branch represents the FORM approach, a method widely used in structure reliability problems. This approach has been applied on dynamic stability problems. Jensen et al. (2017) applied this method for the statistical prediction of parametric roll. Choi et al. (2017) applied the FORM approach to analyze the stability of the ship under dead ship condition. Jensen (2007) applied FORM method to estimate extreme nonlinear roll motions.

One of the most important assumption behind the different probabilistic approaches is the independence of the events. The independence is not always guaranteed for the upcrossing of general stochastic process. Stochastic processes, such as roll angle or wave elevation for example have some inertia. Therefore, the instantaneous value of the process cannot change abruptly.

At the current stage of development of SGISC, the standard method in direct stability assessment is based on time to failure using the time to first event approach. We have seen that, we can achieve the same results using other statistical approaches if the assumptions behind these methodologies are verified.

ACKNOWLEDGEMENT

The author wish to thank Quentin Derbanne and Guillaume De Hauteclocque of Bureau Veritas for their guidance and their support for the investigation and compilation of these approaches.

The present study was partly supported by the Cooperative Research Ships (CRS) under the Direct Dynamic Stability Assessment (DYNASTY) Working Group.

REFERENCES

Campbell, B., Belenky, V., 2010, "Assessment of Short-Term Risk with Monte Carlo Method", Proceedings of the 11th International Ship Stability Workshop

Choi, J., Jensen, J., J., Kristensen, H., O., Nielsen, U., D., Erichsen, H., 2017, "Intact Stability Analysis of Dead Ship Conditions using FORM", *Journal of Ship Research*, Vol. 61, No. 3, pp. 167-176

IMO SDC 6/WP6 2019, "Report of the Expert's Group", 7 February

Jensen, J., J., 2017, "Efficient Estimation of Extreme Non-linear Roll Motions using the First-order Reliability Method (FORM)", *J. Mar. Sci. Technol*. 12(4), pp. 191-202

Jensen, J. J., Capul, J., 2006, "Extreme Response Predictions for Jack-up Units in Second Order Stochastic Waves by FORM", *Probabilistic Engineering Mechanics*, Vol. 21, No 4

Jensen J., J., Choi, J., Nielsen, U., D., 2017, "Statistical Prediction of Parametric Roll using FORM", *Ocean Engineering* 144, pp. 235-242

Wandji, C., 2018, "Investigation on IMO Second Level Vulnerability Criteria of Parametric Rolling", Proceedings of 13th International Conference on the Stability of Ships and Ocean Vehicles, (STAB2018), pp. 202-212

Wandji, C., Corrignan, P., 2012, "Test Application of Second Generation IMO Intact Stability Criteria on a Large Sample of Ships", Proceedings of 11th International Conference on the Stability of Ships and Ocean Vehicles, (STAB2012), pp. 129-139

Computational fluid dynamics prediction of hydrodynamic derivatives for maneuvering models of a fully-appended ship

Shawn Aram, *David Taylor Model Basin (NSWCCD)* shawn.aram@navy.mil

Kevin M. Silva, *David Taylor Model Basin (NSWCCD)* kevin.m.silva1@navy.mil

ABSTRACT

The utilization of Computational Fluid Dynamics (CFD) in the field of ship hydrodynamics is increasing. With the development of more robust and efficient solvers and growing computational resources at high-performance computing centers, more CFD is being utilized in everyday design. However, the computational burden still limits the efficiency of utilizing CFD for predicting long-running time-accurate seakeeping simulations in waves that are required to perform statistical analysis of extreme and rare ship motion events. The presented study builds upon previous work presented by Silva and Aram (2018) and calculates the hydrodynamic derivatives of the fully-appended Office of Naval Research Tumblehome (ONRTH). The hydrodynamic derivatives are then implemented within a maneuvering model and used to simulate a turning circle.

Keywords: *CFD, Maneuvering Models.*

1. INTRODUCTION

CFD is increasingly being utilized in the field of ship hydrodynamics due to its ability to include a broader range of the physics involved in the ship-water interaction and is becoming a popular compliment and even alternative to traditional model testing. However, the computational cost of CFD is still its largest hindrance and it is currently impractical to simulate the long hours (1+ hours per condition) of ship motion that are typically required in dynamic stability assessments and the prediction of rare and extreme ship motion events. An effective and practical use of CFD is in the development of ship-specific inputs into maneuvering models that approximate the viscous contributions within other ship hydrodynamic simulations. The utilization of maneuvering models is typically heavily dependent on a series of experiments that are tailored to calculate hydrodynamic derivatives or coefficients that help describe the forces acting on the hull. Traditionally, these hydrodynamic derivatives are calculated with captive model tests or full-scale trials, but these require the physical construction of a model or ship and the depend on the availability and cost of facilities. CFD is an attractive alternative to these expensive tests due to the relatively straight-forward simulations required to calculate the hydrodynamic derivatives and the ability to easily change fluid and ship properties.

Maneuvering models have been utilized to assess a variety of aspects related to a ship's performance, but a particularly important area of implementation is in the prediction of extreme events. Simulations for the statistical analysis of extreme ship motion events are required to be computationally efficient but must include enough physical phenomena to make accurate and meaningful predictions. Leveraging CFD to tune the maneuvering models allows them to remain computationally efficient while including ship-specific hydrodynamic contributions.

This study builds upon the previous work of Silva and Aram (2018) presented at STAB2018 and calculates hydrodynamics derivatives for the fully-appended ONRTH, as well demonstrates the utilization of the hydrodynamic derivatives within turning circle simulations. The CFD simulations are revisited and a more accurate prediction of hydrodynamic coefficients are obtained.

2. NUMERICAL METHODOLOGY

CFD Solver - NavyFOAM

A United States Navy in-house CFD software, NavyFOAM, in this study performs a series of

Reynolds Averaged Navier-Stokes (RANS)-based simulations of the ONRTH model. NavyFOAM is a suite of CFD codes developed with a C++ based open-source continuum mechanics software called OpenFOAM®. OpenFOAM/NavyFOAM makes use of object-oriented programming techniques offered by C++ language that allow maximization of code re-use, adopt layered development, expedite building top-level applications, and make runtime-selection of numerical schemes, solution algorithms, physical models, and file I/O. NavyFOAM offers additional libraries in areas such as discretization schemes and physical models. Several top-level solvers for single- and multi-phase flows have also been added in NavyFOAM aiming at marine applications including underwater vehicles, surface ships, and propulsors (Gorski et al., 2014). Solvers have also been developed to replicate conditions experienced during captive model tests including static drift, rotating arm, and rotating arm at a drift angle. NavyFOAM has been validated for various ship hydrodynamics applications (Gorski et al., 2014, Kim et al., 2017, Aram and Field, 2016, Aram and Kim, 2017, Bhushan et al., 2018).

The continuity and momentum equations are the governing equations for the incompressible single-phase flow in NavyFOAM:

$$\nabla \cdot \mathbf{u} = 0 \tag{1}$$

$$\frac{\partial \mathbf{u}}{\partial t} + \nabla \cdot (\mathbf{uu}) = \frac{1}{\rho} \nabla \cdot \{ - p\mathbf{I} + \boldsymbol{\tau} \} \tag{2}$$

where $\mathbf{u}$ is the fluid velocity, p is the fluid pressure, $\boldsymbol{\tau} = \mu_{eff}\left(\nabla \mathbf{u} + \nabla \mathbf{u}^T\right) - \frac{2}{3}\mathbf{I}\rho k$ is the viscous/turbulent stress with $\mu_{eff} = \mu + \mu_t$ the effective dynamic viscosity, and k turbulent kinetic energy.

A cell-centered finite-volume method based on a multi-dimensional linear reconstruction scheme is adopted to discretize the Navier-Stokes equations in NavyFOAM, that permits use of arbitrary polyhedral cells. The advection term in the momentum equation is discretized by the 2nd-order upwind scheme with skewness correction employed for the diffusion term. The continuity, momentum, and turbulence equations are solved implicitly in a segregated manner. The Wilcox's k-ω (Wilcox, 2008) model models the turbulence.

Maneuvering Model

A number of maneuvering models have been developed for hydrodynamic simulations of ships, but typically they are driven by a set of hydrodynamic derivatives or coefficients that describe the relationship between forces and moments to quantities like lateral and yaw velocity. Each implementation of a maneuvering model can vary how the terms are non-dimensionalized and utilized, so tailoring the calculation of the coefficients to the intended maneuvering model is important. The maneuvering model selected for this study is a simple model of horizontal motion:

$$(M + A)\ddot{\vec{X}} + F_I\left(\dot{\vec{X}}\right) + F_H\left(\dot{\vec{X}}\right) + F_{RP}\left(\dot{\vec{X}}\right) = 0 \tag{3}$$

where $\ddot{\vec{X}}$ and $\dot{\vec{X}}$ are the second and the first derivative of the state vector defined in the ship-fixed coordinate system:

$$\dot{\vec{X}} = \begin{pmatrix} u \\ v \\ r \end{pmatrix} \quad \ddot{\vec{X}} = \begin{pmatrix} \dot{u} \\ \dot{v} \\ \dot{r} \end{pmatrix} \tag{4}$$

where u is the surge speed, v is the sway speed, and r is the yaw rate. M in Equation (3) is a mass matrix:

$$M = \begin{pmatrix} m & 0 & 0 \\ 0 & m & m \cdot x_g \\ 0 & m \cdot x_g & I_z \end{pmatrix} \tag{5}$$

where m is the mass of a ship, x_g is the position of the center of gravity and I_z is the moment of inertia about the z axis.

A in Equation (3) is the added mass matrix:

$$A = \begin{pmatrix} -X_{\dot{u}} & 0 & 0 \\ 0 & -Y_{\dot{v}} & -Y_{\dot{r}} \\ 0 & -N_{\dot{v}} & -N_{\dot{r}} \end{pmatrix} \tag{6}$$

$F_I\left(\dot{\vec{X}}\right)$ is a vector-valued function expressing the inertial forces:

$$F_I\left(\dot{\vec{X}}\right) = F_{IL}(u,v,r) + F_{IN}(u,v,r) = m\begin{pmatrix} 0 \\ -uv \\ -x_g uv \end{pmatrix} + m\begin{pmatrix} vr + x_g v^2 \\ 0 \\ 0 \end{pmatrix} \tag{7}$$

where F_{IL} corresponds to the linear-only model, while F_{IN} describes the nonlinear correction. For a linear model, u is constant, as it is assumed that there is no speed loss on the turn, so the term F_{IL} is, in fact, linear.

$F_H\left(\dot{\vec{X}}\right)$ is a vector-valued function expressing the hydrodynamic forces on the hull:

$$F_H\left(\dot{\vec{X}}\right) = F_I(u,v,r) = -\begin{pmatrix} X_H \\ Y_H \\ N_H \end{pmatrix} \quad (8)$$

The hydrodynamic reaction forces (X_H and Y_H) and moment (N_H) are approximated with the hydrodynamic derivatives based on Taylor series expansion from Spyrou and Tigkas (2007) and originally formulated in Mikelis (1985):

$$X_H = X_{\dot{u}}\dot{u} - Y_{\dot{v}}vr - Y_{\dot{r}}r^2 + X_{vr}vr + R(u) \quad (9)$$

$$Y_H = Y_{\dot{v}}\dot{v} + Y_{\dot{r}}\dot{r} + Y_v vU + Y_r rU + Y_{vv}v|v| + Y_{vr}v|r| + Y_{rr}r|r| \quad (10)$$

$$N_H = N_{\dot{r}}\dot{r} + N_{\dot{v}}\dot{v} + N_r rU + N_v vU + N_{rr}r|r| + N_{rrv}\frac{r^2v}{U} + N_{vvr}\frac{v^2r}{U} + N_\phi \phi U^2 + N_{v\phi}v|\phi|U + N_{r\phi}r|\phi|U \quad (11)$$

where $R(u)$ is a resistance in calm water and U is the ship speed. $R(u)$, $(Y_v v + Y_r r)U$, and $(N_r r + N_v v)U$ are linear terms in Equation (9) - (11), and the rest are nonlinear corrections. $F_{RP}\left(\dot{\vec{X}}\right)$ in Equation (3) is a vector valued function for the rudder and propeller forces and moments.

The traditional methodology of generating the hydrodynamic derivatives is through a series of captive model tests that are designed to isolate the force and moment dependency of certain variables. Three of the most common captive model tests are the static drift, rotating arm, and rotating arm with drift. The static drift test is operated by setting the vessel at numerous drift angles relative to the flow and towing it with a constant forward resultant speed. Performing the towing in this manner allows for a relation between the sway speed, v and the forces and moments to be developed.

Another traditional captive model test is the rotating arm, where the vessel is fixed at a prescribed distance from a central point and is oriented perpendicular to the moment arm. The vessel is then rotated around the central point at a constant rate that corresponds to a tangential speed that is equivalent to the desired forward speed. The rotating arm test allows for a relationship between forces, moments and the yaw rate. A variation of the rotating arm test with drift determines the relationship between the joint dependence of forces and moments on both v and r. The rotating arm with drift test is performed similarly to the rotating arm except the vessel is set at a drift angle and not set perpendicular to the moment arm.

By performing the steady state simulations of static drift, rotating arm and rotating arm with drift conditions, all the terms containing the time derivatives of velocity vector are eliminated from Equation (3). This equation now only boasts terms like Y_v, Y_{vv} and N_v that come directly from the static drift cases, Y_r, Y_{rr}, N_r and N_{rr} that come from the rotating arm case, and Y_{vr}, N_{rrv} and N_{vvr} that come from the cross-dependence of v and r derived in the rotating arm with drift test.

3. PROBLEM DESCRIPTION AND SETUPS

The main objective of this study is to obtain the hydrodynamic derivatives of a hullform by performing a series of captive model CFD simulations and use the resultant coefficients to evaluate the maneuvering model.

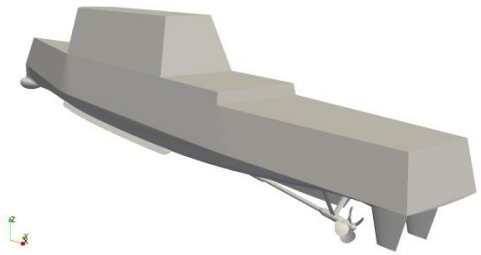

Figure 1: ONRTH model 5613.

Figure 1 shows the ONRTH model 5613, which is a fully appended 1/49 scale model equipped with a skeg, bilge keels, twin rudders, shafts and shaft brackets. Except the propeller geometry, the rest of appendages are considered in the current study. The main particulars of the model are presented in Table 1.

Table 1: Particulars of ONRTH model scale hull

Main Particulars	Model Scale
Displacement, Δ (kg)	72.6
Waterline Length, L (m)	3.147
Waterline Beam, B_{WL} (m)	0.384
Draft, T (m)	0.112
Wetted Surface Area, S (m^2)	1.5
L_{CB} (m aft of FP)	1.625
V_{CG} (m from keel)	0.156
Yaw Inertia (I_{yy}/L)	0.246
Propeller Diameter, D_p (m)	0.1066
Propeller Shaft Angle (deg)	5

Table 2 summarizes the CFD simulation conditions considered in this study, which includes the static drift and steady turn conditions. β and R are the drift angle and moment arm, respectively. All the simulations are performed to match the model scale Froude number of Fr = 0.2 and Reynolds Number of Re = 3.48×10^6. The results of static drift simulations calculate the hydrodynamic derivatives that are dependent on v (Y_v, Y_{vv} and N_v). Results of rotating arm simulations at zero drift angle obtain dependent derivatives of r (Y_r, Y_{rr}, N_r and N_{rr}), and results of the entire run matrix are applied to generate the cross-dependent hydrodynamic derivatives including Y_{vr}, N_{vvr} and N_{rrv}.

The resultant hydrodynamic derivatives obtained from the CFD simulations are then employed within the potential flow simulation framework to predict ship stability and extreme events. Therefore, ignoring the free surface effects is necessary for calculating hydrodynamic derivatives. Removing the free surface effects warrants utilizing a single-phase scheme that only considers the static submerged geometry. This requirement indicates the advantage of numerical approach over the model tests for the presented maneuvering models. Only the underwater geometry shown in Figure 2: is considered in developing the computational domain.

HEXPRESS™, a commercial meshing software package from NUMECA generates non-conformal body-fitted full hexahedral unstructured meshes. Quadrilateral elements predominantly construct the hull surface in combination with the local refinements to properly capture the sharp edges (see Figure 3). A refinement region around the hull as shown in Figure 4 increases the grid resolution in the vessel's wake region and allow for a smoother transition of cell sizing from the thin boundary layer cells with a y^+ (the average distance between the first cell center and vessel surface, in viscous unit) of 45 to the outer domain. The largest cell size (edge length) of the background grid is 0.75 m (~L/4) in all three directions. As depicted in Figure 5, the domain size is set to 16L, 12L, and 3.2L in the x, y, and z directions respectively, where x is positive aft, y is positive starboard, and z is positive up. The domain size is set to be large enough to accommodate all of the simulation conditions and resulted in a cell count of 2.86 million. The sensitivity of the computational results to the grid resolution is also examined by refining the grids on important regions, such as volumes around bow, stern, and wakes. The total number of elements of this refined grid is 7.13 million.

Table 2: Simulation conditions

Type	Case no.	β (deg)	R/L	r (rad/s)
Static Drift	1	0	∞	0
	2	2	∞	0
	3	4	∞	0
	4	6	∞	0
	5	8	∞	0
	6	10	∞	0
Steady Turn	7	0	2	0.176
	8	0	3	0.117
	9	0	4	0.088
	10	0	5	0.007
	11	0	10	0.035
	12	-2	2	0.176
	13	-6	2	0.176
	14	-2	3	0.117
	15	-6	3	0.117
	16	-2	4	0.088
	17	-6	4	0.088
	18	-2	5	0.007
	19	-6	5	0.007
	20	-2	10	0.035
	21	-6	10	0.035

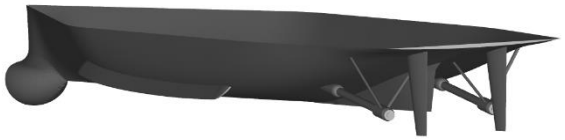

Figure 2: Underwater geometry of ONRTH.

Figure 3: Quadri-lateral surface grid elements on the ONRTH hull.

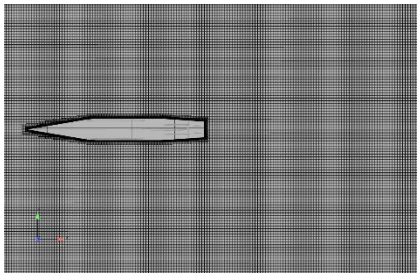

Figure 4: Depiction of the grid refinement regions around the ONRTH.

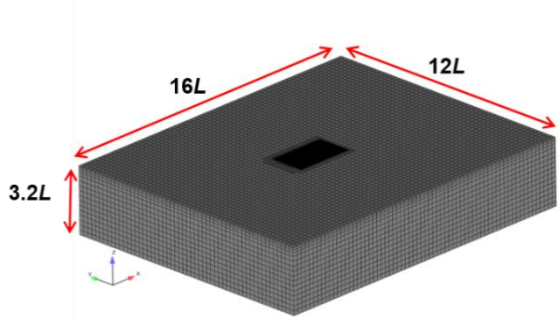

Figure 5: Isometric view of computational domain.

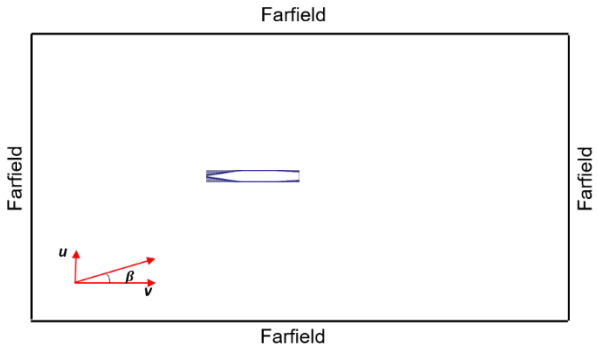

Figure 6: Illustration of velocity boundary condition for static drift cases.

Since the simulations are only considering the underwater geometry, the free surface boundary utilizes a symmetry condition, also referred to as the "double-body" condition. Treating the free surface in this manner neglects the wavemaking effects and focuses on capturing the viscous contributions.

To simulate a captive model at a static drift condition, the *x*- and *y*-components of the velocity, *u* and *v*, on all boundaries of computational domain are set as illustrated in Figure 6 to reflect a drift angle of interest, β. Through this study, $\beta = \tan^{-1}(v/u)$.

The rotating arm captive model simulations are accomplished in NavyFOAM by adopting the single rotating frame (SRF) approach that solves the flow equations in a reference frame rotating at a constant rpm. Since this approach solves the equations for the absolute velocity instead of the relative velocity, a special type of boundary condition for velocity needs to be specified on the body surface that rotates with the SRF. The same computational domain as the static drift case is used for this case. The captive rotating arm simulation with a drift angle could be achieved by rotating the computational domain by the drift angle around the center of buoyancy (CB), as illustrated in Figure 7.

To reduce the computational time, all the simulations are performed by the steady-state solvers in NavyFOAM without any time dependence in the momentum equations.

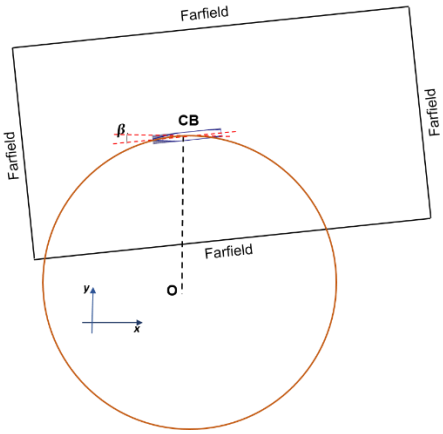

Figure 7: Computational domain for rotating arm simulation.

4. RESULTS AND DISCUSSION

Figure 8 compares the side force and yaw moment obtained from the two grid resolutions under the static drift condition. *Y* and *N* do not show any tangible difference in their results for the range of drift angles studied here. Based on this comparison, the original (coarse) grid is used for the rest of simulations.

The iso-surface of non-dimensional *Q* criterion ($QL^2/U^2 = 8$) colored by the velocity magnitude for 0^o and 10^o static drift conditions is presented in Figure 9. A clear distinction is observed between the two cases, as large vortices extend from the bulbous bow and appendages for the higher drift angle. This is consistent with generation of large side force and yaw moment at the 10^o drift angle.

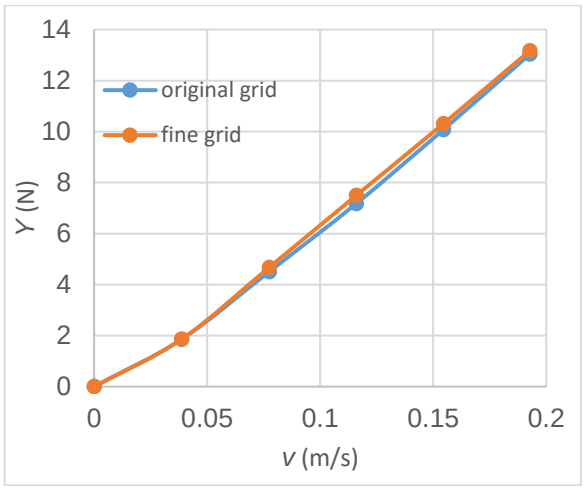

(a)

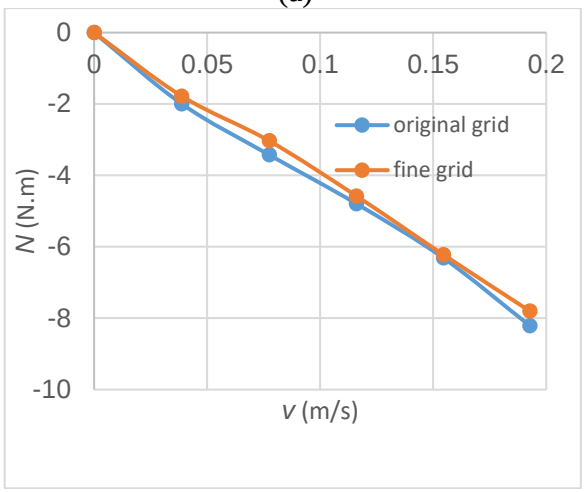

(b)

Figure 8: (a) Side force Y and (b) yaw moment N for static drift condition using two grid resolutions.

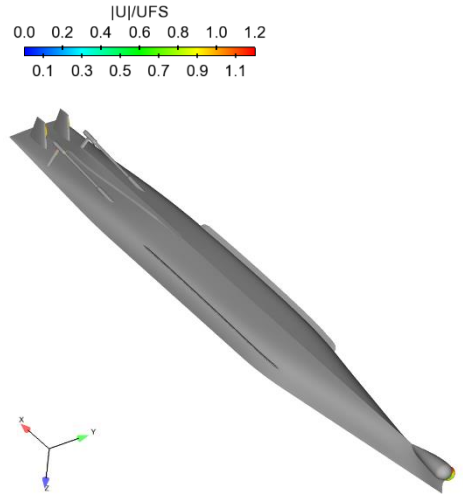

(a)

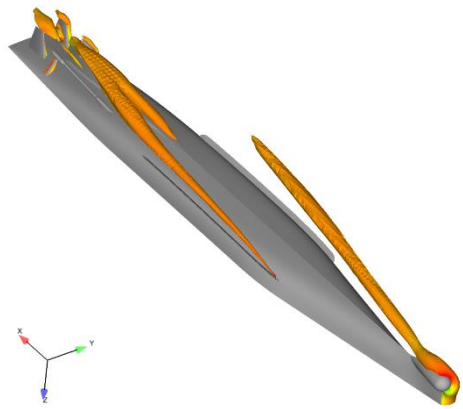

(b)

Figure 9: Iso-surface of non-dimensional Q criterion (QL2/U2 = 8) colored by the velocity magnitude for (a) 0o and (b) 10o at static drift.

Figure 10 shows the contours of absolute velocity magnitudes non-dimensionalized by the ship speed, $|U|/U_{FS}$ for the rotating arm condition at $R = 2L$ and 0° and 6° drift angles, as well as $R = 10L$ at 6° drift. A clear effect of drift angle in turn on the flow fields around the hull and in the wake of the ship is observed between Figure 10(a) and 10(b). As anticipated, changing the turning radius from $2L$ to $10L$ introduces significant effect on the ship wake.

Figure 11 plots the variation of the side force and yaw moment with the v velocity under the static drift condition. The figure also includes the regression for calculation of the hydrodynamic coefficients Y_v, Y_{vv}, and N_v. The trends of the CFD results match the empirical trends (presented by dotted lines).

The results of steady turn at zero drift versus the angular velocity shown in Figure 12 are used to calculate Y_r, Y_{rr}, N_r, and N_{rr}. Similar to the static drift simulation, the regression indicates that the trends of predicted force and moment for both captive model conditions closely match the theoretical trend. The results of the entire run matrix are employed to extract the rest of coefficients including Y_{vr}, N_{vvr} and N_{rrv}.

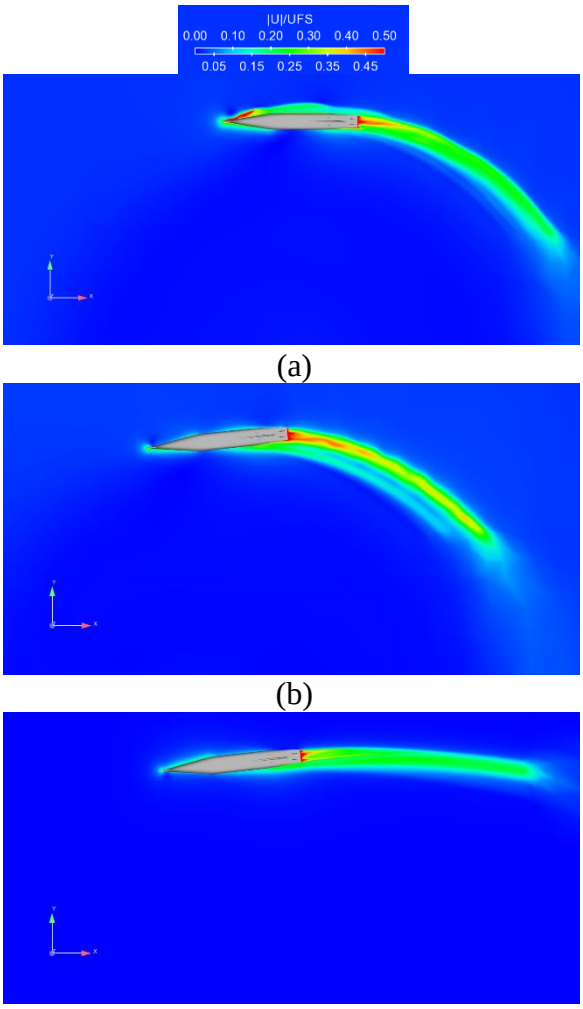

(a)

(b)

(c)

Figure 10: Comparison of velocity magnitude contours between (a) 2L at 0o drift, (b) 2L at 6o drift and (c) 10L at 6o drift.

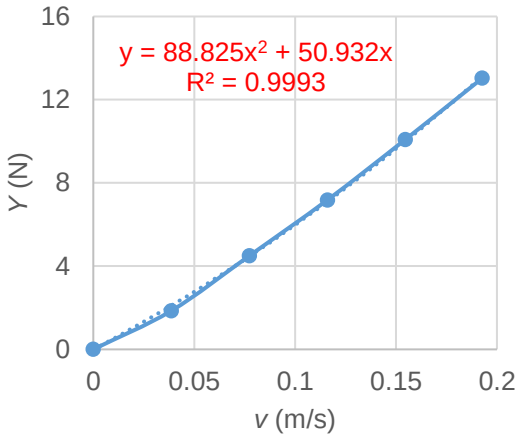

(a)

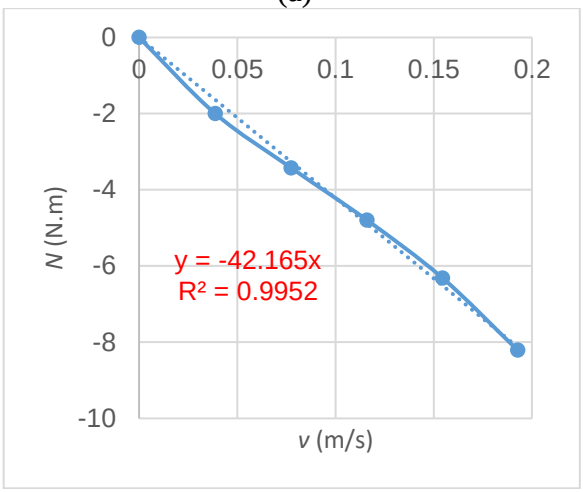

(b)

Figure 11 (a) Side force Y and (b) yaw moment N for static drift condition.

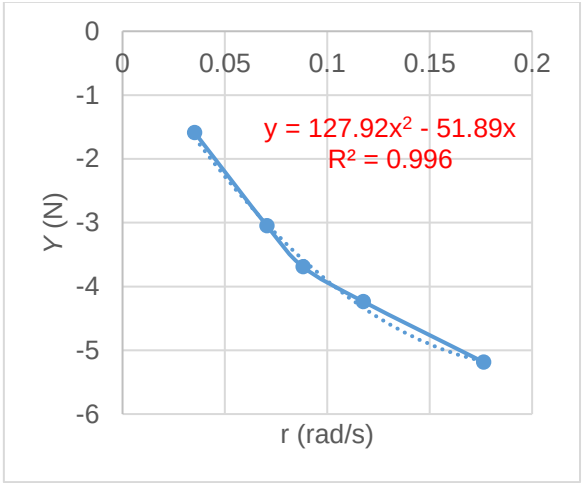

(a)

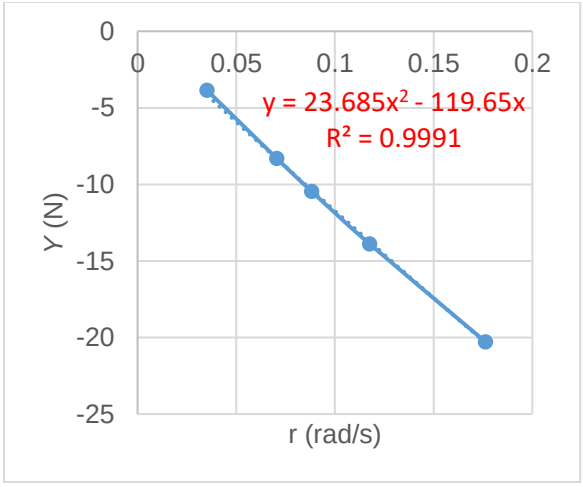

(b)

Figure 12: (a) Side force Y and (b) yaw moment N for static drift condition.

Figure 13 shows comparison of the hydrodynamic side force and yaw moment obtained from CFD under the rotating arm condition at three drift angles of 0°, -2° and -6° and selected angular velocities with those calculated from Equation (3). Close correlation between the CFD predictions and calculated derivatives are observed for both quantities, which is an indication of accuracy in the CFD results. Dependence of force and moment with *r* and *v* seen in these plots is also consistent with maneuvering behaviour of a ship under a steady turn.

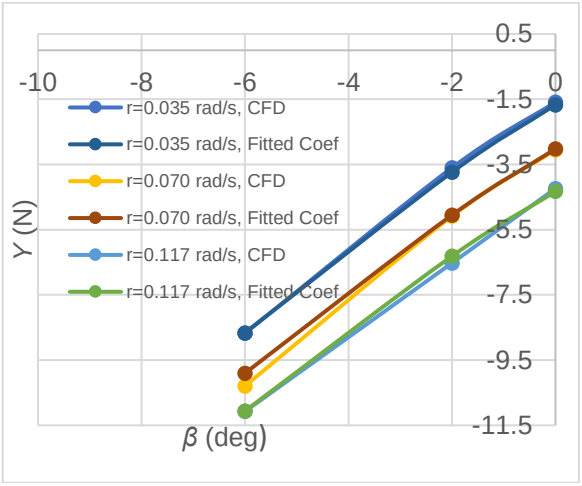

(a)

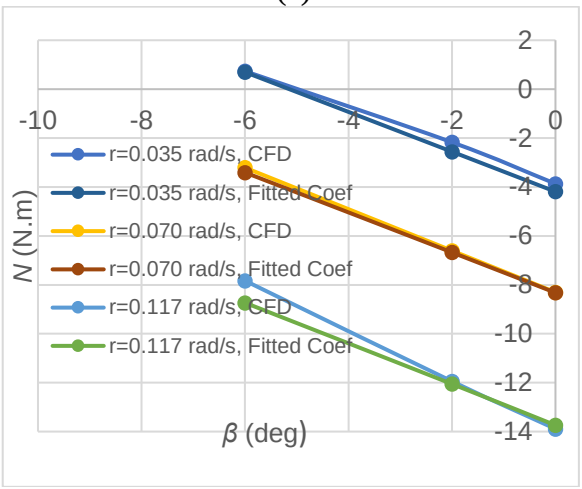

(b)

Figure 13: (a) Side force Y and (b) yaw moment N for rotating arm with selected angular velocities and drift angles.

The hydrodynamic coefficients obtained from the regression of the CFD results are summarized in Table 3. These results only utilized the underwater geometry of the ONRTH, therefore are applicable to any of the ONR Topside Series hullforms. The computational time to perform the simulations needed to develop the hydrodynamic derivatives presented in this study is around 80,000 CPU hours, relatively computationally inexpensive for CFD in naval applications. The proposed methodology could be applied to develop larger matrices of testing conditions for numerous vessel configurations (e.g. with and without certain appendages). The analysis performed can also be used for additional post-processing analysis such as extracting sectional cross-flow drag characteristics as proposed in Hughes, et al. (2019).

Table 3: Predicted hydrodynamic derivatives

Value	Non-dimensional
$\mathbf{X_{vr}}$	-0.000166206
$\mathbf{Y_{v}}$	-0.00903874
$\mathbf{Y_{vv}}$	-0.0175004
$\mathbf{Y_{r}}$	0.0029267
$\mathbf{Y_{rr}}$	-0.00254482
$\mathbf{Y_{vr}}$	0.00171603
$\mathbf{N_{r}}$	-0.00214442
$\mathbf{N_{v}}$	-0.00237815
$\mathbf{N_{rr}}$	0.000149726
$\mathbf{N_{rrv}}$	0.00080805
$\mathbf{N_{vvr}}$	-0.000961908

The predicted hydrodynamic derivatives listed in Table 3 from model-scale CFD simulations are then employed to simulate a turning maneuver of both the model-scale and full-scale fully appended ONRTH. Figure 14 depicts the trajectory of model-scale and full-scale fully appended ONRTH by the linear-only maneuvering model described in Section 2.2. The rudder angle deflected to a maximum angle of 35°. Reasonable behaviour of the ship is observed with about 2.2*L* in turning diameter for model-scale and 2.6*L* for the full-scale ship.

The trajectory of the model-scale and full-scale ONRTH obtained from simple model with non-linear corrections is plotted in Figure 15. A more realistic trajectory is observed in this case compared to the linear-only model and due to the speed loss during turn, the turning diameter is reduced for both model- and full-scale ships.

Figure 16 shows the effect of *Fr* on the trajectory of the full-scaled ONRTH. As anticipated, increasing the *Fr* from 0.2 to 0.4 leads to an increase in the turning diameter.

The ship trajectories presented here could indicate that the hydrodynamic derivatives are properly predicted by CFD.

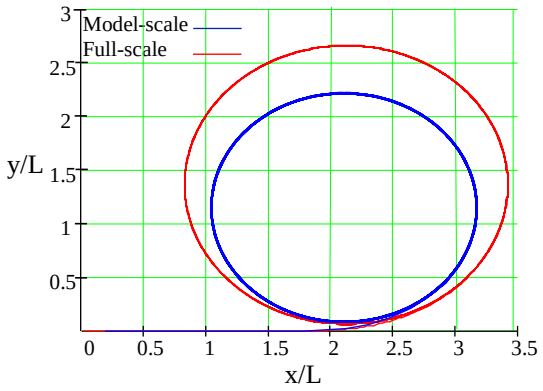

Figure 14: Sample trajectory with linear-only model, computed in model-scale and full-scale: Fr = 0.2, maximum rudder angle 35o.

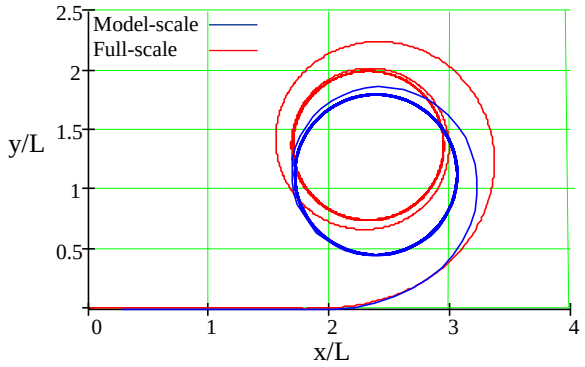

Figure 15: Sample trajectory obtained from simple model with non-linear corrections, computed in model-scale and full-scale: Fr = 0.2, maximum rudder angle 35o.

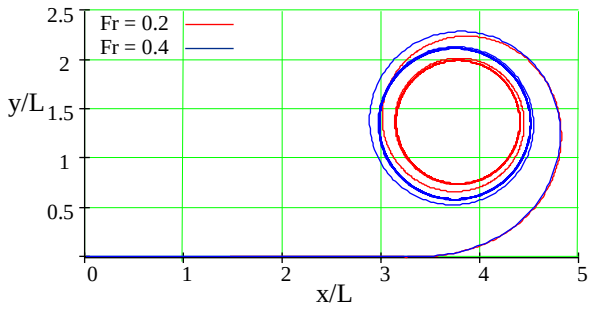

Figure 16. Sample trajectory obtained from simple model with non-linear corrections, computed in full-scale for Fr = 0.2 and 0.4, maximum rudder angle 35o.

5. CONCLUSIONS

The objective of this study was to showcase a simple procedure for a CFD-based prediction of hydrodynamic derivatives, so horizontal ship dynamics can be simulated with computational methods.

The described CFD calculations were completed for a model-scale fully appended hull and the results are significantly better compared to the previous attempt, performed for a bare hull.

However, including those appendages may not be the only reason for success. Performing CFD for fully appended hull may lead to double counting of the forces on control forces and how this double counting affects the results.

Another issue that became apparent is the influence of the multivariable regression. Some criteria for goodness of regression could be useful for reliability of procedure.

In the future, the presented computational results will be validated against the available numerical and experimental data.

6. ACKNOWLEDMENTS

The presented work was sponsored by the Naval Surface Warfare Center Carderock Division (NSWCCD) Independent Applied Research (IAR) and In-house Laboratory Independent Research (ILIR) Programs under Dr. Jack Price.

Authors also would like to thank Ken Weems, Vadim Belenky, and Kostas Spyrou for their help with the maneuvering model.

REFERENCES

Aram, S., and Field, P. L., 2016, "CFD-Based Maneuvering Prediction of a Trimaran with Two Side Hull Configurations in Calm Water," SNAME Maritime Convention, Bellevue, Washington, USA.

Aram, S., and Kim, S. E., 2017, "A Numerical Study of Added Resistance, Speed Loss and Added Power of a Surface Ship in Regular Head Waves Using Coupled URANS and Rigid-Body Motion Equations," VII International Conference on Computational Methods in Marine Engineering, MARINE 2017, Nantes, France.

Bhushan, S., Yoon, H., Stern, F., Guilmineau, E., Visonneau, M., Toxopeus, S., Simonsen, C., Aram, S., Kim, S. E., and Grigoropoulos, G., 2018, "Assessment of CFD for Surface Combatant 5415 at Straight Ahead and Static Drift β = 20º," Journal of Fluids Engineering, doi:10.1115/1.4041229.

Gorski, J., Kim, S. E., Aram, S., Rhee, B., and Shan, H., 2014, "Development of a CFD Framework for Prognoses of Resistance, Powering, Maneuvering, and Seakeeping of Surface Ships," Proceedings of 30th Symposium of Naval Hydrodynamics, Tasmania, Australia.

Hughes, M. J., Kopp, P. J., and Miller, R. W., 2019, "Modelling of Hull Lift and Cross Flow Drag Forces in Large Waves in a Computationally Efficient Dynamic Stability Prediction Tool," Chapter 5 of Contemporary Ideas on Ship Stability. Risk of Capsizing, Belenky, V., Spyrou, K., van Walree F., Neves, M. A. S., and Umeda, N. editors., Springer, ISBN 978-3-030-00514-6., pp 77-90.

Kim, S. E., Shan, H., Miller, R., Rhee, B., Vargas, A., Aram, S., and Gorski, J., 2017, "A Scalable and Extensible Computational Fluid Dynamics Software Framework for Ship Hydrodynamics Applications: NavyFOAM," Computing in Science & Engineering, Vol. 19, No. 6, pp. 33-39.

Mikelis, N., 1985, "A Procedure for the Prediction of Ship Manoeuvring Response for Initial Design," Proceedings of International Conference of Shipyard Operation and Ship Design, ICCAS, Banda, P., and Kuo, C., Elsevier Publishers B. V., North Holland.

Silva, K. M., and Aram, S., "Generation of Hydrodynamic Derivatives for ONR Topside Series Using Computational Fluid Dynamics," Proceeding of the 13th International Conference on the Stability of Ships and Ocean Vehicles, STAB2018, Kobe, Japan.

Spyrou, K. J., and Tigkas, I., 2007, "Dynamics of a ship steering win wind revisited," Journal of Ship Research, Vol. 51, No. 2, pp. 160-173.

Wilcox, D. C., 2008, "Formulation of the K-Omega Turbulence Model Revisited," AIAA Journal, Vol. 46, No. 11, pp. 2823-2838.

Time domain realization of extreme responses of a bilinear oscillator

Wenzhe Xu, *University of Michigan, Ann Arbor,* wenzhe@umich.edu
Kevin J. Maki, *University of Michigan, Ann Arbor,* kjmaki@umich.edu

ABSTRACT

In this paper, we present a method to observe the extreme response of a nonlinear dynamic system in the time domain. The goal of the research is to provide short-time-window environments for a ship in a seaway such that different dynamical extreme events can be simulated. Although much work focuses on a means to determine the probability of an extreme, this work seeks to observe the extreme in the time domain such that causal relationships can be uncovered and the design can be improved. Previous work has shown how the Design-Loads Generator (DLG) method works for different ship processes such as heave, slamming, and roll, but due to the complicated nature of these processes, and the lack of truth about the probability distribution of the process, there are still open questions about the accuracy of the method, particularly with regard to application to nonlinear systems. In this paper we study a very simple problem that has nonlinear behavior but is simple enough that the distribution of extreme response can be obtained to evaluate the DLG method. Specifically, a bilinear oscillator under Gaussian band-limited white noise force is studied. The results from the proposed method are compared with the long-time Monte Carlo Simulation. As part of this study the sensitivity of extreme response distribution to the initial conditions, and the length of time around the extreme that should be simulated is analyzed for this problem.

Keywords: *Bilinear Oscillator, Extreme Response, Design Loads Generator, Neural Networks.*

1. INTRODUCTION

Naval architects are interested in extreme ship responses when designing marine vessels. Extreme responses like large roll, large vertical bending moment, and etc. can bring failure to the vessel during its operation. Though the wave or wind loading can be regarded as Gaussian stochastic processes, the response might not be as simple as Gaussian due to nonlinearity of the dynamic systems. It is fundamental to accurately predict and simulate extreme responses of nonlinear dynamic systems.

To capture the extreme response associated to a long exposure time window which lasts years or decades, a brute-force long-time Monte Carlo Simulation (MCS) using high-fidelity numerical tools is not possible. For example, the Navier-Stokes equation solver in computational fluid dynamics (CFD) can take days to complete a simulation window of minutes, not to mention that the large number of deterministic simulations that are required in order to describe the distribution clearly. One advantage of being able to model the extreme response in time domain is that it allows for observation of the events and environment that leads to an extreme such that the design can be improved. Also, high-fidelity tools that are expensive should only be used when necessary, which is namely when the dynamical system exhibits strong nonlinearity. For example, rms motion for a ship can be estimated by linear or weakly nonlinear potential-flow methods, but the largest motion excursions should be studied using full-scale Reynolds number computational fluid dynamics simulations.

In this paper, short-time MCS are prescribed for a bilinear oscillator as a surrogate for a ship dynamical response. The bilinear oscillator model is chosen since it is simple enough to efficiently evaluate the response using long-time MCS, and it can be significantly nonlinear to produce a fully non-Gaussian response. In addition, many marine behaviors, like offshore mooring system, can be suitable modeled as bilinear oscillators (Thompson, 1983). The current paper demonstrates the DLG process and discusses the effect of the nonlinearity, the sensitivity of the initial condition, and the

computational cost of the current method when modeling extreme responses in the time domain.

2. TECHNICAL APPROACH

The Design-Loads Generator has been used to predict extreme ship responses (Alford et. al., 2009, 2011, Kim et. al., 2012, Xu, et. al., 2019). A very brief summary of the method is presented here for a generic dynamical system.

Given the design time window length T_L which is too long to directly simulate, the largest response during the time, denoted as $M_X(T_L)$, is a random variable. They are many studies to determine the distribution of $M_X(T_L)$. A generalized extreme value distribution (GEVD) can fit well to asymptotic behavior of distributions belonging to Fréchet, Weibull or Gumbel families. With Poisson assumption, a Peaks-over-Threshold (POT) model is developed to determine the extreme value distribution (Smith, R.L., 1987). The sub-asymptotic behavior can be fitted to the tail of extreme values by a parametric model (Naess A, Gaidai O. 2008). In the current paper, an affordable medium-long time window, denoted by T_m, is simulated to collect local maximas and spectrum of oscillator's response. The local maximas are then used to extrapolate the extreme value distribution from window T_m to window T_L.

Once the extreme value distribution for T_L and response energy spectrum are achieved, the Design Loads Generator (DLG) method (Kim, 2012) is applied to generate short-time response waveforms around the extremes. The DLG method, which is an Acceptance-Rejection based filter algorithm, is able to generate phases such that the resultant extremes follow the extrapolated distribution of $M_X(T_L)$.

$$M_X(T_L) = \sum_{i=1}^{N} A_{Xi} cos\phi_i \tag{1}$$

where $M_X(T_L)$ is the extreme response random variable, N is the number of Fourier components, A_{Xi} are the response ith Fourier amplitudes for frequency η_i, and ϕ_i are the response random phases generated by the DLG that correspond to an extreme from the distribution at a focusing time ($\tau = \tau^*$).

After the phases that lead to extreme response ϕ_i are generated, the corresponding extreme response waveforms are determined, each with time length, T_s. Since the dynamic system is often nonlinear and the explicit ODE is not available in many cases, a neural network is used to infer the system input (external force in this case) that leads to each waveform (Xu et. al., 2018). The neural net can be trained using system input and output from the medium-length (T_m) simulation results.

A bilinear oscillator is used as the nonlinear dynamic system to illustrate the method to be introduced. The nonlinearity comes with the different stiffnesses under different response regions. More specifically, when the displacement of the oscillator is larger than or equal to zero, the stiffness coefficient is k_1, and when the displacement of the oscillator is smaller than zero, the stiffness coefficient is k_2. The governing dimensional ordinary differential equation (ODE) is written as follows.

$$mx'' + cx' + \begin{cases} k_1 \\ k_2 \end{cases} x = \sum_{i=1}^{N} a_i \cos(\omega_{fi} t + \varphi_i) \tag{2}$$

where m is the mass of the oscillator, c is the damping coefficient, x, x', x'' are the displacement, velocity, and acceleration of the oscillator respectively. The external driving force is represented as Fourier series with ω_{fi} as the frequencies, a_i, φ_i as the corresponding amplitudes and phases of the ith component.

A dimensionless form of the equation is determined by first defining a characteristic period and the corresponding frequency as:

$$T = \pi\sqrt{m/k_1} + \pi\sqrt{m/k_2}$$
$$\omega = \frac{2\pi}{T} = \sqrt{K/m} \tag{3}$$

where $K = \frac{4k_1k_2}{(\sqrt{k_1}+\sqrt{k_2})^2}$. The discretized Fourier frequencies and time are be non-dimensionalized as:

$$\eta_i = \omega_{fi}/\omega, \tau = t\omega \tag{4}$$

Furthermore, the dimensionless displacement and the force amplitude are defined as:

$$X = x/(\sum_{i=1}^{N} a_i /K), A_i = a_i / \sum_{i=1}^{N} a_i \tag{5}$$

Finally, the dimensionless ODE is written as:

$$\ddot{X} + 2\zeta\dot{X} + \begin{cases} (1+\sqrt{\alpha})^2/(4\alpha) \\ (1+\sqrt{\alpha})^2/4 \end{cases} X = \sum_{i=1}^{N} A_i \cos(\eta_i \tau + \varphi_i) \quad (6)$$

where $\zeta = c/(2m\omega)$ is the damping ratio, and $\alpha = k_2/k_1$is the stiffness ratio. Without losing generality, $\alpha \geq 1$ is assumed, which means the negative half region has larger stiffness.

The external force is a Gaussian process with a band-limited white noise energy spectrum,

$$S(\eta) = \begin{cases} S_0, & 0 \leq \eta \leq 1 \\ 0, & otherwise \end{cases} \quad (7)$$

The dimensionless frequencies are determined as $\eta_i = \frac{1}{N-1} i$, and the corresponding dimensionless amplitudes are $A_i = 1/N, (i = 0,1,\cdots,N-1)$. The random phases φ_i are independently and uniformly distributed from $-\pi$ to π.

In this paper, the results at different level of nonlinearity (different values of α) from the proposed method are compared with the long-time MCS results. The sensitivity of the extreme distribution to various initial conditions are discussed. The required length of time used in short-time (T_s) simulations will also be analyzed in the workshop.

3. RESULTS

The oscillator's responses are all simulated using MATLAB ode45. One realization of such responses under random external force is shown in Fig. 1.

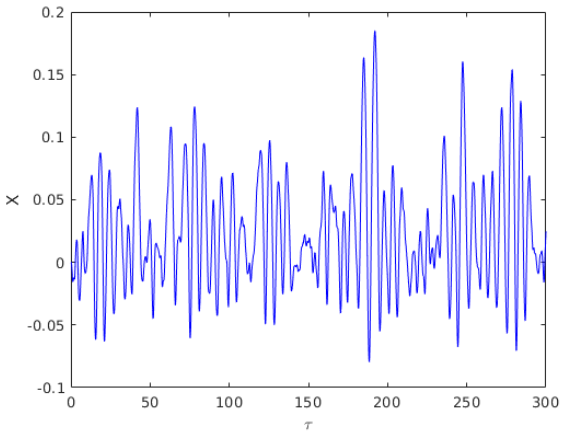

Figure 1: One realization of oscillator's response under random external force ($\alpha = 5, \zeta = 0.1, (X_0, \dot{X}_0) = (0,0)$)

The response is smaller in the negative region as expected due to the larger stiffness in this regime. Fig. 2 shows a 2000-realization ensemble of extreme waveforms with extreme time shifted to $\tau - \tau^* = 0$, where $\tau^*$is the time when extreme response occurs.

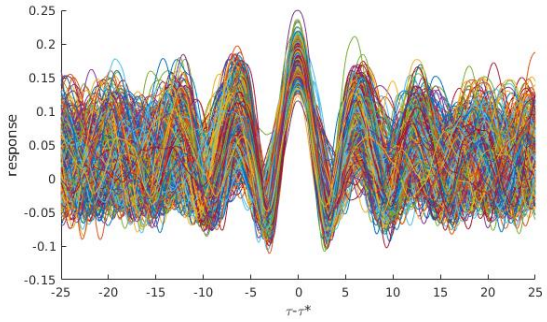

Figure 2: A 2000-realization ensemble of extreme waveforms with extreme time shifted to $-\tau^* = 0, (X, \dot{X}) = (0,0)$.

Fig. 3 plots the same data from Figure 2 in the form of a histogram that shows how the distribution of response evolves before, at, and after the extreme occurrence.

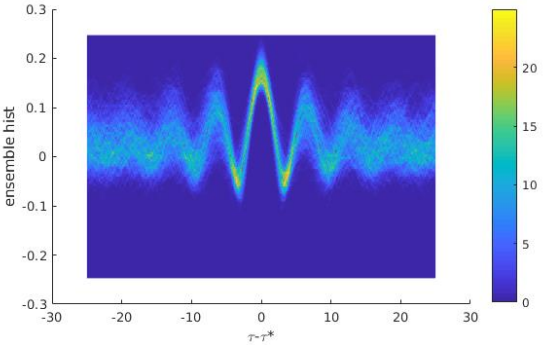

Figure 3: Waveforms have smaller variance when extreme happens.

The histogram of extreme values at the focusing time ($\tau - \tau^* = 0$) is plotted in Fig. 4. To measure the sensitivity of extreme response values to different initial conditions, a grid scan of initial conditions $(X, \dot{X})$is conducted and their histograms are plotted together with same transparency (=0.05) in Fig. 5. The blurriness in the edge qualitatively shows the dependency on the initial condition. (Larger dependency for more blurry edge). A quantitative measure for the dependency can be defined as the quantity

$$D = \frac{1}{B}\sum_{j=1}^{B} \sigma_j \quad (8)$$

where B is the number of histogram bins, and σ_j is the standard deviation among all histogram's counts in bin j. The dependency measure will be compared at different levels of nonlinearity.

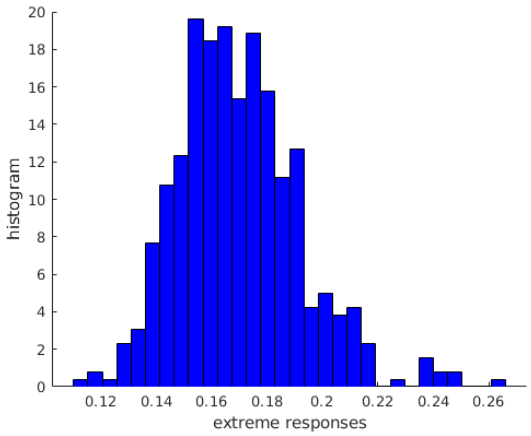

Figure 4: Extreme value histogram for the initial condition $(\boldsymbol{X}, \dot{\boldsymbol{X}}) = (\mathbf{0}, \mathbf{0})$.

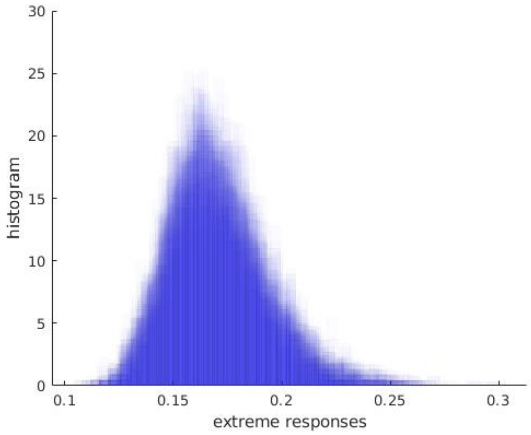

Figure 5: An overlap of histograms corresponding to different initial conditions.

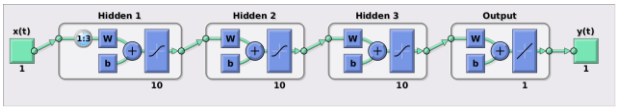

Figure 6: Neural Network architecture to infer the driving force time series. (3 hidden layer, each with 10 neurons)

The response spectrum and extreme response distribution will be compared at different nonlinearity. The distribution of waveforms at extreme time will be compared between long-time MCS and DLG-generated waveforms. A neural network shown in Fig. 6 is trained to infer the external forces producing each waveform. Finally, the simulated responses under inferred forces are compared with long-time MCS results.

REFERENCES

Naess, A. and Gaidai, O., 2008. Monte Carlo methods for estimating the extreme response of dynamical systems. *Journal of Engineering Mechanics*, *134*(8), pp.628-636.

Kim, D.H., 2012. Design Loads Generator: Estimation of Extreme Environmental Loadings for Ship and Offshore Applications.

Smith, R.L., 1987. Estimating tails of probability distributions. *The annals of Statistics*, *15*(3), pp.1174-1207.

Xu, W., Filip, G. and Maki, K.J., 2019. A Method for the Prediction of Extreme Ship Responses Using Design–Event Theory and Computational Fluid Dynamics. *Journal of Ship Research*.

Filip, G., Xu, W. and Maki, K., 2017. *URANS Predictions of Resistance and Motions of the KCS in Head Waves*

Alford, L.K. and Troesch, A.W., 2009. Generating extreme ship responses using non-uniform phase distributions. *Ocean Engineering*, *36*(9-10), pp.641-649.

Thompson, J.M.T., Bokaian, A.R. and Ghaffari, R., 1983. Subharmonic resonances and chaotic motions of a bilinear oscillator. *IMA Journal of Applied Mathematics*, *31*(3), pp.207-234.

Xu, W. and Maki, K., 2018. A method for the prediction of extreme roll suitable for nonlinear time-domain realization.

On regulatory consistency of criteria for dead ship condition and pure loss of stability

William S. Peters, *Office of Design and Engineering Standards, USCG,* william.s.peters@uscg.mil
Vadim Belenky, *David Taylor Model Basin,* vadim.belenky@navy.mil

ABSTRACT

The paper examines different aspects of consistency between the levels 1 and 2 of vulnerability assessment within the second generation IMO intact stability criteria (SGISC). Dead ship condition and pure loss of stability failure modes are considered. The most important aspect of consistency for dead ship condition is its possible influence on integrity of the existing mandatory stability regulations, as the consistency between the levels of vulnerability criteria is in fact representative of consistency between the 2008 IS Code and SGISC. The paper describes possible solution for the between-the-levels consistency of the pure loss of stability.

The main idea is to assess the safety level of the deterministic level-1 criterion. Then, the standard for the probabilistic level-2 criterion has to be set to higher level than the assessed level 1 safety level. For this approach to work, both level 1 and 2 should use the same mathematical models of the stability failure or the model for the level 1 should be inherently more conservative compared to the level 2.

Keywords: *dead-ship condition, pure loss of stability, second generation intact stability criteria (SGISC), vulnerability criteria, Weather Criterion 2008 IS Code.*

1. INTRODUCTION

The tiered sctucture of the second generation intact stability criteria (SGISC) in the final stages of development by the International Maritime Organization (IMO) allows effective management of the complexity of calculations. If the vulnerability of a ship to a particluar mode of dynamic stability failure is not indicated on the lower lever, there is no need for further assessment. On the other hand, the criteria for the same mode of failure must be consistent for the different levels: if the level one assessment shows no vulnrability, so also should be the result of the level 2 assessment.

Unfortunately, it is not always the case. Since the correspondence group on intact stablity has started systematic sample calculations, the reports on the inconsistencies were fairly frequent as well the attempts to resolve these inconsitencies, e.g. see Tompuri, *et al.* (2017).

This paper considers between-the-level inconsistency for both the dead ship condition and the pure loss of stability modes of failure, continuing and extending the approach formulated by the authors in the previous workshop (Peters & Belenky, 2017).

2. DEAD SHIP CONDITION

There are several aspects of inconsistency of vulnerability criteria for dead ship conditions as described in Annex 3 SDC 6/WP.6: application consistency, probabilistic consistency and physical consistency.

Application Consistency

The dead ship condition is the only mode of failure included in the second generation intact stability criteria that also is covered in Part A of the 2008 IS Code. The severe wind and rolling criterion (weather criterion), described in the section 2.3 of the 2008 IS Code has loading condition limitations for use of the formula and table for calculation of the roll back angle in the paragraph 2.3.5. These limitations are described in the paragraphs 2.3.5 and include breadth to draft ratio, KG to draft ratio and natural roll period.

To address these applicability limitations, MSC Circular 1200 (MSC.1/Circ.1200) describes an alternative way to obtain the roll-back angle through the performance of model tests. However, the assessment of the weather criterion is unchanged.

The level 1 vulnerability criterion uses the extended roll period table from MSC.1/Circ.1200, so the limitation for two other parameters remain to be addressed at the level 2 assessment, which is a probabilistic long-term criterion based on an averaged upcrossing rate. As the level 2 assessment does not provide the roll back angle outside the applicability range of the weather criterion, the level 2 assessment is essentially an alternative outside of the current stability regulatory framework.

Probabilistic Consistency

Consistency between the level 1 and level 2 criteria has been considered, apart from the applicability and general regulatory issues. As the level 1 vulnerability criterion is the weather criterion with an extended table for the roll period, the consistency problem essentially focuses on the probabilistic interpretation of the weather criterion. The problem attracted attention of Naval Architects long ago (e.g. Dudziak & Buczkowski, 1978) abridged version available in (Belenky & Sevatsianov, 2007).

One of the authors touched this problem in an attempt to assess probability capsizing of a series of ships in KG-critical condition based on the criteria to be included in the 2008 IS Code (Belenky, 1995). With some surprise at the time, the value of the capsizing probability had shown significant variation. This outcome meant that compliance with the weather criterion does not necessarily mean that a probability of stability failure will fall within a certain range.

Annexes 1, 7 and 12 of IMO document SDC 5/INF.4 describe a probabilistic study, that addresses the inconsistency between the levels of vulnerability criteria for dead ship condition.

A data sample satisfied the following conditions:

- Weather criterion is fully applicable: B/d≤3.5, $0.3 \leq \mathrm{KG/d} - 1 \leq 0.5$ and T≤20 s.
- Area a exactly equals area b or the static angle equals to 16 degrees.

This data sample can be created by using a ship loading condition within the applicability range of the weather criterion and simultaneous adjusting the KG value and windage area to achieve the equivalency. The sample contained 74 points (i.e., loading conditions). Fig. 1 shows a histogram of the level 2 criteria value, computed as described in Annex 3 of SDC 6/WP.6. The "weighted data" refers to the adjustment of statistical weight to match the distribution of ship lengths in the world fleet.

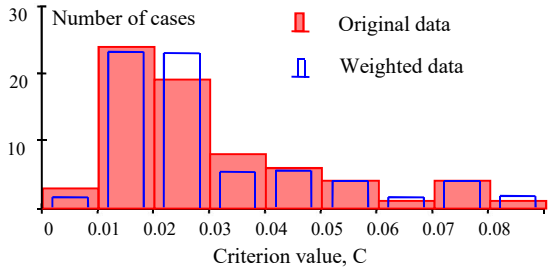

Figure 1: Distribution of the criterion value C based on original and weight data

The inconsistency between the levels manifests itself in the form of a distribution, while consistency would look like a deterministic function.

The histogram in Fig. 1 can be approximated with log-normal distribution and then used to set the standard with specified "probability of inconsistency" that may be treated in a similar way as safety level, see for details Annexes 7 and 12 of SDC 5/ INF.4.

Physical Consistency

The second possible source between the levels is the difference in a mathematical model describing stability failure in a dead ship condition. Annex 15 of SDC 4/INF.4/Add.4 and Annex 1 of SDC 5/ INF.4 contain formulations of an alternative level 2 criterion, which uses the same general scheme of application of the weather criterion, but in which the input parameters are given a probabilistic interpretation, see Fig. 2.

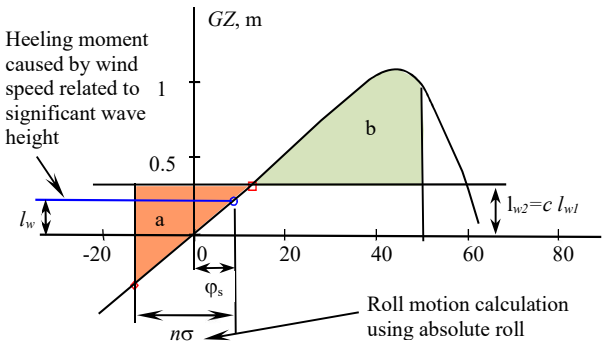

Figure 2: On the formulation of the alternative level 2 vulnerability criterion

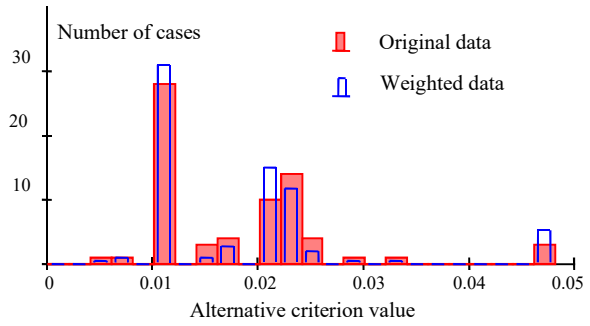

Figure 3: Distribution of the alterative criterion value based on original and weight data

The alternative criterion helped to decrease the amount of inconsistency, but did not resolve it completely. Being applied to the data sample, described in the previous subsection, it still produced the distribution, see Fig. 3. Its "randomness", however seems to be decreased, compare to the one shown in Fig. 1.

Calculations, presented in Annex 12 of SDC 5/INF.4, have shown that a standard has to be largely non-conservative, unless some degree of inconsistency is allowed. Having in mind that this inconsistency is associated with mandatory criteria, this approach is not attractive. Thus, it makes sense to change the role of the level 2 vulnerability criteria to be considered as an independent assessment of safety level in dead ship condition.

3. PURE LOSS OF STABILITY

Now we consider a theoretical reason for inconsistency between levels 1 and 2 of vulnerability criteria for pure loss of stability. The level 1 criterion is essentially a GM value approximated for a wave of steepness of 0.0334 in which the wave length is considered to be equal to the ship length (Paragraph 1.2.2 of Annex 3 of SDC 6/WP.6). The level 2 criterion is an estimate of a long-term probability that the static angle caused by a specified heeling moment or angle of vanishing stability to exceed required boundary values. Both angles are computed for worst GZ curve during a wave pass. Thus, level 1 criterion is deterministic and the level 2 criterion is probabilistic. This difference, by itself, can lead to an inconsistency between the levels, unless special provisions are considered.

Probabilistic Consistency

To gain insight into the probabilistic aspect of inconsistency, we consider a notional pure loss of stability criterion: a static or dynamic angle of heel achieved under a specified heeling moment with the worst GZ curve during the passing of a longitudinal wave (i.e., a wave pass). This criterion is applied for both level 1 and level 2. To compute this criterion, one needs to know wave length and wave height.

Following the procedure agreed for the level 2 vulnerability criteria for the pure loss of stability failure mode, as described in draft explanatory notes (paragraph 7.3.1 of Annex 19 of SDC 5/INF.4/Add.1), Grim's effective wave is used to represent stability variation in a particular sea state. As the length of the Grim's effective wave is equal to ship length, there is only one random variable left – the wave height. Thus, for a given ship length, each cell of a wave scatter table (e.g IACS Recommendation 34) corresponds to a particular value of the effective wave height, H_{eff}:

$$H_{eff} \approx 5.97\sqrt{V_H} \tag{1}$$

V_H is the variance of the effective wave:

$$V_H = \int_{\omega_1}^{\omega_2} RAO_{eff}^2(\omega) s(\omega|H_S, T_z) d\omega \tag{2}$$

Here, $s(\omega|H_S,T_z)$ is a spectral density of the wave elevations, ω is a frequency, $\omega_{1,2}$ are the limits of integration, H_S is the signficiant wave height, T_z is the mean wave zero-crossing period and RAO_{eff} is the RAO of the effective wave amplitude:

$$RAO_{eff}(\omega) = \frac{\omega^2 Lg^{-1} \cdot sin(0.5\omega^2 Lg^{-1}\cdot)}{\pi^2 - 0.5\omega^2 Lg^{-1}} \tag{3}$$

where L is a ship length and g is gravity acceleration.

As each cell of the scatter also corresponds to a statistical frequency, one can easily compute an estimate of the cumulative distribution function (CDF) by sorting the effective wave heights in ascending order and integrating all the statistical frequencies below the current value:

$$P(H_{eff}) = P(H_S, T_z) \tag{4}$$

$$P_1(H_{eff}) = sort(P(H_{eff}), H_{eff}) \tag{5}$$

$$CDF(H_{eff}) = \int_0^{H_{eff}} P_1(h)\, dh \tag{6}$$

The CDF, shown in Fig. 4, also can be interpreted as a dependence between the safety level for the level 1 criterion and a wave steepness for a ship with length of 260 m. The safety level of a deterministic criterion is a probability that a ship satisfying this criterion will nevertheless suffer from the failure. As the ship stability is a subject of random meteorological factors, the safety level theoretically cannot be zero.

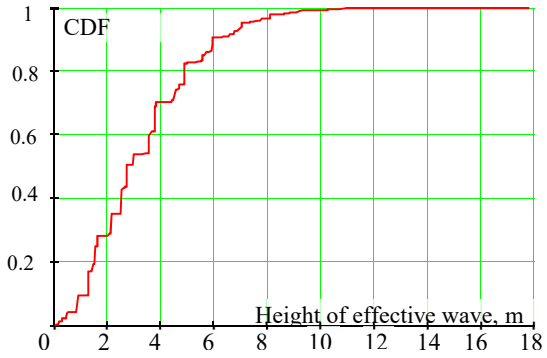

Figure 4: Estimate of CDF of the effective wave height computed for ship length L=260 m.

For example, we set the safety factor to 1%. Then, the effective wave height corresponding to the 99 percentile equals approximately 9.2 m for a ship length of 260 m. Thus, the steepness of the effective wave is 9.2 m /260 m = 0.035. If the ship satisfies the level 1 criterion for the wave steepness 0.035, there is only 1% probability over the lifetime that the stability will not be sufficient to withstand the pure loss of stability failure. Keeping the safety level constant, one will get another wave stiffness for another length, coming to an idea of the level-1 wave steepness that depends on a ship length. Originally, this idea was proposed in SDC 5/6/5.

It is assumed here that the heeling moment is created by wind. The relation of mean wind speed U_{Wm} is taken from paragraph 4.3.2.2 of Annex 3 of SDC 6/WP.6:

$$U_{Wm} = \left(\frac{H_S}{0.06717}\right)^{2/3} \tag{7}$$

Then the aerodynamic pressure p_A can be computed as:

$$p_A = \frac{\rho_A U_{Wm}^2}{2} \cdot C_m \tag{8}$$

where C_m is wind heeling moment coefficient. Its value is taken as 1.22 from paragraph 4.3.2.2 of Annex 3 of SDC 6/WP.6, while ρ_A is density of air.

This pressure is also a random variable, as it depends on the significant wave height. As each value of significant wave height in the scatter diagram has an associated statistical frequency, one can compute the CDF for the significant wave height:

$$CDF(H_S) = \int_0^{H_S} P_H(h)\, dh \tag{9}$$

P_H is a statistical frequency of the significant wave height, available from a wave scatter table (e.g., IACS Recommendation 34). The CDF of the wind pressure is essentially a rescaling of the CDF (9) with the formula (8), see Fig. 5. The values of mean wind pressure can be expressed as a function of the safety level:

$$SL = 1 - CDF \tag{10}$$

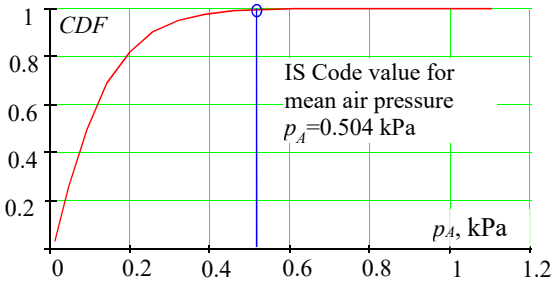

Figure 5: CDF for mean wind pressure

Fig. 5 shows the pressure value of 0.504 kPa that is used in the weather criterion in section 2.3 of the 2008 IS Code. The CDF for this value is interesting because it is actually quite high 0.993, when using the scatter diagram from IACS Recommendation 34, so that the safety level is only 0.007.

The setting the safety level for the level 1 criterion will define both the wave steepness and the wind pressure. Beyond these, there are no more random parameters involved in the level 1 criterion. Now, if the standard for level 2 criterion is established above the safety level for the level 1 criterion, the criteria always will be consistent between the two levels.

Physical Consistency

The second reason for the inconsistency between the level of the pure loss vulnerability criteria is actually the oversimplification of the level 1 criteria. The reason is that GM alone does not well characterize stability at large heel angles (a well known fact among naval architects). Thus, the level 1 criteria should include enough information to characterize stability at large heel angles. At the same time, it should be more conservative while perhaps less accurate than the level 2 criterion.

This idea can be implemented by formulating the level 1 criterion for the GZ curve in the worst possible position of ship on a wave (which is not necessarily when the midship section is located at exactly at the wave crest). Then, the level 2 criteria can be defined based on the stability variation throughout a complete wave pass (see Fig. 6). The conservatism of the level 1 criterion is then ensured by the simple fact that the worst GZ curve does not last too long during a wave pass.

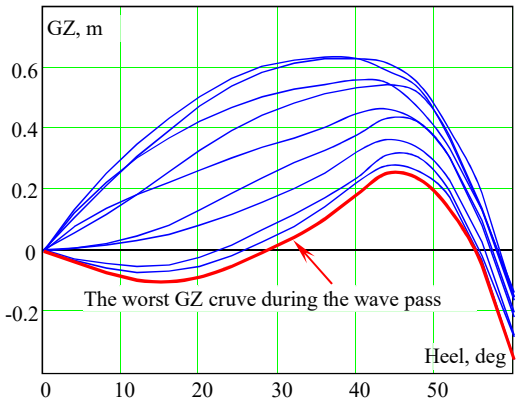

Figure 6: GZ Curve During Wave Pass, C11-class containership, wave steepness 0.012, KG=19.92 (IS Code critical)

Indeed, in this consideration, the level 1 criterion becomes more complex compared to a GM based-formulation that has been in consideration since 2011, including as currently contained in Annex 3 of SDC 6/WP.6 (Peters, *et al.* 2011). The new level 1 criterion proposal requires computation of GZ curve over the wave pass; these calculations do require a computer program with software suited for this purpose. This approach, however, seems to be inconsistent with the original intention (Peters *et al.* 2011) to limit level 1 efforts to spreadsheet-type calculations. However:

- GZ curves in longitudinal waves can be computed with most standard ship hydrostatic software. The level 1 criterion without any simplification can still be applied using a spreadsheet if the worst-case GZ curve during wave pass can be produced by the standard ship hydrostatic software;
- It may be possible to approximate the worst GZ curve during pass with the worst GM during the wave pass. If this will be found possible, the level of complexity of the proposed level 1 criterion will be on the same level as originally envisioned.

Consistent Criteria

Following the concept of the weather criterion, we consider a dynamic angle as a level 1 criterion. The GZ curve is selected as the worst GZ curve during the wave pass (see Fig. 3). The GZ curves in waves are computed for the effective wave height, corresponding to the agreed safety level that must be below the standard accepted for the level 2 criterion. Currently, the value of the level 2 standard equals to 0.06 per paragraph 1.3.1 of Annex 3 of SDC 6/WP.6. If the safety level for the level 1 criterion is taken as 0.02, the steepness of the effective wave for a 260 m long ship is 0.0328, which is slightly lower than the 0.0334 proposed in Annex 3 of SDC 6/WP.6.

The mean wind pressure, corresponding to the safety level of 0.02 is p_A = 0.407 kPa (see Fig.2 and subsection 3.1). A few more assumptions are needed to compute the heeling lever:

The pure loss of stability failure mode occurs in stern quartering and following waves in which it will be too conservative to consider beam wind: it is assumed that the wave has a β = 20 degrees angle with ship heading .

Little roll motion is expected in following and stern quartering seas and, in this case, the roll back angle may be assumed to be zero.

No developed wind drift is assumed because the relative wind angle is small (20°), which means that the hydrodynamic resistance to wind drift is also small. This has the effect of making the lever of the wind force as the distance from the waterline to the center of wind pressure, which, of course, is different from the assumption made in the weather criterion.

Following the weather criterion assumption (see paragraph 2.3.2 of the 2008 IS Code), the sudden increase of the wind force (i.e., the sustained gust) above the mean value is taken as 1.5.

As a result of these assumptions, the lever of the heeling moment in the considered loading condition is computed as follows:

$$l_w = 1.5 \cdot \frac{p_A \cdot A \cdot Z}{g \cdot \Delta} \cdot \sin(\beta) \qquad (11)$$

where A is the projected lateral area of the ship and deck cargo above the waterline, Z vertical distance from the center of A to the waterline, Δ is mass displacement in metric tonnes, and g is the gravitational acceleration.

The level 1 criterion can be formulated as follows

$$\phi_d \leq R_{PL2} \qquad (12)$$

where ϕ_d is a dynamic angle of heel calculated by equalizing area a and area b, as shown in Fig. 7. R_{PL2} = 15 degrees for passenger vessels and 25 degrees otherwise.

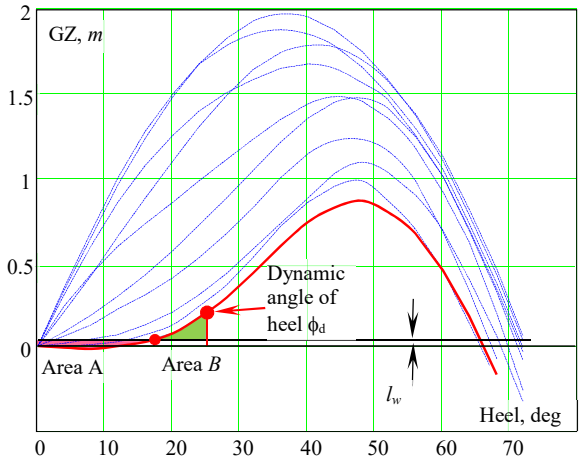

Figure 7: GZ Curve During Wave Pass, C11-class containership, KG=18.55 wave steepness 0.0328

To be consistent, the level 2 criterion is formulated for the same scenario, but takes into account time, i.e. that the GZ curve changes during the wave pass and does not remain at the worst case throughout the wave pass. Computation of the dynamic angle is carried out by numerical integration of the equations of motions, describing surging x and rolling ϕ:

$$\begin{cases} (\Delta + A_{11})\ddot{x} + R_x(\dot{x}) - T(\dot{x}, n) = F_x(x,t) \\ (I_x + A_{44})\ddot{\phi} + R_\phi(\dot{\phi}) + \Delta g GZ(\phi, x) = \Delta g l_w \end{cases}$$

where, I_x is the moment of inertia in roll; A_{11} and A_{44} are the added mass in surge and roll, respectively; R_x is the ship resistance in calm water; T is the ship thrust, achieved with commanded number of propeller revolutions, n; F_x is the Froude-Krylov wave force in direction of surge and R_ϕ is the roll damping.

The GZ curve in waves is precomputed and then is interpolated for the particular values of roll angle and position on the wave – see also paragraphs 3.3.2.4 of Annex 19 of SDC5/INF.4/Add.1, while the description of the calculation of the Froude-Krylov force can be found in (Belenky, *et al.* 2019)

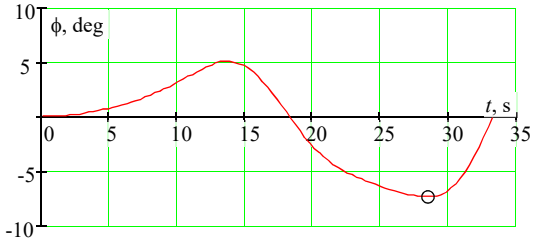

Figure 8: Roll during the Wave Pass; C11-class containership, KG=18.55 m wave steepness 0.034

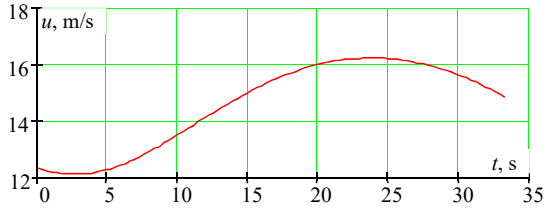

Figure 9: Surging Velocity during the Wave Pass; C11-class containership, KG=18.55 m wave steepness 0.034

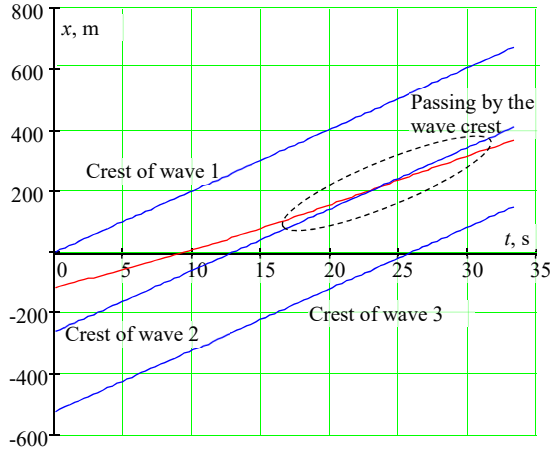

Figure 10: Distance travelled during the wave pass; C11-class containership, KG=18.55 m wave steepness 0.034

A numerical integration is performed for the duration of one wave pass and largest encountered roll angle for that one wave pass is recorded, see the example in Fig. 8-10.

Sample Calculations: Consistency

The numerical demonstration of consistency of the considered criteria is presented in Table 1. Calculations were performed for a RoPax ship, for which the particulars are presented in Table 2.

Table 1 is configured in order to test and compare the consistency of the four criteria, which are presented in four numbered columns. The base loading condition is the maximum KG for which the criteria of the 2008 IS Code are satisfied (column 1) – termed the "limiting 2008 IS Code critical condition". Column 2 shows the level 1 criterion as proposed in Annex 2 IMO SDC 6/WP.6 (column 2: "simplified GM"); column 3 shows the previously proposed level 1 criteria that involved the direct calculation of GM in a longitudinal wave; and column 4 that presents the dynamic angle criterion considered above in 3.3 for level 1.

Table 1: Considered Criteria for Sample RoPax Ship

Criteria →		2008 IS Code	Simpl. GM	Direct calc. for GM in waves	Considered dynamic angle criteria
Column →		1	2	3	4
ΔKG, m		0	-1.33	-0.147	-0.692
Level 1	Simpl. GM, m	-1.28	0.05	-1.134	-0.589
	Direct calc. for GM in waves, m	-0.097	1.23	0.05	0.596
	Considered criteria	44.3°	6.3°	37.6°	15.0°
Level 2	CR1	0	0	0	0
	CR2	0.537	$2\ 10^{-4}$	0.366	0.055
	Considered criteria	0.173	0	0.142	$8.28\ 10^{-3}$

Table 2: Principal Particulars for a Sample RoPax Ship

Length BP, m	140.4
Breadth molded, m	20.27
Draft amidships, m	5.77
KG (critical 2008 IS Code), m	9.622
GM (critical 2008 IS Code), m	0.702
Speed, kt	19
Windage area, A, m^2	2,739
Center of pressure above WL, h, m	9.92

The second line shows the required change of KG relative to the 2008 IS Code critical condition KG. This value also shows how conservative the criteria are relative to each other by indicating the amount of a decrease in KG needed to satisfy the other criteria in columns 2 through 4. As expected, the ”simplified GM” criterion is the most conservative, while the ”direct GM” is the least conservative. The considered dynamic angle criteria is about half way between columns 2 and 3.

Inconsistency can be observed in column 3. Here, the level 1 criterion is a critical condition: GM = 0.05m, while the level 2 criterion indicates vulnerability with a significant margin $CR_2 = 0.366$.

On the contrary, column 4 shows consistency for the dynamic angle criteria. The level 1 criterion is shown to be critical: a dynamic angle equal to 15 degrees, while the level 2 criterion is shown to pass with significant margin: $0.0083 < 0.06$.

The currently proposed criterion in column 2 of Table 1, “the simplified GM”, is also consistent, but the required KG must be reduced about 0.6 m from that shown for the considered criteria in column 4.

Sample Calculations: Separation Capability

To test the separation capability of the considered criteria, we consider the C11 container carrier (see Table 3) as a typical representative of the “old” post-panamax container ship. Built in the early 1990s, this class is known, *inter alia*, for significant variation of the GZ curve in waves leading to parametric roll (France, *et al.* 2003). We are not aware of any potential issues of pure loss of stability of any ship in this class, while they have been in service for about 30 years. Results of the calculations are presented in Table 4.

On the other hand, the observed vulnerability to pure loss of stability for a RoPax carrier may be well justified; as this ship is similar to a ship that suffered from a stability accident that may be attributed to pure loss of stability (Maritime New Zealand, 2007).

Table 3: Principle Particulars for a C11 Class Containership

Length BP, m	262
Breadth molded, m	40
Draft amidships, m	11.5
KG (critical 2008 IS Code), m	19.93
GM (critical 2008 IS Code),m	0.38
Speed, kt	24
Windage area, A , m2	7,887
Center of pressure above WL,h, m	14.73

The ability to differentiate the C11-class containership with the RoPax carrier is a good “stress-test” for the vulnerability criteria for pure loss of stability. To complete this test, the critical ΔKG values are also computed for the proposed level 2 criteria (as described in Annex 3 of SDC 6/WP.6) and the level 2 criteria, considered in this paper, see Table 5.

Both sample ships were found to be vulnerable to pure loss of stability by both the criteria in 2008 IS Code KG-critical condition, see column 1 in Tables 1 and 4.

Table 4: Considered Criteria for a C11 Class Containership

Criteria →		2008 IS Code	Simpl. GM	Direct calc. for GM in waves	Considered criteria
Column →		1	2	3	4
ΔKG, m		0	-3.69	-1.578	-1.374
Level 1	Simpl. GM, m	-3.643	0.05	-2.065	-2.269
	Direct calc. for GM in waves, m	-1.528	2.165	0.05	-0.153
	Considered criteria	-	1.7°	18.1°	25°
Level 2	CR1	0.057	0.057	0.057	0.057
	CR2	0.849	0	0.086	0.0128
	Considered criteria	0.18	0	$6.05\ 10^{-4}$	$6.58\ 10^{-5}$

Table 5: Critical KG for Level 2 Criteria

	Ropax R_{PL2} = 15°	C11 w/o weathertight volume R_{PL2}= 25°
Proposed Level 2 Criteria (Annex 3 of SDC 6/WP.6)	-0.39	-0.81
Considered Level 2 Criterion (this paper)	-0.41	-0.22

However, the minimum operational GM for C11-class containership is about 1 m (likely due to damage stability criteria requirements). The value of 0.9 m is the smallest GM mentioned by France, *et al.* (2003). As seen in the Table 5, the level-2 criterion from Annex 3 of SDC 6/WP.6 suggests that the GM for the C11 should be 1.19 m in order to avoid pure loss of stability failure.

The proposed level 2 criterion requires only GM = 0.6 m, which includes the entire operational range of GM, which indicates that the C11 is not vulnerable to pure loss of stability, which does not contradict existing operational experience and shows some separation capability of the proposed criterion.

4. SUMMARY AND CONCLUSIONS

The consistency of vulnerability assessments between levels 1 and 2 of the dead ship condition and pure loss of stability failure modes have been considered.

The level 2 vulnerability criterion for the dead ship condition is a probabilistic long-term criterion, which assesses dynamic stability in waves with an upcrossing rate or probability of upcrossing during a given exposure time. The level 1 vulnerability criterion replicates the weather criterion with an extended table for the natural roll period. Following other studies, it was found that consistency between the two levels cannot be guaranteed and that a certain probability of inconsistency has to be accepted.

As currently formulated, the level 2 criterion does not provide the roll back angle for the weather criterion, thus it cannot be used to extend applicability of the weather criterion within the current stability regulatory framework. However, it can be used for independent assessment of the safety level in dead ship conditions.

The consistency of vulnerability assessments between levels 1 and 2 for the pure loss of stability failure mode can be achieved by satisfying two conditions:

- Level 1 and 2 criteria use same mathematical model (like a dynamical angle of heel) or mathematical level for level 2 is less conservative compare to level 1 (e.g. level 1 is a dynamical angle computed with for the worst GZ curve during the wave pass, while level 2 accounts for variation of the GZ curve during the wave pass);
- Safety level for the deterministic level 1 criterion is set below the standard for the probabilistic level-2 criterion.

The possibility of considering consistent vulnerability criteria for pure loss of stability is suggested as a possible alternative for the future refinement of the second generation intact stability criteria.

ASKNOWLEGEMENT

The work described in this paper has been funded by the Office of Design and Engineering Standards of the US Coast Guard (CG-ENG) under the guidance of Mr. Jaideep Sirkar. The authors are grateful to Mr. K. Weems (NSWCCD) for his help with calculations and to Prof. K. Spyrou for fruitful discussions on the methodology of calculations.

REFERENCES

Belenky, V., Spyrou, K. and K. Weems (2019) "Modeling of Surf-Riding in Irregular Seas", Chapter 20 of Contemporary Ideas on Ship Stability. Risk of Capsizing, Belenky, V., Spyrou, K., van Walree F., Neves, M.A.S., and N. Umeda, eds., Springer, ISBN 978-3-030-00514-6., pp 347-358

Belenky, V.L. and N.B. Sevastianov (2007) Stability and Safety of Ships: Risk of Capsizing. Second edition SNAME, Jersey City, ISBN 0-939773-61-9.

Belenky, V.L. (1995) "Analysis of probabilistic balance of IMO stability regulation by piece-wise linear method", Marine Technology Trans., Polish Academy of Sciences, Branch in Gdansk, Vol. 6, pp. 5-55.

Dudziak, J., Buczkowski, A. (1978). "Probability of ship capsizing under the action of the beam wind and sea as a background of stability criteria", Polish Register of Ships, Prace Studialno-Roswojowe, Zeszyt Nr. 13, Gdansk.

IACS Recommendation No. 34 Standard Wave Data, November 2001

IMO MSC.1/Circ.1200 Interim Guidelines for Alternative Assessment of the Weather Criterion. 24 May 2006.

IMO SDC 5/6/5 Proposal on Improving Consistency of Pure Loss of Stability Vulnerability Criteria. Submitted by China, 17 November 2017.

IMO SDC 4/INF.4/Add.2 Correspondence Group on Intact Stability. Submitted by Japan, 9 December 2016

IMO SDC 5/INF.4 Information collected by the Correspondence Group on Intact Stability. Submitted by Japan, 15 November 2017

IMO SDC 5/INF.4/Add.1 Information collected by the Correspondence Group on Intact Stability. Submitted by Japan, 15 November 2017.

IMO SDC 6/WP.6 Finalization of Second Generation Intact Stability Criteria. Report of the Expert's Group on Intact Stability, 7 Februaury 2019.

France, W. M, M. Levadou, T. W. Treakle, J. R. Paulling, K. Michel & C. Moore (2003). An Investigation of Head-Sea Parametric Rolling and its Influence on Container Lashing Systems. Marine Tech., 40(1):1–19.

Maritime New Zealand (2007), Incident Report Heavy Weather/Cargo Shift Aratere 3 March 2006. Maritime New Zealand Investigation Report 06-201, vi+57 p, 2007

Peters, W., Belenky, V., Bassler C., Spyrou, K., Umeda, N., Bulian, G. and B. Altmayer (2011) "The Second Generation of Intact Stability Criteria, An Overview of Development", SNAME Trans. Vol. 119. pp. 225-264.

Peters, W. and V. Belenky (2017) "Challenges of Dead Ship condition Vulnerability Criteria Development" Proc. 16th Intl. Ship Stability Workshop, Belgrade, Serbia, pp. 15-19.

Tompuri, M., Ruponen, P. and D. Lindroth (2017) "On the Consistency of the Level 1 and 2 Vulnerability Criteria in the second generation Intact Stability", Proc. of the 16th Intl. Ship Stability Workshop, Belgrade, Serbia, pp 3-8.

Surf-riding failure mode: from IMO criterion to Direct Assessment procedure and application on Systematic Series D

Maria Acanfora, *University of Naples Federico II,* maria.acanfora@unina.it
Ermina Begovic, *University of Naples Federico II,* begovic@unina.it
Barbara Rinauro, *University of Naples Federico II,* barbara.rinauro@unina.it

ABSTRACT

The paper follows contemporary development of the second generation IMO intact stability criteria and describes application of vulnerability criteria for surf-riding / broaching to Systematic Series D parent hull. Model D1 is a semi-displacement twin-screw round-bilge hull by Kracht and Jacobsen (1992) representative of several naval ships built during 90ties. The modern hull form and the complete set of resistance and self-propulsion results available for the Systematic Series D models offer a possible benchmark case to support scientific community for further criteria verification.

More in particular, the Direct Assessment of surf-riding failure mode has been addressed by two approaches. The first one is based on the 1 DoF nonlinear differential equation for surge motion solved analytically and the occurrence of homoclinic bifurcation is examined.

The second approach is based on a 6DoF ship dynamics simulation taking into account wave, propeller and maneuvering forces and moments. Instantaneous wetted surface is considered for restoring and Froude-Krylov forces while ship resistance, thrust and maneuvering are based on the calm water performances.

Calculations are performed for four ship speeds at the wave with $\lambda/L = 1$ for different wave steepness. A condition where the occurrence of the surf-riding by 1DoF has been verified, is further analyzed by 6DoF, exploring the effect of the nonlinearity in the Froude Krylov force. The limit wave steepness is found for each considered ship speed.

Keywords: *Surf-riding, IMO SGISC, Direct Assessment, Systematic Series D, Bifurcation analysis, 6DoF ship dynamics*

1. INTRODUCTION

The second generation intact stability criteria (SGISC) are developing since 2002 and now are close to their final approval. This new generation of criteria is structured as a multi-level approach; when vulnerability is detected the next level is performed.

Surf-riding/broaching criteria is one of the failure modes SGISC IMO deals with. Level 1 and Level 2 vulnerability criteria are defined by IMO and are based on surf-riding 2nd threshold, while the Direct Assessment procedure is still in development.

This paper focuses on the vulnerability of surf-riding criteria applied on the Systematic Series D parent hull D1. Level 1 and Level 2 following IMO have been verified previously. A further analysis of the surf-riding phenomena, towards the direct assessment, is described and perfomed comparing two different approaches: one based on the 1DoF nonlinear surge equation, the second is based on a 6DoF time domain simulation of ship dynamics in wave.

In particular, the 1DoF equation of surge motion is solved analytically to find the manifolds of surf riding occurrence. The 6DoF time domain model, which combines seakeeping and maneuvering motions of the ship, allows simulating surf-riding phenomenon up to broaching-to instability.

The comparison of the results obtained by the application of the two different methods is performed for several speeds and steepness.

2. IMO SURF-RIDING CRITERION

Level 1 and Level 2 calculation procedures for surf-riding criteria are defined in IMO documents SDC 2 WP 4 and SDC 3 WP 5.

Umeda (1990) studied the surf riding probability as the “probability for ship to meet peak to peak wave whose height and length are satisfied for the condition for the surf riding in regular waves”. Based

on this approach, IMO defines Level 1 vulnerability as limit values of Froude number (Fn>0.3) or ship length (L<200 m).

Spyrou (2006) derived the close form of the Melnikov method for asymmetric surging and surf-riding in extreme following seas, inspired by work of Kan (1990). The main outcome of this work combined with the probability of wave occurrence as previously shown by Umeda (1990), is currently used as IMO SGISC procedure of surf-riding and broaching failure mode.

Level 2 vulnerability is detected if the value of Index *C* is greater than limit value of 0.005.

3. 1 DoF MODEL OF SURGE MOTION EQUATION

The mathematical model for 1 DoF describing surge motion equation is derived from Newton second law:

$$(m + m_X)\dot{u} + R(u) - T(u,n) = F_X \quad (1)$$

m is the ship displacement, m_X is the added mass, and u is the ship speed.

R is the calm water resistance approximated with a 5th order polynomial equation.

$$R = r_0 + r_1 u + r_2 u^2 + r_3 u^3 + r_4 u^4 + r_5 u^5 \quad (2)$$

T is the thrust delivered by the propulsor, expressed by:

$$T = N_P(\tau_0 n^2 + \tau_1 n u + \tau_1 u^2) \quad (3)$$

F_X is the wave excitation calculated considering only the Froude Krylov component f_X in calm water determined with the strip theory method (Belenky 2007, IMO SCD 3 WP.5):

$$F_X = f_X \sin(\omega_e t - kx)$$

$$f_X = \rho g k \zeta_A \sqrt{Fc_i^2 + Fs_i^2} \quad (4)$$

For Surf-riding equilibrium the encounter frequency ω_e is equal to zero therefore the time dependence is neglected.

Defining x_G the distance between center of gravity of the ship and wave trough, equation (1) can be expressed as function wave celerity, c, and ship and wave relative speed in relationship:

$$\dot{x}_G = u - c$$

$$\ddot{x}_G = \frac{1}{(m+m_X)}\left[T_C - R_C - (A_1\dot{x}_G + A_2\dot{x}_G^2 + A_3\dot{x}_G^3 + A_4\dot{x}_G^4 + A_5\dot{x}_G^5\right] \quad (5)$$

Where:

$$A_1 = r_1 + 2(r_2 - N_P\tau_2)c + 3r_3c^2 + 4r_4c^3 + 5r_5c^4 - N_P\tau_1 n$$
$$A_2 = r_2 + 3r_3c + 6r_4c^2 + 10r_5c^3 - N_P\tau_2$$
$$A_3 = r_3 + 4r_4c + 10r_5c^2$$
$$A_3 = r_4 + 5r_5c \quad (6)$$
$$A_5 = r_5$$
$$T_C = N_P(\tau_0 n^2 + \tau_1 nc + \tau_2 c^2)$$
$$R_C = r_0 + r_1 c + r_2 c^2 + r_3 c^3 + r_4 c^4 + r_5 c^5$$

This second order nonlinear differential equation has been transformed in a first order system with Runge-Kutta method, and then studied numerically analyzing the stability of the possible fixed points, by the definition of Jacobian matrix, its trace and the determinant.

Furthermore, the surge motion equation has been numerically solved in time domain simulations. The results have been plotted in phase plan diagrams and approximated trajectories of the stable and unstable manifold have been defined in order to represent the first and second threshold of surf-riding phenomena.

4. NUMERICAL SIMULATION 6 DOF MODEL

The numerical model has been developed for the dynamics in waves of the displacement ship. It combines seakeeping and manoeuvring motions. The ship is considered as a rigid intact body.

The main coordinate systems used for describing ship motion are presented in Figure 1, i.e. the inertial system fixed to Earth, with the *X*-*Y* plane coincident with the still water level, and the body-fixed reference frame having its origin at ship centre of gravity.

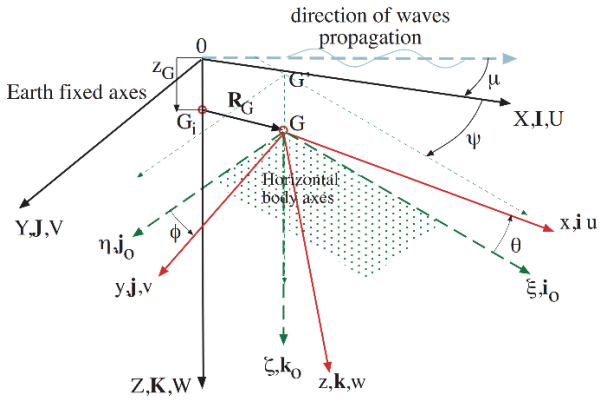

Figure 1: Co-ordinate systems used in ship dynamics (Matusiak 2013).

The hull surface is discretized by means of triangular panels. For each panel, the surface and the normal vector are known. In Eq. 7 the regular wave is calculated in the control points of the hull surface X_c and Y_c (referring to the center of each panel), given in the Earth fixed co-ordinate system by means of a transformation matrix. The coordinates X_c and Y_c take into account the ship's position in waves.

$$\zeta(t) = A\cos[k(X_c cos\beta - Y_c sin\beta) - \omega t] \quad (7)$$

It is important to underline that ω in Eq. 7 is the wave frequency since the longitudinal coordinate X_c depends on ship forward speed. The angle β is the wave heading.

The non-linear 6DoF model is based on the equations of motions in Eq.8. The numerical model can be defined as hybrid or blended (i.e. non-linearities are accounted for restoring and Froude-Krylov actions, while radiation and diffraction actions are obtained by linear strip-theory potential method), and it is based on the assumptions explained in (Matusiak 2013).

$$\begin{aligned}
&(m + a_{11})\dot{u} + m(qw - rv) + a_{15}\dot{q} = \\
&\quad -mgsin\theta + X_{wave} + X_{man} - b_{15}q + X_{prop} + X_{resist} \\
&(m + a_{22})\dot{v} + m(ru - pw) + a_{24}\dot{p} + a_{26}\dot{r} = \\
&\quad mgcos\theta sin\phi + Y_{wave} + Y_{man} - b_{22}v - b_{24}p \\
&(m + a_{33})\dot{w} + m(pv - qu) + a_{35}\dot{q} = \\
&\quad mgcos\theta cos\phi + Z_{wave} - b_{33}w - b_{35}q \\
&(I_x + a_{44})\dot{p} + (I_z - I_y)qr + a_{42}\dot{v} + a_{46}\dot{r} = \\
&\quad K_{wave} + K_{man} - b_{44}p - b_{42}v - b_{46}r \\
&(I_y + a_{55})\dot{q} + (I_x - I_z)rp + a_{15}\dot{u} + a_{53}\dot{w} = \\
&\quad M_{wave} - B_{55}q - b_{53}w - b_{51}u \\
&(I_z + a_{66})\dot{r} + (I_y - I_x)pq + a_{62}\dot{v} + a_{64}\dot{p} = \\
&\quad N_{wave} + N_{man} - b_{66}r - b_{64}p
\end{aligned} \quad (8)$$

The terms a_{ij} and b_{ij} are respectively the added mass and damping coefficients at the encounter wave frequency. The terms with the subscript *"wave"* include Froude-Krylov, diffraction and restoring forces and moments, while the terms with the subscript *"man"* refer to manoeuvring actions (i.e. further forces acting in the transversal direction and not included in the hull-wave interaction). The term X_{prop} and X_{resist} models ship propeller actions and hull resistance, respectively, at a given speed.

The inertia, Froude-Krylov and restoring forces and moments are evaluated accounting for all the pertinent non-linearities. The pressure profile is assumed by applying the so called "stretched distribution" above the waterline:

$$p = g\zeta e^{-k(Z_c+\zeta)} + Z_c \quad (9)$$

Where ζ is the wave profile, k is the wave number and Z_c is the depth of any panel, accounting for the actual ship motions.

This approach is a kind of extension of the linear wave theory to incorporate the nonlinear effects associated with the variation of a ship's wetted surface in the Froude-Krylov and hydrostatics forces and moments. Damping, added mass and diffraction forces and moments are calculated beforehand by a potential strip theory code (Faltinsen 1990 and Salvesen et al. 1970) and then implemented in the numerical model.

The numerical model accounts for ship velocity given by the propeller behavior, together with ship resistance in waves. Propeller actions are expressed in body fixed reference frame and move with the hull (see Fig.1).

The total thrust provided by the propellers is evaluated from a known open water characteristic of the propeller, $K_T = K_T(J)$, as follows:

$$X_{prop} = N_P \rho n^2 D^4 K_T \quad (10)$$

where J is the advance ratio, N_P is the number of the propellers, n is the propeller revolutions per second and D is the propeller diameter.

The required propeller revolution n, for still water and constant forward speed, is set in order to obtain the condition:

$$X_{prop} = X_{resist}$$

where:

$$X_{resist} = \frac{R_T}{1-t} = -0.5\rho u^2 S C_T/(1-t) \quad (11)$$

In (11), R_T is the total resistance, t is the thrust deduction factor, S is the static wetted surface and u is the forward velocity of the ship in the body-fixed co-ordinate system.

Propeller revolution is kept constant during the simulations in waves. Therefore, ship speed will modify from still water value, due to added resistance in waves. This is evaluated as a result of dynamic pressures forces, acting on the wetted panel on the ship, projected on x-direction.

Maneuvering actions are estimated by semi-empirical model. The so-called *slow motion hydrodynamic derivatives* for maneuvering motions are evaluated for the still water condition. The argument is that these terms include the effects that are related to slow motion, and they are mainly governed by the non-potential flow effects. This way of modelling ship manoeuvring may be questioned for the ship operating in waves. However, it proved to yield reasonable results. A good compromise is to preserve only the terms related to velocities such as Y_v, Y_r, N_v and N_r without including added mass contribution in the manoeuvring model, as these are already included in the radiation forces model. (Acanfora and Matusiak 2016).

In the current simulations, the potential damping terms related to yaw and sway motions in wave are neglected. Dealing with surf-riding, which involves encounter frequencies close to zero, the above assumption is supported by the evidence that in such condition, potential damping tends to null values.

The linear model for ship maneuvering limits the maneuvering forces only to the linear coefficients (i.e. to the motion derivatives). These can be easily estimated from the semi-empirical formulae obtained by the regression analysis. The linear maneuvering coefficients are given in Eq. 12, where T is the ship draft:

$$Y_v = -\pi(T/L)^2\ [1 + 0.4C_B(B/T)]$$
$$Y_r = -\pi(T/L)^2\ [-0.5 + 2.2(B/L) - 0.08(B/T)]$$
$$N_v = -\pi(T/L)^2\ [0.5 + 2.4(T/L)]$$
$$N_r = -\pi(T/L)^2\ [0.25 + 0.039(B/T) - 0.56(B/L)] \quad (12)$$

The assumptions on maneuvering model do not concern surf-riding developments; indeed they will affect the development of broaching instability.

5. SYSTEMATIC SERIES D OF FAST TWIN SCREW DISPLACEMENT SHIPS

The systematic Series D is originated from a semi-displacement twin-screw round-bilge hull form, initially made by the German yard Howaldtswerke-Deutsche Werft, with the necessity of having resistance and power predictions on a shorter and wider ship as this was a new and developing trend of ship design. (Kracht 1992, Kracht and Jacobsen, 1992).

The D-Systematic Series has seven models, derived from two parent hull forms D1 and D5. Resistance and propulsion tests have been performed in calm water in a speed range of Froude's number from 0.15 to 0.80.

6. IMO LEVEL 1 AND LEVEL 2 CRITERIA RESULS

The body plans of Systematic series D and ship main dimensions scaled to 90 m length are reported in (Begovic et al. 2018, Rinuaro and Begovic. 2019). All seven models result vulnerable to level 1 and level 2 criteria at given ship service speed of Fn = 0.433. Therefore, Froude number limit values, over which surf-riding is likely to occur, have been defined and reported in Begovic et al. (2018). Performing level 2, Froude number limit is around 0.325-0.34, depending on the type of hull, instead of 0.30 defined by the 1st level. With this result, an increase of ship speed of about 1 - 2 knots is obtained without been vulnerable to surf-riding and broaching. It has been shown that in the case of hull forms with the same length and tested with the same propeller, models with the lower calm water resistance resulted less vulnerable to the surf riding occurrence.

7. TOWARDS DIRECT ASSESSMENT

Based on the results found applying IMO criteria, similar for all Systematic Series D models, a further analysis towards direct assessment has been performed for hull D1.

The 1DoF and 6DoF models have been performed for $\lambda/L = 1$ wave case and for four Froude number cases. The limit value of steepness, to avoid surf riding, has been defined for each ship speed.

It is important to point out the implicit difference between the two methods: 1Dof model analytically finds the equilibrium points considering the ship speed equal to celerity and identifies stable and unstable manifolds from the unstable equilibrium points by numerical simulation in time to assess surf-riding developments.

On the other hand, 6DoF model simulates the effective speed of the ship in waves caused by the solution of the dynamic problem in time domain. Therefore surf-riding is observed in the simulation if the ship speed at a certain time equals the wave celerity.

1 DoF methodology

The analytical study of the surge motion equation brings to the definition of equilibrium points between the three forces acting on the ship: T_C, R_C and F_X, where T_C, and R_C are calculated for the wave celerity value c equal to 11.85m/s.

Figure 2 shows different equilibrium conditions for $\lambda/L = 1$ and $Fn = 0.335$ ($u = 9.95$m/s) and three different steepness. The input number of revolutions per second n is imposed to reach ship nominal speed; for Fn=0.335, n is equal to 2.9107 rps.

For $H/\lambda = 1/50$ no fixed points are found and the only possible motion is surging. As steepness increases, $H/\lambda = 1/45$ and 1/40, surf-riding phenomenon becomes possible, defined by infinite points of equilibrium.

By numerical simulation of the surge motion, the phase plan can be used to study the occurrence of surf-riding. Figure 3 to 6 show the phase plans, with displacement and cosine function of displacement, reporting the trajectories of the manifold that divide the different domains of attractions. Figures 3 and 5 report wave steepness case that generates surf-riding condition between 1st and 2nd threshold (for definition of surf-riding thresholds see Belenky 2011), where the stable manifold (continuous line) defines the only surf-riding domain, while the rest of the plane defines surge motion, and the unstable manifold (dashed line) converge to the stable equilibrium point. Figures 4 and 6 report surf-riding over 2nd threshold. The phase plans with cosine function, given in Figures 5 and 6 show the homoclinic bifurcation occurring for surf-riding 2nd threshold, as reported in Spyrou (1996).

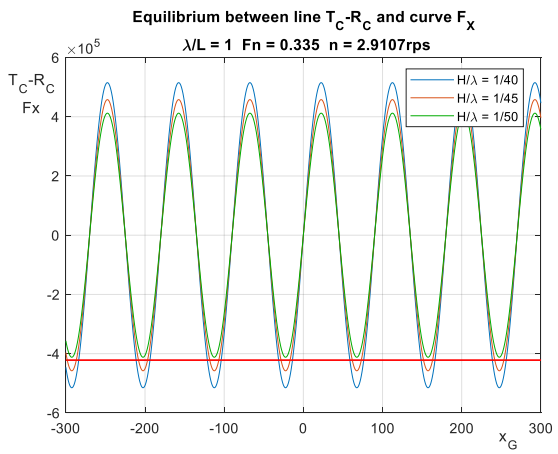

Figure 2: Equilibrium between T_C-R_C and F_X, for λ/L=1, Fn=0.335 and 3 steepness

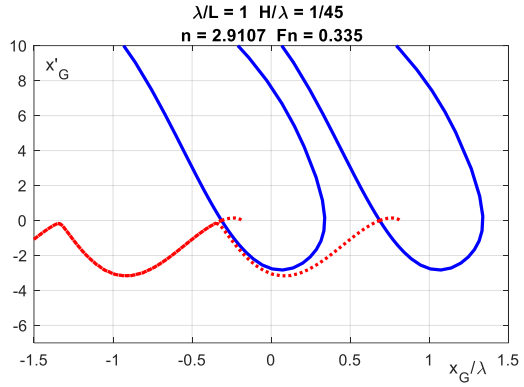

Figure 3: Phase plan for λ/L=1, Fn=0.335 and H/λ=1/45 - between 1st and 2nd threshold

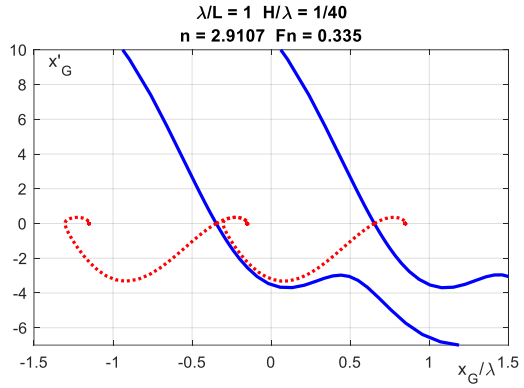

Figure 4: Phase plan for λ/L=1, Fn=0.335 and H/λ=1/40 – over 2nd threshold

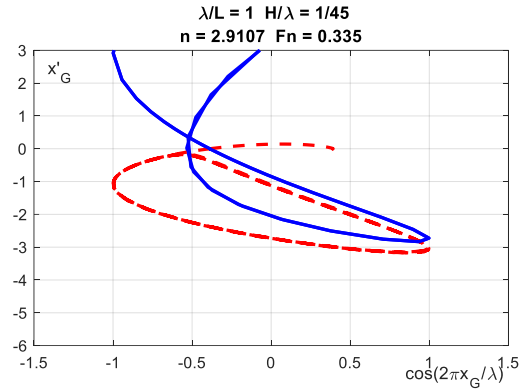

Figure 5: Phase plan with cosine function for λ/L=1, Fn=0.335 and H/λ=1/45 - between 1st and 2nd threshold

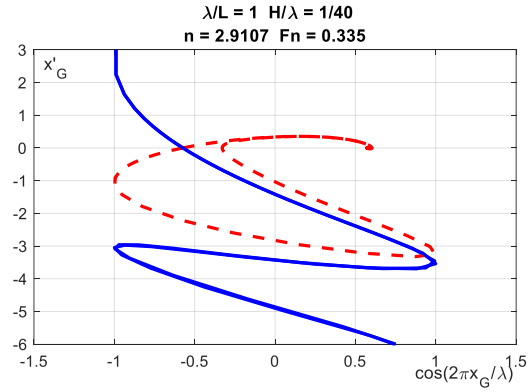

Figure 6: Phase plan with cosine function for λ/L=1, Fn=0.335 and H/λ=1/40 – over 2nd threshold

6 DoF methodology

Time domain simulations work on a sinusoidal wave, defined by length and steepness, starting with initial Froude number, Fn_{int}, that sets the propeller revolution and the initial encounter frequency (for radiation and diffraction forces).

Calculations have been performed for two cases, based on different pressure integrations for the Froude-Krylov Forces. The first case considers linear Froude-Krylov Forces integrated on the wetted surface coincident with the calm water one; the second case (nonlinear Froude-Krylov) considers the effective wetted surface due to wave elevation and ship dynamics. However, in both cases, restoring forces include the pertinent nonlinearities.

Figures 7 through 9 show time domain simulations for X_{prop}-$X_{Resistance}$ and FK_L (linear Froude Krylov), ship speed u, and yaw angle ψ for wave case λ/L = 1, H/λ = 1/50 and Fn_{int} = 0.35 corresponding to n=3.0726 rps. This case features the dynamic equilibrium of surging, where all forces oscillate in time.

Increasing the steepness to H/λ = 1/40 after a certain number of oscillations surf-riding phenomenon can be observed form figures 10 to 12, when X_{prop}-$X_{Resistance}$ and FK_L equilibrate and Fn and yaw angle remain constant. The ship will experience surf-riding until yaw angle increases and generates instability corresponding to broaching phenomena.

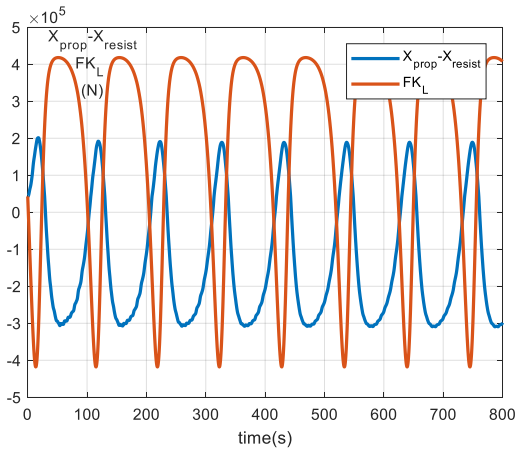

Figure 7: X_{prop}-X_{Resist}, and FK_L time domain simulation for λ/L=1, Fn_{int}=0.35 and H/λ=1/50 , for Linear Froude Krylov case– surging condition

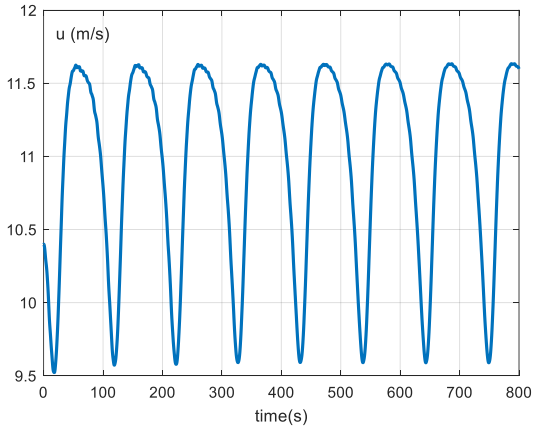

Figure 8: Speed time domain simulation for λ/L=1, Fn_{int}=0.35 and H/λ=1/50, for Linear Froude Krylov case – surging condition

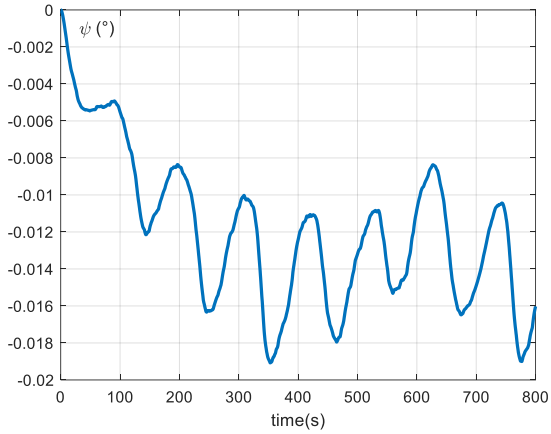

Figure 9 Yaw angle time domain simulation λ/L=1, Fn_{int}=0.35 and H/λ=1/50, for Linear Froude Krylov case – surging condition

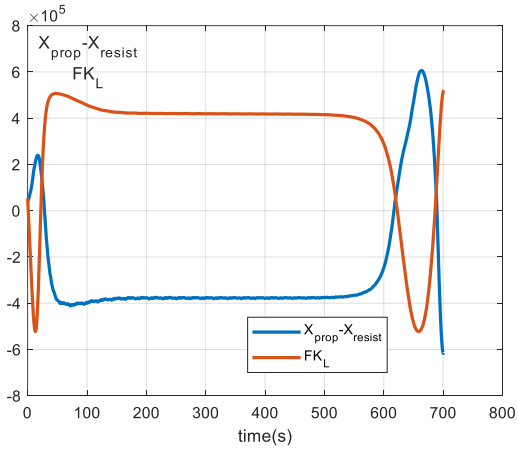

Figure 10: X_{prop}-X_{Resist}, and FK_L time domain simulation for λ/L=1, Fn_{int}=0.35 and H/λ=1/40, for Linear Froude Krylov case – surf-riding/broaching phenomena

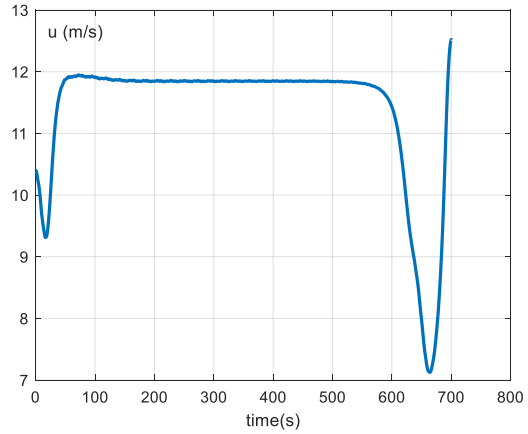

Figure 11: Speed time domain simulation for λ/*L*=1, *Fn*$_{int}$=0.35 and *H*/λ=1/40, for Linear Froude Krylov case – surf-riding/broaching phenomena

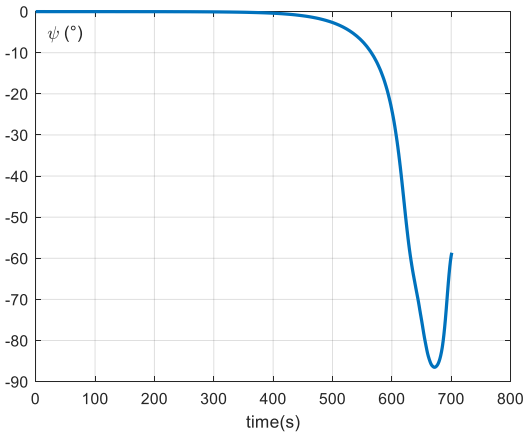

Figure 12: Yaw angle time domain simulation for λ/*L*=1, *Fn*$_{int}$=0.35 and *H*/λ=1/40, for Linear Froude Krylov case – surf-riding/broaching phenomena

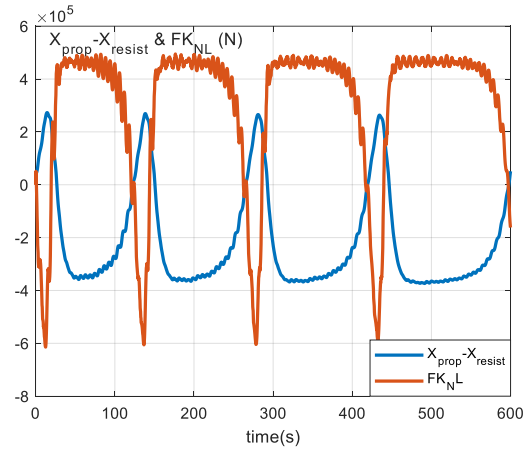

Figure 13: X_{prop}-X_{Resist}, and FK_{NL} time domain simulation for λ/*L*=1, *Fn*$_{int}$=0.35 and *H*/λ=1/50 – surging condition

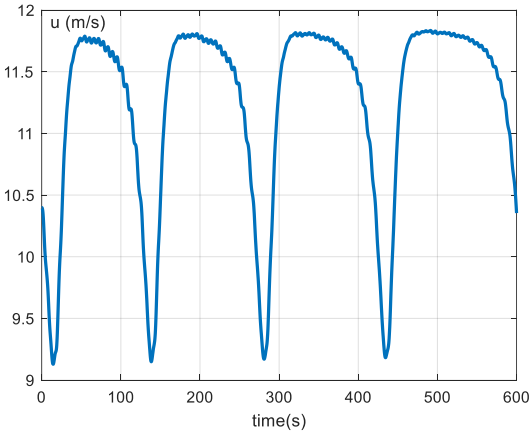

Figure 14: Speed time domain simulation for λ/*L*=1, *Fn*$_{int}$=0.35 and *H*/λ=1/40, for Nonlinear Froude Krylov case – surging condition

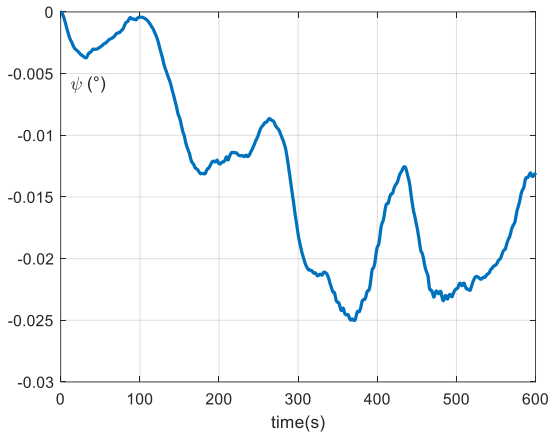

Figure 15 Yaw angle time domain simulation λ/*L*=1, *Fn*$_{int}$=0.35 and *H*/λ=1/50, for Nonlinear Froude Krylov case – surging condition

Figures 13 to 15 represent time domain simulations for X_{prop}-$X_{Resistance}$, FK_{NL} (nonlinear Froude Krylov), *F*n, and yaw angle, by nonlinear Froude Krylov forces, for wave case λ/*L* = 1, *H*/λ = 1/40 and *Fn*$_{int}$ = 0.35. It can be seen how considering the nonlinearity of Froude Krylov forces, surf-riding is not detected for the same conditions of linear Froude Krylov case.

Comparison of 1 DoF and 6 DoF results

Figure 16 summarizes the main results for four Froude number cases comparing the different approaches discussed above. The ship is identified as vulnerable to surf-riding if the wave steepness exceeds the value above the limit line:

- Blue line, square markers for 6DoF approach with nonlinear Froude-Krylov forces
- Red line, triangle markers for 6DoF approach with linear Froude-Krylov forces
- Grey line, round markers for 1Dof approach

It can be observed that 1 DoF method is more conservative than the 6 DoF ones (both linear and nonlinear Froude Krylov cases). However, for ship speed *u* converging to wave celerity *c*, all methods predict the surf-riding phenomenon at the same steepness, around 0.006. Concerning the 6 DoF approach, all nonlinearities due to instantaneous wetted surface, for small wave amplitudes, are converging to their linear values.

For ship speeds far from the wave celerity, the adopted methods provide distinct threshold values. The 1DoF linear and the 6DoF linear outcomes are closer to each other than 6DoF nonlinear.

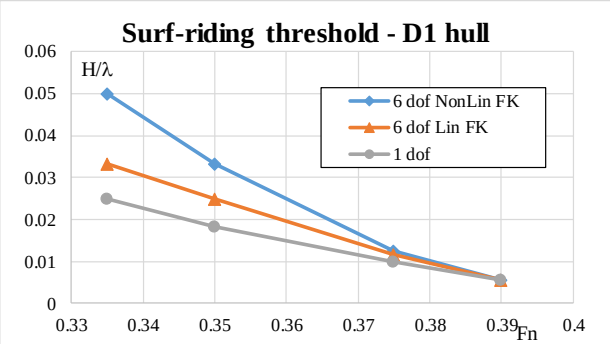

Figure 16: Comparison of 1 DoF and 6 DoF results

8. CONCLUSIONS

The present work explores the possibility of Direct Assessment approaches for surf riding phenomenon by bifurcation analysis of 1 DoF surge motion equation and 6 DoF ship dynamics simulation, considering two cases: linear and nonlinear Froude-Krylov Forces.

The different methodologies have been applied on Systematic Series D parent hull, for four nominal Froude numbers and wave case $\lambda/L=1$ and surf riding thresholds have been defined through wave steepness.

As expected, 1 DoF method is more conservative than the 6 DoF ones. A possible explanation in the different results between 1DoF and 6DoF linear Froude-Krylov model can be attributed to the non-linarites in restoring forces. Moreover, the 6DoF approach with nonlinear Froude-Krylov forces leads to the less conservative thresholds.

Based on the above considerations, a two-fold approach can be envisaged applying 1DoF and 6DoF nonlinear: 1DoF approach, faster and easier to implement, might be used to set the initial steepness value for the 6DoF simulations.

Further step towards direct assessment can be the implementation of resistance and thrust forces calculated in waves by CFD simulations.

REFERENCES

Acanfora, M., and J. Matusiak. 2016. "On the Estimations of Ship Motions during Maneuvering Tasks in Irregular Seas." In Proceedings of 3rd International Conference on Maritime Technology and Engineering, MARTECH 2016. Vol. 1.

Begovic, E., C. Bertorello, G. Boccadamo, and B. Rinauro. 2018. "Application of Surf-Riding and Broaching Criteria for the Systematic Series D Models." Ocean Engineering 170 (December). Pergamon: 246–65. https://doi.org/10.1016/J.OCEANENG.2018.08.062.

Belenky V., Bassler C.C., Spyrou K.J., 2011, "Development of second generation intact stability criteria", Naval surface warfare center Carderock division -50-TR-2011/065, Hydromechanics department report

Belenky V., Sevastianov V., 2007, "Stability and safe of ships, risk of capsizing", The society of naval architects and marine engineers (SNAME), Jersey City NJ

Dunwoody A.B., 1989, "Roll of a Ship in Astern Seas – Response to GM Fluctuations", *Journal of Ship Research* 33(4), pp. 284-290.

Faltinsen, O.M. 1990. "Sea Loads on Ships and Offshore Structures". Cambridge University Press. Vol. 1. https://doi.org/9780521458702.

IMO SDC 3 /WP 5 – Report of the working group (part 1). London, 21 Gen 2016

IMO SDC 2 /WP 4 – Report of the working group (part 1). London, 19 Feb 2015

IMO 2006, "MSC.1/Circ.1200 - Interim Guidelines for Alternative Assessment of the Weather Criterion", 24 May.

Kan, M. (1990), "A Guideline to Avoid the Dangerous Surf-riding", Proceedings of the 4th International Conference on Stability of Ships and Ocean Vehicles, University Federico II of Naples (Naples), pp.90-97

Kawahara, Y., Maekawa, K., Ikeda, Y., 2009, "A Simple Prediction Formula of Roll Damping of Conventional Cargo Ships on the Basis of Ikeda's Method and Its Limitation", Proceedings of the 10th International Conference on Stability of Ships and Ocean Vehicles, (STAB2009), St. Petersburg, Russia, pp. 387-398.

Kracht A., 1992, internal report – VWS-Bericht Nr. 1202/92

Kracht A. M., Jacobsen A., 1992, "D-series Systematic Experiments with Models of Fats Twin-screw Displacement Ship", SNAME transactions, Vol. 100, pp. 199-222

Matusiak, Jerzy. 2013. Dynamics of a Rigid Ship. SCIENZE +. Aalto University publication series. https://aaltodoc.aalto.fi/handle/123456789/24408.

Rinauro B., and Begovic E., 2019, "Vulnerability assessment of surf-riding/broaching and pure loss of stability for Systematic Series D1 model", Ships and Offshore Structures, DOI: 10.1080/17445302.2019.1596545

Salvesen N., Tuck E. O., Faltinsen O., 1970, "Ship Motions and sea loads", The society of naval architects and marine engineers

Spyrou K.J., 1996, "Dynamic instability in quartering seas: The behavior of a ship during broaching", Journal of ship research, 40, No 4, 326-336

Umeda, N. (1990), "Probabilistic Study on Surf-riding of a Ship in Irregular Following Seas", Proceedings of the 4th International Conference on Stability of Ships and Ocean Vehicles, University Federico II of Naples (Naples), pp.336-343.

Wave radar application to the simplified parametric roll operational guidance at actual sea

Takehiro Yano, *Osaka University*, mn846048@gmail.com
Naoya Umeda, *Osaka University,* umeda@naoe.eng.osaka-u.ac.jp
Keiichi Hirayama, *Japan Radio Co. Ltd.*, hirayama.keiichi@jrc.co.jp
Mitsunori Baba, *Japan Radio Co. Ltd.*, baba.mitsunori@jrc.co.jp
Masahiro Sakai, *Osaka University,* sakai@naoe.eng.osaka-u.ac.jp

ABSTRACT

The authors executed measurements of the encounter waves by an X band wave radar and the roll angles by a gyro sensor on board for a Ropax ship. By using the measured wave spectrum, the roll amplitude is estimated by using the simplified method for parametric rolling, which is used for the draft IMO vulnerability criteria. The estimated roll angle shows reasonably good agreement with the measured roll angle. Therefore, the wave-radar-assisted simplified operational guidance could be promising for practical uses on board.

Keywords: *IMO second generation intact stability criteria, RoPax ship, parametric rolling, wave radar, operational guidance.*

1. INTRODUCTION

Current stability safety of ships is realised not only with good ship design but also with appropriate operation. Based on this understanding, the International Maritime Organization (IMO) is going to develop the operational guidance, other than the stability design criteria, as a part of the second generation intact stability criteria those dealing with the five failure modes, i.e., pure loss of stability, parametric rolling, dead ship stability, broaching and excessive acceleration. Both design criteria and operational guidance are based on physics reflecting the state-of-the-art methodology (IMO, 2019).

IMO developed a guidance to the master for avoiding dangerous situations in following and quartering seas as MSC/Circ 707 (IMO, 1995), which was superseded by MSC/Circ. 1228 (IMO, 2007) for covering all wave directions. By using the wave information including the wave height, wave period and wave direction, the master can select appropriate ship course ad speed. This guidance is also based on physics but does not utilise the ship dependent data, such as hull forms and loading conditions. As a result, the dangerous zones specified by this guidance could be often too wide for ships having sufficient intact stability.

For overcoming such drawback, the new operational guidance will be developed to fully utilise the ship conditions, which are used for the new design criteria as well (IMO, 2019). The new design criteria mentioned here is called as direct stability assessment, and evaluate safety level against the specified failure mode by using a numerical tool for simulating ship behaviours in irregular waves in the time domain, which should be validated with model experiments based on the ITTC recommended procedure. While the ship stability failure probabilities under different sea states are summed up in the direct stability assessment, the operational guidance requests the ship master to utilise only the ship stability failure probabilities under the sea state that he or she meets. Even so, for providing the operational guidance, the same computational efforts are required for the ship designers because the guidance should cover all possible encounter sea states during the life of ships.

However, for accurately evaluating such safety level, required computational efforts are not so small that the operational guidance is not always a feasible solution for most of smaller ships. Ironically such smaller ships are more relevant to intact stability failure. Thus, the IMO also agreed to provide a way for the simplified operational guidance, which uses simplified methodologies for the simplified design criteria named as the vulnerability criteria. In the

simplified methodologies for parametric rolling, as an example, the safety level is calculated as the probability of encountering dangerous sea states and the dangerous sea states is judged by a comparison of the roll amplitude with the acceptable angle. The roll amplitude is calculated by using an uncoupled but nonlinear roll model in representative regular waves determined from the wave spectrum. Thus, the method still involves nonlinearity of ship dynamics and randomness of wave environment. However, the coupling effect from heave and pitch is ignored so that the final judgement could be conservative to some extent. This nature is suitable for regulatory purpose and the computation could be made even with a spread sheet software.

The use of operational guidance, even in case of its simplified one, is rather new for mariners. In particular, wave information, such as the significant wave height, the mean wave period and the main wave direction, is not easily determined by visual observation on board. In the simplified method, often the shape of wave spectrum is assumed but it could be different from actual one. On the other hand, nowadays the wave radars are available for obtaining the wave information by using reflection of electric waves at the inclined wave surface (e.g. Hirayama et al. , 2010 and Suzaki et al., 2017). In the case of the wave radar, firstly the directional wave spectrum is determined from the spatial distribution of water elevation and then the significant wave height and so on are straightforwardly determined. If this approach is feasible, the use of operational guidance can be a promising beyond the limitation of the capability of mariners on board. Furthermore, the directional wave spectrum data could be directly used for the simplified operational guidance.

Based on this understanding, the authors attempt to apply the simplified method to a Ropax ship at seas. Here the wave information is determined from the directional wave spectrum obtained by the wave radar on the Ropax ship and her ship roll motion simultaneously is recorded by a gyro sensor. By comparing these two data, the feasibility of the simplified operational guidance using the wave radar is investigated. In this paper, we focus on parametric rolling as its first step. Similar research was reported by Suzuki et al. (2014) but focused on synchronous rolling.

2. SUBJECT SHIPS AND USED WAVE RADAR

The subject ship used by the authors is a Ropax ship operated in the coastal area around the Japanese Isle. Its principal particulars and the restoring arm curve are shown in Table 1 and Figure 1, respectively. Because of high freeboard, almost no possibility of capsizing but the danger of cargo shift on the vehicle deck may exist if the roll motion is significant.

Table 1: Principal particulars of the Ropax ship under the designed full load condition.

Items	Ship
Length	208.0 m
Breadth	26.0 m
Depth	20.4 m
Draft	7.4 m
Metacentric height	1.49 m
Natural roll period	15.5 s
Bilge keel area	41.6 m^2

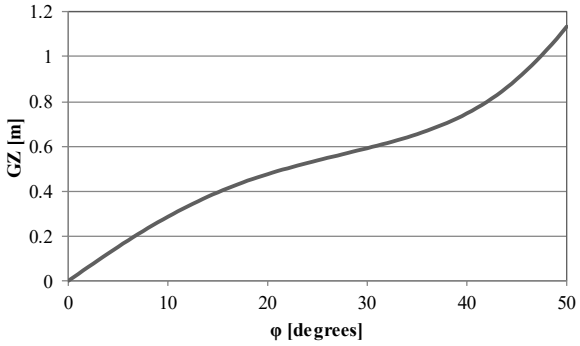

Figure 1: GZ curve of the Ropax ship in still water.

The ship is equipped with a wave radar system, which consists of an X band antenna, a radar display and a computer. Its measuring range is 3.8 km and measuring direction is about 190 degrees. For obtaining the wave measurement, a square 1920 m on a side, which corresponds to 256 meshes, is used so that the wavelength of 40 m or over can be detected. Every one rotation of the radar antenna, i.e. 2 or 3 s, the raw sea clutter image is recorded. An example of the obtained image is shown in Figure 2. Then the 2 dimensional Fourier transformation is applied to the images and their cross spectra are calculated for determining the wave spectrum removing noise spectrum by using a wave dispersion relationship. The average of 50 cross spectra is used

for the output having sufficient sound noise ratio. An example of comparison between the visual and radar-measured wave height is shown in Figure 3 (Hirayama et al., 2015). The accuracy of the wave radar is not perfect but could be used for practical purpose.

The second check of the level 2 vulnerability criteria for parametric rolling was applied to this subject ship as shown in Table 3. Here the probability of encountering dangerous sea states in the North Atlantic is required to be calculated as the C2 index. Since this work was done before SDC 6 in 2019, the details used here is based on older version: the number of ship speeds is seven and the averaging method is used so that the standard is 0.06 (IMO, 2015). The results indicate that the limited number of loading conditions, i.e. those having deeper drafts with medium metacentric heights, slightly exceed the standard. The criteria are requested to use the wave scatter table for the operational water area. Since the water area around the Japanese Isles is not so severe as that in the North Atlantic, the identified vulnerability could be removed (Usada et al., 2016). Thus, we can say that no real danger exists for this Ropax ship in the Japanese water area but tendency of parametric rolling may exist.

Table 3: C2 index of the second check of the draft level 2 vulnerability criteria for parametric rolling applied to the RoPax ship. Here d and GM indicate draft (m) and metacentric height (m), respectively.

d＼GM	1.49	1.5	1.6	1.7	1.8	1.9	1.93
6.2	1.29.E-02	1.29.E-02	1.88.E-02	1.93.E-02	1.88.E-02	1.53.E-04	2.07.E-04
6.3	1.88.E-02	1.88.E-02	2.22.E-02	2.30.E-02	2.23.E-02	3.69.E-04	3.69.E-04
6.4	1.93.E-02	1.93.E-02	2.30.E-02	2.47.E-02	2.32.E-02	3.72.E-04	7.02.E-04
6.5	2.29.E-02	2.30.E-02	2.48.E-02	2.49.E-02	2.51.E-02	9.43.E-04	9.51.E-04
6.6	2.46.E-02	2.48.E-02	2.49.E-02	3.59.E-02	2.55.E-02	1.03.E-03	1.79.E-03
6.7	2.48.E-02	2.48.E-02	3.59.E-02	3.99.E-02	3.60.E-02	1.79.E-03	1.84.E-03
6.8	2.48.E-02	2.49.E-02	3.97.E-02	4.22.E-02	4.25.E-02	1.82.E-03	2.35.E-03
6.9	3.57.E-02	3.57.E-02	4.19.E-02	4.42.E-02	4.47.E-02	2.32.E-03	2.37.E-03
7	3.96.E-02	3.97.E-02	4.38.E-02	4.44.E-02	4.54.E-02	2.41.E-03	2.58.E-03
7.1	4.16.E-02	4.16.E-02	4.39.E-02	4.53.E-02	4.54.E-02	2.57.E-03	4.28.E-03
7.2	4.15.E-02	4.18.E-02	4.39.E-02	6.07.E-02	4.61.E-02	4.89.E-03	4.24.E-03
7.3	3.96.E-02	4.15.E-02	4.38.E-02	6.04.E-02	6.15.E-02	4.62.E-02	5.85.E-03
7.4	4.15.E-02	4.15.E-02	4.44.E-02	6.03.E-02	6.58.E-02	2.47.E-02	6.68.E-03

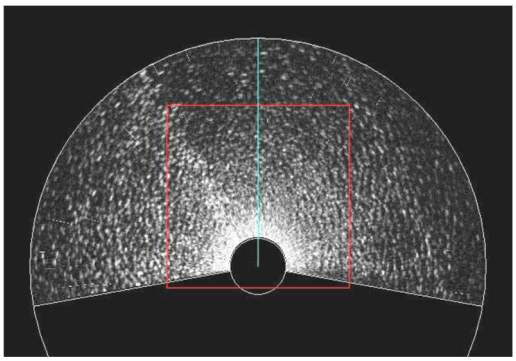

Figure 2: An example of sea clutter. (Hirayama et al., 2015)

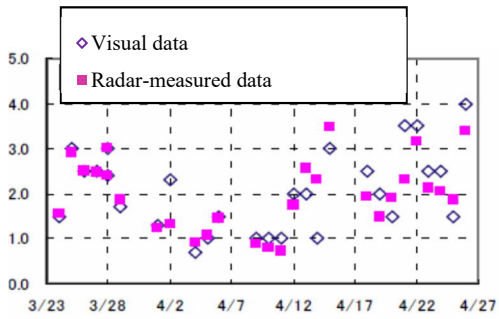

Figure 3: Comparison in wave height (m) between the visual and the radar-measured data on a containership in the North Atlantic and North Pacific for several weeks. (Hirayama et al., 2015)

3. SIMPLIFIED ESTIMATION METHOD FOR PARAMETRIC ROLLING FOR A SHORT-TERM SEA STATE

In this work, a simplified estimation method is used, which is based on an averaging method applied to an uncoupled roll equation with time-dependent roll restoring variation in regular oblique waves (Sakai et al., 2017). The used wave is determined from the directional wave spectrum (Umeda & Yamakoshi, 1994) by using Grim's effective wave concept (Grim, 1961). Further simplified version of this calculation method was adopted for the second check of the vulnerability level 2 criteria for

parametric rolling (IMO, 2019). While the IMO criteria deals with the longitudinal waves only, the current method takes account of waves from all possible directions as well. IMO decided to use time-domain simulation by using the Runge-Kutta method but the current method uses the averaging method. It was already confirmed that these two provide the same solution for most of cases if we pay sufficient attentions on the initial value dependence of the time-domain simulation.

4. RESULTS AND DISCUSSION

By using the wave radar and the gyro sensor on board, we automatically recorded the wave spectra and the roll angles for about five years. During the measurement, one of largest roll case is selected for validating the wave-radar-based simplified operational guidance. The selected case is the 9th February 2015 at 10:25 am JST. At this time, the subject ship heading southward off Akita in the Sea of Japan with the Froude number of 0.33. According to weather map, the wind velocity of about 20m per second from the south to the low pressure system situated in Sakhalin. The on-board wave radar outputted the wave spectrum as shown in Figure 4, which results in the significant wave height of 2.15m and the mean wavelength of 177m. Under this situation, the maximum roll angle that she experienced was 12.7 degrees, which is half the critical roll angle that the Japanese administration requested for RoPax ships for avoiding cargo shift. Thus, no actual danger existed for this ship.

The ship was almost fully loaded so that the ship draft is about 7.4m but the metacentric height is not certain. Thus, the simplified method for calculating the representative roll amplitude is applied for different metacentric height, as shown in Figures 5-10. It covers almost all possible metacentric height range, i.e. from 1.49m to 1.9m. The natural roll period is estimated by Morita's formula, which is used in the IMO weather criterion (IMO, 2008) using the relevant metacentric height.

Besides uncertainty in the metacentric height, these comparisons show reasonable agreement between the wave radar-assisted simplified operational guidance and the actually measured roll angle. Therefore, we cannot say that the wave radar-assisted simplified operational guidance does not have practical importance. In addition, this guidance suggests that the roll motion could be significantly reduced if the ship course is changed with just 15 degrees. This information is not relevant to ship capsizing or cargo shift very much but is useful for passengers' comfort.

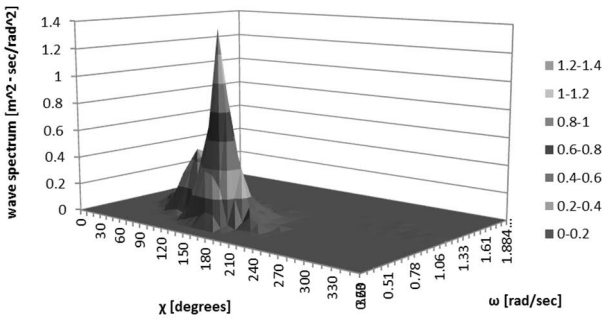

Figure 4: Wave spectrum measured by the wave radar as a function of the wave frequency, ω (rad/s), and directional angle, χ (degreees).

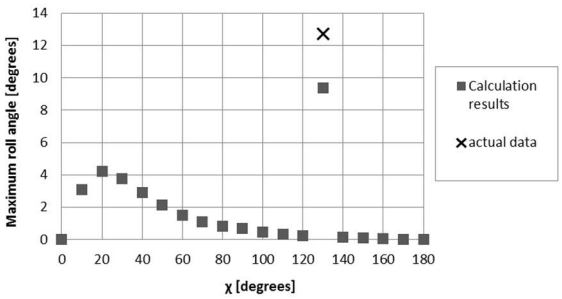

Figure 5: Roll angles estimated by the wave radar-assisted simplified operational guidance and the actually measured roll angle with the metacentric height is 1.49m.

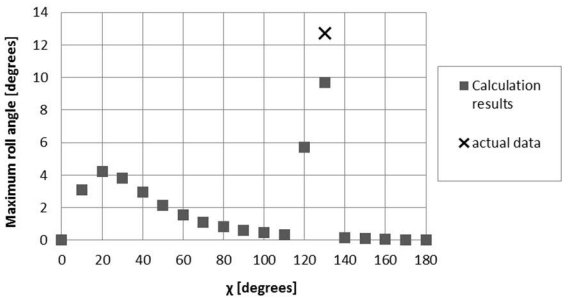

Figure 6: Roll angles estimated by the wave radar-assisted simplified operational guidance and the actually measured roll angle with the metacentric height is 1.50m.

The reason why parametric rolling occurs here is that the mean wavelength is comparable to the ship length and the mean encounter period can be almost half the natural roll period. Whether the fin stabilizer was used under this situation was not recorded so that this is another uncertainty. However, the good agreement with the estimation excluding the fin stabilizer effect suggests that the fin stabilizer was not used during the measurement.

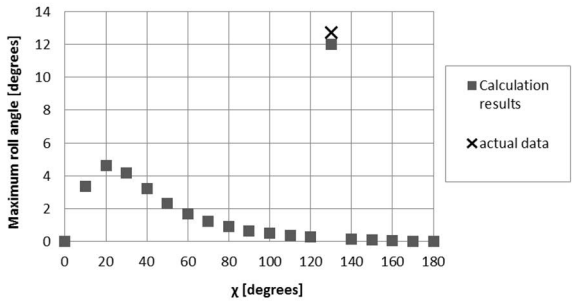

Figure 7: Roll angles estimated by the wave radar-assisted simplified operational guidance and the actually measured roll angle with the metacentric height is 1.60m.

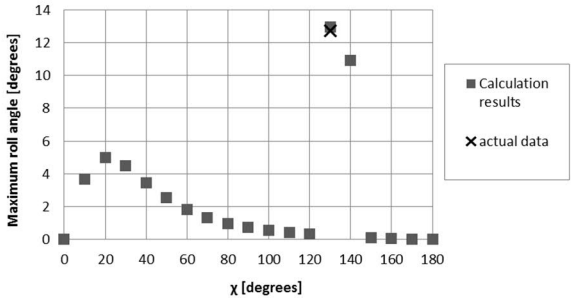

Figure 8: Roll angles estimated by the wave radar-assisted simplified operational guidance and the actually measured roll angle with the metacentric height is 1.70m.

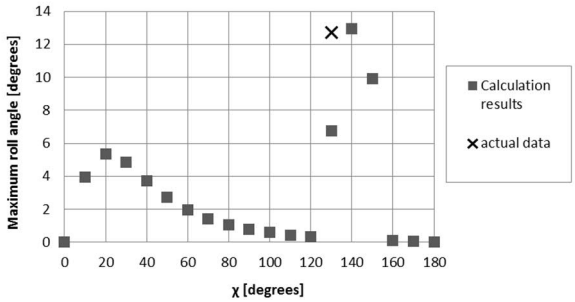

Figure 9: Roll angles estimated by the wave radar-assisted simplified operational guidance and the actually measured roll angle with the metacentric height is 1.80m.

5. CONCLUDING REMARKS

The authors executed measurements of the encounter waves by the wave radar and the roll angles by the gyro sensor on board for a Ropax ship. By using the measured wave spectrum, the roll amplitude is estimated by using the simplified method, which is used for the draft IMO vulnerability criteria. The estimated roll angle shows reasonably good agreement with the measured roll angle. Therefore, we may conclude that the roll angle of 13 degrees that the ship experienced seem to be parametric rolling and the wave-radar-assisted simplified operational guidance could be promising for practical uses on board. In any case this Ropax ship does not have any danger due to parametric rolling if the ship is operated in the water areas around the Japanese Isle. In addition, the guidance suggests that the parametric roll motion can be significantly reduced only if the ship course is changed with only 15 degrees. Further validation study should be encouraged.

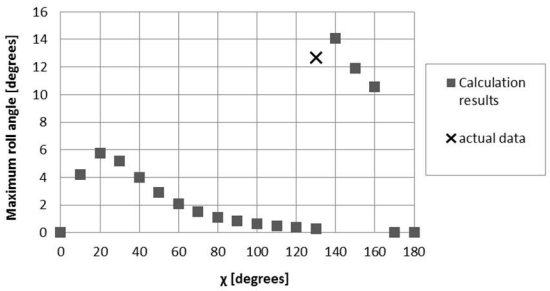

Figure 10: Roll angles estimated by the wave radar-assisted simplified operational guidance and the actually measured roll angle with the metacentric height is 1.90m.

ACKNOWLEDGEMENTS

This work was supported by a Grant-in Aid for Scientific Research from the Japan Society for Promotion of Science (JSPS KAKENHI Grant Number 19H02360). The authors are grateful to the shipbuilder and operator of the subject ship allowing the publishing the obtained data.

REFERENCES

Grim, O. (1961). "Beitrag zu dem Problem der Sicherheit des Schiffes in Seeegang", Schiff und Hafen, Heft. 6, S. 490-497.

Hirayama, K., Oka, K. and Baba, M. (2010). "Marine Wave Observation System with Radar", Technical Report of Japan Radio, No. 10, pp. 229-234, (in Japanese).

Hirayama, K., Baba, M. and Iseki, T. (2015). "Wave Monitoring on Board", Proceedings of Marine Dynamics Symposium on Ship Performance Monitoring in Actual Seas, The Japan Society of Naval Architects and Ocean Engineers, pp. 229-234, (in Japanese).

IMO (1995). "Guidance to the Master for Avoiding Dangerous Situations in Following and Quartering Seas", MSC/Circ. 707, IMO.

IMO (2007). "Revised Guidance to the Master for Avoiding Dangerous Situations in Adverse Weather and Sea Conditions", MSC.1/Circ. 1228, IMO.

IMO (2008). "Explanatory Notes to the International Code on

Intact Stability, 2008", MSC.1/Circ. 1281, IMO.

IMO (2015). "Report of the Working Group (Part 1)", SDC 2/WP.4, Annex 2, pp. 1-7.

IMO (2019). "Report of the Experts' Group on Intact Stability", SDC 6 /WP.6, Annex 3, pp. 1-5.

Sakai, M., Umeda, N., Yano, T., Maki, A., Yamashita, N., Matsuda, A. and Terada, D. (2017). "Averaging Methods for Estimating Parametric Roll in Longitudinal and Oblique Waves", Journal of Marine Science and Technology, Vol. 23, pp. 413-424.

Suzaki, H., Hirakawa, Y., Takayama, T. and Hirayama, T. (2017). "Acquision and Prediction of Wave Surface by Marine Radar for the Safety of Small Ships", Proceedings of the 16th International Ship Stability Workshop, Belgrade, pp. 49-56.

Suzuki, K., Nihei, Y., Ikeda, Y. and Suzumura, R. (2014). Journal of the Academic Society for Cruise & Ferry, Japan, No. 4, pp.15-22, (in Japanese).

Umeda, N. and Yamakoshi .Y (1994). "Probability of Ship Capsizing due to Pure Loss of Stability in Quartering Seas ", Naval Architecture and Ocean Engineering,Vol.30, pp. 73-85.

Usada, S. and Umeda, N. (2016). "Safety Assessment of Broaching for a Large Domestic RoPax Ship", Journal of the Academic Society for Cruise & Ferry, Japan, No.6, pp.1-8, (in Japanese).

On the uncertainties of the weather routing and support system against dangerous conditions

Teemu Manderbacka, *NAPA,* teemu.manderbacka@napa.fi

ABSTRACT

Better operational efficiency by fuel savings can be achieved by applying voyage optimization. Weather routing can improve the safety of operation. The route selection is dependent on the weather forecast, which contains uncertainty. Response of the ship and vulnerability to dynamic stability failures in certain sea conditions can be very different depending on the loading condition of the ship. The ship loading condition may not be exactly known for some ship types, introducing another source of uncertainty. Besides these, the methods used to assess the vulnerability also have some level of uncertainty. Taking all these factors into account, some level of safety margin should be introduced, which would in some cases narrow down the benefit of the fuel saving. In this paper the sources of uncertainties from the point of voyage optimization and weather routing are discussed.

Keywords: *Voyage Optimization, Operational Safety, Dynamic Stability Failure, Weather Routing, Operational Conditions.*

1. INTRODUCTION

Voyage optimization can provide significant savings in consumed fuel. It can also help to choose safe navigation route to avoid dangerous conditions. The duration of trans-oceanic voyages can be several weeks. Typically, a trans-pacific voyage of a container vessel takes approximately 2 weeks and a trans-Atlantic voyage around 10 days. Uncertainty in the weather forecast increases, the longer in the future it is extended. New updated forecasts will be received during the voyage, still some route selections in the beginning have effect on the later stages of the voyage.

Loading condition of the ship has important contribution to the motion response in waves. In the real operation, there is an uncertainty in the values of initial stability of the ship, namely GM and mass distribution and consequent rotational inertias, which affect the ship responses. Also, the applied methods to calculate the forces and motion response have limited accuracy in all realistic conditions. Total uncertainty of the estimated motions is a result of all these factors: uncertainty in:

- environmental conditions,
- ship mass distribution
- and calculation method.

In some route selections the fuel efficiency and safety might be conflicting. Some of the most fuel-efficient routes may not be the safest, or vice versa, the safest route may not be the most fuel efficient. Captain of the ship would emphasize the safety in route selection, because it is his responsibility. The operating company and the charter would emphasize timely arrival and total fuel oil consumption. Generally, in this order, because the compensation of late arrival generally would result more costly than excessive fuel oil consumption. Both factors are important for economical operations, where their weight depends on the type of transportation.

However, it is possible and essential to fulfill all the requirements, safe, punctual and energy efficient navigation. The question is, how much margin of safety need to be allowed in the planning of the voyage? Some choices in the route selection cannot be easily reverted, or at least not without compromising the planned arrival time or without excessive fuel consumption. As an example, voyages departing from the North Sea area would have alternatives of passing either north of Great Britain or through the English Channel. If the northern route is selected and the weather forecast changes, so that it would no more result as a feasible safe option, then changing the route could lead into arriving later than what was planned. The

uncertainty and the related risk in safety and economical risk easily leads into conservative and possibly not the most energy efficient route selections.

Bačkalov et al. (2016) studied the opportunity to improve the safety of navigation by mitigating the risks through operational measures. This paper aims at clarifying the related uncertainties and their sources. In this way paving way to approach on the planning and execution of energy efficient and safe voyages. Identification of uncertainties in the weather routing become essential also if and when the rules will allow navigation for ships that are susceptible to some failure modes but are allowed to operate in limited conditions or under operational guidance (Hashimoto et al. 2017). Huss (2016) point out the possibility to improve the stability by operational measures and possibility to avoid dangerous condition with help of decision support system (DSS), mentioning that even ships vulnerable to stability failures do not need to be less safe when would be operated with more active management, support and care.

2. CHALLENGES IN ROUTE SELECTION

If we optimize the fuel consumption of a sea passage, the optimal route with respect of minimum fuel consumption can be such that the ship would navigate with strong tail winds, but also with following waves, see Figure 1. This kind of conditions, following or stern quartering waves, may result difficult in terms of maneuvering and even stability, by introducing possibility to pure loss of stability, surf riding and broaching or parametric roll resonance.

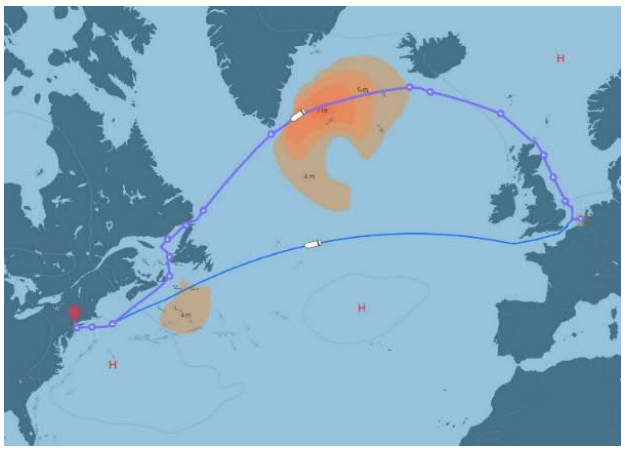

Figure 1: An example of fuel-efficient route without considering risk of stability failures vs shortest route.

To overcome the possibility of the route optimization algorithm to suggest a fuel-efficient but potentially dangerous route we can introduce limits to the allowed conditions. Most simple way is by limiting the allowed predicted wave height on the planned route. Which is an approach, that many of the operators choose in practice for the sake of simplicity. However, some of the stability failure modes, are not only dependent on the wave height, but the period and encounter angle, together with ship speed play an important role (Hashimoto et al 2017). For this reason, it would be possible to safely navigate at certain speed and heading in conditions that would result dangerous at different heading and speed for the same ship. Thus, by introducing the limits of heading and speed in certain wave height and period conditions to avoid stability failures taking into account the ship properties, we could in theory find the optimal route without compromising safety (Kobayashi et al., 2015).

The challenge is in defining what is an acceptable and reasonable margin of safety. The margin of safety should allow room for all the uncertainties; in the

- weather forecast,
- ship loading condition
- and calculation methods.

The naval architecture hydrodynamics and stability research has concentrated on improving the calculation methods and thus reducing the uncertainties originated from assessment of motion responses in waves. However, in real operation, the ship mass distribution is not exactly known. Depending on the ship type, even the initial stability, metacentric height GM, can vary significantly. Container ships can have very different GM values at same draft and similar number of containers, depending on their mass distribution. In theory the masses of containers loaded on board the ship should be well known, but in practice the weights vary from the announced ones, in this way causing uncertainty in the actual load case of the ship.

In ship design, and regulatory approval as well as in the regulation development the environmental conditions that the ship is required to withstand without compromising its safety are well defined. The designer can assess the ship's vulnerability to dynamic stability failure by applying Second Generation Intact Stability Criteria, SGISC (Umeda

and Francescutto, 2016) regulation to ensure the compliance of the ship to the rules. However, the methods used to check compliance at levels 1 and 2 are simplified and the ship not passing the first level L1 SGIS criteria should pass the second level L2 and if failing to pass the second level then Direct Stability Assessment (DSA) methods (Shigunov 2016, 2017) should be applied. The first level is intended to be the most conservative one. DSA methods are still under development, and many of the weather routing methods take the approach to constrain the allowable weather conditions. Whereas Yoon et al. (2018) are considering also the potential risks of dangerous motions in the selected route.

3. UNCERTAINTIES

Weather forecast

The weather routing services rely on the prediction of weather conditions, namely wave, wind and ocean current predictions. Currents consists of larger, prevailing ocean current systems with smaller variations, and tidal currents, which are well predicted and more important at the coastal areas. The effect of currents is relatively more important to the fuel consumption and efficient navigation of slower ships, nonetheless they do not generally pose any significant safety issue to a normally functioning ship.

The wave conditions, combination of wave height, period and encounter angle can result dangerous to the stability of the ship. Wind gusts may compound the situation, however generally the wind alone is not a stability risk. Wave conditions are dependent on the wind, however the wave propagation is well predicted since it takes time to transfer energy from the wind to ocean waves. Prediction of wind often bears larger uncertainty.

All the main international wave forecast providers have similar accuracy, as seen in yearly study by Bidlot (2017), who compare hundreds of globally positioned wave buoy measurement during the year 2016 with the forecasted wave conditions. Comparison on the forecasts at the location of wave buoys show how much in average the forecasts deviate from the measured real conditions. Globally, prediction of significant wave height Root Mean Square Error RMSE ranges from around 0.3 meters (nowcast) to around 0.6 to 0.8 meters for forecasts to five days ahead (Figure 2). Wave peak period RMSE does not seem to be so much affected by the extent of the forecast, the RMSE for wave peak period ranges from around 1.8 seconds to around 2.4 seconds for most of the weather providers. The wind speed forecast RMSE starts at around 0.9 to 1.5 m/s at 0 days ahead nowcast and increases nearly threefold to five days forecast having RMSE around 3.0 m/s to 3.4 m/s.

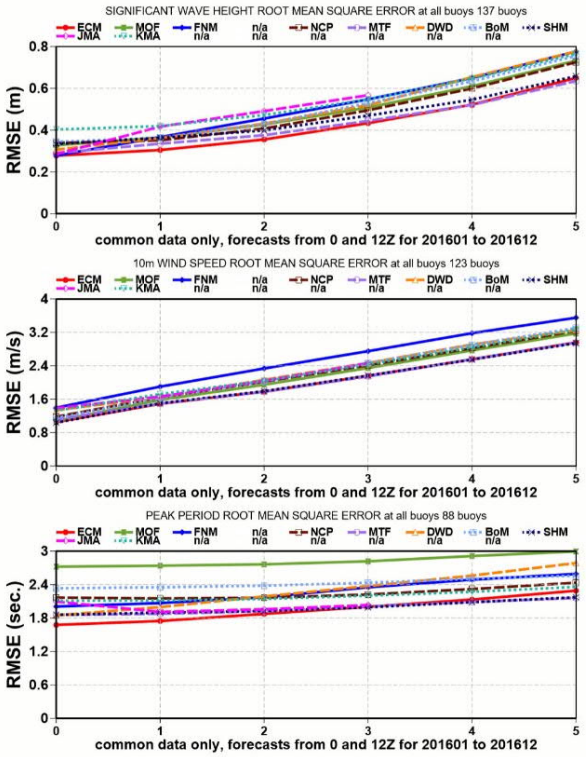

Figure 2: Root Mean Square Errors of forecasted Significant wave height (upper), Wind speed (middle), and Wave peak period (lower), figure adopted from Bidlot (2017).

Ship loading condition

The container vessel can have large variations in initial stability. In general, a container vessel has larger GM at smaller drafts. The GM can be very high for a container vessel in ballast condition in some cases. However, even at the same draft the initial stability can vary significantly. As an example of GM variation for a container vessel of ~5000TEU of capacity and length of nearly 300 m is presented in Figure 3. All recorded loading conditions are shown in non-dimensional format.

Motion response calculation methods

For the voyage or route optimization or weather routing purposes the calculation methods need to be efficient. Several scenarios of route and speed combinations with respect to the predicted weather

need to be studied to find the fuel efficient, optimal route, which is safe to navigate. Wind resistance calculation is generally straight forward, basing on predefined wind force and moment coefficients for the ship in question or as general coefficient for different ship types. Thus, the wind effect calculation does not require huge computational effort. Of course, the wind effect can also be calculated in a very detailed manner applying CFD calculations (Luquet et al. 2017) e.g. for all different load cases, however more simple approaches provide reasonably good results for wind effect.

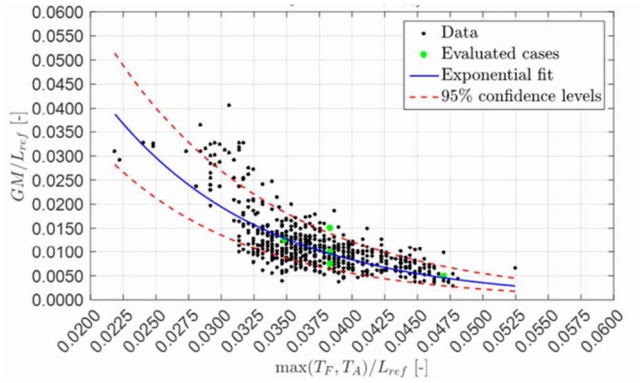

Figure 3: Recorded container vessel load cases.

The wave added resistance in turn is more complicated to estimate. Significant amount of research effort has been addressed to develop methods to estimate the wave added resistance, the state-of-the art methods still give relatively different results in some wave conditions according to the benchmark study performed within the EU funded SHOPERA (2016) project. The route optimizing algorithms generally use precalculated results for the wave added resistance. Sophisticated methods can be applied to pre-calculate added resistance, which can be tabulated and parametrized for fast availability for the optimization. The uncertainties related to the factors affecting on the consumption do not directly affect the uncertainty in safety, however the suggested candidate routes are dependent on the models that calculate the consumption.

Similarly, to the added resistance in waves, ship motion response calculation is challenging and bear uncertainty in the results. The assessment of vulnerability to stability failures is also dependent on the uncertainties in the modelling, like the in case of calculated surf riding probability shown to be dependent on the accuracy of calm water resistance and wave induced surge force modelling (Umeda et al. 2015). Calculation methods can vary in their level of accuracy, however generally it is preferred to use robust and efficient calculation methods, such as presented by Kalske and Manderbacka (2017), to avoid unnecessary long computational times and to have better coverage valid conditions of calculation.

4. CONCLUSIONS

Using weather routing and voyage optimization can help to reduce fuel oil consumption and improve operational efficiency. The safety of navigation can also be improved by better preparedness to avoiding dangerous conditions. Attention should be paid to the uncertainties in the planning of voyages through a safety margin. The uncertainties can be divided into three different categories. Arising from the uncertainty in the weather forecast, uncertainty in the actual loading condition affecting the initial stability and rotational inertias of the ship, and from the uncertainties in the methods assessing the responses of the ship in the seaway. The latter is paid a lot of attention by the naval architects and the researchers in the field of ship hydrodynamics. Weather forecasts are also improving, and a significant amount of research is carried by the meteorological institutes, also providing comparisons of the realized forecasts. With this, a need can be identified to further combine the meteorological information with the operational information into the assessment of responses and dangerous conditions. Such research is welcome addition and could be expected to help in practice the uptake of the voyage optimization, by clarifying the required range of the safety margin and to reduce the possible hesitation of the captains to approve the of voyage and route optimization suggestions.

REFERENCES

Bačkalov, I., Bulian G., Rosén, A., Shigunov, V., Themelis, N., 2016, “Improvement of ship stability and safety in intact condition through operational measures: challenges and opportunities”, Ocean Engineering, 120, pp.353-361.

BIDLOT J.-R. (2017), Intercomparison of operational wave forecasting systems against buoys: data from ECMWF, MetOffice, FNMOC, MSC, NCEP, MeteoFrance, DWD, BoM, SHOM, JMA, KMA, Puerto del Estado, DMI, CNR-AM, METNO, SHN-SM January 2016 to December 2016, European Centre for Medium-range Weather Forecasts (ECMWF),

https://www.jcomm.info/index.php?option=com_oe&task=viewDocumentRecord&docID=18333

Hashimoto, H., Taniguchi, Y. and Fujii, M., 2017, "A case study on operational limitations by means of navigation simulation", Proceedings of ISSW 2017, pp. 41-48.

Huss, M., 2016, "Operational stability beyond rule compliance", Proceedings of ISSW 2016, pp. 193-200.

Kalske, S., Manderbacka, T. 2017. Development of a new practical ship motion calculation method with forward speed. Proceedings of the International Ocean and Polar Engineering Conference (ISOPE 2017). San Francisco, CA, USA.

Kobayashi, H., Hashimoto, H., Taniguchi, Y., Yoneda, S., 2015, "Advanced Optimized Weather Routing for an OceanGoing Vessel", Proceedings of the 2015 International Association of Institutes of Navigation World Congress

Liwång, H., Rosén, A., 2018, "A framework for investigating the potential for operational measures in relation to intact stability", Proceedings of the 13th International Conference on the Stability of Ships and Ocean Vehicles, 16-21 September 2018, Kobe, Japan.

Luquet R., Vonier P., Prior A., Leguen J. F., 2015, "Aerodynamics Loads on a Heeled Ship", Proceedings of STAB 2015, pp. 735-744.

Papatzanakis, G., Papanikolaou, A., Liu, S., Optimization of Routing Considering Uncertainties, Journal of Marine Science and Application, March 2012, 11: 10-17, DOI: 10.1007/s11804-012-1100-y

Shigunov, V., 2016, "Probabilistic direct stability assessment", Proceedings of ISSW 2016, pp. 17-26.

Shigunov, V., 2017, "Possible simplifications of direct stability assessment", Proceedings of ISSW 2017, pp. 27-38

SHOPERA. 2016. SHOPERA Energy Efficient Safe Ship Operation EU FP-7 Project.

Umeda, N., Ihara, T., Usada, S., 2015, "An Investigation into the Factors Affecting Probabilistic Criterion for Surf-Riding", Proceedings of STAB 2015, pp. 319-329

Umeda, N., Francescutto, A., 2016, "Current state of the second generation intact stability criteria - achievements and remaining issues", Proceedings of ISSW 2016, pp. 3-9.

Yoon, H.K., Nguyen, V.M., Nguyen, T.T. 2018, "Development of Solution for Safe Ship Considering Seakeeping Performance", TransNav Vol 12, no 3, 2018, DOI: 10.12716/1001.12.03.10
http://www.transnav.eu/Article_Development_of_Solution_for_Safe_Yoon,47,835.html

Pure loss of stability in stern quartering waves: revisited with numerical simulations reproducing accidents

Naoya Umeda, *Osaka University,* umeda@naoe.eng.osaka-u.ac.jp
Mizuki Osugi, *Osaka University,* Haruka Nagato, *Osaka University,*
Yuito Ikenaga, *Osaka University*, Kazuma Matsubara, *Osaka University*,
Atsuo Maki, *Osaka University* and
Akihiko Matsuda, *National Research Institute of Fisheries Engineering*

ABSTRACT

For identifying the accident case suitable for validation of direct stability assessment for pure loss of stability failure modes, three accidents known as those due to pure loss of stability in stern quartering waves were examined with comparative numerical simulations using a surge-sway-yaw-roll coupled model. They include the large heel accidents of a RoPax ship in 2009, capsizing of an ocean research vessel in 1986 and a torpedo boat in 1934. As a result, we confirmed that major cause of these three accidents was not roll restoring variation due to waves but rather the coupling effect of sway-yaw motion to roll.

Keywords: *IMO second generation intact stability criteria, RoPax ship, ocean research vessel, torpedo boat, dynamic loss of stability.*

1. INTRODUCTION

The International Maritime Organization (IMO) agreed to develop the second generation intact stability criteria those dealing with the five failure modes by using physics-based approaches. Their standards are to be preferably based on known accidents. For example, the known accidents for parametric rolling and pure loss of stability are the cargo loss accident of the C11 class post-Panamax containership in the North Pacific and the fatal accident of the containership "Chicago Express" off Hong Kong, respectively. In case of the pure loss of stability, accidents of large heel of the RoPax ships in Japan (Japan Transport Safety Board, 2011) and New Zealand (New Zealand Transport Accident Investigation Commission, 2007) are mentioned. Other than these RoPax ships, capsize of an ocean research vessel (Umeda et al., 2017) and a torpedo boat in Japan (Maki et al., 2018) are often mentioned as candidates of accidents of pure loss of stability in stern quartering waves. In this paper, the authors attempt to reexamine whether these can be regarded as pure loss of stability or not.

Pure loss of stability in astern waves is defined by Oakley et al. (1974) as follows: a ship encounters one or more very steep high waves, with little or no preliminary rolling motion, simply loses all stability when a crest moves into the amidships position and "flops" over. They observed capsizing due to this phenomenon in free-running model experiments in San Francisco Bay. Kan et al. (1990 and 1994), de Kat and Thomas (1998) and others also realised capsizing due to this phenomenon by free-running model experiments in seakeeping and manoeuvring basins. Here key factors could be the magnitude and duration of roll restoring moment reduction due to the relative longitudinal wave profile. The magnitude depends on the wave height, wavelength and heading angle and the duration does on the relative forward speed of a wave crest to the ship. Thus, a surge-roll coupled simulation model was initially used for estimating the failure probability for pure loss of stability (e.g. Umeda & Yamakoshi, 1994). Such model was well validated with a towing model experiment of the ONR tumblehome topside vessel in regular following waves with the bias of roll angle of 4 degrees (Hashimoto, 2009). The danger increases with the increasing forward speed because the duration of restoring reduction is longer.

It failed, however, to explain the free-running model experiment of a containership in regular and irregular stern quartering waves. While the danger in the experiment increases with the increasing the forward speed, the danger in the numerical simulation does not. Thus, a surge-sway-yaw-roll

model was applied and then succeed to explain its qualitative tendency observed in the experiment. This was thought to be because, once large heel occurs due to restoring reduction, the underwater hull becomes unsymmetrical so that hydrodynamic sway force and yaw moment act on the ship. As a result, the lateral motion shall be induced so that the additional heel moment due to the lateral motion, which can be regarded as a centrifugal force effect and are proportional to the square of the ship forward speed. Since this additional effect seems to be essential to explain the speed dependence for danger of pure loss of stability in stern quartering waves (Kubo et al., 2012). Based on this understanding, the IMO (2019) agreed to take account of the moment due to centrifugal force as a function of the forward speed, in the level 2 vulnerability criteria for pure loss of stability.

Then the standard of the level 2 vulnerability criteria for pure loss of stability was determined with the large heel accident of the Ropax ship in stern quartering waves (Umeda et al., 2013). Since similar large heel incidents often reported for large RoPax ships in stern quartering waves (Japan, 2015), the danger modelled in the IMO level 2 vulnerability criteria for pure loss of stability surely exists. Indeed, seven cases of large heel angles in following and stern quartering waves were reported during the five years. The reported roll angles were 25 degrees or over, which happened for more than 7,000 gross tonnage ship in the North Pacific with the Froude number close to 0.3. As a result, some on board vehicles and containers were transversely moved. Therefore, the criteria could be effective for avoiding such danger.

As the next stage, it is necessary to validate a time-domain numerical simulation code to be used for the direct stability assessment with model experiments preferably relevant to actual accidents due to pure loss of stability. Therefore, the authors attempt to compare the numerical simulations using a surge-sway-roll-yaw model (Kubo et al., 2012) and the free-running model experiments for the accidents of the Ropax ship, the ocean research vessel and the torpedo boat mentioned above. These three accidents occurred when they ran in stern quartering waves with higher speed. For identifying the reason of the accidents, the numerical simulation was executed without and with key elements in the simulation model.

2. NUMERICAL MODEL

The accidents often occurred when ships ran in stern quartering waves. Under such situation the encounter wave frequency is low so that the heave and pitch, of which the natural frequencies are much higher, can be regarded to just trace their static equilibria and the hydrodynamic lift forces are more important than high-frequency wave making forces. Therefore, a coupled surge-sway-roll-yaw model based on manoeuvring model with heave and pitch motions as constraints is suitable for simulating such accidents. Here the wave forces should be estimated with a slender body theory based on the low encounter frequency assumption and the auto pilot should be included for keeping the commanded. In this paper, as one of such models, the model proposed by Kubo et al. (2012) is used. This model was based on the model used by Umeda (1999) for broaching prediction but the roll restoring moment, which is essential to pure loss of stability, is estimated using with Grim's effective wave concept (Grim, 1961) and the manoeuvring coefficients in calm water were determined by captive model experiments using the circular motion technique. The wave effects on the manoeuvring forces are ignored as higher order terms under the assumption of small wave steepness and the linear relationships between the forces and waves. Nonlinearity essential here is the position dependence of wave forces, in other words, the wave forces proportional to the sinusoidal function depending on the horizontal ship motions. This is indispensable for surf-riding at the wave downslope and riding on a crest.

3. ROPAX SHIP ACCIDENT CASE

The accident of large heel of the RoPax ship in Japan (Japan Transport Safety Board, 2011) occurred when the ship ran with the Froude number of 0.275, the significant wave height of 4.59 m, the wave period of 10.0 s and the heading angle of 35 degrees from the wave direction. The waves came from the port side. The ship is equipped with two propellers, one rudder and a pair of the fin stabilizer but at the accident the fin stabilizer was utilized.

The accident report says that the ship suffered the heel angle of 25 degrees because of roll restoring moment due to the decrease of water plane area as a result of a wave. Then the cargo shift occurred so that the heel angle increased up to 40 degrees by the

action of the following waves and turning motion due to the heel. This means that pure loss of stability is mentioned as one of primary reason of the initial large heel of 25 degrees. The principal particulars are shown in Table 1.

For this accident condition, the numerical simulation is executed with and without the roll restoring variation due to waves. The wave spectrum here is assumed to be unidirectional ITTC spectrum and the autopilot is simulated with the rudder gain of 1.0. Although the hull manoeuvring coefficients including propulsion ones are determined by the captive model experiment at the seakeeping and manoeuvring basin of National Research Institute of Fisheries Engineering, some of the rudder parameters are estimated from the experimental data of a similar ship (Kondo et al., 2015). These details will be published later. For this accident condition, Ueno et al. (2012) executed a free-running model experiment in short-crested irregular waves at the seakeeping and manoeuvring basin of National Maritime Research Institute, and reported that the maximum roll was about 30 degrees before the cargo shift so that they succeeded to realise roughly similar heel angle occurred at the accident. In their experiment, the fin stabilizer was not actively used.

Table 1: Principal particulars of the Ropax ship.

Items	Values
Length	150.0 [m]
Breadth	22.80 [m]
Draft	6.26 [m]
Trim	1.68 [m]
Metacentric height	1.80 [m]
Natural roll period	17.1 [s]

An example of the numerical simulation results using the fore-mentioned model with the roll restoring variation due to waves is shown in Figure 1. The wave elevation at the midship and the roll angle are shown as time series: the negative wave elevation indicates the wave elevation from the calm-water surface and the positive roll angle does the roll towards starboard. The roll period is generally the same as the wave encounter period so that the obtained roll motion is harmonic. When the ship meets a wave crest or shortly before a wave crest, the ship significantly rolls towards starboard side. This seems to be a typical pure loss of stability but significant rolls towards port side also happens. If the phenomenon is harmonic, the significant rolls also for port side is natural and the restoring variation could be a major source of large roll.

For directly investigating this hypothesis, the numerical simulation without the restoring variation is also executed and its result is shown in Figure 2. The maximum roll angle here, as well as the qualitative nature of the relationship between the roll and waves, is the almost the same as the simulation with the restoring variation. This suggests that the roll restoring variation is not a major cause of the significant roll.

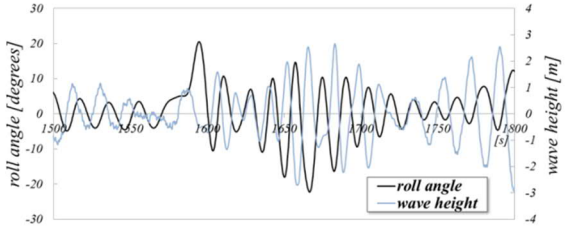

Figure 1: Numerical simulation of the RoPax ship with the roll restoring variation.

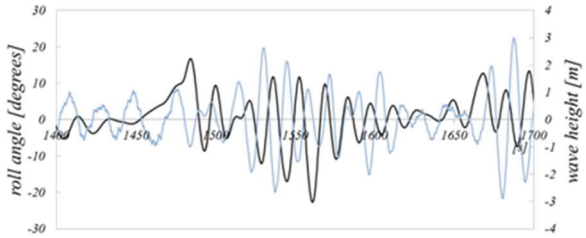

Figure 2: Numerical simulation of the RoPax ship without the roll restoring variation.

The simulated results also indicate that the wave encounter period is about 17.5 s, which is close to the natural roll period of 17.1 s. Thus we may suppose that the significant roll could be a simply harmonic resonance of uncoupled roll motion in stern quartering waves. If so, the major course could be a wave exciting roll moment. For examining this hypothesis, the numerical simulations with and without the effects of sway and yaw to roll are executed and their results are shown in Figures 3-4. Here the yaw rate and the roll angle are shown as time series: the positive yaw rate indicates the increase of yaw angle towards a starboard turn. It is clearly seen in Figure 4 that large yaw rate towards port results in a large starboard heel and the large yaw rate towards starboard does in a large port heel. This is well known tendency as a result of yaw-roll coupling. On the other hand, if we ignore such

coupling effect, no significant roll as well as no significant yaw rate cannot be found. Therefore, we should conclude that the significant roll that the Ropax ship experienced is a harmonic resonance due to coupling from the yaw motion. More systematic numerical investigation including the ensemble average of the maximum roll and the effect of fin stabilizer was published in Osugi et al. (2019). The yaw-roll coupling mentioned here seems to be identical to "dynamic loss of stability due to surge-roll-yaw coupling" identified by de Kat and Thomas (1998) in their experiment of a frigate model with the artificially lowered GM in stern quartering waves, in which the model typically capsized at a wave crest. They also noted that this phenomenon is different from "quasi-static loss of transverse stability in wave crest" that they also found. Since both phenomena occurred at a wave crest, they are not easily distinguished. Indeed, Kan et al. (1990) regarded rather dynamic phenomenon observed in their experiment of a containership model at a wave crest as "pure loss of stability". Further discussion is needed.

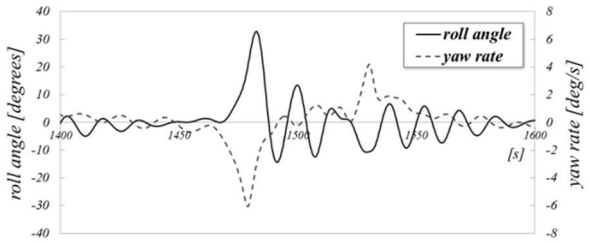

Figure 3: Numerical simulation of the RoPax ship with the roll restoring variation and the coupling effect from sway and yaw to roll.

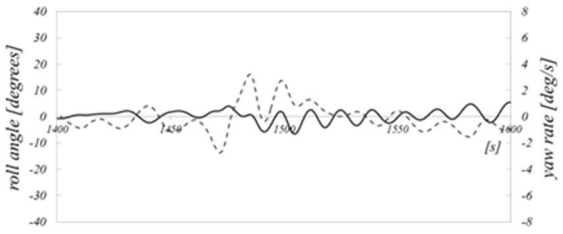

Figure 4: Numerical simulation of the RoPax ship with the roll restoring variation and the coupling effect from sway and yaw to roll.

4. OCEAN RESEARCH VESSEL ACCIDENT CASE

The accident of an ocean research vessel in stern quartering waves was examined by the maritime court (the Japan Association of Marine Safety, 1990), which suggests that this accident was triggered with loss of roll restoring moment in stern quartering waves. In June 1986, the ocean research vessel sank off Fukushima in Japan on its maiden voyage without any emergency call. The maritime court concluded that the height of centre of gravity was increased due to several changes of design during construction and then during her maiden voyage the ship heeled significantly when she ran in severe stern quartering waves. The principal particulars of the ship and the estimated condition at the accident are shown in Table 2 (Umeda, Osugi et al., 2017).

Table 2: Principal particulars of the ocean research vessel and its accident condition.

Items	Values
Length	22.00 [m]
Breadth	5.00 [m]
Depth	2.20 [m]
Mean draft	1.75 [m]
Metacentric height	0.41 [m]
Natural roll period	7.11 [s]
Ship speed	10 [kts]
Wave height	3.0 [m]
Wave period	5~6 [s]
Encounter angle from wave direction	-45 [degrees]

For investigating the reason why large roll occurs, comparative simulations were executed. Firstly, the time series of numerical simulation with and without the roll restoring variation for a typical case are shown in Figures 5 and 6, respectively. Here the wave elevation indicates its value at the midship and its minima correspond to a wave crest. The positive roll angle means the starboard downwards, the positive yaw angle does the starboard turn and the positive rudder angle normally induces the starboard turn. As shown in Figure 5, a large roll angle of about 35 degrees towards port side occurs shortly after the wave crest amidship. This seems to be relevant to a pure loss of stability. However, it is noteworthy here that at the moment the yaw rate towards starboard side becomes very large. It could induce large centrifugal force due to this large yaw rate, which could result in large heel towards the port side. Indeed, the numerical simulation without the restoring variation, as shown in Figure 6, shows that

slightly smaller but still more than 20 degrees roll occurs at the relevant moment. Therefore, we should conclude the roll restoring variation is not the only reason of large roll.

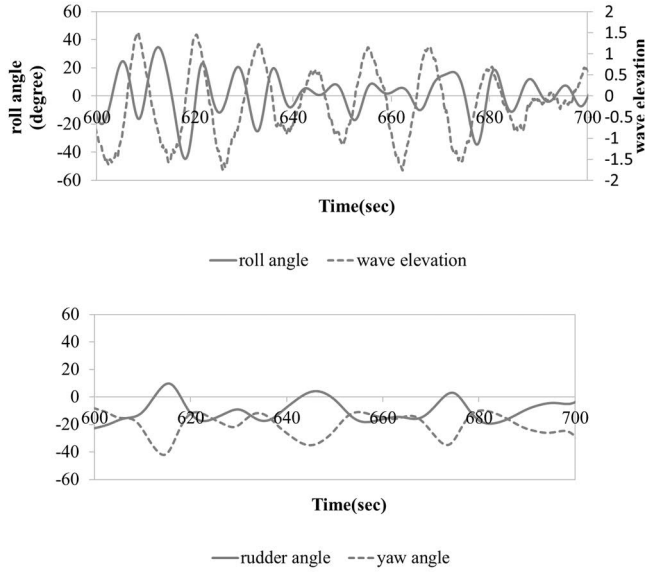

Figure 5: Numerical simulation of the ocean research vessel with the restoring variation.

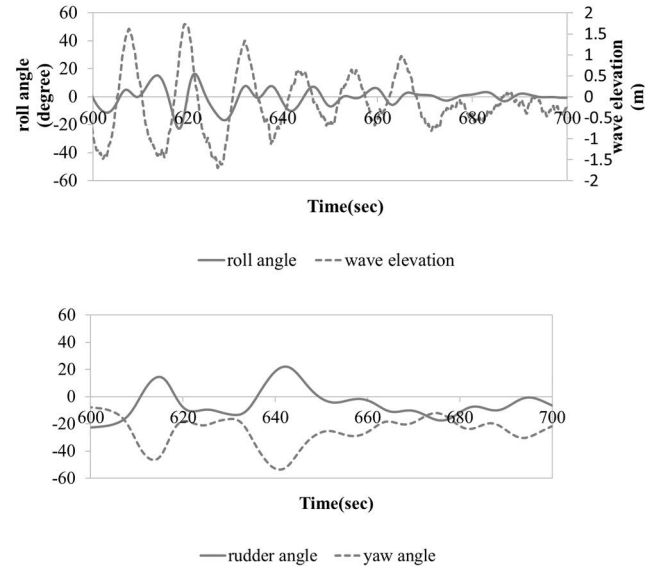

Figure 6: Numerical simulation of the ocean research vessel without the restoring variation.

For more directly confirming the reason of large heel, the numerical simulation without roll damping components due to sway velocity and yaw angular velocity was executed as shown in Figure 7. This indicates that the roll angle becomes further reduced from about 35 degrees to about 7 degrees. Thus, we can conclude that the coupling between sway/yaw and roll is also a major reason of the large heel at the wave crest amidship. Therefore, we can presume that both roll restoring variation and the roll-sway/yaw coupling are important for large heels in stern quartering waves.

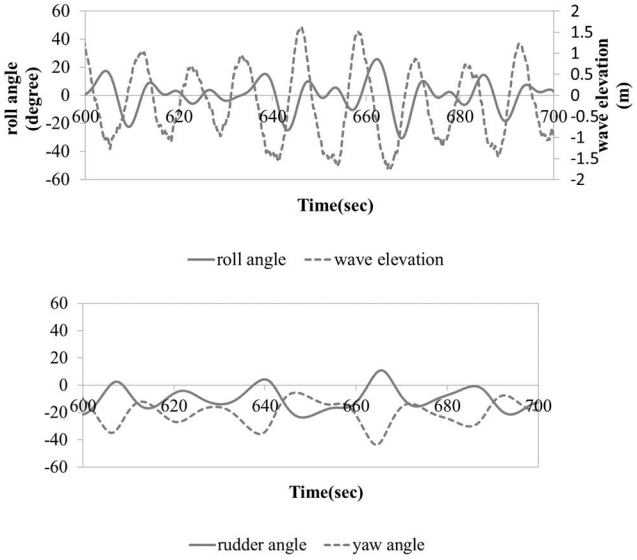

Figure 7: Numerical simulation of the ocean research vessel without the roll damping components due to sway velocity and yaw angular velocity.

5. TORPEDO BOAT ACCIDENT CASE

On March 12, 1934, a torpedo boat conducted a military training outside Sasebo port. Returning to the port after the training, she made a sharp turn to starboard and capsized to the port side in heavy wind and waves. After the accident, IJN (Imperial Japanese Navy) intensively investigated the reason of the accident. Its accident report in1934 concluded the accident was caused by high KG values due to her excessive armament, insufficient GZ and significant decrease of her restoring variation due to bulge-exposure. After the WWII, Matsumoto (1954) released the IJN report to public domain.

In 1978, Takaishi introduced this Matsumoto's article and emphasized the effect of GM decrease in waves. After Takaishi's introduction, Japanese research community of naval architecture believed that the major cause of her accident was restoring decrease in waves, which is known as pure loss of stability in following waves. Therefore, in this research, we attempted to verify the above hypothesis on her accident by conducting captive model experiments and numerical simulations.

The torpedo boat had bulges for compensating high KG due to heavy armament so that the ship was regarded as having sufficient GM. The principal

particulars are shown in Table 3. The estimated condition at the capsize accident is shown in Table 4.

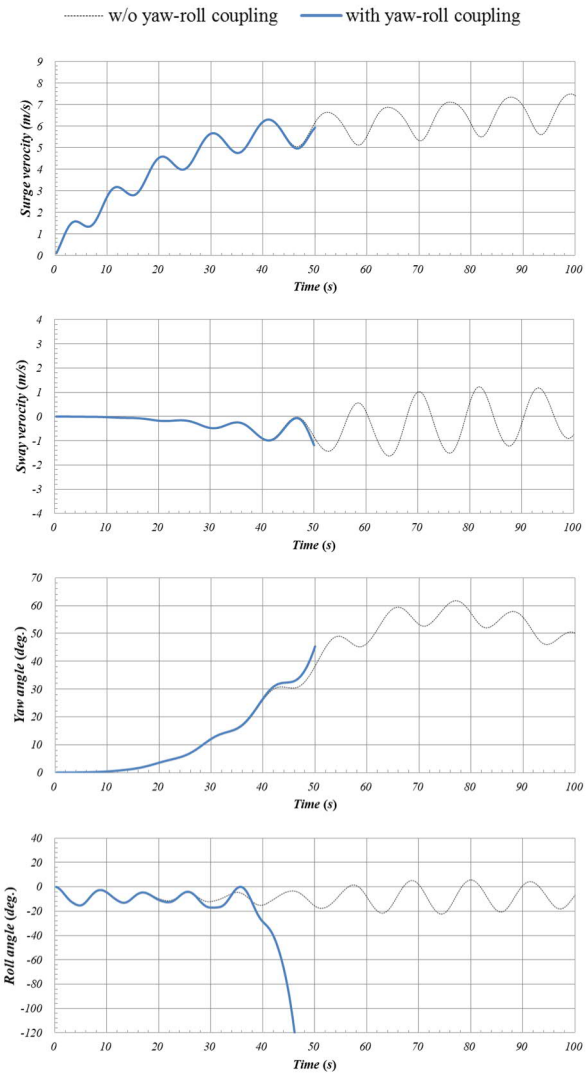

Figure 8: Numerical simulation of the torpedo boat with and without yaw-roll coupling. Here the wave steepness of 0.06, the wavelength to ship length ratio of 1.0, the Froude number of 0.26 and the heading angle of 50 degrees from the wave direction.

In order to explain the accident, the 4 DoF (surge-sway-yaw-roll) numerical simulation model mentioned before was utilized with the wave and operational conditions at the accident. A constant heel angle due to wind was also considered. Figure 8 shows the simulated results with and without the yaw-roll coupling.

The simulated result with yaw-roll coupling demonstrates that the ship rapidly turns to starboard side and then capsizes to port side. This is the same as the accident report (Matsumoto, 1954). On the other hand, the ship does not capsize if we ignore yaw-roll coupling in the numerical model. Therefore, we presume that the reason of capsizing could be considered yaw-roll coupling.

Table 3: Principal particulars of the torpedo boat at the accident.

Items	Values
Length	80.12 [m]
Breadth	8.01 [m]
Draft	2.25 [m]
Block coefficient	0.502
Natural roll period	7.86 [s]
Metacentric height	0.698 [m]
Propeller diameter	1.99 [m]
Rudder area	2.331 [m^2]

Table 4: Conditions of the accident.

Item	Values
Froude number	0.257
Wave height	3~4 [m]
Wind speed	15~20 [m/s]
Encounter angle	50 [degrees]

6. CONCLUDING REMARKS

For identifying the accident case suitable for validation of direct stability assessment for pure loss of stability failure modes, three accidents known as those due to pure loss of stability in stern quartering waves were examined with numerical simulations together with model experiments. As a result, we confirmed that major cause of these three accidents was not roll restoring variation but rather the coupling effect of sway-yaw motion to roll. Since the current draught level 2 vulnerability criteria for pure loss of stability take account for both roll restoring variation and the coupling effect of sway-yaw motion to roll and are tuned with the Ropax ship accident, the criteria could work for the stability failure examined here. However, it is noteworthy here that the countermeasures for the roll restoring variation, e.g. the avoidance of excessive bow flare and transom stern, are not so effective for the stability failure examined here. The increase of rudder area, improvement of directional stability and appropriate steering could be solutions.

Further discussion on pure loss of stability should be expected. The large roll at a wave crest in stern quartering waves is not necessarily a result of transverse stability loss. The relationship with the

quasi-static large roll that observed by de Kat and Thomas (1999) and Hashimoto (2009) at a wave crest still may remain as a discussion item.

ACKNOWLEDGEMENTS

This work was supported by a Grant-in Aid for Scientific Research from the Japan Society for Promotion of Science (JSPS KAKENHI Grant Number 19H02360). It was partly carried out as a research activity of Goal-based Stability Criteria Project of Japan Ship Technology Research Association in the fiscal years of 2017 and 2018 funded by the Nippon Foundation. The authors are grateful for kind support from Dr. Takako Kuroda of National Maritime Research Institute for the use of ship model of the RoPax ship. They also thank Messrs. Thet Zaw Htet and Myo Zin Aung as well as Ms. Su Sandy Htun for their support during the experiment.

REFERENCES

Grim, O. (1961). “Beitrag zu dem Problem der Sicherheit des Schiffes in Seeegang”, Schiff und Hafen, Heft. 6, S. 490-497.

Hashimoto, H. (2009). "Pure Loss of Stability of a Tumblehome Hull in Following Seas", Proceedings of the 19th International Offshore and Polar Engineering Conference, Osaka, Vol.3, pp.626-631.

IMO (2019). “Report of the Experts' Group on Intact Stability”, SDC 6 /WP.6, Annex 3, pp. 1-5.

Japan (2015). “The rationale of 15 degrees as the appropriate stable heel angle requirement in draft vulnerability criteria for pure loss of stability in waves”, SDC 2/5/5, IMO, pp.1-3.

Japan Transport Safety Board (2011). Ferry ARIAKE hull heeling, Ship Accident Investigation Report, MA2011-2.

Kan, M., Saruta, T., Taguchi, H., Yasuno, M. and Takaishi, Y. (1990). “Model Tests on Capsizing of a Ship in Quartering Seas”, Proceedings of the 4th International Conference on Stability of Ships and Ocean Vehicles, Naples, Vol. 1, pp. 109-116.

Kan, M., Saruta, T. and Taguchi, H. (1994). “Comparative Model Tests on Capsizing of Ships in Quartering Seas”, Proceedings of the 5th International Conference on Stability of Ships and Ocean Vehicles, Melbourne, Vol. 3, pp. 1-20.

Kat, J. O. de and Thomas, W.L. (1998). “Extreme Rolling, Broaching and Capsizing –Model Tests and Simulations of a Steered Ship in Waves”, Proceedings of the 22nd Symposium of Naval Hydrodynamics, Washington DC.

Kondo, M., Yano, H., Fukui, Y. and Yoshimura, Y. (2015). “Simple Simulation Model for Manoeuvring Ship Motion of Twin-propeller and Single-rudder Ships”, The Journal of Japan Institute of Navigation, Vol. 133, pp.28-33, (in Japanese).

Kubo, H., Umeda, N., Yamane, K. and Matsuda, A. (2012). ”Pure Loss of Stability in Astern Seas -Is It Really Pure?-“ , Proceedings of the 6th Asia-Pacific Workshop on Marine Hydrodynamics, Johor, pp. 307-312.

Maki, A., Umeda, N., Nagato, H. and Matsuda, A. (2018). “Capsize of a torpedo boat in following waves in 1930`” , Proceedings of the 13th International Conference on Stability and Ocean Vehicles, Kobe, pp. 25-26.

Matsumoto, K. (1954). “Some Problems of War Ship Technology (Parts 3-4)”, Senpaku, Vol. 27, pp. 940-944, 1009-1021, (in Japanese).

New Zealand Transport Accident Investigation Commission. (2007). Passenger freight ferry Aratere heavy weather incident resulting in cargo shift on 3 March 2006, Report 06-201.

Oakley O.H., J.R. Paulling and P.D. Wood (1974). “Ship Motions and Capsizing in Astern Seas”, Proceedings of the 22nd Symposium on Naval Hydrodynamics, Cambridge, pp.1-51.

Osugi, M., Umeda, N., and Matsuda, A. (2019). “Investigation into a Large-Roll Accident of RoPax Ship in Astern Waves”, Journal of the Academic Society for Cruise & Ferry , Japan, No.9, pp.1-5, (in Japanese).

Takaishi, Y. (1978). “Ship Stability Research: State-of-the-Art”, Bulletin of the Society of Naval Architects of Japan, No. 594, pp. 571-578, (in Japanese).

The Japan Association of Marine Safety (1990). “Disaster of the submarine support vessel Herios”, *Sea and Safety*, No. 375, pp. 2-11, (in Japanese).

Ueno, M., Miyazaki, H., Taguchi, H., Kitagawa,Y., Tsukada,Y., (2012). “Model experiment reproducing an incident of fast ferry”, Journal of Marine Science and Technology, Springer, Vol. 18, No. 2, pp. 192-202.

Umeda, N. and Yamakoshi .Y (1994). ”Probability of Ship Capsizing due to Pure Loss of Stability in Quartering Seas “, Naval Architecture and Ocean Engineering ,Vol.30, pp73-85.

Umeda, N.. (1999). “Nonlinear Dynamics on Ship Capsizing due to Broaching in Following and Quartering Seas”, Journal of Marine Science and Technology , Vol.4, pp.16-26.

Umeda, N., Sakurada, A., Yamane, K. and Kubo, H. (2013). “A RoPax Ship Accident due to Pure Loss of Stability on a

Wave Crest and Intact Stability Criteria", Proceedings of the 5th International Maritime Conference on Design for Safety, Shanghai, pp. 118-125.

Umeda, N., Osugi, M., Sakai, M and Matsuda, A. (2017). "Model experiment on pure loss of stability for a ship in astern waves and its relationship with the Second Generation Intact Stability Criteria", Proceedings of the 16th International Ship Stability Workshop, Belgrade, pp. 21-26.

On parametric roll predictions

Geert Kapsenberg, *MARIN,* g.k.kapsenberg@marin.nl
Bastien Abeil, *MARIN,* b.abeil@marin.nl
Sungeun (Peter) Kim, *ABS,* sukim@eagle.org
Clève Wandji, *BV,* cleve.wandji@bureauveritas.com
Eivind Ruth, *DNV-GL,* eivind.ruth@dnvgl.com
Antoine Pages, *SIREHNA/Naval Group,* antoine.pages@sirehna.com

ABSTRACT

Experiments have been carried out with a model of the KCS container vessel. The model tests focussed on three out of five stability failure modes of the Second Generation Intact Stability Criteria that are currently being developed by the IMO. This paper focusses on two aspects of the prediction of the risk on parametric roll in regular waves. The first aspect is a check on the assumption of the IMO that simulation programs exist that properly can predict the risk on parametric roll; the second aspect is the effect of the roll damping model on the predicted parametric roll amplitudes.

The first aspect has been investigated by asking members of the CRS community[1] to do simulations using proprietary programs. Five members responded to this request. The paper shows that a prediction of the roll damping based on exclusively geometrical information results in quite different answers. If the coefficients of a quadratic damping model are fixed in the input, the predictions of parametric roll angles in regular waves as a function of the wave amplitude are quite close for the different simulation programs. However, there is a significant discrepancy between simulations and experimental results with respect to the threshold wave amplitude at which the parametric roll phenomenon starts. An investigation in the modelling of the damping shows that this has some effect, but it does not explain the large difference. A final conclusion is, that the studied simulation programs will benefit from further improvements to predict all aspects of parametric roll events accurately. A good understanding of these aspects is considered important for a reliable Direct Stability Assessment.

Keywords: *Parametric roll, roll damping, simulation, direct stability assessment.*

1. INTRODUCTION

As the Second Generation Intact Stability Criteria (SGISC) are now in the final phase, it is now the appropriate time to verify if the existing simulation tools are indeed ready for the Level 3 Direct Stability Assessment. Work has been done in the Cooperative Research Ships consortium that focused on three out of five failure modes: parametric roll, loss of stability and dead ship. This paper focusses on parametric roll in regular waves only. Results of different simulation programs are compared to results of experiments. The hull form chosen for this study is the Korean Container Ship (KCS) since this is a public hull form.

This work adds to existing benchmark cases like those published by France *et al.* (2003), Spanos and Papanikolaou (2009) and Reed (2011). The added value of this work is the effort put in accurately determining the roll damping, also for larger amplitudes, and in the availability of results both in regular waves (one wave length and increasing amplitude) and irregular seas (not presented here).

2. NOMENCLATURE

Symbol	unit	Description
$A_{\varphi\varphi}$	ton.m^2	Roll added moment of inertia
B_1	kNms	Linear comp. of roll damping
B_2	kNms^2	Quadr. comp. of roll damping
B_3	kNms^3	Cubic comp. or roll damping

[1] CRS – Cooperative Research Ships, www.crships.org

Symbol	unit	Description
B_{eq}	kNms	Equivalent roll damping
B_{cr}	kNms	Critical roll damping
$C_{\varphi\varphi}$	kNm	Roll restoring moment
g	m/s^2	Acceleration due to gravity
GM	m	Metacentric height
$I_{\varphi\varphi}$	$ton.m^2$	Roll moment of inertia
KG	m	Height CoG above keel
T	m	Draft
T_e	s	Wave encounter period
T_φ	s	Roll natural period
k_{xx}	m	Roll gyradius
k_{xx}^*	m	Roll gyradius incl. added mass
Vs	kn	Ship speed
Vs av	kn	Average ship speed
Δ	ton	Displacement
φ	rad	Roll angle
φ_a	rad	Roll angle – amplitude
ζ_a	m	Wave amplitude
ω_0	rad/s	Earth fixed wave frequency
ω_e	rad/s	Wave encounter frequency

3. SUBJECT VESSEL

The subject vessel is the KCS hull form. The main dimensions and loading condition are given in Table 1, the hull form is fully specified on the SIMMAN2008 website, SIMMAN (2008).

A model was constructed at scale 1:37.89. the model was equipped with bilge keels, height 0.40 m, length 68.82 m (St 6 – 14) and a rudder (span 9.90 m, mean chord 5.54 m). An autopilot kept the model on course.

Table 1: Main dimensions and loading conditions of the KCS for the parametric roll experiments.

Parameter	symbol	LC-1	units
Length perp.	Lpp	230.00	m
Beam	B	32.20	m
Draft	T	10.80	m
Displacement	Δ	53389	ton
Vertical CoG	KG	13.67	m
Metacentric height	GM	1.22	m
Roll nat. period	$T\varphi$	23.6	s
Roll gyradius	k_{XX}	11.90	m
Pitch gyradius	k_{YY}	57.50	m
Yaw gyradius	k_{ZZ}	57.50	m

4. SIMULATION PROGRAMS

Five different simulation programs have been used in this paper, the programs are owned by the companies of the respective authors. The programs have identical basics: the hydrodynamics are calculated by a linear potential flow theory and the linear restoring and excitation due to the incoming wave are replaced by non-linear Froude-Krylov and restoring forces. Specifics about the programs used are detailed in Table 2.

Table 2: Characteristics of the simulation programs used in this study.

	Sim-1	Sim-2	Sim-3	Sim-4	Sim-5
Wave model	S5	L	L	L	L
Hydrodynamics	R	ZG	R	S	ZG
Rel. motion	I	I	I	I	I
Pressure for z>0	H	H	H	HW	HW
Pressure integration	M	M	M	M	M
Course control	SD	F	R	R	R
Speed control	S	C	S	C	C
DoF	6	6	6	6	6

Key to Table 2:

Wave model: most programs use linear waves (L), one program uses Stokes 5th order (S5).
Hydrodynamics: The hydrodynamics are based on Rankine source panels (R), Green functions for zero speed with an encounter frequency correction (ZG) or on strip theory (S).
Rel. motion: To determine the wetted surface, the relative motion is based on the incoming wave only (I) or incoming + diffracted wave (ID).
Pressure for z>0: The pressure above the calm water surface is usually determined by the hydrostatic pressure only (H). In two cases Wheeler stretching is added for the dynamic pressure (HW).
Pressure integration: the pressure integration is in all cases performed over a mesh (M), also in case the dynamics are calculated by a strip method.
Course control: Course control can be realized by springs and dampers (SD), by freezing the yaw degree of freedom (F) or by a rudder controlled by an auto-pilot (R).
Speed control: For these simulations, the speed is kept constant (C) or first order surge motions are allowed by means of a soft spring system (S).
DoF: The number of degrees of freedom that are solved by the equations of motion. For all cases all 6 DoF are solved, but the average speed is fixed.

A critical aspect is the determination of the roll damping. Usually this is an input value for the simulation program determined either by Ikeda's method or by CFD. One program uses a translation of the Ikeda method to the time domain to better capture non-linear effects.

5. ROLL DAMPING – CALCULATED

Calculations of the roll decay in calm water were made before doing experiments. The predictions were made by the various programs on basis of just the geometrical parameters. Not all programs have a procedure to estimate the damping of the rudder and bilge keels. In particular program 'Sim-3' uses only the potential flow damping of the naked hull. In general damping from CFD calculations would be added, but this was not done for this case.

Results of roll decay tests at Vs = 0 and 10 kn are given in Figure 1 and Figure 2 respectively. Especially at speed Sim-3, with only potential flow damping, is an outlier, but there is also a great variety in the roll damping for the other programs.

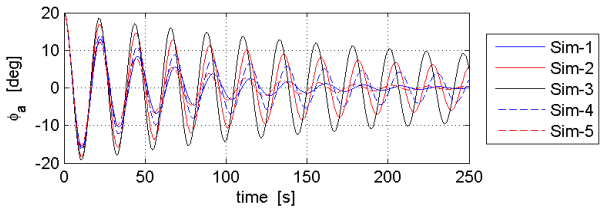

Figure 1: Result of the blind roll damping simulations. Initial angle 20 deg, Vs = 0 kn.

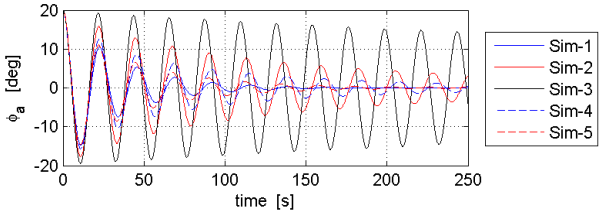

Figure 2: Result of the blind roll damping simulations. Initial angle 20 deg, Vs = 10 kn.

6. THE EXPERIMENTS

Experiments were carried out in the Seakeeping and Manoeuvring Basin of MARIN, measuring 170*40*5 meters. Tests were carried out with a target speed of 8 kn. This speed was considered to be the minimum speed to maintain course in large waves. The required thrust to achieve this speed in varying wave heights was estimated based on added resistance. The vessel was propelled by an electrical motor and a propeller. To avoid any influence of varying propeller RPM on the results, this was kept constant during each run. It was found that with the onset of parametric rolling, the added resistance increased significantly and the speed dropped from 8 to 5.5 knots. It was tried to increase the initial RPM to achieve a speed of 8 knots during parametric rolling. However, in these cases the initial speed was too high for parametric rolling to start due to a too large difference between roll period and twice the encounter frequency and a higher roll damping.

7. ROLL DAMPING - EXPERIMENTAL

Quite some effort was spent on measuring the roll damping since this is a critical parameter in most of the SGISC failure modes. Roll decay experiments were carried out at different speeds and different initial angles, repeat experiments were done for critical cases and forced roll experiments were done. This latter experiment was carried out by fitting an electrical motor with a flywheel inside the model. This motor was mounted on a 6 DoF force balance. The motor has the rotation axis in the longitudinal direction of the model and was forced in a harmonically changing RPM. The rotational acceleration of the flywheel provides the roll moment. Experiments were done with various amplitudes, all at the natural roll frequency.

The roll decay's were done for different initial angles: 6, 12 and 15 deg and several repeat tests were done. They were analysed using a fitting procedure for a 2nd order, 1 DoF roll damping model, eq. (1), as proposed by Lewandowski (2011). Note that the restoring moment in eq. (1) is defined by just the linear (hydrostatic) coefficient.

The forced roll tests were done with different values of the roll moment, all at the roll resonance frequency. The experiments were analysed using the measured roll moment by the 6 DoF force balance and using the phase angle between roll motion and moment produced by the motor.

$$\left(A_{\varphi\varphi} + I_{\varphi\varphi}\right)\ddot{\varphi} + B_1\dot{\varphi} + B_2\dot{\varphi}\left|\dot{\varphi}\right| + C_{\varphi\varphi}\varphi = 0 \qquad (1)$$

The linear and nonlinear damping coefficient were combined to arrive at an amplitude dependent equivalent damping coefficient, eq. (2).

$$B_{eq} = B_1 + \frac{16}{3} B_2 \frac{\varphi_a}{T_\varphi} \tag{2}$$

Often the damping parameters B_1 and B_2 are expressed in non-dimensional coefficients p and q. These coefficients are defined in eq. (3). These definitions make use of the critical roll damping B_{cr} that is defined in eq. (4).

$$p = 2\pi \frac{B_1}{B_{cr}}, \quad q = \frac{32\pi}{3T_\varphi} \frac{B_2}{B_{cr}} \tag{3}$$

$$B_{cr} = 2\Delta k_{xx}^{*} \sqrt{g\,GM} \tag{4}$$

The results of the roll damping experiments at Vs = 8 kn are shown in Figure 3. This figure shows the results of the roll decay tests over the range of roll angles that were used in the analysis of that particular test. It appeared not to be possible to have results at large roll amplitudes, but such results could be obtained from the forced roll tests. It appears that the results of the two methods give consistent results, but for large roll angles the forced roll experiment is the way to go.

Figure 3 also demonstrates a fundamental problem; it is not possible to accurately model the roll damping with just a quadratic model. The plot shows the equivalent linear damping as a function of the roll amplitude, so a quadratic roll damping model as defined in eq. (1) is displayed as a straight line following from eq. (2) and illustrated in Figure 4.

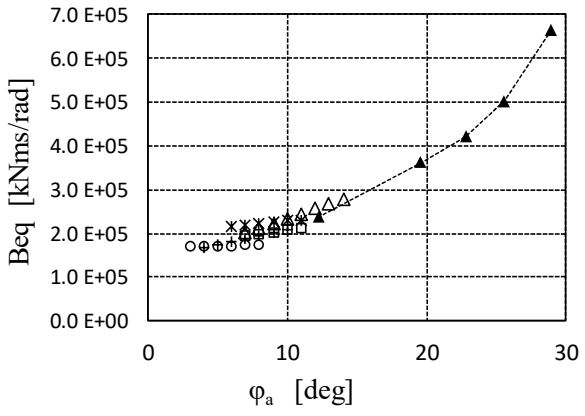

Figure 3: Roll damping at ω_φ = 0.273 rad/s and Vs = 8 kn. Results of forced roll tests (filled triangles connected by dashed line) and of roll decay tests (other symbols).

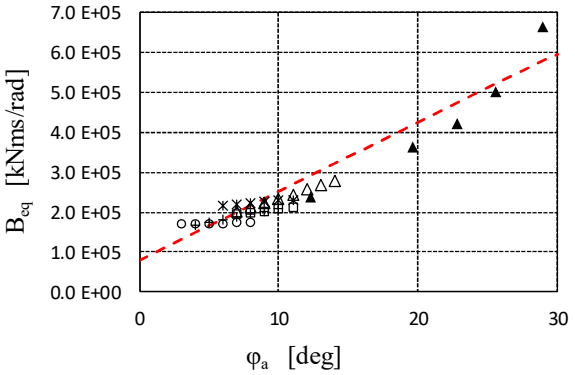

Figure 4: Roll damping at ω_φ = 0.273 rad/s and Vs = 8 kn. Experimental data (symbols), 2nd order model (red dashed line).

8. PARAMETRIC ROLL IN REGULAR HEAD WAVES

Experiments

The experiments in head seas were carried out at a speed that was selected as a minimum value to keep the vessel under (heading) control in a severe sea state: Vs = 8 kn. The wave condition was based on simulations to maximize the probability of parametric roll. This resulted in a wave length of λ/L=1.07. Together with a speed of 8 kn this results in an encounter period of Tφ/Te=2.2, which is slightly higher than the 'ideal' ratio Tφ/Te=2.0. An explanation might be, that the speed reduces when parametric roll occurs and hence the encounter period increases. This reduces the Tφ/Te ratio to a value of 2.1 for the last two cases given in Table 3.

Table 3: Results from the experiments in regular head waves, KCS – LC1.

ω_0 [rad/s]	ζ_a [m]	φ_a [deg]	Vs av [kn]	ω_e [rad/s]
0.50	1.0	0.3	7.9	0.60
	1.5	0.2	8.2	0.61
	2.0	0.2	8.4	0.61
	2.5	25.8	5.6	0.57
	3.0	26.9	5.5	0.57

The wave amplitude was increased such that the two highest waves showed large parametric roll angles. It was noticed that in the experiments the cross-over from no parametric roll to significant parametric rolling was very abrupt.

Results of the simulation programs

The choice was made to derive a linear and a quadratic damping coefficient from the experimental results. Since roll decay and forced roll results were available for 0 and 8 kn speed, p and q values were chosen for these speeds and it was agreed to use linear interpolation for intermediate speeds. The values used by all programs are listed in Table 4. The result of the p, q model for Vs = 8 kn is plotted in Figure 4 (the red dashed line) together with the results of the experiments.

A comparison of the various programs with the experiments is shown in Figure 5. It is apparent that all programs can model parametric roll. However, the calculations seem to onset parametric roll at lower wave heights than the experiments. This could be due to more idealized conditions in the calculations. For some programs the onset is significantly delayed at the lower wave heights and require a very long time to develop.

Table 4: Choice of p and q coefficients for the parametric roll simulations in LC-1.

Vs [kn]	p [-]	q [1/deg]
0	0	0.0235
8	0.107	0.0230

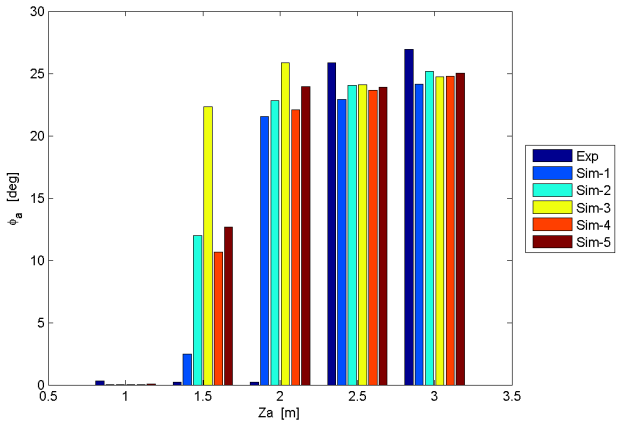

Figure 5: Comparison of roll amplitudes in regular head waves.

The results of the simulations and experiments are compared in Figure 5. Parametric roll occurred in the experiments only for a wave amplitude of 2.5m and higher, most programs predict the phenomenon to start at a wave amplitude of 1.5m.

The experiments in 1.5 and 2.0m wave amplitude showed no signs of parametric roll, although the length of the run was 540 s full scale. The measured wave and roll motion of the run in 2m waves are shown in Figure 6, the roll motion is very low, the roll period is the same as the wave period and there is no sign of any build-up of the amplitude. In a wave with a little higher amplitude, ζa=2.5m, there is however a significant amount of parametric roll with the characteristic factor 2 between the roll and the wave encounter periods, Figure 7.

For these simulations, it appeared that a 'water on deck' module in the programs needed to be switched off. Although in hydrostatic conditions there is a considerable amount of water on deck, the experiments showed that even at a speed of 5.5 kn and in a wave of 3.0m amplitude this was hardly the case for these dynamic conditions, Figure 8.

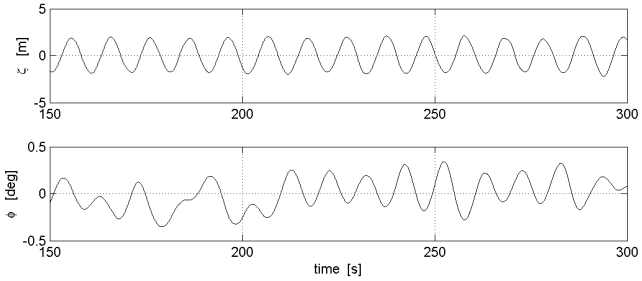

Figure 6: Measured roll motion in regular head waves, ζa = 2.0 m, ω = 0.50 rad/s. Vs = 8.4 kn.

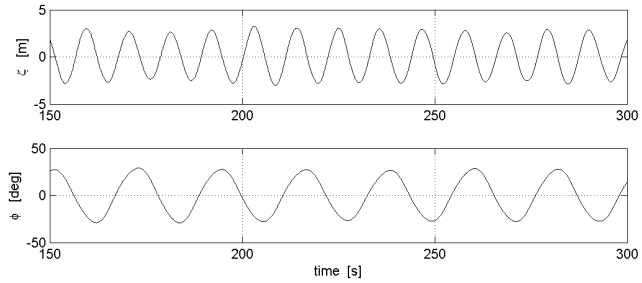

Figure 7: Measured roll motion in regular head waves, ζa = 2.5 m, ω = 0.50 rad/s. Vs = 5.6 kn.

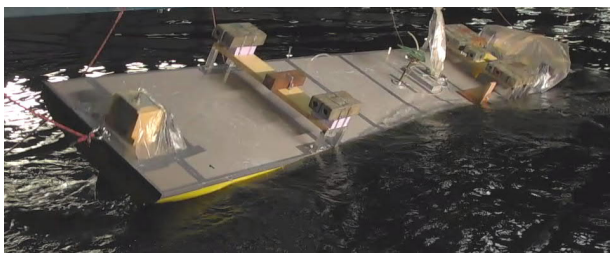

Figure 8: Still from the experiment in regular head waves at maximum roll angle: ζa = 3.0 m, ω = 0.50 rad/s. Vs = 5.5 kn.

9. VARIATION OF THE DAMPING MODEL

The comparison between the different simulation programs has been made with a medium fit, Figure 4, of the experimental damping data. This means that the damping is good for φ_a around 10 deg, but it is too low for both $\varphi_a < 5$ and $\varphi_a > 25$ deg. This might mean that the predicted wave amplitude for which the phenomenon starts might be too low and also that the final amplitude of the parametric roll motion in higher waves might be too low. Both are bad aspects for a prediction method.

In order to check the effect of the choice of the roll damping model and the value of the coefficients, two variants were tested:

1. Fit a 2nd order model on the roll damping at low amplitudes
2. Fit a 3rd order model on the full range of damping values.

The third order model is defined in eq. (5), the B_3 coefficient is usually presented as a non-dimensional factor r, eq. (6). The fits are illustrated in Figure 9 for Vs = 8 kn.

$$B_{eq} = B_1 + \frac{16}{3} B_2 \frac{\varphi_a}{T_\varphi} + 3\pi^2 B_3 \left(\frac{\varphi_a}{T_\varphi} \right)^2 \quad (5)$$

$$r = \frac{6\pi^2}{T_\varphi^{\,2}} \frac{B_3}{B_{cr}} \quad (6)$$

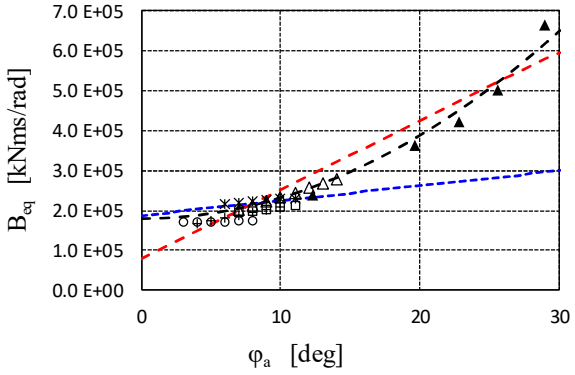

Figure 9: Roll damping of the KCS at Vs = 8 kn. Experimental data (symbols), 2nd order model based on all data (red dashed line), 2nd order model fitted on values at low amplitudes (blue dotted line) and 3rd order damping model (black dashed line).

Simulations with the Sim-4 program were carried out for these 3 models for the roll damping. Since initial results were surprising, small steps on the wave amplitude axis were made. The results are given in Figure 10. The figure shows that indeed the value of the roll damping at $\varphi_a = 0$ has some effect on the threshold wave amplitude at which parametric roll starts. Secondly, the figure shows that a lower roll damping at large roll angles results in larger parametric roll amplitudes. Both effects are however smaller than expected and the large discrepancy with the experimental results is not explained by any of these variations. The third order model blends the two second order models as expected.

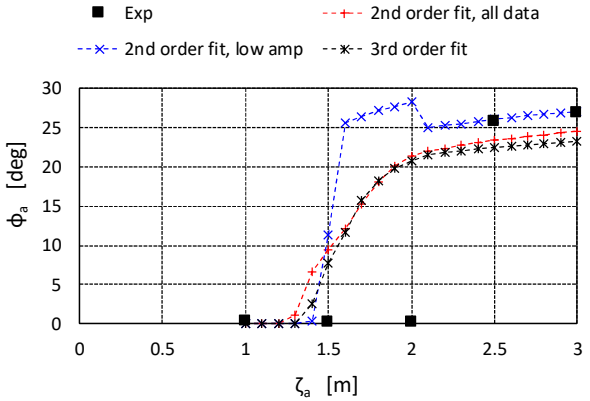

Figure 10: Results of simulations using a 2nd order damping model based on all data points (red dashed line), a 2nd order model fitted on values at low amplitudes (blue dotted line) and 3rd order damping model (black dashed line). Experimental data are indicated by black square markers.

10. DISCUSSION AND CONCLUSIONS

The IMO has published qualitative and quantitative criteria for simulation programs in document SDC 6/WP.6 dated 7 Feb 2019. It has been verified that the programs used in this study satisfy these criteria. Noted is, that these criteria specify limits for under-prediction of the roll angle, not for over-prediction. This means that only the results for wave amplitudes 2.5 and 3.0 m are relevant in this respect.

It can be argued that this work is not relevant for the SGISC since this vessel in this loading condition did not suffer from parametric roll using the criterion of a roll angle larger than 40 deg (in this case a lower angle would be applicable since the edge of the deck submerges at $\varphi > 22$ deg). However, large roll angles were measured and are also predicted. It is the opinion of the authors that these predictions should also be accurate in order to predict parametric roll angles of more than 40 deg.

The prediction of the roll damping inside the simulation programs appears to be very unreliable,

this is a matter of concern. However, when this problem is avoided by using measured values for the roll damping, the predictions of five different simulation programs show little variation. It appeared that, although roll angles were larger than the angle at which there is water on deck in static conditions, the effect of water on deck should be ignored in simulations for this vessel at this speed.

The prediction of the threshold wave amplitude at which the parametric roll phenomenon starts appeared to be severely underestimated. Large roll angles were predicted for wave amplitudes in the range 1.5 – 2.0m while no parametric roll was measured in the wave basin. On the other hand, predictions appeared to be accurate for waves that showed parametric roll in the basin.

The roll damping is taken from experiments in calm water. Although there might be differences to the damping in waves, it is suggested that the problem in predicting the threshold wave amplitude correctly is mainly due to shortcomings in the mathematical model for the excitation of parametric roll. This problem is fundamental, it is present in all simulation programs.

A final conclusion is therefore that the studied simulation programs will benefit from further improvements to predict all aspects of parametric roll events accurately. A good understanding of these aspects is considered important for a reliable Direct Stability Assessment.

ACKNOWLEDGMENT

Permission to publish these results from the Cooperative Research Ships group is gratefully acknowledged. The simulations at MARIN were carried out by Julio Polo. The paper benefitted a lot from discussions with Bulent Duz and Frans van Walree.

REFERENCES

Lewandowski E.M., “Comparison of Some Analysis Methods for Ship Roll Decay Data”, 12th Int. Ship Stability Workshop, (STAB2011), 12-15 Jun 2011, Washington DC, USA.

SIMMAN (2008), MOERI Container Ship (KCS), geometry http://www.simman2008.dk/KCS/kcs_geometry.htm

France W., Levadou M., Treakle T.W., Paulling J.R., Michel R.K., and Moore C., “An investigation of head-sea parametric rolling and its influence on container lashing systems”, Marine Techn., Vol 40, No 1, pp1-19, Jan 2003.

Hashimoto, H., Umeda, N., Matsuda, A. and Nakamura, S., “Experimental and Numerical Studies on Parametric Roll of a Post-Panamax Container Ship in Irregular Waves”, Proc. of the 9th Int. Conf. on Stability of Ships and Ocean Vehicles, (STAB2006), 25-29 Sep 2006, Rio de Janeiro, Brazil.

IMO, Report of the Experts' Group on Intact Stability, Finalization Of Second Generation Intact Stability Criteria, IMO document SDC 6/WP.6, 7 Feb 2019.

Reed A.M., “26th ITTC Parametric Roll Benchmark Study”, 12th Int. Ship Stability Workshop, (STAB2011), 12-15 Jun 2011, Washington DC, USA.

Spanos, D. and Papanikolaou, A., 2009, “Benchmark Study on Numerical Simulation Methods for the Prediction of Parametric Roll of Ships in Waves”, Proc. of the 10th Int. Conf. on Stability of Ships and Ocean Vehicles, (STAB2009), 22 - 26 Jun, St. Petersburg, Russia.

Direct counting method and its validation

Vladimir Shigunov, *DNV GL SE, Hamburg, Germany,* vladimir.shigunov@dnvgl.com

ABSTRACT

Direct counting of stability failures, required to define failure rate (or probability) in direct stability assessment and operational measures, is possible for a stationary Poisson process. This paper proposes measures to ensure that numerical simulations or model tests satisfy the requirements of such process and develops efficient procedure, illustrated in application examples, to define the 95%-confidence interval of failure rate, which is required for assessment.

Keywords: *Poisson process, Failure rate, Direct stability assessment.*

1. INTRODUCTION

Direct counting, i.e. counting of the number of stability failures per given exposure time, is used in the probabilistic direct stability assessment (DSA) in design situations, as well as (in combination with statistical extrapolation, which itself uses direct counting) in the full probabilistic DSA and in operational measures (OM). Such counting is based on the model of a stationary Poisson process (frequently without knowing this), which raises two questions: first, whether real stability failures can be assumed a Poisson process and if they can, second, how should numerical simulations or model tests be performed to ensure that the resulting process is a Poisson process.

Stationarity seem questionable since ships are sailing in conditions (sea state, ship speed and course) that often change quicker than the time required for roll motion to be considered stationary; in some applications (e.g. transient flooding), also the hydrodynamic model changes too quickly for the stationarity assumption. This apparent contradiction is easy to resolve since design assessment (and operational measures) do not consider a ship operating in a sequence of changing sea states, forward speeds and courses but consider ensemble statistics over a large number of ships, each of which operates unlimited time in stationary conditions.

A Poisson process requires that failures do not occur simultaneously and that failures happen independently, i.e. that the occurrence of one failure does not affect the probability of occurrence of a second failure. The former requirement seems trivial, while the latter is known to be not valid for roll motion since big roll motions tend to appear in groups. The justification is the *clumping heuristic*: although big roll motions tend to appear in groups, occurrence of such groups may be independent, which, in turn, is based on the heuristic that rare events tend to be independent. However, no strict proof is possible.

This paper summarises properties of a Poisson process, illustrates the validity of the Poisson process assumption and proposes direct counting procedures to define the boundaries of the 95%-confidence interval of the failure rate, which is used in the probabilistic DSA and OM.

2. POISSON PROCESS

A *counting process* is a stochastic process $N(t)$, where the integer random variable N counts the total number of some defined events, e.g. stability failures (or more general, exceedances of some reaction level), tasks, phone calls, customers etc. (the usual term in mathematics is *arrivals*) that have occurred in the time interval from 0 up to and including time t. The number of arrivals per time interval $(s,t]$, $N(t)-N(s)$, is called an *increment*. Consider counting processes in which increments are *independent* (i.e. numbers of arrivals in non-overlapping time intervals are independent) and *stationary* (i.e. the number of arrivals depends only on the length of a time interval and not on its location in time).

There are several equivalent definitions of a Poisson process; one, which is convenient for mathematical derivations, defines a Poisson process with a rate $r>0$ as a counting process $N(t)$ which has stationary independent increments and satisfies the following requirements:

$$p\{N(\mathrm{d}t)=1\}=r\,\mathrm{d}t+o(\mathrm{d}t) \qquad (1)$$

$$p\{N(\mathrm{d}t) \geq 2\} = o(\mathrm{d}t) \quad (2)$$

$$p\{N(\mathrm{d}t) = 0\} = 1 - r\,\mathrm{d}t + o(\mathrm{d}t) \quad (3)$$

where the Landau's notation $o(x)$ means that if $f(x) = o(x)$, then $\lim_{x\to 0} f(x)/x = 0$.

Another definition, more useful in applications, defines a Poisson process with a constant rate $r > 0$ as a counting process $N(t)$ which has independent increments and where the number of arrivals $N(t)$ in any time interval of length t satisfies the Poisson distribution with the mean rt, i.e.

$$p\{N(t) = k\} = (rt)^k \cdot e^{-rt}/k! \text{ for } k = 0, 1, \ldots \quad (4)$$

(it automatically implies stationary increments).

A Poisson process has several useful properties. The *superposition property* (which is convenient for summing failure rates due to different failure modes) means that a sum of independent Poisson processes $N_1, \ldots, N_k$, i.e. $N_1 + \cdots + N_k$, is a Poisson process with the rate $r_1 + \cdots + r_k$ (conversely, if the sum of two independent random variables is Poisson distributed, so are each of these two variables). The *random split property* means that if each arrival of a Poisson process $N(t)$ with rate r is randomly tagged as either process $N_1(t)$, with probability p, or $N_2(t)$, with probability $1-p$, then the two resulting processes $N_1(t)$ and $N_2(t)$ are independent Poisson processes with rates rp and $r(1-p)$, respectively. Similarly, the *thinning property* means: if each arrival of a Poisson process with rate r is randomly marked, with probability p, then the marked process is a Poisson process with rate rp. In both the random split and thinning properties, the probability p can depend on time as $p(t)$, then the above properties are valid assuming that $p = (1/t)\int_0^t p(u)\mathrm{d}u$.

The probability density function of the Poisson distribution $f(k) = p\{N(t) = k\}$, eq. (4), expresses the probability of occurrence of k arrivals during a time interval t. A special case of eq. (4) is when $k = 0$ (which corresponds to the probability that no failures occur from time 0 to time t):

$$p \equiv p\{N(t) = 0\} = e^{-rt} \quad (5)$$

From eq. (5), the probability that at least one failure happens during time t, i.e. that $k > 0$, (loosely formulated: "probability of stability failure during time t") is

$$p^* \equiv p\{N(t) > 0\} = 1 - p\{N(t) = 0\} = 1 - p = 1 - e^{-rt} \quad (6)$$

For small rt, p^* from eq. (6) can be linearised as

$$p^* \approx rt \quad (7)$$

The mean of a Poisson process, i.e. the mean number of arrivals per interval t, is

$$E\{N(t)\} = \int_0^\infty t f(t)\mathrm{d}t = rt \quad (8)$$

i.e. r is equal to the expected number of arrivals per time unit. The variance of the Poisson process is equal to the mean, $Var\{N(t)\} = rt$.

Instead of looking at the number of arrivals $N(t)$, a Poisson process can be seen as a sequence of time intervals T_1 (time between $t = 0$ and the first arrival), T_2 (time between the first and second arrival) etc., which are also random variables.

Note that the probability that the time until the first arrival exceeds t, i.e. that $p\{T_1 > t\}$, is the same as $p\{N(t) = 0\} = e^{-rt}$, eq. (5), i.e. T_1 is exponentially distributed (similarly, it can be shown that all time intervals T_i are exponentially distributed random variables with the same rate r).

Therefore, a Poisson process can also be defined as a counting process $N(t)$ in which time intervals between arrivals are independent random variables, exponentially distributed with rate r:

$$p\{T > t\} = e^{-rt} \text{ for } t > 0 \text{ and 0 otherwise} \quad (9)$$

(note that this definition automatically implies independent and stationary increments).

An important property of the exponential distribution is its *memoryless property*: a memoryless random variable T is a variable for which

$$p\{T > t + \tau\} = p\{T > t\} \cdot p\{T > \tau\}, \quad (10)$$

which also can be written in the following form: $p\{T > t + \tau \,|\, T > t\} = p\{T > t\}$, which means that if an arrival has not occurred until time τ, the distribution of the remaining waiting time is the same as the distribution of the original waiting time, which means that the remaining waiting time has no memory of previous waiting time.

Moreover, the exponential distribution is the only continuous distribution with the memoryless property: if the time intervals between arrivals are not exponential, the process will not be a Poisson

process since it does not satisfy the requirements of stationary and independent increments. The memoryless property of the exponential distribution is what makes the Poisson process unique (sometimes called a *purely* or *completely random process*).

Correspondingly to a sum of Poisson processes, if $T_1, \ldots, T_k$ are independent exponentially distributed random variables with rates $r_1, \ldots, r_k$, then $\min(T_1, \ldots, T_k)$ is exponentially distributed with rate $r_1 + \cdots + r_k$. The index of the variable that achieves the minimum is distributed according to the law $p\{i \mid T_i = \min(T_1, \ldots, T_k)\} = r_i / (r_1 + \cdots + r_k)$.

From eq. (9), the cumulative density function of time to failure is

$$F(t) = p\{0 < T < t\} = 1 - p\{T > t\} = 1 - e^{-rt} \tag{11}$$

for $t > 0$ and 0 otherwise. In the reliability theory, the *survival function* is frequently used, defined as $R(t) = p\{T > t\} = 1 - F(t) = e^{-rt}$.

The probability density function of an exponential distribution, i.e. of the time intervals between arrivals in a Poisson process, is

$$f(t) = \mathrm{d}F(t)/\mathrm{d}t = re^{-rt} \text{ for } t > 0 \text{ and } 0 \text{ otherwise} \tag{12}$$

The mean of an exponentially distributed random variable T (i.e. mean time between arrivals) is

$$E\{T\} \equiv \overline{T} = \int_0^\infty tre^{-rt}\mathrm{d}t = 1/r \tag{13}$$

The second moment $E\{T^2\} = \int_0^\infty t^2 re^{-rt}\mathrm{d}t = 2/r^2$, and thus the variance and the standard deviation are

$$Var\{T\} = E\{T^2\} - E^2\{T\} = 1/r^2 \tag{14}$$

$$\sigma\{T\} = (Var\{T\})^{1/2} = 1/r = \overline{T} \tag{15}$$

respectively, i.e. $\sigma\{T\}$ is equal to the mean. Shigunov (2016, 2017a) verified eq. (15) by numerical simulations, Fig. 1.

To define parameters of distributions from a series of numerical simulations or model tests, time intervals T_i to each failure should be defined; for a set of N values T_i, i=1, 2, …, N, the *sample mean time to failure* is

$$\hat{T} = (1/N)\sum_{i=1}^{N} T_i \tag{16}$$

and the *maximum likelihood estimate of the stability failure rate* is

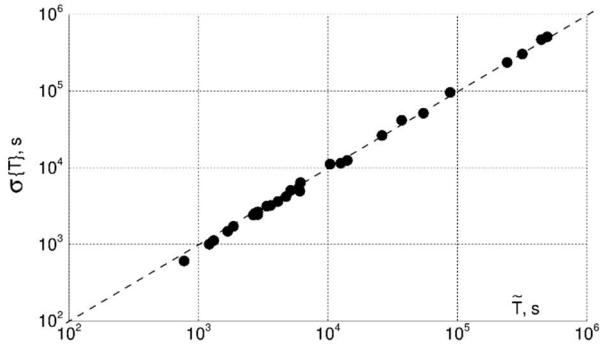

Figure 1: An estimate of the standard deviation of the time to failure vs. estimate of the mean time to failure from 200 simulated failures (from Shigunov, 2017a).

$$\hat{r} = 1/\hat{T} \tag{17}$$

The variance of the individual time intervals T_i to stability failure is

$$Var\{T_i\} = \overline{T}^2 \tag{18}$$

thus the standard deviation of the individual times to stability failure is

$$\sigma\{T_i\} = (Var\{T_i\})^{1/2} = \overline{T} \tag{19}$$

To estimate the confidence interval for the rate, Shigunov (2017) proposed an approximation based on the central limit theorem, according to which, for a sufficiently big sample, the sample mean can be assumed normally distributed with the standard deviation $\sigma_T = \sigma\{T_i\} N^{-1/2}$, i.e. $\sigma_T = \overline{T} N^{-1/2}$, eq. (19). Then, a 95%-confidence interval for the failure rate can be defined as

$$\hat{r}(1 - 1.96N^{-1/2}) < r < \hat{r}(1 + 1.96N^{-1/2}) \tag{20}$$

Fig. 2, based on numerical simulations of several cases of parametric (P1, P2) and synchronous (S1 to S4) resonance, Shigunov (2017), confirms that $\sigma_T / \sigma\{T_i\}$ really decreases as $N^{-1/2}$ with increasing N, and that this happens already for small sample sizes N.

Here, as a more general approach, it is proposed to define the $(1 - \alpha)\cdot 100\%$-confidence interval (note that α denotes some small value: e.g. for a 95%-confidence interval, $\alpha = 0.05$) for the rate r of an exponential distribution as

$$\frac{2N}{\hat{r}\chi^2_{1-\alpha/2,2N}} < \frac{1}{r} < \frac{2N}{\hat{r}\chi^2_{\alpha/2,2N}} \tag{21}$$

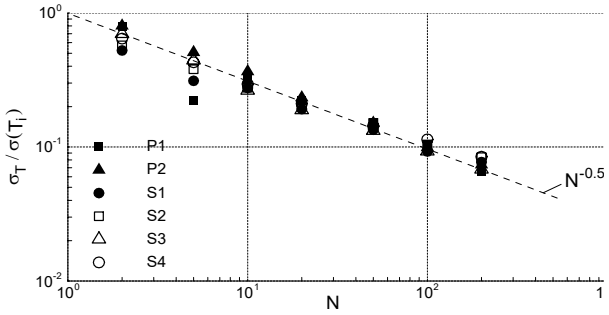

Figure 2: The standard deviation of the estimate of the mean time to failure vs. the number of counted failures from Shigunov (2017)

or, resolving eq. (21) with respect to r,

$$0.5\chi^2_{\alpha/2,2N} / N < r / \hat{r} < 0.5\chi^2_{1-\alpha/2,2N} / N \qquad (22)$$

where $\chi^2_{p,f}$ is the quantile function (corresponding to a lower tail area, equal to the cumulative probability p) of the χ^2 distribution with f degrees of freedom. The function $\chi^2_{p,f}$ is available in many software packages: e.g. in MS Excel, it can be calculated as chisq.inv(p;f) or, alternatively, as chisq.inv.rt(1-p;f). Correspondingly, the upper-tail quantile function $\chi^2_{1-p,f}$ can be calculated as chisq.inv.rt(p;f) or chisq.inv(1-p;f), Fig. 3. Eqs. (20) and (22) are compared in section 5.

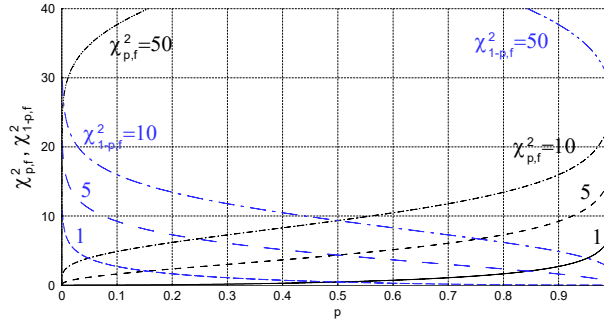

Figure 3: Examples of functions $\chi^2_{p,f}$ and $\chi^2_{1-p,f}$, calculated with MS Excel as chisq.inv(p;f) and chisq.inv.rt(p;f), respectively, for $f = 1$, 5, 10 and 50 degrees of freedom vs. cumulative probability p

3. NON-STATIONARY PROCESSES

Section 2 considered the Poisson process with a constant rate r, which is called a *stationary* (or *homogeneous*) Poisson process. The definition of the Poisson process can be generalised to a *non-stationary* (*non-homogeneous*) process by letting the rate to change in time (which happens due to changing sea state, forward speed and course) as $r(t)$: a non-stationary Poisson process is a counting process $N(t)$ which has independent increments and, for any $\mathrm{d}t > 0$, satisfies the following conditions:

$$p\{N(t+\mathrm{d}t) - N(t) = 1\} = r(t)\,\mathrm{d}t + o(\mathrm{d}t) \qquad (23)$$

$$p\{N(t+\mathrm{d}t) - N(t) \geq 2\} = o(\mathrm{d}t) \qquad (24)$$

$$p\{N(t+\mathrm{d}t) - N(t) = 0\} = 1 - r(t)\,\mathrm{d}t + o(\mathrm{d}t) \qquad (25)$$

The mean of a non-stationary Poisson process (i.e. mean number of arrivals) per infinitesimally small time interval $(t, t+\mathrm{d}t]$, can be calculated as $E\{N(t+\mathrm{d}t) - N(t)\} = \sum_{k=0}^{\infty} k \cdot p\{N(t+\mathrm{d}t) - N(t) = k\} = r(t)\mathrm{d}t + o(\mathrm{d}t)$, and, therefore, the mean number of arrivals in a finite time interval from t to $t+\tau$ is

$$E\{N(t+\tau) - N(t)\} = E\left\{\int_t^{t+\tau} [N(u+\mathrm{d}u) - N(u)]\right\} = \int_t^{t+\tau} E\{N(u+\mathrm{d}u) - N(u)\} = \int_t^{t+\tau} r(u)\mathrm{d}u = \bar{r}\tau \qquad (26)$$

where

$$\bar{r} = (1/\tau)\int_t^{t+\tau} r(u)\mathrm{d}u \qquad (27)$$

which is the average rate in the time interval $(t, t+\tau]$. Comparison of eq. (26) with eq. (8) shows that $N(t+\tau) - N(t)$ is a Poisson-distributed random variable with the mean $\bar{r}\tau$ and the rate $\bar{r}$, i.e. all properties of a Poisson distribution apply by using the mean rate $\bar{r}$. In particular, the distribution of the number of arrivals in a time interval $(t, t+\tau]$, i.e. the probability of k arrivals in this time interval, is

$$p\{N(t+\tau) - N(t) = k\} = (\bar{r}\tau)^k e^{-\bar{r}\tau} / k! \qquad (28)$$

Similarly, the probability that no failures occur from time t to time $t+\tau$ is

$$p \equiv p\{N(t+\tau) - N(t) = 0\} = e^{-\bar{r}\tau} \qquad (29)$$

and the probability that at least one failure happens between time t and time $t+\tau$ ("probability of failure during time τ") is

$$p^* \equiv p\{N(t+\tau) - N(t) > 0\} = 1 - e^{-\bar{r}\tau} \qquad (30)$$

One way of looking at long-term statistics is to consider the ship as operating a "long time" in a changing sequence of stationary situations, each of which is specified by a stationary sea state and constant ship forward speed and course. This allows considering the "long-term" operation as a non-stationary Poisson process with variable failure rate $r(t)$, thus allowing using the usual formulae like eq. (28) - (30), where the mean "long-term" rate $\bar{r}$ is, according to eq. (27),

$$\bar{r} = (1/t_o)\int_0^{t_o} r(u)\mathrm{d}u \approx (1/t_o)\sum_i r_i t_i = \sum_i r_i p_i \qquad (31)$$

where t_i is the duration of each stationary "short-term" situation (specified by a stationary sea state and constant ship forward speed and course), t_o is the total time at sea and $p_i = t_i / t_o$ are the probabilities of each stationary "short-term" situation.

A more correct treatment is to consider the "long-term" operation as a stationary Poisson process with a constant rate $\bar{r}$, consisting of an infinite number of stationary Poisson processes with constant rates r_i, each of which happens in stationary "short-term" conditions with probability p_i; then, the application of either the splitting property of a stationary Poisson process or, alternatively, sum and tagging properties, leads to the same formula (30).

Thus, the problem reduces to the definition of a constant rate r_i in each stationary situation from numerical simulations or model tests in a way ensuring a stationary Poisson process.

4. PRACTICAL PROBLEMS

In practice, ensemble statistics in stationary conditions is replaced by time history statistics using the ergodicity property. Thus, in principle, it is required to run one, long enough, simulation of roll motion, updating (after each failure) the number N of failures, the total simulation time t_t, the estimate of failure rate

$$\hat{r} = N / t_t \tag{32}$$

and the estimate of the upper boundary r_U of the 95%-confidence interval of failure rate, eq. (22),

$$r_U = 0.5 \hat{r} \chi_{0.05/2,2N} / N \tag{33}$$

Once r_U reduces below the acceptance standard, the simulation can be stopped and the loading condition can be considered acceptable.

However, if the sea state is modelled, following Longuet-Higgins (1952), as a finite sum of harmonic components,

$$\zeta(t) = \sum_{i=1}^{M} a_i \cos(\omega_i t + \varepsilon_i) \tag{34}$$

where $a_i = \{2 S_{\zeta\zeta}(\omega_i) D(\mu_i) \Delta\omega_i \Delta\mu_i\}^{1/2}$ are amplitudes, ω_i frequencies, μ_i directions and ε_i phases of components, collecting sufficient statistics in one sufficiently long run is impossible because of self-repetition effects, which violate the requirement of independence of failures (note that exact repetition is not required: a partial repetition in a relevant band of encounter frequencies is bad enough). A solution is to generate multiple independent *realisations* of the same sea state, randomly varying phases ε_i in the interval $[0, 2\pi)$ for each realisation, and to simulate ship motions for a limited time in each such realisation (in model tests, the duration of each realisation is limited also by wave reflection effects). Note that eq. (32) still can be used, so that N and t_t are the total number of failures and total simulation time, respectively, over all realisations.

In the examples in this paper, also frequencies ω_i and directions μ_i of components were randomly varied between realisations (using normal distributions with specified standard deviations). Some authors recommend also using a random variation of amplitudes a_i. To generate random values, pseudo-random number generators are frequently used, which apply a user-specified integer as a seed number; in the examples in this paper, the internal computer timer was used as the seed number. Short-crested seaway with a JONSWAP wave energy spectrum was used (with the peak parameter equal to 3.3 and the $\cos^2$-wave energy spreading), discretised by 19 wave directions with 10^3 harmonic components of equal amplitudes per direction.

Another problem is the transient hydrodynamic effects at the beginning of each simulation, which violate the stationarity requirement. To address this, some time after the start of each simulation (in the examples in this paper, 50 roll periods were used) was excluded from post-processing, i.e. not included in t_t, and failures during this time were not counted in N in eq. (32). Note that whereas it is useful to increase the number and reduce duration of random realisations using parallel simulations, this will also increase wasted simulation time.

Finally, the independence of stability failures in numerical simulations is violated by autocorrelation of large roll motions: large roll amplitudes tend to appear in groups (note that neglecting this effect would lead to an over-estimation of the stability failure rate, i.e. a conservative error). One way to neutralize this effect is to run each simulation up to the first encountered failure; another way is to switch off both the simulation timer t_t and the failure counter N after an encountered failure until the envelope of the autocorrelation of roll motion reduces to a specified level. These two options lead to similar unproductive losses: in the former method, due to transient effects at the start of a new simulation, in the latter, for the decay of the autocorrelation

function of roll motion. However, the former method (which was used in the examples in this paper) is simpler and, besides, another benefit is that restarting also takes care of repeatability effects.

After removing portions of time histories of roll motion affected by repeatability effects, initial transients and stability failures, the remaining pieces can be treated as a single stationary Poisson process: removed pieces do not matter due to the memoryless property, durations of the remaining pieces may be arbitrary, and it does not matter whether a failure was encountered in each simulation or not, Fig. 4.hus, eq. (32) can be used for the most likelihood estimate of the failure rate, with N and t_t summed over all remaining pieces of the simulations. Similarly, the sample mean time to failure can be calculated as $\hat{T} = t_t / N$, eq. (16), and all formulae from section 2 can be directly applied.

To investigate repeatability effects, parametric resonance in head waves and synchronous resonance in beam waves were simulated for a systematically varied significant wave height in two types of simulations. In one, denoted 'limited' for brevity, the simulation time was limited to 3 hours (while simulations were stopped after first failure), and in the other ('unlimited'), simulations were run always until first failure. Thus, after each 'limited' simulation, N was increased by 1 in case of failure (t_t was increased by the time to failure) and by 0 if simulation ended in 3 hours without failure (t_t was increased by 3 hours). After each 'unlimited' simulation, N was increased by 1 and t_t was increased by the time to failure. Fig. 5 compares the sample mean time to failure from these simulations, plotted vs. the number of failures, together with the boundaries of the 95% confidence interval of the mean time to failure, eq. (22), for examples with mean time to failure above and below 2 hours.

Fig. 5 shows no clear difference; for more insight, Fig. 6 shows quantile diagrams (QQ diagrams) derived from these simulations. Since the cumulative density function of an exponentially distributed time to failure is $F(t) = 1 - e^{-rt}$ for $t > 0$, $T_i / \bar{T}$ should be equal to $-\ln(1 - F_i)$. The cumulative density function F_i was calculated from the sample data as $i/(N+1)$, where i is the index of a stability failure when stability failures are sorted in ascending order of T_i. Fig. 6 shows that the 'unlimited' simulations over-estimate failure time compared to the exponential distribution for simulations with large time to failure due to self-repetition effects: the same 'uncritical' realisation repeats itself again and again (since repetition is not exact, failure may eventually happen but much later than it should).

This means that simulations that are too long lead to deviation from the Poisson process in relevant sea states, i.e. the notion of failure rate and the formulae from section 2 are not applicable (note that using these formulae as if the process were Poisson would lead to an under-estimation of the failure rate, i.e. a non-conservative error). Thus, the maximum duration of simulations should be limited: when at least 10^3 frequencies per wave direction are used, simulations up to 3 hours seem acceptable. More general recommendations require further studies; until that, quantile plots can be used to verify the absence of repetition effects.

To check whether the considered measures are sufficient to assume the Poisson process, the χ^2 goodness-of-fit test was applied to several cases of parametric and synchronous resonance in head and beam, respectively, waves at systematically varied significant wave height, using 'limited' simulations of 3-hour duration (or until failure if it happened).

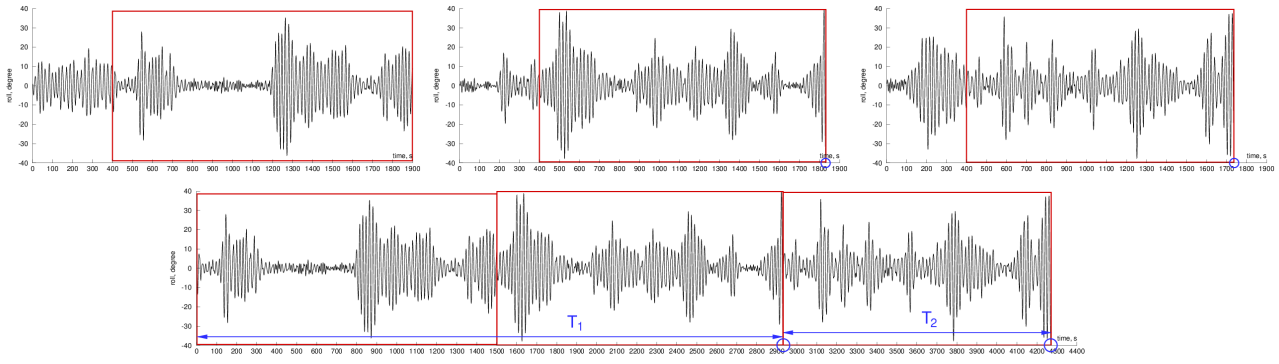

Figure 4: Roll motions in multiple realisations of a sea state (top) and the resulting Poisson process (bottom)

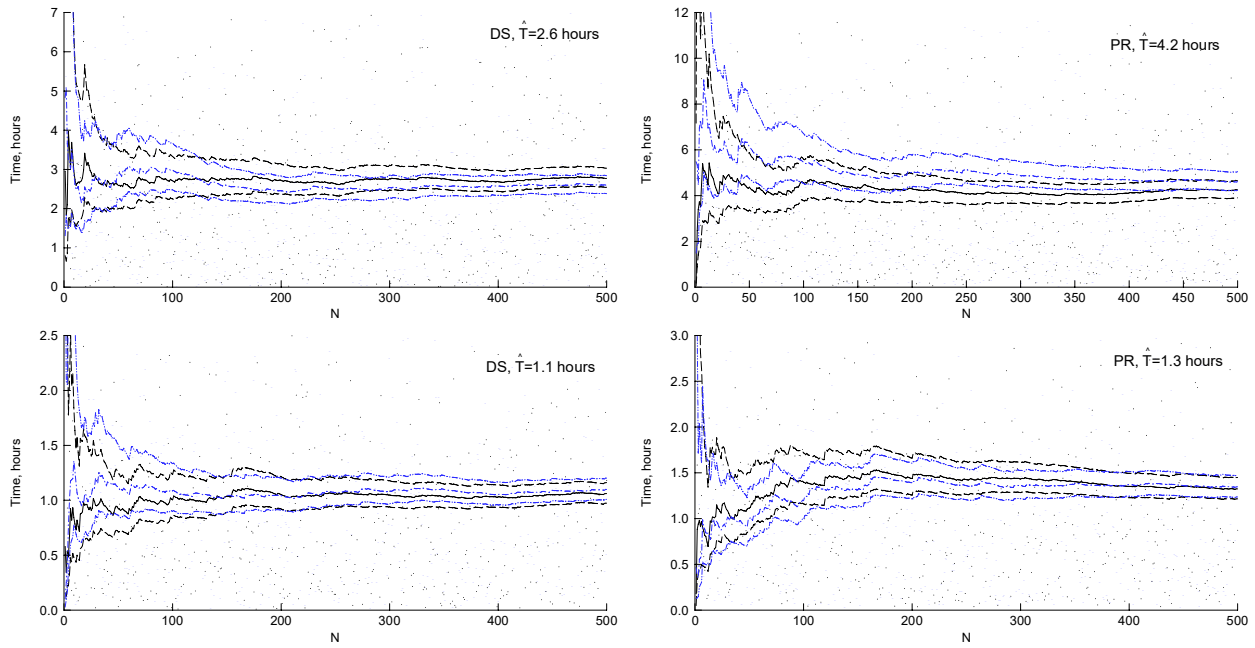

Figure 5: Time until failure (dots) and sample mean time to failure (lines) from 'limited' (solid black lines) and 'unlimited' (dash-dot lines) simulations together with bounds of the 95%-confidence interval of mean time to failure vs. the number of counted failures for synchronous (left) and parametric (right) resonance cases

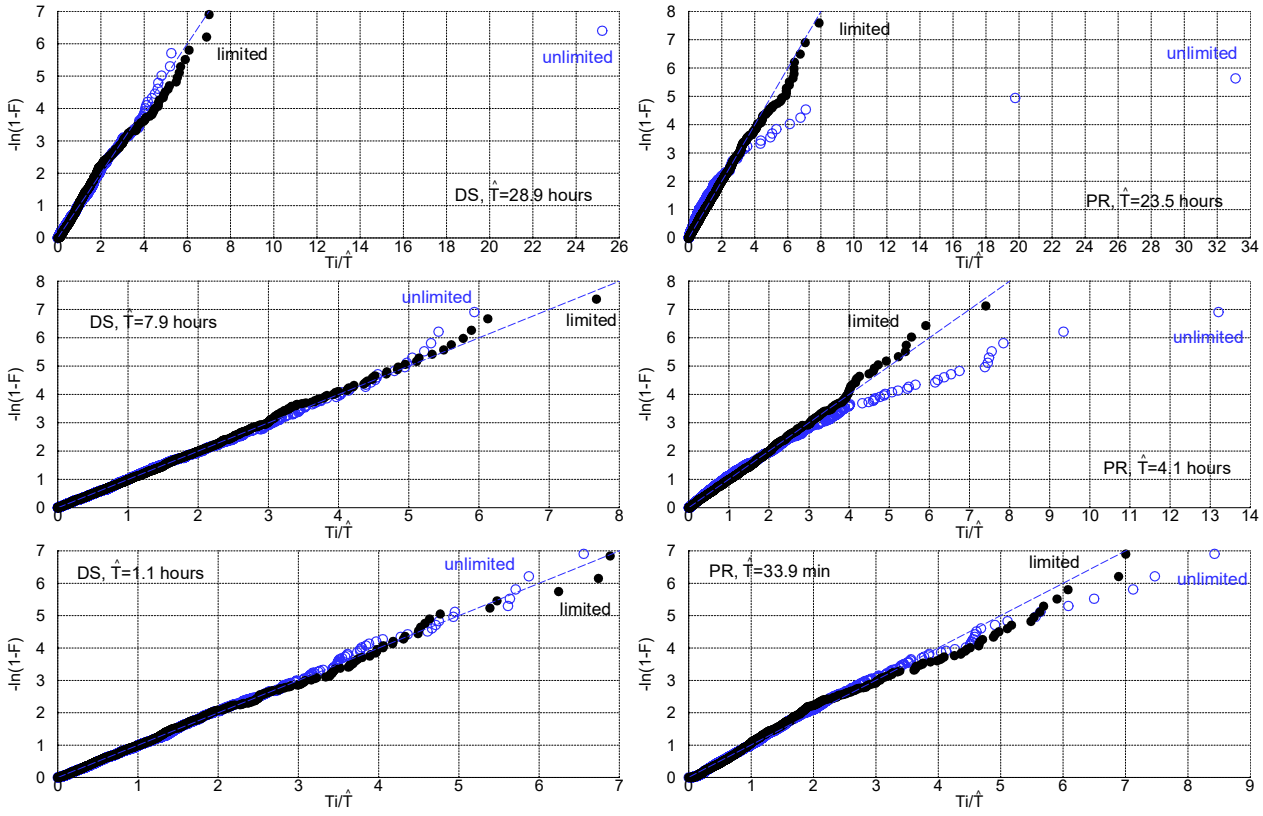

Figure 6: Quantile diagrams from 'limited' and 'unlimited' simulations (black full and empty blue circles, respectively) for synchronous (left) and parametric (right) resonance cases

Random realisations of the same sea state were repeated until about 10^3 failures were encountered in each sea state. Observed times to failure were compared with the exponential distribution (which used the most likelihood estimate $\hat{r} = 1/\hat{T}$ for the failure rate). The full range $t \geq 0$ of time to failure was sub-divided into $k \geq 5$ intervals of equal probability $\Delta F = \Delta(1 - e^{-rt}) = 1/k$; the number of intervals was systematically increased up to a maximum $k = N/5$.

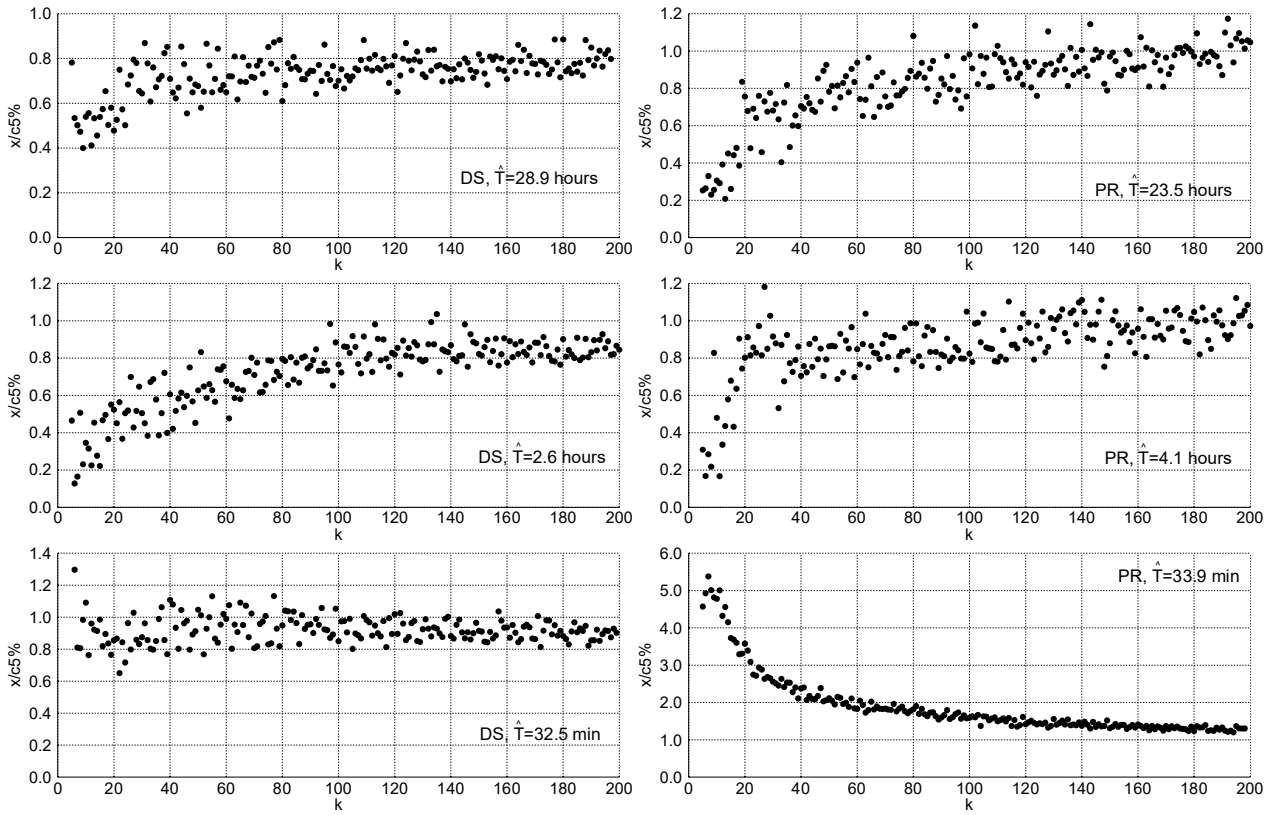

Figure 7: The ratio of χ^2-test statistic to critical value $\chi^2_{1-\alpha,k-2}$ for significance level $\alpha=5\%$ vs. number of intervals k of time to failure for synchronous (left) and parametric (right) resonance for varied mean time to failure

The number O_i of the observed times to failure within each interval i was counted, and the expected number E_i was calculated, according to the assumed distribution, as N/k; then, the *test statistic* was calculated as

$$x = \sum_{i=1}^{k} (O_i - E_i)^2 / E_i \qquad (34)$$

The *critical value* of the test statistic, at the *significance level* $\alpha=0.05$, was defined as $c_{5\%} = \chi^2_{1-\alpha,f}$, i.e. the value of the χ^2 distribution at the cumulative probability $1-\alpha=0.95$ with the number of degrees of freedom $f=k-p-1$, where $p=1$ is the number of parameters of the assumed distribution estimated from the sample. Fig. 7 shows ratio $x/c_{5\%}$ vs. the number of intervals k: when $x/c_{5\%}<1$, the *null hypothesis* that the data follow the assumed distribution cannot be rejected at the significance level 5%. Fig. 8 shows ratio $x/c_{5\%}$ at $k=200$ as a function of the sample mean time to failure. For synchronous resonance, the Poisson process model is acceptable (at the 5% significance level) in all studied cases. On the other hand, for parametric resonance, the results disagree with the Poisson process assumption: marginally at $\hat{T} \approx 2$ hours and greater and increasingly for $\hat{T}$ decreasing below 2 hours. Note, however, that the χ^2 test is considered as very strict when the amount of data is large.

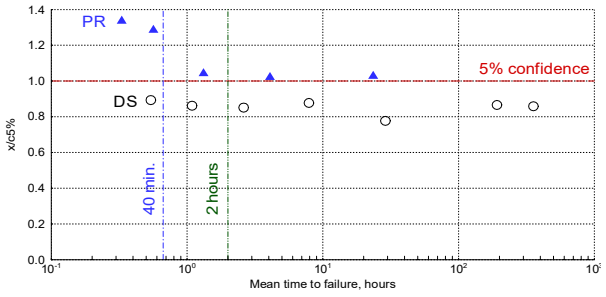

Figure 8: The ratio $x/c_{5\%}$ at $k=200$ for synchronous (○) and parametric (▲) resonance vs. sample mean time to failure

5. APPLICATION

In the *probabilistic assessment in design situations*, Annex 1 of IMO (2019), section 5.3.3, the *acceptance* requirement is that in all design sea states the upper boundary of the 95%-confidence interval of the failure rate should not exceed a *standard* λ (note that since the remaining 5% outside of the confidence interval include both tails, this means that failure does not happen with the probability 97.5%); the standard is equal to one

Table 1. Significant wave heights for design sea states with probability density 10^{-5} (m·s)$^{-1}$ for unrestricted service, according to Annex 1 of IMO (2019), section 5.3.3

T_z, s	4.5	5.5	6.5	7.5	8.5	9.5	10.5	11.5	12.5	13.5	14.5	15.5	16.5
h_s, m	2.8	5.5	8.2	10.6	12.5	13.8	14.6	15.1	15.1	14.8	14.1	12.9	10.9

failure in 2 hours in sea states with probability density 10^{-5} (m·s)$^{-1}$. For parametric roll assessment, design situations are defined by 0° and 180° mean wave directions, zero forward speed, all wave periods and significant wave heights vs. zero-upcrossing period per Table 1.

This means that for the acceptance of a loading condition, the upper boundary of the 95%-confidence interval of the failure rate should be estimated and compared with the standard λ in all design situations. To save simulation (or model testing) time, it is useful to estimate also the lower boundary of the 95%-confidence interval of the failure rate and stop further simulations or tests (and consider the loading condition as *unacceptable*) once this estimate exceeds the standard λ in at least one design situation.

The upper r_U and lower r_L boundaries of the 95%-confidence interval of the failure rate can be estimated from eq. (22) as

$$r_U = 0.5\chi^2_{1-\alpha/2,2N}\hat{r}/N \tag{36}$$

$$r_L = 0.5\chi^2_{\alpha/2,2N}\hat{r}/N \tag{37}$$

where N is the number of counted stability failures, $\alpha = 1-95/100 = 0.05$ and $\hat{r} = 1/\hat{T}$.

For *acceptance*, it should be required that r_U is less than λ, which leads to the following condition:

$$\hat{T} > \hat{T}_A \equiv \beta_1(N)/\lambda \tag{38}$$

where $1/\lambda = 2$ hours and $\beta_1(N) = 0.5\chi^2_{1-\alpha/2,2N}/N$; β_1 is shown as a function of N in Fig. 9; $\chi^2_{1-\alpha/2,2N}$ was calculated with MS Excel as chisq.inv.rt(α/2;2*N).

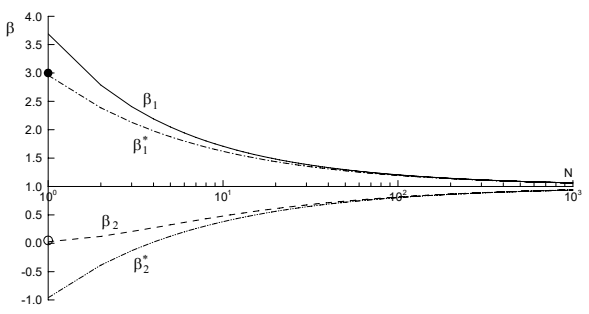

Figure 9: χ^2 vs. normal approximation for r_U and r_L: β_1, β_2, β_1^* and β_2^* together with approximations for N=1 from Shigunov (2016), $3/\lambda$ (●) and $0.05/\lambda$ (○)

For *not acceptance*, it can be required that r_L is greater than λ, which leads to the condition

$$\hat{T} < \hat{T}_F \equiv \beta_2(N)/\lambda \tag{39}$$

where $\beta_2(N) = 0.5\chi^2_{\alpha/2,2N}/N$, Fig. 9; $\chi^2_{\alpha/2,2N}$ was calculated with MS Excel as chisq.inv(α/2;2*N).

In Shigunov (2016), conditions of *acceptance*

$$\hat{T} > \beta_1^*(N)/\lambda \tag{40}$$

and *not acceptance*

$$\hat{T} < \beta_2^*(N)/\lambda \tag{41}$$

respectively, were derived using the central limit theorem (i.e. normal distribution approximation for the sample mean). For the estimate of the 95%-confidence interval for the failure rate, eq. (20), this leads to $\beta_1^*(N) = 1+1.96N^{-1/2}$, $\beta_2^*(N) = 1-1.96N^{-1/2}$; Fig. 9 shows $\beta_1^*(N)$ and $\beta_2^*(N)$ for comparison.

If, after the start of the first simulation, the first failure has not occurred yet, it is useful to know when the achieved simulation time is already sufficient for acceptance. Applying eq. (38), in which it is conservatively assumed that $N=1$ and, correspondingly, $\hat{T} = t$, yields that simulations can be stopped (with the acceptance decision) when the simulation time without failure satisfies the following condition:

$$t \geq t_A \equiv \beta_1(1)/\lambda \tag{42}$$

i.e. when $t > 3.7/\lambda$ (Shigunov, 2016, proposed a similar approximation $t > 3/\lambda$).

It is useful to extend this idea on the second and further failures: by rearranging, in eq. (38), the definition (16) as $\hat{T} = \hat{T}_{N-1}\cdot(1-1/N) + T_N/N$, where $\hat{T}_{N-1}$ is the sample mean time to failure for N-1 previous failures and assuming, conservatively, $T_N = t$, we obtain that simulation for N-th failure can be stopped with the *acceptance* decision when the simulation time without failure achieves

$$t \geq t_A \equiv \beta_1(N)\cdot N/\lambda - \hat{T}_{N-1}\cdot(N-1) \tag{43}$$

Examples of the assessment using eq. (38,39) for a 1700 TEU container ship in loading conditions with GM=1.7 m, 1.8 m, …, 2.2 m are shown in Fig. 10 (for each loading condition, only one result is shown, corresponding to the smallest $\hat{T}$ over all T_z). Table 2 shows the number of failures required until a decision can be made; note that a large number of failures was required only in one case (GM=1.9 m).

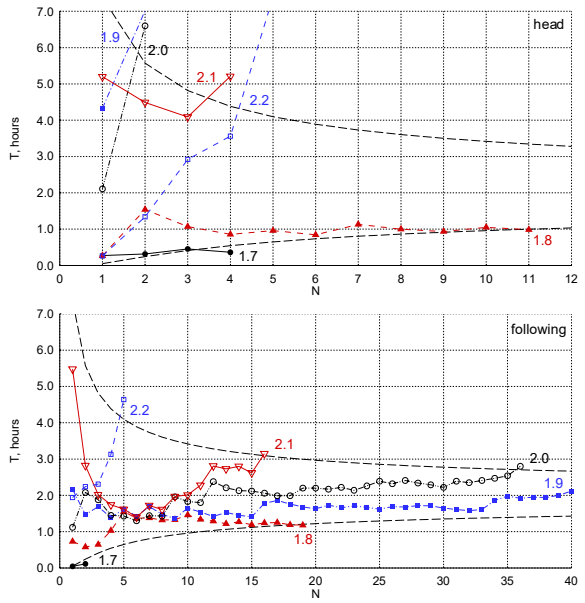

Figure 10: Sample mean time to failure vs. the number of simulations together with the *acceptance* $\beta_1(N)/\lambda$ and *not acceptance* $\beta_2(N)/\lambda$ boundaries in head (top) and following (bottom) waves; values along lines indicate *GM*

Table 2. The number of failures counted until the acceptance (+) or not acceptance (-) for parametric roll assessment in design situations

GM, m	Head waves	Following waves
1.7	-4	-1
1.8	-11	-19
1.9	+2	+175
2.0	+2	+36
2.1	+4	+16
2.2	+5	+5

6. CONCLUSIONS

Counting the number of stability failures, required to define the failure rate and the failure probability, makes sense for a stationary Poisson process. To ensure that stability failures in numerical simulations or model tests satisfy the assumptions of a Poisson process, the procedure should avoid self-repetition effects, transient hydrodynamic effects and the auto-correlation of large roll motions. To avoid self-repetition effects, the duration of simulations should be limited to about 3 hours if about 10^3 frequencies per wave direction are used for discretisation of the wave energy spectrum. During the initial transients at the beginning of simulations, the counter of stability failures and the simulation timer should be switched off. An effective way to avoid the auto-correlation effects is to stop a simulation after the first failure. These measures are sufficient to assume that the process is Poisson for the assessment of synchronous resonance in relevant conditions, whereas for parametric resonance, the process still significantly deviates from the Poisson process when the mean time to failure is less than about 2 hours.

Efficient procedures are proposed to define the 95%-confidence interval of the failure rate, required for the assessment; application examples show that small number of simulations is sufficient in most cases; in few cases (near the acceptance threshold), large number of simulations may be required.

REFERENCES

IMO (2019) Report of the Experts' Group on Intact Stability, Document SDC 6/WP.6, International Maritime Organization, London.

Longuet-Higgins, M.S., 1952, "On the statistical distribution of the heights of sea waves", J. of Marine Research.

Shigunov, V., 2016, "Probabilistic direct stability assessment", Proc. 15th Int. Ship Stability Workshop, 13-15 June, Stockholm, Sweden.

Shigunov, V., 2017, "Direct stability assessment: pragmatic solutions", *Ship Technology Research (Schiffstechnik)* 64(3), pp. 144-162.

Shigunov, V., 2017a, "Possible simplifications of direct stability assessment, Proc. 16th Int. Ship Stability Workshop, 5-7 June, Belgrade, Serbia.

* * *

Model experiments and direct stability assessments on pure loss of stability of the ONR tumblehome in following seas

Jiang Lu, *China Ship Scientific Research Center,* lujiang1980@aliyun.com
Min Gu, *China Ship Scientific Research Center,* gumin702@163.com

ABSTRACT

The guidelines for direct stability assessment of pure loss of stability are currently under development at the International Maritime Organization (IMO) for the second generation intact stability criteria. A surge-heave-pitch-roll coupled equation named as 4 DOF is newly established for predicting pure loss of stability in following seas. Firstly, the thrust and the resistance of calm water are varied with the ship forward speed and the excited surge force by waves is varied with the relative position between the ship and waves. Secondly, the heave and pitch motions obtained by a strip method with an enhanced integrating method applied to an upright hull, in which the ship speed variation due to the surge motion is also newly considered, are used to determine the simultaneous relative position of the ship to waves in time domain, and then the nonlinear Froude-Krylov roll restoring variation is calculated by integrating the wave pressure up to the wave surface. Thirdly, the initial heeling angle, the nonlinear roll damping and the heel-induced hydrodynamic forces for large heeling angle in calm water are considered in the 4 DOF mathematical model, and the effect of the constant ship speed, the surge motion, the initial heeling angle, the heel-induced hydrodynamic forces and the heave and pitch motions on pure loss of stability are studied for direct assessment of pure loss of stability. Finally, the new numerical approach on pure loss of stability in following seas are verified by experimental results using the standard ONR tumblehome provided by an IMO's intercessional corresponding group.

Keywords: *Pure loss of stability, IMO, second generation intact stability criteria, direct stability assessment, surge-heave-roll-pitch.*

1. INTRODUCTION

The guidelines for direct stability assessment of pure loss of stability are currently under development at the International Maritime Organization (IMO) for the second generation intact stability criteria (IMO SDC 4, 2017). As one of the problems related to the roll restoring force variation, pure loss of stability in following seas has been studied for many years (Umeda & Yamakoshi , 1986), which is a nonlinear phenomenon involving a large amplitude roll motion, or even capsizing when the crest of a large wave passes the midship section of a ship with a slightly higher speed than the ship speed and the state of stability loss at the crest exists long enough. It is urgently required to establish reliable guidelines for developing accurate but sufficiently simple methods to predict pure loss of stability in following seas

Pure loss of stability is a nonlinear phenomenon involving a large amplitude roll motion and it is still difficult to be predicted quantitatively. Hashimoto carried out experiments on pure loss of stability in following seas with one surge-roll coupled mathematical model (Hashimoto, 2009). Umeda firstly pointed out that it could be not really pure for pure loss of stability in astern seas (Kubo et al., 2012). Japan delegation (IMO SLF 55, 2013) noted that predicting pure loss of stability with their newly 4 degrees of freedom (DOF) mathematical model is more accurate than the 2 DOF mathematical model. An experiment with a fishing vessel was carried out for further study on pure loss of stability (Umeda et al., 2017).

For drafting guidelines for direct stability assessment, several crucial elements for predicting parametric roll were investigated with simulations and experiments by the authors (Lu et al., 2017). Several crucial elements for pure loss of stability were investigated with experiments and one established mathematical model which refers a

MMG standard method for ship maneuvering predictions and existing mathematical models for broaching (Lu & Gu., 2017; Lu et al., 2018).

The capsizing due to pure loss of stability happens at a high speed in following and astern seas. In that case, the encounter frequency is much lower than the natural frequencies of heave and pitch, and the coupling with heave and pitch motions is almost static (Matsuda & Umeda, 1997). The above methods for pure loss of stability and existing mathematical models for broaching (Umeda, 1999; Umeda & Hashimoto, 2002; Hashimoto et al., 2011; Umeda et al., 2016) are based on a static balance assumption for heave and pitch motions.

The large amplitude roll motion and capsizing due to pure loss of stability are related to seakeeping, maneuvering, thrust and resistance. Unfortunately, they are still separated at this stage and the improvement of predicting methods for pure loss of stability are limited by the development of seakeeping and maneuvering. The above existing mathematical models are apt to maneuvering mathematical models in which the maneuvering coefficients are difficult to be obtained accurately except for expensive experiments at this stage. Therefore it is urgent to obtain a unified method to predict pure loss of stability with a seakeeping mathematical model combined with some essential maneuvering coefficients. In the seakeeping field, strip methods can obtain reasonable heave and pitch motions in the frequency domain when the ship speed is not very high, such as Ordinary Strip Method (OSM), New Strip Method (NSM) and STF Method (STFM). For predicting added resistance, Kashiwagi (Kashiwagi, 1995; Kashiwagi et al, 2010) developed an enhanced unified theory from the unify theory (Newman, 1978) in which an enhanced integrating method of a direct line integral is developed to solve the velocity potential to replace the traditional collocation method.

For predicting the large amplitude roll motion during pure loss of stability in following seas, a more accurate mathematical model is newly established with a surge-heave-pitch-roll coupled equation in which heave and pitch motions at each constant forward speed are obtained by a strip method with an enhanced integrating method of direct line integral applied to an upright hull. The non-uniform forward speed due to the surge motion is also newly considered by an interpolation method. Then the effect of the constant speed, the surge motion, the initial heeling angle, the heel-induced hydrodynamic forces and the heave and pitch motions on pure loss of stability are studied. The new numerical approach on pure loss of stability in following seas are verified by experimental results using the standard ONR tumblehome hull form which is provided by an IMO's intersessional correspondance group as one of standard ships for developing the second generation intact stability criteria.

2. MATHEMATICAL MODEL

Coordinate systems

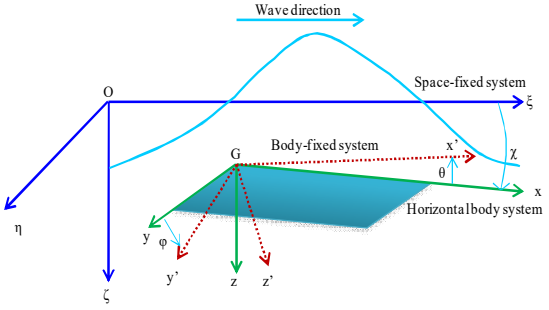

Figure 1: Coordinate systems

A space-fixed coordinate system $O-\xi\eta\zeta$ with the origin at a wave trough, a body-fixed system $G-x'y'z'$ with the origin at the center of gravity of the ship, and a horizontal body coordinate system $G-xyz$ (Hamamoto & Kim, 1993), which has the same origin with the body-fixed system but does not rotate around the x-axis and y-axis, are adopted as shown in Fig. 1.

The relationships between the horizontal body coordinate system $G-xyz$, the body-fixed system $G-x'y'z'$ and the space-fixed system $O-\xi\eta\zeta$ are shown in Eq. (1) and Eq. (2), respectively.

$$\begin{bmatrix} x \\ y \\ z \end{bmatrix} = \begin{bmatrix} \cos\theta & \sin\phi\sin\theta & \cos\phi\sin\theta \\ 0 & \cos\varphi & -\sin\varphi \\ -\sin\theta & \sin\varphi\cos\theta & \cos\varphi\cos\theta \end{bmatrix} \begin{bmatrix} x' \\ y' \\ z' \end{bmatrix} \quad (1)$$

$$\begin{bmatrix} \xi-\xi_G \\ \eta-\eta_G \\ \zeta-\zeta_G \end{bmatrix} = \begin{bmatrix} \cos\theta\cos\chi & \sin\varphi\sin\theta\cos\chi & \cos\varphi\sin\theta\cos\chi \\ & -\cos\varphi\sin\chi & +\sin\varphi\sin\chi \\ \cos\theta\sin\chi & \sin\varphi\sin\theta\sin\chi & \cos\varphi\sin\theta\sin\chi \\ & +\cos\varphi\cos\chi & -\sin\varphi\cos\chi \\ -\sin\theta & \sin\varphi\cos\theta & \cos\varphi\cos\theta \end{bmatrix} \begin{bmatrix} x' \\ y' \\ z' \end{bmatrix} \quad (2)$$

Mathematical Model

The 4 DOF mathematical model is expressed by surge, roll, heave and pitch motions as shown in Eq. (3) to Eq. (6), respectively. The time domain of ship positions in surge, heave and pitch are shown in Eq. (7), (8) and (9), respectively. The subscripts H, P and W refer to hull, propeller and wave, respectively.

$$(m + A_{11})\dot{u} = X_H + X_P + X_W \tag{3}$$

$$\begin{aligned}(I_{xx} + A_{44})\ddot{\varphi} &= K_H - D(\dot{\varphi}) \\ &- W \cdot [GZ_W(\xi_G / \lambda, \zeta_G(t), \theta(t), \chi, \varphi) - GZ(\varphi)]\end{aligned} \tag{4}$$

$$\begin{aligned}&(m + A_{33}(u))\ddot{\zeta} + B_{33}(u)\dot{\zeta} + C_{33}\zeta + A_{35}(u)\ddot{\theta} \\ &+ B_{35}(u)\dot{\theta} + C_{35}\theta = F_3^{FK}(u) + F_3^{DF}(u)\end{aligned} \tag{5}$$

$$\begin{aligned}&(I_{yy} + A_{55}(u))\ddot{\theta} + B_{55}(u)\dot{\theta} + C_{55}\theta + A_{53}(u)\ddot{\zeta} \\ &+ B_{53}(u)\dot{\zeta} + B_{53}\zeta = F_5^{FK}(u) + F_5^{DF}(u)\end{aligned} \tag{6}$$

$$\xi_G = \int\int_0^t \dot{u}(t)dtdt \tag{7}$$

$$\zeta_G(t) = \zeta_{Ga}(u)\cos(\omega t - k\xi_G \cos\chi + \delta_H(u)) \tag{8}$$

$$\theta(t) = \theta_a(u)\cos(\omega t - k\xi_G \cos\chi + \delta_\theta(u)) \tag{9}$$

where m: ship mass; u: surge velocity; X_H, K_H: surge force and roll moment around center of ship gravity acting on ship hull; X_P: surge force due to propeller; X_W: surge force due to waves; I_{xx}, I_{yy}: moment of inertia in roll and pitch; φ: roll angle; $D(\dot{\varphi})$: roll damping moment; W: ship weight; GZ_W: righting arm in waves; GZ: righting arm in calm water; t: time; $\zeta_G(t)$: heave displacement; $\theta(t)$: pitch angle, ξ_G: instantaneous ship longitudinal position; λ: wave length; χ: heading angle; F_3^{FK}, F_3^{DF}: wave exciting force on heave direction including Froud-Krylov component and diffraction component. F_5^{FK}, F_5^{DF}: wave exciting moment on pitch direction including Froud-Krylov component and diffraction component. $\zeta_{Ga}(u)$, $\delta_H(u)$: amplitude and initial phase of heaving when the ship forward speed is u; $\theta a(u)$, $\delta_\theta(u)$: amplitude and initial phase of pitching when the ship forward speed is u; ω: wave frequency; k: wave number; The dot denotes the differentiation with time. A_{ij}, B_{ij}, C_{ij} are coupling coefficients, and 1,3,4,5 denote the direction in surge, heave, roll and pitch, respectively.

Hydrodynamic forces acting on a ship

The hull forces in still water X_H and K_H are expressed as follows:

$$X_H = -R(u) \tag{10}$$

$$K_H = \frac{1}{2}\rho L_{pp} d^2 u^2 K'_\varphi \cdot \varphi \tag{11}$$

where, $R(u)$: ship resistance in calm water; ρ: water density; d: ship draft; K'_φ: the non-dimensional derivative for roll moment with respect to roll angle.

Propeller thrust and the hull resistance in still water

The surge force due to propeller thrust X_P with twin propellers is expressed as follows.

$$X_P = 2 \times (1 - t_P)T \tag{12}$$

$$T = \rho {n_P}^2 D_P^4 K_T(J_P) \tag{13}$$

$$J_P = \frac{(1 - w_P)\,u}{n_P D_P} \tag{14}$$

The hull resistance in still water R in the surge motion is expressed as follows:

$$R = \frac{1}{2}\rho S_F u^2 C_T\left(\frac{u}{\sqrt{gL_{PP}}}\right) \tag{15}$$

where, t_P: thrust deduction factor; T: propeller thrust; n_P: propeller revolution number; D_P: propeller diameter; K_T: thrust coefficient of propeller; J_P: propeller advanced ratio; w_P: wake fraction at propeller position; S_F: wetted hull surface area; C_T: total resistance coefficient in calm water; g: gravitational acceleration.

Initial values for numerical integration with time are set as follows:

$$t = 0\ ; \xi_G = 0, u = 0, n = n^* \tag{16}$$

where, n^*: denotes the desired propeller revolution rate.

Excited surge force by waves

The wave-induced forces as the sum of the Froude-Krylov force (W_FK) and the diffraction force (W_Dif) including hydrodynamic lift forces acting on the hull are used for broaching by Umeda and Hashimoto (Umeda & Hashimoto, 2002), and only Froude-Krylov force in the surge direction is considered and it is expressed as follow.

$$\begin{aligned}&X_W(\xi_G / \lambda, u, \chi) = X_{W\_FK}(\xi_G / \lambda, u, \chi) \\ &= -\rho g \zeta_w k \cos\chi \\ &\cdot \int_{AE}^{FE} C_1(x) S(x) e^{-kd(x)/2} \sin k(\xi_G + x\cos\chi)dx\end{aligned} \tag{17}$$

$$C_1 = \frac{\sin(k \sin\chi \cdot B(x)/2)}{k \sin\chi \cdot B(x)/2} \tag{18}$$

where, *AE, FE*: after section and forward section; ζ_w: amplitude of incident waves; *B(x)*: sectional breadth; *S(x)*: sectional area.

Roll restoring force variation

Pure loss of stability is one of the problems related to the roll restoring force variation. The restoring force variation can be calculated by integrating the pressure around the instantaneously wetted hull surface with static balance of heave and pitch which is based on a Froude-Krylov assumption (Hamamoto & Kim, 1993) and it is widely used to predict parametric roll using heave and pitch motions obtained by Ordinary Strip Method (Lu et al., 2017). Here non-uniform forward speed due to the surge motion in following seas is further considered. As a result, the following formula is used.

$$\begin{aligned} W \cdot GZ_{FK} &= \rho g \int_L y(x, X_G, t) \cdot A(x, \xi_G, t)\, dx \\ &+ \rho g \sin\chi \cdot \int_L z(x, \xi_G, t) \cdot F(x) \cdot A(x, \xi_G, t) \\ &\cdot \sin(\xi_{G0} + (X_G + x)\cos\chi - c \cdot t) dx \end{aligned} \tag{19}$$

$$F(x) = \zeta_w\, k \frac{\sin(k \frac{B(x)}{2} \sin\chi)}{k \frac{B(x)}{2} \sin\chi} e^{-k\, d(x)} \tag{20}$$

where, $A(x,\xi_G,t)$: the submerged area of local section of the ship; $y(x,\xi_G,t)$: the transverse position of buoyancy centre of local section; $z(x,\xi_G,t)$: the vertical position of buoyancy centre of local section; ξ_{G0}=0: the initial longitudinal position of a ship centre from a wave trough.

Heave and pitch motions

The large amplitude roll motion and capsizing due to pure loss of stability are related to low encounter frequency of heave and pitch motions. For finding a method to obtain stable heave and pitch motions in following seas at a high speed, firstly, the authors calculated heave and pitch motions with Ordinary Strip Method (OSM) using the collocation method to solve the velocity potential and a strip method using an enhanced integrating method of direct line integral (Kashiwagi et al., 2010) to solve the velocity potential named as EStrip in this paper for the modified Wigley model (Kashiwagi et al., 2010) in head seas. Then the calculated results are compared with the model experiments published by Kashiwagi and their results of Enhanced Unified Theory (EUT) (Kashiwagi et al., 2010) as shown in Figs. A1-A2. Both OSM and EStrip methods show reasonably good agreement in heave and pitch motions in head seas at low speeds. The heave and pitch motions calculated by OSM and EStrip methods are further compared in head seas at high speed as show in Fig. A3. Both OSM and EStrip methods can generate stable heave and pitch motions at Fn=0.4. For obtaining stable heave and pitch motions for pure loss of stability, the heave and pitch motions in following seas with OSM and EStrip methods are further investigated as shown in Figs. A4-A5. Both OSM and EStrip methods could generate the same results at a low speed, but the pitch motion calculated by the EStrip method is more stable than that calculated by the OSM method at a high speed. Since pure loss of stability could happen at a high speed in following seas, the EStrip method is used to calculate heave and pitch motions at each constant forward speed applied to an upright hull while non-uniform forward speed is considered by an interpolation method in this paper.

Roll damping force

Roll damping is one of essential terms for predicting roll motion, especialy large amplitude roll motions. Linear and cubic nonlinear roll damping coefficients are used for predicting parametric roll and linear and squared nonlinear roll damping coefficients are used for predicting dead ship stability in the vulnerability criteria (IMO SDC 4, 2017). Linear and cubic nonlinear roll damping coefficients are adopted as shown in Eq.(21) for predicting pure loss of stability.

$$D(p) = (I_{xx} + J_{xx})(\alpha \cdot p + \gamma \cdot p^3) \tag{21}$$

3. EXPERIMENTS

The free running experiment with a 1/40.526 scaled model of the ONR tumblehome vessel was conducted in the seakeeping basin (length: 69m, breadth: 46m, depth: 4m) of China Ship Scientific Research Center, which is equipped with flap wave makers at the two adjacent sides of the basin.

The ship model was driven by twin propellers in regular following seas in the free running experiment. The roll angle, pitch angle and yaw angle were measured by the MEMS (Micro Electro-Mechanical System)-based gyroscope placed on the

ship model and the roll angle, pitch angle, yaw angle, rudder angle and propeller rate were recorded by an on-board system which is connected with an on-shore control computer by a wireless connection. The wave elevation was measured at the middle position of the basin by a servo-needle wave height sensor attached to a steel bridge which is 78m in length and spans over the basin.

Roll damping is very important for predicting large amplitude roll motions and even capsizing due to pure loss of stability, and here free roll decay tests in calm water are conducted to obtain roll damping coefficients. The speed is a key factor for pure loss of stability, and here the nominal Froude number (Fn) is used for the experiment of pure loss of stability in following seas by using the same specified propeller rate in calm water. The specified propeller rate corresponding to one nominal speed in calm water is determined by measuring instantaneous position of the model ship with a total station system, and the total station system consists of a theodolite and a prism attached to the model ship as shown in Fig.2.

First the model is kept near the wave maker by hands of two workmen sitting on the carriage and the initial heading of the model is kept referring to the steel bridge which can rotate about its center, up to 45 degree. Next, the wave-making system starts to generate waves. Then the propeller revolutions increase up to specified value after receiving the order from the on-shore control computer. When the wave train propagates far enough, the model is released free near one wave crest with its initial heading, and then the model automatically runs in following or quartering seas with its specified propeller rate and auto pilot course.

Figure 2: The theodolite and the prism attached on the model ship

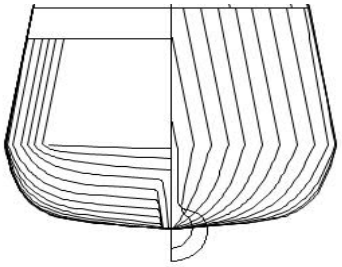

Figure 3: The ONR Tumblehome lines

The subject ship is the ONR Tumblehome vessel. The principal particulars and the lines of the ONR Tumblehome vessel are shown in Table 1 and Fig. 3, respectively. The ship model in the free running experiment is shown in Fig. 4.

Table 1: Principal particulars of the ONR tumblehome

Items	Ship	Model
Length: L	154.0 m	3.8 m
Draft: d	5.494m	0.136 m
Breadth: B	18.8 m	0.463 m
Depth: D	14.5 m	0.358 m
Displ.: W	8507 ton	0.1278 ton
C_b	0.535	0.535
GM	1.48 m	0.037 m
OG	-2.729 m	-0.067 m
L_{CB}	-2.569 m	-0.063 m
T_φ	14.0 s	2.199 s
κ_{yy}	0.25 L	0.25 L
K_{zz}	0.25 L	0.25 L
$2\times A_R$	$2\times23.74m^2$	2×0.0145 m^2
D_p	5.22m	0.129m
δ_{max}	35degs	35degs

Figure 4: The ship model in the free running experiment

4. RESULTS AND DISCUSSIONS

The effect of speed on the heave and pitch motions

Pure loss of stability could happen in following seas at a high speed, and it is related to seakeeping problems of the high speed and low encounter frequency. The methods for pure loss of stability mostly are based on a static balance assumption for heave and pitch motions. As discussed in paragraph 2.7 and the appendix, one strip method with an enhanced integrating method of a direct line integral for solving the velocity potential is used to calculate heave and pitch motions at each constant forward speed applied to an upright hull. Then the non-uniform forward speed due to the surge motions is considered by an interpolation method in this paper. Here the effect of forward speed on the heave and pitch motions for the ONR tumblehome ship is further investigated. As shown in Fig. 5, the amplitude and initial phase of heave motions obtained by the EStrip method at zero forward speed are almost the same as that obtained by the static method and the OSM method, while small differences exist with increasing forward speeds.

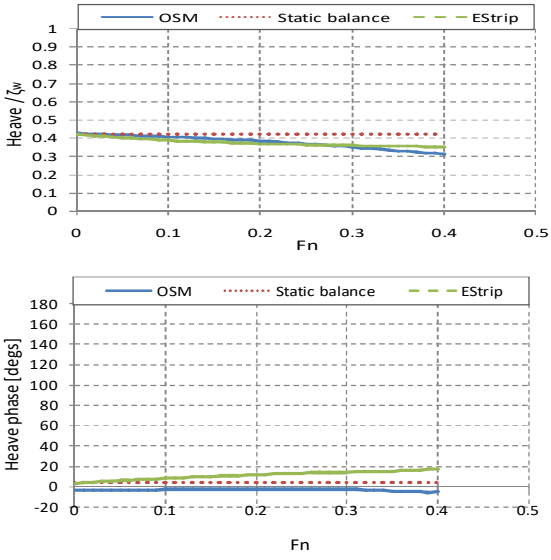

Figure 5: Heaving motion as a function of the Froude number in following seas with φ=0^0 and λ/Lpp=1.25.

As shown in Fig. 6, the amplitude and initial phase of pitch motions obtained by the EStrip method at zero forward speed are almost the same as that obtained by the static method and the OSM method, while the amplitude of pitch motions obtained by the OSM method obviously becomes small with increasing forward speeds. The critical Froude number of pure loss of stability is much smaller than 0.4, and the heave and pitch motions obtained by the Estrip method can be used to predict pure loss of stability for the ONR tumblehome vessel.

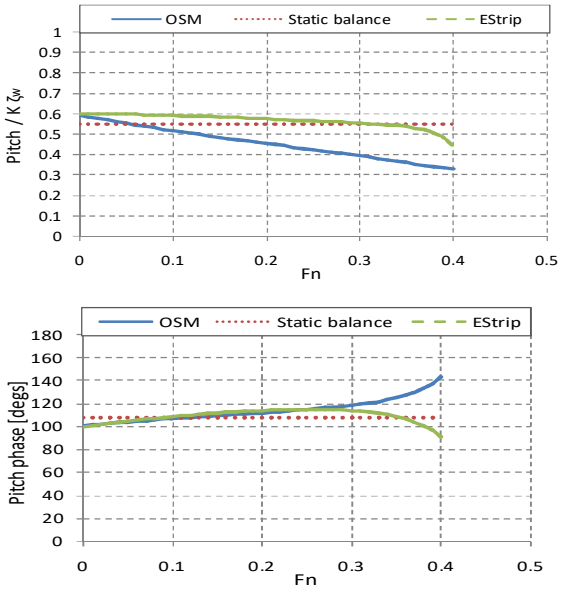

Figure 6: Pitching motion as a function of the Froude number in following seas with φ=0^0 and λ/Lpp=1.25.

The effect of wave on roll restoring variation

When the midship section is located on the crest in following seas, the metacentric height is reduced and may be negative. The righting arm in calm water GZ, the restoring variations in waves with static balance method GZ_W-static and with the strip method at different constant forward speeds GZ_W(Fn=0.0/0.1/0.2/0.3) are shown in Fig. 7. The stability loss at the crest is heavy, and if the state of stability loss at the crest exists long enough, capsizing could happen.

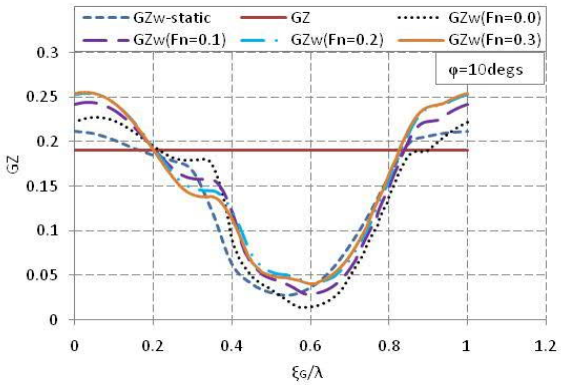

Figure 7: Restoring variation in following seas with φ=10^0 , λ/Lpp=1.25, H/Lpp=0.05, and χ=0^0

The effect of constant speed on pure loss of stability

The righting arm in calm water GZ and the restoring variations in waves GZ_W at different constant forward speed are shown in Fig. 8. The

encounter period becomes larger as the ship increasing forward speed, and the state of stability loss at the wave crest becomes larger.

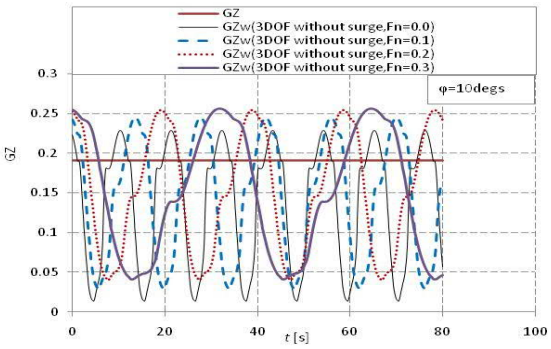

Figure 8: Time domain restoring variation in following seas with φ=10⁰, *λ/Lpp*=1.25, *H/Lpp*=0.05, and χ=0⁰.

The roll angle due to pure loss of stability at different constant forward speeds are shown in Fig. 9, and the roll angle becomes larger as the ship forward speed increases because the state of stability loss at crest becomes larger as shown in Fig. 8. But the state of stability loss at crest is not long enough to result in capsizing.

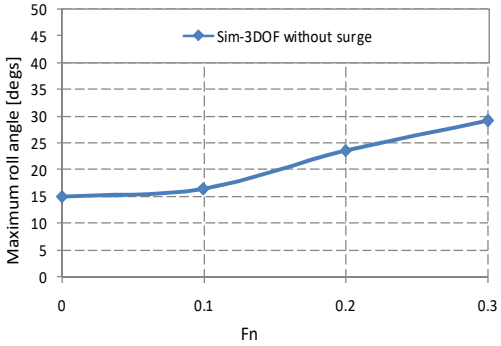

Figure 9: The effect of the constant speed on pure loss of stability with an initial heeling φ=8.6° , *λ/Lpp*=1.25, *H/Lpp*=0.05, and χ=0°.

The effect of surge motion on pure loss of stability

The nominal velocity of ship with Fn=0.3, the actual velocity of ship and the wave velocity are shown in Fig. 10. The nominal velocity of ship is much smaller than the wave velocity, and the maximum actual velocity of ship is also smaller than the wave velocity. The forward speed is varied in a large range around the nominal speed of ship due to the surge motion, and the state at the crest exists longer than that at the trough.

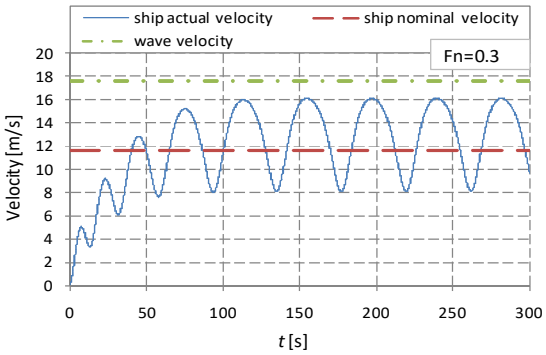

Figure 10: Comparison between ship velocity and wave velocity with nominal *Fn*=0.3, *λ/Lpp*=1.25, *H/Lpp*=0.05, and χ=0⁰.

The righting arm in calm water GZ, the restoring variations in waves GZ_W with surge and without surge are shown in Fig. 11. The state of stability loss at the crest exists longer than that at the trough because the surge motion causes the state at the crest to exist longer than that at the trough as shown in Fig. 10.

As shown in Fig. 12, the mathematical model with 3 DOF of heave-roll-pitch coupled motions fails to predict capsizing because the state of stability loss at the crest is not long enough while that with 4 DOF of surge-heave-roll-pitch coupled motions could appropriately estimate the pure loss of stability in following seas. One key reason is that the state at the crest exists longer than that at the trough due to the surge motion and then the state of stability loss at the crest exists long enough. Therefore, the surge motion is important for predicting pure loss of stability in following seas.

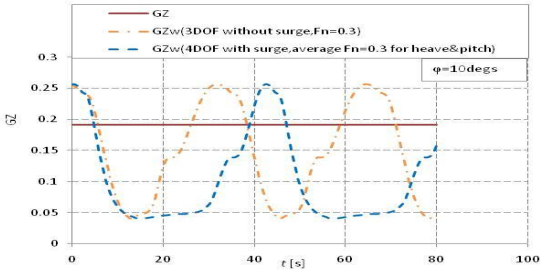

Figure 11: The effect of surge motion on restoring variation with *φ*=10°, *λ/Lpp*=1.25, *H/Lpp*=0.05, and χ=0°.

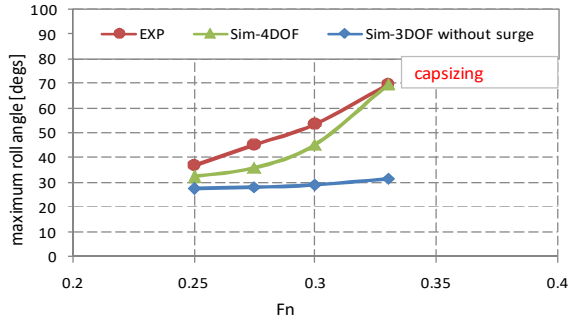

Figure 12: The effect of the sure motion on pure loss of stability with an initial heeling φ=8.6 , *λ/Lpp*=1.25, *H/Lpp*=0.05 and χ=0º.

The effect of initial heel angle on pure loss of stability

Without an external heeling moment, once the wave crest passes the ship, the ship will finally return to the upright position with regained stability in following seas as shown in Fig. 13 with $\varphi=0^0$. The initial heeling angle is set as 8.6 degrees by cargo shift in the experiment and capsizing happens due to pure loss of stability as shown in Fig.12. For investigating the effect of initial heeling angle on pure loss of stability, simulations with different initial heeling angles are carried out as shown in Fig. 13. The roll angles become larger as the initial heeling angles increases, and capsizing happens at the critical speeds due to pure loss of stability. However, the ship could be captured by a wave crest when the ship has a very small initial heeling angle in following seas at a high speed. That is to say, the ship reaches the speed of the wave in this case.

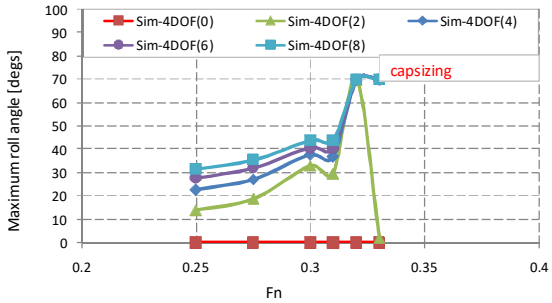

Figure 13: The effect of initial heeling angles on pure loss of stability with *λ/Lpp*=1.25, *H/Lpp*=0.05, and χ=0⁰（φ=0⁰, φ=2º, φ=4º, φ=6º, φ=8º）

The effect of heel-induced hydrodynamic forces for large heeling angle in calm water

Pure loss of stability is accompanied with large amplitude roll motions. The heel-induced hydrodynamic forces for large heeling angle in calm water, which are hydrodynamic lift due to underwater non-symmetry induced by heeling angle with the forward velocity, could affect the prediction of pure loss of stability.

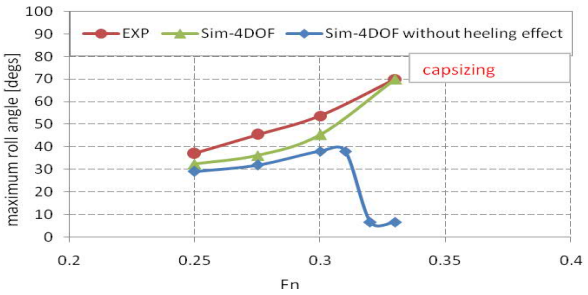

Figure 14: The effect of the heel-induced hydrodynamic forces on pure loss of stability with an initial heeling *φ*=8.6, *λ/Lpp*=1.25, *H/Lpp*=0.05 and χ=0⁰.

The linear heel-induced hydrodynamic forces in calm water are investigated as shown in Fig. 14. The 4 DOF mathematical model without linear heel-induced hydrodynamic forces could fail to predict capsizing at critical ship speeds due to pure loss of stability.

The effect of heave and pitch motions on pure loss of stability

The non-uniform forward speed due to the surge motion is newly considered for the heave and pitch motions in the surge-heave-pitch-roll coupled 4 DOF mathematical model for predicting pure loss of stability. The righting arm in calm water GZ, the restoring variations in waves GZ_W with the uniform and non-uniform forward speeds for the heave and pitch motions are shown in Fig. 15 and the predictions of pure loss of stability are shown in Fig. 16.

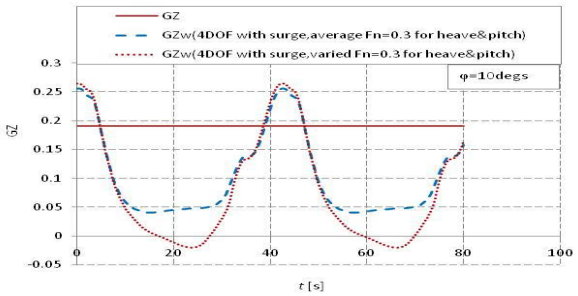

Figure 15: The effect of heave and pitch motions on restoring variation with φ=10º, *λ/Lpp*=1.25, *H/Lpp*=0.05 and χ=0º.

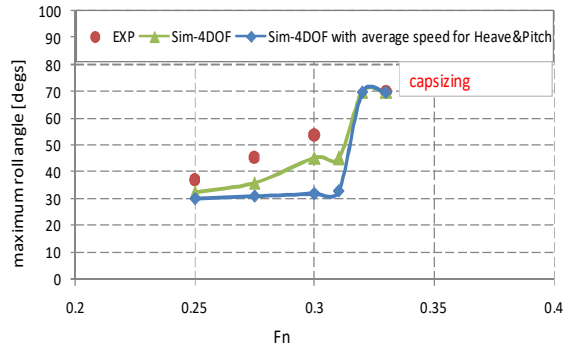

Figure 16: The effect of heave and pitch motions on pure loss of stability with φ=8.6°, λ/Lpp=1.25, H/Lpp=0.05 and χ=0°.

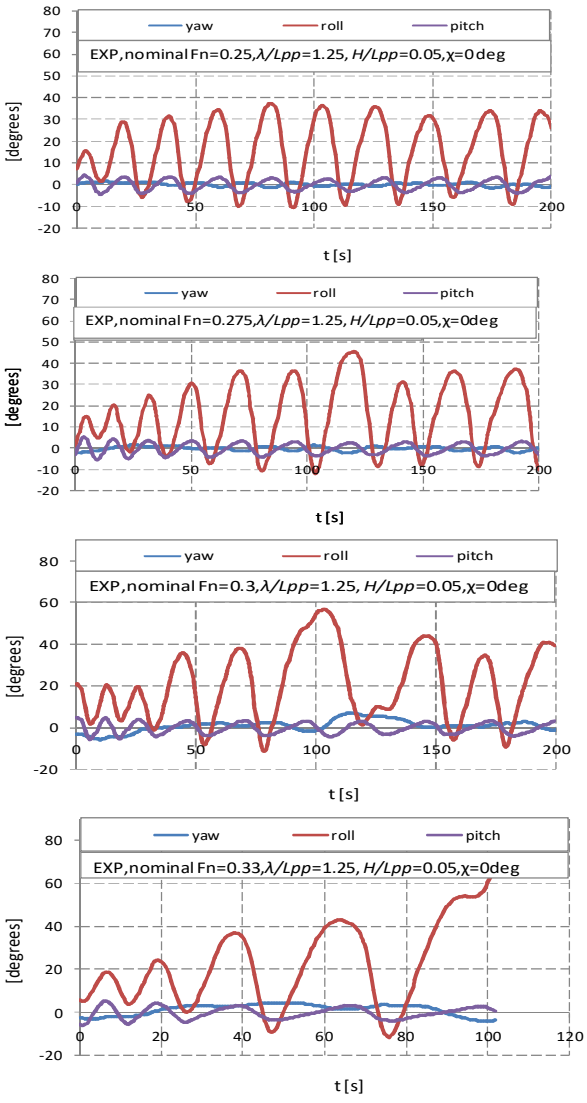

Figure 17: Yaw, roll and pitch motions in the free running experiment with an initial heeling φ=8.6°, λ/Lpp=1.25, H/Lpp=0.05 and χ=0°.

The method considering uniform forward speeds for the heave and pitch motions can predict capsizing due to pure loss of stability at the critical forward speed, but it could underestimate the roll angles at speeds below the critical forward speed. This because the stability loss at the crest with the non-uniform forward speed for the heave and pitch motions are larger than that with the uniform forward speed for the heave and pitch motions, as shown in Fig. 15.

The type of roll motions during pure loss of stability

The experimental results of yaw, roll and pitch motions in following seas are shown in Fig. 17. The roll motions become unstable when she ship speed near the critical speed of pure loss of stability. The capsizing happens due to pure loss of stability when the ship speed reaches the critical speed as shown in Fig. 17.

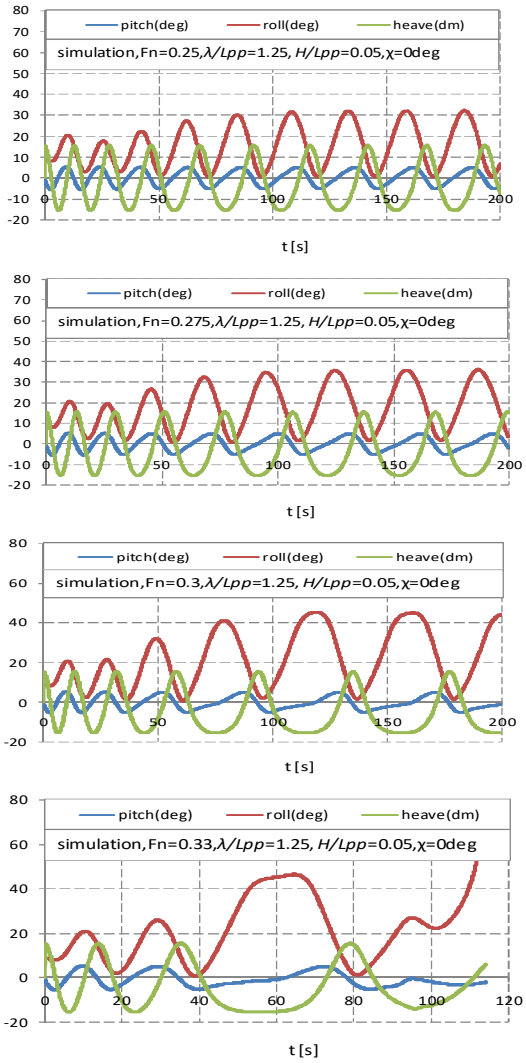

Figure 18: Pitch, roll and heave motions in the simulations with the 4 DOF mathematical model with an initial heeling φ=8.6°, λ/Lpp=1.25, H/Lpp=0.05 and χ=0°.

The calculated results of pitch, roll and heave motions in following seas with the 4 DOF mathematical model are shown in Fig. 18. The roll motions become large with the ship speed increasing,

and capsizing happens due to pure loss of stability when the ship speed reaches the critical speed. The roll amplitudes are agreed well with the experimental results, while the unstable roll motions cannot be completely repeated in the simulations. Pure loss of stability is more complicated than our previous understanding, although the roll angle and capsizing due to pure loss of stability can be predicted.

5. CONCLUSIONS

On the basis of the new numerical approach on pure loss of stability in following seas with one experiment by using the ONR tumblehome vessel, the following remarks can be made:

1) The new numerical approach with surge- -heave-pitch-roll coupled 4 DOF mathematical model considering the non-uniform forward speed for the heave and pitch motions obtained by a strip method with an enhanced integrating method applied to an upright hull could appropriately estimate pure loss of stability in following seas.
2) The encounter period becomes larger with increasing forward speed, while the surge motion further extends the state of stability loss at the crest. The effect of surge motion with varied forward speed on pure loss of stability in following seas should be considered.
3) The effect of linear heel-induced hydrodynamic forces in calm water on pure loss of stability in following seas should be taken into account for the ONR tumblehome vessel.

A unified method to predict pure loss of stability in astern waves with a seakeeping mathematical model combined with some essential maneuvering coefficients will be further investigated in future.

ACKNOWLEDGMENTS

Some contents used in this research were once guided by Prof. Naoya Umeda during the first author's Ph.D course at Osaka University supported by China Scholarship Council [No.2008606031]. Prof. M. Kashiwagi from Osaka University once provided the first author with his useful lecture and textbook on enhanced unified theory. The research is supported by Ministry of Industry and Information Technology of China (No. [2016] 25, 26; [2017] 614) and China research fund (No. B2420132001; No. 51509124). These supports are gratefully acknowledged.

REFERENCES

Hamamoto M., Kim Y.S., 1993, "A New Coordinate System and the Equations Describing Manovering Motion of a Ship in Waves", *Journal of the Society of Naval Architects of Japan*, 173: 209-220.

Hashimoto H., 2009, "Pure Loss of Stability of a Tumblehome Hull in Following Seas", Proceedings of the 19th International Offshore and Polar Engineering Conference Osaka, Japan, June 21-26.

Hashimoto H., Umeda N., Matsuda A., 2011, "Broaching Prediction of a Wave-piercing Tumblehome Vessel with Twin screws and Twin Rudders", *Journal of Marine Science and Technology*, 16:448-461.

IMO SLF 55, 2013, "Development of Second Generation Intact Stability Criteria", INF. 15. Annex 12

IMO SDC 2017, "Finalization Second Generation Intact Stability Criteria", Report of the working group, SDC 4/WP4.

Kashiwagi M, 1995, "Prediction of Surge and Its Effect on Added Resistance by Means of the Enhanced Unified Theory", *Trans. West-Japan Society of Naval Architects*, 89:77-89.

Kashiwagi M., Ikeda T. Sasagawa T., 2010, "Effect of Forward Speed of a ship on Added Resistance in waves", *International Journal of Offshore and Polar Engineering*, 20(2):1 -8.

Kubo H., Umeda N., Yamane K., Matsuda A., 2012, "Pure Loss of Stability in Astern Seas -Is It Really Pure?", Proceedings of the 6th Asia-Pacific Workshop on Marine Hydrodynamics, pp. 307-312.

Lu J., Gu M., Umeda N., 2017, "Experimental and Numerical Study on Several Crucial Elements for Predicting Parametric Roll in Regular Head Seas", *Journal of Marine Science and Technology*, 22:25-37.

Lu J., Gu M., 2017, "Study on Standard Mathematical Model of Pure Loss of Stability in Stern-quartering Waves", Proceedings of the 16th International Ship Stability Workshop, Belgrade, Serbia, pp. 181-190.

Lu J., Gu M., Wang T., Chao S., 2018, "Experimental and Numerical Study on Standard Mathematical Model of Pure Loss of Stability", Proceedings of the 14th International Conference on Stability of Ships and Ocean Vehicles, (STAB2018), Kobe, Japan, pp. 164-178.

Matsuda A., Umeda N., 1997, "Vertical Motions of a Ship Running in Following and Quartering Seas", *Naval Architecture and Ocean Eng.* 227:47-55 (in Japanese).

Newman J. N., 1978, "The theory of ship motions", *Advances in Applied Mechanics*, 18:221-83

Umeda N. and Yamakoshi Y., 1986, "Experimental study on Pure Loss of Stability in Regular and Irregular Following Seas", Proc. of the 3rd International Conf. on Stability of Ships and Ocean Vehicles, (STAB1986), pp. 93-99.

Umeda N., 1999, "Nonlinear Dynamics of Ship Capsizing due to Broaching in Following and Quartering Seas", *Journal of Marine Science and Technology*, 4:16-26.

Umeda N. and Hashimoto H., 2002, "Qualitative Aspects of Nonlinear Ship Motions in Following and Quartering Seas with High Forward Velocity", *Journal of Marine Science and Technology*, 6:111-121.

Umeda N., Usada S., Mizumoto K., Matsuda A, 2016, "Broaching Probability for a Ship in Irregular Stern-quartering Waves: Theoretical Prediction and Experimental Validation", *Journal of Marine Sci. and Techn.*, 21:23-37.

Umeda N., Osugi M., Sakai M., Matsuda A., Terada D., 2017, "Model Experiment on Pure Loss of Stability for a Ship in Astern Waves and Its Relationship with the Second Generation Intact Stability Criteria", Proceedings of the 16th International Ship Stability Workshop, Belgrade, Serbia, pp. 21-26.

APPENDIX: VALIDATION OF THE CALCULATION OF HEAVE AND PITCH MOTIONS WITH DIFFERENT METHODS

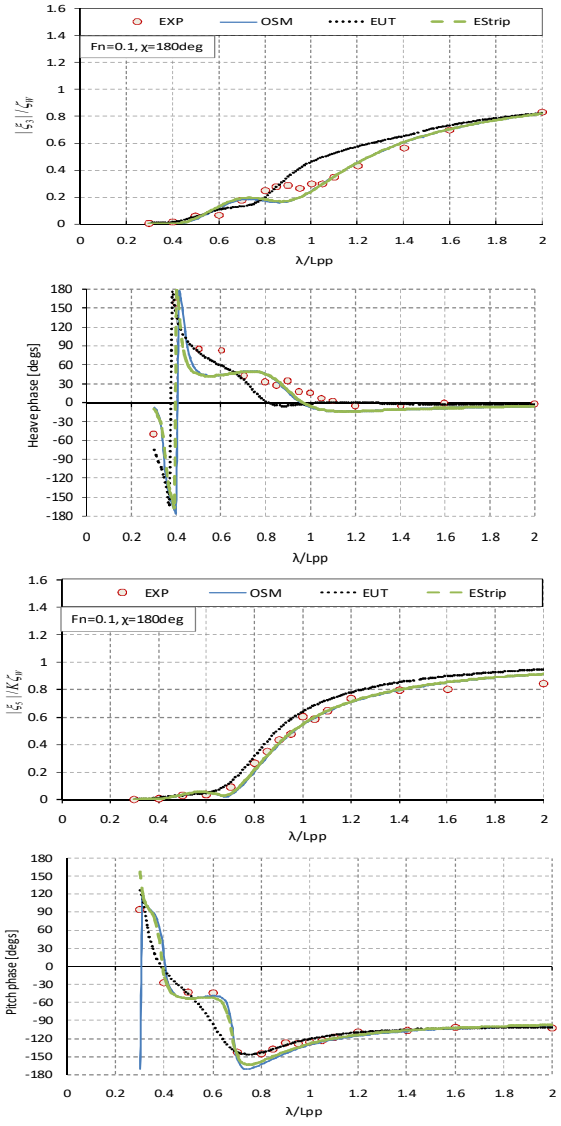

Figure A1: Heave and pitch motions of the modified Wigley ship model with different methods and experimental (EXP) and theoretical (EUT) results by Kashiwagi et al.(2010) at Fn=0.1 in head seas.

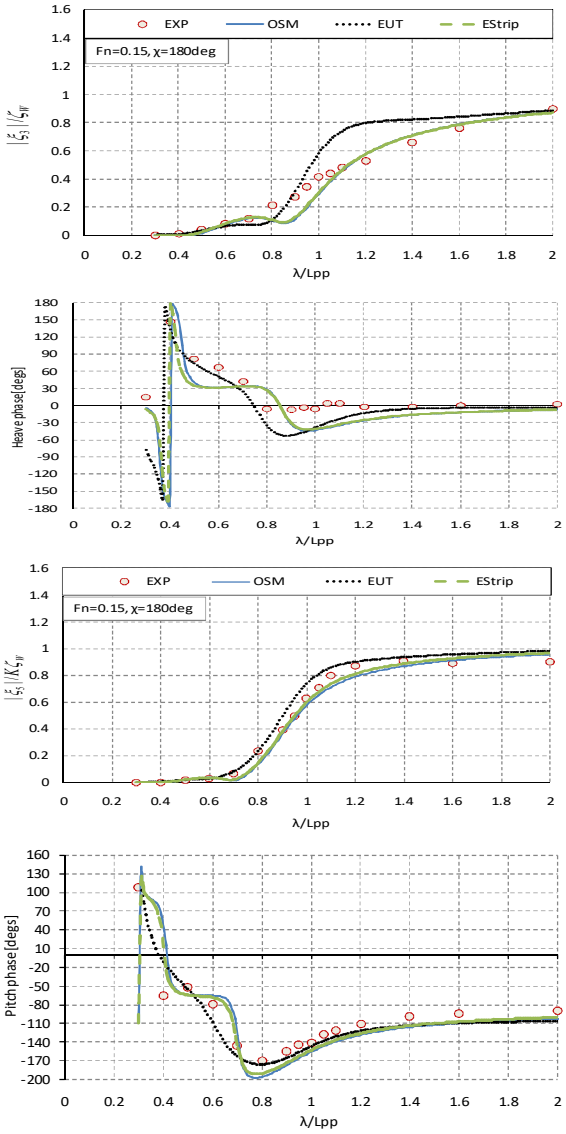

Figure A2: Heave and pitch motions of the modified Wigley ship model with different methods and experimental (EXP) and theoretical (EUT) results by Kashiwagi et al. (2010) at Fn=0.15 in head seas.

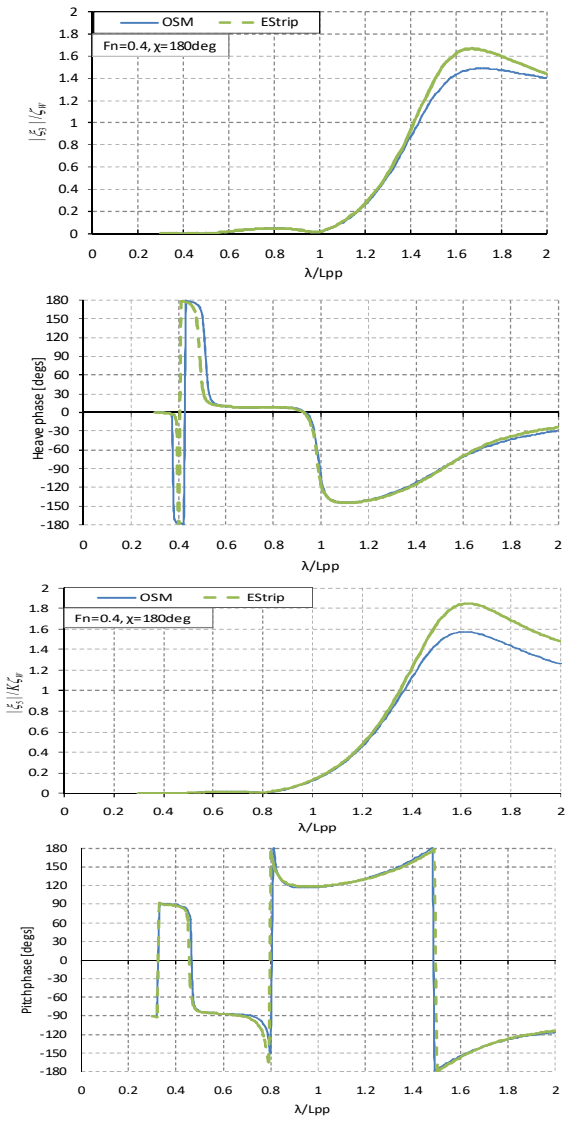

Figure A3: Heave and pitch motions of the modified Wigley ship model with different methods at Fn=0.4 in head seas.

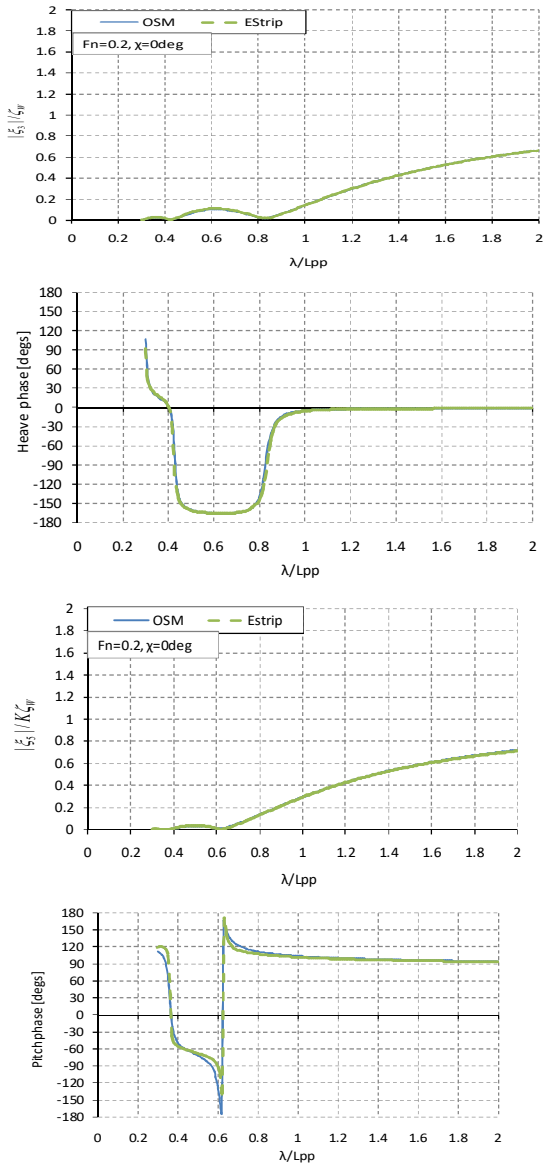

Figure A4: Heave and pitch motions of the modified Wigley ship model with different methods at Fn=0.2 in following seas.

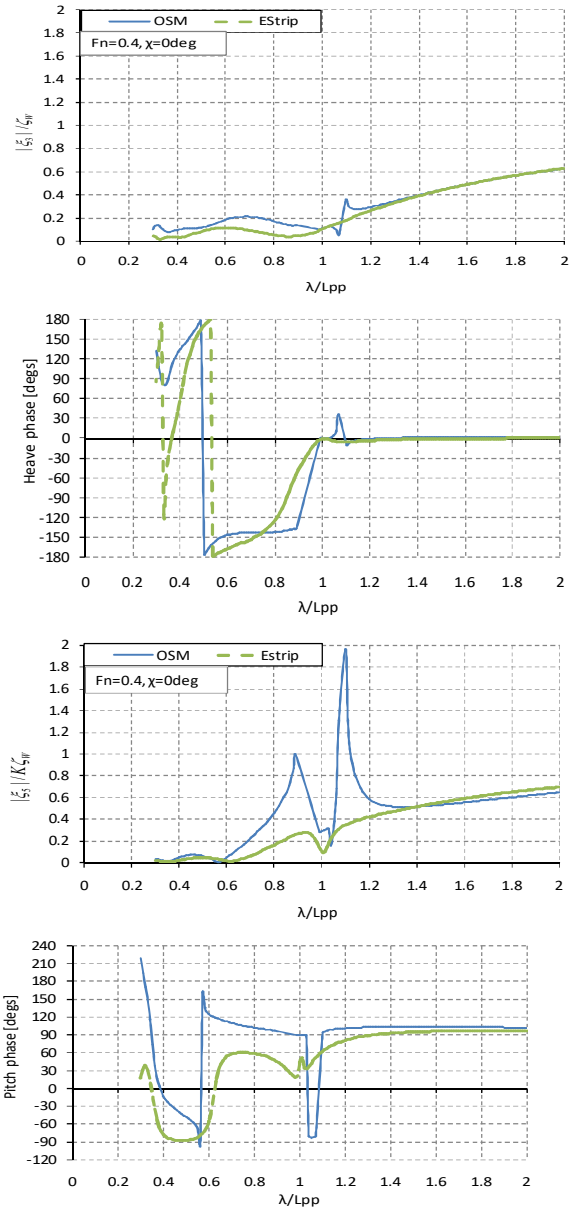

Figure A5: Heave and pitch motions of the modified Wigley ship model with different methods at Fn=0.4 in following seas.

Envelope Peaks Over Threshold (EPOT) application and verification

Kenneth Weems, *David Taylor Model Basin,* kenneth.weems@navy.mil
Vadim Belenky, *David Taylor Model Basin,* vadim.belenky@navy.mil
Bradley Campbell, *David Taylor Model Basin,* bradley.campbell@navy.mil
Vladas Pipiras, *University of North Carolina at Chapel Hill,* pipiras@email.unc.edu
Themis Sapsis, *Massachusetts Institute of Technology,* sapsis@mit.edu

ABSTRACT

The paper considers the application of the Envelope Peaks Over Threshold (EPOT) method for physics-informed statistical extrapolation of large-amplitude roll motion beyond values observed in the sample data. The area of application is direct stability assessment within the framework of the 2nd generation International Maritime Organization (IMO) intact stability criteria. The paper also describes the statistical validation of the EPOT method in the context of requirements for direct stability assessment procedures as specified in the draft interim IMO guidelines.

Keywords: *Extrapolation, Direct Stability Assessment, 2nd Generation IMO Intact Stability Criteria.*

1. INTRODUCTION

The development of advanced numerical codes for the time-domain simulation of large-amplitude ship motions (Beck and Reed, 2001; Reed and Beck, 2016) has provided new capabilities for assessing the dynamic stability of a ship in waves. The procedures for performing this type of simulation-based assessment, which is referred to as Direct Stability Assessment (DSA), have become a central part of the second generation of the International Maritime Organization (IMO) intact stability criteria, as described in Annex 1 of SDC 6 /WP.6 (IMO, 2019).

Unless deterministic criteria are used (paragraph 5.3.4 of Annex 1 SDC 6 /WP.6, IMO, 2019), the stochastic nature of ocean waves forces DSA to incorporate a statistical characterization of the ship's response in irregular waves. If a response sample of sufficient volume (*i.e.* simulated motion histories of sufficient duration) is available, a direct counting procedure can be applied (section 5.4 Annex 1 SDC 6 /WP.6, IMO, 2019). To obtain a sample of sufficient volume is impractical or even impossible; consequently, extrapolation methods are expected to be applied to the obtainable data.

Peaks over threshold / envelope peaks over threshold (POT/EPOT) is one of the extrapolation methods mentioned in paragraph 5.5.3.1 of Annex 1 SDC 6 /WP.6 (IMO, 2019). The present paper attempts to provide essential information concerning the development, application, and validation of POT/EPOT methods.

The basic idea of the POT method is to fit a Generalized Pareto Distribution (GPD) to the observed data above a particular threshold value of the response. The mathematical background of the method is the second extreme value theorem, which states that the tail of an extreme value distribution can be approximated with GPD above a "large enough" value (Pickands, 1975). A key feature of the POT extrapolation is that it can capture the nonlinearity of the large amplitude response, such as that caused by the changes in the restoring at large roll angles and in waves.

However, the POT method is only applicable to independent data points, while the roll motions of a ship are correlated because of the ship's inertia, correlated wave excitation, and "memory" in the hydrodynamic forces. The application of POT, therefore, requires an extraction of independent points from the time history, a process known as "de-clustering."

Fitting an envelope to the time history of the roll motion, as illustrated in Figure 1, is a convenient way to de-cluster the data, as the peaks of the

envelope of the roll response are sufficiently far from each other to provide the necessary independence.

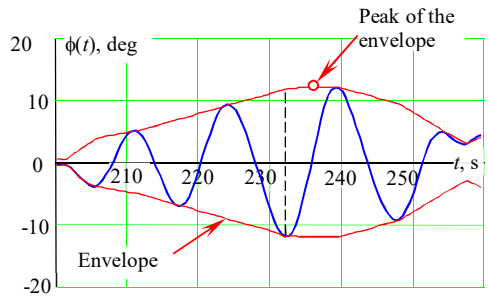

Figure 1: De-clustering using an envelope (Belenky *et al.* 2018)

The use of an envelope to de-cluster the roll motion provides the additional letter in the name of the method, so POT becomes EPOT – Envelope Peaks Over Threshold.

The fitting procedure for EPOT with GPD is described in Campbell *et al.* (2016). This fitting includes an assessment of uncertainty, which is required by paragraph 5.5.1.3 of Annex 1 SDC 6 /WP.6 (IMO, 2019). The statistical validation of the method was described by Smith and Zuzick (2015) with some details further corroborated in Weems *et al.* (2018). This procedure for the statistical validation of EPOT satisfies the requirements laid out in section 5.6 of Annex 1 SDC 6 /WP.6 (IMO, 2019).

The GPD-based EPOT method should be further improved. The upper boundary of its confidence interval is, at times, too large, making the assessment too conservative (Figure 1 of Smith and Zuzick 2015). Also, five cases occurred for which the passing rate fell short of the required value: one roll case and four acceleration cases. These failures, however, were not that dramatic: the worst passing rate was 0.84 versus the minimally required 0.90 for 100 samples. Smith (2019) provides a justification of this requirement; paragraph 5.6.7 of Annex 1 SDC 6 /WP.6 (IMO, 2019) sets the passing rate to 0.88 for 50 samples.

A way to improve the GPD-based EPOT method has become available with the determination of a relationship between the nonlinearity of roll motions and the structure of the tail of its distribution (Belenky *et al.* 2016, 2019). Including physical information into the statistical model of the tail helps to decrease the uncertainty and increase the reliability of the fitting. This approach is called a "physics-informed solution."

2. TYPES OF DISTRIBUTION TAILS

The first extreme value theorem (a.k.a. Fisher-Tippett-Gnedenko theorem) proves that a distribution of the largest value in a sample has a limit in the form of a Generalized Extreme Value (GEV) distribution. The second extreme value theorem (a.k.a. Pickands-Balkema-deHaan theorem) shows that the GEV distribution can be approximated by GPD above a threshold. Coles (2001). The tail ($y>u$) of *any* distribution can be approximated with GPD above a sufficiently large threshold. The GPD is defined by three numbers – a shape parameter ξ, a scale parameter σ, and threshold value u – and has the following form:

$$\mathrm{pdf}(y) = \begin{cases} \frac{1}{\sigma}\left(1+\xi\frac{y-u}{\sigma}\right)^{-\left(1+\frac{1}{\xi}\right)} & \xi \neq 0 \\ \frac{1}{\sigma}\exp\left(-\frac{y-u}{\sigma}\right) & \xi = 0 \end{cases} \quad (1)$$

$$\mathrm{cdf}(y) = \begin{cases} 1-\left(1+\xi\frac{y-u}{\sigma}\right)^{-1/\xi} & \xi \neq 0 \\ 1-\exp\left(-\frac{y-u}{\sigma}\right) & \xi = 0 \end{cases} \quad (2)$$

The objective of the present application is to estimate a rate of exceedance $\hat{\lambda}(c)$ of a target value $c>u$ above the threhold u:

$$\hat{\lambda}(c) = \hat{\lambda}(u)\widehat{\mathrm{cdf}(c)} \quad (3)$$

where $\hat{\lambda}(u)$ is the rate of upcrossing of the threshold u, estimated through the direct counting procedure as descibed in paragraph 5.4 of Annex 1 of SDC 6 /WP.6 (IMO, 2019).

For application of GPD, three parameters must be found: shape ξ and scale σ and threshold u. The shape and scale parameter are estimated by the maximum likelihood method. The threshold is found from a condition of GPD applicability; Campbell *et al.* (2016). The scale parameter σ is positive, while the shape parameter ξ can be either positive or negative. A negative shape parameter imposes a limitation on the expressions in parenthesis of equations (1) and (2) and formally introduces a right bound to the distribution:

$$\mathrm{pdf}(y) = 0, \quad if \quad y > u - \frac{\sigma}{\xi} \text{ and } \xi < 0 \quad (4)$$

The shape parameter defines the type of tail: heavy, exponential, or light, as shown in Figure 2[1].

The exponential tail (ξ=0) describes the extreme values of a normal distribution. The heavy tail (ξ>0) is above the exponential tail, while the light tail (ξ<0) is below. As the exponential tail is the smallest infinite tail, the light tail has a limit, which is its right bound. The heavy tail is unbounded.

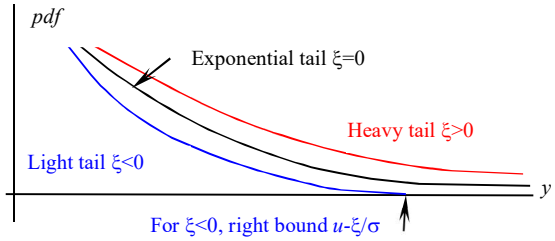

Figure 2: Types of tails (Belenky *et al.* 2018)

3. STRUCTURE OF ROLL TAIL

The roll restoring arm (GZ) curves of most ships have a limited range of stability, leading to the appearance of an unstable equilibria at the angle of vanishing stability, as well a maximum value of GZ. This configuration leads to a heavy tail after the maximum of the GZ curve, which switches to a light tail in the immediate vicinity of the angle of vanishing stability. Figure 3 shows such a distribution, computed for a dynamical system with piecewise linear (PWL) restoring.

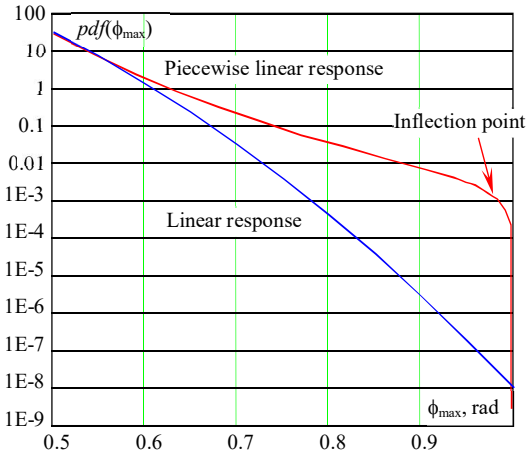

Figure 3: PDFs of peaks of linear response and PWL response (Belenky *et al.*, 2016)

The piecewise linear approximation of the GZ curve allows a closed-form solution for the tail of the distribution of the peaks and instantaneous values of the roll angle (Belenky *et al.* 2016, 2019). Belenky *et al.* (2018) presents an argument for why the piecewise linear result can be generalized for any dynamical system with softening stiffness, including the roll motions of many ships.

The roll angles associated with dynamic stability failures (*e.g.* 50 degrees per paragraph 2.3.1 of the 2008 IS Code, IMO, 2008) are usually located around and beyond the angle of the maximum of the GZ curve. Therefore, to assume a heavy tail appears appropriate for extrapolation problems associated with dynamical stability failures.

4. FITTING HEAVY TAIL FOR ROLL

When the shape parameter ξ>0 (heavy tail) and threshold value $u = \sigma/\xi$, the GPD is equivalent to a Pareto distribution with scale $y_m = \sigma/\xi$ and shape $\alpha = 1/\xi$:

$$\mathrm{pdf}(y) = \frac{\alpha y_m^{\alpha}}{y^{\alpha+1}} \tag{5}$$

The conditional probability of exceedance of a target value y associated with dynamic stability failure is expressed as:

$$\mathrm{P}(Y > y | Y > u) = \left(\frac{u}{y}\right)^{\alpha} = \left(\frac{y}{u}\right)^{-\frac{1}{\xi}} \tag{6}$$

Here, the threshold u does not have to be the same as in the GPD case. A method for finding the threshold and estimating the shape parameter is proposed in Belenky *et al.* (2018), which is based on Beirlant, *et al.* (2004), Dupuis and Victoria-Feser (2006), and Mager (2015).

To extrapolate with equation (6), the threshold is found from applicability considerations so only one parameter needs to be fitted. Decreasing the number of parameters from two (in case if the GPD is used) to one decreases the statistical uncertainity. This is how the physical understanding of the process propagates into a statistical model.

The input data for fitting is designated ϕ_e and consists of N independent peaks extracted from the envelope of the roll time histories (Figure 1). The method is applied to a sample sorted in descending order – a.k.a. order statistics:

$$\mathrm{Y} = \mathrm{sort}_{\mathrm{desc}}(\phi_e) \tag{7}$$

[1] No universally accepted definition of heavy and light tail exists. Other souces may use heavy/light tail in a different context.

The Hill estimator provides the shape parameter ξ:

$$\hat{\xi}_k = \frac{1}{k}\sum_{i=1}^{k} \log\left(\frac{Y_i}{Y_k}\right) \quad (8)$$

where the index k refers to the number of upper order statistics used in the estimation. Mager (2015) suggests the first index $k = \min(40, 0.02N)$, while the last (largest) value for the index taken as $0.2N$.

The threshold u is found by an index that corresponds to a minimum of the mean squares prediction error function (Figure 4):

$$\hat{\Gamma}(k) = \frac{1}{\hat{\xi}_k^{\,2} k^1}\sum_{i=1}^{k} \frac{\left(\log\left(\frac{Y_{i-1}}{Y_{k-1}}\right) + \hat{\xi}_k \log\left(\frac{i}{k+1}\right)\right)^2}{\left(\sum_{j=i}^{k} j^{-2}\right)} + \frac{2}{k}\sum_{i=1}^{k} \frac{\left(\log\left(\frac{i}{k+1}\right)\right)^2}{\left(\sum_{j=i}^{k} j^{-2}\right)} - 1 \quad (9)$$

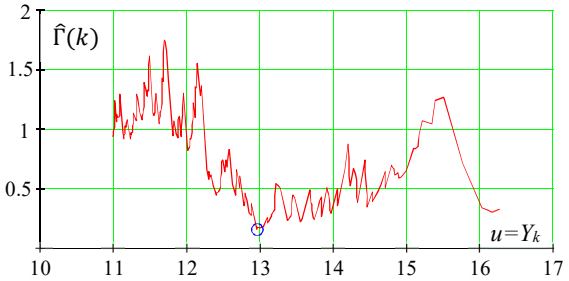

Figure 4: Mean squares prediction error function

Once the index k corresponding to a minimum of $\hat{\Gamma}$, is found, the threshold is set as:

$$u = Y_k \quad (10)$$

The confidence interval for the extrapolated value is computed assuming a normal distribution for the estimate of the shape parameter $\hat{\xi}$. Its variance estimate is expressed as:

$$\widehat{Var}(\hat{\xi}) = \frac{\hat{\xi}^2}{k} \quad (11)$$

The boundries of the confidence interval of the estimate are:

$$\hat{\xi}_{up,low} = \hat{\xi} \pm K_\beta \sqrt{\widehat{Var}(\hat{\xi})} \quad (12)$$

where K_β is a half of a non-dimensional confidence interval computed as a normal quantile of $0.5(1+\beta)$, where β is the confidence probability. For β=0.95, K_β=1.96.

The extrapolated estimate of the exceedance rate of target value c can be computed as:

$$\hat{\lambda}(c) = \hat{\lambda}(u)\left(\frac{c}{u}\right)^{-1/\hat{\xi}} \quad (13)$$

where $\hat{\lambda}(u)$ is the rate of upcrossing of threshold u, estimated through the direct counting procedure with its confidence interval, as described in paragraph 5.4 of Annex 1 of SDC 6 /WP.6 (IMO, 2019).

Boundaries for the extrapolated value are computed through the lower and upper boundaries of the upcrossing rate estimate $\hat{\lambda}_{low,up}(u)$ and the shape parameter estimate $\hat{\xi}_{low,up}$:

$$\begin{cases} \hat{\lambda}_{low}(c) = \hat{\lambda}_{low}(u)\left(\frac{c}{u}\right)^{-1/\hat{\xi}_{low}} \\ \hat{\lambda}_{up}(c) = \hat{\lambda}_{up}(u)\left(\frac{c}{u}\right)^{-1/\hat{\xi}_{up}} \end{cases} \quad (14)$$

Equations (14) contain a product of the boundaries of two estimates. If the desired confidence probability for the entire extrapolated estimate $\hat{\lambda}(c)$ is to be β = 0.95 as recommended in 5.4 of Annex 1 of SDC 6 /WP.6 (IMO, 2019), then the confidence probabilities for each estimate $\hat{\lambda}(u)$ and $\hat{\xi}$ must be set as:

$$\beta_1 = \sqrt{\beta} = \sqrt{0.95} = 0.975 \quad (15)$$

In order to account for the difference in the confidence probability, K_β is set to 2.236 in equation (12) and the confidence 0.975 is used in the direct counting procedure (paragraph 5.4.4 of Annex 1 of SDC 6 /WP.6, IMO, 2019) instead of 0.95.

5. STATISTICAL VALIDATION

A statistical validation of heavy tails was carried out following the recommendations of section 5.6 of Annex 1 of SDC 6 /WP.6 (IMO, 2019).

Per the recommedation in paragraph 5.6.3, a reduced order mathematical model in the form of volume-based 3-DOF calculations was applied as described in Weems *et al.* (2018). This fast code creates very large samples of data in which large roll angles associated with rare failures are observable. The observations estimates a "true value" from direct counting.

A series of validation data sets was computed for the ONR tumblehome configuration (Bishop *et al.* 2005) with KG = 7.5 m, resulting in GM = 2.2 m. Simulations were performed with independent pseudo-random realizations of a seaway by a Bretschneider spectrum with a significant wave height of 9 m and a modal period of 15 seconds. The ship speed was set to 6 knots. Other simulations parameters, including the total simulation time determined the true value, are presented in Table 1.

Section 5.6 of Annex 1 of SDC 6 /WP.6 (IMO,

2019) does not specifiy the target values, which would be the angle associated with dynamic stability failure. This value may be different for different ships, depending on considerations such as the location of the floodable opening. Thus, a number of target angles will be examined.

Table 1: "True value" calculations

Headings Deg.	Total time, hrs	Number of targets	Largest target	Number of exceedances of largest target
15	570,000	5	20	14
22.5	200,000	7	27.5	16
30	200,000	13	45	9
37.5	200,000	15	60	7
45	690,000	15	70	8
60	600,000	15	70	12
90	690,000	9	37.5	12
135	690,000	3	20	6

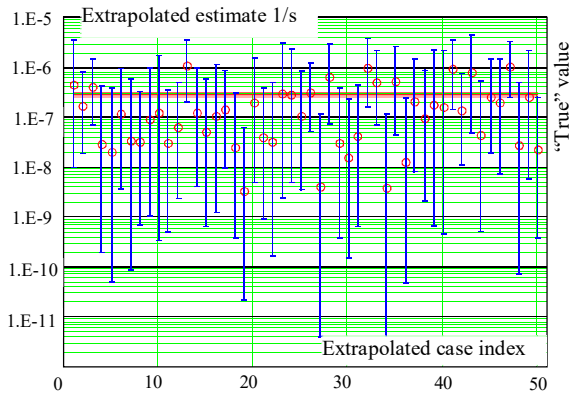

Figure 5: Example of extrapolation validation for a heading of 45 degrees and target value of 45 degrees

The extrapolation procedure was applied to a series of small subsets of this large sample, and the extrapolated estimates were compared with the "true value." Figure 5 shows an example comparison for a 45 degree heading (stern quartering seas) and a target roll value of 45 degrees. Fifty (50) extrapolation estimates occur, each computed from 100 hours of data. The main index of performance is the passing rate, which indicates the percentage of successful extrapolations. An extrapolation is considered successful if the confidence interval of the extrapolated exeedence rate includes the "true value." The example shown in Figure 5 has 45 successful extrapolations, resulting in a passing rate of 90%.

In the three-tiered validation methodology of Smith and Zuzick (2015), the tiers are defined as:

1) all extrapolations for a single target value,

2) extrapolations for all available target values, and

3) extrapolations for all available operational and environmental conditions.

The tier 1 validation is a set of comparisons of extrapolated estimates with the true value. Its example is shown in Figure 5.

The second tier of statistical validation considers all available target angles. The passing rates are shown in Figure 6. An acceptable passing rate for 50 extrapolation data sets is from 0.88 to 1 (Smith, 2019, and paragraph 5.6.7 of Annex 1 of SDC 6 /WP.6, IMO, 2019). This variation of the passing rate can be explained by the natural variability of the statistical estimates. The extrapolations are acceptable for all targets, excluding 50 and 60 degrees, for which the passing rates fell to 0.86. The average passing rate for the 45 degrees heading is 0.90, which is within the acceptable range.

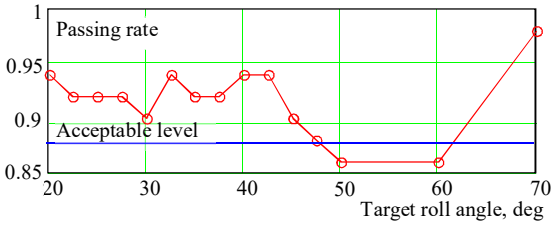

Figure 6: Passing rate for heading of 45 degrees

The third tier of validation assesses the performance over all available conditions. The passing rates are shown in Figure 7. Two lines are shown: one corresponds to an averaged passing rate over all target values, while the other corresponds to the smallest passing rate value encountered among all the target values. For a 45 degree heading, the latter corresponds to a minimum shown in Figure 6. Obviously, the extrapolation did not work for the heading of 135 degrees.

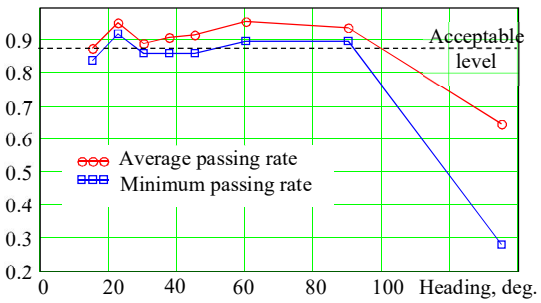

Figure 7: Passing rate for all headings

Belenky *et al.* (2018) looked into the reasons why the validation at the heading of 135 degrees failed. The reason is very likely to be insufficient data in the nonlinear region. That work considers possible indications of sufficient/insufficient data for extrapolation.

Belenky *et al.* (2018) also considered other performance indicators of the EPOT method. The average conservative distance (measure of practical statistical uncertainty) does not exceed an order of magnitude, in terms of the exceedance rate. This performance seems to be sufficient to distinguish between realistic and distant chances of dynamic stability failure.

Overall, the validity of EPOT, except for the 135 degree heading, can be characterized as "almost there." The passing rate falls short of the required 0.88 for a few cases, but not by much. The averaged passing rates stay above 0.88 for all the cases except for the heading of 135 degrees. The decrease of uncertainty in comparison with the two-parameter GPD is substantial and brings EPOT closer to practical application.

6. SUMMARY AND CONCLUSIONS

The paper considers an EPOT extrapolation method for roll motion in the context of direct stability assessment (DSA) and the second-generation IMO intact stability criteria. The main objective was how to make EPOT method a practical tool for DSA.

An envelope of the motion time histories generates a set of independent peak values, and a Generalized Pareto Distribution approximates the tail of the peak distribution above a threshold. The GPD model is completely data-driven, and its statistical uncertainty reflects the volume of the available sample. For rare events and extreme values, the statistical uncertainty of the prediction may be large. To reduce the uncertainty without having to increase the sample volume, physical information can be incorporated into the statistical model.

Based on previous research, the tail of the distribution of roll peaks must be heavy because of the softening nonlinearity of roll stiffness. The application of the tail of the Pareto distribution within the framework of the EPOT method provides an effective physics-informed statistical model.

The paper describes statistical validation carried out following the requirements of the draft interim IMO guidlines on the specification of direct stability assessment procedures.

ACKNOWLEDGEMENT

The work described in this paper has been funded by the Office of Naval Research (ONR) under Dr. Woei-Min Lin and by the NSWCCD Independent Applied Research (IAR) program under Dr. Jack Price. The participation of Prof. Sapsis was facilitated by the NSWCCD Summer Faculty Program, while the participation of Prof. Pipiras was facilitated by NSWCCD Summer Faculty and Sabbatical Programs, both of which are also managed by Dr. Jack Price.

The authors are very grateful for the support that made this work possible.

REFERENCES

Beck, R. F., and A. M. Reed (2001). "Modern Computational Methods for Ships in a Seaway". *SNAME Trans.* Vol. 109, pp. 1–51.

Beirlant, J., Y. Goegebeur, J. Teugels, and J. Segers (2004). *Statistics of Extremes*, Wiley Series in Probability and Statistics. John Wiley & Sons, Ltd., Chichester.

Belenky, V., D. Glotzer, V. Pipiras, and T. Sapsis (2016). "On the Tail of Nonlinear Roll Motions". *Proc.* 15th Intl. Ship Stability Workshop, Stockholm (ISSW2016), Sweden, pp. 109-114.

Belenky, V., K. Weems, V. Pipiras, D. Glotzer, and T. Sapsis (2018). "Tail Structure of Roll and Metric of Capsizing in Irregular Waves". *Proc.* 32nd Symp. Naval Hydrodynamics, Hamburg, Germany.

Belenky, V., D. Glotzer, V. Pipiras, and T. Sapsis (2019). "Distribution tail structure and extreme value analysis of constrained piecewise linear oscillators". *Probabilistic Engineering Mechanics* (to appear).

Bishop, R. C., W. Belknap, C. Turner, B. Simon, and J. H. Kim (2005). "Parametric Investigation on the Influence of GM, Roll damping, and Above-Water Form on the Roll Response of Model 5613", Report NSWCCD-50-TR-2005/027.

Campbell, B., V. Belenky, and V. Pipiras (2016). "Application of the Envelope Peaks over Threshold (EPOT) Method for Probabilistic Assessment of Dynamic Stability", *Ocean Engineering,* Vol. 120, pp. 298-304.

Coles, S. (2001). *An Introduction to Statistical Modeling of Extreme Values*. Springer, London.

Dupuis, D. J., and M.-P. Victoria-Feser (2006). "A robust prediction error criterion for Pareto modelling of upper tails," *Canadian Journal of Statistics*, Vol. 34, 2006, pp. 639–658.

International Maritime Organization (2008). *International Code on Intact Stability, 2008* ("2008 IS Code").

International Maritime Organization (2019). IMO SDC 6 /WP.6 Finalization of Second Generation Intact Stability Criteria. Report of the Expert's Group on Intact Stability, 7 February 2019.

Mager, J. (2015). "Automatic threshold selection of the peaks over threshold method", Master's Thesis, Technische Universitat Munchen.

Pickands, J. (1975). "Statistical Inference Using Extreme Order Statistics," *The Annals of Statistics*, Vol. 3, No. 1, pp. 119-131.

Reed, A. M., and R. F. Beck (2016). "Advances in the Predictive Capability for Ship Dynamics in Extreme Waves", *SNAME Trans.,* Vol. 124.

Smith, T. C., and A. Zuzick (2015). "Validation of Statistical Extrapolation Methods for Large Motion Prediction," *Proc.* 12th Intl. Conf. on Stability of Ships and Ocean Vehicles (STAB2015), Glasgow, UK, pp. 1127-1140.

Smith, T.C. (2019). "Validation Approach for Statistical Extrapolation", Chapter 34 of *Contemporary Ideas on Ship Stability*, Belenky, V., Neves, M., Spyrou, K., Umeda, N., van Walree, F., eds., Springer, ISBN 978-3-030-00514-6, pp. 573-589.

Weems, K., V. Belenky, and K. Spyrou (2018). "Numerical Simulations for Validating Models of Extreme Ship Motions in Irregular Waves" *Proc.* 32nd Symp. Naval Hydrodynamics, Hamburg, Germany.

On extending multifidelity uncertainty quantification methods from non-rare to rare problems

Brendan Brown, *University of North Carolina at Chapel Hill*
Vladas Pipiras, *University of North Carolina at Chapel Hill*

ABSTRACT

When modeling a random phenomenon (e.g. ship motions in irregular seas), data are often available from multiple sources, or models, of varying fidelity, those with higher fidelity carrying higher costs. Multifidelity uncertainty quantification (UQ) offers tools that allow using lower-fidelity and lower-cost models to inform decisions being made about high-fidelity models. With a few exceptions though, much of the focus of the multifidelity UQ literature has been on characterizing uncertainty related to averages, in the context of non-rare problems where data are available to estimate these averages directly. In this work, we extend some multifidelity UQ methods to estimation of probabilities of rare events, possibly those that have not been observed in high-fidelity data. The suggested approach is based on bivariate extreme value theory, applied to simultaneously large observations from low-fidelity and high-fidelity models. The ideas are illustrated on simulated data associated with ship motions. It is not assumed that the reader is familiar with multifidelity UQ, with the discussion focusing on the most basic setting and building naturally from the recalled methods for non-rare problems.

Keywords: *Uncertainty Quantification, Multifidelity Estimators, Bivariate Extremes, Sampling Variability, Probability of Rare Event, Nonlinear Random Oscillator, Ship Motions.*

1. INTRODUCTION

When studying random phenomena of interest, it is common to examine data from multiple sources or models. For example, ship motions or loads data can be collected from a model basin or sea trials, or generated from various computer programs, e.g. SimpleCode (Weems and Wunrow, 2013), LAMP (Lin and Yue, 1991). With data at hand, a common goal is to estimate some quantities of interest, for example, mean, single significance amplitude (SSA), etc. In this case, how should different estimates of the same quantities of interest obtained across multiple models be interpreted? If one of the models is less "expensive" to run but less accurate, how can it be used in conjunction with the more expensive and more accurate models in order to estimate better the quantities of interest? What does this say about differences among the models?

These questions have been studied from various angles as part of the Uncertainty Quantification (UQ) literature, in particular, in the direction of the so-called multifidelity (MF) methods. See, for example, a recent survey paper by Peherstorfer *et al.* (2018). As above, at the most basic level, the underlying assumption of these methods is the availability of two sets of data, one associated with the variable X_e and the other with the variable X_s, referring to expensive (true, high-fidelity, etc.) model and simple (low-fidelity, surrogate, etc.) model, respectively. (We shall use the terms and subscripts for "expensive" and "simple" throughout this work, in lieu of perhaps more sophisticated "high-fidelity" and "low-fidelity.") For example, X_e could refer to CFD and X_s to LAMP calculations. The interest is in estimating the mean (or the expected value) $\mathbb{E}(X_e)$ of the expensive response, or some function thereof, having the data from both expensive and simple models. Construction and calibration of simple models also make an important part of MF methods, but these will not be our focus here. That is, we suppose that data on X_e and X_s are given and ask questions about implications of this setting.

Estimation of the mean through available MF methods concerns non-rare behavior of the studied random phenomenon in that there is enough variability in collected data to make an informed decision about behavior of the mean. In this work, we are interested in analogous MF methods but for

rare problems. A working example throughout this paper is that of estimating an exceedance probability $\mathbb{P}(X_e > x)$ for some large threshold x, so that $X_e > x$ is a rare event. The latter event might be so rare that it is not even observed in the data from the expensive model. It should be noted nevertheless that in the latter case, the rare probability could, in principle, still be estimated through the approach of the statistical Extreme Value Theory (EVT); see e.g. Coles (2001). This approach for extreme ship motions, capsizing and other rare phenomena has been studied quite extensively by the second author of this work and collaborators over the past number of years (e.g. Campbell *et al.*, 2016; Belenky *et al.*, 2018, Belenky *et al.*, 2019).

In the context of estimating a rare exceedance probability $\mathbb{P}(X_e > x)$, we are thus interested in whether and how the data for the variable X_s from the simple model might be useful. For example, since the simple model is thought to be inexpensive to run, the events $X_s > x$ could, in principle, be observed in really long records of the model. Then, could one use the direct estimate of the probability $\mathbb{P}(X_s > x)$ for that of $\mathbb{P}(X_e > x)$? These are the kind of questions that will be discussed in this work, within an introduced mathematically justified framework.

We are not aware of other works pursuing this exact line of investigation. The closest are perhaps MF methods for failure probabilities as in e.g. Peherstorfer *et al.* (2017). These failure probabilities though are still estimated directly, perhaps in conjunction with importance sampling, whereas in this work, we do so indirectly through EVT. For this reason, the reader should also expect our approach to appear more complex, especially to those unfamiliar with EVT.

The MF methods discussed in this work will be illustrated on synthetic data generated from a non-linear random oscillator mimicking ship rolling. It should be noted that the synthetic data framework is for illustration purposes only; there is nothing more expensive or simpler about either model in the synthesis.

The rest of this work is organized as follows. Section 2 sets some notation and introduces the more probabilistic notions used throughout this work. In Sections 3 and 4, we discuss and illustrate the most basic available MF estimator when making inference about the expected value (mean) in non-rare problems. Sections 5 and 6 extend this MF approach to estimating probabilities of rare events. Basic bivariate EVT is recalled and employed in developing the approach in Section 5. Section 7 concludes.

2. BASIC SETTING AND NOTATION

At the most basic level, we assume the following setting. We observe two signals: $X_e(t)$, $t \in [0, T_e]$, from an expensive, true, high- (or maybe engineering-level) fidelity model, and $X_s(t)$, $t \in [0, T_s]$, from simple, surrogate, low-fidelity model. Again, the terms "expensive" and "simple" will be used exclusively below. The observation window sizes T_e and T_s are such that $T_e \ll T_s$, reflecting the idea that the simple model can be run for a much longer period of time at low cost, though the exact costs will be mostly ignored here. More importantly, we assume that the expensive and simple models are run under the same "conditions" in that the error process

$$\epsilon(t) = X_e(t) - X_s(t), \; t \in [0, T_e], \tag{1}$$

is meaningful over the smaller observation window $[0, T_e]$.

Furthermore, the following notation will be used: $\mu(Z) = \mathbb{E}(Z)$, $\sigma^2(Z) = Var(Z)$ will stand for a theoretical mean and variance, respectively, of a variable Z or a stationary process $Z(t)$; $\hat{\mu}(Z)$, $\hat{\sigma}^2(Z)$ will denote statistical estimators of the latter quantities from data; $\bar{Z}_T$ will refer to the sample average of $Z(t)$ over time interval $[0, T]$. The hats used for other quantities will also refer to estimators. For example, $\widehat{\mathbb{P}}$ will refer to a probability estimate.

3. METHODS FOR NON-RARE PROBLEMS

In the setting described in Section 2, suppose that one is interested in estimating the mean $\mu(X_e)$ of X_e. A multifidelity (MF) estimator of the mean is defined as

$$\hat{\mu}_{mf}(X_e) = \bar{X}_{s,T_s} + \bar{\epsilon}_{T_e} \tag{2}$$

or, equivalently, as

$$\begin{aligned} \hat{\mu}_{mf}(X_e) &= \bar{X}_{s,T_s} + \left(\bar{X}_{e,T_e} - \bar{X}_{s,T_e}\right) \\ &= \bar{X}_{e,T_e} + \left(\bar{X}_{s,T_s} - \bar{X}_{s,T_e}\right), \end{aligned} \tag{3}$$

where the last expression is a simple rearrangement of the previous one. For comparison, let also

$$\hat{\mu}_0(X_e) = \bar{X}_{e,T_e} \tag{4}$$

be the baseline estimator of the mean that uses only the expensive data.

We make several observations that might be useful to readers unfamiliar with MF estimators. Note that $\hat{\mu}_{mf}(X_e)$ is unbiased for $\mu(X_e)$ even if $\mu(X_e) \neq \mu(X_s)$. This follows from Eq. (3) since

$$\mathbb{E}\hat{\mu}_{mf}(X_e) = \mathbb{E}\bar{X}_{s,T_s} + \left(\mathbb{E}\bar{X}_{e,T_e} - \mathbb{E}\bar{X}_{s,T_e}\right) = \mu(X_s) + \left(\mu(X_e) - \mu(X_s)\right) = \mu(X_e). \quad (5)$$

Another key observation and the crux of MF methods is that $\hat{\mu}_{mf}(X_e)$ can potentially do better in estimating the mean than the baseline estimator $\hat{\mu}_0(X_e)$, in the sense that

$$Var\left(\hat{\mu}_{mf}(X_e)\right) < Var\left(\hat{\mu}_0(X_e)\right). \quad (6)$$

Indeed, suppose for simplicity that the two terms in Eq. (2) are independent so that the variance of their sum is the sum of the variances. The variance of the sample average $\bar{Z}_T$ of a stationary process $Z(t)$ behaves for large T as

$$Var(\bar{Z}_T) \approx \frac{\Pi(Z)}{T}, \quad (7)$$

where the so-called long-run variance $\Pi(Z) = \int_{-\infty}^{\infty} \gamma_Z(u)du$ accounts for temporal dependence in the process $Z(t)$ having the auto-covariance function $\gamma_Z(u) = Cov(Z(t+u), Z(t))$ at lag u. Then, Eq. (5) is equivalent (for large T_e and T_s) to

$$\frac{\Pi(X_s)}{T_s} + \frac{\Pi(\epsilon)}{T_e} < \frac{\Pi(X_e)}{T_e}, \quad (8)$$

which provides a verifiable condition for the MF estimator to outperform the baseline. As seen from Eq. (8), this will happen if

$$T_e \ll T_s \quad \text{and} \quad \Pi(\epsilon) < \Pi(X_e). \quad (9)$$

The first relation of Eq. (9) is natural in the scenario of low costs for the simple model. The second relation in Eq. (9) states effectively that the error between the signals of the simple and expensive models has to be small compared to the original expensive signal. This is also intuitive as the simple model should be useful only if it approximates the expensive model well. We should also note that the key consequence of Eqs. (6) and (8) is that a normal confidence interval for the mean $\mu(X_e)$ would be smaller when using $\hat{\mu}_{mf}(X_e)$ as its length is determined by $Var(\hat{\mu}_{mf}(X_e))$.

In practice, the above discussion also suggests how to proceed in estimating the mean with the simple and expensive model data. First, estimate the long-run variances $\Pi(\epsilon)$ and $\Pi(X_e)$. Estimation of these quantities is discussed in detail in e.g. Pipiras *et al.* (2018). Second, compare the resulting estimates $\widehat{\Pi}(\epsilon)$ and $\widehat{\Pi}(X_e)$. If $\widehat{\Pi}(\epsilon)$ is smaller than $\widehat{\Pi}(X_e)$, then the MF estimator should be preferred to for sufficiently large T_s. Again, this would translate into smaller confidence intervals for $\mu(X_e)$.

It should also be stressed that though the case of the mean seems simplistic, it is at the core of estimation of many quantities. For example, the variance $Var(X_e) = \mu(X_e{}^2) - (\mu(X_e))^2$ is expressed through the means of a process and its square and can be dealt with similarly.

4. ILLUSTRATION FOR NON-RARE PROBLEMS

To illustrate the procedure of Section 3, we use synthetic data from a non-linear random oscillator model describing qualitatively ship rolling. More specifically, suppose the dynamics of a stationary process $X(t)$ is governed by the equation

$$\ddot{X}(t) + 2\delta\dot{X}(t) + r\big(X(t)\big) = Z(t), \quad (10)$$

where $\delta > 0$ is a damping parameter, $r(x)$ is a restoring force and $Z(t)$ is a zero-mean random excitation. The excitation $Z(t)$ is commonly assumed to be a Gaussian stationary process, with the spectral density suggested by e.g. the Bretschneider spectrum for wave elevations. We further assume a piecewise linear restoring force $r(x)$, given by

$$r(x) = \begin{cases} \omega_0^2 x, & \text{if } |x| \le x_m, \\ -k\omega_0^2(x - x_m) + \omega_0^2 x_m, & \text{if } |x| > x_m, \end{cases} \quad (11)$$

where ω_0 is a natural frequency of the system, x_m is referred to as a knuckle point (separating the linear and nonlinear regimes) and $k > 0$ enters into the negative slope of the nonlinear part. The restoring force has a softening shape for $|x| > x_m$, typical in modeling ship motions.

Figure 1 presents time plots of two realizations of the random oscillator model in Eq. (10), labeled expensive and simple. For the expensive signal X_e, the values $w_0 = 0.6$, $\delta = 0.15w_0$, $k = 1$, $x_m = 30\pi/180$ are taken. The same values were used for the simple signal X_s, except that $k = 0.3$ and the variance for the excitation is smaller. We emphasize again that these expensive and simple signals are called so for illustration purposes only; there is nothing more expensive or simpler, or high- or low-fidelity about either of the signals. The signals were generated for $T_e = 3600$ seconds (1 hour) and $T_s =$

36000 seconds (10 hours). Figure 2 depicts the time plot of the error process $\epsilon(t)$ between the two signals for the first 360 seconds. Note that the vertical scale in Figure 2 is much smaller compared to that in Figure 1, suggesting that the simple model might be a good approximation for the expensive model.

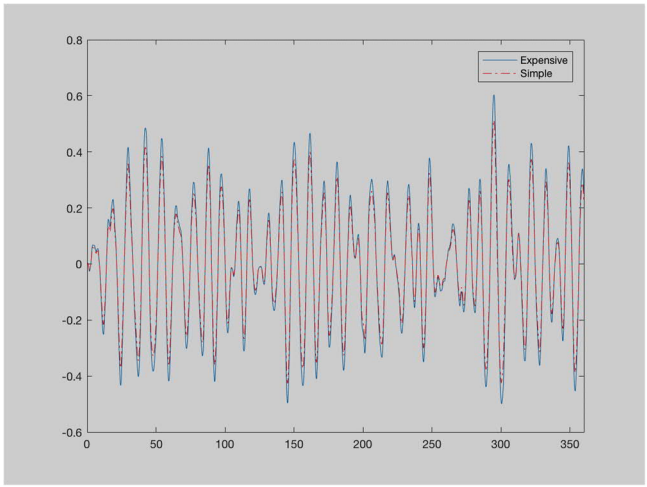

Figure 1: Two realizations of random oscillator model.

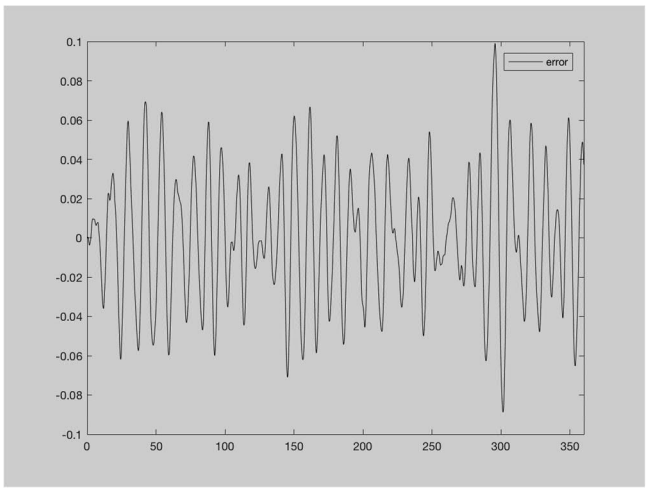

Figure 2: The error process for two realizations in Figure 1.

For the two signals, the long-run variances estimated through triangular kernel and "decorrelation time" bandwidth (see Pipiras *et al.*, 2018) were $\widehat{\Pi}(\epsilon) = 0.0001$ and $\widehat{\Pi}(X_e) = 0.0051$. Clearly, $\widehat{\Pi}(\epsilon)$ is smaller than $\widehat{\Pi}(X_e)$ by an order of magnitude. In this case, the MF estimator is preferred for T_s larger than T_e. The confidence interval for the mean resulting from the MF estimator is depicted in Figure 3 (the right vertical segment) in comparison to the confidence interval if the baseline estimator is used (the left vertical segment). The two mean estimates are indicated as circles on the two confidence intervals.

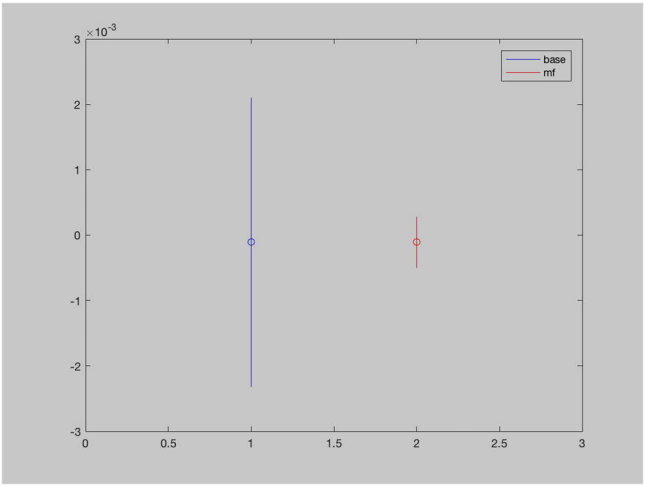

Figure 3: Confidence intervals for the mean based on the baseline and the MF estimator.

Figure 3 shows a clear benefit of the MF estimator and the simple signal in this case. Again, what makes this possible is a relatively small variance of the error process for the two signals and the fact that $T_s > T_e$. This should not be taken for granted in a given situation and might require proper calibration of the simple and expensive models.

5. METHODS FOR RARE PROBLEMS

We would like to extend the methods described in Sections 3 and 4 to estimation of an exceedance probability $\mathbb{P}(X_e > x)$ for large target x. For oscillating signals related to ship dynamics, X_e in the exceedance probability typically represents suitable peaks of the signal, perhaps even peaks of an envelope (e.g. Campbell *et al.*, 2016). To simplify the discussion and for technical reasons, we shall further assume that X_e represents block maxima of the peaks. If needed, block maxima exceeding a critical value could be translated to peak exceedances per unit time.

Figure 4 illustrates the notions of peaks and block maxima on the same synthetic data as in Section 3, where 10 hours of data are used with both expensive and simple models. The figure depicts a scatterplot of peaks from the expensive and simple signals, and in a darker shade, the respective block maxima are marked for 39 blocks of size 30. In this setting, for example, one might be interested to estimate $\mathbb{P}(X_e > 1.5)$, with no occurrences of the event $X_e > 1.5$ in the data as can be seen from Figure 4. Would having potentially larger simple model data for X_s help in this case, and through what method?

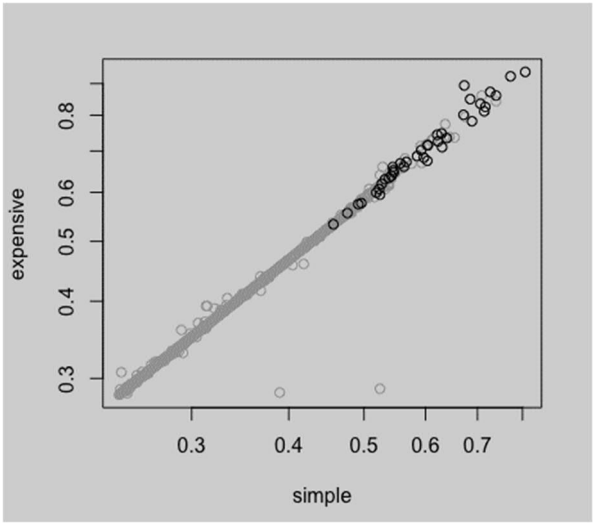

Figure 4: Scatterplot of peaks and block maxima for the simple and expensive models.

Before addressing these questions, it is instructive to discuss what the baseline estimator for $\mathbb{P}(X_e > x)$ is, without the availability of X_s from the simple model. It is known from the statistical Extreme Value Theory (EVT) that the distribution of the block maxima follows approximately that of a generalized extreme value (GEV) distribution as

$$\mathbb{P}(X_e \le z_1) = e^{-y_1}, \qquad (12)$$

where

$$y_1 = y_1(z_1) = \left(1 + \xi_1 \frac{z_1 - \mu_1}{\sigma_1}\right)_+^{-1/\xi_1} \qquad (13)$$

with location, scale and shape parameters μ_1, σ_1 and ξ_1, respectively, and the subscript + indicating the positive part of the function. After fitting these parameters to the data, the GEV distribution in Eq. (12) would be used to "extrapolate" into the tail $X_e > x$. A confidence interval for $\mathbb{P}(X_e > x)$ could also be provided.

Suppose now that the block maxima X_s are available for the simple model as well. To see how they could be used together with X_e, we need an analogue of Eq. (5). At the population (theoretical) level, consider

$$\mathbb{P}(X_e > x) = \mathbb{P}(X_s > y) + (\mathbb{P}(X_e > x) - \mathbb{P}(X_s > y))$$

and, after rewriting the difference in the parentheses,

$$\mathbb{P}(X_e > x) = \mathbb{P}(X_s > y) + \mathbb{P}(\epsilon), \qquad (14)$$

where

$$\mathbb{P}(\epsilon) = \mathbb{P}(X_e > x, X_s \le y) - \mathbb{P}(X_e \le x, X_s > y). \qquad (15)$$

We view Eqs. (14) and (15) as analogues of Eq. (5). That is, $\mathbb{P}(X_e > x)$ for the expensive model is being replaced by $\mathbb{P}(X_s > y)$ for the simple model, with the error probability $\mathbb{P}(\epsilon)$. The error probability in Eq. (15) is expressed in terms of the joint behavior of X_e and X_s, and could be expected small if the simple model is a good approximation to the expensive model at the extremes. The value y could but does not have to be equal to x; in fact, in analogy to Eq. (5) where $\mu(X_e)$ and $\mu(X_s)$ can be different, having different y and x can be critical.

Turning to estimation, the probability $\mathbb{P}(X_s > y)$ in Eq. (14) could, in principle, be estimated directly if needed, by taking a large enough T_s. The probabilities in Eq. (15), however, need to be estimated from the data on X_e and X_s gathered under the same conditions over the smaller observation window of size T_e. This is where bivariate GEV distributions come in, as those modeling the joint behavior of X_e and X_s. As in Eqs. (12) and (13), let

$$\mathbb{P}(X_s \le z_2) = e^{-y_2}, \qquad (16)$$

where

$$y_2 = y_2(z_2) = \left(1 + \xi_2 \frac{z_2 - \mu_2}{\sigma_2}\right)_+^{-1/\xi_2} \qquad (17)$$

with a similar set of parameters. The cross-dependence between the two variables X_e and X_s of a bivariate GEV is described through a dependence function A, for example, as in

$$\mathbb{P}(X_e \le z_1, X_s \le z_2) = e^{-(y_1+y_2)A\left(\frac{y_1}{y_1+y_2}\right)}, \qquad (18)$$

where y_1 and y_2 are given in Eqs. (13) and (17). The function $A(t)$ is defined for $t \in [0,1]$, is convex and satisfies $\max(t, 1-t) \le A(t) \le 1, A(0) = A(1) = 1$. (See Figure 5 for a plot of such functions.) The case of $A(t) = 1$ for all $t \in [0,1]$ corresponds to independence of X_e and X_s, since in this case $\mathbb{P}(X_e \le z_1, X_s \le z_2) = e^{-(y_1+y_2)}$ is the product of the marginals in Eqs. (12) and (16), and that of $A(0.5) = 0.5$ to their complete dependence. There are parametric models for $A(t)$ that can be fitted in practice.

After a bivariate model is fitted to X_e and X_s, one could obtain an estimate $\widehat{\mathbb{P}}(\epsilon)$ of the error probability, and also the estimate $\widehat{\mathbb{P}}(X_s > y)$ of the error probability (in the same way as the baseline estimator $\widehat{\mathbb{P}}(X_e > x)$), leading to the MF estimator

$$\widehat{\mathbb{P}}(X_e > x) = \widehat{\mathbb{P}}(X_s > y) + \widehat{\mathbb{P}}(\epsilon). \qquad (19)$$

A confidence interval can be constructed to go with $\widehat{\mathbb{P}}(\epsilon)$. For large enough T_s, the variability of $\widehat{\mathbb{P}}(X_s > y)$ can be thought negligible in comparison. If the variability expressed through a confidence

interval on $\widehat{\mathbb{P}}(\epsilon)$ is smaller than that of the baseline estimate $\widehat{\mathbb{P}}(X_e > x)$, then the MF estimate in Eq. (19) should be preferred. In practice, we suggest choosing y as the point corresponding to x through the regression line of X_e on X_s.

6. ILLUSTRATION FOR RARE PROBLEMS

We illustrate the ideas of Section 5 on the same synthetic data used in Section 4 and also in Figure 4. For this example, the estimated marginal parameters (and their standard errors in parentheses) are: $\hat{\mu}_1 = 0.5475\ (0.0083)$, $\hat{\sigma}_1 = 0.0471\ (0.0060)$, $\hat{\xi}_1 = 0.3876\ (0.1118)$ and $\hat{\mu}_2 = 0.6431\ (0.0102)$, $\hat{\sigma}_2 = 0.0577\ (0.0075)$, $\hat{\xi}_2 = 0.3963\ (0.1128)$. Figure 5 presents estimation of the function $A(t)$ entering Eq. (18) and modeling dependence through four parametric models. (For reference, the function $\max(t, 1-t)$ is also plotted in Figure 5.) Since $A(0.5)$ are close to 0.5 (see the discussion following Eq. (18)), the resulting plot suggests that the bivariate block maxima of X_e and X_s are quite strongly correlated. This is also consistent with the scatterplot of the block maxima (in a darker shade) in Figure 4.

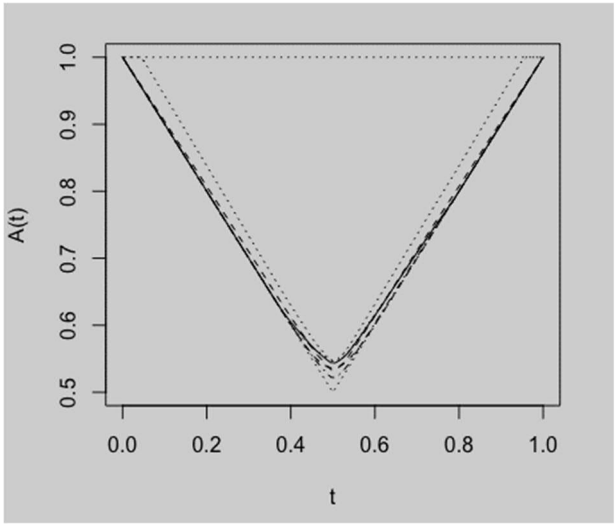

Figure 5: Estimation of $A(t)$ through four parametric models.

Figure 6 depicts the resulting baseline and MF probability estimates and their variability in vertical segments for the target $x = 1.5$. In producing the plot, we treated the fitted bivariate GEV model as the truth, with the horizontal line and the middle circle in the first vertical segment as the baseline estimator representing the true GEV probability $\mathbb{P}(X_e > 1.5)$. Variability is measured by generating data from the bivariate GEV model, re-estimating the probability $\mathbb{P}(X_e > 1.5)$, either through the baseline or the MF estimator, and taking the 0.025th and 0.975th quantiles of the obtained estimates as the endpoints of the vertical segments.

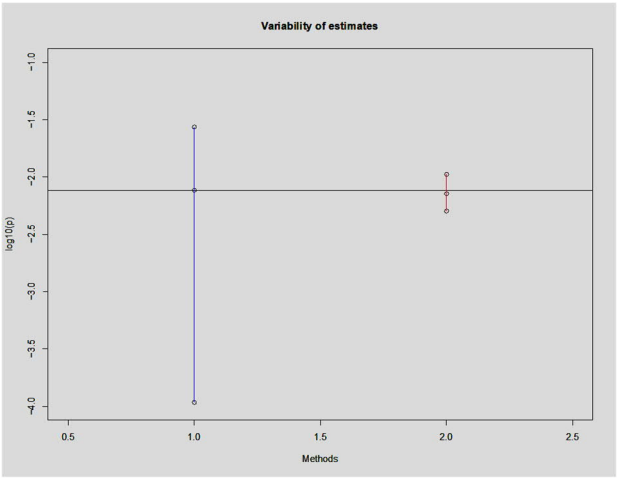

Figure 6: The baseline (left) and MF (right) probability estimates with confidence intervals.

Since the variability of the MF estimator is smaller than that of the baseline, the MF estimator is preferred. It should also be stressed that this is very much a result of strong extremal dependence in the simple and expensive models. Were the dependence not as strong (as expressed through the function $A(t)$ and which can be checked easily), the effect seen in Figure 6 would not be present.

7. CONCLUSIONS

In this work, we showed how a basic MF estimator for low-fidelity and high-fidelity models for non-rare problems could be adapted to estimate probabilities of rare events, especially those that are not observed in high-fidelity data. At a technical level, our approach was rooted in bivariate EVT, that allows modeling simultaneously extremes from the low-fidelity and high-fidelity models. The ideas were illustrated on synthetic data mimicking ship roll motion.

Several directions related to this work could be pursued in the future. First, the methodology should be applied to more realistic models of ship dynamics. Our first attempt in this direction was to compare roll extremes from SimpleCode and LAMP, but their dependence was not strong enough to warrant the use of MF methods. This could partly be a result of the lack of calibration between the two models, which is a topic of its own interest. Second, an even more mathematical treatment of the issues presented in Sections 5 and 6 should also be undertaken, for example, with the introduction of costs, a more

careful construction of confidence intervals, and the use of bivariate peaks-over-threshold methods instead of block maxima, etc.

ACKNOWLEDGMENT

This work has been funded by the Office of Naval Research grant N00014-19-1-2092 under Dr. Woei-Min Lin. The authors also thank Drs. Vadim Belenky and Kenneth Weems at NSWC Carderock Division for their comments on this work.

REFERENCES

Campbell, B., Belenky, V. and V. Pipiras (2016), "Application of the envelope peaks over threshold (EPOT) method for probabilistic assessment of dynamic stability," *Ocean Engineering*, Vol. 120, pp. 298–304.

Coles, S. (2001), *An Introduction to Statistical Modeling of Extreme Values*. Springer, London.

Belenky, V., Weems, K., Pipiras, V., Glotzer, D. and T. Sapsis (2018), "Tail structure of roll and metric of capsizing in irregular waves," *Proceedings of the 32th Symposium of Naval Hydrodynamics*, Hamburg, Germany.

Belenky, V., Glotzer, D. Pipiras, V. and T. Sapsis (2019), "Distribution tail structure and extreme value analysis of constrained piecewise linear oscillators," *Probabilistic Engineering Mechanics,* To appear.

Lin, W. M. and D. K. P. Yue (1991), "Numerical solutions for large amplitude ship motions in the time-domain," *Proceedings of the 18th Symposium on Naval Hydrodynamics*, Ann Arbor.

Peherstorfer, B., Kramer, B. and K. Willcox (2017), "Combining multiple surrogate models to accelerate failure probability estimation with expensive high-fidelity models," *Journal of Computational Physics*, Vol. 341, pp. 61–75.

Peherstorfer, B., Willcox, K. and M. Gunzburger (2018), "Survey of multifidelity methods in uncertainty propagation, inference, and optimization," *SIAM Review*, Vol. 60, pp. 550–591.

Pipiras, V., Glotzer, D., Belenky, V., Levine, M. and K. Weems (2018), "On confidence intervals of mean and variance estimates of ship motions," *Proceedings of the 13th International Conference on the Stability of Ships and Ocean Vehicles*, Kobe, Japan.

Weems, K. and D. Wundrow (2013), "Hybrid models for fast time-domain simulation of stability failures in irregular waves with volume-based calculations for Froude-Krylov and hydrostatic forces," *Proceedings of the 13th International Ship Stability Workshop*, Brest.

On the application of change detection techniques for the stability monitoring of fishing vessels

Lucía Santiago Caamaño, *Integrated Group for Engineering Research, University of A Coruña A Coruña, Spain,* lucia.santiago.caamano@udc.es
Marcos Míguez González, *Integrated Group for Engineering Research, University of A Coruña A Coruña, Spain,* mmiguez@udc.es
Roberto Galeazzi, *Department of Electrical Engineering, Technical University of Denmark, DTU Electrical Engineering, Kgs. Lyngby, Denmark*, rg@elektro.dtu.dk
Ulrik D. Nielsen, *Department of Electrical Engineering, Technical University of Denmark, DTU Electrical Engineering, Kgs. Lyngby, Denmark*, udn@mek.dtu.dk
Vicente Díaz Casás, *Integrated Group for Engineering Research, University of A Coruña A Coruña, Spain,* vdiaz@udc.es

ABSTRACT

This work includes the description of a novel way to tackle the problem of real time stability monitoring. Instead of taking natural roll frequency as the only variable to estimate the stability level of the vessel, a methodology based on the use of signal-based methods with statistical change detection tools is used for detecting changes in the vessel stability and differentiating between safe and non-safe situations. This methodology also includes a colour coded risk alarm that informs the crew about the current state of the vessel. Moreover, in the proposed work, the behaviour and performance of this method is analysed using roll motion data of a stern trawler generated by a one degree of freedom nonlinear model in irregular beam waves. In addition, the obtained results are compared to those from the application of a Fast Fourier Transform (*fft*)-based methodology previously developed by the authors. The performance of this new proposal has been good, both regarding the estimation of the vessel natural roll frequency and the change detection schemes, showing a better performance than the *fft*-based method. However, further analysis is needed to validate these results under more wave conditions and sailing situations.

Keywords: *Fishing vessels, intact stability, stability monitoring, guidance systems.*

1. INTRODUCTION

Medium and especially small fishing vessels have historically suffered a large amount of stability-related accidents, which led to one of the highest fatality rates among all industrial sectors. It has been acknowledged by administrations and the research community, that this very high accident rate could be related not only to the lack of (common) regulatory framework, but also to the lack of crew training programs or formation in vessel stability. In the last two decades, the use of simplified stability guidance systems has been proposed as a possible solution to try to reduce the number of accidents by providing the crew with simple, easy to understand information regarding the stability situation of their vessel. These approaches include the use of simplified stability posters (Wolfson Unit, 2004; Womack, 2003), the analysis of residual freeboard (Scarponi, 2017), or the real time estimation of stability parameters (Wawrzynski and Krata, 2016; Terada et al. 2018 and 2019; Galeazzi et al., 2011).

On this matter, some of the authors of this work have been working on the development of a computer based stability guidance system for small and medium sized fishing vessels, which operates in real time and provides information regarding the stability of the ship with no need of crew interaction, thus reducing the uncertainty of the stability estimations. The state of development of this system has been previously presented, in its different stages, in Santiago Caamaño et al. (2018), Míguez González

et al. (2017) and Míguez González et al. (2018). In these works, the performance of a methodology based on the sequential application of the Fast Fourier Transform (*fft*) for the real time estimation of the natural roll frequency of the vessel (and so of its metacentric height and initial stability), was tested using both a nonlinear mathematical model of roll motion and data from a real scale test campaign onboard a stern trawler, obtaining satisfactory results. If this methodology is applied, the stability level of the vessel could be evaluated based on the last available metacentric height estimation, or on the median value of a set of metacentric height estimations obtained during a given time period (which should be as small as possible to avoid missing possible sudden changes in stability). Due to this fact, the performance of this method, including the appearance of false alarms or stability over predictions, only depends on the precision of the obtained metacentric height estimations and their stability in time.

In this work, a novel way to tackle the problem of stability monitoring is presented. Instead of taking natural roll frequency as the only variable to estimate the stability level of the vessel, a methodology based on the combined use of signal-based methods (Empirical Mode Decomposition and Hilbert-Huang Transform) with statistical change detection tools (Weibull - Generalized Likelihood Ratio Test) are used for detecting changes in the vessel stability and differentiating between safe and non-safe situations.

The use of change detection tools has been already applied in the maritime sector, even including some applications within ship stability, such as the approach included in Galeazzi et al. (2015), where these type of tools are used for predicting the appearance of parametric rolling. Other uses include the detection of faults in mooring systems (Fang et al., 2015) or the detection of incoming vessels within marine traffic (Pradhan and Gupta, 2017).

The main objective of the proposal presented herein is to include in the stability evaluation a tool which provides an indication of whether a loading condition is safe or not, and which is less dependent on metacentric height estimations than the one previously described. In this new methodology, the *fft* is substituted by the EMD+HHT, providing better resolution and performance for estimating the vessel natural roll frequency in short time records. Moreover, the direct stability evaluation obtained from this frequency estimations, done in the previous proposal, is substituted by a probabilistic detector, which should provide a more robust stability level indication.

2. CONDITION MONITORING SYSTEM ARCHITECTURE

The proposed methodology consists of an estimator which, applying the Empirical Mode Decomposition method and the Hilbert Huang Transform (EMD + HHT), obtains from a given time record of the vessel roll motion, information about its natural roll frequency and possible variations of this parameter over time. These estimates are then modelled following a Weibull distribution and used as input of a statistical change detector, based on the Generalized Likelihood Ratio Test (W – GLRT), which determines if a change between a safe and a non-safe situation is taking place.

In addition to the above, a situation awareness system has been also included, with the objective of informing the crew about the stability level of their vessel following a colour coded pattern, in a similar way as it has been done in previous works by the authors (Míguez González et al., 2012).

In Figure 1, a block diagram describing the structure of the proposed stability monitoring system has been included.

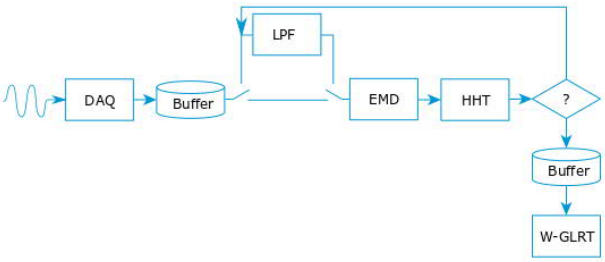

Figure 1. Structure of the stability monitoring system.

EMD + HHT estimator

The EMD technique is applied to decompose the roll motion signal of the time record under analysis into its main oscillatory components, the *IMF*s (Intrinsic Mode Functions) ((Dätig and Schlurmann, 2004; Gupta et al., 2014; Huang et al., 1998)). After its application, the vessel roll motion $\phi(t)$ could be represented as:

$$\phi(t) = \sum_{i=1}^{N_{IMF}} IMF_i(t) + R(t) \qquad (1)$$

where *R(t)* is a monotonic function, $IMF_i(t)$ is each of the Intrinsic Mode Functions obtained from the time series after the application of the EMD and N_{IMF} is the number of obtained *IMF*s. In the typical situation of a vessel sailing under the effect of wind, waves and other external excitations, the IMFs usually include those corresponding to these excitations, plus the one related with the ship natural oscillation and some others. Once the *IMF*s have been obtained from the original signal, the Hilbert-Huang Transform (HHT) is applied to them (Dätig and Schlurmann, 2004; Huang et al., 1998). This transform, designed for representing a signal in a time-frequency-energy basis, is used in this work for providing an estimate of the instantaneous frequency of each *IMF*. From these values, and for a given time record, the mean instantaneous frequency ($\hat{\omega}_j$) for each *IMF* is computed according to Xie and Wang (2006) and stored in a vector Ω_{IMF}

$$\Omega_{IMF} = [\hat{\omega}_1, \hat{\omega}_2, ..., \hat{\omega}_{N_{IMF}}] \tag{2}$$

where $\hat{\omega}_1 > \hat{\omega}_2 > ... > \hat{\omega}_{N_{IMF}}$.

In the case of a vessel rolling under external excitations, the extracted *IMF*s from the roll motion time series, and so its corresponding mean instantaneous frequencies, usually include the oscillatory modes due to these excitations, as well as the mode corresponding to the vessel natural frequency, sensor noise and other possible components. The chosen estimate of the natural roll frequency of the vessel for that given time record will be one of these values. In order to carry out this selection firstly, from the whole set of obtained values, all of those which are over and under a given value are disregarded. This range is determined by the maximum expected roll natural frequency of the vessel (previously determined, for example, by considering a maximum stability condition), and a minimum value (which in this case is associated with the minimum stability level necessary to keep heel beyond 15 degrees under a 30 knot lateral wind). After this process, the estimated natural roll frequency is selected as the maximum value from the remaining ones, based on observations and some experience, which showed that the first and second largest values usually concentrate most of the energy. However, this assumption is arguable, and more testing is needed to confirm such an hypothesis.

W-GLRT detector

In order to take into consideration that there is some level of uncertainty in the estimation of the natural roll frequency done by the EMD+HHT, these values have been statistically characterized. After some previous testing in different load cases and sea states, it has been concluded that the distribution which best fits the natural roll frequency estimates is the Weibull, which main parameters are the shape (κ) and the scale parameter (λ). If the probabilistic median of this distribution is taken as the estimator of the natural roll frequency ($\hat{\omega}_0$)

$$\hat{\omega}_0 = \lambda \cdot (\ln 2)^{1/\kappa} \tag{3}$$

and considering that both scale and shape parameters change with the vessel loading condition, the proposed detector has been designed to track their variations and subsequently, those in the vessel roll natural frequency. The detection problem under consideration is then to decide between two hypotheses; the null one (H_0), which corresponds to a safe condition, and the alternative one (H_1), which is related to a non-safe condition,

$$\begin{aligned} H_0 &: \lambda_0 \cdot (\ln 2)^{1/\kappa_0} \geq \omega_{0_c} \\ H_1 &: \hat{\lambda}_1 \cdot (\ln 2)^{1/\hat{\kappa}_1} < \omega_{0_c} \end{aligned} \tag{4}$$

where ω_{0_c} is defined as the critical natural roll frequency, and is the one corresponding to a $\overline{GM}$ equal to the minimum required by IMO for this type of ships ($\overline{GM} = 0.350$ m).

Taking into consideration that $\hat{\omega}_0$ depends on the Weibull parameters, the detection problem above could be reduced to a standard parameter test, where the decision between the two different hypotheses is done using the Generalized Likelihood Ratio Test (GLRT) (Kay, 1998). This statistical test, based on the Neyman-Pearson theorem, maximizes the probability of detection for a desired probability of false alarms (γ). The GLRT would decide that the H_1 hypotheses is fulfilled if:

$$L_G(\Omega_0) = \frac{Weibull\left(\Omega_0; \hat{\theta}_1, H_1\right)}{Weibull\left(\Omega_0; \theta_0, H_0\right)} > \gamma \tag{5}$$

where Ω_0 is the vector containing the estimations of natural roll frequency under analysis, $\theta = [\lambda, \kappa]^T$ is the vector containing the characteristic parameters of

the Weibull distribution, θ_0 is its realization for the null hypotheses and $\hat{\theta}_1$ is the maximum likelihood estimate (MLE) of the parameter vector θ for the H_1 hypotheses, which is obtained by maximizing $Weibull(\Omega_0;\theta)$ under H_1.

In addition to deciding between the two previous hypotheses, and so to deciding if the sailing situation under analysis is safe or not from a stability point of view, the value of $\hat{\omega}_0$ is used for generating stability – related information to the crew. This information is obtained by comparing $\hat{\omega}_0$ with ω_{0_c}, in a similar way as it has been proposed in Míguez González et al. (2017) or Caamaño Santiago et al. (2018). However, there is a remarkable difference between both proposals. While in the previous ones the stability estimation relied on the instantaneous estimations of the natural roll frequency, in this case it is done based on a probabilistic approach which, in principle, should represent a more robust approach.

3. TEST CASE

Fishing vessel model

In order to evaluate the performance of the proposed methodology, a nonlinear mathematical model of roll motion of a stern trawler in irregular beam seas has been applied for generating the roll motion time series.

The model, shown in equation (6), is described in detail in Bulian and Francescutto (2004), and has been already applied to the same vessel in Míguez González et al. (2017).

$$\ddot{\phi} + 2\cdot\upsilon\cdot\omega_0\cdot\dot{\phi} + \beta\cdot\dot{\phi}\cdot\left|\dot{\phi}\right| + \omega_0^2\cdot\frac{\overline{GZ}(\phi)}{\overline{GM}} = \\ = \omega_0^2\cdot\left(m_{wave}(t)\right) \qquad (6)$$

In this model, υ and β are the linear and nonlinear quadratic damping coefficients, ω_0 is the natural roll frequency of the vessel, $\overline{GM}$ is the still water metacentric height and $\overline{GZ}(\phi)$ is the nonlinear righting lever in calm water. The irregular beam wave excitation ($m_{wave}(t)$) has been modelled applying the Absolute Roll Angle Model (Bulian and Francescutto, 2006), as shown in Equation (7).

$$m_{wave}(t) = \sum_{i=1}^{n} \pi\cdot r(\omega_i)\cdot s(\omega_i)\cdot\cos(\omega_i t + \xi_i) \qquad (7)$$

In this equation, $r(\omega_i)$ is the effective wave slope coefficient (computed for the tested vessel using linear hydrodynamics), $s(\omega_i)$ is the wave slope and ω_i and ξ_i are the wave frequency and phase of each wave component (i). Wave excitation has been modelled using a Bretschneider spectrum and the vessel has been considered to be sailing at zero speed which, due to the typical operational profile of these type of stern trawlers, is a quite frequent condition.

The vessel under consideration is a mid-sized stern trawler, which has been already used by some of the authors in previous works (Míguez González et al., 2017; Míguez Gonzálezand Bulian, 2018), and which main characteristics, hull forms, arrangement and $\overline{GZ}(\phi)$ and $r(\omega)$ curves for the critical condition with $\overline{GM} = 0.350$ m are shown in Table 1 and in Figures 2, 3 and 4.

Table 1. Test vessel: main characteristics.

Overall Length	34.50 m
Beam	8.00 m
Depth	3.65 m
Linear Roll Damping Coefficient (υ)	0.0187
Quadratic Roll Damping Coefficient (β)	0.393 1/rad

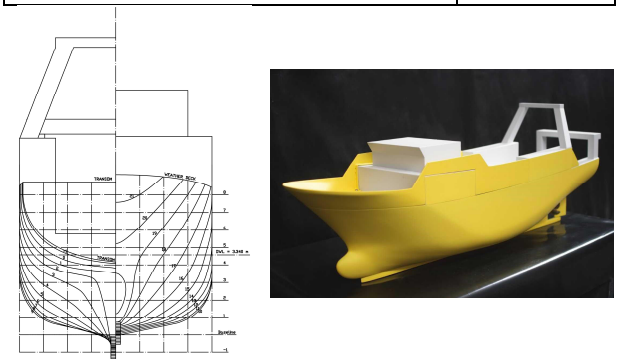

Figure 2. Test vessel: hull sections and scale model.

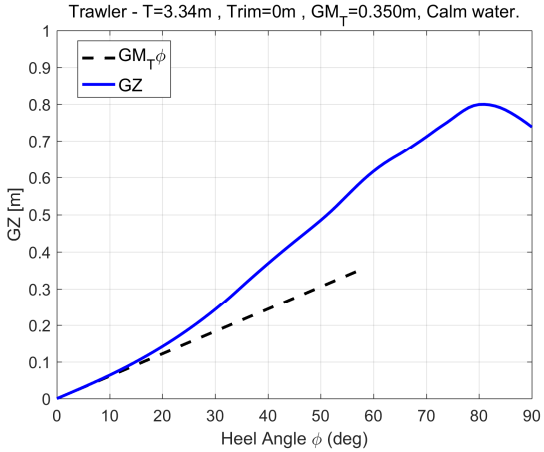

Figure 3. Test vessel: *GZ* curve in calm water.

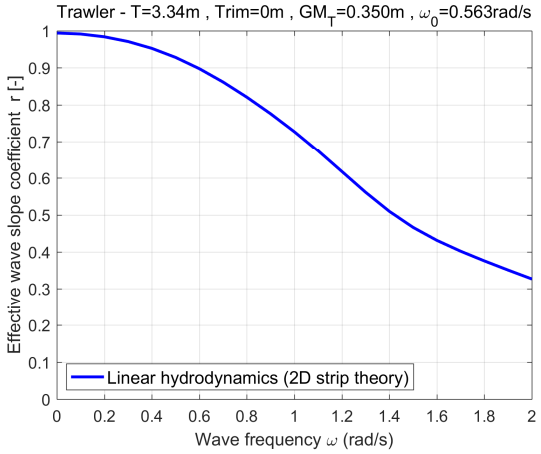

Figure 4. Test vessel: effective wave slope coefficient.

Test condition

In order to test the performance of both the EMD+HHT and the W-GLRT schemes, two time series of 4200 seconds of roll motion have been generated, for the same wave parameters but for different loading conditions, and have been stitched together. The resulting time series is a 8400 seconds long roll motion time series, where a change in loading condition (but also in waves, as both cases have been randomly generated) takes place approximately after 4200 seconds, going from an initial loading condition which fulfils all stability requirements (LC1), to another one with a low $\overline{GM}$, which is supposed to represent a non-safe situation (LC2). The parameters characterizing these two loading conditions are included in Table 2. The safe condition, LC1, has been obtained directly from the stability booklet of a very similar vessel, so that it represents a realistic sailing condition. The non-safe condition, LC2, has been defined by the authors to represent a sailing situation with a slightly lower $\overline{GM}$ than the IMO minimum required value.

Regarding the wave situation under analysis, wave conditions (T_P, H_S) have been selected to represent a heavy seas condition, according to prevailing conditions in Spanish north-western coastal area. These wave parameters are shown in Table 3. The roll motion time series, obtained from stitching those corresponding to the two loading conditions is shown in top of Figure 6, where it can be appreciated the time instant where conditions have changed. From this time series, the first 20 minutes are used for the calibration/adjusting stage of the detector; during this time, the detector does not generate any result; from this moment on, a result is generated every 3 minutes.

Table 2. Tested loading conditions.

	LC1	LC2
Displacement	489 t	448 t
Metacentric Height (*GM*)	0.501 m	0.331 m
Natural Roll Frequency (ω_0)	0.701 rad/s	0.548 rad/s
Natural Roll Period (s)	8.963 s	11.466 s
Draft	3.484 m	3.294 m
Roll gyradius (k_{xx}) / B	0.395	0.411

Table 3. Tested wave conditions.

Significant wave height (H_S)	8.520 m
Peak period (T_P)	12.8 s

Regarding the estimation of natural roll frequency, the EMD+HHT work in time records of 3 minutes with an overlap between consecutive measures of 75%, thus making a new estimation every 45 seconds. Regarding the detector, its operation time window has been set to 5 minutes with an overlapping of a 40 %, thus generating a new measurement every 3 minutes (which is supposed to be, for this type of vessel, a short enough time as to detect possible sudden changes in stability).

4. RESULTS

In order to analyse the performance of the proposed system, the aforementioned algorithms have been applied to the roll motion time series described above. In Figure 6, the obtained results are displayed.

In Centre top of Figure 6, the green dots illustrate the natural roll frequency estimates obtained by applying the EMD+HHT. In Centre bottom of Figure 6, the results of the W-GLRT detector are included as blue dots. In this figure, the red line represents the limit between safe (values under this line) and non-safe conditions (values over this line). At the Bottom of Figure 6, the results obtained from the colour awareness alarm are included. Finally, in Figure 7, results of the estimations of natural roll frequency obtained by applying the *fft*-based methodology developed by the authors, as described in Míguez González et al. (2017), have been included.

If the obtained results are analysed, it can be appreciated that regarding the estimations of natural roll frequency (Table 4), a very good agreement between the obtained values and the target ones has been observed, not only regarding the median values, but also between the 95% percentiles and the

5% percentiles and the target values. This fact is especially remarkable if results are compared to those obtained with the *fft*-based methodology (Table 6). In these last case, the system had previously shown a tendency to over predicting the natural roll frequency of the vessel, which can be also appreciated in these results (deviations between the 95% percentile and target value close to the 12 %). The newly developed EMD+HHT estimators seem to reduce these values (maximum deviations between the 95% percentile and target value of the 5 %), thus leading to the favourable effect of reducing the tendency of the system to overestimate the stability of the vessel.

On the other hand, at least in the case under analysis, the EMD+HHT has shown a larger tendency to under predicting the vessel stability (bigger differences between the 5% percentile and the target value than in the *fft* case), although this issue is less important, at least from the safety point of view and if under predictions are kept under reasonable levels, than the previous one.

In addition to the above, it also has to be said that the novel approach performs better than the *fft* based one even in those situations (as the one represented by LC1), where roll natural period and wave peak period are far from each other. On this same line, it is also worth to mention that those situations, although safe from a dynamic stability point of view (as wave and natural roll frequencies are far from each other and pure roll resonance are not expected to take place), could be suffering from reduced stability levels and so, they have to be considered as also relevant while stability is being monitored.

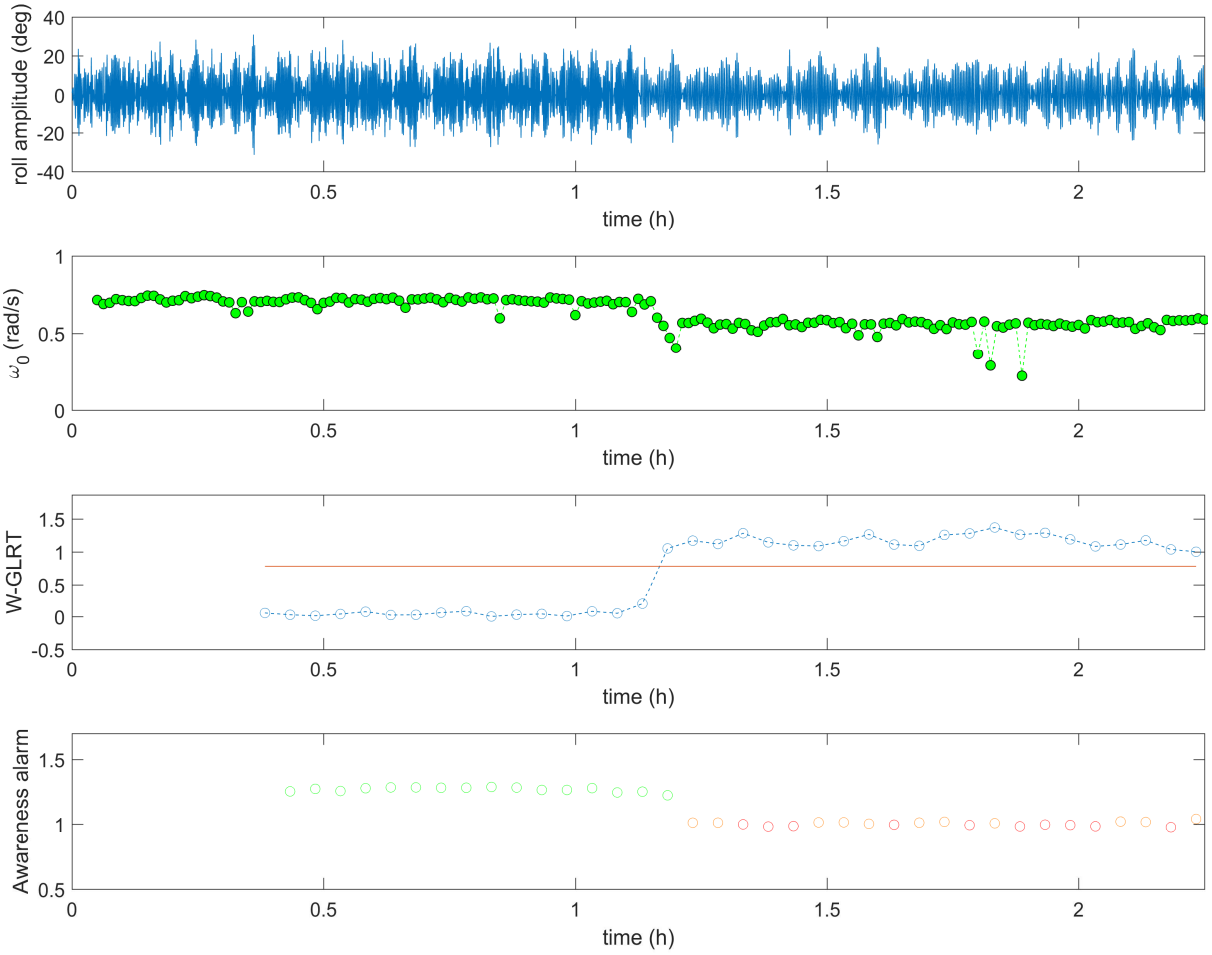

Figure 6. Top: roll motion time series under analysis. Centre top: estimations of natural roll frequency from the EMD+HHT. Centre bottom: output of the W-GLRT detector. Values under the red line indicate a safe situation, while values over the red line generate an alarm due to low stability levels. Bottom: output of the colour – coded situation awareness algorithm.

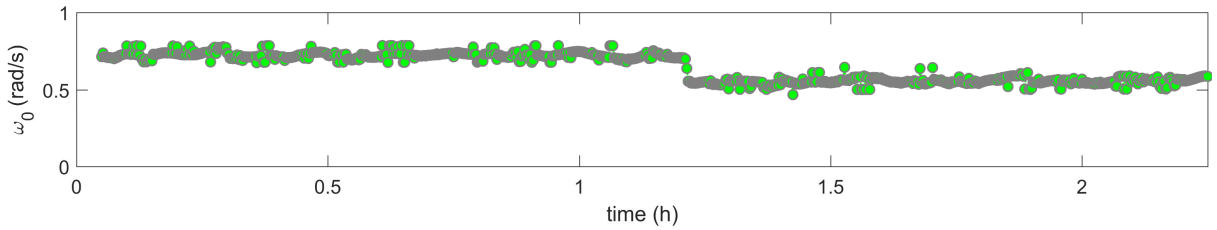

Figure 7. Estimations of natural roll frequency from the *fft* methodology (as described in Míguez González et al., 2017).

Regarding the results obtained from the detector (included in Table 5), it has shown to timely track the changes between the safe and the non-safe condition and has not generated any false alarms (classifying a safe condition as unsafe) or miss-detections (classifying as safe an unsafe condition). Subsequently, the results from the awareness alarm are also quite accurate, although some variation in colour is observed for the second half of the time series, where the detector results tend to slightly oscillate with time.

It is necessary to say that one of the advantages of this proposal is that in addition to the evaluation of the vessel $\overline{GM}$ that could be done from the natural roll frequency estimates (following the same concept that was applied in Míguez González et al., 2017), the detector provides a rougher evaluation of the level of stability (safe / non-safe condition), but that at the same time is less dependent of the level of accuracy of the frequency estimators and represents the minimum information the crew needs for evaluating the level of safety of their vessel.

Table 4. Estimations of natural roll frequency. EMD+HHT.

	LC1	LC2	Deviations to target value (%)	
			LC1	LC2
ω_0 Target Value ($\omega_{0\ target}$) [rad/s]	0.701	0.548	-	-
Estimated ω_0 Median ($\omega_{0\ median}$) [rad/s]	0.695	0.545	0.86	0.55
5% Percentile Estimated ω_0 ($\omega_{0\ 5\%}$)[rad/s]	0.643	0.448	8.27	18.25
95% Percentile Estimated ω_0 ($\omega_{0\ 95\%}$)[rad/s]	0.720	0.575	2.71	4.93

Table 5. W-GLRT detector performance.

	LC1	LC2
True Detections	16	22
False Detections	0	0

Table 6. Estimations of natural roll frequency. *fft*-based methodology (Míguez González et al., 2017).

	LC1	LC2	Deviations to target value (%)	
			LC1	LC2
ω_0 Target Value ($\omega_{0\ target}$) [rad/s]	0.701	0.548	-	-
Estimated ω_0 Median ($\omega_{0\ median}$) [rad/s]	0.725	0.556	3.40	1.45
5% Percentile Estimated ω_0 ($\omega_{0\ 5\%}$)[rad/s]	0.685	0.516	2.28	5.84
95% Percentile Estimated ω_0 ($\omega_{0\ 95\%}$)[rad/s]	0.784	0.613	6.70	11.86

5. CONCLUSSIONS

In this work, a novel proposal for carrying out a real time evaluation of the stability of a vessel has been presented. This proposal relies on two main different methodologies; on one hand, one algorithm aimed at estimating the natural roll frequency of the vessel (EMD+HHT). And on the other hand, a probabilistic detector which analyzes if the current loading condition is safe or not from a stability point of view (W-GLRT).

In order to evaluate the performance of this proposal, a nonlinear mathematical roll model of a stern trawler in irregular beam waves has been used to simulate the vessel roll motion sailing in two different loading conditions, one which represents a safe one, and another which is supposed to be non-safe from an initial stability point of view.

The estimations of the natural roll frequency of the vessel obtained by the EMD+HHT, have shown to be quite accurate, performing better than the *fft*-based estimator previously proposed by the authors, at least in the wave conditions under analysis. Regarding the detector, its behaviour has been very satisfactory in the tested wave conditions, accurately differentiating between safe and non-safe

conditions, and timely detecting the changes in the vessel loading condition.

Although the results are very promising, and could represent a step forward compared to the previous developments of some of the authors of this work, additional testing is needed to verify this behaviour in more wave conditions and vessel speeds and headings.

ACKNOWLEDGEMENTS

This work was supported by University of A Coruña and INDITEX SA under the "Collaboration agreement between UDC and INDITEX for the internationalization of doctoral studies" (grant number 04.00.47.00.01 422D48001).

REFERENCES

Bulian, G., Francescutto, A., 2004, "A simplified modular approach for the prediction of the roll motion due to the combined action of wind and waves", *Proceedings of the Institution of Mechanical Engineers, Part M: Journal of Engineering for the Maritime Environment* 218, pp. 189-212.

Bulian, G., Francescutto, A., 2006, "Safety and Operability of Fishing Vessels in Beam and Longitudinal Waves", *The Transactions of The Royal Institution Of Naval Architects. Part B, International Journal of Small Craft Technology* 148, pp. 1-16.

Dätig, M., Schlurmann, T., 2004, "Performance and limitations of the Hilbert-Huang transformation (HHT) with an application to irregular water waves", *Ocean Engineering* 31, pp. 1783-1834.

Fang, S., Blanke, M., Leira, B.J., 2015, "Mooring system diagnosis and structural reliability control for position moored vessels", *Control Engineering Practice* 36, pp. 12-26.

Galeazzi, R., Perez, T., 2011, "A Nonlinear Observer for Estimating Transverse Stability Parameters of Marine Surface Vessels", *IFAC Proceedings Volumes* 44, Issue 1, pp. 2967-2971.

Galeazzi, R., Blanke, M., Falkenberg, T., Poulsen, N.K., Violaris, N.,Storhaug, G., Huss, M., 2015, "Parametric roll resonance monitoring using signal-based detection", *Ocean Engineering* 109, pp. 355-371.

Gupta, R., Kumar, A., Bahl, R., 2014, "Estimation of instantaneous frequencies using iterative empirical mode decomposition", *Signal, Image and Video Processing* 8, pp. 799 - 812.

Huang, N., Shen, Z., Long, S.,Wu, M., Shih, H., Zheng, Q., Yen, N., Tung, C., Liu, H., 1998, "The empirical mode decomposition and the Hilbert spectrum for nonlinear and non-stationary time series analysis", *Proceedings of the Royal Society A: Mathematical, Physical and Engineering Sciences* 454, Issue 1971, pp. 903-995.

Kay, S.M., 1998, *Fundamentals of statistical signal processing: detection theory,* Prentice-Hall, Inc., Englewood Cliffs.

Míguez González, M., Caamaño Sobrino, P., Tedín Álvarez, R., Díaz Casás, V., Martínez López, A., López Peña, F., 2012, "Fishing vessel stability assessment system", *Ocean Engineering* 41, pp. 67-78.

Míguez González, M., Bulian, G., Santiago Caamaño, L. and Díaz Casás, V., 2017, "Towards real-time identification of initial stability from ship roll motion analysis", Proceedings of the 16th International Ship Stability Workshop (ISSW 2017), Belgrade, Serbia, pp. 221-230.

Míguez González, M., Bulian, G., 2018, "Influence of ship dynamics modelling on the prediction of fishing vessels roll response in beam and longitudinal waves", *Ocean Engineering* 148, pp. 312-330.

Míguez González, M., Santiago Caamaño, L. and Díaz Casás, V., 2018, "On the applicability of real time stability monitoring for increasing the safety of fishing vessels", Proceedings of the 13th International Conference on the Stability of Ships and Ocean Vehicles (STAB 2018), Kobe, Japan.

Pradhan, C., Gupta, A., 2017, "Ship detection using Neyman-Pearson criterion in marine environment", *Ocean Engineering* 143, pp. 106-112.

Santiago Caamaño, L., Míguez González, M. and Díaz Casás, V., 2018, "On the feasibility of a real time stability assessment for fishing vessels", *Ocean Engineering* 159, pp. 76-87.

Scarponi, M., 2017, "Use of the Wolfson stability guidance for appraising the operational stability of small fishing vessels", Proceedings of the 16th International Ship Stability Workshop (ISSW 2017), Belgrade, Serbia, pp 213-220.

Terada, D., Hashimoto, H., Matsuda, A., Umeda, N., 2018, "Direct estimation of natural roll frequency using onboard data based on a Bayesian modeling procedure", Proceedings of the 13th International Conference on the Stability of Ships and Ocean Vehicles (STAB 2018), Kobe, Japan.

Terada, D., Tamashima, M., Nakao, I., Matsuda, A. 2019, "Estimation of metacentric height using onboard monitoring roll data based on time series analysis", *Journal of Marine Science and Technology* 24, Issue 1, pp. 285–296.

Wawrzynski, W., Krata, P., 2016, "Method for ship's rolling period prediction with regard to non-linearity of GZ curve", *Journal of theoretical and applied mechanics* 4, 54, pp. 1329-1343.

Wolfson Unit, 2004, "MCA Research Project 530. Simplified presentation of fishing vessels stability information. Phase 1. Final Report", Wolfson Unit, University of Southampton, U.K.

Womack, J., 2003, "Small commercial fishing vessel stability analysis: Where are we now? Where are we going?", *Marine Technology*, Vol. 40, 4, pp. 296-302.

Xie, H., Wang, Z., 2006, "Mean frequency derived via Hilbert-Huang transform with application to fatigue EMG signal analysis", *Computer Methods and Programs in Biomedicine* 82, pp. 114-120.

Fatal stability loss of a small craft on a wave crest – based on a real safety investigation

Risto Haimila, *Safety Investigation Authority Finland,* risto.haimila@om.fi
Tapani Salmenhaara, *University of Applied Sciences South Eastern Finland,* Tapani.Salmenhaara@xamk.fi
Jerzy Matusiak, *Aalto University*, jerzy.matusiak@aalto.fi

ABSTRACT

The capsizing of a pilot boat in average weather conditions has generated questions about sufficient stability regulations and uncertainty in pilot boat operations. Abnormal wave formation due to the interaction of a turning vessel and sea surface waves raised particular problems associated with the special operational conditions of the pilot boat. Investigation of the accident has shown that the V-bottom shaped boat may lose 70% of the righting arm maximum on a crest of a typical steep sea surface wave compared to the calm water line situation. This, combined with the external loads and other dynamic effects, caused capsizing of the pilot boat.

Keywords: *pilot boat, V-shaped bottom, boat stability, stability on wave crest.*

1. INTRODUCTION

This paper is based on the investigation of the pilot boat accident which took place in the Gulf of Finland, south of Emäsalo, on 8 December 2017 at approximately 5 PM, Safety Investigation Authority Finland (2018).

Meteorological conditions

Based on the Finnish Meteorological Institute's information the wind in the area was 190º/10…12 m/s with gusts of maximum 15 m/s. The significant wave height was 2 meters. The maximum wave height was 3.8 meters. Waves were coming from 205°. It was dark during the occurrence. The conditions were considered safe for the use of the pilot boat.

Sequence of events leading to the accident

A pilot boat prepared to collect a pilot from a tanker proceeding with the speed of about 9 knots in rough seas in the Gulf of Finland off Emäsalo in December 2017. The pilot boat had followed the tanker *Sten Nordic* at about 20…50 meters from the stern where it was sheltered from the sea waves. The tanker started to prepare for the disembarkment of the pilot by making lee for the operation. When *Sten Nordic* was turning hard to port the pilot boat was to proceed towards the port side of the vessel. The pilot boat was at the distance of 20…30 meters from the stern of the tanker and became exposed unexpectedly to high, steep recurring waves caused by the combined effect of the vessel and the sea waves. The path travelled both by the tanker and that of the pilot boat *L-242* are shown in Figure 1.

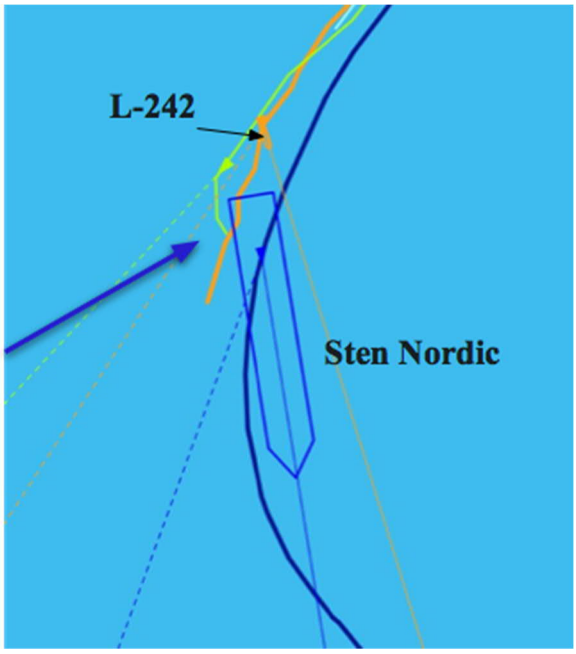

Figure 1: The paths travelled by the tanker and the pilot boat L-242 shortly before the boat capsizing.

The situation prior to the boat capsizing is shown. The blue arrow depicts the prevailing direction of the sea waves' propagation. The speed of the boat was approximately 9 knots.

The stability accident

Suddenly the pilot boat rolled, lost stability and capsized to the port (left) side. After floating for 10 minutes the boat turned upside down.

No signs of the pilot boat's crew were seen during the six hour rescue operation. Eventually the pilot boat sank into the 30 meter deep water. During the inspection dive the crew was found in the cabin wearing survival suits. The Safety Investigation Authority Finland commenced a marine safety investigation in which one of the main safety issues was to find out why the pilot boat lost stability and capsized in prevailing conditions. This issue has wider importance to enhance the general safety of small boats operating in heavy seas.

2. MAIN PARTICULARS AND STABILITY OF THE BOAT

Particulars of the pilot boat

The pilot boat was a high-speed pilot boat of the Kewatec Pilot 1500 type. The boat's LOA was 14.5 meters, breadth 5.1 meters and it was powered by two Scania DI13 Marine Engines of 331 kW (450 hp) connected to two axis driven propellers. The boat had two rudders. The displacement of the boat was 19 m^3 and maximum speed 27 knots.

The hull was divided into five watertight sections below the main deck. The wheelhouse was attached on the deck with vibration damping devices and had only cables running through holes into the hull. The boat was supposed to survive with one watertight section flooded but all the inlets, locks and bulkheads should have been closed. A photograph of the boat is shown in Figure 2.

Figure 2: Pilot boat L-242 investigated after the accident. (Source: SIAF)

The stability of the pilot boat

The risk of the pilot boat capsizing had not been previously identified. The pilot boats were regarded as safe in all conditions and were generally assumed by the crew to be self-righting, due to which the capsizing was a surprise. The users were not sufficiently aware of the boat's stability characteristics in strong waves.

The pilot boat was designed and constructed according to category B requirements of the Finnish Maritime Administration (FMAW, version 2009.1). Finnish VTT Expert Services Oy had inspected the boat based on the Category B requirements and issued an inspection report including the stability information.

The pilot boat was supposed to be capable of operating in conditions where the significant wave height is 4 meters and the maximum wind speed is 21 m/s as well as be to endure a maximum heel of about 75°. The pilot boat had not gone through the inclination test, but the stability information based on the calculated information (presented in Figure 3) was obtained from the previous tests of its sister vessels. The investigation group decided to verify this information.

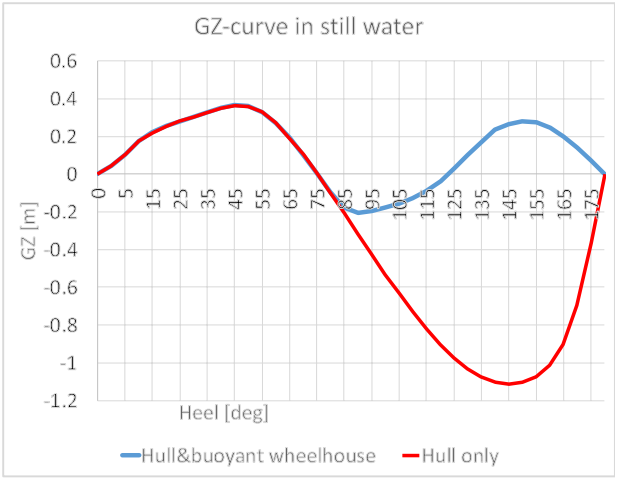

Figure 3: Righting moment curve (*GZ*-curve) of the pilot boat.

The Safety Investigation Authority Finland ordered an inclination test to be carried out for one of the sunken pilot boat's sister vessel in a loading condition much the same as the sunken pilot boat to verify the results of the calculations. This was conducted by Beacon Finland Oy under the supervision of the investigation team. The results of this inclination test were in line with and validated the results of the calculated stability values but did

not explain why the pilot boat capsized. The Safety Investigation Authority Finland ordered a simulation from Napa Oy modelling the factors effecting the pilot boat in different wave conditions.

It was observed that the restoring moment of the pilot boat can temporarily lose up to 70% of its maximum in steep waves, during which a sudden, strong external force can capsize the boat. Such an external force can occur due to a rudder movement or a powerful gust of wind. No account of these factors had been taken in the design, manufacture or use of the boat. On the basis of the investigation, there is also reason to believe that the crew of the pilot boat *L-242* had no grounds for believing that the boat would capsize.

Risk management

In the investigation, it emerged also that in Finland no clear official standards exist with regard to commercial craft, which has led to the interpretation and adaptation of a wide range of rules. This creates the risk that insufficient account is taken of special standards applying to various intended uses of commercial craft and the conditions in which they will be used, during the vessels' design and manufacture, and when ensuring their safe use.

The users were not sufficiently aware of the boat's stability characteristics in strong waves. The orientation of pilot boat operators varies and is not necessarily sufficient in terms of the challenging nature of the work or ensuring safety. Risk identification and safe practices are largely based on "silent" knowledge rather than documentation and systematic risk assessment.

3. THE WAVES ENCOUNTED BY THE BOAT

Wave conditions, at the time of accident, were typical for the Gulf of Finland at this time of a year and characterized by two-directional wave propagation and a double-peaked wave spectrum. The significant wave height was H_S= 2 m and the zero-crossing period T_Z=4.7 s. Waves of length 50 m to 150 m propagated in the 240° direction while the direction of shorter waves was directly from the south.

The initial heading of the tanker was 240° and thus it provided a good shelter for the pilot boat. Turning of *Sten Nordic* to port exposed the pilot boat to the sea waves (refer to Figure 1). Moreover, interaction of sea waves with the tanker hull resulted in formation of steep waves that were sweeping along the hull downstream astern to the region where the pilot boat was located. These waves, interacting with the open sea waves, were encountered by the pilot boat.

Qualitatively the formation of steep and breaking waves downstream of a turning ship due to interaction of the turning vessel and the sea waves can be explained by the observations made during earlier tests conducted in the multi-functional model basin of Aalto University. Turning circle tests were conducted in irregular long-crested waves. The primary goal of the tests was to reveal roll resonance motion of a RoPax in stern quartering seas (Acanfora & Matusiak, 2016). A still photo capture of the video taken during the tests is shown in Figure 4.

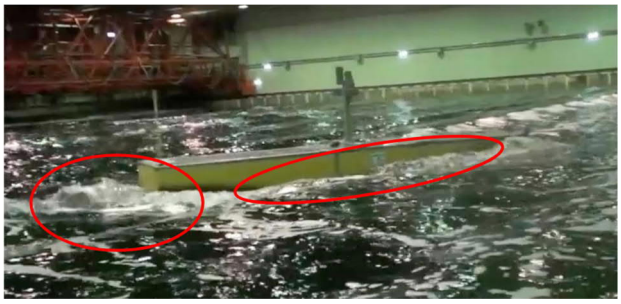

Figure 4: Model of a RoPax vessel in long-crested irregular waves in the multi-functional basin of Aalto University.

The waves used in the model tests were higher and longer (H_S= 4.8 m and T_1=5.9 s) than the ones that were present during the accident. However, a similar effect on the waves formed downstream due to turning of *Sten Nordic* can be expected.

4. QUASI-STATIC ANALYSIS OF THE BOAT STABILITY

A thorough and reliable dynamic analysis of the pilot boat behavior and capsizing in such a complex wave environment proved to be impossible. There are several reasons for this. The V-shaped, shallow draft hull of the boat differs much from the displacement ship hull forms. Large and slow variations of the wetted surface in waves contradict the linearity assumptions of the radiation and diffraction forces of traditional seakeeping methods and also of so-called hybrid models. Thus, the available tools used in analyzing vessel motions in waves, proved to be insufficient.

Assumptions of the quasi-static approach

The relatively low speed and the heading of the boat, combined with waves much longer than the boat length, resulted in a period of encounter higher than the roll resonance period (approx. 2.4 s). This made a quasi-static analysis of the boat floatation and stability feasible and relevant for the investigation of accident. The assumption is that the boat follows well the waves and its position is governed by the weight and the hydrostatic pressure. The latter takes the wave profile into account. Large variations of the wetted surface result in drastic and highly non-linear variations of the restoring moment given in the form of a *GZ*-curve. The dynamic effects related to the boat motion, such as inertia, radiation and diffraction forces, are disregarded. The effect of forward speed (approximately 9 knots in this case) on dynamic pressure and wave-making are disregarded as well.

Tool used in evaluation of stability change in waves

The tool for evaluation pure loss of stability on a wave crest, being a part of the second-generation intact stability ship criteria (Tompuri et al, 2017), was used. Calculations were conducted with the NAPA software.

Sinusoidal deep-water waves of lengths (λ) from 40 m to 150 m and heights (H) from 1.5 m to 4.5 m were used. Wave heights were limited by the wave breaking criterion $H/\lambda<0.1$. The considered heading angles were from 20° to 60° with head waves corresponding to zero heading. For each heading and wave case, the boat was set in a wave at different positions and the one with the minimum stability was selected as a reference. For each case the static equilibrium position of the boat and it's *GZ*-curve were evaluated. An example of the static equilibrium position of the boat, with substantially weakened stability, in a regular wave is shown in Figure 5.

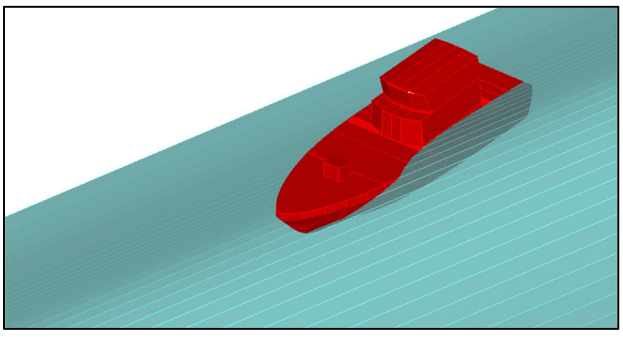

Figure 5: Position of static equilibrium of the pilot boat in regular sinusoidal wave of length 40 m and height 3 m. Heading 50°.

The knowledge of the *GZ*-curve in different situations made it possible to evaluate the boat response to both static and dynamic external loads.

External loading

Apart from possible dynamic effects related to boat motion, the most relevant external loading was caused by the rudders. The rudders of the capsized boat were turned 40° to port. The heeling moment M_{ext} caused by turning both rudders by 40° was evaluated using the methodology of Molland (2007) and resulted in the lever of external loading

$$l_{ext} = M_{ext} / \Delta = 0.0834 \text{ m}, \quad (1)$$

where Δ is buoyancy.

Two types of rudder loading on the boat were considered, namely the static one and the dynamic one given as a step function. The latter is treated in a similar manner as the wind gust loading of the weather criteria, i.e. knowing the *GZ*-curve and the arm of the dynamic loading the areas made-up by both are compared. If the work done by the external loading exceeds the work done by the restoring moment the vessel capsizes. This is illustrated in Figure 8 in the following paragraph.

Results of the analysis

For the static loading, the cases with the external loading exceeding the maxima of the *GZ*-curves were identified, that is

$$l_{ext} > GZ_{MAX} \ . \quad (2)$$

The results of this static, i.e. slowly increasing, loading by rudders on the boat in the critical waves are presented in Figure 6.

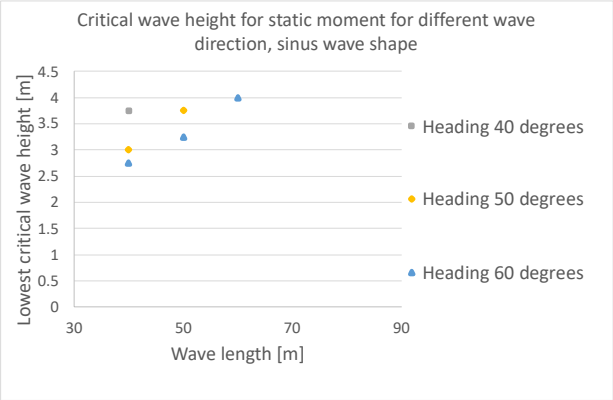

Figure 6: Critical wave heights for static loading caused by turning rudders by 40°.

In Figure 7 the critical waves and headings for rapid (step function form) rudder load are presented.

An example of the boat capsizing due to a rapidly changed rudder angle in the critical wave and heading condition is illustrated in Figure 8. The static balance of the boat in this condition yields a heel of 24°.

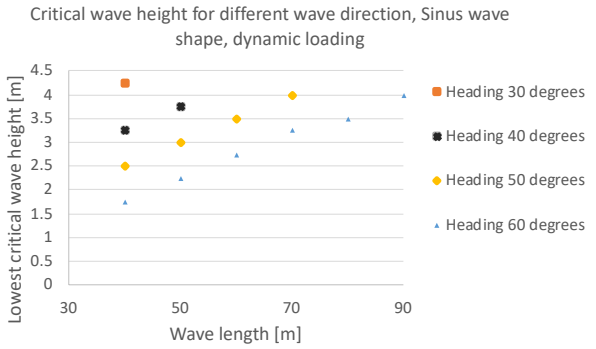

Figure 7: Critical wave heights for dynamic (step function) loading caused by turning rudders by 40°.

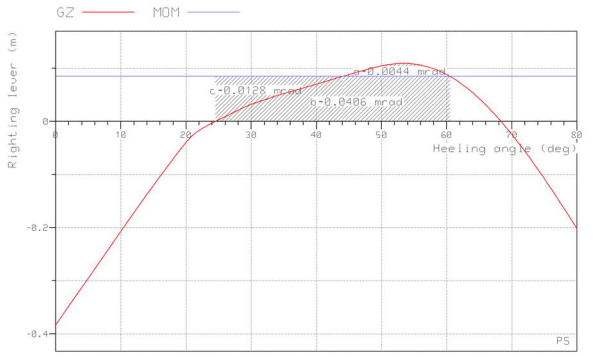

Figure 8: Dynamic loading due to rapidly turned rudders capsizes the boat in 40 m long and 3.5 m high wave, heading 40°.

A substantial decrease of the GZ-curve maximum, stability range and the capability to withstand dynamic loads is noted. The latter is not enough to resist dynamic load of the rudders.

It is clearly seen that the dynamic rudder command substantially increases the risk of capsizing. A nearly linear increase of critical wave height with length suggests that wave steepness is the primary reason for capsizing. The critical wave steepness depends upon heading. The most dangerous heading capsizing the boat in waves of smallest steepness is 60^0.

Static and step function type loading approximations are idealized realizations of the rudder action. It is impossible to find out what was the actual rudder command prior to capsizing. Most likely the loading caused by them was something in between.

5. CONCLUSIONS

Qualitatively, the conducted quasi-steady analysis of the boat's behavior in waves taking into account the effect of rudder heeling moment agrees with the observations and testimonies in the conducted investigation. In the actual critical situation, which in this case led to the accident, the pilot boat was subjected most likely to steep and breaking waves. Because the environment of such waves is difficult to evaluate and to reconstruct a simple regular wave model was used to demonstrate the effect of surface waves on the boat's stability.

The conducted investigation clearly shows that the restoring moment drops rapidly when the boat is affected by steep waves. In particular, relatively long, beam-quartering waves may be dangerous.

Evaluating the semi-displacement pilot boat stability solely on the basis of GZ-curve in still water seems not to be sufficient. The logical development of stability criteria for this type of boat, often operating in harsh weather conditions, would be checking the boat's stability in waves, as presented in the paper. Actually, such a check is a part of the second-generation of intact ship stability criteria.

The only difference between the pure loss of ship stability on a wave crest check and checking the stability of a boat in waves is the range of headings. The ship criteria consider stern and stern quartering waves of a length close to the ship length, while in case of a boat the range of headings should be larger and the considered waves longer.

To improve maritime safety in the use of the similar type craft as the capsized pilot boat, the Safety Investigation Authority Finland (SIAF) recommends that the regulatory authority should draw up regulations for special-purpose craft. The regulations should take into account the various purposes for which the craft is designed as well as the special requirements related to the conditions in which the craft is used.

The Safety Investigation Authority also pointed out that the owners should improve the orientation processes and professional competencies of the craft users in such a manner, so that the seaworthiness and

safe handling of different types of craft can be guaranteed in all operating conditions.

REFERENCES

Acanfora, M. Matusiak, J. 2016, "On the estimations of ship motions during maneuvering tasks in irregular seas", Proceedings of 3rd International Conference on Maritime Technology and Engineering, MARTECH 2016, Volume 1, Pages 227-234.

Molland,, A. F. 2007, Marine Rudders and Control Surfaces. Principles, Data, Design and Applications. Elsevier. ISBN 978-0-75-066944-3

Safety Investigation Authority Finland 2018, https://www.turvallisuustutkinta.fi/en/index/tutkintaselostukset/vesiliikenneonnettomuuksientutkinta/tutkintaselostuksetvuosittain/2017/m2017-04luotsiveneenl-242finkaatuminenjauppoaminensuomenlahdellaemasalonetelapuolella8.12.2017.html

Tompuri, M et al 2017, "On the consistency of the level 1 and 2 vulnerability criteria in the Second Generation Intact Stability", Proceedings of the 16th International Ship Stability Workshop, 5-7 June 2017, Belgrade, Serbia.

Impulsive loads on and water ingress in a landing craft: model tests and simulations

F. van Walree, *MARIN,* F.v.Walree@marin.nl
D. Sgarioto, *DST Group,* Daniel.Sgarioto@dst.defence.gov.au

ABSTRACT

This paper describes the use of two potential flow simulation tools, of varying degrees of non-linearity, for predicting landing craft motions, impulsive loads and water ingress. A comparison between experimental and simulation results for a landing craft hull form operating in irregular seas is provided. During the experiments, severe wave impacts against the bow door are recorded, with water ingress occurring through the bow door. Simulation results for these phenomena are compared with corresponding experimental results. The results from both non-linear and semi-linear versions of the simulation tool are discussed, together with measures adopted in the semi-linear method to yield results that approach the more representative non-linear results.

Keywords: *Model tests, Impulsive wave loads, Water ingress, Simulation methods.*

1. INTRODUCTION

For assessing the safety of ships in waves by means of simulations, advanced prediction methods are required. The advanced prediction method should be capable of handling six degrees of freedom, large motion amplitudes, non-linear waves, non-constant wetted geometry, water on deck effects, forward speed effects, impulsive wave loads and propulsion and steering.

Prediction methods that are capable of handling the above are in principle suited to simulate phenomena like resonant large roll motions, parametric roll, capsize due to loss of stability in waves, capsize after broaching and surf riding (van Walree and Carette 2011). Computational Fluid Dynamics (CFD) and fully non-linear potential flow methods require large amounts of computer time. For safety assessment purposes, many simulations are required to cover all combinations of speed, heading, loading condition and environmental conditions. This makes fully non-linear simulation tools (i.e. body-exact) less suitable for timely safety assessment purposes. As a compromise, simulation tools that are non-linear in only certain aspects of the hydrodynamic problem, such as wave excitation and restoring forces, are typically employed.

The Landing Craft (LLC) operating out of the Australian Defence Force (ADF) Landing Helicopter Dock (LHD) were procured as a Military off The Shelf (MoTS) vessel for performing a sea-shore connector role for the LHD. LLC seakeeping is influenced by a number of challenges associated with their operation within complex non-linear wave environments as well as their requirement for delivering large payloads at relatively high speed.

The Defence Science and Technology (DST) Group were requested by the ADF to assist with an examination of the operability of the LLC. Partnering with the Maritime Research Institute Netherlands (MARIN), a scope of work was established that combined a model scale test program with numerical simulation development. The objective of the MARIN/DST collaboration was to develop a validated numerical simulation capability. This capability could be used by the ADF for determining operational guidance for LLC operations via the development of operability guidance plots. These polar plots, presented in a format similar to the Ship Helicopter Operating Limit (SHOL) polar plots, can be used to depict LLC operability over a range of vessel speeds and headings, loading conditions and sea states using a variety of limiting criteria.

Capability improvements through enhanced understanding of LLC operability will provide a force multiplier for ADF amphibious forces and deliver important safeguards for embarked personnel and materiel. Together with the provision of significant improvements to the operating envelope of the existing LLC, the ability to evaluate the operability of future LLCs will facilitate the sustainment of Australia's amphibious assault capability into the foreseeable future.

The paper discusses the model test arrangement, the main test results and the use of the simulation tools to generate operational guidance.

2. MODEL TESTS

Seakeeping test facilities throughout the world are typically designed to test ship models at scale factors between 1/36 and 1/22. As a result, the wave makers in the test facility have been designed to generate moderate to large seaways at these scale ratios.

Unfortunately, small vessel model testing at the aforementioned range of scale factors would require small models which are too small for instrumentation and are subject to scale effects.

The model scale used for the present vessel (1/6.5) was dictated by the maximum wave height that can be generated in the seakeeping basin, space and weight considerations.

A carbon fibre model was constructed with main dimensions as given in Table 1. Propulsion and steering was by means of twin water jet units with steerable nozzles. Figure 1 shows a photo of the model.

Table 1: Main particulars

Item	Magnitude	
	Medium Load	Full Load
Lpp (m)	21.3	21.3
B-wl (m)	6.40	6.40
Tf (m)	1.19	1.29
Ta (m)	1.10	1.22
Vol (m^3)	117.7	131.9
GMt (m)	2.07	1.65
Tφ (s)	3.68	4.15

In order to measure global loads the model was segmented in four parts which were connected through an instrumented aluminium beam. At the three segment cuts the vertical shear force and torsional and vertical bending moments were calculated. The beam dimensions were chosen such that the natural frequencies for the one and two node mode shapes were approximately scaled.

Care has been taken to include the outer stiffener structure on the bow door since this was expected to affect the occurrence of water intake through the bow door louver openings, see Figure 2. Pressure gauges were used to record local pressures in the bow region.

Figure 1: Model photo

Figure 2: Bow door detail

The tests were performed in the Seakeeping and Manoeuvring Basin of MARIN. The basin measures 170 x 40 x 5 m in length, width and depth. Wave making is achieved using 331 flaps that are all individually driven by an electronic motor along the lengths of two sides of the basin. This facilitates generation of regular and long- and short-crested irregular waves from any direction. A

main carriage (x-direction) and a sub-carriage (y-direction) follow the free-sailing model. An optical motion tracking system sends position information to the on-board autopilot.

Test conditions consisted of:

- Nominal speeds of 8 and 12 knots (Froude numbers 0.28 and 0.56);
- Moderate irregular waves with $H_{1/3}$=1.25 m and T_p=5.50 s (top SS3) and $H_{1/3}$=2.50 m and T_p=6.95 s (top SS4) with directions between and including head and following seas.
- Two load conditions: 119 tonnes (t) and 134 t, representing 50 and 65 t cargo payloads.

3. MODEL TEST RESULTS

Model testing was performed for various combinations of loading condition, sea state, wave direction and speed to examine the operability of the LLC in terms of motions, accelerations, slamming and water ingress onto the loading deck. Occasionally, nominal operational limits are reached in Sea State 3 and more frequently in Sea State 4. Relevant notable findings arising from the test program include:

- Roll angles in SS4 exceed generic NATO STANAG 4154 limits in beam seas;
- Loss of course control is not observed, however heavy use of the steering nozzles is required for course keeping at lower speeds in stern quartering seas (SS3 and SS4) indicating that in higher sea states course keeping will be problematic;
- Water ingress through the bow door occurs in head and bow quartering seas, especially for the higher speed conditions. However the amount of water ingress did not compromise the stability of the vessel as it was discharged quickly through the freeing ports;
- In bow quartering SS4 conditions the vessel may occasionally be subject to breaking waves spilling over the side on to the loading deck;
- Slamming occurs frequently at high speed in bow and bow quartering seas. Impact pressures up to 320 kPa (full scale value) have been measured which is equivalent to a head of water of 32 m;
- The wave loads acting on the vessel are substantial in head and bow quartering seas due to wave impacts on the blunt bow shape.

4. SIMULATION TOOLS

The time domain panel methods are used for predicting hydrodynamic loads and seakeeping behaviour of high speed craft operating in waves. Characteristics of these simulation methods include:

- 3D transient Green functions to account for linearized free surface effects, exact forward speed effects on radiation and diffraction forces and a Kutta condition at ventilated transom sterns;
- 3D panel method to account for Froude-Krylov forces on the instantaneous submerged body;
- Cross flow drag method for viscosity effects;
- Resistance (in waves) is obtained from pressure integration at each time step;
- Propulsion and steering using propeller open water characteristics, semi-empirical lifting-surface characteristics and propeller-rudder interaction coefficients. Also a semi-empirical water jet propulsion and steering method is incorporated;
- Empirical viscous roll damping by either the FDS or Ikeda methods;
- Autopilot steering.

There are two versions of the simulation tool: a linear (PanShip) and a nonlinear one (PanShipNL). In PanShip, it is assumed that the motions of the craft are small, i.e. the submerged geometry does not change in time. Furthermore, the speed and heading are assumed to be constant so that the Green functions can be computed *a priori* for use at each time step in the simulation. In effect, the radiation and diffraction problems are then solved in a linearised manner while the wave excitation and restoring forces are treated in a nonlinear way by using the actual submerged hull geometry under the disturbed incident wave. The disturbed wave is obtained from the pressure at waterline panels.

In PanShipNL the motions may be large while the speed and heading are not necessarily constant. The discretisation of the submerged geometry and the computation of the Green function convolution integrals are performed at each time step. This approach is still not fully nonlinear due to the use of the Green functions which satisfy the linearised free surface condition. By discretising the actual submerged hull form and using the submergence relative to the undisturbed incident wave surface

rather than the calm water surface, a semi-nonlinear approach is obtained. More detailed information can be found in Van Walree et al (2016).

The hull form of MARIN model M10009 was discretised into a surface mesh consisting of 1400 panels below the still water level and 900 above the still water level panels. Figure 3 shows the mesh with a typical pressure distribution. The bow wave is clearly discernible.

During the simulations the ship was free running and self-propelled and kept on course using an autopilot. The impeller RPM was set such that the mean speed in waves was approximately equal to that of the model tests. The autopilot gains were the same as used for the model tests.

For all PanShip simulations the effect of forward speed on sinkage and trim was taken into account by determining the calm water equilibrium position a priori and adapting the hull mesh accordingly. For the PanShipNL simulations this was automatically achieved during the simulation since the mesh was adapted to the instantaneous motions and incident wave profile at each time step. The disturbed wave profile is not included in the adapted mesh; it is used for a hydrostatic correction of the pressure at each time step.

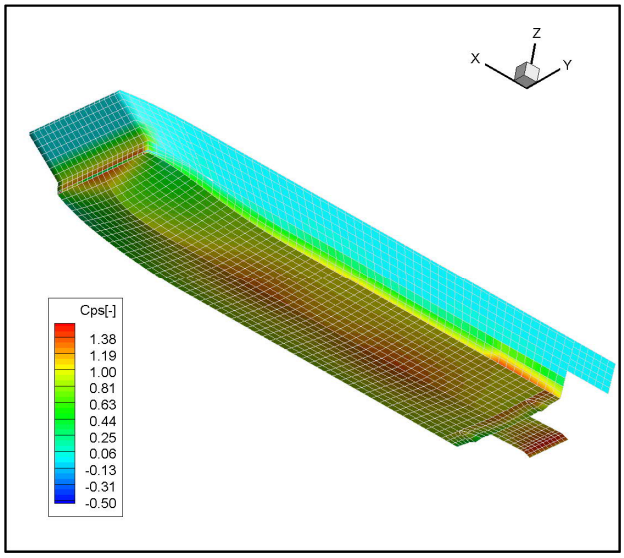

Figure 3: Discretised hull form M10009

Linear lift roll damping is included by means of the IHT method, see Ikeda (1978). For the Landing Craft model considered in this paper, quadratic roll damping was found to be well represented by the cross-flow drag method used to estimate viscosity effects in the horizontal plane for course keeping and manoeuvring.

5. SIMULATION RESULTS

Motions

Figures 4 through 7 show a comparison of motion responses for the 119 t load condition in SS4 at 8 knots speed for five wave directions where 180 deg is head seas. The response is defined here as the standard deviation of the motion divided by that of the wave height.

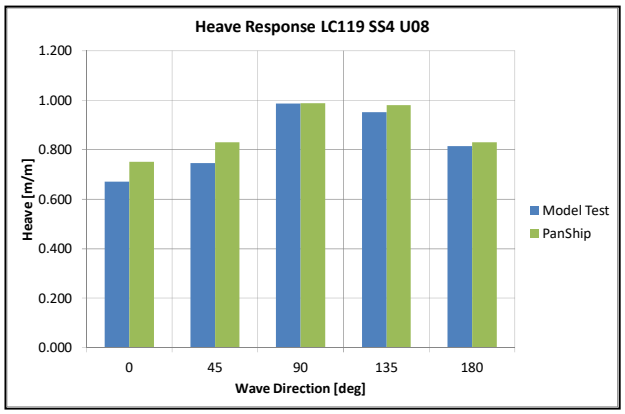

Figure 4: Comparison of heave

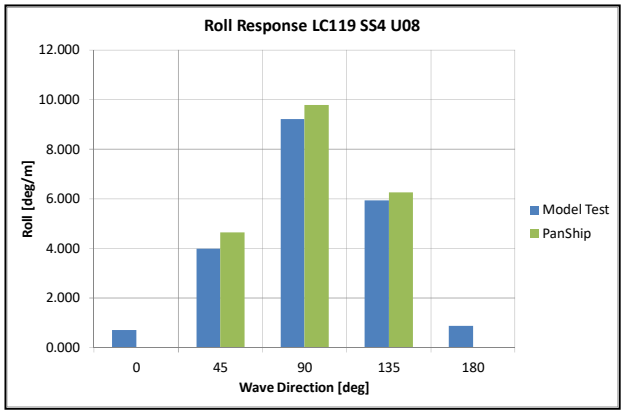

Figure 5: Comparison of roll

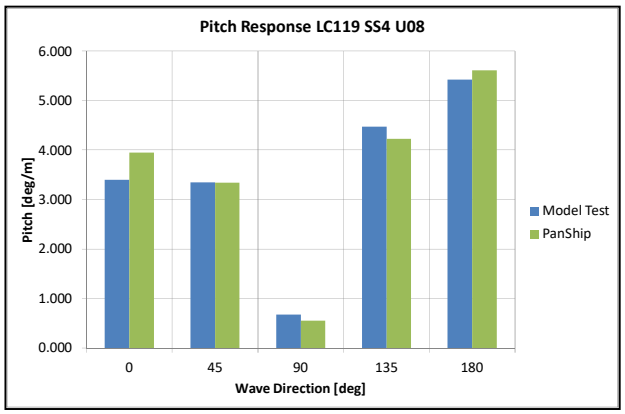

Figure 6: Comparison of pitch

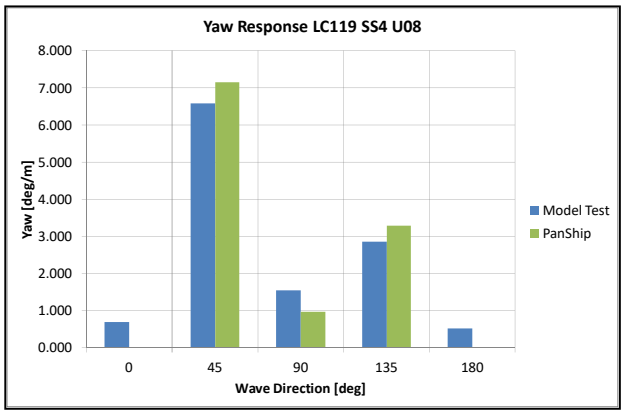

Figure 7: Comparison of yaw

The figures show that the motions are adequately predicted by the linear PanShip method. As a ship-to-shore connector for the LHD, the LLC is expected to be fully loaded on 0-90 deg headings most often as it transits from ship to shore, then most likely unladen on 180-90 deg headings on its way back to the LHD.

Wave loads

Although there are no criteria formulated for wave loads it can be an important aspect of the operability of landing craft. Figures 8 through 10 show a comparison of the mid-ship vertical shear force, torsion moment and vertical bending moment response. For this case the speed is 12 knots in SS3 and the 119 t loading condition. The uncertainty of the measurements is indicated by the error bars. It is seen that in bow seas the vertical shear force is overpredicted and the vertical bending moment is underpredicted by PanShip. This is unsurprising since the linear PanShip method cannot predict wave impact and hydro-elastic effects.

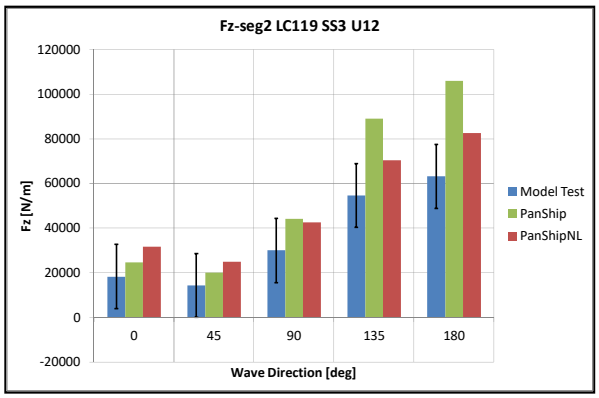

Figure 8: Comparison of vertical shear force

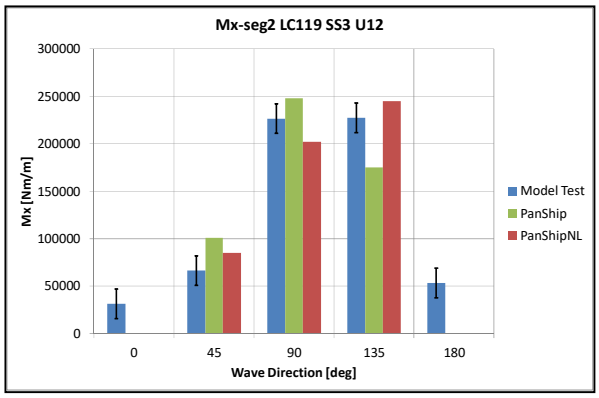

Figure 9: Comparison of torsion moment

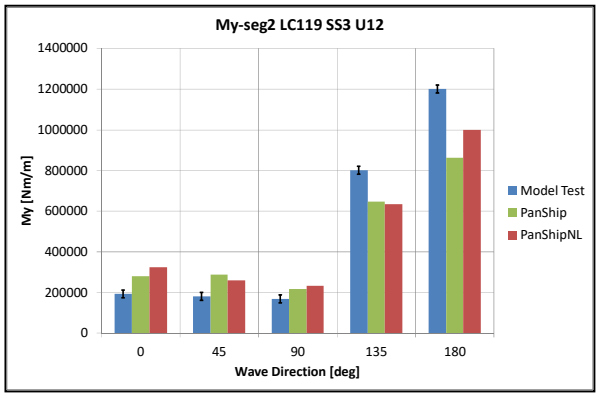

Figure 10: Comparison of vertical bending moment

The non-linear version PanShipNL does include wave impacts but still lacks hydro-elastic effects. Figures 8 through 10 show improved predictions using PanShipNL for some, but not all conditions. It is expected that the inclusion of hydro-elastic effects would improve the wave impacts prediction capabilities of PanShipNL.

Water entry

The next item of interest is water entry through the bow door louver openings. The model tests show that water may enter through these openings in head and bow quartering seas, especially at higher speeds and for heavier load conditions, see Figure 11. This phenomenon cannot be accurately predicted by PanShip due to the massive breaking bow wave and the flow blocking effect of the bow door stiffener structure. A CFD-based method is required here but would be too time consuming for generating operability information. The same is true for the non-linear PanShipNL method.

Figure 11: Model shipping water

As a compromise the following approach has been taken: depending on speed and wave direction, an additional factor (0.35 to 0.65 m) is added to the threshold relative wave height in PanShip (2.00 m above the water line) so that the predicted probability of water ingress better matches experimental observations. The probability is defined as the percentage of wave encounters that result in a water level on the deck of 0.10 m or more. Figure 12 shows a comparison between experimental, non-tuned and tuned water entry probabilities. The non-tuned simulation data are clearly much too conservative while the simple tuning does result in realistic water entry probabilities.

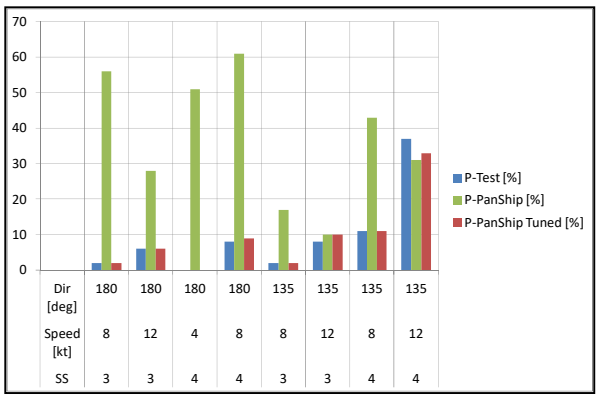

Figure 12: Water entry probabilities

Slamming

Figures 13 and 14 show the effect of a slam on the vertical acceleration and vertical bending moment. The condition is bow quartering seas SS4 at 12 knots for the 119 t loading condition. The wave frequent signal (WF) has been obtained by low-pass filtering of the measurement signal (HF). The whipping vibrations can be clearly seen in the HF signal.

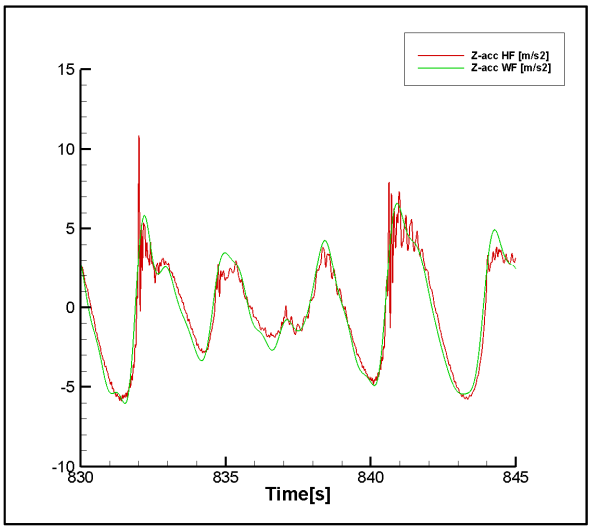

Figure 13: Vertical acceleration at the bow

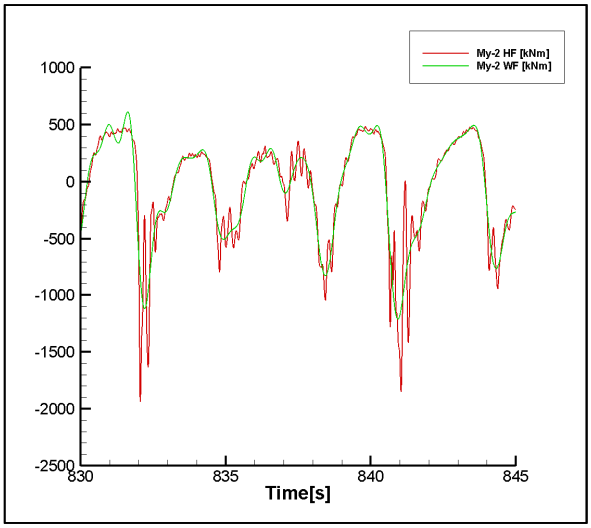

Figure 14: Midship vertical bending moment

For determining the effect of slamming on operability, one needs to define what a slam is and how much slamming can be allowed. To define a slam one can inspect time traces such as those shown in Figure 13-14 and declare an event with a significant peak followed by whipping response to be a slam. But what is significant in this respect? Another approach is to define a pressure recording above a certain threshold a slam. This approach has been adopted here, with a threshold value of 30 kPa (full scale value), related to the forebody impact pressure specified in the relevant Classification Society structural design documentation. Although not employed in this work, alternate slam identification approaches are available, see Thomas (2003) and Magoga et al. (2017) for details. The linear PanShip simulations have been tuned on the basis of the model test results with an Ochi-type

approach, see Ochi (1973). An exceedance of a threshold value for the relative vertical velocity between the pressure gauge locations and the water surface is counted as a slam. The default Ochi threshold is $V_{rel} = C\sqrt{gL}$ with a value for C of 0.093 and where L is the length between perpendiculars. Figure 15 shows the experimental slamming probabilities and corresponding C-values which result in the same probability in PanShip. The C-values are seen to be fairly constant and higher than the default Ochi value.

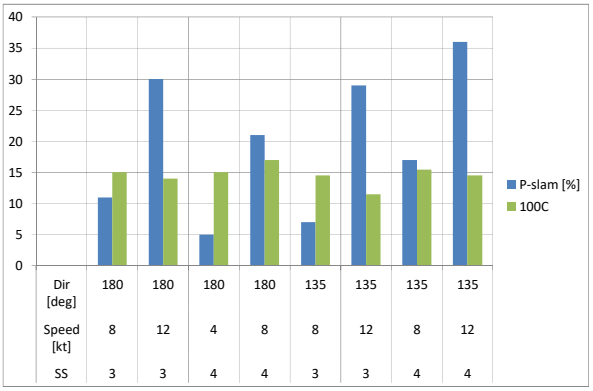

Figure 15: Slamming probabilities

The non-linear PanShipNL method can predict impact pressures. Using the same slam determination method as utilised on the model test data, the slamming probabilities predicted by PanShipNL are shown in Figure 16 for a selection of conditions. The correlation is considered to be satisfactory.

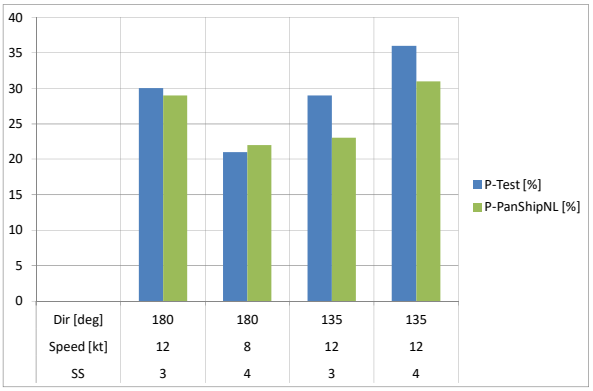

Figure 16: Slamming probabilities

6. OPERATIONAL GUIDANCE

The tuned linear PanShip method has been used to generate operability data for a large number of conditions. The conditions consisted of four sea states, three loading conditions, four speeds and thirteen wave directions, in total 624 conditions. For each condition half hour simulations were performed. The challenge is to define suitable operability criteria. In consultation with a range of stakeholders the following criteria are applied to the simulation results to generate the operational guidance plots:

- Standard deviation of roll 4-8 degrees;
- Probability of water ingress 5-10%;
- Probability of slamming 5-10%;
- Standard deviation of horizontal and vertical acceleration pilot house 1 and 2 m/s^2, respectively.

The operability guidance plots show three zones:

- Green: normal risk;
- Yellow: higher risk, consider additional controls;
- Red: urgent operational requirement only.

An example plot is shown in Figure 17.

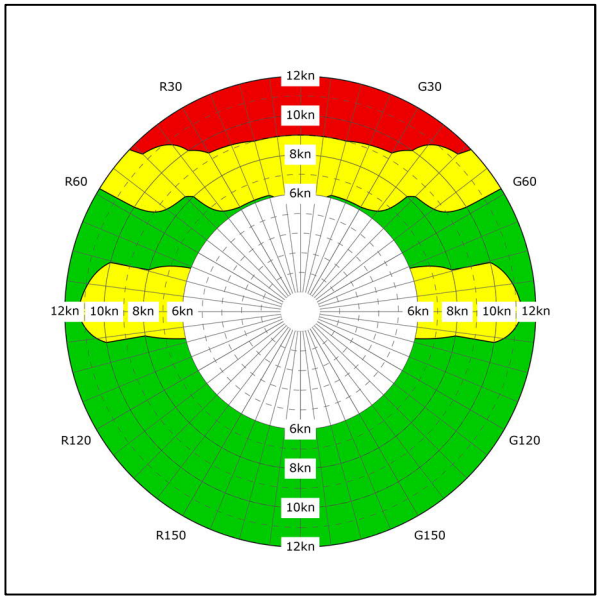

Figure 17: Example operability guidance plot

7. CONCLUDING REMARKS

The paper has addressed the use of the combination of model tests and simulation tools for generating operability data for a landing craft. The linear simulation tool PanShip can be used for the prediction of motions in waves. For predicting the occurrence of slamming and water entry through the bow door experimental data for tuning purposes is required. Predictions for wave loads are reasonable for conditions without slamming.

For improved wave load predictions in head seas the non-linear tool PanShipNL is required.

This tool can predict slamming loads without the need for tuning by using experimental results.

For the prediction of water entry through the bow door, experimental data for tuning purposes is required when using potential flow based simulation tools. CFD based tools would be better suited for this scenario, but are not presently practical for generating operability information due to lengthy simulation runtimes.

REFERENCES

Ikeda Y., Himeno Y. and Tanaka N. (1978), "Components of Roll Damping of Ship at Forward Speed", ISSN 0514-8499.

Magoga, T., Aksu, S., Cannon, S., Ojeda, R., & Thomas, G. (2017). Identification of slam events experienced by a high-speed craft. *Ocean Engineering, 140*, 309-321. doi: https://doi.org/10.1016/j.oceaneng.2016.07.017

Ochi M.K. and Motter L.E. (1973), "Prediction of Slamming Characteristics and Hull Responses for Ship Design", Transactions SNAME Annual Meeting, November 15-17, New York, 1973.

Thomas G. (2003) "Wave Slam Response of Large High Speed Catamarans", PhD thesis, University of Tasmania.

Van Walree F. and Carette N.F.A.J. (2011), "Validation of Time Domain Seakeeping codes for a Destroyer Hull Form Operating in Steep Stern Quartering Seas", International Journal of Naval Architecture and Ocean Engineering, Vol. 3, Issue 1, March 2011, pp. 9-19.

Van Walree F., Sgarioto D. and Turner T.G. (2016), "Validation of a Time Domain Panel Code for Prediction of Impulsive Loads on High Speed Ships", 31th Symposium on Naval Hydrodynamics, Monterey, California, 11-16 September.

Probabilistic damage stability of small passenger ships

S.L. van der Voort, *Rotterdam Mainport Institute, Department of Maritime Engineering, The Netherlands*
s.l.van.der.voort@hr.nl
M.K.S. Krol, *Rotterdam Mainport Institute, Department of Maritime Engineering, The Netherlands*
F.M. de Wit, *Rotterdam Mainport Institute, Department of Maritime Engineering, The Netherlands*

ABSTRACT

The IMO has set a new standard for the probabilistic damage stability requirements for passenger ships. One of the major changes is a new formula for the required subdivision index R which will result in a higher required subdivision index for new passenger ships. Whether very small passenger ships can meet this requirement was never investigated. This study aims to give a general indication of the possibilities for small passenger ships with a length of approximately 40 meters to meet the new required subdivision index. The scope of the study is limited to adjustments to the openings and changes of the internal subdivision. External hull form, displacement and GM' were not varied and the cost effectiveness of the changes were not investigated.

Keywords: *Probabilistic damage stability, very small passenger ships, SOLAS, required subdivision index R, attained subdivision index A, internal subdivision, weathertight openings.*

1. INTRODUCTION

The IMO Maritime Safety Committee (MSC) agreed in her 98th session (IMO, Report of the Maritime Safety Commission on its ninety-eighth session, 2017) on a revision of damage stability requirements. Part of this revision is a new method for calculating the required subdivision index for passenger ships. In the current SOLAS the required subdivision index for passenger ships depends on the length of the ship, the number of passengers and the lifeboat capacity. As of January 2020, the required subdivision index R will depend only on the number of passengers the ship is designed to carry. The formulation of R was extensively discussed in the IMO subcommittee Ship Design and Construction (SDC). In particular for smaller passenger ships widely different views were expressed as to what extent raising the required subdivision index would be a cost effective measure to improve the safety of these ships. Where raising the R value for passenger ships carrying 400 passengers or more has been justified by several studies and publications, the possibilities for smaller ships are hardly investigated. In this paper two small passenger ships with a length of approximately 40 meters are modelled with various internal subdivisions to investigate to what extent compliance with the new R value is possible for very small passenger ships.

2. INTERNATIONAL LEGAL CONTEXT

As part of the IMO working program, the damage stability requirements in SOLAS Chapter II-1 have been revised by the SDC subcommittee during several sessions. Part of this revision was the establishment of a formule for the required subdivision index R as defined in SOLAS CH II-1, regulation 6.

The SDC sub-committee vividly discussed various formulas for the required subdivision index, based on extensive feasibility studies into values for R, including detailed cost analyses for RoRo passenger ships and cruise vessels (GOALDS Consortium, 2012), (Japan, 2013). Where these studies focused on the effects of raising R for small passenger ships, it is observed that the lower limit of the ships studied lies at 400 passengers (Danish Maritime Authority, 2015) (DNV GL AS Maritime, 2015) (Japan, 2015). Based on the proposals made by the SDC sub-committee, the Maritime Safety Committee of the IMO agreed to set the value for R at 0.722 for ships carrying 12 up to 400 persons on board (IMO, Report of the Maritime Safety Commission on its ninety-eighth session, 2017). For passenger ships designed to carry more than 400 persons the revised SOLAS contains formulas in Chapter II-1 regulation 6 to calculate the value of R.

For ships engaged in international voyages the 400 persons limit may seem reasonable as passenger ships with less than 400 passengers are normally not engaged in international voyages. However, in this respect two things should be observed. The first is that the SOLAS passenger ship requirements are, by definition, applicable to all ships carrying 12 or more passengers. It would be illogical to set a requirement that cannot reasonably be met by the all ships it applies to. The other observation is that (inter)national legislators tend to harmonize different sets of regulations, for which SOLAS requirements are often used as basis. For passenger ships with a length of 24 meter or more in national EU trade, the EU directive 2009/45 (EC, 2009) is applicable. Although the current damage stability requirements of EU/2009/45 are identical to the old, deterministic, SOLAS requirements, it is expected that the directive will be aligned with the new probabilistic SOLAS requirements as soon as the directive is revised.

3. SCOPE OF THIS PAPER

In order to investigate to what extent smaller passenger ships can be subdivided to meet the SOLAS 2020 subdivision requirements, various subdivisions were made for two different hull forms. For each subdivision the attained subdivision index was calculated and compared with the required subdivision index.

For this study the attained subdivision index A was calculated according SOLAS CH II-1; part B-1. Consequently the calculations were made for the three draughts prescribed in regulation 6 and 7, and permeabilities and openings were modelled in accordance with the specific requirements. A compliance check with SOLAS Ch. II-1 regulation 6.1 was made for each of the three partial indices and with regulation 7.1 for the weighted summation of A over the three draughts.

Limitations and boundaries of the scope

The aim of this study is to determine whether small passenger ships can meet the SOLAS probabilistic damage stability index R. Other damage stability requirements from SOLAS CH II-1, with a more deterministic nature, must also be met. These requirements include, but are not limited to SOLAS CH II-1 regulation 8 (Special requirements concerning passenger ship stability) and regulation 9 (Double bottoms in passenger ships and cargo ships other than tankers). Even though it is known that the deterministic requirements may, in many cases, be limiting for passenger ship damage stability, they are not included in this study.

For this study, modifications for improving the attained subdivision index are limited to the openings and internal subdivision. External geometry, draughts, GM' and trims were not varied. The cost effectiveness of the changes to the model were not investigated.

4. SHIP DESIGNS

For the purpose of this paper, two hull forms were created in the stability calculation program PIAS[1]. PIAS is a calculation tool for hydrostatic calculations and has, amongst others, modules for intact and probabilistic stability calculations.

Design of Model A

The first hull is based on an existing, Netherlands flagged, sailing passenger ship2, certified under the EU directive 2009/45. The external geometry, draughts, GM and internal watertight decks and bulkheads provide a subdivision standard complying with the regulations of EU 2009/45 and the SOLAS (1990) deterministic 1-compartment subdivision standard. An overview of the external hull form of model A is presented in Figure 1. The displacement and position of the center of gravity are taken from the original ship. Draughts, trims and GM' values are presented in Table 1.

The internal subdivision of model A-0 is represented in Figure 2.

Table 1: Subdivision loading conditions Model A.

Subdivision loading condition	Draught [m]	Trim [m]	GM' [m]
Light	2.000	-1.000	1.20
Partial	2.138	0.000	1.10
Deepest	2.230	0.000	1.10

[1] PIAS is a naval architecture design software package designed by SARC B.V. based in The Netherlands. PIAS can be used for design and stability purposes. PIAS is accepted by major classification societies and statutory authorities.

[2] For reasons of privacy the name and details of the ship are not disclosed.

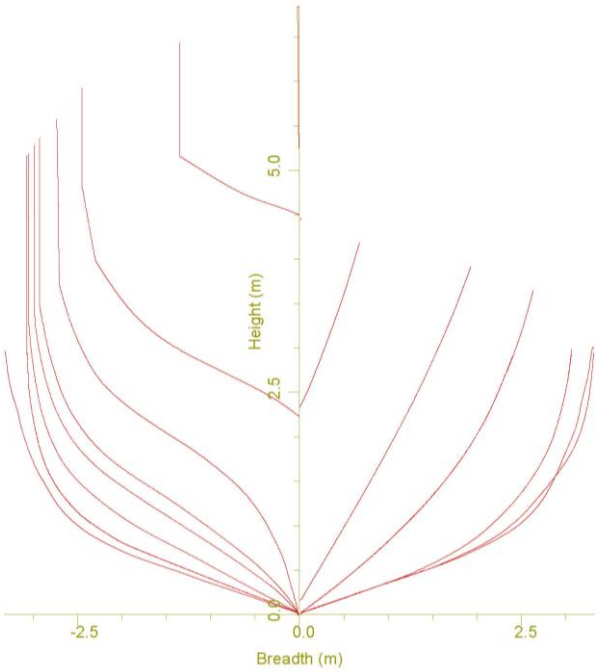

Figure 1: Frames fore and aft ship of Model A.

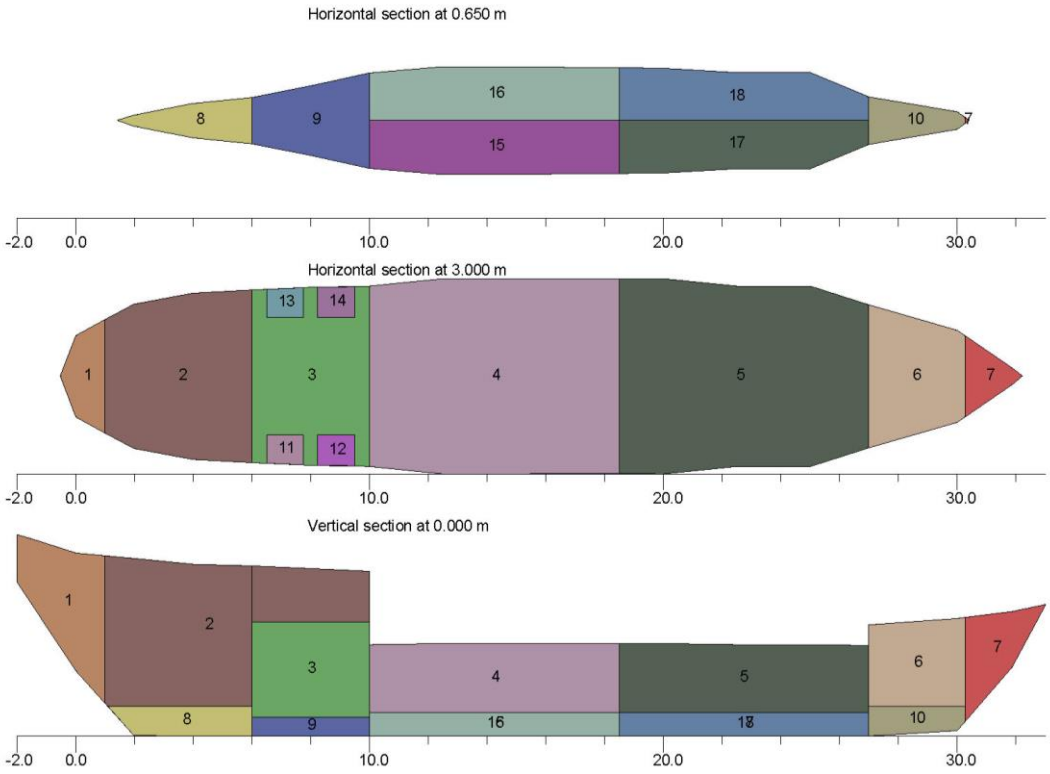

Figure 2: Internal subdivision of Model A-0.

Design of Model B

The second hull is based on the external geometry of a fishing vessel. The initial internal subdivision was chosen to provide ample subdivision for compliance with the 1 compartment standard. Hull form and subdivision of Model B are presented in Figure 3 and Figure 4. The displacement and position of the center of gravity are based on the original fishing vessel, whereby the weight of fishing gear and fish in the holds is replaced with a weight for passengers. Draughts, trims and GM' values are presented in Table 2.

Table 2: Subdivision loading conditions of Model B.

Subdivision loading condition	Draught [m]	Trim [m]	GM' [m]
Light	2.700	-1.000	0.609
Partial	2.940	0.000	0.503
Deepest	3.100	0.000	0.539

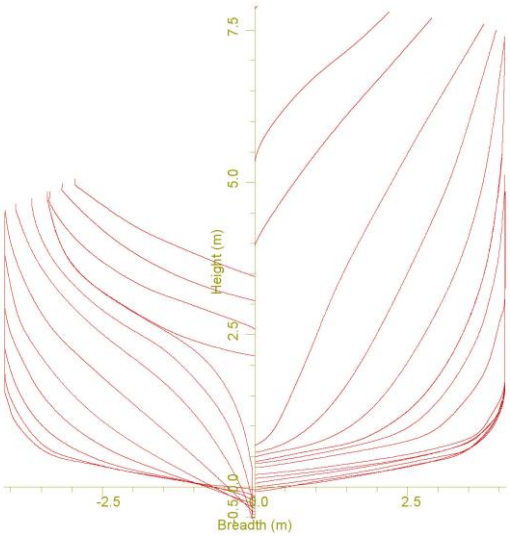

Figure 3: Frames fore and aft ship of Model B.

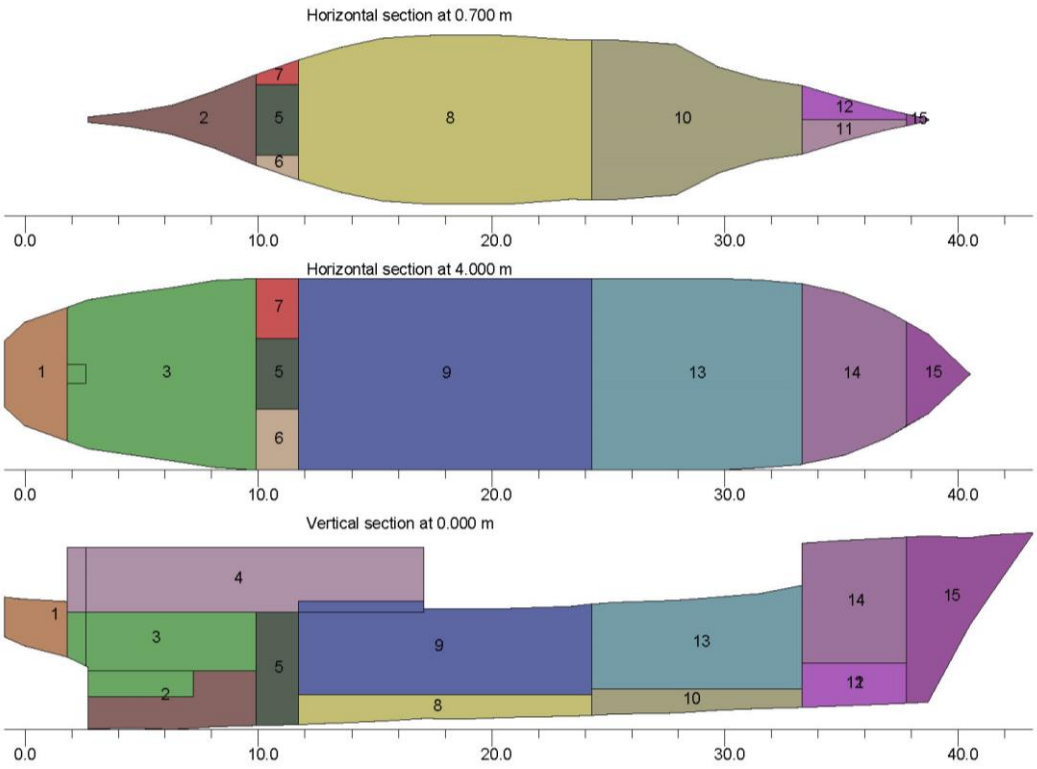

Figure 4: Internal subdivision of Model B-0.

5. MODIFICATIONS AND RESULTS MODEL A

Design changes

In order to investigate possibilities of improving the attained subdivision index, five alterations of the openings and internal subdivision of model A were investigated:

A-1) Improved openings: openings are raised and/or moved towards the center line;
A-2) Improved tanks engine room: the existing tanks in the sides of the engine room are extended to form a continuous double hull;
A-3) Increased double bottom accommodation: the height of the double bottoms is enlarged;
A-4) Six tanks under two holds: the existing tank arrangement (two tanks under each hold) is changed. Two tanks are added. One starboard and one portside, both partially under the fore and aft hold;
A-5) The existing two tanks under each hold are subdivided into four tanks under each hold.

An overview of the subdivision of Model A-5 is presented in Figure 5. The design choices made in model A-1 up to A-5 are arbitrary which is unavoidable because it was not possible to investigate all possible changes within the scope of this study. A-1 was chosen as adjusting (de-aeration) openings has limited impact during the design stage but may improve the attained subdivision index considerably. The same applies to a certain extent to the changes in model A-2, creating a double hull. Fitting a continuous double hull will not be much more complicated than creating separate tanks. Raising the height of the double bottom in model A-3 will result in more room to construct and maintain the tanks. The height of the compartments above the tanks remains sufficient for the passenger accommodation areas. Model A-4 with six tanks in the double bottom under the two holds, is the first step in decreasing the volume of the individual double bottom tanks. The same applies to model A-5 with eight tanks under the two holds.

Attained subdivision indices

The attained subdivision index of the original model A is relatively close to the required subdivision index. Normally only small design changes would be necessary to raise A sufficiently. For the purpose of this study more thorough design changes have also been tried, some of which resulted in a decrease of A. An overview of the attained indices is presented in Table 3. In this table, the attained subdivision index is the weighted sum of the three partial indices calculated in accordance with SOLAS CH II-2 regulation 7.1. The rightmost column (A/R) indicates to which extent the attained subdivision index meets the required subdivision index; each model with A/R > 1 is compliant.

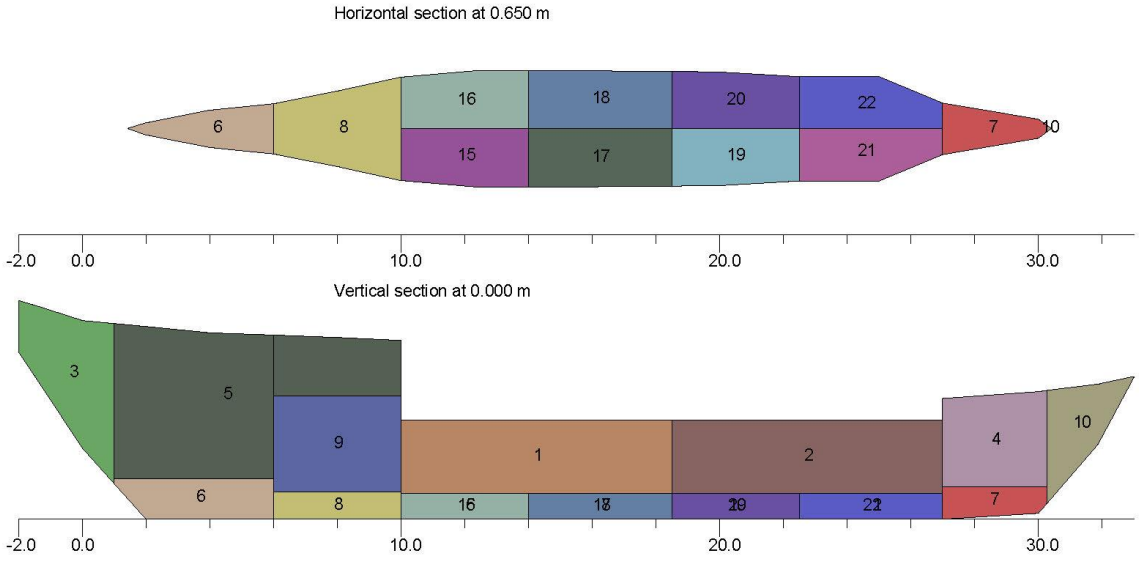

Figure 5: Internal subdivision of Model A-5.

Table 3: Attained subdivision indices of Model A.

description	Damage cases	A	A/R
Model A-0	58	0.6899	0.96
Model A-1	58	0.7602	1.05
Model A-2	49	0.7623	1.06
Model A-3	49	0.7627	1.06
Model A-4	65	0.7041	0.98
Model A-5	65	0.7630	1.06

For compliance with SOLAS regulation 6.1, the attained subdivision index of each partial draught shall be greater than 0.9 times R. Table 4 presents the results of the 6 different designs of model A. Here a ratio of A/0.9R above one indicates that the attained subdivision index for that specific draught complies with regulation 6.1. The results in Table 3 and 4 indicate that Models A-2, A-3 and A-5 comply with both regulation 6.1 and 7.1.

Table 4: Attained partial subdivision indices of Model A.

description	$A_l/_{0.9R}$	$A_p/_{0.9R}$	$A_s/_{0.9R}$
Model A-0	1.22	1.05	0.99
Model A-1	1.22	1.32	0.99
Model A-2	1.24	1.24	1.07
Model A-3	1.24	1.24	1.07
Model A-4	1.24	1.12	0.97
Model A-5	1.24	1.24	1.07

6. MODIFICATIONS AND RESULTS MODEL B

Design changes

For model B, an internal subdivision complying with a 1-compartment was created. In order to investigate possibilities of improving the attained subdivision index, six alterations of the openings and internal subdivision of model B were investigated:

B-1) The fuel tanks are relocated from transverse oriented tanks in front of the engine room to double hull side tanks in the engine room;

B-2) Both single tanks under the holds are subdivided in six separate tanks; two SB, two PS and two center tanks;

B-3) The SB and PS double bottom tanks under the accommodation holds are connected with a cross-flooding device;

B-4) Both accommodation holds are fitted with side tanks in line with the double bottom tanks. In order to avoid large heel after damage, the side tanks are fitted with a cross over;

B-5) The side tanks are only fitted in the aft hold;

B-6) Only the aftermost two side tanks (One SB, one PS) are fitted in the aft accommodation.

An overview of the subdivision of Model B-6 is presented in Figure 6.

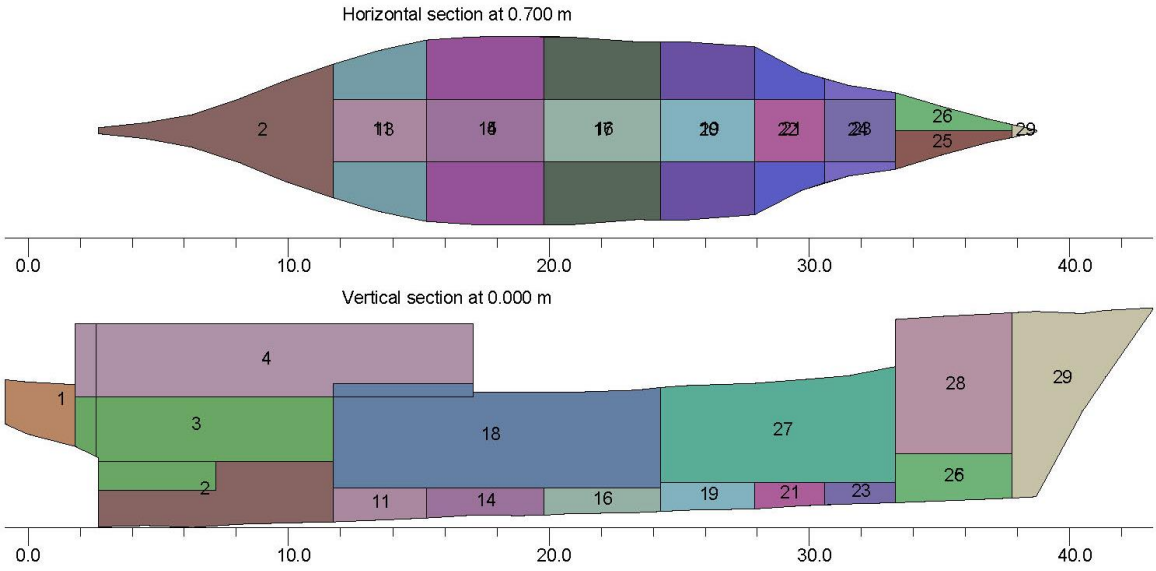

Figure 6: Internal subdivision of Model B-6.

For the same reasons as for model A the chosen subdivisions for model B are arbitrary. Moving the fuel tanks as proposed for model B-1 has serious impact on the design of piping and engine room lay out. Changes proposed in model B-2 and B-3 have a smaller impact as construction elements for the subdivision of tanks are already in place for structural integrity, which limits the design impact to piping and (watertight) welding. Design changes B-4, B-5 and B-6 do have more impact on the design, both in terms of construction weight as in terms of reduced available space for passengers.

Attained subdivision indices

The original Model B-0 does not meet the required subdivision index. The index of all designs is presented in Table 5. It is obvious that adding a continuous double hull in the accommodation area in model B-4 has a large positive effect on the attained subdivision index. The results of Model B-3 show that a cross over between double bottom tanks has, for this ship, a negative impact on the attained subdivision index. Apparently the increase of volume of the combined compartments has a bigger influence on the stability in damaged condition than the reduction of heel. Table 4 shows that a partial double hull in one hold (model B-5) or even one third of the hold (model B-6) raises the attained subdivision index to a value above the required subdivision index.

Table 5: Attained subdivision indices of Model B.

description	Damage cases	A	A/R
Model B-0	100	0.6071	0.84
Model B-1	118	0.6096	0.84
Model B-2	256	0.6824	0.95
Model B-3	254	0.6656	0.92
Model B-4	201	0.8789	1.22
Model B-5	191	0.8688	1.20
Model B-6	197	0.7587	1.05

Also for model B compliance with SOLAS regulation 6.1 was checked. The results of this check are presented in Table 6. These results indicated that Model B-4, B-5 and B-6 comply with both regulation 6.1 and 7.1.

Table 6: Attained partial subdivision indices of Model B.

description	$A_l/_{0.9R}$	$A_p/_{0.9R}$	$A_s/_{0.9R}$
Model B-0	0.90	0.91	0.97
Model B-1	0.87	0.86	1.05
Model B-2	1.11	1.01	1.06
Model B-3	1.13	0.92	1.08
Model B-4	1.40	1.33	1.36
Model B-5	1.34	1.35	1.33
Model B-6	1.23	1.13	1.18

7. DISCUSSION

This study focussed on existing hull forms. As a consequence, only changes in the internal subdivision and deck openings have been investigated. When all parameters of the design could have been adjusted for improvement of the attained subdivision index, other solutions may also have been interesting to investigate. Following examples of such changes are indicative, and should not be considered as exhaustive:

- Increase of beam;
- Increase of depth;
- Increase of GM; (note: GM of the model A already is rather high as the design is a sailing ship)
- Increase of buoyant volume on deck such as forecastle, deckhouse, etc;
- External additions to the buoyant hull such as duck tails or sponsoons.

Another possibility, only taken into account to a limited extent in this study, is to investigate the effects of small changes of the position of bulkheads. Minor transverse shifts of longitudinal bulkheads may be very effective in reducing heel after damage. This may increase the survivability after damage, while the influence on the probability of that damage is relatively small. The same applies in principle to the longitudinal position of transverse bulkheads.

In a further study the effect of the proposed measures such as adding or replacing bulkheads, on the light ship weight and the position of the centre of gravity of the ship should be taken into account and the values of the light service draught, VCG' (or GM') should be adjusted accordingly

Both models presented in this study require more or less significant changes in the internal subdivision to meet the new R index. In other, more detailed studies (DNV GL AS Maritime, 2015), The life time costs of all suggested changes are calculated in order to validate whether the proposed improvements are cost effective. The determination of the costs of the

proposed measures are beyond the scope of this study. It would be interesting to quantify costs and effects of these measures. However, the majority of the changes proposed are, from a structural point of view, rather limited. Repositioning a bulkhead in the first stages of the ship design hardly affect the final costs for building or operating a ship. With respect to more extensive changes such as adding a double hull, these do affect the building price significantly and should be carefully considered.

This study only focused on the required and attained subdivision index. Compliance with other revised requirements of SOLAS Chapter II-1 are outside the scope of this paper. It may be expected that other parts of the revised damage stability requirements such as the ban on open watertight doors at sea, have a significant impact on the design and operation of smaller passenger ships.

A second interesting topic for further research would be the whether the factor s_i[3] with a value of 1 does represent a sufficient probability of survival for small ships.

8. CONCLUSION

This study proves that it is possible to meet the new increased SOLAS probabilistic damage stability required subdivision index with small passenger ship designs. Whether the measures necessary for compliance are cost effective was not investigated. Some changes in the internal subdivision such as adding a double hull, will most certainly affect the costs of operation and construction. Others, such as raising openings, will probably have a smaller impact.

To meet the required subdivision index, the original designs had to be refined to a certain extent. For model A, the necessary adjustments affect the design to a limited extent. For model B, the necessary changes include the fitting of a double hull in the engine room and a partial double hull in the under deck passenger area. These measures have quite an impact on the design and would possibly not be cost effective.

Other likely effective design changes such as raising the GM' were not investigated in this study, but may prove to be highly effective in reaching the required subdivision index.

The results of the calculated indices show that, in general, the required subdivision indices for the partial draughts A_l, A_p and A_s are also met when the combined index A is met.

It can be concluded that meeting the required subdivision index is possible for small passenger ships. Whether the additional deterministic requirements from SOLAS Chapter II-1 regulation 8 an 9 can also be met is not investigated.

REFERENCES

Danish Maritime Authority. (2015). *Small Ro/pax Vessel stability study.* Valby: DMA.

DNV GL AS Maritime. (2015). *Combined assessment of cost effectiveness of previous parts, FSA compilation and recommendations for decision making.* Høvik: DNV-GL.

EC. (2009). *2009/45 safety rules and standards for passenger ships* . Brussels: EU.

GOALDS Consortium. (2012). *Development of new damage stability requirement based on Cost-Benefit assesment.*

Group, R. E. (2019). *Red Ensign Group Yacht Code.* United Kingdom: Red Ensign Group.

IMO. (2008). *Code on safety for Special Purpose Ships -SPS-Code.* London: IMO.

IMO. (2017). Report of the Maritime Safety Commission on its ninety-eighth session. (p. Annex 3). London: IMO.

Japan. (2013). *SDC1/INF.7 Review of the damage stability regulations for Ro-Ro passenger ships.* London: IMO.

Japan. (2015). *SDC 3/3/8; Proposal on the required* subdivision *index 'R' taking into account the risk level of small passenger ships.* london: IMO.

[3] The factor s_i accounts for the probability of survival after flooding. S_i is defined in SOLAS CH II-1 regulation 7-2 and depends on the stability characteristics after damage.

GM limiting curve for operation in brackish water

Petri Pennanen, *NAPA,* petri.pennanen@napa.fi
Daniel Lindroth, *NAPA,* daniel.lindroth@napa.fi
Pekka Ruponen, *NAPA,* pekka.ruponen@napa.fi

ABSTRACT

Onboard a passenger or dry cargo ship, the statutory compliance related to intact and damage stability criteria is most conveniently determined by using GM limiting curves. The actual GM of the loading condition is compared to a required value, read from a curve for the actual draught/trim combination. The GM limit values are calculated for the full operating range of draught and trim. However, in practice the GM limiting curves do not cover draughts greater than the deepest subdivision draught or the maximum sea water draught of the ship. When the ship is operated on a sea area of brackish water, like the Baltic Sea, there is no common understanding on how to use the GM limiting curves, and it is not clear whether the ship is allowed to submerge the Plimsoll mark. Furthermore, the definition of the required GM value is not clear since the limit curve does not exceed to that draught. The problem affects many ships built according to different editions of the SOLAS. The authorities and classification societies have different approaches, but a common and well-grounded way is needed. The problems are highlighted by presenting real life practical examples.

Keywords: *damage stability, statutory compliance, loading computer, load line, sea water density.*

1. BACKGROUND

The GM limiting curves are very practical for determining the statutory compliance for passenger or dry cargo ships, especially onboard. These curves are calculated by the designer, and presented in the stability booklet of the ship. According to the SOLAS, the GM limit information shall be presented as consolidated data and encompass the full operating range of draught and trim. In practice, however, the curves do not cover draughts exceeding the deepest subdivision draught or the maximum sea water draught of the ship.

When the ship is operated on a sea area of brackish water, like the Baltic Sea, there is no common understanding on how to use the GM limiting curves. Brackish water is water having more salinity than freshwater, but not as much as seawater, and consequently density is between 1.0 and 1.025 t/m^3. This condition commonly occurs when fresh water meets seawater such as estuaries, where a river meets the sea. However, there are also brackish seas and large lakes, such as Baltic Sea, Black Sea and Caspian Sea.

When a ship arrives from the North Sea to the Baltic Sea, the draught of the ship increases, possibly exceeding the summer load line draught. In these cases, it is not clear, how to define the minimum required GM for the sea passage on the Baltic. Some classification societies have not approved the calculation of the curves beyond the summer load line draught, whereas some require separate "fresh water limiting curves" to be used. Some classification societies request the use of the equivalent draught, calculated in sea water, to be used instead of the actual draught in brackish water.

This paper discusses the problems by presenting four real life cases related to the use of a loading computer applying GM limiting curves in brackish water navigation. In addition, the relevant damage stability calculations are briefly referred with examples.

2. REGULATORY ASPECTS

International Convention of Load Lines (ICLL)

The International Convention of Load Line (ICLL), as amended, declares limitations to how much a ship can be loaded based on freeboard, and was signed on April 5th 1966, ICLL (1966). The convention received a significant update in the Protocol of 1988, ICLL (1988), and in Resolution MSC.143(77) in 2003, IMO (2003). Use of basic freeboard tables, as is done in the convention, dates

back more than a century, and regardless of the latest amendments, the convention would still benefit from further revision, as is discussed in Kobylínski (2006).

The requirement not to submerge the Plimsoll mark in Article 12 is part of the original text of ICLL from 1966. Unfortunately, still today the convention does not provide a clear answer to if it is acceptable to submerge the Plimsoll mark, for example in the Baltic Sea. The original intention in the convention was likely to allow a temporary submersion of the mark when sailing into, or from, sheltered estuaries, rivers and lakes. However, brackish water areas, like the Baltic Sea, are not sheltered, and the operating conditions can be very harsh, FMI (2019).

Ships designed to be operated solely in the Baltic Sea traffic, like the cruise ferries between Finland and Sweden, have their stability documentation done for sea water with a density of 1.005 t/m^3, and are not allowed to submerge the summer load line.

Ships designed for unrestricted service and oceans, like international cruise ships, are however typically allowed to "slightly" submerge the summer load line mark in the Baltic Sea since their visit is considered "temporary". However, these cruise ships may be operating in the Baltic Sea for the whole summer season, which can last over three months.

From a loading computer point of view, "slightly" is not a precise enough definition to be applied in a software that is used for confirming statutory compliance. Therefore, a clearer definition, or at least a common interpretation, is needed.

International Convention for the Safety of Life at Sea (SOLAS)

A practical way for the master to check compliance with the intact and damage stability requirements is to compare the current loading condition to a limiting GM curve. This information is required to be supplied to the master by the current Chapter II-1 Part B-1 Reg. 5-1 of the International Convention for the Safety of Life at Sea (SOLAS), as amended, IMO (2006).

The limiting GM curves are, for damage stability compliance, calculated for a draught range from the lightest service condition up to the deepest subdivision draught, at different trims if needed. SOLAS Chapter II-1 Part A Reg. 5-1.4 further explains that for draughts in between the calculated ones, the limiting values are to be obtained by linear interpolation, IMO (2006). Regulation 5-1.5 right after continues that if the curve could be considered not appropriate for a condition, possibly for situations when the operating condition falls outside of the limiting curve range, the master is required to operate using an already studied condition or to verify by calculation that the condition is acceptable.

According to the definition in SOLAS Chapter II-1 Part A Reg. 2.10, the deepest subdivision draught is *the waterline which corresponds to the summer load line draught of the ship*, IMO 2006. Deadweight, on the other hand, is according to SOLAS Chapter II-1 Part A Reg. 2.20 defined as "*the difference in tonnes between the displacement of a ship in water of a specific gravity of 1.025 at the draught corresponding to the assigned summer freeboard and the lightweight of the ship*". Following these definitions, ships operating in waters with a smaller density than 1.025 t/m^3, like the Baltic Sea, cannot be loaded with their full deadweight, without submerging the summer load line mark.

Looking a little deeper into SOLAS, Chapter II-1 Part A-3 Reg. 18.5 states for passenger ships that: *"In no case shall any subdivision load line mark be placed above the deepest load line in salt water as determined by the strength of the ship or the International Convention on Load Lines in force".*

Additionally Reg. 18.6 immediately after states that: *"Whatever may be the position of the subdivision load line marks, a ship shall in no case be loaded so as to submerge the load line mark appropriate to the season and locality as determined in accordance with the International Convention on Load Lines in force".* Consequently the interpretation of if or how much the mark can be submerged is here passed to ICLL.

Looking a little into the future, the most recent amendments for SOLAS Resolution MSC.421(98), IMO (2017a), and the corresponding Explanatory Notes Resolution MSC.429(98), IMO (2017b), do offer some guidance to this situation. According to the new Explanatory Notes for SOLAS 2020 Reg. 5-1.4 Paragraph 5: *"Ships may be permitted to sail at draughts above the deepest subdivision draught ds according to the International Convention on Load Lines, e.g. using the tropical freeboard. In these*

cases, for draughts above ds the GM limit value at ds is to be used". The Baltic Sea is, however, defined to be a normal winter or summer load line seasonal area according to Annex II Reg. 51 in ICLL, ICLL (1966).

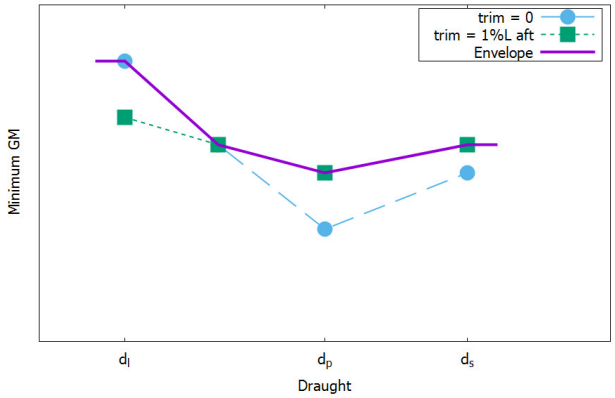

Figure 1: Illustration of envelope GM limit curve with SOLAS 2020, including the extensions of the draught range

3. DAMAGE STABILITY CALCULATIONS AND WATER DENSITY

Calculation of a damage case

When the initial condition before flooding is defined as the floating position (draught and trim) and center of gravity (or metacentric height), and the final condition is calculated with the lost buoyancy method, the water density has no effect at all. The results are solely dependent on the hull form, damaged compartments and the center of gravity. For intermediate flooding stages, a common practice is to consider constant volumes of floodwater in the calculation of the righting lever, see Ruponen et al. (2018).

Let us consider a single degree of freedom model for the transverse stability and heel angle ϕ of the ship, Figure 2. The static righting moment is:

$$M_{st}(\phi) = -\Delta\overline{GZ}(\phi) = -\rho g \nabla \overline{GZ}(\phi) \qquad (1)$$

where ρ is density of water, g is gravitational acceleration, ∇ is volume of displacement and $\overline{GZ}$ is righting lever.

The heeling moment, caused by the floodwater, depends on the water density:

$$M_w(\phi) = \rho g V_w(\phi)\big(y_w(\phi) - y_G(\phi)\big) \qquad (2)$$

where V_w is the volume of floodwater and y_w and y_G are the centre of floodwater and centre of gravity in a global coordinate system.

At equilibrium heel angle ϕ, the sum of these two moments is zero:

$$M_w(\phi) + M_{st}(\phi) = 0 \qquad (3)$$

Substituting equations (1) and (2) results in:

$$\rho g V_w(\phi)\big(y_w(\phi) - y_G(\phi)\big) - \rho g \nabla \overline{GZ}(\phi) = 0 \qquad (4)$$

Or simply:

$$V_w(\phi)\big(y_w(\phi) - y_G(\phi)\big) = \nabla \overline{GZ}(\phi) \qquad (5)$$

Obviously, the solution is not dependent on the density of the water.

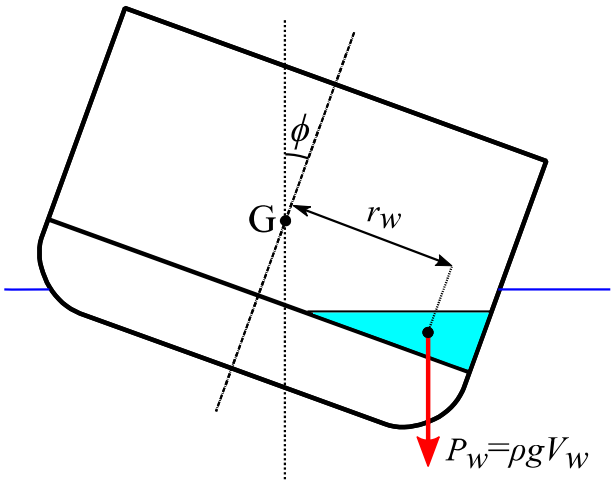

Figure 2: Heeling moment due to floodwater

Calculation of GM limiting curve

When evaluating the minimum GM at given draught (and trim), the form stability lever is unchanged, and only the center of gravity KG is iterated so that the stability requirements are passed.

The s-factor in SOLAS depends on the characteristics of the righting lever (GZ) curve, in particular:

- heel angle
- immersion angle of unprotected openings
- range of positive stability
- maximum righting lever

In principle, all of these are geometric quantities, dependent on the hull form and the center of gravity. The density of water does not have a direct effect on the righting lever values. Naturally, the displacement, and subsequently the static righting

moment, are directly proportional to the density. The only exception is the s-mom factor that is used for passenger ships since the external heeling moments (passenger, wind and survival craft) are independent of the water density, but in fresh water the displacement that corresponds to the same draught value is smaller than in salt water.

4. PRACTICAL EXAMPLES

SOLAS 1992 (Reg. 25-1) ro-ro ship in Baltic and North Sea operation

This ship has been built in the early 2000s, and is operating between ports at the northern end of the bay of Bothnia in the Baltic Sea and the North Sea. All the loading conditions presented in the original stability booklet have been calculated using 1.005 t/m^3 as the sea water density. Also the maximum displacement has been defined at the summer draught in that density.

After installation of a scrubber, the cargo capacity of the ship was naturally decreased. In order to compensate this, a new stability booklet was suggested, with one full load loading condition calculated in fresh water. Also the maximum deadweight would be defined based on this loading condition. The idea was to be able to load the ship at the FW load line, when departing from the Bay of Bothnia, where the water is brackish, although not completely fresh. The owner requested the loading computer to be updated in order to show this as a legal departure loading condition. However, the flag administration could not deliver a clear answer, whether this would be such a case.

The new stability booklet still presented the original GM limiting curve, calculated up to the maximum summer draught (in density 1.025 t/m^3). Even in case it would be allowed to submerge the Plimsoll mark for a voyage of several days on the Baltic Sea, there would not be a value of required GM to compare the actual GM with, at that draught.

The owner even had damage stability calculations performed at the fresh water maximum draught and in fresh water. However, these calculations did not provide required GM value for that draught – only a confirmation of a sufficient A-index

Finally, the class advised that the Plimsoll mark may be submerged at the Baltic, according to ICLL and that the SOLAS 2020 method could be used for the required GM at the draughts above the maximum summer load line.

At the deeper end of the GM limiting curves, the governing values are derived from the intact stability criteria with an upwards trend. These should be extended by 0.12 m horizontal line in the loading computer, although not shown in the stability booklet.

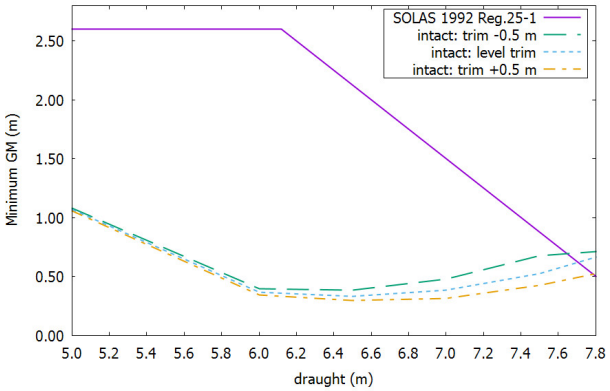

Figure 3: GM limiting curves for a ro-ro ship, ending at the maximum draught in sea water

SOLAS 2009 ro-ro ship in the Baltic Sea

The second example is also typical ro-ro ship in traffic between ports at the Baltic Sea, but designed according to the probabilistic damage stability requirements of SOLAS 2009. The ship has a typical GM limit curve for a ro-ro, Figure 4, with the damage stability results governing at the deeper draughts. The curve shows decreasing requirement for the GM as the draught is increased.

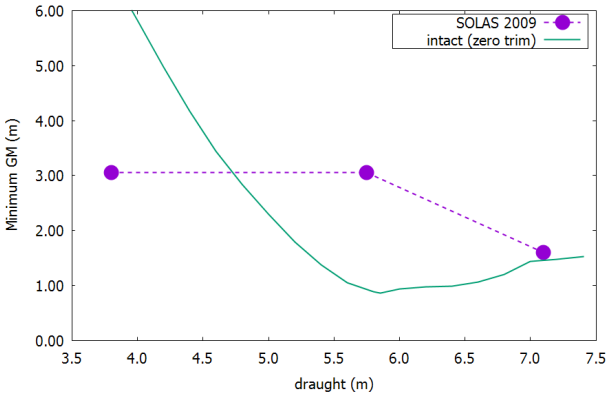

Figure 4: GM limiting curve of a Baltic ro-ro ship, according to SOLAS 2009

For some unknown reason, it was not allowed to use this curve in the loading computer in sea water densities below 1.025 t/m^3. Instead, it was requested that the GM should be compared using a draught corresponding to an equivalent loading condition in

the density of 1.025 t/m^3 as a substitute of the actual draught in brackish water.

This suggested approach will result in a more conservative requirement, but based on the calculations shown earlier, this is not justified, since the density of the sea water does not affect the calculation of the GM limiting curve.

SOLAS 90 cruise ship in the Baltic Sea

The deterministic damage stability results are usually calculated for a set of trims covering the operational loading conditions. The required GM is found by interpolating between the curves. For deterministic damage stability requirements, it is easy to calculate the minimum GM at any combination of draught and trim.

An example of GM limiting curves, which has been calculated well beyond the summer load line draught of the ship is presented in Figure 5. This way it is possible to utilize the curves also in fresh water situations and the approach also gives flexibility for future draught increases based on weight growth over the life span of the ship.

The loading computer gives relevant warnings of possible overloading of the ship, based on summer load line draught and the set density of the sea water.

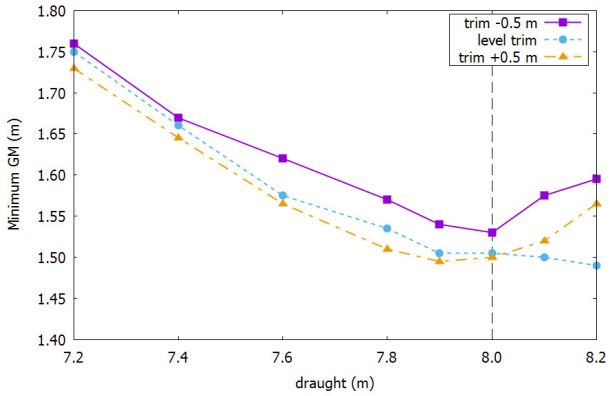

Figure 5: GM limiting curves of a SOLAS 90 cruise ship, the vertical line marks the maximum draught in sea water

SOLAS 2020 cruise ship in the Baltic Sea

For this kind of a ship, the single GM limiting curve is derived from the calculation of three draughts and compiled to cover the whole trim range. In addition to that, the explanatory notes of the rule state that the ship may be permitted to sail at draughts above the deepest subdivision draught according to the ICLL. In these cases, for draughts above ds, the GM limit value at ds is to be used.

Rule-wise, it is clear how to handle the GM requirement at draughts above the summer load line draught, provided that it is clearly legal to exceed this draught because of the sea water density. An example of the limit curves is presented in Figure 6.

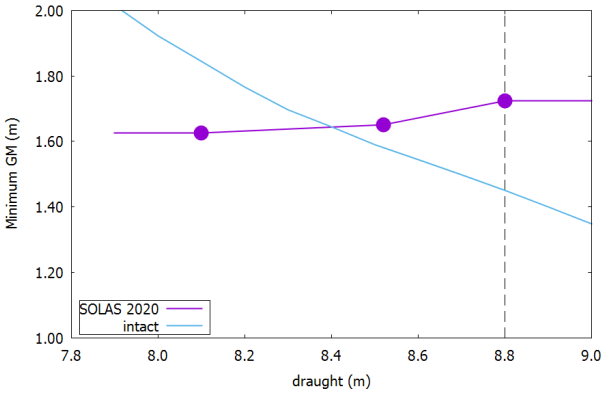

Figure 6: GM limiting curves of a SOLAS 2020 cruise ship, the vertical line marks the maximum draught in sea water

5. LIMIT CURVES WITH PROBABILISTIC DAMAGE STABILITY CALCULATIONS

In order to illustrate the effect of different sea water densities on the limiting GM curves, a case study calculation was performed using NAPA software for a generic ro-ro cargo ship ($L_S \approx 180$ m) and a cruise ship ($L_S \approx 300$ m).

In this study, for simplicity, it is assumed that the damage stability requirements are the governing ones, and the intact requirements are therefore left out. To simulate the effect of the ships entering or leaving brackish waters, draughts corresponding to a constant weight while the sea water density changes from 1.025 t/m^3 to 1.005 t/m^3, or 1.005 t/m^3 to 1.025 t/m^3 were used, and compared against the results from the actual draughts (constant density). The draughts calculated are presented in Table 1 and Table 2.

Table 1 - Draughts calculated for the ro-ro ship

Original draught	Draughts for δ: 1.005 t/m^3 → 1.025 t/m^3	Draughts for δ: 1.025 t/m^3 → 1.005 t/m^3
4.00 m	3.935 m	4.066 m
5.20 m	5.116 m	5.285 m
6.00 m	5.905 m	6.097 m

Table 2 - Draughts calculated for the cruise ship

Original draughts	Draughts for δ: 1.005 t/m^3 → 1.025 t/m^3	Draughts for δ: 1.025 t/m^3 → 1.005 t/m^3
8.10 m	7.975 m	8.227 m
8.52 m	8.390 m	8.651 m
8.80 m	8.666 m	8.936 m

For the probabilistic damage stability calculation according to SOLAS, IMO (2006), there is a global requirement that the attained subdivision index A shall be larger than the required subdivision index R. This requirement do however offer some freedom in choosing the GM values for the individual draughts, and is therefore not suitable to use when the actual limiting value at each draught is sought. The regulation on the other hand does also set a requirement for the individual draughts, that each partial attained subdivision index A_i shall be at least 0.5R for cargo ships, and at least 0.9R for passenger ships, IMO (2006). These criteria are more useful for an iteration searching to find the actual limit, and used in this case study as well.

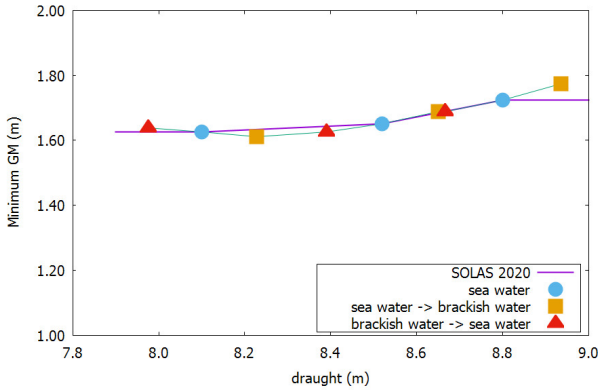

Figure 7: GM limiting curve for a cruise ship according to SOLAS 2020 and at actual draught changes due to water density

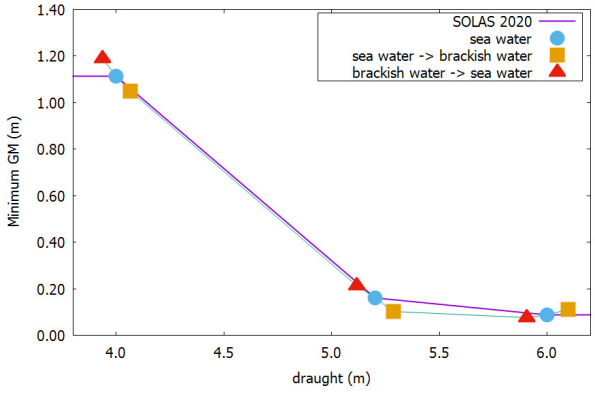

Figure 8: GM limiting curve for a ro-ro ship according to SOLAS 2020 and at actual draught changes due to water density

The calculation was set up in an iteration loop where new GM values were used to re-define the initial conditions until the difference for a new GM value was less than 2 cm and the A_i criteria for the ship type passed. In each iteration loop a new attained subdivision index for each draught was calculated.

The results of the GM limit iteration for the two calculated ships are presented in Figure 7 and Figure 8. Compared to the ro-ro ship, the original draughts for the cruise ship are closer to each other, and consequently, it operates with a smaller relative deadweight. This can also be one of the reasons for that the variation in limiting GM values is smaller for the cruise ship compared to the ro-ro ship. It is good to remember that as these GM limit values now represent the partial subdivision index requirements only, they do not as such comply with the overall attained subdivision index requirement of A being greater than R. It is also notable that the limiting GM values for draughts outside the original draught range are not exactly following the extrapolated values according to the Explanatory Notes for Reg. 5-1.4 of SOLAS 2020, IMO (2017b).

6. CONCLUSIONS

Based on the presented examples and underlying physics of damage stability, the most important finding of the study is that:

- The only relevant parameter when defining and applying the minimum GM values is the draught of the vessel in the sea water density of the operation area.

The big question for ships operating in sea areas with brackish water is whether it is allowed to submerge the Plimsoll mark. Provided that submerging the summer load line mark in brackish sea water areas is allowed by interpretation of the ICLL, the following conclusions can be drawn from the presented real life practical examples:

- Using the expanded GM limiting curves over the whole draught range, up to the maximum fresh water draught, with the draught (and possibly trim) as the only parameter would erase all problems related to the interpreting the effect of the sea water density
- SOLAS 2020 offers a solid rule-wise solution, which is easy to apply. The same could be expanded to cover SOLAS 2009 ships since the calculation methodology is the same
- However, this may not always be realistic, and alternatively a minimum GM curve could be extended based on calculations at additional

draught values. With this approach, the requirement for partial attained subdivision index must be met

- For SOLAS 90 ships with deterministic damage stability, it would be an easy task to expand the GM limiting curves, by calculating the requirements for one additional draught representing the maximum draught in fresh water

Finally, it should be noted that ships designed for operation at the brackish sea, like the Baltic Sea, should not be allowed to submerge the Plimsoll mark, since this operation cannot by any means considered to be a temporary situation.

REFERENCES

FMI 2019, "Wave height records in the Baltic Sea", visited March 20th, 2019, https://en.ilmatieteenlaitos.fi/wave-height-records-in-the-baltic-sea

IMO 2003, "Resolution MSC.143(77) – Adoption of Amendments to the Protocol of 1988 Relating to the International Convention on Load Lines, 1966", Adopted on 16 June 2003.

IMO 2006, "Resolution MSC.216(82) Adoption of Amendments to the International Convention for the Safety of Life at Sea, 1974, as Amended", Adopted on 6 December 2006.

IMO 2017a, "Resolution MSC.421(98) Amendments to the International Convention for the Safety of Life at Sea, 1974, as Amended", Adopted on 9 June 2017.

IMO 2017b. "Resolution MSC.429(98) Revised Explanatory Notes to the SOLAS Chapter II-1 Subdivision and Damage Stability Regulations", Adopted on 9 June 2017.

ICLL 1966, "International Convention on Load Lines, 1966", Adopted on 5 April 1966.

ICLL 1988, "Protocol of 1988 relating to the International Convention on Load Lines, 1966", November 11th 1988.

Kobylínski, L., 2006, "New Load Line Rules – Success or Failure?", EXPLO-SHIP 2006, ISSN 1733-8670

Ruponen, P., Manderbacka, T., Lindroth D., 2018, "On the calculation of the righting lever curve for a damaged ship", *Ocean Engineering* 148, pp. 313-324.

Ro-Ro passenger ships – from Stockholm Agreement to SOLAS2020

Jakub Cichowicz, University of Strathclyde, jakub.cichowicz@strath.ac.uk
Odd Olufsen, DNV GL, odd.olufsen@dnvgl.com
Dracos Vassalos, University of Strathclyde, dracos.vassalos@strath.ac.uk

ABSTRACT

In June 2016, the European Commission (EC) appointed a consortium comprising several research and commercial organisations, to conduct an "*assessment of specific EU stability requirements for ro-ro passenger ships*". The primary aim of the study was to compare the regional requirements as specified by Directive 2003/25/EC (commonly known as Stockholm Agreement) with the provisions of the amended SOLAS regulations (SOLAS 2020). The two predominant changes in SOLAS lead to significant increase in the required index of subdivision, R, and the calculation of the survivability factor (s-factor) for the flooding cases involving vehicle/large open spaces of ro-ro passenger ships. In this paper the authors discuss various elements of the regulations that need to be considered while comparing both frameworks.

Keywords: *RoPax ships, SOLAS2020, Stockholm Agreement, damage stability, survivability.*

1. BACKGROUND

The legislation considered in this study is based on Directive 2003/25/EC (applicable to ships on international voyages visiting European ports) and Directive 2009/45/EC which makes the Directive 2003/25/EC mandatory for all new ships of classes A, B and C on domestic voyages.

The Directive 2003/25/EC is based on some assumptions fundamentally different from other regulations concerning damage stability. The main assumption is that water may accumulate on the ro-ro deck in case of a damage. Hence, the Directive requires that the stability is assessed by assuming a certain amount of water on deck in the flooded condition. The water accumulated on deck is quantified based on the freeboard after damage and the limiting wave height applicable for the area of operation.

The criteria and requirements of the Directive 2003/25/EC were introduced at a time when the deterministic damage stability standard of SOLAS90 was in force. The probabilistic damage stability concept was introduced also for passenger ships by SOLAS2009. However, the Directive was kept applicable as it was not considered evident that the amended requirements of SOLAS2009 would ensure the same safety level as Stockholm Agreement[1]. When the newly adopted SOLAS2020 enters into force, the requirements will become stricter for new ships both in terms of the formulation of survivability when the roro space (and other open spaces) is involved in a damage case as well as in terms of the required subdivision index R.

2. OUTLINE OF THE REGULATORY FRAMEWORKS

Stockholm agreement

The Stockholm Agreement provisions require demonstration of survivability in a specific damage with

- 0.5 m water head accumulated on deck if the residual freeboard is less than 0.3 m and
- 0.0 m if the residual freeboard is 2.0 m or more

with linear interpolation in between.

[1] For brevity the Stockholm agreement is referred to as SA in the following

The height of water accumulated on deck can be adjusted depending on the significant wave height (with a 10% probability of exceedance) in the specific area of operation. For areas where the significant wave height is 4.0 m or above, the height of accumulated water is as in the residual freeboard formulations while it is assumed to be 0.0 m when the significant wave height is 1.5 m or less, with linear interpolation in between.

SOLAS

The damage stability framework of SOLAS[2] is mostly probabilistic with the deterministic provisions for minor and bottom damages. The overall objective of the framework is to ensure that the attained index of subdivision, A, is equal or larger than the required index, R, that is

$$A \geq R \tag{1}$$

The attained index is nothing else than the weighted average of expected probabilities of survival (given as the so-called s-factors), namely

$$A_j = \sum_i p_i s_i$$

and (2)

$$A = \sum_j w_j A_j$$

Where

- A_j Partial subdivision index at j[th] loading condition (with the additional requirement that $A_j \geq 0.9R$)
- w_j Weighting factor representing proportion of time the ship operates in one of the three loading conditions (light draught, partial subdivision draught and deepest subdivision draught)
- p_i Weighting factor representing probability of occurrence of the specific damage case
- s_i The survival factor (s-factor) representing expected probability of survival

However, the above relationships present only the high-level and clear-cut picture of the framework. The actual implementation is, for number of reasons, much more convoluted:

- The factor s for the final stage of flooding, s_{final} is modified by two multipliers - s_{mom} and k; the former is essentially a deterministic measure accounting for (the largest of) external heeling moments due to passenger crowding, launching of life-saving appliances and wind. The factor k is an arbitrary and deterministic linear model accounting for detrimental impact of heel on ability to evacuate the ship (with $k = 0$ for heel angles in damage equilibrium equal to or larger than 15 degrees).
- The factor s used in A-index calculations is taken as the smaller of two - s_{final} (including k and s_{mom}) and $s_{intermediate}$, both calculated by the very similar models (with the latter being less stringent)
- Additional, deterministic, requirements for the minor (in terms of length and transverse penetration) damages are specified by SOLAS Ch. II-1 Reg. 8.
- Bottom damages are regulated by semi-deterministic requirements specified by SOLAS Ch. II-1 Reg. 9.

3. MAIN ISSUES PERTAINING TO COMPARING SA WITH SOLAS

Comparison of any regulatory frameworks is always a challenging task, even if the frameworks stem from the same root. In case of SA and probabilistic regulations of SOLAS the undertaking is particularly difficult because the regulations are of fundamentally different origins and they differ even in the part promising the biggest overlap (i.e. minor damages provision of SOLAS Ch. II-1 Reg. 8). The main issues can be summarised as in the follows

- SA was intended as a purely deterministic addition to the existing set of deterministic regulations whereas SOLAS2009 is primarily a probabilistic instrument with some deterministic elements (such as k, s_{mom} or the content of Ch. II-1 Reg.8)
- SA is selectively targeting a specific damage scenario whereas SOLAS is comprehensive, accounting for the entire watertight subdivision

[2] For brevity the probabilistic framework for damage stability of SOLAS will be in the following referred to simply as SOLAS.

and all damage scenarios deriving from it. These features are a direct consequence of the regulations stemming from distinctive roots. As a result, it is easy to identify the SOLAS damages that correspond to SA and verify if they meet the SA requirements, but the opposite is not true. The SA damages are a mere (and small) subset of probabilistic damages and the compliance with SA says little more about the overall survivability other than that *all the less severe* damages should also result in survival in the wave height in question

- SA is prescriptive and sets specific requirements with respect to the combination of residual freeboard and the height of floodwater on the vehicle deck that defines the scenario in which the survival needs to be demonstrated. SOLAS is, in its main part, goal-oriented and does not consider any specific scenarios for as long as the weighted proportion of all surviving cases is larger than the required index. This implies that the SOLAS compliant ship may still fail the SA requirements.
- The SA requirements are wave-height scalable, i.e. the exact requirements can be changed depending on the prevailing wave conditions in the specific area of operation. SOLAS (for the reasons that will be discussed in the following) does not offer such possibility.
- SA compliance can be demonstrated either by calculations or by model tests. This is a unique feature of the SA. For obvious reasons, SOLAS allows proof of compliance by calculations only.

Nevertheless, considering a larger sample of vessels allows for drawing, with some confidence, conclusions about the high-level relationship between the standards. In the case of SA and SOLAS the following aspects need to be examined in order to measure how these standards relate:

- equivalence of the stability criteria by comparing the limiting sea states of the SA to the critical significant wave height, HS_{crit} (a concept implicitly present in SOLAS s-factor formulation);
- equivalence of safety levels provided by the regulations which can be achieved by comparing the attained indices of subdivision of SA-compliant ships to the required index of subdivision of SOLAS2020;
- how the operational wave-height limitations can be captured by the probabilistic framework

These will be discussed in detail in the following section.

4. COMPARISON OF SURVIVAL CRITERIA

The SA survival criteria are based on a combination of the residual freeboard and height of the floodwater accumulated on the ro-ro deck (if the freeboard is lower than 2 meters). SOLAS, on the other hand, uses the s-factor to estimate the expected probability of surviving specific damage *in waves*. The GZMAX and RANGE requirements in the s-factor formula are the measures of the ship resilience against capsize caused by the action of waves.

Customarily, the s-factor models are derived in a two-step process (Figure 1), see for example (Bird & Browne, 1973), (Project HARDER, 2000-2003). The first step involves determining the relationship between ship parameters and the critical significant wave height, HS_{crit} (the limiting sea state below which the ship can be considered safe). The critical significant wave height is damage-case and loading-condition specific. Furthermore, because the HS_{crit} is expressed as a function of ship parameters it can be considered as an attribute of the ship rather than the environment (i.e. HS_{crit} measures ability of the ship to survive a specific damage in waves).

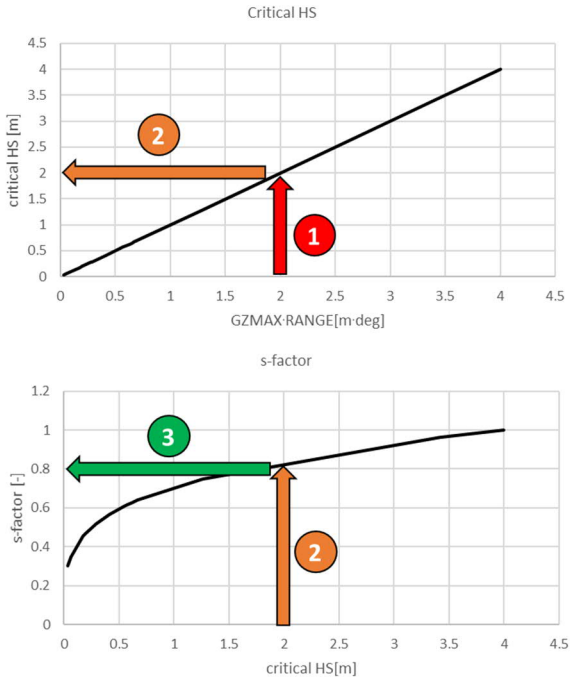

Figure 1: Two-step algorithm for calculating the s-factor. Top graph – estimating the critical HS based on the GZ curve characteristics. Bottom graph – use of the critical HS to determine the s-factor

The implicit, two-step, modelling behind the s-factor allows to isolate the HS_{crit} from the formula and use it as a yard stick against SA (noting however, that both instruments are arbitrary).

The following formula describes the relationship between the s-factor and the critical *HS* (Jasionowski, 2009):

$$s = \left(\frac{HS_{crit}}{4.0}\right)^{0.25} \quad (3)$$

Thus, the critical *HS* is given as

$$HS_{crit} = 4.0 \cdot \frac{GZMAX}{TGZMAX} \cdot \frac{RANGE}{TRANGE} \quad (4)$$

Where

RANGE – is the range of positive stability (up to the flooding angle) of the damaged ship

GZMAX – is maximum righting lever within the RANGE

TGZMAX and TRANGE – are *target* values for the maximum righting lever and range, respectively

Presently in SOLAS2009 the target values are given as 0.12 m for TGZMAX and 16 degrees for TRANGE. However, in a bid to mitigate the risk of capsize due to accumulation of floodwater on the vehicle, the latest amendments to SOLAS2020 bring higher requirements for the damages involving the ro-ro spaces. These new requirements are 0.2m and 20 degrees, respectively. Thus, bearing in mind that it is the concern about the vulnerability to the ro-ro-deck flooding that is addressed by Directive 2003/25/EC it is reasonable to use the following model to calculate the critical HS for relevant damages

$$HS_{crit} = 4.0 \cdot \frac{GZMAX}{0.2} \cdot \frac{RANGE}{20} \quad (5)$$

When it comes to comparing critical *HS* to the limiting sea states the fact that SA compliance can be demonstrated by model tests is of great assistance. This is because the results of physical tests are generally representative and hence not affected by the arbitrariness of simple formulae. A significant number of SA model tests is reported in (Vassalos & Papanikolaou, 2002) and these results were used as basis for comparing the critical *HS* against the SA. The results, presented in Figure 2, show clearly that the values calculated with the SOLAS2020 target values demonstrated much higher correlation with the SA limiting wave height than the results calculated with the SOLAS2009 values. Specifically, nearly all the results based on SOLAS2009 are more lenient than SA whereas the SOLAS2020-based predictions show much better agreement with SA (although with quite significant scatter). These results indicate that the more stringent requirements of SOLAS2020 have similar effect on survivability to the requirements of SA (in terms of trends – the scatter is a consequence of the systematic uncertainty, irreducible with the present, lacking robustness, formula for the critical *HS*). Based on this it can be concluded that the new SOLAS requirements for the righting lever and range constitute survival criteria comparable to SA.

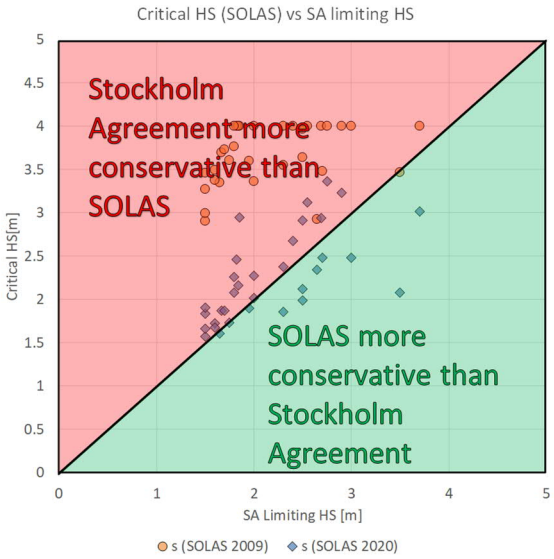

Figure 2: Comparison of the critical HS calculated with SOLAS2020 target values for GZMAX and RANGE with the experimentally derived SA limiting HS as reported in (Vassalos & Papanikolaou, 2002)

It is also noteworthy, that the present requirements are consistent with the earlier proposal made following the second EMSA study, which claimed that increase of the GZMAX and RANGE requirements to 0.25 meter and 25 degrees, respectively would make the s-factor a conservative measure with 90% confidence, see Figure 3 below.

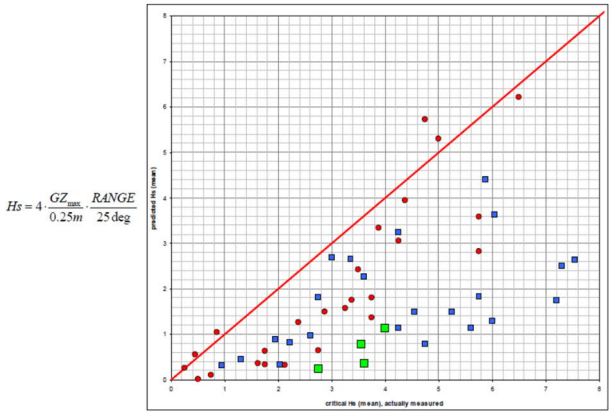

Figure 3 Comparison between critical wave height based on s-factor proposed within EMSA2 and measured during the model experiments for a sample of conventional RoRo/RoPax ships (Jasionowski, 2009).

5. COMPARISON OF SAFETY LEVELS

For a ship of passenger capacity in excess of 400 persons on board[3](POB) SA may be considered as a "2+ compartment equivalent standard[4]". This is a consequence of the additional freeboard/water-on-deck requirements imposed on the worst 2-compartment SOLAS90 damage. Obviously, for the reasons discussed in the foregoing it is impossible to establish the one-to-one correspondence between the standards. Furthermore, the actual designs are often optimised for the specific set of rules they need to comply with, hence their performance measured against another set of rules may be suboptimal. Nevertheless, it can be argued that high-enough safety standards (goal) in terms of R would eliminate most of the "blind spots" and local vulnerabilities from the design leading inadvertently to consistent and uniform safety levels.

Generally, in comparison to SOLAS2009, SOLAS2020 represents significant increase in standard, delivered primarily by the change in required index of subdivision R. In fact, the analysis carried out in the study (European Commission, 2019)[5] demonstrates that most of the sample ships carrying more than 1350 POB (in compliance with SA and SOLAS 2009 or SOLAS90) would fail to meet the requirements of the new regulations (SOLAS2020) even if the optimised GM was used in A-index calculations. This implies that the "2+ compartment equivalent standard" as delivered by SA is not high enough to meet the required index of subdivision.

The situation is, however, different in case of smaller capacity ships (carrying less than 1350 POB), where the tendency is that the majority of sample ships are able to achieve compliance with the new regulations (European Commission, 2019).

This is a notable fact for two reasons: firstly, previous research, e.g. (Project GOALDS, 2009-2012), indicates that present SOLAS s-factor model tends to overestimate survivability of smaller (in terms of dimensions) ships. The SOLAS 2020 amendments to the s-factor model result in a shift in the survivability prediction but the model remains less stringent for the small ships. Secondly (and more importantly), the level of R as adopted for SOLAS2020 is a political compromise which saw the level or R as recommended by EMSA 3 study (so-called EMSA 3.2 proposal reflecting the study involving calculations of costs of averting fatality, CAF) was reduced by IMO twice.

The first compromise was made by SDC3 whilst the second, final change was done by MSC98; in both cases the changes affected mostly the ships of smaller passenger capacity (below 1,000 POB).

Table 1: Level of *R* formulations

	POB	R
EMSA 3.2	All	R=1-(C1 x 6200)/(4 x N+20,000) with C1=0.8-(0.25/10,000) x (10,000-N)
SDC3	$N \leq 1{,}000$	R=0.000088 x N+0.7488
	$1{,}000 < N \leq 6{,}000$	R=0.0369 x ln(N+89.048)+0.579
	$N > 6{,}000$	R=1-(C1 x 6200)/(4 x N+20,000) with $C1 = 0.8 - 0.25(10{,}000 - N)/10{,}000$
SOLAS 2020	$N < 400$	$R = 0.722$
	$400 \leq N \leq 1{,}350$	$R = \frac{N}{7{,}580} + 0.66923$
	$1{,}350 < N \leq 6{,}000$	$R = 0.0369\, ln(N + 89.048) + 0.579$
	$N > 6{,}000$	$R = 1 - \frac{852.5 + 0.03875N}{N + 5000}$

[3] For brevity the number of persons on board is referred to as POB in the following

[4] For the ships of capacity smaller than 400 POB SA can be considered a single compartment standard

[5] https://ec.europa.eu/transport/modes/maritime/studies/maritime_da

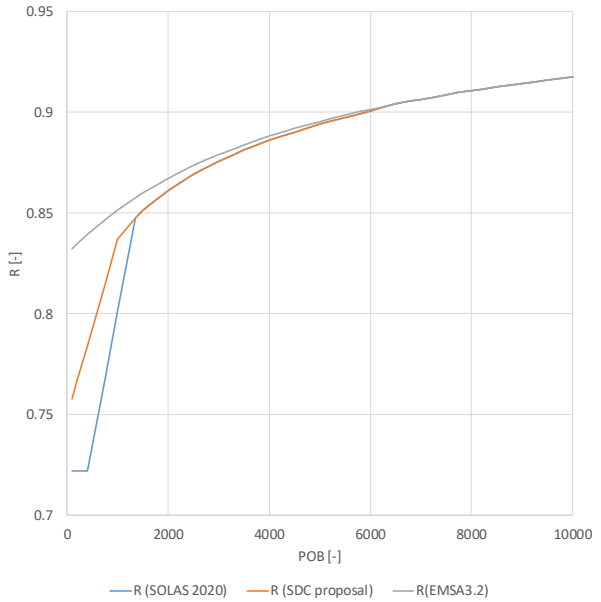

Figure 4: Alternatives for level of R

The observations made during the project can be summarised as follows (European Commission, 2019):

- The ships of capacity in excess of 1350 POB designed to comply with SA (and in conjunction with SOLAS90 or SOLAS2009) are likely to fail to meet the SOLAS2020 required index of subdivision even **with** the optimised GM (→ indication that SOLAS2020 provides **equal or higher** safety level to SA for this group of ships)
- The ships of capacity smaller than 1350 POB and in compliance with SA (and in conjunction with SOLAS90 or SOLAS2009) may comply with the SOLAS2020 required index of subdivision **without** the need to reduce the original GM margins (→ indication that SA provides **higher** safety level for the **significant proportion** of ships in this group)
- The SOLAS2020 increase of s-factor requirements led to a significant number of sample ships failing the compliance with the deterministic provision for minor damages (SOLAS Ch. II-1 Reg.8)

6. OPERATIONAL WAVE-HEIGHT LIMITATIONS

One of the important features of SA is that it allows for scaling the requirements according to the typical sea conditions in the area of operation (represented as significant wave height with 10% probability of exceedance). Since there is no similar instrument in SOLAS, the study considered including the critical wave-height limitations within the probabilistic framework by means of either

- the normalised s-factor, where both the HS_{crit} and the s-factor formulae are modified to accommodate for the operational wave heights less than 4 meters HS;
- the expected critical sea-state, the critical wave heights for all damages are averaged (with w and p being the weighting factors, just like the case of A-index) to calculate the expected value of HS_{crit}.

Normalised s-factor

The s-factor formulation estimates the average (expected) probability of surviving specific damage with the averaging carried out with respect to sea state the ship is likely to encounter during the collision incident. The normalisation accounts for the fact that the ship may be limited to operate in the areas where the normal wave heights are considerably lower than the 4 meters HS assumed by SOLAS.

By analogy with the target values for GZMAX and RANGE the denominator in the s-factor formulation as given by (3) can be interpreted as the target sea state (e.g. THS). Hence, the base in (3) is the ratio of critical HS to the target HS. In the s-factor formulation the target sea state is taken as 4.0 meters HS because virtually all collision incidents occurred in sea states below 4.0 meters HS. Thus, the normalisation of the s-factor can be achieved by replacing the target sea state of 4.0 meters HS with the corresponding limiting HS. This allows for expressing the normalised s-factor as follows:

$$s_{norm} = \left(\frac{\min(HS_{crit}, HS_{limit})}{HS_{limit}}\right)^{0.25} \qquad (6)$$

The s-factor normalisation accommodates for the fact that the ship will not operate in sea states exceeding the S_{limit} , as Figure 5 illustrates.

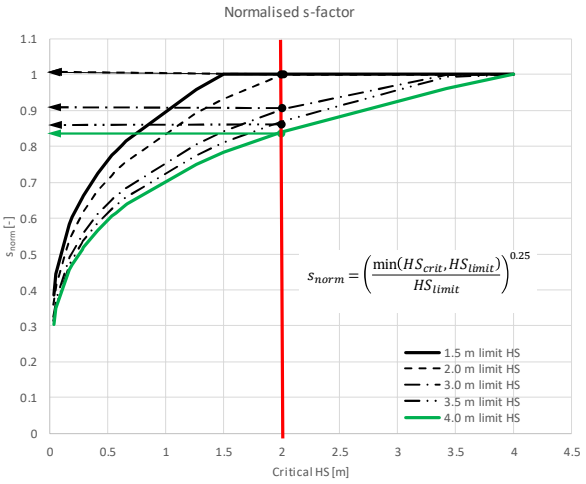

Figure 5: Effect of s-factor normalisation. The red line marks the critical HS corresponding to given damage. Should the ship be limited to operate in sea states not exceeding the 2 metres HS, the normalised s-factor formula would yield 1, while the probability of surviving the damage calculated by SOLAS s-factor would be about 0.84.

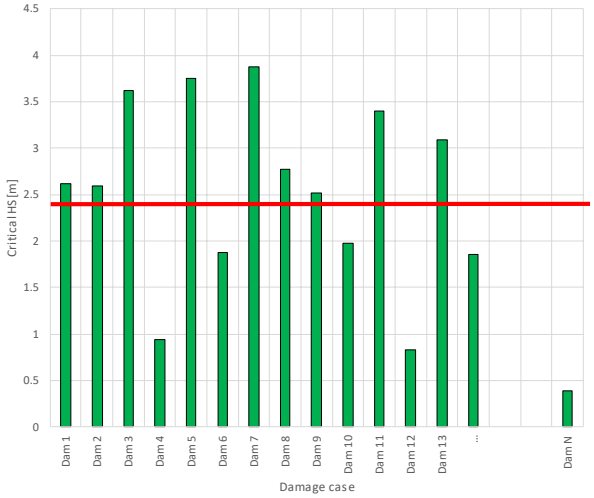

Figure 6: The calculation of expected HS_{crit} (the red line) involves calculating critical HS for individual damage cases and averaging it with respect to p and w-factors.

The attained index of subdivision with the wave-height operational limits could be calculated as in the SOLAS with the only difference that the normalised s-factor would be used in place of the regular s-factor.

$$A = \sum_j w_j \sum_i p_i s_{norm_i} \qquad (7)$$

Expected critical wave height

An alternative way to account for the operational wave-height limitations is to calcluate the expected critical HS by averaging the HS_{crit} characterising invidual damage cases (as given by (4)) with respect to probability of damage occurence (p) and operation in specific loading condition (w) (i.e., by replicting the process the s-factors are averaged to calculate the A-index).

$$\overline{HS_{crit}} = \sum_j w_j \sum_i p_i HS_{crit_i} \qquad (8)$$

This process is illustrated by Figure 6.

The criterion for compliance with the wave-height operational limits could read simply as shown next:

$$\overline{HS_{crit}} \geq HS_{limit} \qquad (9)$$

Notes on incorporating wave height limitations to the probabilistic framework

Both methods are equivalent in that they utilise the core concepts of survivability assessment present within the probabilistic framework. Furthermore, both can be calculated alongside the typical A-index calculations.

However, the application of both methods to the sample ships demonstrated that - generally - they do not have a significant effect when accounting for operational wave heights. In particular, the use of normalised s-factors has a negligible impact on the attained index of subdivision. This is also caused by the aforementioned factors k and $s_{mom.}$. This is an important observation because the normalisation of the s-factor is an analogy to introducing the distribution of wave heights (for averaging the probability of surviving specific damage) less stringent that the one behind the regular SOLAS s-factor (i.e. distribution of sea-states recorded during the collision accidents). However, since the "SOLAS distribution" is already more biased towards the lower wave heights than most of the wave scatter data for geographical locations, it is perfectly justifiable to question the rationale for lowering it even further.

The second technique is free of such controversy as $\overline{HS_{crit}}$ is a parameter derived directly from the characteristics of the damaged ship, without any form of modification. The underlying concept is also well linked to the s-factor methodology; hence it is not an entirely foreign inclusion to the framework.

However, it should be noted that by definition[6] the probability of survival (i.e. "s-factor") calculated based on $\overline{HS_{crit}}$, would be equal to or higher than the A-index. That is, since the attained index of subdivision is as an "average s-factor" (i.e. $A = \overline{s(HS_{crit})}$ the following relationship holds[7]

$$s(\overline{HS_{crit}}) \geq A \qquad (10)$$

Finally, the proposal for use of the $\overline{HS_{crit}}$ might require establishing additional compliance criteria supplementing the A ≥ R criterion.

7. CONCLUSIONS

The study as presented in (European Commission, 2019) includes technical evaluation of the safety levels provided by SA and SOLAS by sample ship investigations and impact assessment studies. Some conclusions can be highlighted:

Survival factor

- The new requierements for the target values for residual maximum GZ and range of positive stability for the damages involving ro-ro cargo spaces have an effect on survivability (as measured by Hscrit) similar to the freeboard and water on deck requirements of SA
- The impact of new s-factor on the attained index of subdivision is in general relatively small, resulting in decrease of the A-index not exceding a few percentage points

Required index of subdivision

- SOLAS2020 level of R will provide safety standard at least equal to the requirements of Directives 2009/45/EC and 2003/25/EC stability frameworks for ships of capacity exceeding 1,350 POB.
- For ships having a capacity less than 1,350 POB, SOLAS2020 may not ensure the same safety standard as the requirements of Directives 2009/45/EC and 2003/25/EC. In this case it may be necessary to implement the level of R matching the SDC3 proposal or to retain the SA requirements.

Operational wave-height limitations

- The sample ship calculations did not show that wave-height limitations accounted for by either the normalised s-factor or expected critical wave height had significant impact on the overall survivability as expressed by the attained index A. Based on this there is little merit in introducing separate requirements with respect to the operational wave-height limitations for damage stability in a probabilistic concept.

ACKNOWLEDGEMENTS

This work was carried out as part of the study "Assessment of specific EU stability requirements for ro-ro passenger ships" funded by the European Commission, Directorate-General for mobility and transport. The work was carried out by a consortium led by DNV GL with the following partners listed in alphabetical order: Brookes Bell, Foreship, Herbert Engineering Company, INTERFERRY, LMG Marine, Maritime Safety Research Centre (MSRC), Meyer Turku, Meyer Werft and NAP Engineering.

DISCLAIMER

Even though the study was funded by the European Commission it is to be duly noted that the information and views set out in this paper are those of the authors and not necessarily reflect the official opinion of the Commission. The Commission does not guarantee the accuracy of the data included in this study. Neither the Commission nor any person acting on the Commissions' behalf may be held responsible for the use which may be made of the information contained therein.

The views as reported in this paper are those of the authors and do not necessarily reflect the views of the respective members of the consortium.

REFERENCES

Bird, H., & Browne, R. (1973). Damage stability model experiments. *The Transactions of RINA*, 69-91.

Cichowicz, J., Tsakalakis, N., Vassalos, D., & Jasionowski, A. (2016). Damage Survivability of Passenger Ships - Re-Engineering the Safety Factor. *Safety, 4*(2).

European Commission. (2019). *Assessment of specific EU*

[6] According to so-called Jensen's inequality

[7] The relationship reflects the so-called Jensen's inequality and it states simply that the average s-factor (i.e. A-index) is equal to or smaller than the s-factor calculated with the average HS_{crit}

stability requirements for ro-ro passenger ships. Final report - study. Directorate-General for Mobility and Transport. Brussels: European Commision. doi:10.2832/968505

IMO. (1976, November 20). Resolution A.265(VIII). *Regulations on Subdivision and Stability of Passenger Ships as an Equivalent to Part B of Chapter II of the International Convention For the Safety of Life at Sea, 1960*. London: International Maritime Organization.

IMO. (1996). *Resolution 14 Agreement Concerning Specific Stability Requirements for Ro-Ro Passenger Ships Undertaking Regular Scheduled International Voyages Between or To or From Designated Ports in North West Europe and the Baltic Sea*. London, UK: IMO.

Jasionowski, A. (2009). *Study of the specific damage stability parameters of Ro-Ro passenger vessels according to SOLAS 2009 including water on deck calculation.* Lisbon: European Maritime Safety Agency. Retrieved from http://www.emsa.europa.eu/implementation-tasks/ship-safety-standards/download/1774/1457/23.html

Project GOALDS. (2009-2012). Goal-Based Damage Stability. (D. Research, Ed.) European Commision, FP7.

Project HARDER. (2000-2003). Harmonization of Rules and Design Rationale. (D. XII-BRITE, Ed.) European Commission.

Vassalos, D., & Papanikolaou, A. (2002). Stockholm Agreement -- Past, Present , Future. *Marine Technology, 39*(3), 137-158.

Study on the damaged ship motion coupled with damaged flow based on the unified viscous/potential prediction model

Shuxia Bu, *China Ship Scientific Research Center*, bushuxia8@163.com
Min Gu, *China Ship Scientific Research Center*, gumin702@163.com

ABSTRACT

The behaviour of a damaged ship is very complex because of the interaction between the ship motion and the flow inside the damaged compartment. Therefore, a feasible prediction method for the damaged ship stability considering the interactions between the damaged ship and the floodwater is very important. In this paper, one nonlinear time domain unified prediction model for the damaged ship motion is proposed, which combines the advantages of potential theory in calculating ship motion and viscous theory in calculating the floodwater flow. In this unified prediction model, the three-dimensional hybrid time domain panel method which is used to calculate the large amplitude motion of damaged ship and the CFD method which is used to calculate the flow in the compartments are coupled with each other in time domain. Two boundary condition forms for the damaged opening are studied. The unified model is verified by comparing the CFD simulation results with ITTC benchmark model. The research show that the proposed unified model captures both the large amplitude motion and the details of floodwater flow very well. The efficiency of the calculation of damaged ship motion in waves is improved as the mesh quantity for CFD simulation is considerably reduced.

Keywords: *Damaged ship motion coupled with damaged flow, 3D time domain hybrid source method, far-field boundary condition, hatch pressure boundary condition.*

1. INTRODUCTION

The damaged ship stability in waves is very complex and the evaluation of the damage ship motion is a difficult task. The performance of a damaged ship in waves is influenced not only by waves but also by the internal loads of the fluid flow and sloshing. The inflow of floodwater causes the change of ship parameters (mass, buoyancy, etc.) and the sloshing of liquid inside the damaged compartment. The load generated by the sloshing of liquid will further affect the motion characteristics of the ship. The motion of damaged ship and the damaged floodwater are coupled with each other. Water flowing into the compartment has a significant effect on the ship stability and safety.

Generally, there are three basic problems related to damaged ship motion (ITTC, 2005): ship with zero forward speed moving on the free surface under the excitation of waves; the flooding phenomenon itself, namely the process of water inflow and outflow through damage openings and progressive flooding through internal spaces; the behavior of the accumulated floodwater inside the ship`s compartments and its interaction with the ship.

The dynamic performance of damaged ships in waves are constantly changing, which leads to high nonlinearity of the dynamic system. Therefore, an effective method to reproduce the high nonlinearity of the ship motion and the process of the damaged flow is to solve it in time domain. Up to now, many works have been devoted to the study of the damaged ship motion in waves (Jasionowski and Vassalos, 2011; Umeda et al., 2004; Spanos and Papanikolaou, 2007; Van Walree et al., 2007).

The assessment of damaged ship motion is normally based on potential theory. However, the potential theory cannot accurately capture hydrodynamic loads caused by floodwater; sloshing is usually ignored; the internal water surface is assumed to be horizontal or a free-moving plane; the inflow and outflow of water through the damaged opening are calculated by the modified empirical Bernoulli`s equation. Furthermore, the roll damping and damping forces due to floodwater are usually calculated by empirical. Some researchers also use shallow water equation to simulate the physical characteristics of the internal flow (Chang et al., 1998; Santos et al., 2006, 2008). Although the improved model can display the nonlinear characteristics of the flow inside the compartment,

yet the method still fails to characterize flow through external (damage) and internal openings.

CFD method is deemed to be a better choice that can offer a detailed description of the dynamic characteristics of flow. Indeed, it has been used by several researchers to study the flooding process of damaged ships (Cho et al., 2006; Nabavi et al., 2006; Strasser, 2010; Gao and Vassalos, 2015). The research prove that CFD is successful to describe the flow and its characteristics pretty well. However, it should be pointed out that it is hard to simulate the entire damaged ship motion only by CFD method due to high computational costs.

The coupling between the damaged ship motion in waves and damaged floodwater is a very complex problem. The in-waves calculations need to consider not only the motions of damaged ship but also the strong non-linear floodwater dynamics as well as progressive flooding. Particularly, despite a number of studies that focused on the relationship between flooding water and the motion response of damaged ship, the effects of flooding dynamics on the motion of a damage ship is not yet clearly understood.

Considering that CFD method can simulate most of the flow characteristics and parameters, potential flow method has a strong advantage in solving seakeeping problems. Therefore, the coupling method of CFD and potential theory can be used to reduce the computational cost on one hand, and to simulate the flow problem more efficiently on the other hand. In this method, CFD is used to simulate the flow in the damaged compartment whilst the potential flow method is used to calculate the forces due to action of waves. Cho et al. (2006) developed a numerical method that can take into account the internal flow, in which the ship motion is solved by the three-dimensional frequency domain panel method, and the internal fluid motion is solved by the modified VOF method, taking into account the effect of sloshing. Gao et al. (2013) simulated the motion of one damaged Ro-Ro ship coupled with damaged flow, in which the ship motion in waves were calculated with use of strip theory and flows inside the damaged compartment were calculated by RANS equation. Hashimoto et al. (2015) simulated the transient behavior of ships by coupling the three-dimensional MPS method with the conventional 2D strip method.

The above inspire us to establish a method that combines CFD and potential theory to investigate the hydrodynamics of floodwater and its effects on the damaged ship motions. Firstly, a unified viscous/ potential prediction model is proposed, in which the three-dimensional time-domain hybrid source method is used for the calculation of damaged ship motion in waves, and viscous CFD method is used for the simulation of floodwater. Two boundary condition forms for damaged opening are introduced. Then the time domain coupling between damaged ship motion and damaged floodwater are simulated based on this method.

2. RESEARCH OBJECT

The ITTC benchmark model for progressive flooding is selected as the research object. The model made available by NAPA and HUT Ship Laboratory provides experimental data for the validation of numerical simulation method (Ruponen et al., 2007). The model is a barge with eight interconnected compartments, as shown in Fig. 1. Its principal dimensions are shown in Table 1.

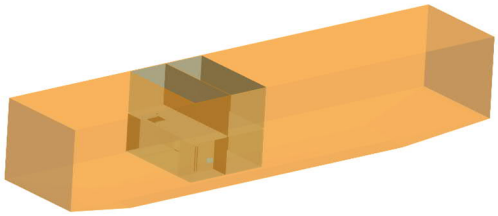

Figure 1: The shape model of damaged barge.

The damaged compartments are located in the middle of the hull towards the bow of the ship. The compartments and compartment connections are shown in Fig. 2 and Table 2. The damage opening is located at mid-length of the side wall of compartment R21S, 185mm below the waterline. In the study presented in this paper, DB1 and DB2 in the lower compartment are not connected with the upper compartment and therefore they are not flooded during the simulations.

Table 1: Main dimensions of damaged barges and cabins

Items	Values	Items	Values
Length	4m	Vol	1.45m3
Breadth	0.8m	KB	0.27m
Height	0.8m	BM	0.118m
Draft	0.5m	GM	0.11m
Cb	0.906	KG	0.278m

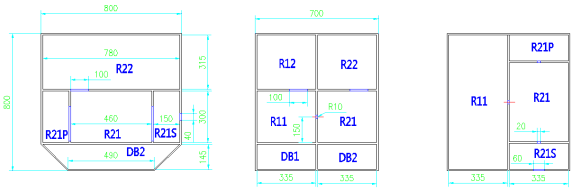

(a) Front view **(b) Side view** **(c) Top view**

Figure 2: Section diagram of damaged compartment

Table 2: Compartment connections

Opening	Connected compartment	Dimension
FDP	R21↔R21P	20mm×200mm
FDS	R21↔R21S	20mm×200mm
DP	R21↔R11	Φ20mm
SC1	R11↔R12	100mm×100mm
SC2	R21↔R22	100mm×100mm
DAS	R21S↔Sea	60mm×40mm

3. UNIFIED VISCOUS / POTENTIAL PREDICTION MODEL

Mathematical model

Three degrees of freedom (heave-roll-pitch) mathematical model is used for the simulation of damaged ship motion, as follows:

$$\begin{aligned}
&(m + A_{33})\ddot{x}_3 + B_{33}\dot{x}_3 + \sum_{j=4,5}\left[A_{3j}\ddot{x}_j + B_{3j}\dot{x}_j\right] \\
&= F_3^{\mathrm{FK+H}} + F_3^{\mathrm{DF}} + F_3^{\mathrm{In}} \\
&(I_{44} + A_{44})\ddot{x}_4 + B_{44}\dot{x}_4 + \sum_{j=3,5}\left[A_{4j}\ddot{x}_j + B_{4j}\dot{x}_j\right] \\
&= F_4^{\mathrm{FK+H}} + F_4^{\mathrm{DF}} + F_4^{\mathrm{In}} \\
&(I_{55} + A_{55})\ddot{x}_5 + B_{55}\dot{x}_5 + \sum_{j=3,4}\left[A_{5j}\ddot{x}_j + B_{5j}\dot{x}_j\right] \\
&= F_5^{\mathrm{FK+H}} + F_5^{\mathrm{DF}} + F_5^{\mathrm{In}}
\end{aligned} \tag{1}$$

where m is the mass of the hull; I_{ii} is the moment of inertia about an i-axis; A_{ij} is the added mass coefficient of the hull; B_{ij} is the damping coefficient of the hull; x_i is the displacement in the i-direction; $\dot{x}_i$ is the velocity in the i-direction; $\ddot{x}_i$ is the acceleration in the i-direction; the roll damping coefficient is calculated based on to the critical rolling damping coefficient:

$$B_{44} = \varsigma \cdot 2\sqrt{(I_{xx} + A_{44})mg} \tag{2}$$

where ς is the critical roll damping coefficient (Ruponen et al., 2007); $F_i^{\mathrm{FK+H}}$ is the Froude-Krylov force and hydrostatic force, obtained by integrating the incident wave pressure over the instantaneous wetted surface of the hull; F_i^{DF} is the diffraction force, integrated over the average wetted surface of the hull; the hydrodynamic coefficients related to radiation force such as A_{ij} and B_{ij} are also integrated over the average wetted surface of the hull; F_i^{In} is the force acting on the interior wall due to floodwater (including sloshing) and incorporating the pressure and shear force generated by viscous flow.

Three Dimensional Hybrid Source Method

Three dimensional time-domain hybrid source method is used for the calculation of damaged ship motions. The field domain is divided into two sub-domains by an arbitrary virtual control surface S_c, as shown in Figure 3. The inner field I is a closed area surrounded by the wetted surface S_b, the partial free surface S_{f1} and the control surface S_c, while the outer field II is a closed area surrounded by the control surface S_c, the remaining free surface S_{f2} and the infinite boundary S_∞ (Bu et al., 2019a, 2019b).

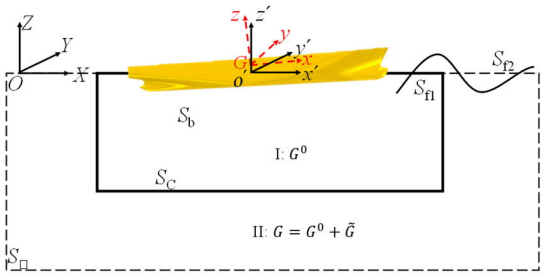

Figure 3: Diagram for the field domains in the three dimensional hybrid source method.

The total perturbation potential in the inner field domains $\Phi_I(P,t)$ satisfies the following conditions in the earth-fixed coordinate system:

$$\begin{aligned}
&\nabla^2\Phi_I = 0 && \text{Inner} \\
&\frac{\partial^2\Phi_I}{\partial^2 t} + g\frac{\partial\Phi_I}{\partial Z} = 0 && \text{on } S_{f1},\ t>0 \\
&\frac{\partial\Phi_I}{\partial\vec{n}} = \vec{V}_n - \frac{\partial\Phi_w}{\partial\vec{n}} && \text{on } S_b,\ t>0 \\
&\Phi_I = \frac{\partial\Phi_I}{\partial t} = 0 && \text{at } t=0
\end{aligned} \tag{3}$$

The boundary integral equation of Rankine source in the inner field I can be written as follows:

$$2\pi\Phi_I(P) + \iint_{S_I}(\Phi_I G_n - \Phi_{In} G)dS = 0 \tag{4}$$

where $\vec{x} = P(X(t), Y(t), Z(t))$ is field point; $\vec{\xi} = Q(\xi(t), \eta(t), \zeta(t))$ is source point; $G = 1/r_{PQ}$ is simple Green function, with r_{PQ} given as:

$$r_{PQ} = |P - Q| = \sqrt{(X-\xi)^2 + (Y-\eta)^2 + (Z-\zeta)^2}$$

The total perturbation potential $\Phi_{II}(P,t)$ satisfies the following conditions in earth-fixed coordinate system:

$$\begin{aligned} &\nabla^2\Phi_{II}=0 && \text{Outer}\\ &\frac{\partial^2\Phi_{II}}{\partial^2 t}+g\frac{\partial\Phi_{II}}{\partial Z}=0 && \text{on } S_{f2}\\ &\nabla\Phi_{II}\to 0 && \text{on } S_{\infty}\\ &\Phi_{II}=\frac{\partial\Phi_{II}}{\partial t}=0 && \text{at } t=0 \end{aligned} \tag{5}$$

The boundary integral equation of time domain Green function in the outer field II can be expressed as follows:

$$\begin{aligned} &2\pi\Phi_{II}+\iint_{S_C}(\Phi_{II}G_n^0-\Phi_{IIn}G^0)dS\\ &=\int_0^t d\tau\left\{\begin{array}{l}\iint_{S_C}(\Phi_{IIn}\tilde{G}-\Phi_{II}\tilde{G}_n)dS\\ +\frac{1}{g}\oint_{w(\tau)}(\Phi_{II\tau}\tilde{G}-\Phi_{II}\tilde{G}_\tau)\vec{V}_N dl\end{array}\right\} \end{aligned} \tag{6}$$

The continuity conditions on the control surface are the following:

$$\begin{aligned} &\Phi_I=\Phi_{II}\\ &\frac{\partial\Phi_I}{\partial n}=-\frac{\partial\Phi_{II}}{\partial n}\quad(\text{on } S_c) \end{aligned} \tag{7}$$

Then, the fluid force F and moment M acting on the panel can be get by integrating the pressure obtained from Bernoulli`s equation along the wetted surface:

$$\begin{aligned} &\vec{F}=\iint_{S_b}p\vec{n}dS\\ &\vec{M}=\iint_{S_b}(\vec{r}\times\vec{n})pdS \end{aligned} \tag{8}$$

where, $\vec{r}$, $\vec{n}$:the radial and normal vectors, defined in the ship-fixed coordinate system.

Viscous method

The internal force and moment due to the viscous flows of floodwater are given as:

$$\begin{aligned} &\overrightarrow{F}^{\text{In}}=\int_S(\vec{f}_p+\vec{f}_s)\cdot\vec{n}dS\\ &\overrightarrow{M}^{\text{In}}=\int_S\vec{r}_f\times(\vec{f}_p+\vec{f}_s)\cdot\vec{n}dS \end{aligned} \tag{9}$$

Where, $\vec{f}_p$ and $\vec{f}_s$ are the pressure and shear force acting on the compartment wall, respectively. These forces calculated by commercial CFD software solving by the unsteady RANS (Reynolds time-averaged Navier-Stokes) equation with VOF (Volume of Fluid) multiphase flow model.

The governing equations of flow field include continuity equation, momentum equation and phase volume fraction equation are expressed as follows:

$$\left\{\begin{array}{l}\frac{\partial}{\partial t}\int_V\rho dV+\int_S\rho(\vec{u}-\vec{u}_g)\cdot\vec{n}dS=0\\ \frac{\partial}{\partial t}\int_V\rho\vec{u}dV+\int_S\rho\vec{u}(\vec{u}-\vec{u}_g)\cdot\vec{n}dS\\ +\int_V(\vec{\omega}\times\vec{u})dV=-\int_S p\vec{I}'\cdot\vec{n}dS\\ +\int_V\rho g dV+\int_S\mu(\nabla\vec{u}+\nabla\vec{u}^T)\cdot dS\\ \frac{\partial}{\partial t}\int_V\alpha dV+\int_S\alpha(\vec{u}-\vec{u}_g)\cdot\vec{n}dS=0\end{array}\right. \tag{10}$$

where, ρ: mixture density, can be defined as $\rho=\alpha\rho_w+(1-\alpha)\rho_g$, α: volume fraction of liquid phase, ρ_w, ρ_g: densities of liquids and gases, respectively; μ: average effective dynamic viscosity coefficient of phase volume fraction, in accordance with the definition of density; $\vec{u}$: the velocity of fluid micro-clusters; $\vec{u}_g$:the velocity of gird nodes; p: fluid pressure; $\vec{I}'$: the unit matrix; g: the acceleration of gravity; $\vec{\omega}$: the angular velocity of rotation. SST k-ω turbulent model is chosen for the closure of the equation.

In viscous flow calculations, motions of the internal compartment are determined by the translation velocity $\vec{u}_g(\dot{x}_i, i=1..3)$ and angular velocity $\vec{\omega}(\dot{x}_i, i=4..6)$ obtained by solving the equation (1). The momentum equation, turbulent kinetic energy k, dissipation rate ω or other transport equations are associated with volume fraction through density ρ and viscous coefficient μ in the whole viscous flow calculation region. Once the force and moment acting on the compartment wall are calculated they serve as initial condition for the next iteration of the equation (1).

Calculating Process

In the numerical simulation, the CFD method is only used to solve the floodwater motions and the resultant force acting on the compartment is applied to the ship's equations of motions in the time domain and the equations are solved by the potential theory solver. The inviscid flow solver can afford longer time steps because of the larger mesh size compared with viscous flow solver requiring shorter time steps. As a result it is necessary to introduce distinct time scales for CFD and inviscid solvers and use the

method of multi-step superposition. For example, if the time step associated with potential solver is given as Δt, then the viscous flow is solved in N inner time steps Δt_1 (where $\Delta t = N\Delta t_1$ and the value of N depends on the courant number). The floodwater forces after the N inner time steps is applied to the ship's equations of motion to ensure the unification of the two methods in calculation time. The calculation of damaged ship also need to consider the floodwater inflow and outflow the corresponding hydrodynamic force. This requires accurate calculation of the flowrates through the damaged opening and consequently a special boundary condition for the opening. This will be discussed in detail in the next section.

The calculation process of the unified viscous/potential prediction model is the following (Fig. 4):

(1) Initialization of ship motion by time domain potential flow solver, including initial time meshing and calculation of hydrodynamic coefficients;

(2) Initialization of the CFD flow field within damaged compartment, including the pressure and velocity fields, free surface, etc.

(3) The time-domain potential flow solver calculates the hydrodynamic and wave induced forces to solve the ship equations of motions. This steps involves also establishing of the boundary conditions of the flow field in the RANS solution, such as the boundary conditions of the computational domain or the damaged opening.

(4) The boundary conditions calculated by time domain potential method are transferred to CFD.

(5) After the boundary conditions are transferred to the viscous flow solver, it initializes the calculations of the floodwater ingress/egress and sloshing inside the damaged compartment. After a series of internal iterations, when the steady state is reached the solver computes the internal forces and moments due to floodwater flow and sloshing.

(6) The internal forces calculated by CFD are transferred to the time domain potential solver.

(7) The hydrodynamic loads due to floodwater are added to the external forces acting on the hull and the ship's equations of motions are solved by the fourth-order Runge-Kutta method.

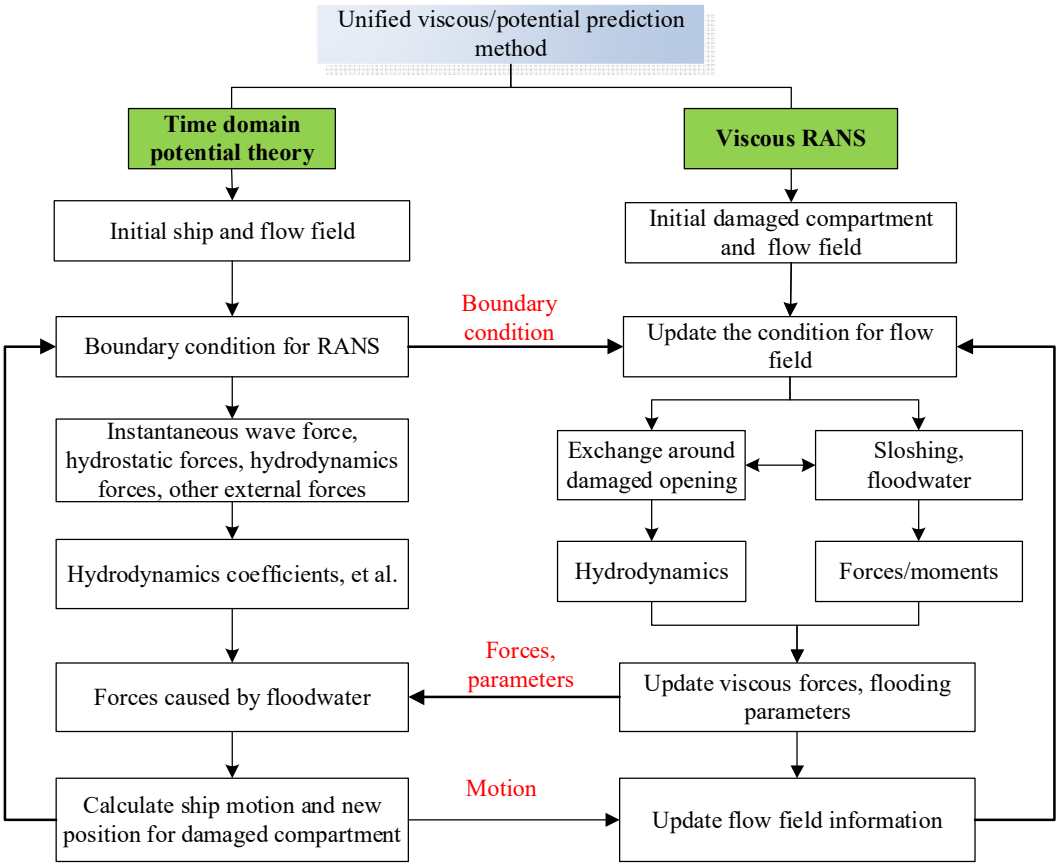

Figure 4: Flow chart for calculation of unified viscous/potential prediction model

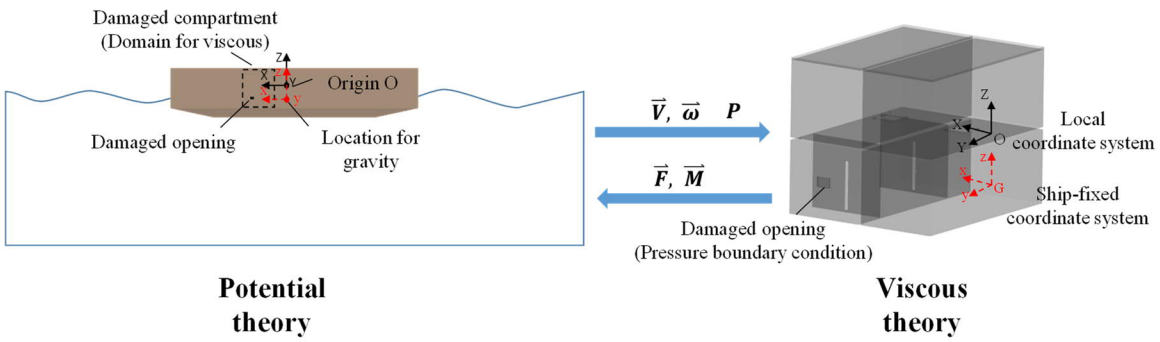

Figure 5: Diagram for the computing domain and coordinate systems

(8) The updated motions of the damaged compartment obtained from the inviscid solver are transferred to the CFD method.

(9) Repeat (3) - (8) until the calculation is completed.

The local coordinate system of the CFD solver is aligned with the inertial coordinate system used in the calculation of ship motions. As shown in Fig. 5, the force acting on the compartment is calculated based on the instantaneous position of the center of gravity.

Treatment for the damaged opening

The unified viscous/potential prediction model utilises three different methods for handling of the boundary condition at the damage openings:

(1) Far-field pressure boundary

The far field pressure boundary is applied to the domain constructed by constraining the entire CFD domain with two parallel planes aligned with the fore- and aft-most limits of the damaged compartments (Gao, et al., 2015). The front and back sections of the computational domain are slip wall boundary conditions while the upper and lower boundary conditions are far-field pressure boundary conditions. The corresponding pressure conditions are determined according to the position of the free surface. The interior and exterior walls of the compartment are the wall boundary conditions.

(2) Near-field pressure boundary

The idea of near-field pressure boundary originates from the observations made during CFD simulations, namely that the velocity field in the proximity of damage opening represents a "hemispherical" transition zone. Therefore, the computational domain consists of the interior region and a hemispherical region near the damage opening. The CFD solver does not need to set the free surface position in this domain because there is no inconsistency of the free surface between viscous flow and potential flow.

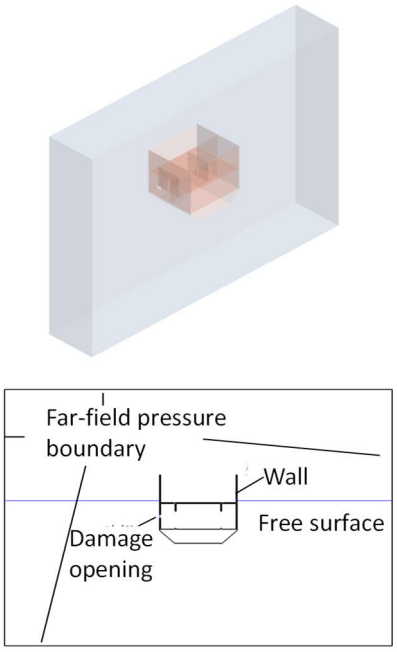

Figure 6: Diagram for the far-field pressure boundary

(3) Hatch pressure boundary

The idea of hatch pressure boundary stems from the problem of orifice and pipeline flow. The computational domain of this method includes only the interiors of the damaged compartment. The pressure inlet boundary condition at the damage opening is calculated by the potential solver. This coupling method has no external flow field and the flow into the compartment is entirely determined by the pressure applied at the damage opening. Therefore, in order to account for the influence of the floodwater flow, the hatch pressure needs to be corrected for the pressure loss, which is similar to the setting of the local pressure loss coefficient in the small outlet flow.

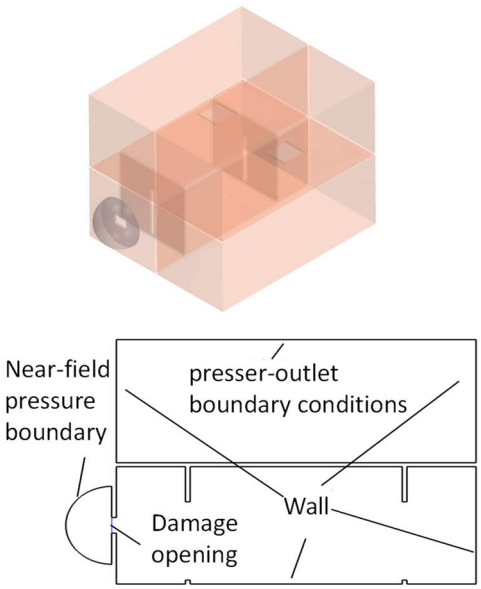

Figure 7: Diagram for the near-field pressure boundary

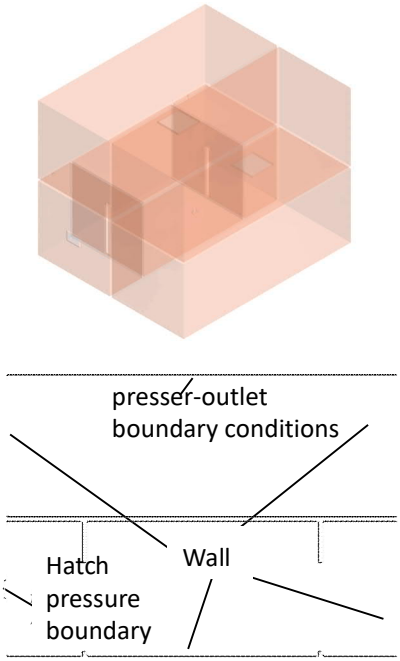

Figure 8: Diagram for the hatch pressure boundary

Herein, the hatch pressure boundary conditions in viscous flow calculations are given by modifying the hatch pressure obtained from potential flow calculation. Hence, pressure at the damage opening in CFD calculations is given as:

$$p_v = K \cdot p_0 \tag{11}$$

where p_v is the pressure at the damage opening in CFD calculation; p_0 is the pressure near the damaged opening in potential flow calculation, including the first and second order pressure caused by incident wave and disturbance potential; K is the local loss coefficient.

The results presented in this paper include the snapshots of velocity and pressure fields calculated by full CFD method, comparison of unified viscous/potential prediction model coupled with different boundary conditions at the damage opening (far-field pressure boundary, near-field pressure boundary and hatch pressure boundary condition). Initial value of the coefficient K is 0.6 and it increases gradually after 10s. Of course, further research is needed for the selection of the coefficient.

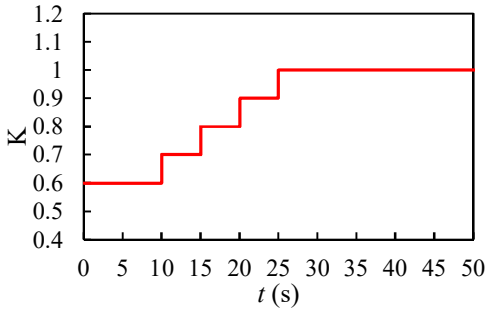

Figure 9: Values for the coefficient K.

4. RESULTS AND ANALYSIS

CFD simulation and validation

The dimensions of the computational domain are 15m×15m×10m. The meshing utilises the technique of overlapping grid. The wall boundary condition is used for the ship surface, and the pressure outlet condition is used for the external computational domain. There are two sets of grids in the computational domain (as shown in Fig. 10): background grid which contains the whole flow field and the overlapping grid containing the hull and the surrounding flow field. Data exchange between two sets of grids is carried out by interpolation near the interface. The total grids contain 1.3 million cells.

The calculations of floodwater levels in different compartments are in good agreement with model test results, as shown in Fig. 11, which validates the feasibility of the method.

Analysis of flowing process

In order to verify the reliability of the nonlinear time-domain unified viscous/potential prediction model presented in this paper, the numerical results calculated with different methods for handling boundary conditions at the damage opening, are compared with the experimental data.

The mesh quantity used for calculations are: 1.3 million cells for CFD simulation; 620,000 cells for unified prediction model with the far-field pressure boundary condition; 320,000 cells for unified prediction model with near-field pressure boundary condition and 300,000 for unified prediction model with hatch pressure boundary.

Fig. 12 shows the flow inside the compartment calculated with different methods. It can be seen from the figures that the transient inflow shows strong non-linear characteristics at t=5s. The near-field pressure boundary and hatch pressure boundary can better simulate the non-linear transient inflow than the far-field boundary condition. When t=25s, the floodwater begins to flow to the other side. The hatch pressure boundary offers the closest match to the calculation results of CFD simulation at this time instant. The far-field pressure boundary overestimated the inflow water, while the near-field pressure boundary proposed in this paper underestimated the inflow water. The inflow water is relatively small at this time, hence its impact on the ship behaviour may be relatively small. Overall, the three methods capture the flow process very well.

Fig. 13 shows the comparison of velocity fields calculated with different boundary conditions. It can be seen from the figures that, the near-field pressure boundary calculates the velocity field well, but the velocities calculated by the hatch pressure boundary are relatively small at t=5s. However, the accuracy become better with time. Overall, there is little difference in velocity fields calculated with the full CFD method, near-field pressure boundary, far-field pressure boundary and hatch pressure boundary which further validates the applicability of the boundary conditions in this problem.

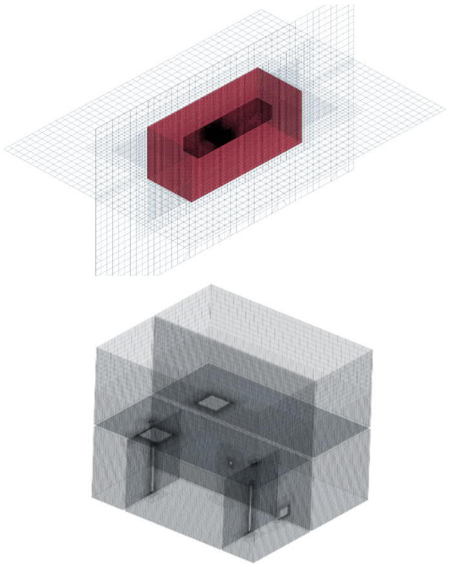

Figure 10: Diagram for CFD computation domain and meshes

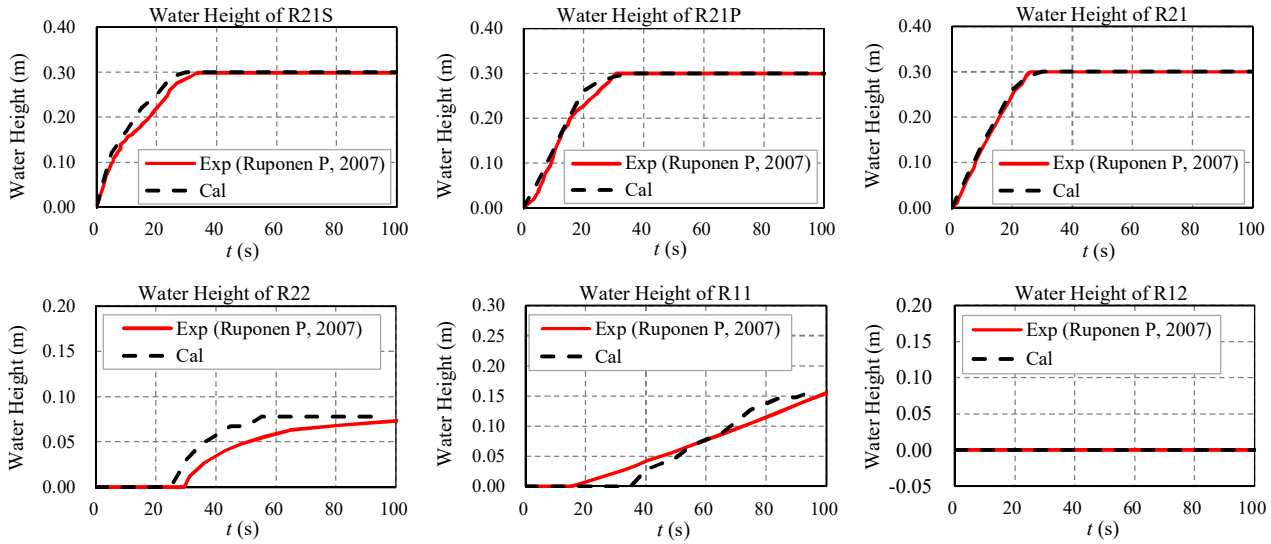

Figure 11: Comparisons of the variation of water level in different compartments

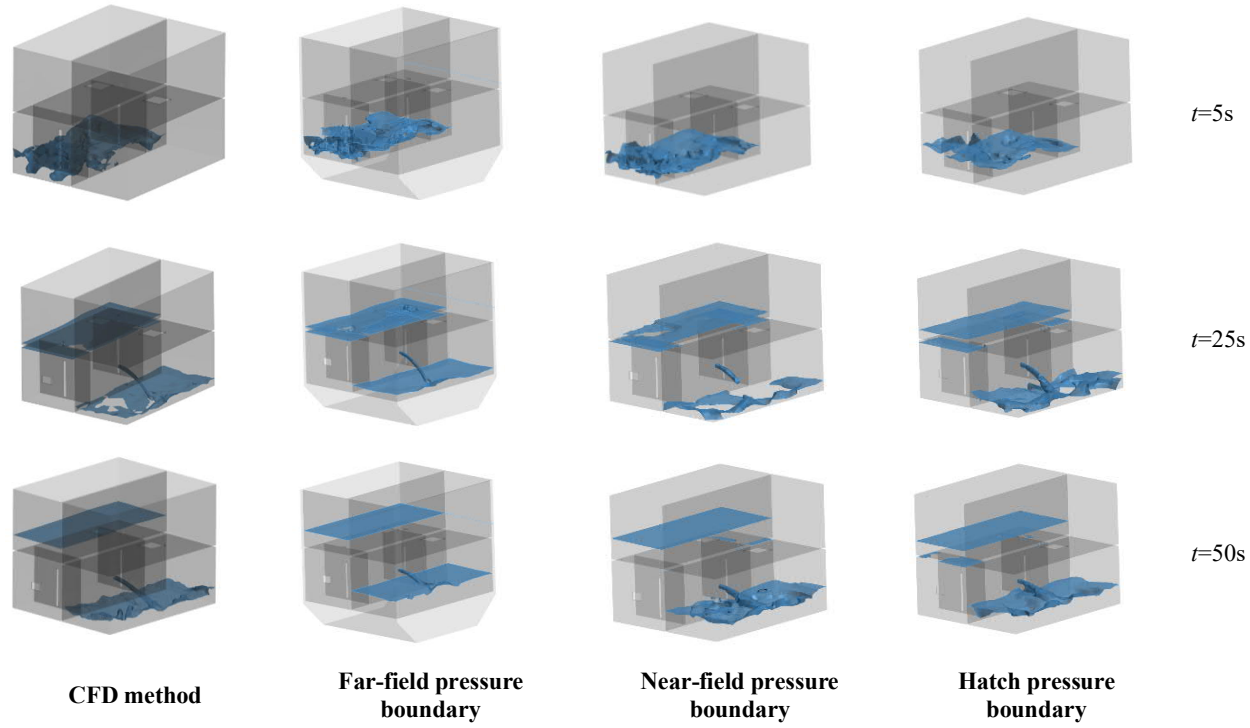

Figure 12: Flowing process calculated by different boundary conditions

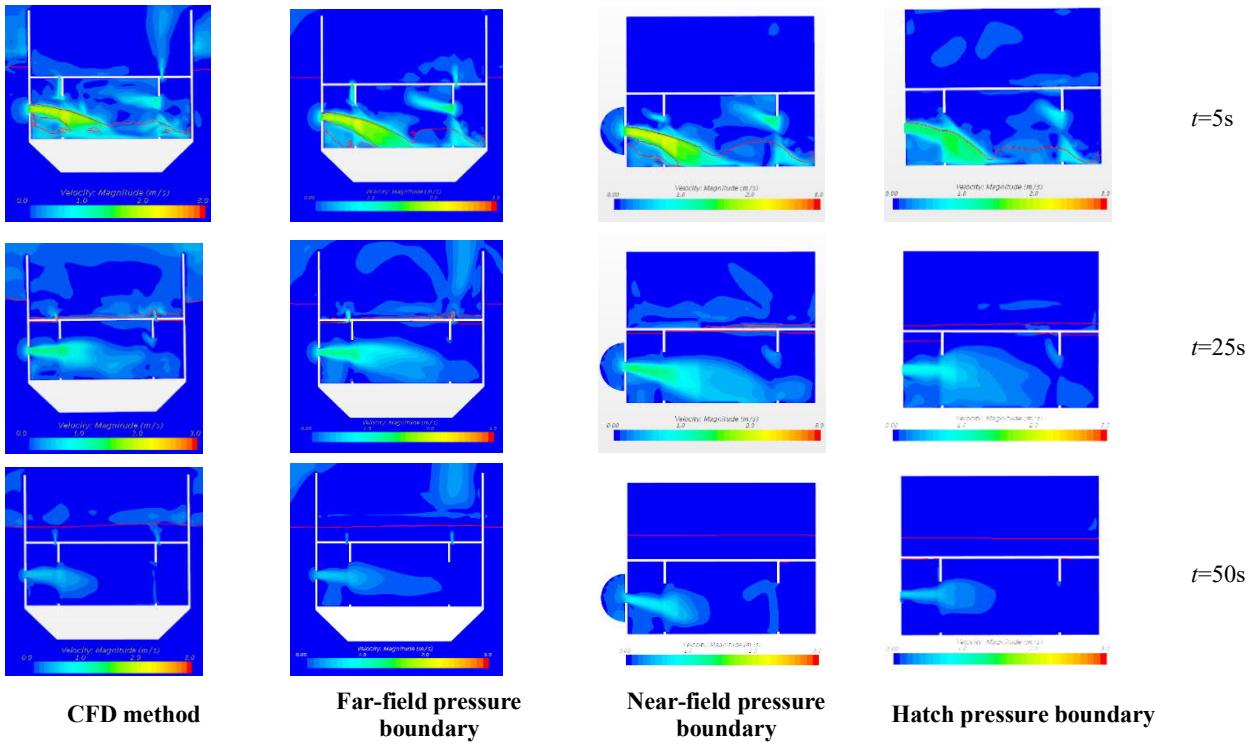

Figure 13: Velocity contour of hatch section calculated by different boundary condition

Analysis of damaged ship motion

The results of unified viscous/potential prediction model, CFD simulations and model test are compared in Fig. 14.

For the roll motion, the errors by hatch pressure boundary at the initial stage are relatively large, possibly caused by the errors in calculations of floodwater inflow, roll damping, etc, and can be neglected. For the heave and pitch motions, the calculated results of CFD simulation, far field pressure boundary, near field pressure boundary and hatch pressure boundary are all in good agreement with the model tests.

The comparison of the time-domain motions calculated by unified viscous/potential prediction model with different methods for handling of boundary conditions prove that CFD, the near-field pressure boundary and hatch pressure boundary proposed in this paper can calculate motions of the damaged ship well.

Considering that the calculation of far-field pressure boundary needs to include a relatively large computational domain outside the damaged opening, the mesh quantity is much larger than that of near-field boundary conditions and hatch pressure boundary conditions. Furthermore, there exists a problem of inconsistency between the potential and viscous solutions in the calculation of wave conditions under far-field boundary conditions, especially when the incoming flow is parallel or intersecting with the damaged opening. The near-field pressure boundary and hatch pressure boundary on the other hand, can be used to calculate damaged ship motion under different wave directions and ship speeds.

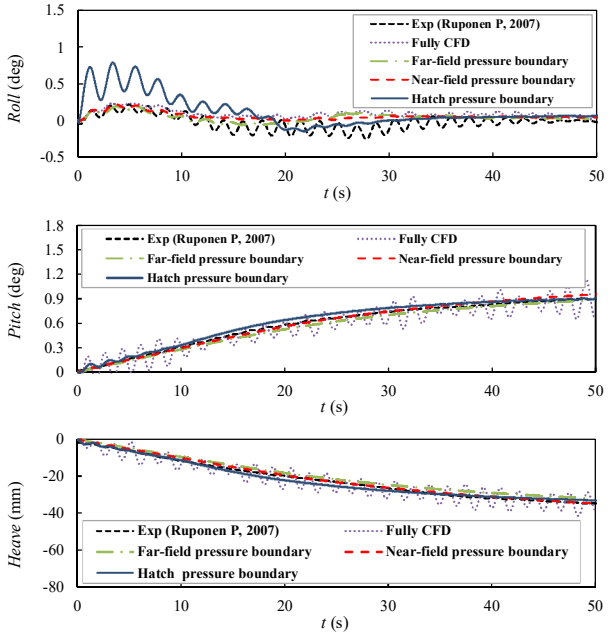

Figure 14: Time history of motions calculated by different methods

5. CONCLUSION

In this paper, a unified viscous/potential prediction model for stability in waves is proposed based on the real-time interactive iteration of three dimensional time domain hybrid source method and viscous CFD method. The unified model combines the advantages of the three dimensional time domain hybrid source method in calculating extreme motions of ships in waves, and the advantages of CFD method in detailed simulations for hull-floodwater interactions. Two time scales, fast scale and slow scale, are introduced and two boundary condition forms for damage opening in the unified model are also proposed. The research and analysis show that:

(1) The unified viscous/potential prediction model established in this paper can be effectively applied to the study of real-time coupled damaged flow of damaged ships.

(2) The comparisons of flow process, velocity, pressure with full CFD method and model tests verify the effectiveness of the proposed unified viscous/potential prediction model for the prediction of damaged ships stability in waves.

(3) The proposed near-field pressure boundary and hatch pressure boundary for the damaged opening can significantly reduce mesh quantity and improve computation efficiency without compromising the accuracy of calculations.

6. ACKNOWLEDGEMENTS

The experimental campaign for ITTC benchmarked model used in this paper was carried out at HUT (Aalto University), which was funded by NAPA Ltd and Tekes. The experimental data used in this paper were shared by Dr. Pekka Ruponen for the research purpose.

Part of the research was conducted in the institute of fluid dynamic and ship theory during the first author's study in Hamburg University of Technology. Prof. M. Abdel-Maksoud from Hamburg University of Technology provided the author with useful advices.

The authors sincerely thank the above organization and individuals.

7. REFERENCES

Bu S, Gu M, Lu J, Zeng K. Time domain prediction of the damaged ship motion in waves [J]. Shipbuilding of China [J]. 2018, 59(2): 80-80.

Bu S, Gu M, Lu J, Abdel-Maksoud M, Effects of radiation and diffraction forces on the prediction of parametric roll [J], Ocean Engineering. 175(2019a):262-272

Bu S, Gu M, Abdel-Maksoud M. Study on roll restoring arm variation using a three-dimensional hybrid panel method [J], Journal of Ship Research. 2019b,

https://doi.org/10.5957/JOSR.09180078

Cho S K, Hong S Y, Kyoung J H. The numerical study on the coupled dynamics of ship motion and flooding water[C]// Proc. 9th STAB, Rio de Janeiro, Brazil, 2006:599-605.

Chang B C, Blume P. Survivability of damaged Ro-Ro passenger vessels-ship technology research [J]. Schiffstechnik, 1998, 45(3): 105-117.

Gao Q, Vassalos D. The dynamics of the floodwater and the damaged ship in waves [J]. Journal of Hydrodynamics, 2015, 27(5): 689-695.

Gao Z, Gao Q, Vassalos D. Numerical simulation of flooding of a damaged ship [J]. Ocean Engineering, 2011, 38(14): 1649-1662.

Gao Z, Gao Q, Vassalos D. Numerical study of damaged ship flooding in beam seas [J]. Ocean Engineering, 2013, (61): 77-87.

Hashimoto H, Kawamura K, Sueyoshi M. Numerical simulation of ship transient behavior coupled with water flooding [C]// Proc. 25th ISOPE, Koan, USA. 2015:1251-1258.

ITTC. Final report and recommendation to the 24th ITTC [R]. The specialist committee on stability in waves, 2005 (II): 369-408.

Jasionowski A, Vassalos D. Numerical modelling of damage ship stability in waves[C]//5th International Workshop on Stability and Operational Safety of Ships, Trieste, 2001:7.3.1-7.3.7

Nabavi Y, Calisal S M, Akinturk A, et al. A computational investigation of the three dimensional geometric parameters' effects on the discharge rate of a ship opening [C]// Proc. 9th STAB, Rio de Janeiro, Brazil, 2006: 617–624.

Ruponen P, Sundell T, Larmela M. Validation of a simulation method for progressive flooding [J]. International Shipbuilding Progress, 2007, 45:305-321.

Spanos D, Papanikolaou A. On the time to capsize of a damaged RoRo/passenger ship in waves[C]//Proc. 9th ISSW, Germany. 2007.

Santos T A, Guedes Soares C. Study of the dynamics of a damaged passenger Ro-Ro ship[C]//Proc. 9th STAB, Rio de Janeiro, Brazil, 2006: 25-29.

Santos T A, Soares C G. Study of damaged ship motions taking into account floodwater dynamics [J]. Journal of Marine Science and Technology, 2008, 13(3): 291-307.

Strasser C. Simulation of Progressive Flooding of Damaged Ship by CFD [D]. Ph.D. Thesis. Universities of Glasgow and Strathclyde, 2010.

Umeda N, Kamo T, Ikeda Y. Some remarks on theoretical modeling of damaged stability [J]. Marine Technology, 41(1), 2004:45-49.

Van Walree F, de Kat J O, Ractliffe A T. Forensic research into the loss of ships by means of a time domain simulation tool [J]. International Shipbuilding Progress, 2007, 54(4): 381-407.

Modelling of compartment connectivity and probabilistic assessment of progressive flooding stages for a damaged ship

Kristian Bertheussen Karolius, *Maritime Safety Research Centre,* kristian.karolius@strath.ac.uk
Jakub Cichowicz, *Maritime Safety Research Centre*, jakub.cichowicz@strath.ac.uk
Dracos Vassalos, *Maritime Safety Research Centre*, d.vassalos@strath.ac.uk

ABSTRACT

Large cruise vessels have subdivision and compartment connectivity of unique complexity, making predictions of floodwater propagation a particularly challenging task. Evermore so, the plethora of internal openings leads to a large number of opening status combinations, a well-known problem in identifying flooding paths and assessing progressive flooding stages. This paper presents a novel approach aiming at reducing the problem to manageable size. The method enables a fully probabilistic approach for assessing progressive flooding stages and the examples presented demonstrate that it converges to a practical number of possible realisations even in the case of a realistic model of a large cruise vessel. The result show clearly that the methodology will render overly simplified models for assessment of vulnerability from internal openings obsolete and that it may be further refined for implementation to a range of applications.

Keywords: *Damage stability, Compartment connectivity, Progressive flooding, Opening modelling, Progressive flooding stages.*

1. INTRODUCTION

Large cruise vessels have an internal subdivision and compartment connectivity of unparalleled complexity. This makes predicting floodwater propagation in damaged condition a particularly challenging task with the number of possible flooding paths growing exponentially with the number of internal openings. This problem was highlighted in the European research project EMSA III (EMSA, 2016), addressing the contribution to risk from watertight doors, for Cruise and RoPax ships in collision flooding emergencies and considering door opening frequencies (from historical data), crew actions and door reliability.

The assessment of the impact of a single open watertight door on stability carried out by the project, led to the observation that the impact of any one single open door was small in comparison with the impact of combinations of multiple open doors. Furthermore, the impact on stability was proved insensitive to the opening's allowance category (as defined in MSC.1/Circ. 1380 (IMO, 2010) and summarised in Table 1) of doors comprising that particular combination (e.g. an opened door of category C would degrade stability, on average, to the similar extent as a door of category A).

Due to the combinatorial character of the problem the opening (doors in particular) statuses result in an immense number of possible combinations, N, increasing exponentially with the number of n doors available which is governed by Eq. 1 below.

$$N = 2^n \tag{1}$$

It is clear that the stability assessment involving all possible combinations of doors is infeasible, thus resulting in the necessity for developing simplified models, such as the one proposed within the EMSA project. Notably, such simplified models may neglect potentially critical combinations of doors. However, the number of possible initial damage extents is limited, and for every one of these, there are also a limited number of directly connected compartments. This entails that only the status of doors directly within the boundary of a specific initial damage extent needs to be considered in the first (and all subsequent flooding stages). This view enables to limit the problem and has been the basis for the development of a novel modelling approach presented in this paper.

Table 1: Opening allowance categories for watertight doors according to MSC.1/Circ. 1380 (IMO, 2010).

Categories	Opening allowance
Category A	Permitted to remain open during navigation by the Administration according to SOLAS regulation II-1/22.4.
Category B	May be opened during navigation when work in the immediate vicinity of the door necessitates it being opened, according to SOLAS regulation II-1/22.3.
Category C	May be opened during navigation to permit the passage of passengers or crew, according to SOLAS regulation II-1/22.3.
Category D	Shall be closed before the voyage commences and shall be kept closed during navigation according to SOLAS regulation II-1/22.1.

2. PROGRESSIVE FLOODING

Deterministic representation

Traditionally, and in contrast to the overall probabilistic damage stability regulations laid out in Reg. II-1/7 of SOLAS (IMO, 2006) progressive flooding stages are deterministic, determined by the openings watertightness alone rather than the opening frequencies. The underlying assumption is that watertight openings prevent progressive flooding even if they are allowed open in specific circumstances as seen in Table 1, simply because they can be *closed in time* by crew.

Considering separate progressive flooding stages is required only for non-watertight openings seriously restricting equalisation (with the equalising time over 60 seconds) as is laid out in the explanatory notes of SOLAS (IMO, 2017). Instantaneous equalisation (below 60s) assumes immediate flooding and allows including the progressively flooded compartments in the initial damage extent without a separate stage.

The non-watertight structural elements and doors seriously restricting the floodwater ingress are typically represented by A-class fire rated bulkheads and doors. In a single watertight zone, there may be a range of A-class boundaries leading to the exponential combinatorial problem on a local scale. Simplified approaches have been suggested to tackle the problem, such as the *neighbouring approach* as implemented in the stability software NAPA (NAPA, 2018), where the next connections (or stages) are considered as all the neighbouring compartments sharing a limit (bulkhead) with the currently damaged rooms and grouping those in a single combined stage.

Probabilistic representation

Deterministic approach is not suitable to address the risk contribution from watertight doors simply because it does not cater for random statuses of the actual openings. The first-principles probabilistic models, in addition to considering the damage breaches (initial extent) as a statistical variable, need to capture the stochastic behaviour of the internal connectivity of the vessel. The latter involves dynamically changing opening status with the associated opening frequencies as well as the uncertainty inherent in the openings resistance to leak and collapse when closed (progressive extent), as is illustrated in Figure 1. Both, the openings status frequencies and leak/collapse hydrostatic head distributions will influence the probability of progressive flooding through the opening. Similarly, if the stochastic nature of the vessel movements in waves is not accounted for directly, e.g. by time-domain simulations, it may be introduced as a probabilistic model within the traditional static assessment (e.g. as the probability of the internal water-elevation exceeding the vertical opening position or leak/collapse heads). Such governing variables may be represented as a total probability of progressive flooding and they will determine various realisations of progressive flooding stages, related to each initial damage extent, as will be discussed in the next section.

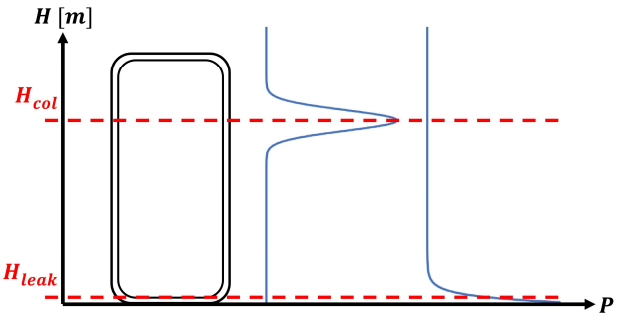

Figure 1: Example of leak and collapse pressure heights modelled with probability distributions (Norm./Exp.) to account for inherent uncertainty and to enable a fully probabilistic consideration.

Progressive extent realisation

A simple event (probability) tree, as shown in Figure 2 below, can illustrate the various realisations of initial and corresponding progressive extents. The top event represents any breach resulting from a collision damage (or contact/grounding), which branches out to all the possible initial damage extents.

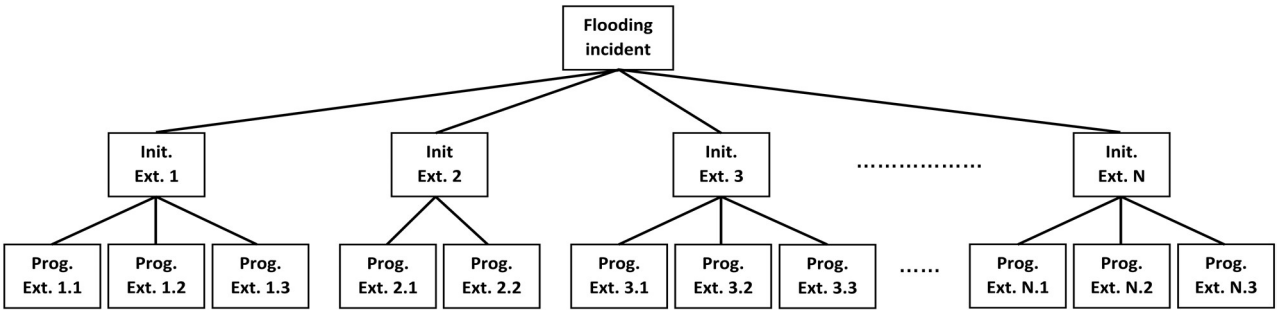

Figure 2: Event (probability) tree of damage extents (First row: breach resulting from collision damage or contact/grounding, second row: possible initial extents of damage, third row: possible progressive extents of damage).

A range of respective progressive damage extents may originate from each of these initial extents depending on the openings open/closed state, leak/collapse resistance and the openings position in relation to the floodwater elevation during the flooding evolution. All branches of progressive extents stemming from each of the initial extents, should sum to the initial extent probability according the total probability theorem, as given by Eq. 2, where $x = initial, y = progressive$.

$$P(x) = \int_y P(x|y)P(y)dy \qquad (2)$$

For example, the progressive extents in the leftmost branch are representing all possible progressing extent originating from the initial damage extent number one (if there is no progressive extent the initial extent remains unchanged and considered as total extent which would still be represented with a separate branch in the tree). The actual number of possible realisations of progressive extents will be governed by the number of connections in direct contact with the initial damage extent, and subsequent connections thereafter. An initial damage extent comprising a single compartment with just a couple connections would therefore be expected to have a smaller number of possible progressive extents than an initial damage extent comprising several compartments and multiple connections.

This being said, it would not necessarily be so as the probability of progressive flooding will be governing, e.g. if all the doors leading from the extent with several compartments connected had a progressive flooding probability of 1, the progressive extent where all connected compartments were progressively flooded would in fact be the only realisation possible. The various realisations are highly related to the combinatorics problem as was discussed in the foregoing.

To illustrate the combinatorial problem with multiple permutations, we may consider an example compartmentation shown in Figure 3. The compartmentation comprises six rooms (compartments): *A, B, C, D, E* and *F*, and six watertight doors: *a, b, c, d, e* and *f*. Compartment *F*, marked in yellow, is breached and considered as the initial damage extent. For simplicity, we assume that the probability of progressive flooding is solely governed by the door opening status (frequency), disregarding other variables as was mentioned in the previous section.

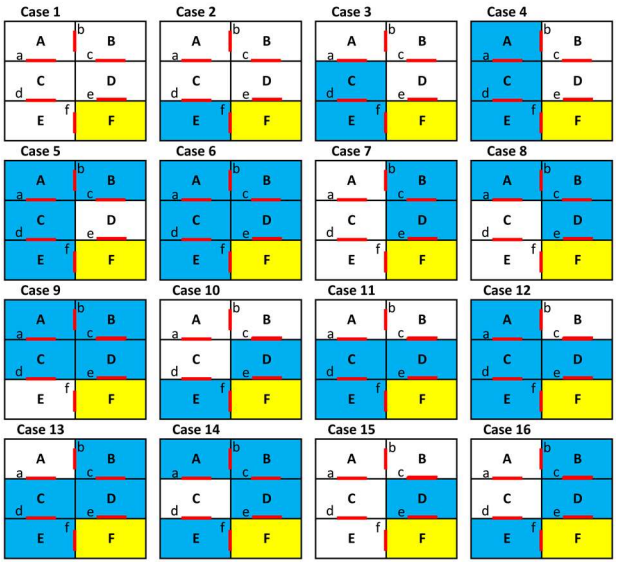

Figure 3: Example compartmentation with doors and possible flooding realisations (Doors are marked in red, initial flooding is marked in yellow, and progressively flooded compartments are marked in blue).

A door's opening status may be modelled by a *Bernoulli process* with the opening frequency represented by the parameter λ, as shown by Eq. 3.

$$P(open) = \lambda, P(closed) = 1 - \lambda \qquad (3)$$

The assumed opening frequency for the example compartmentation is summarised in Table 2.

Table 2: Assumed opening frequencies for example compartmentation.

Door	Opening frequency, λ
a	0.90
b	0.95
c	0.10
d	0.30
e	0.05
f	0.70

To calculate the realisation probability of *Case 1*, all the various door status combinations that are possible needs to be considered. In total, there are $2^6 = 64$ possible permutations (combinations) of door statuses in this specific case. Out of these, 16 permutations result in *Case 1* being realised (i.e. there is 16 progressive flooding scenarios originating in room *F*). Probability of *Case 1* may therefore be calculated by summing all these realisations as shown by Eq. 4, where n is the number of realisations resulting in a specific initial damage extent x.

$$P(X = x) = \sum_{i=1}^{n} P_{x_i} \tag{4}$$

It may be shown that this results in a probability of: $P(X = Case\ 1) = 0.285$. Another way to calculate the realisation probability may be illustrated as in the following. For *Case 1* to be realised, doors *e* and *f* have to be closed ($open = 1, closed = 0$) whilst the status of the remaining doors status is not affecting the outcome. Hence, the probability of this particular case is simply the joint probability of the two relevant doors being closed (using the probability rule of conditionality governed by Eq. 5 and calculated in Eq. 6).

$$P(X = x) = P(e, f) = P(e)P(f) \tag{5}$$

$$\begin{aligned} P(X = Case\ 1) &= P(e = 0, f = 0) \\ &= (1 - \lambda_e)\,(1 - \lambda_f) \\ &= (1 - 0.05)\,(1 - 0.70) \\ &= 0.285 \end{aligned} \tag{6}$$

The second case, *Case 2* may be calculated by the same method (it is only governed by doors *d*, *e* and *f*). For the case to be realised, doors *d* and *e* have to be closed and door *f* has to be open whilst the status of the remaining doors statuses does not affect the realisation. The probability of *Case 2* may again simply be calculated as the joint status probability of the three relevant doors.

$$\begin{aligned} P(X = Case\ 2) &= P(d = 0, e = 0, f = 1) \\ &= (1 - \lambda_d)\,(1 - \lambda_e)\lambda_f \\ &= (1 - 0.30)(1 - 0.05)70 \\ &= 0.4655 \end{aligned} \tag{7}$$

The process can be repeated for all 16 cases, but we will consider *Case 6*, with all doors part of the progressive boundary, as a final example. This case may result from flooding progression by two routes with multiple door realisations leading to the same case. In fact, seven realisations will result in *Case 6;* summarised below by Eq. 8 to 14 with the total probability as given by Eq. 15.

$$\begin{aligned} P_1(X_1 = Case\ 6) &= P(a, b, c, d, e, f = 1) = \cdots \\ \cdots &= \lambda_a\lambda_b\lambda_c\lambda_d\lambda_e\lambda_f = \cdots \\ \cdots &= 0.90 \cdot 0.95 \cdot 0.10 \cdot 0.30 \cdot 0.05 \cdot 0.70 = \cdots \\ \cdots &= 0.0009 \end{aligned} \tag{8}$$

$$\begin{aligned} P_2(X_2 = Case\ 6) &= P(a, b, c, d, e = 1, f = 0) = \cdots \\ \cdots &= \lambda_a\lambda_b\lambda_c\lambda_d\lambda_e(1 - \lambda_f) = \cdots \\ \cdots &= 0.90 \cdot 0.95 \cdot 0.10 \cdot 0.30 \cdot 0.05 \cdot (1 - 0.70) = \cdots \\ \cdots &= 0.0004 \end{aligned} \tag{9}$$

$$\begin{aligned} P_3(X_3 = Case\ 6) &= P(a, b, c, d, f = 1, e = 0) = \cdots \\ \cdots &= \lambda_a\lambda_b\lambda_c\lambda_d(1 - \lambda_e)\lambda_f = \cdots \\ \cdots &= 0.90 \cdot 0.95 \cdot 0.10 \cdot 0.30 \cdot (1 - 0.05) \cdot 0.70 = \cdots \\ \cdots &= 0.0171 \end{aligned} \tag{10}$$

$$\begin{aligned} P_4(X_4 = Case\ 6) &= P(a, b, c, e, f = 1, d = 0) = \cdots \\ \cdots &= \lambda_a\lambda_b\lambda_c(1 - \lambda_d)\lambda_e\lambda_f = \cdots \\ \cdots &= 0.90 \cdot 0.95 \cdot 0.10 \cdot (1 - 0.30) \cdot 0.05 \cdot 0.70 = \cdots \\ \cdots &= 0.0021 \end{aligned} \tag{11}$$

$$\begin{aligned} P_5(X_5 = Case\ 6) &= P(a, b, d, e, f = 1, c = 0) = \cdots \\ \cdots &= \lambda_a\lambda_b(1 - \lambda_c)\lambda_d\lambda_e\lambda_f = \cdots \\ \cdots &= 0.90 \cdot 0.95 \cdot (1 - 0.10) \cdot 0.30 \cdot 0.05 \cdot 0.70 = \cdots \\ \cdots &= 0.0081 \end{aligned} \tag{12}$$

$$\begin{aligned} P_6(X_6 = Case\ 6) &= P(a, c, d, e, f = 1, b = 0) = \cdots \\ \cdots &= \lambda_a(1 - \lambda_b)\lambda_c\lambda_d\lambda_e\lambda_f = \cdots \\ \cdots &= 0.90 \cdot (1 - 0.95) \cdot 0.10 \cdot 0.30 \cdot 0.05 \cdot 0.70 = \cdots \\ \cdots &= 0.0001 \end{aligned} \tag{13}$$

$$\begin{aligned} P_7(X_7 = Case\ 6) &= P(b, c, d, e, f = 1, a = 0) = \cdots \\ \cdots &= (1 - \lambda_a)\lambda_b\lambda_c\lambda_d\lambda_e\lambda_f = \cdots \\ \cdots &= (1 - 0.90) \cdot 0.95 \cdot 0.10 \cdot 0.30 \cdot 0.05 \cdot 0.70 = \cdots \\ \cdots &= 0.0001 \end{aligned} \tag{14}$$

$$P(X = Case\ 6) = \sum_{i=1}^{n=7} P_{X_i} = \cdots \quad (15)$$

$$\cdots = P_1 + P_2 + P_3 + P_4 + P_5 + P_6 + P_7 = \cdots$$

$$\cdots = 0.0009 + 0.0004 + 0.0171 + 0.0021 + \cdots$$

$$\cdots + 0.0081 + 0.0001 + 0.0001 = \cdots$$

$$\cdots = 0.0287$$

Table 3 below summarises the probability calculations for all example cases. The second calculation methodology comprises less combinations of doors, as only the doors located within the flooding boundary is of interest. However, *Case 1* and *2* are the simplest of the example cases, and it is relatively easy to calculate their realisation probability by manual calculations, being governed by a few doors. If more doors are governing, such as in *Case 6*, increasing various realisations of doors may result in the same progressive damage extent, which will complicate the problem. Nevertheless, the manual calculations method cannot be applied to a realistic case of a large cruise vessel with thousands of possible initial damage extents and numerous connections, hence an alternative approach is essential.

3. GRAPH MODEL OF COMPARTMENT CONNECTIVITY

The problem of opening permutations can be addressed more efficiently than the direct calculations with the help of *Graph Theory*. Graph Theory is a well-known mathematical modelling technique for representing pairwise connections between objects (nodes) with the relationship maintained by edges (lines). The application of graphs ranges from the evacuation modelling software *Evi* (Vassalos et al, 2001) through social networks (Zweig, 2016) to navigational- and road-networks (Thomson et al, 1995). Any exhaustive review of theory and applications of graph theory is outside the scope of this paper, but reference is made to introductory texts such as (Bondy et. al., 1976).

In modelling of compartment connectivity as a graph, the compartments are simply represented by the nodes (points) and openings are represented by edges (lines). For example (Dankowski & Krüger, 2013) represented compartment connectivity by deterministic directed graphs (i.e. without the ability to account for probabilities). Graph model of the example compartmentation from Figure 3 is presented in Figure 4 below. For the purpose of compartment connectivity, we are not interested in distances between locations (as is often used for road networks); instead we may rather use the weights representing the probability of progressive flooding between compartments, or opening frequencies, depending on how we define the problem.

Representing the edges by probabilities turns the graph into an *uncertain graph*, a well-known technique utilised for example in network reliability (Khan, 2018). In the compartment connectivity example, existence of the edge implies possible progressive flooding between the nodes (compartments). However, progressive flooding only occurs if at least one of the edges is connected to the initial damage extent (the source node).

Table 1: Probability summary of case realisations for example compartmentation.

Case, i	Calculation formulae	Result
$P_{Case\ 1} =$	$(1.00 - 0.05) \cdot (1.00 - 0.70)$	$= 0.2850$
$P_{Case\ 2} =$	$(1.00 - 0.30) \cdot (1.00 - 0.05) \cdot 0.70$	$= 0.4655$
$P_{Case\ 3} =$	$(1.00 - 0.90) \cdot (1.00 - 0.05) \cdot 0.30 \cdot 0.70$	$= 0.0200$
$P_{Case\ 4} =$	$(1.00 - 0.95) \cdot (1.00 - 0.05) \cdot 0.90 \cdot 0.30 \cdot 0.70$	$= 0.0090$
$P_{Case\ 5} =$	$(1.00 - 0.10) \cdot (1.00 - 0.05) \cdot 0.90 \cdot 0.95 \cdot 0.30 \cdot 0.70$	$= 0.1535$
$P_{Case\ 6} =$	$0.0009 + 0.0004 + 0.0171 + 0.0021 + 0.0081 + 0.0001 + 0.0001$	$= 0.0287$
$P_{Case\ 7} =$	$(1.00 - 0.70) \cdot (1.0. - 0.95) \cdot 0.10 \cdot 0.05$	$= 0.0001$
$P_{Case\ 8} =$	$(1.00 - 0.70) \cdot (1.00 - 0.90) \cdot 0.95 \cdot 0.10 \cdot 0.05$	$= 0.0001$
$P_{Case\ 9} =$	$(1.00 - 0.30) \cdot (1.00 - 0.70) \cdot 0.05 \cdot 0.10 \cdot 0.95 \cdot 0.90$	$= 0.0009$
$P_{Case\ 10} =$	$(1.00 - 0.30) \cdot (1.00 - 0.10) \cdot 0.05 \cdot 0.70$	$= 0.0220$
$P_{Case\ 11} =$	$(1.00 - 0.90) \cdot (1.00 - 0.10) \cdot 0.30 \cdot 0.05 \cdot 0.70$	$= 0.0009$
$P_{Case\ 12} =$	$(1.00 - 0.95) \cdot (1.00 - 0.10) \cdot 0.90 \cdot 0.30 \cdot 0.70 \cdot 0.05$	$= 0.0004$
$P_{Case\ 13} =$	$(1.00 - 0.90) \cdot (1.00 - 0.95) \cdot 0.30 \cdot 0.70 \cdot 0.05 \cdot 0.10$	$= 0.0000$
$P_{Case\ 14} =$	$(1.00 - 0.30) \cdot (1.00 - 0.90) \cdot 0.70 \cdot 0.05 \cdot 0.10 \cdot 0.95$	$= 0.0002$
$P_{Case\ 15} =$	$(1.00 - 0.70) \cdot (1.00 - 0.10) \cdot 0.05$	$= 0.0135$
$P_{Case\ 16} =$	$(1.00 - 0.30) \cdot (1.00 - 0.95) \cdot 0.70 \cdot 0.05 \cdot 0.10$	$= 0.0001$
$Sum =$	$\sum_{i=1}^{n} P_{Case\ i}$	$= 1.0000$

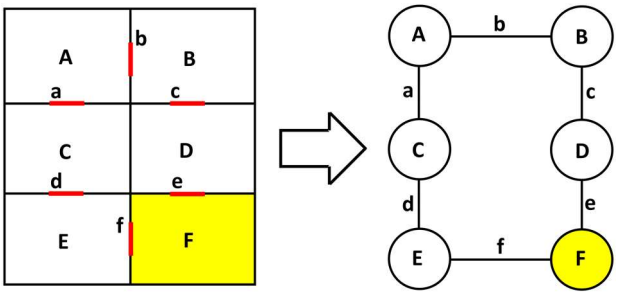

Figure 4: Compartments mathematical abstraction as graph (compartment or node marked in yellow is initial damage extent, or source node).

This conditionality can be accounted for readily by implementing search algorithms for traversing the graph structure. Such algorithms comprise Breadth-First-Search (BFS) (Moore, 1959), and Depth-First Search (DFS) (Trémaux, 1859–1882). In the example compartmentation the opening frequencies can be used to sample (create) the connections (edges) between the compartments (nodes) for multiple instances (samples). An example of such sampled realisations is shown in Figure 5 below, where dashed lines represent non-existing edges and continuous lines represent existing edges.

The nodes (compartments), having existing edges and a valid connection to the source node (initial extent) are part of the progressive extent (blue nodes in the figure). The sampling process, if done sufficient number of times, should result in accurate approximation of the realisation probability of the openings, while search algorithms account for the conditionality of the connections (i.e. they return only the relevant progressive stages with connection to the source node, representing the initial extent of damage). The sum of each flooding realisation (initial and progressive combined), divided by the number of samples, represents the estimate of the respective case-realisation probabilities. In order to verify the approach, the example flooding cases are sampled with $N = 100{,}000$ samples. The results shown in Table 4 demonstrate good agreement with the calculated probabilities.

Table 4: Progressive flooding case (realisation) probability from manual calculation and sampling scheme.

Case, i	P, calculation	P, sampling
$P_{Case\ 1}$ =	0.2850	0.2847
$P_{Case\ 2}$ =	0.4655	0.4650
$P_{Case\ 3}$ =	0.0200	0.0201
$P_{Case\ 4}$ =	0.0090	0.0091
$P_{Case\ 5}$ =	0.1535	0.1542
$P_{Case\ 6}$ =	0.0287	0.0287
$P_{Case\ 7}$ =	0.0001	0.0001
$P_{Case\ 8}$ =	0.0001	0.0001
$P_{Case\ 9}$ =	0.0009	0.0009
$P_{Case\ 10}$ =	0.0220	0.0220
$P_{Case\ 11}$ =	0.0009	0.0010
$P_{Case\ 12}$ =	0.0004	0.0004
$P_{Case\ 13}$ =	0.0000	0.0000
$P_{Case\ 14}$ =	0.0002	0.0002
$P_{Case\ 15}$ =	0.0135	0.0135
$P_{Case\ 16}$ =	0.0001	0.0001
Sum =	1.0000	1.0000

4. REAL-CASE EXAMPLE

The ship model selected for case study is based on a large modern cruise vessel of 100,000 GT, currently in operation. The vessel main particulars are presented in Table 5 below. The vessel internal compartment connectivity comprises a total of 894 openings, covering doors, hatches, etc. The model of the internal arrangement is shown in Figure 6 below.

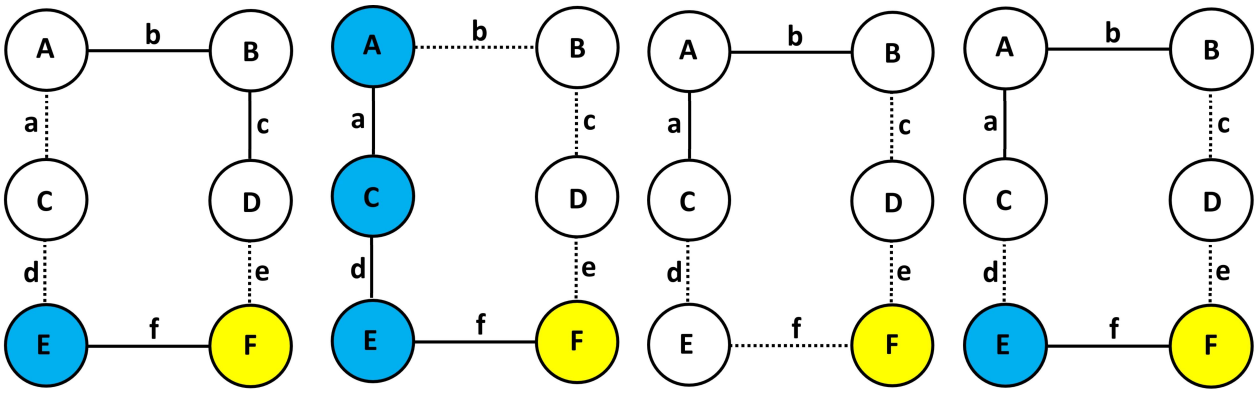

Figure 5: Sampled edge existence in example compartmentation represented as uncertain graph (Dashed lines represent non-existing edges or no progressive flooding realization, and continuous lines represent existing edges or progressive flooding realization. Initial flooding is marked in yellow, and progressively flooded compartments are marked in blue).

Table 1: Particulars of the sample ship

Parameter (symbol)	Value [designation]
Length between perp. (L_{BP})	273 [m]
Breadth (B)	36 [m]
Depth (D)	21 [m]
Gross tonnes (GT)	100000 [tonnes]
Number of passengers (-)	2800 [persons]
Number of crew (-)	1050 [persons]

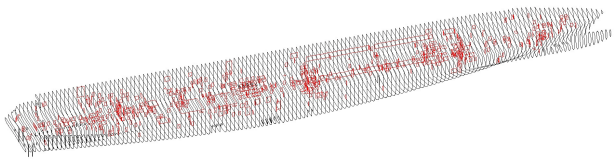

Figure 6: Test-Vessel stability model with internal openings.

Due to lack of actual data, the opening frequencies are based on their opening allowance category (supported by data adopted from the EMSA project, which has been derived from onboard records of various vessel types). Protected, non-watertight openings not imposed by any category, has been given an assumed opening frequency of 0.5 for the purpose of illustration. The frequencies are shown in Table 6 for the various opening categories.

In reality, such values would vary with specific doors depending on compartment type and crew/passenger traffic. The probability of doors being closed in time by crew is represented by a correction factor. In the EMSA project, such a correction has been modelled as a function of time, however, for illustration purposes, this has been taken as constant 90% success rate (only for watertight doors). In this specific example the correction factor accounts also for reliability of the doors.

Table 2: Assumed opening frequencies for test vessel per allowance category.

Ope. Allow. category	Ope. Freq.	Corrected
A	0.850	0.085
B	0.600	0.060
C	0.100	0.010
Protected non-WT	0.500	0.500
Unprotected non-WT	1.000	1.000

To limit the result, a single initial damage extent has been chosen to be implemented with the sampling methodology, to produce progressive extent realisations. Furthermore, for the purpose of illustration, we have considered the opening frequencies alone disregarding other variables such as leak/collapse heads and position of openings in relation with the floodwater elevation (this will obviously result in compartments being marked as part of the progressive extent (lost buoyancy), but not necessarily flooded). The initial damage case selected for illustration is a 2-zone damage, comprising 2 compartments and is illustrated in Figure 7 below.

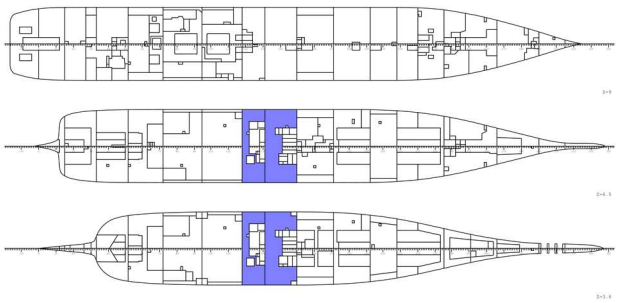

Figure 7: Initial damage extent of the case study.

For implementation of the sampling methodology, we generated $N = 1{,}000$ samples using the Bernoulli process, resulting in a corresponding number of graphs representing the state-space. The traversing search algorithm (BFS in this specific example), identified 86 unique progressive extents originating from specific initial extent, stemming from 6 openings with direct connection to the initial extents boundary. In order to rank the cases we make use of traditional statistical methods such as confidence intervals (CI). In the discrete domain, the CI may be represented as the number of cases with the largest probability, that results in a specific proportion of the total probability. The summary results of CI-based ranking are shown in Table 7. For example, the 90% CI simply indicate that there is a 90% probability that following a damage breach comprising the initial extent, the progressive extent would result in one out of nine cases as is seen in Table 8 below.

Table 7: Confidence Intervals (CI) and corresponding number of related progressive extents for 1,000 samples.

Confidence Interval, CI [%]	Number of prog. extents
50	3
80	6
90	10
95	36
99	76
100	86

Table 8: Progressive extents representing a 90% Confidence Interval (CI), including initial extent (two leftmost comp.).

Case	**P**	**Compartments**
1	0.233	R070101 R080116 EX070101 R070102
2	0.206	R070101 R080116 EX070101 EX080101 R070102
3	0.115	R070101 R080116
4	0.112	R070101 R080116 EX080101
5	0.072	R070101 R080116 R070102
6	0.055	R070101 R080116 EX080101 R070102
7	0.052	R070101 R080116 EX070101
8	0.046	R070101 R080116 EX070101 EX080101
9	0.005	R070101 R080116 EX070101 EX080101 R070102 R080201
SUM	0.902	

All case realisations representing the 90% CI are illustrated in Appendix I, including also realisation No. 36, corresponding to the transition to the 95% CI for illustrating a less probable, but larger progressive extent. Case No. 3 represents the initial stage alone, where no additional compartments are progressively flooded. From the various progressive extent realisations presented in Appendix I, it is seen that the 90% CI are mostly comprising smaller A-class boundary compartments within the watertight boundaries as would be expected, simply due to the assignment of a 50% opening rate. More substantial progressive extents with compromised watertight boundaries are only seen above the 90% CI, as is represented by case realisation 36 in figure I-10.

5. CONCLUDING REMARKS

This paper presents a fully probabilistic methodology for modelling compartment connectivity with the help of graph theory. The method utilises state-of-the art search algorithms for maintaining the probabilistic conditionality of connection to source (initial extent). This simplifies the problem, as non-existing connections to the source are disregarded. A simple example has been provided to demonstrate that the method converges to the actual probabilities. The fully probabilistic modelling approach enables the use of traditional statistical methods and probabilistic evidence for quantifying the choices of progressive flooding extents in place of analysis of all possible combinations, which is highly infeasible (impossible in most cases). The realistic case study presented in this paper demonstrates that the method identifies a manageable number of possible progressive flooding extents. The choice of detail, and number of resulting cases are governed by the confidence interval and number of samples used. The methodology is capable of rendering the overly simplified models for assessment of vulnerability from internal openings obsolete. Apart from the survivability assessment the method may also be employed in emergencies to avoid compartments imposed by floodwater, smoke, or fire in a range of emergency situations, and may therefore provide a tool in identifying optimal evacuation routes.

REFERENCES

EMSA, 2015, EMSA/OP/10/2013 (EMSA III), Project No. PP090623, “Evaluation of risk from watertight doors”, Report No. 2015-0167 Rev 7.

International Maritime Organisation, IMO, 2010, MSC.1/Circ. 1380, “Guidance for watertight doors on passenger ships which may be opened during navigation” Ref. T4/3.01.

International Maritime Organization, 2009, “Reg. II-1/7 of SOLAS Consolidated Edition 2009”, as adopted in IMO Res. MSC 216(82)), 2006.

International Maritime Organisation, IMO, 2017, “Revised Explanatory Notes to the SOLAS Chapter II-1 Subdivision and Damage Stability Regulations”, as adopted by Res. MSC.429(98), 2017.

NAPA Ltd, 2018, “NAPA for Design Manuals 2018.3”

D. Vassalos, H. Kim, G. Christiansen, J. Majumder, 2001, “A Mesoscopic Model for Passenger Evacuation in a Virtual Ship-Sea Environment and Performance-Based Evaluation”, Pedestrian and Evacuation Dynamics – April 4-6, 2001 – Duisburg.

K. A. Zweig, M. Abufouda, 2016 “A theoretical model for understanding the dynamics of online social networks decay”, arXiv preprint arXiv:1610.01538, 2016.

R. C. Thompson, D. E. Richardson, 1995, ”A Graph Theory approach to road network generalization”, Proceedings of the 16th International Cartographic Conference, Barcelona, Spain, 3–9 September 1995.

J. A. Bondy and U. S. R. Murty, 1976, “Graph Theory with Applications”, Elsevier Science Publishing Co., Inc., 1976.

H. Dankowski, S. Krüger, 2013, “Progressive Flooding Assessment of the Intermediate Damage Cases as an Extension of a Monte-Carlo based Damage Stability Method”, Proceedings of the PRADS201320-25, October 2013 CECO, Changwon City, Korea

A. Khan, F. Bonchi, F. Gullo, A. Nufer, 2018, “Conditional Reliability in Uncertain Graphs”, IEEE Transactions on Knowledge and Data Engineering, Volume: 30 , Issue: 11, November 1st, 2018.

E. F. Moore, 1959, "The shortest path through a maze", Proceedings of the International Symposium on the Theory of Switching. Harvard University Press. pp. 285–292. As cited by Cormen, Leiserson, Rivest, and Stein.

C. P. Trémaux (1859–1882) École polytechnique of Paris (X:1876), French engineer of the telegraph in Public conference, December 2, 2010 – by professor Jean Pelletier-Thibert in Académie de Macon (Burgundy – France) – (Abstract published in the Annals academic, March 2011).

APPENDIX I

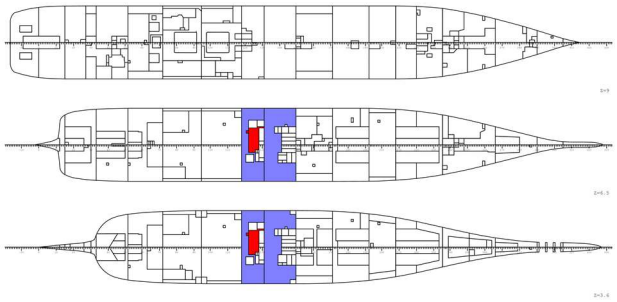

Figure I-1: Progressive flooding realization 1, P = 0.2219

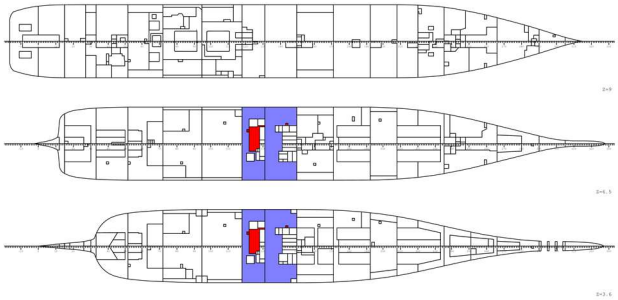

Figure I-2: Progressive flooding realization 2, P = 0.1964

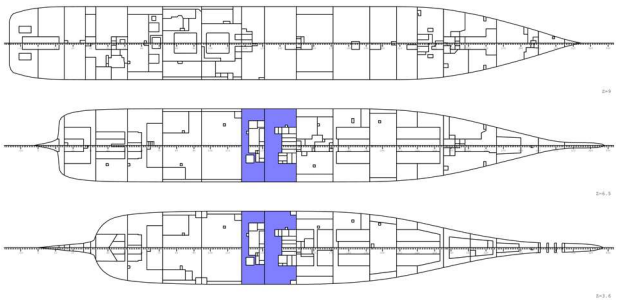

Figure I-3: Progressive flooding realization 3, P = 0.1212

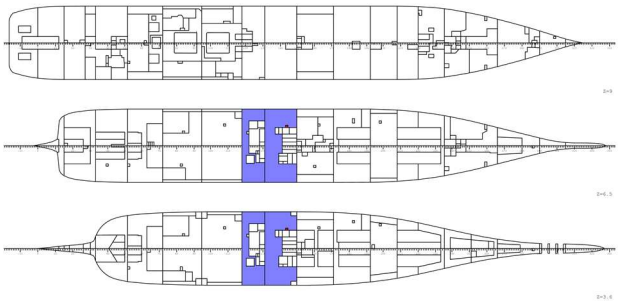

Figure I-4: Progressive flooding realization 4, P = 0.1152

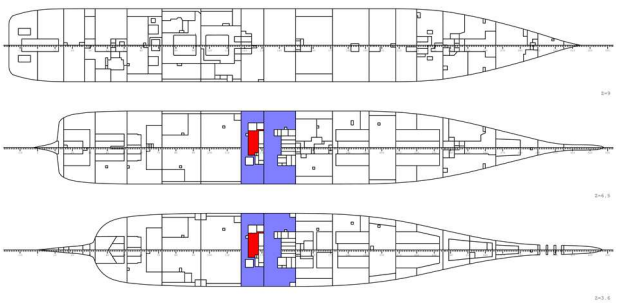

Figure I-5: Progressive flooding realization 5, P = 0.0603

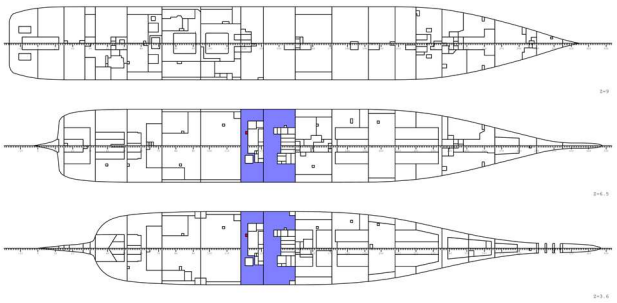

Figure I-6: Progressive flooding realization 6, P = 0.0552

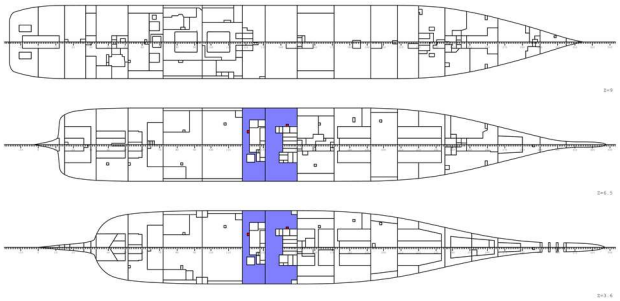

Figure I-7: Progressive flooding realization 7, P = 0.0534

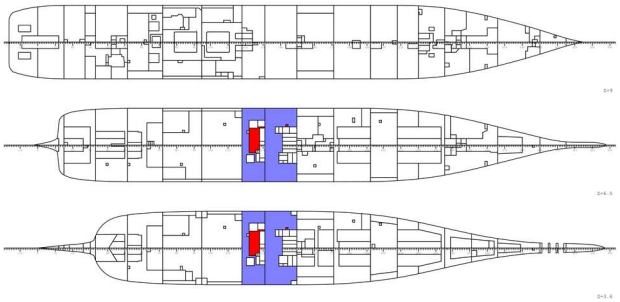

Figure I-8: Progressive flooding realization 8, P = 0.0058

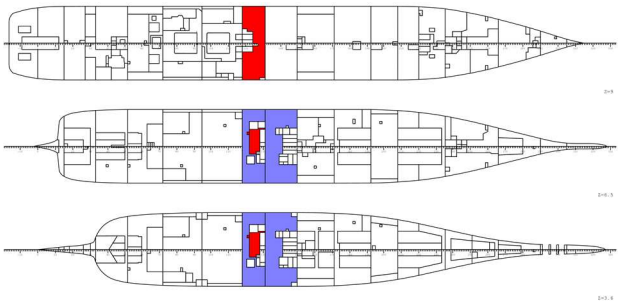

Figure I-9: Progressive flooding realization 9, P = 0.0046

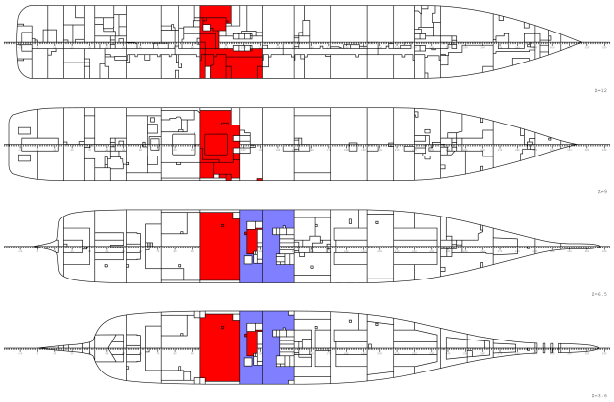

Figure I-10: Progressive flooding realization 36, P = 0.001

Ship stability-related effects on a critical distance of collision evasive action

Mateusz Gil, Gdynia Maritime University, m.gil@wn.umg.edu.pl
Jakub Montewka, Gdynia Maritime University, j.montewka@wn.umg.edu.pl
Przemysław Krata, Gdynia Maritime University, p.krata@wn.umg.edu.pl
Tomasz Hinz, Aalto University, Tomasz.Hinz@aalto.fi, Deltamarin Ltd, Waterborne Transport Innovation

ABSTRACT

Numerous solutions have been developed to facilitate collision avoidance process and safety assessment at sea. These are based on proximity indicators, defined as an area around own ship that is to be kept clear from other vessels. One of such indicators is referred to as a ship's domain. Therein, a domain violation is recognized as an unsafe operation and needs to be avoided. However, the concept of a ship's domain does not originate from the collision avoidance field, rather it is rooted in the field of waterway's capacity assessment. Thus, the problem of transferability of the concept from one field to another emerges, resulting in the need for proper evaluation of the domain's characteristics that are suitable for the field of collision avoidance. Therein such features as ship's manoeuvrability and stability conditions seem to be indispensable since those affect the minimum area required for a ship to perform collision evasive manoeuvre.

The aim of the paper is three-fold. First, it sketches the minimum requirement for an area around own ship that needs to be kept free from other objects to ensure the safe passage of the ship. Second, it discusses the significance of stability-related effects on this area. Third, it is to provoke a discussion on the subject.

To this end extensive literature review is performed summarizing available domains, then to determine the safe area around own ship, a 6DoF ship motion model (*LaiDyn*) is adopted, along with encounter simulator.

Keywords: *ship collision avoidance, minimum distance to collision, ship operational stability.*

1. INTRODUCTION

From the operational viewpoint, a number of collision avoidance system (CAS) methods have been proposed, in line with developments in *e-Navigation*, [1]. However, the most widely used CAS is the *Automatic Radar Plotting Aid* (ARPA). This technology tracks several targets and displays proximity indicators, called CPA *(closest point of approach*) and TCPA (time to CPA), used for operational risk assessment. However, the passing distance does not translate into the required area for a safe and efficient evasive manoeuvre. Another type of proximity indicator stems from a concept of *ship domain*. Where *ship domain can be thought of as the sea area around the ship which a navigator would like to keep free, with respect to other ships and fixed objects*, see [2]. Nevertheless, the concept was initially developed for the purpose of waterway capacity evaluation and strategic risk assessment [2]–[4]. Despite that, it migrated to the field of operational risk assessment and collision avoidance, as used by [5]–[8]. Another concept called *arena* has been introduced in [9], defined as *the area around the own ship which when infringed causes the mariner to consider whether to make a collision-evasive manoeuvre*. However, all those proximity indicators are subjective, referring to the comfort area defined by a navigator rather than a safety-critical area for a ship to perform evasive action. The difference between these two areas is substantial, and a navigator handling a ship should be aware of the safety area's dimension. It would be rather helpful when planning an evasive manoeuvre in an encounter, where the other, give-a-way vessel is not acting as supposed. This critical area depends on numerous factors, where the ship's dynamics is one of them. Interestingly, only a few studies take into account ship dynamics, as a factor determining the safe area for a given type of a manoeuvre, see for example [10]–[15]. However, those models face serious limitations, by considering one type of

manoeuvre for fixed rudder settings (turning circle at 20° rudder angle), one type of ship, fixed, presumably favourable stability condition. Adoption of maximum rudder angle for the collision evasive manoeuvre is not always advisable. Obviously, this results in the smallest turning radius for evasive action. However, it may lead to the development of significant roll angle, ultimately leading to an incident or even to ship capsizing, if the stability conditions are poor, see for example an accident of *m/s Hoegh Osaka* as described in [16]. In our earlier work [17], [18], a model determining the critical area for a Ro-Pax ship is presented, accounting for her dynamics, preselected stability conditions and simplified encounter conditions. The models stem from the concept of *Minimum Distance To Collision* (MDTC), as introduced in [19], [20]. Therefore in this paper, we discuss the minimum requirements for an area around own ship that needs to be kept free from other objects to ensure the safe passage of the ship in an encounter. Moreover, we discuss the significance of stability-related effects on this area. As a case study, we demonstrate the safe area for a container ship.

The structure of the paper is as follows: Section 2 introduces the concept of the safe area around own ship, Section 3 presents the methods adopted in the study and the developed model. In Section 4 the results are elaborated and discussed, while Section 5 concludes.

2. CONCEPT

Operational stability characteristics of selected vessels

Collision avoidance manoeuvres are usually planned with regard to the ship turning characteristics, as per wheelhouse poster. The stability issues are usually not considered, despite the effect of the ship's stability on her behaviour while exposed to the external force developed on the rudder and hull. Since the stability characteristics may affect the way the safe evasive action is conducted in an encounter, it is important for a bridge officer to be aware of its magnitude. Therefore, the feasible range of ship stability indicators for a given ship needs to be known, along with their effect on the size of the required minimum safe area for an evasive manoeuvre. A ship type that faces significantly different loading conditions in operation is container vessel. In Figure 1 ships' metacentric height (GM) variations are shown for a set of such ships. The data is collected by the students of *Gdynia Maritime University* during their sea practices, and it covers a period of five years 2013-3018. The values of container vessels' GMs are spanning over 0.2- 4.5 m.

The series of ships operated by *Cosco* company is a good example of stability variations since the 300 m long vessels loaded down to their draft of around 10.5 - 11.6 m faces the GM ranging between 1.66 - 4.56 m. Thus, despite the same draft of the same ships, stability conditions govern her behaviour in the seas. The second characteristics of analysed ships is the area under the GZ curve calculated from zero up to an angle of heel 30°, as presented in Figure 2. Therein the significant spread of this parameter is seen. The stability of container vessels vary significantly in their daily operations, thus the behaviour of the ship and her response will vary. This should be accounted for in any research addressing the stability-related areas, e.g. manoeuvring and its derivatives such as collision avoidance. Therefore, a set of manoeuvring data shown on the bridge in the form of turning circles (relevant for ballast conditions and for fully loaded ones) are not enough to cover all practical loading conditions, and a better solution needs to be found, like a minimum safe area for an evasive manoeuvre.

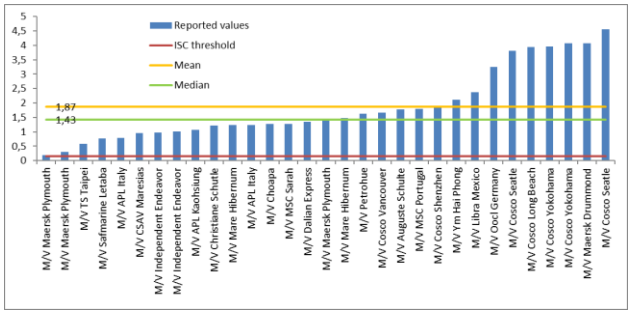

Figure 1: GM reported during routine operation of examined container vessels.

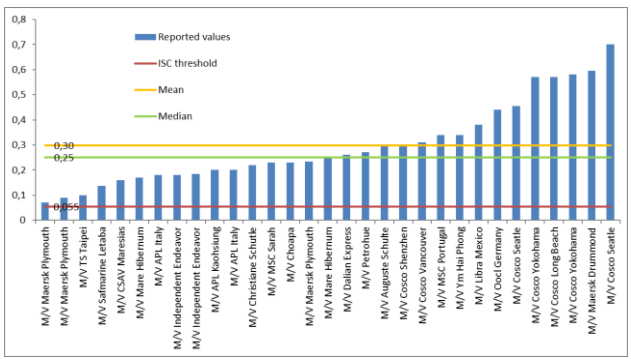

Figure 2: Area under GZ curve up to 30 degrees, reported during routine operation of examined container vessels.

Safe manoeuvring area definition

The minimum safe area for evasive manoeuvre is understood here as an area around own ship, which must be kept free from any objects that are on collision course with the own ship. The dimensions of the area are based on the ship's manoeuvring capabilities under given stability conditions, ensuring safe evasive actions. The latter denotes such manoeuvre, where the collision encounter is resolved and there is no harm to ship, crew or cargo. This means that the ship does not experience excessive roll angle or accelerations in the course of collision evasive action.

According to the assumptions of MDTC concept, as per [19]–[21], for each navigational scenario that can be interpreted as an arrangement of two vessels in the two-dimensional coordinate system only one MDTC exists. Safe area for the vessel can be obtained by computation of mentioned value for each navigational scenario and selected hydro-meteorological conditions. Because of utilization vessels' trajectories that include 6DoF motion model, stability issues and criteria can be directly incorporated into the subject of collision avoidance.

Determination of MDTC values for many scenarios and cases allows defining the general area where the last moment of evasive manoeuvre execution by the vessel is still feasible. To this end, a wide range of ships' headings and weather conditions needs to be accounted for resulting in a considerable number of combinations. The projection of the MDTC values in the function of the wave direction and relative bearing between the vessels creates around the ship the safe manoeuvring area. Due to the time-consumption of proposed calculations for a large sample of input data, the computer application is developed, called ships encounter simulator.

3. METHODS

6DoF ship's motion model

The study focuses on effects resulting from coupling between the ship manoeuvrability and her stability response to external forces due to seas. Thus, the most convenient approach is not to separate these both characteristics and rather consider them as a complex response to all relevant forces like seas, wind and rudder action. To comprise them, the state-of-the-art 6DoF ship motion model called *LaiDyn* is utilized, which is developed as a hybrid non-linear simulation model for a ship being considered a rigid body in the time domain, [22], [23]. Hence the assumption of small amplitude oscillatory motions are adopted [24], the radiation and diffraction forces are calculated according to the linear approach. The non-linear part, for example, hydrostatics (hull shape), wave force, manoeuvring, and propulsion, were taken into consideration [25]. Especially the two latter ones are crucial for our research since rudder action and propulsion during the ship turn to remain core issues for collision avoidance problems.

The model is validated in two-fold. First in the course of the towing tank model tests conducted at Aalto University [26], [27], second through the numerous external benchmark studies [28], [29]. The results of those are found satisfactory for the purpose of this research, where *LaiDyn* produces ship's trajectories for varying hydro-meteorological conditions defined by significant waves (H_s) and angle of wave's attack on the ship's hull.

Ships encounter simulator

Subsequently, the trajectories generated by *LaiDyn* are fed into an encounter simulator, where different navigational scenarios are modelled, resulting in the mutual arrangement of the vessels and their angular positions (ships' headings and bearings), as well as the hydro-meteorological conditions considered. The general principle of encounter simulator's operation, as presented in Figure 3, is based on causing the collision between the vessels which are figures on a 2D coordinate system that estimate projections of ships' hulls at the given angle. Afterwards, ships are successively moving apart in the straight line by given time step. For each iteration, according to the simulation case and navigational scenario, into the position of the particular vessel, the trajectory is loaded and set. The simulator validates the realisation of the evasive manoeuvre and if the collision between the ships still exists, the next backward step is executed. The loop is processed as long, as the set trajectories cause the collision. At the first position where tracks allow for the safe passage (collision-avoidance is successful), the application is breaking the loop and computes the safety parameters of ships' encounter. These include MDTC value, positions of the ships and the relative

bearings to the target, for manoeuvre execution moment.

Before the trajectories are set into the simulator, tracks are filtered out according to the adopted safety-related criteria. In the research presented here, a criterion of rolling angle is taken into account. The input files are screened for the threshold for roll angle exceedance. In case its value, as computed by *LaiDyn*, exceeds the threshold, the trajectory is considered unsafe and is rejected from the dataset to be processed.

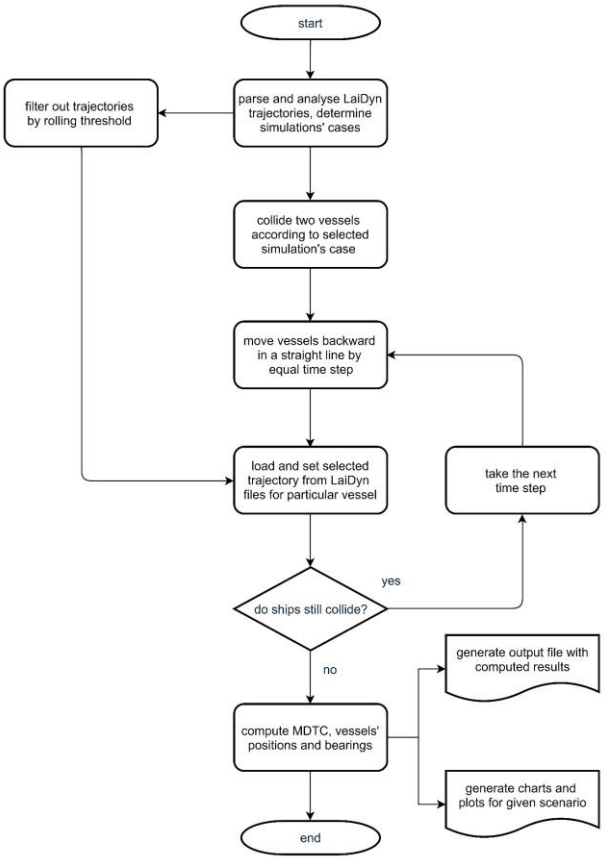

Figure 3: Flowchart of ships encounter simulator.

Simulations' cases and ship's model characteristic

The simulation cases analysed here attempt to cover two aspects. First is the evaluation of the influence of waves in the course of ships' encounter on the MDTC, where a fixed rudder angle is applied. Therein the MDTC values are calculated for the following navigational scenario:

- Own Ship (OS) proceeds to the North (heading = 000°) and executes the manoeuvre by set the rudder to 20° on the starboard side.
- Target Ship (TS) proceeds the course 225° and she keeps her course and speed.

Second, is the influence of the ship's stability (especially vertical centre of gravity resultant roll motion) on the safe rudder angle and resulting manoeuvring area. To determine the MDTC, which corresponds to the last moment for execution of evasive manoeuvre in the function of the vessel's relative bearing, the following scenarios are considered:

- Own Ship (OS) proceeds to the North (heading = 000°) and executes the manoeuvre by set the rudder to a maximum allowable value resulting from rolling threshold separately for port and starboard side for two considered VCGs.
- Target Ship (TS) proceeds on different starting courses from 000° up to 315° for each 45° interval. For each heading vessel keeps her course and speed.

Characteristic of the analysed container vessel's model is presented in Table 1, while waves parameters used in simulation cases are tabulated in 2. Projection of estimated vessels' hulls on the plotting sheet for the scenario of waves' direction impact is depicted in Figure 4.

Table 1: Characteristic of a used ship model.

LOA [m]	Beam [m]	VCG [m]	Draft [m]	Mass [t]	Speed [kts]
262.0	40.0	14.92	12.3	76027.6	20.0
262.0	40.0	17.91	12.3	76027.6	20.0

Table 2: Waves parameters used in the study.

Waves parameters			
Significant height [m]	Period [s]	Angle interval [°]	Number of angles
3.0	7.0	45.0	8
7.1	10.9	45.0	8
13.0	14.7	45.0	8

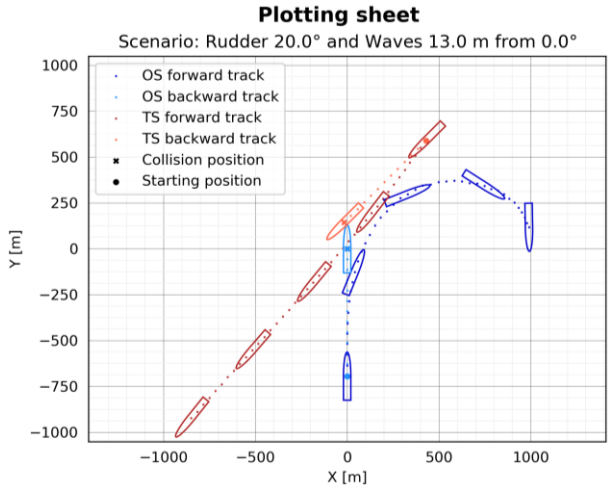

Figure 4: Scatter plot from the simulator for one of the considered navigational scenarios.

Roll angle filtering

Due to various heights and relative directions of waves with respect to ship's hull, her rolling magnitude differs. Thus, depending on the wave's parameters, trajectories that result in roll angle lower than the threshold are allowed, those where the threshold is exceeded are rejected. Depending on the wave parameters, the same manoeuvre where the same rudder angle is applied result in different roll angles in the course of the manoeuvre. The threshold value for roll angle, as a stability indicator for a ship, is arbitrary taken as 20°.

Totally, the 1872 input files from *LaiDyn* describing the ship's trajectories are generated. Because the realisation of waves for given parameters in the software is stochastic, each case is obtained three times. The trajectories where the rolling threshold is exceeded are considered unsafe from the operational perspective thus rejected from the database. The result of filtering is depicted in Figure 5. Therein the total number is shown however, the percentage of rejection differs across values of VCG. For VCG = 17.92 only 3 cases are rejected, whereas for VCG = 14.92 in 174 cases the threshold is exceeded. The rejected cases are observed for one out of three wave heights, which is H_s = 13 m – see Table 2. The number of rejected trajectories depends on the relative direction of the wave to the ship, as depicted in Figure 6.

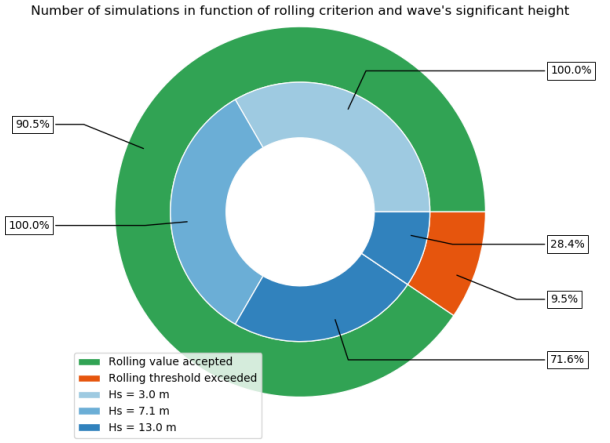

Figure 5: Percentage of rejected simulations according to the exceeding of the rolling threshold for two analysed values of VCG.

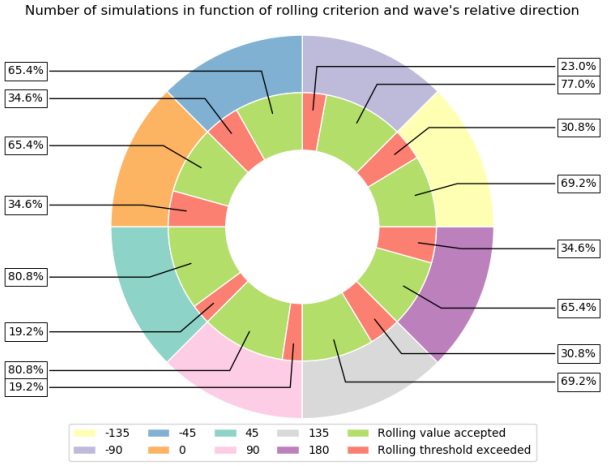

Figure 6: Percentage of rejected simulations according to the roll angle for wave's directions and H_s = 13 m.

4. RESULTS AND DISCUSSION

The effect of ship stability on MDTC at fixed rudder angle

Here we determined the MDTC for a single scenario, taking into account the relative angle of the given wave (H_s = *13 m*) and two VCG values. The realisation of a turn at 20° rudder angle to starboard side is not possible for all wave's direction without an exceedance of the rolling threshold, see Figure 7. Therein the outer scale refers to the relative angle of the wave, the inner scale denotes the MDTC value, and the VCG values are color-coded. The MDTC required for safe evasive manoeuvre (where the roll angle is below the threshold), heavily depends on the relative direction of wave and ship's stability. For a ship with VCG = 17.9 m all relative directions of waves are feasible for collision-evasive action, however in some cases, longer MDTC is required (for the head-on seas), whereas in other cases the

short MDTC suffices (for a wave coming from the relative direction of -45°). However, for the same ship with VCG = 14.9 m, only a tiny sector is feasible, for an evasive manoeuvre where the roll angle is not exceeded, which is the grey area in Figure 7.

Therefore the ship stability and loading conditions are safety critical factors for the collision-avoidance process.

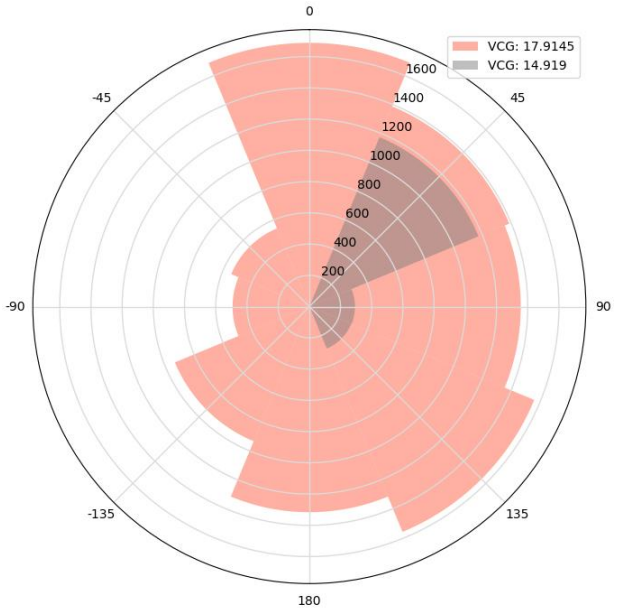

Figure 7: MDTC obtained in the simulations for different wave's directions with H_s = 13 m.

The effect of ship stability on MDTC at safe rudder angle

Subsequently, the MDTC is obtained for the maximum allowable values of rudder angle for two VCGs values. The following parameters are considered: the wave height (13 m) and relative direction (-45 °), eight relative bearing values to the target, eight starting courses of the target.

For each scenario, the admissible rudder angle is determined, as per the rolling criteria. For VCG = 14.92 m, the maximum rudder angle for the port side is determined at 5°, while for starboard side it is 15°. For VCG = 17.915 m, it is possible to make a turn to both sides with full rudder angle of 30° without exceeding the roll threshold. The results are depicted in Figure 9 and 10. Therein two distinct safe manoeuvring areas are shown, that are related to the direction of the ship's turn. The green area denotes a situation where the vessel turns to starboard, whereas the red area means the port side turn. It is evident, that the turn to starboard (green area) should be executed earlier than the turn to port (red area). Obviously, the shape of the areas is governed by the starting relative bearing to the target.

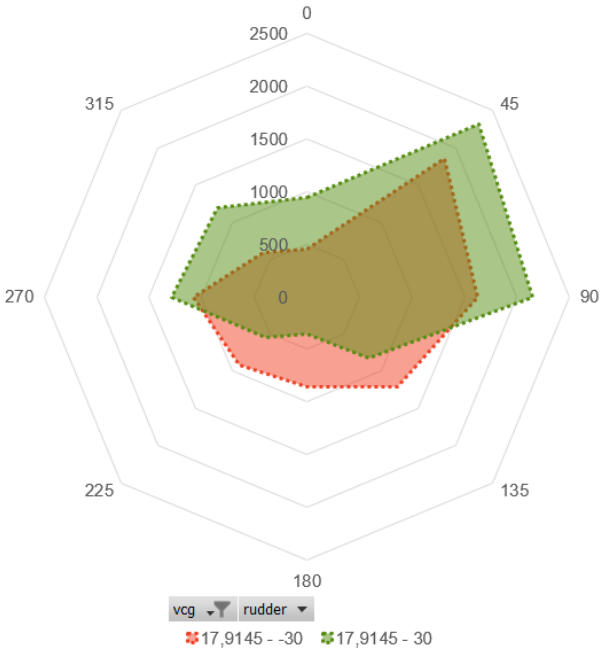

Figure 8: MDTC obtained for different bearings and turning sides for VCG=17.9m. The outer scale refers to the starting relative bearing to the target, while the inner scale denotes the MDTC.

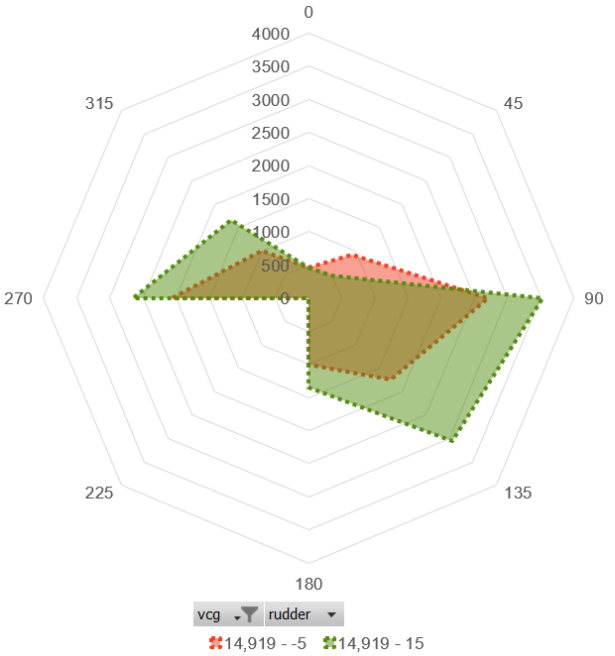

Figure 9: MDTC obtained for different bearings and turning sides for VCG=14.9m. The outer scale refers to the starting relative bearing to the target, while the inner scale denotes the MDTC.

Discussion

As presented, the ship's stability may have a crucial impact on the moment of evasive manoeuvre's execution, especially for the rough seas. The MDTC values differ significantly in the relation of the vessel's loading condition because VCG affects the obtained roll angles. It also varies according to hydro-meteorological conditions, especially the height and direction of the wave's angle of attack on a ship that makes her leeway. The study opens numerous questions to be considered in the course of future works, as follows, see also Table 3.

1. The rolling threshold value for a particular vessel is taken arbitrarily. In the future different approach should be considered. Adjusting the threshold could be obtained e.g. in an empirical way by performing a very large number of simulations. Also introducing the second stability criterion into the simulation software, for instance by computing the accelerations could affect in complementary hybrid-approach to the presented issue. Thus, raised the problem of ship's rolling during anti-collision should be continued and considered in the future works to determine the most realistic approach to stability issues in encounter situation of two vessels.

2. Roll angle values for particular cases exceed the set threshold but not the maximum rudder commands. It affects the rejection of trajectories for the same wave's parameters. For instance, for rudder angle 20° rolling exceeds the threshold, but for 25° or 30°, it does not. This is due to non-linear effects in ship motion during the turning and the time of exposure to the exciting moment plays its role. It means that the largest value of the rolling results mainly from the waves impact, not from the list that is generated during the vessel's turning.

3. The stochastic implementation of waves in *LaiDyn* trajectories should be refactored. Currently, three simulations for each case are generated and included in ships encounter simulator. In the next researches, this number could increase to improve the probability of waves' parameters modelling. It seems to be significant because presented results indicate a big impact of waves in the problem of ships' anti-collision.

Table 3: Issues for future consideration.

Issue to be addressed	Advantages compared to present solutions	Related challenges
Roll threshold adjusting	The threshold can be tuned according to the ship's type and characteristic	Lack of a commonly accepted method for the threshold setting
Accelerations as a complementary criterion for stability incidents	To adjust the acceleration threshold to the cargo lashing system fitted on-board To ensure proper conditions for work on-board	Threshold value not commonly accepted Possible high-frequency oscillations producing high accelerations
Stochastics description of waves' parameters.	To comprise a realistic sea wave thanks to the determination of such number of cases that will include stochastics in waves implementation	Lack of a clearly accepted number of samples Time-consumption during generation of many numbers of the same simulation cases

5. CONCLUSIONS

The aim of this paper is to discuss the minimum requirements for an area around own ship that needs to be kept free from other objects to ensure the safe passage of the ship in an encounter, accounting for the significance of stability-related effects. This has been achieved by developing an encounter simulator and a model based on the set of trajectories obtained from the 6DoF ship motion model. The safe manoeuvring area is demonstrated for a sample container ship.

Preliminary results presented in this paper indicates that the problem of vessels' collision avoidance is much more complex than contemporary considered and it requires a multi-criteria approach. The moment of execution, as well as the type of evasive manoeuvre depends not only on COLREGs (*International Regulations for Preventing Collisions at Sea*), but also on loading condition of the ship, relative position of encountering ships, parameters of the target, and environmental parameters like height or direction of waves.

REFERENCES

[1] D. Patraiko, P. Wake, and A. Weintrit, "e-Navigation and the Human Element," *TransNav, Int. J. Mar. Navig. Saf. od Sea Transp.*, vol. 4, no. 1, pp. 11–16, 2010.

[2] E. M. Goodwin, "A Statistical Study of Ship Domains," *J. Navig.*, vol. 28, no. 03, pp. 328–344, 1975.

[3] Y. Fujii and K. Tanaka, "Traffic Capacity," *J. Navig.*, vol. 24, no. 04, pp. 543–552, Jan. 1971.

[4] E. M. Goodwin, "A Statistical Study of Ship Domains," *J. Navig.*, vol. 26, no. 01, p. 130, 1973.

[5] S.-L. Kao, K.-T. Lee, K.-Y. Chang, and M.-D. Ko, "A Fuzzy Logic Method for Collision Avoidance in Vessel Traffic Service," *J. Navig.*, vol. 60, no. 1, pp. 17–31, 2007.

[6] Z. Pietrzykowski and J. Uriasz, "The Ship Domain – A Criterion of Navigational Safety Assessment in an Open Sea Area," *J. Navig.*, vol. 62, no. 01, pp. 93–108, Dec. 2009.

[7] N. Wang, "An Intelligent Spatial Collision Risk Based on the Quaternion Ship Domain," *J. Navig.*, vol. 63, no. 04, pp. 733–749, Sep. 2010.

[8] A. Lopez-Santander and J. Lawry, "An Ordinal Model of Risk Based on Mariner's Judgement," *J. Navig.*, pp. 1–16, Sep. 2016.

[9] P. V Davis, M. J. Dove, and C. T. Stockel, "A Computer Simulation of Marine Traffic Using Domains and Arenas," *J. Navig.*, vol. 33, no. 02, pp. 215–222, 1980.

[10] B. A. Colley, R. G. Curtis, and C. T. Stockel, "Manoeuvring Times, Domains and Arenas," *J. Navig.*, vol. 36, no. 02, pp. 324–328, 1983.

[11] R. Curtis, "A ship collision model for overtaking," *J. Oper. Res. Soc.*, vol. 37, no. 4, pp. 397–406, 1986.

[12] J. Montewka, F. Goerlandt, and P. Kujala, "Determination of collision criteria and causation factors appropriate to a model for estimating the probability of maritime accidents," *Ocean Eng.*, vol. 40, pp. 50–61, Feb. 2012.

[13] J. Zhang, X. Yan, X. Chen, L. Sang, and D. Zhang, "A novel approach for assistance with anti-collision decision making based on the International Regulations for Preventing Collisions at Sea," *Proc. Inst. Mech. Eng. Part M J. Eng. Marit. Environ.*, vol. 226, no. 3, pp. 250–259, Feb. 2012.

[14] A. Łukaszewicz, "Określanie odległości krytycznej podjęcia manewru ostatniej chwili zgodnie z przepisami konwencji COLREG," in *Międzynarodowa konferencja naukowa Transport XXI wieku*, 2007, pp. 389–396.

[15] R. Szlapczynski and P. Krata, "Determining and visualizing safe motion parameters of a ship navigating in severe weather conditions," *Ocean Eng.*, vol. 158, 2018.

[16] MAIB, "Report on the investigation into the listing, flooding and grounding of Hoegh Osaka Bramble Bank, The Solent, UK on 3 January 2015," Southampton, 2016.

[17] P. Krata and J. Montewka, "Assessment of a critical area for a give-way ship in a collision encounter," *Arch. Transp.*, vol. 34, no. 2, 2015.

[18] J. Montewka and P. Krata, "Towards the assessment of a critical distance between two encountering ships in open waters.," *Eur. J. Navig.*, vol. 12, pp. 7–13, 2014.

[19] J. Montewka, T. Hinz, P. Kujala, and J. Matusiak, "Probability modelling of vessel collisions," *Reliab. Eng. Syst. Saf.*, vol. 95, no. 5, pp. 573–589, May 2010.

[20] J. Montewka, F. Goerlandt, and P. Kujala, "Determination of collision criteria and causation factors appropriate to a model for estimating the probability of maritime accidents," *Ocean Eng.*, vol. 40, pp. 50–61, Feb. 2012.

[21] P. Krata, J. Montewka, and T. Hinz, "Towards the assessment of critical area in a collision encounter accounting for stability conditions of a ship," *Pr. Nauk. Politech. Warsz. Transp.*, no. z. 114, pp. 169--178, 2016.

[22] J. Matusiak, "Towards an unified theoretical model of ship dynamics," in *The Maritime Research Seminar*, 2002.

[23] J. E. Matusiak, "Dynamics of Rigid Body," *Aalto Univ.*, 2017.

[24] J. Journée and W. Massie, "Offshore Hydromechanics," *Electrochim. Acta*, 2002.

[25] J. Matusiak, "On the non-linearities of ships restoring and the froude-krylov wave load part.," *Int. J. Nav. Archit. Ocean Eng.*, vol. 3, no. 1, pp. 111–115, 2011.

[26] J. Matusiak, "On the effects of wave amplitude, damping and initial conditions on the parametric roll resonance," in *8th International Conference on the Stability of Ships and Ocean Vehicles*, 2003.

[27] J. Matusiak and C. Stigler, "Ship Roll Motion in Irregular Waves During a Turning Circle Maneuver," in *11th International Conference on Stability of Ships and Ocean Vehicles*, 2012, pp. 291–298.

[28] ITTC, "The Specialist Committee on Prediction of Extreme Ship Motions and Capsizing Final Report and Recommendations to the 23rd ITTC," in *23rd International Towing Tank Conference*, 2002, vol. II, pp. 619–748.

[29] D. Spanos and A. Papanikolaou, "Benchmark Study on Numerical Simulation Methods for the Prediction of Parametric Roll of Ships in Waves," in *Proceedings of the 10th International Conference on Stability of Ships and Ocean Vehicles (STAB2009)*, 2009.

Permeability of tanks intended for liquids in cruise vessels

Mike Cardinale, *Fincantieri SpA,* mike.cardinale@fincantieri.it
Rodolphe Bertin, *Chantiers de l'Atlantique*, rodolphe.bertin@chantiers-atlantique.com
Henning Luhmann, *Meyer Werft,* henning.luhmann@meyerwerft.de
Anna-Lea Routi, *Meyer Turku,* anna-lea.routi@meyerturku.fi

ABSTRACT

One of the objectives of the eSAFE project was to formulate a proposal for permeability to be used for tanks intended for liquids in cruise vessels. This paper provides a summary overview of the main outcomes, in this respect, based on data collected from real loading conditions of cruise vessels. On the basis of collected data, a simplified formulation is derived for the permeability of tanks intended for liquids, depending on the ship draught. The impact of permeability on the Attained Subdivision Index-A is assessed according to the probabilistic damage stability approach prescribed in SOLAS Ch.II-1, Part B.

Keywords: *eSAFE, tanks, permeability, loading conditions, damage stability, SOLAS.*

1. INTRODUCTION

The permeability prescribed by SOLAS Ch.II-1 reg.7-3.1 for tanks intended for liquids is 0 or 0.95 whichever results in the more severe requirement (IMO, 2019).

On the other hand, for cargo compartments (dry cargo spaces, container spaces, Ro-ro spaces, cargo liquids) SOLAS Ch.II-1 reg.7-3.2 defines a different permeability for each draught, as shown in Table 1 (IMO, 2019).

Table 1: Permeability for cargo compartments as defined in SOLAS Ch.II-1 reg.7-3.2.

Spaces	Permeability at draught d_s	Permeability at draught d_p	Permeability at draught d_l
Dry cargo spaces	0.70	0.80	0.95
Container spaces	0.70	0.80	0.95
Ro-ro spaces	0.90	0.90	0.95
Cargo liquids	0.70	0.80	0.95

Comparing the approach used for compartments containing cargo liquids and the approach for tanks intended for liquids, it is evident that there is a great discrepancy. In particular, for passenger ships and, thus, cruise ships, there are no cargo liquid compartments. Therefore, all tanks are considered as "tanks intended for liquids" and the permeability is assumed equal to 0.95 that results in the more severe requirement.

The data of real loading conditions of cruise ships taken from a wide range of vessels (see Figure 1) demonstrate that abt. 83% of the deadweight of a cruise ship is intended for liquids in tanks.

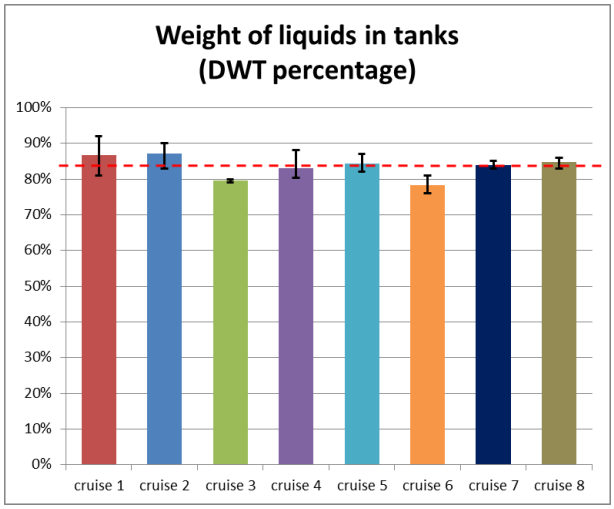

Figure 1: Percentage of deadweight intended for liquids within tanks for cruise vessels of different dimensions (from about 10,000 GRT to more than 200,000 GRT). Intervals reported in the graph for each vessel provide the variation range for different loading conditions according to collected data.

Based on this data, two important facts become apparent:

1) cruise ships never navigate with empty tanks
2) the draught of a cruise ship is strictly related to amount of liquids in tanks

It, therefore, appears that the real permeability of tanks needs a careful investigation.

2. ON BOARD DATA COLLECTION

The first part of the work has been a wide collection of onboard data from 14 cruise ships operating worldwide, with a wide range of dimensions (from about 30,000 GRT to more than 200,000 GRT). This unique collection of data of 317 real loading conditions has been used to obtain a better view of the tanks filling in different operational conditions. For each loading condition, the draughts (aft and fore), the amount of liquids on board for the main tanks purposes and maximum tanks capacity have been provided by the different cruise operators. In particular, the amount of the following liquids has been recorded on board:

- Fuel Oil
- Marine Gas Oil/ Diesel Oil
- Potable Water
- Ballast Water
- Waste Water

Even if the data has not been collected for all tank purposes, the selected categories of liquids cover abt. 90% of the total tank capacity of a cruise ship.

Following this, for each loading condition, the normalized draught (*dn*) and the actual global tank permeability (*tperm*) have been calculated.

The normalised draught (*dn*) was introduced in order to allow for a comparison among different ships. For each ship, *dn* was defined as follows:

$$dn = \frac{T_m - T_l}{T_s - T_l} \tag{1}$$

where

- T_s : maximum draught [m] (corresponding to deepest subdivision draught for ships built under SOLAS 2009);
- T_l : minimum draught [m] (corresponding to light service draught for ships built under SOLAS 2009);
- T_m : draught at mid-ship perpendicular [m].

The tanks permeability for each recorded loading condition was calculated by assuming that the liquid loaded within the damaged tanks is totally replaced by sea water. Therefore the actual global tanks permeability is obtained from the following equation:

$$\sum_{i=1}^{n}(\rho \cdot c_i - m_i) = \rho \cdot tperm \cdot \sum_{i=1}^{n} c_i \tag{2}$$

where

- i : index for the i-th tank;
- ρ : sea water density (1.025 t/m^3);
- c_i : capacity of the i-th tank [m^3];
- m_i : mass of liquid within the i-th tank [t];
- *tperm* : actual global tanks permeability.

It follows that:

$$tperm = 1 - \frac{\sum_{i=1}^{n} m_i}{\rho \cdot \sum_{i=1}^{n} c_i} \tag{3}$$

Two example results are shown in Figure 2 and Figure 3, where the global tank permeability versus the normalized draught are shown for each recorded loading conditions of ship n.2 and ship n.5, respectively. From the results in the figures it can be concluded that there is a very good correlation between tank permeability and normalized draught in both cases. A similar result was found for all the other ships (Cardinale et al., 2017).

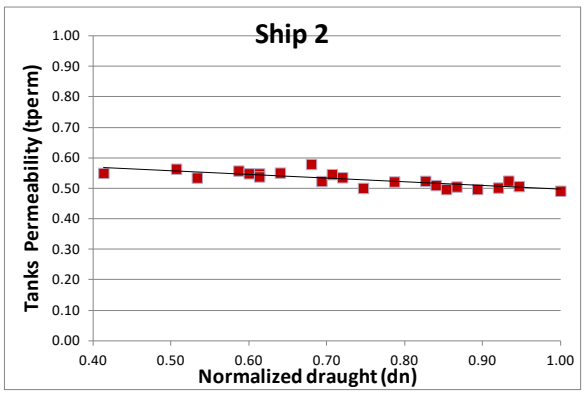

Figure 2: Actual global tanks permeability vs Normalized Draught (cruise ship n.2).

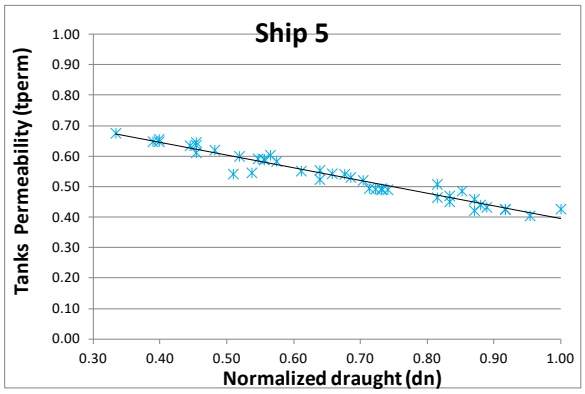

Figure 3: Actual global tanks permeability vs Normalized Draught (cruise ship n.5).

Furthermore, if we look at Figure 4, where all ships are collected in the same graph, we can realise that the SOLAS permeability for tanks is not realistic and very conservative.

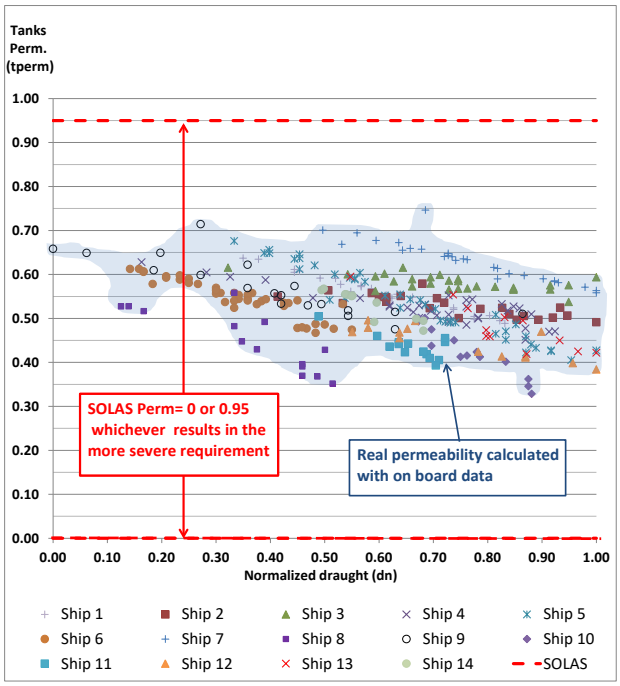

Figure 4: Actual global tanks permeability vs Normalized Draught (all ships).

3. NEW PROPOSAL FOR TANKS PERMEABILITY

A different tank permeability could be defined for each ship based on its real operating loading conditions, but these conditions are not known at the design stage. Therefore, a formula based on data available at an early design stage is needed.

Considering the approach used in SOLAS Ch.II-1 reg.7-3.2 for dry cargo spaces, container spaces, ro-ro spaces and cargo liquids (see Table 1), a similar approach can be used for permeability of tanks intended for liquids on cruise ships, instead of the presently used worst case between 0 or 0.95. Indeed, the calculations of real permeability with results shown in Figure 2, Figure 3 and Figure 4 are sufficient to justify such a different approach. Moreover, "other figures for permeability may be used if substantiated by calculations" as stated in SOLAS Ch.II-1 reg.7-3.3, with more clarifications provided in the relevant Explanatory Notes (IMO, 2017).

A simple proposal is shown in Figure 5, where a linear regression is used to define the permeability of tanks as a function of the normalised draught.

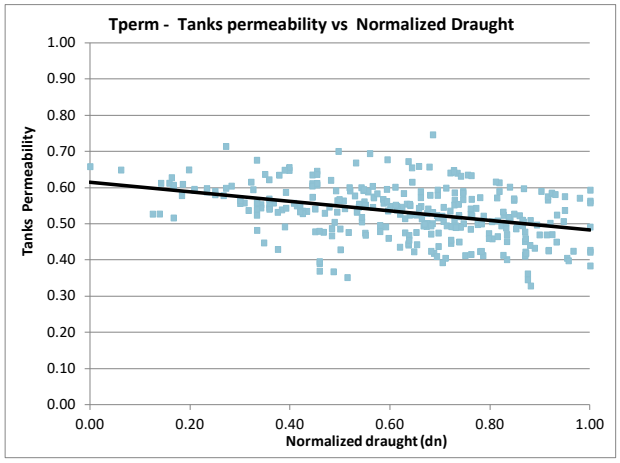

Figure 5: Proposal of regression for tanks permeability.

The proposed formulation takes the following analytical form (Cardinale et al., 2017; Luhmann et al., 2018a,b):

$$Tperm = 0.61 - 0.13\frac{T - T_{min}}{T_{max} - T_{min}} \qquad (4)$$

where:

- $Tperm$: tanks permeability;
- T : mean draught of the initial condition to be calculated [m];
- T_{min} : minimum draught according to stability booklet [m] (corresponding to light service draught for ships built under SOLAS);
- T_{max} : maximum draught according to stability booklet [m] (corresponding to

deepest subdivision draught for ships built under SOLAS).

The notation *Tperm* is used in (4) to differentiate between the permeability directly determined from the on-board data (*tperm*, see (2)) and the permeability from the regression.

This proposal will result in the following values of the tanks permeability (*Tperm*) at the three calculation draughts for attained index calculation defined in SOLAS:

- 0.61 at light service draught (dl);
- 0.53 at partial subdivision draught (dp);
- 0.48 at deepest subdivision draught (ds).

4. IMPACT ON THE ATTAINED INDEX

In order to evaluate the impact of tanks permeability on the assessment of cruise ships safety through the attained subdivision index, six initial conditions have been selected for each sample ship of the eSAFE project. Some of these conditions correspond to real operational loading conditions, while additional loading conditions are taken from the stability booklet. This approach has been used both to evaluate the impact in cases where real filling levels for tanks are used and also to cover a wide range of draughts.

The results of these calculations are dependent on the GM of each loading condition. Therefore, considering the scope of the test, three loading cases have been calculated with the actual GM and three with the minimum GM required by SOLAS 2009.

The loading conditions used for each ship are as follows:

- Ship A: two loading conditions from the stability booklet and three real loading conditions;
- Ship B: three real loading conditions;
- Ship C: three real loading conditions;
- Ship D: three loading conditions from the stability booklet.

All the calculations executed on the four cruise ships (Cardinale et al., 2017; Luhmann et al., 2018a) clearly show that there is a significant gap between A index calculated with the real filling level for tanks and A index calculated with empty tanks (perm=0.95 according to SOLAS), especially when calculations are executed, for design purpose, with the GM of limit curve according to SOLAS 2009 (see Figure 6). As expected, this gap generally increases at partial and heaviest draught, as in these cases the global filling level of the tanks is higher compared to lightest loading condition.

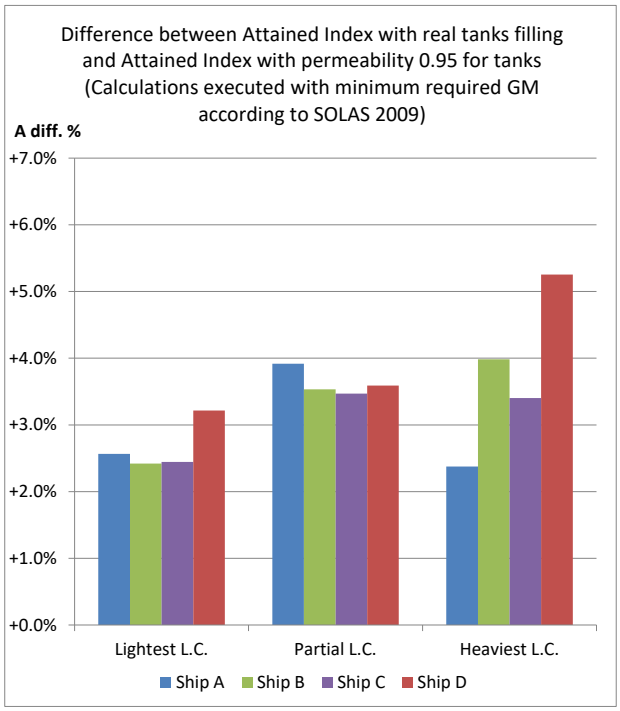

Figure 6: Difference between A index with real filling for tanks vs empty tanks.

Based on these results it is evident that the SOLAS permeability is not realistic for cruise ships and the proposed formula for *Tperm* (equation (4)) has been tested in order to verify its capability to compensate the gap shown in Figure 6.

5. VALIDATION OF THE PROPOSED TANKS PERMEABILITY

The validation of the formula for tanks permeability proposed in section 3 has been performed with two different sets of calculations for each ship. In particular, two different options for permeability of heeling tanks have been calculated:

- Attained Index calculated with permeability 0.95 for heeling tanks and permeability according to *Tperm* (see (4)) for other tanks;
- Attained Index calculated with permeability 0.50 for heeling tanks and permeability according to *Tperm* (see (4)) for other tanks.

Even if the second option (permeability 0.50 for heeling tanks) is much more realistic for cruise ships, also calculations according to the first option have been carried out to evaluate the impact of heeling tanks permeability on the Attained Index.

The calculations executed on the sample ship demonstrated that the *Tperm* formula (4) for tanks permeability is capable to reduce the difference between attained index calculated with real tanks filling and attained index calculated according to SOLAS permeability for tanks (see Figure 7). Furthermore, the results showed that it is necessary to use a permeability of 0.5 for heeling tanks in order to minimize the aforementioned difference, as shown in Figure 8, in particular when calculations are executed with GM of the limit curve.

To cover any different filling of the heeling water tanks during operation, it is necessary to calculate the damages on both sides, port and starboard sides.

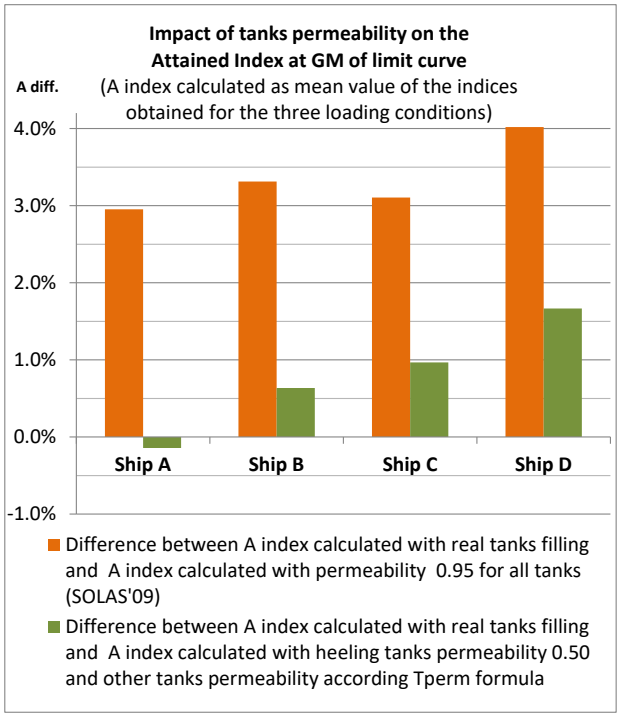

Figure 7: Impact of tanks permeability on A index at GM of limit curve.

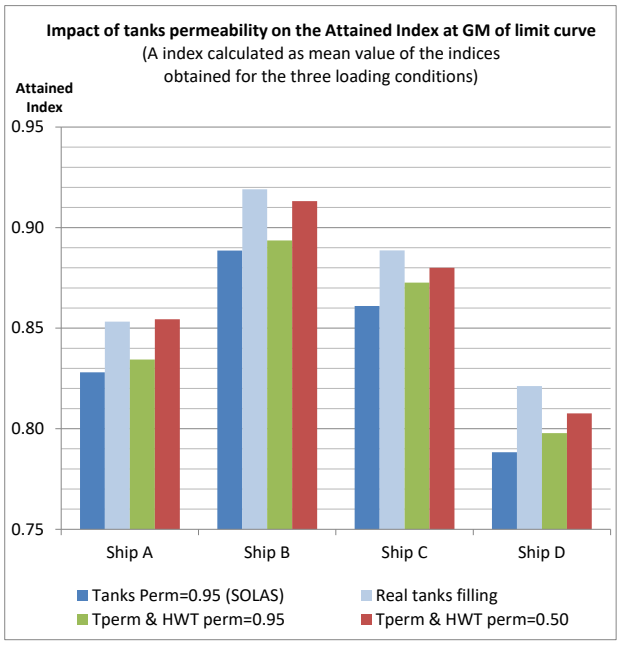

Figure 8: Impact of tanks permeability on A index at GM of limit curve.

6. CONCLUSIONS

The data collected on board (14 cruise ships and 317 loading cases) demonstrate that the SOLAS permeability for tanks is not realistic for cruise ships and it represents a very conservative approach in A-Index calculation.

Furthermore, the results showed that there is a good correlation between tanks permeability and normalised draught; based on this correlation, a simple formula for permeability (*Tperm*), based on linear regression, has been proposed to be applied for all tanks (excluding heeling tanks) of cruise ships.

To evaluate the impact of tanks permeability, the attained index has been calculated for some loading cases of a set of sample ships, using real tanks permeability. The results showed that the difference between A index calculated with the real tanks filling and A index calculated with empty tanks (perm=0.95 according to SOLAS), is significant (from 2.4% to 5.3%), when calculations are executed using GM from the limit curve.

A second round of calculations carried out by using the proposed formula for permeability, showed that the difference between A index calculated with the real tanks filling and A index calculated with empty tanks can be significantly reduced by using a permeability of 0.5 for heeling tanks combined with the value *Tperm* from the proposed formula for the other tanks.

ACKNOWLEDGEMENTS

This work was carried out in the framework of the project "eSAFE – enhanced Stability After a Flooding Event – A joint industry project on Damage Stability for Cruise Ships". The funding partners of eSAFE are: Carnival Corporation Plc, DNV GL, Fincantieri, Lloyd's Register, Meyer Werft, RINA Services, Royal Caribbean Cruises Ltd. and STX France. The financial support from the eSAFE funding partners is acknowledged.

DISCLAIMER

The information and views as reported in this paper are those from the authors and do not necessarily reflect the views of the eSAFE Consortium.

The views as reported in this paper are those of the authors and do not necessarily reflect the views of the respective organizations.

REFERENCES

Cardinale, M., Routi, A., Luhmann, H., Bertin, R., 2017, "eSAFE-D1.2.5 - Proposal for permeability to be used for tanks intended for liquids in cruise vessels", Joint Industry Project "eSAFE - enhanced Stability After a Flooding Event – A joint industry project on Damage Stability for Cruise Ships", 30 May (Rev.0).

IMO, 2017, "Resolution MSC.429(98) – Revised Explanatory Notes to the SOLAS Chapter II-1 Subdivision and Damage Stability Regulations", 9 June.

IMO, 2019, "International Convention for the Safety of Life at Sea (SOLAS)", Consolidated edition.

Luhmann, H., Olufsen, O., Atzampos, G., Bulian, G., 2018a, "eSAFE-D4.3.1 – Summary report", Joint Industry Project "eSAFE - enhanced Stability After a Flooding Event – A joint industry project on Damage Stability for Cruise Ships", 24 October (Rev.4).

Luhmann, H., Bulian, G., Vassalos, D., Olufsen, O., Seglem, I., Pöttgen, J., 2018b, "eSAFE-D4.3.2 – Executive summary", Joint Industry Project "eSAFE - enhanced Stability After a Flooding Event – A joint industry project on Damage Stability for Cruise Ships", 24 October (Rev.3) – available from: https://cssf.cruising.org/projects .

Considering collision, bottom grounding and side grounding/contact in a common non-zonal framework

Gabriele Bulian, *University of Trieste,* gbulian@units.it
Mike Cardinale, *Fincantieri SpA,* mike.cardinale@fincantieri.it
George Dafermos, *National Technical University of Athens*, dafermos@deslab.ntua.gr
Eleftheria Eliopoulou, *National Technical University of Athens,* eli@deslab.ntua.gr
Alberto Francescutto, *University of Trieste,* francesc@units.it
Rainer Hamann, *DNV GL*, rainer.hamann@dnvgl.com
Daniel Lindroth, *NAPA,* daniel.lindroth@napa.fi
Henning Luhmann, *Meyer Werft GmbH & Co. KG*, henning.luhmann@meyerwerft.de
Pekka Ruponen, *NAPA,* pekka.ruponen@napa.fi
George Zaraphonitis, *National Technical University of Athens,* zar@deslab.ntua.gr

ABSTRACT

One of the objectives of the eSAFE project was to develop a holistic probabilistic methodology, as well as an associated NAPA software functionality, for assessing post-damage ship survivability combining, through a sound and consistent generalised approach, collision, bottom grounding and side grounding/contact damages. This paper provides a summary overview of some main outcomes in this respect, namely: the development of a non-zonal approach for collision starting from, and extending, the SOLAS framework; the development and critical analysis of alternative approaches for considering the different attained indices from collision, bottom grounding and side grounding/contact damages; the practical implementation and testing of the framework.

Keywords: *eSAFE, damage stability, non-zonal approach, collision, grounding, contact, SOLAS.*

1. INTRODUCTION

The key objective of the eSAFE activity overviewed in this paper was to develop a holistic probabilistic methodology, as well as an associated NAPA software functionality, for assessing post-damage ship survivability combining, through a sound and consistent generalised approach, collision, bottom grounding and side grounding/contact damages.

During the EMSA 3 study, a probabilistic method was developed, implemented in a software tool and tested on real designs, for addressing survivability following bottom grounding and side grounding/contact in case of passenger vessels (Zaraphonitis et al., 2015; Bulian et al., 2016). The method was based on a non-zonal approach where: a) breaches are directly generated on the basis of the underlying geometrical and probabilistic model for the damage extent; b) "damage cases" are automatically created from the identification of breached compartments; c) associated probabilities of flooding are estimated by collecting the probability contribution from breaches leading to the same "damage case". Survivability for each damage case can then be determined through the usual s-factor, and attained indices are eventually obtained for each calculation draught and corresponding loading condition.

The non-zonal method developed in EMSA 3 has been extended in eSAFE in order to address also collision damages, keeping consistency with present SOLAS (IMO, 2019a). In this context, it was necessary to develop a probabilistic model for the lower edge of the damage, which is missing in the present SOLAS framework (Bulian et al., 2017, 2018). This development, combined with a clear geometrical description of the geometry of the breach, allowed to develop a non-zonal approach for

collision, which could be used alongside those for grounding/contact.

Then, approaches were explored for defining safety metrics in order to combine survivability in case of collision, bottom grounding, and side grounding/contact (Zaraphonitis et al., 2017). To this end, reference has been made to statistical analysis of accidents data and to existing risk-models (Konovessis et al., 2015; Zaraphonitis et al., 2015).

Based on the findings, a new functionality for practical implementation of the non-zonal approach has been made available in NAPA (Lindroth et al., 2017), and the tool has been tested within eSAFE to gain experience and provide feedback.

A procedure for calculation and reporting of results was also envisaged which takes into account the presence of random sampling uncertainty in the application of the non-zonal approach (Zaraphonitis et al., 2017).

This paper provides a summary overview of some main outcomes of the mentioned activity, which is summarised also by (Luhmann et al., 2018a,b). In the following, section 2 provides a summary regarding the development of the non-zonal approach for collision. Afterwards, section 3 summarises the different approaches which have been considered in order to try addressing collision, bottom grounding, and side grounding/contacts in a common framework. Section 4 then provides an overview of the software implementation. Section 5 shows some examples from the testing and application. Finally, section 6 reports some summarising conclusions.

2. NON-ZONAL APPROACH FOR COLLISION

Present damage stability framework in SOLAS Ch.II-1 (IMO, 2019a) allows determining the probabilities of flooding of a compartment (or group of compartments) by using p-, r- and v-factors (SOLAS/II-1/B-1/7-1, SOLAS/II-1/B-1/7-2). In particular, p-factor accounts for transversal subdivision defining so-called “zones”, and this is why the SOLAS approach can be shortly referred to as “zonal”. The analytical formulae for such factors embed the probability distributions of collision damage characteristics (position, length, penetration and vertical extent above waterline) assumed by SOLAS.

It is very well-known that the basic ideas leading to present SOLAS originated from the HARDER project, and are documented in details in HARDER-related documentation (see Lützen (2001, 2002)). Nevertheless, following the HARDER project, some modifications regarding damage distributions have been introduced during the discussion at IMO, leading to the final formulation, as embedded in present SOLAS regulation.

SOLAS, however, does not provide a distribution for the lower limit of vertical extent of damage. Instead, SOLAS uses a “worst-case approach” (often referred to as “damages of lesser extent”), where a systematic variation of the lower limit of damage is carried out in the calculations to find the damage case giving the least s-factor when there are horizontal subdivision boundaries below the waterline (SOLAS/II-1/B-1/7-2/6.2). This approach, by its very nature, is conservative, as it leads to a systematic conservative estimation of the attained subdivision indices (Zaraphonitis et al., 2017; Bulian et al., 2018).

In the EMSA 3 project a different methodology was proposed for addressing bottom grounding and side grounding/contact (Zaraphonitis et al., 2015; Bulian et al., 2016), which was referred to as “non-zonal”. In the “non-zonal” approach, single breaches are generated using a Monte Carlo procedure based on the distributions of damage characteristics. Each individual breach will lead to the flooding of a certain (set of) room(s), which represents what is usually called a “damage case”. Summing up the probabilities associated to all breaches leading to the same damage case, it is possible to estimate the probability of occurrence of each damage case. This can then be directly used in the calculation of A-indices. The logical flow of the non-zonal approach is outlined in Figure 1.

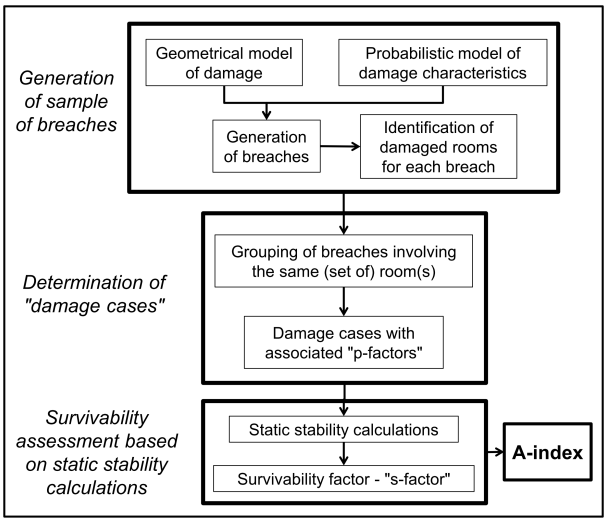

Figure 1: Logic of non-zonal approach.

A schematic graphical representation of the principle of the non-zonal approach is shown in Figure 2. The figure shows different breaches, and different colours identify the (set of) breach(es) leading to the same damage case.

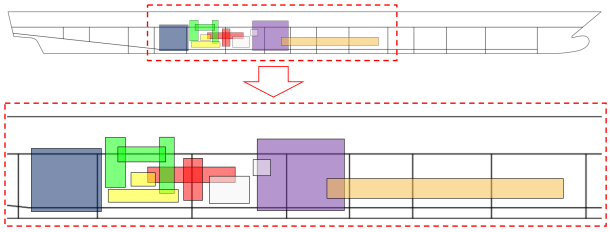

Figure 2: Schematic graphical representation of the principle of non-zonal approach. Top: full longitudinal view. Bottom: zoom of the region where example breaches are shown.

During eSAFE, the EMSA 3 non-zonal approach was extended to cover also collision damages, keeping, as main target, the highest possible consistency with existing SOLAS framework.

To this end, the following main aspects were addressed (Bulian et al., 2017):

- Explicit definition of the geometrical model for collision damages;
- Generation of collision damages using the distributions for damage characteristics according to SOLAS background;
- Development of a probabilistic model for the lower limit of vertical extent of damage, not available from SOLAS.

The geometrical model for collision damage (conventionally referred to as damage of type "C00" in eSAFE) was defined according to the following characteristics:

- The damage penetration is measured orthogonally to the ship's centre plane;
- The longitudinal extent of damage (damage length) is measured parallel to the ship's longitudinal axis;
- The vertical damage extent is measured along the vertical direction;
- The horizontal section (profile) of the damage follows the waterline at the actual calculation draught. As a result, the damage, in general, is not box shaped.

In addition, for consistency with SOLAS (IMO, 20018, 2017), collision damages have been defined to be always crossing the calculation waterline. This means that the upper limit of damage is always above the waterline, and the lower limit of damage is always below the waterline, for each calculation draught.

The distributions of all relevant damage characteristics were taken from the analysis of the SOLAS background, with the exception of the lower limit of damage. In particular (Bulian et al., 2017):

- Damage side: 50% probability on each side, unless the damage side is specified in the calculations.
- Longitudinal position of centre of the extent of damage within the limits of the ship length, X_C: uniformly distributed along the ship length.
- Longitudinal extent of damage (potential damage length), $L_{x,p}$: bilinear probability density function, with characterising coefficients b_{11}, b_{12}, b_{21} and b_{22} (see Lützen (2001, 2002)) from SOLAS/II-1/B-1/7-1/1.1.
- Transversal extent of damage (potential damage penetration), $L_{y,p}$: truncated trapezoidal distribution depending on potential damage length. The cumulative distribution function, before truncation, corresponds to the function $C\left(\bar{z}\right)$ reported by Lützen (2001, 2002).

- Vertical position of upper limit of damage above the waterline, $z_{UL,p} - d$: the cumulative distribution function corresponds to the SOLAS v-factor.

The damage is defined as a potential damage, this meaning that it can also partially extends outside of the vessel.

For consistency reasons, the "ship length" to be considered in the calculations has been taken as the subdivision length of the ship according to SOLAS.

Two points required particular attention in order to derive a methodology consistent with existing SOLAS.

The first point concerned the proper positioning of the damage, given X_C and $L_{x,p}$, in order to be consistent with the analytical and theoretical formulation of zonal SOLAS p-factors for compartments at the extremities of the ship length (Lützen, 2001, 2002; Pawłowski, 2004). When the damage is fully contained within the ship length, the longitudinal coordinate X_C corresponds to the centre of damage. However, if the potential damage partially extends outside the vessel, this is no longer the case, and the longitudinal coordinate of the midpoint of the potential damage differs from X_C (Bulian and Francescutto, 2010; IMO, 2012). The procedure for the longitudinal positioning of the damage is graphically reported in Figure 3.

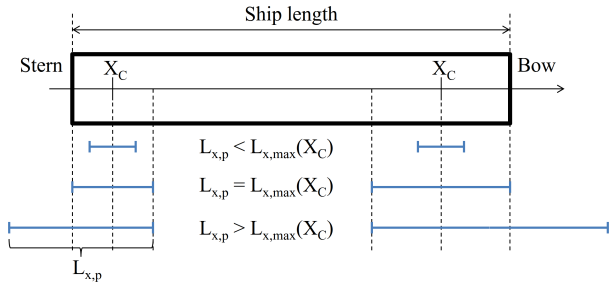

Figure 3: Graphical representation of longitudinal positioning of collision damage.

The second point of attention concerned the proper generation of the potential damage penetration $L_{y,p}$, in order to be consistent with the zonal SOLAS r-factor. The absolute maximum damage penetration according to SOLAS is B/2, where B is the ship breadth, and this limit is directly embedded in the function $C(\bar{z})$ reported by Lützen (2001, 2002), and already mentioned before. However, in addition, the SOLAS framework also implicitly assumes that the ratio between the dimensionless damage penetration and the dimensionless damage length cannot exceed 15 (Lützen, 2001, 2002; Pawłowski, 2004; Bulian and Francescutto, 2010; IMO, 2012). Different equivalent approaches can be used to generate the penetration of damages consistently with the truncation embedded in SOLAS. The following algorithm is an example:

1) Firstly, the potential damage length $L_{x,p}$ is generated.
2) The corresponding maximum potential damage penetration $L_{y,p,\max}$ is then determined as $L_{y,p,\max} = (15 \cdot B / L_S) \cdot L_{x,p}$, where B is the ship breadth and L_S is the ship length.
3) Then, a "raw" potential damage penetration $L_{y,p,raw}$ is generated according to the non-truncated trapezoidal distribution associated with $C(\bar{z})$.
4) Finally, if $L_{y,p,raw} < L_{y,p,\max}$ the potential damage penetration $L_{y,p}$ is taken as $L_{y,p} = L_{y,p,raw}$, otherwise $L_{y,p}$ is taken as $L_{y,p} = L_{y,p,\max}$.

As SOLAS does not provide a probabilistic model for the extent of damage below the waterline, it was necessary to specifically develop one to be embedded in the non-zonal approach. The development of a probabilistic model for the lower limit of vertical extent of damage was based on the analysis of historical accident data. To this end, use has been made of data from the HARDER accidents database as updated in the GOALDS project (Mains, 2010; Bulian and Francescutto, 2010; IMO, 2012). As the underlying distributions of collision damage characteristics in SOLAS is common to passenger and cargo vessels, historical accidents data from both passenger and cargo ships were considered in the analysis. Data from the database were filtered in three stages. Firstly, data were filtered consistently with the HARDER approach, as done in GOALDS (Bulian and Francescutto, 2010; IMO, 2012), by extracting damages due to ship-ship collisions where

the damaged vessel is the struck one. After this, a subsequent filtering was applied, in order to remove some few cases which appeared as having inconsistent data. Then, for consistency with SOLAS (IMO, 2008), the final set of data was extracted by retaining only those cases with sufficient information to unambiguously identify damages crossing the waterline. The final filtered dataset which was eventually used for the analysis comprised a total of 152 samples. More information on the filtering have been reported by Bulian et al. (2017, 2018).

Two probabilistic models for the lower limit of damage below waterline with different levels of complexity were developed, discussed, implemented in the non-zonal approach, and compared (Bulian et al., 2017; Lindroth et al., 2017). One of the two models was eventually selected for describing the vertical position of lower limit of potential damage from the ship bottom, $z_{LL,p}$. The model considers $z_{LL,p}$ to be statistically independent of the other damage characteristics, and to have the following cumulative distribution (Bulian et al., 2017, 2018):

$$\begin{cases} CDF\left(z_{LL,p}\right) = 1.4 \cdot \dfrac{z_{LL,p}}{d} - 0.4 \cdot \left(\dfrac{z_{LL,p}}{d}\right)^2 \\ z_{LL,p} \in \left[0, d\right] \end{cases} \qquad (1)$$

where d is the actual calculation draught. This model can then be used for describing, and hence generating $z_{LL,p}$ in the non-zonal approach.

It is noted that this probabilistic model also allows to easily define a “u-factor” which can be directly embedded in the existing SOLAS zonal framework (see Bulian et al. (2017, 2018) for details).

The developed non-zonal approach was implemented in a NAPA software functionality, and it was successfully verified through comparisons with SOLAS zonal calculations (Bulian et al., 2017; Lindroth et al., 2017; and see section 5).

3. SAFETY METRICS FOR THE COMBINED IMPACT OF COLLISION, BOTTOM GROUNDING AND SIDE GROUNDING/CONTACT

For each type of accident (collision, bottom grounding, side grounding/contact), a corresponding attained subdivision index (A-index) can be obtained from damage stability calculations, namely:

- For collision: A_{CL};
- For bottom grounding: A_{GR-B};
- For side grounding/contact: A_{GR-S}.

The three mentioned A-indices represent ship survivability, separately, in case of specific types of accidents. However, a measure is needed in order to provide a combined quantification of the ship safety. To this end, two different methods to derive a measure of ship survivability, covering all three accident types, have been considered:

- A risk-based safety metric, directly related to societal risk;
- A probability-/survivability-based safety metric, based on the relative frequencies of different types of accident.

The metrics defined by the two approaches share the characteristic that they can be determined as weighted combinations of individual A-indices corresponding to different types of accidents.

Risk-based safety metric - SM

The fundamental ideas and assumptions behind the developed risk-based safety metric have been anticipated in the EMSA 3 project (Konovessis et al., 2015; Vassalos et al., 2015; Zaraphonitis et al., 2015), and are as follows:

- With reference to consequences from flooding accidents, the total societal risk which is accounted for is given by the sum of the risk due to collision, the risk due to bottom grounding, and the risk due to side grounding/contact;
- The risk is measured through the "Potential Loss of Life (*PLL*)", i.e. the expected number of fatalities per ship-year (which, if needed, can be transformed to ship-life);
- The reference risk models which have been used are those developed in the EMSA 3

study and which are relevant for cruise ships.

Starting from the risk models developed in the EMSA 3 study (Konovessis et al., 2015; Zaraphonitis et al., 2015), the potential loss of life (*PLL*) associated with each type of accident can be determined as follows:

$$\begin{cases} PLL_{CL} = POB \cdot c_{CL} \cdot (1 - A_{CL}) \\ PLL_{GR-B} = POB \cdot c_{GR-B} \cdot (1 - A_{GR-B}) \\ PLL_{GR-S} = POB \cdot c_{GR-S} \cdot (1 - A_{GR-S}) \end{cases} \quad (2)$$

where *POB* is the number of persons on board (crew and passengers, considering assumptions with respect to occupancy). The coefficients c_{CL}, c_{GR-B} and c_{GR-S} depend on, and can be directly calculated from, the assumed reference risk models.

More specifically, each coefficient c_{CL}, c_{GR-B} and c_{GR-S}, can be readily determined according to the following procedure. At first, the relevant risk model is selected for each type of accident (collision, bottom grounding, side grounding/contact). Then, by following the various branches of the event tree, *PLL* is expressed explicitly as a function of products of initial frequency, conditional probabilities, assumed percentages of fatalities, $1 - A$, and *POB*. In fact, *A* and *POB* are the ship-specific parameters to be provided for the determination of *PLL* in each of the background risk models. Finally, each coefficient c_{CL}, c_{GR-B} and c_{GR-S}, as appropriate, is determined as the proportionality factor between *PLL* and $POB \cdot (1 - A)$ for each type of accident, as stemming from the described procedure.

The total *PLL* can then be determined by summing up the contribution to risk from the three accidents, as follows:

$$\begin{cases} PLL_{TOT} = PLL_{CL} + PLL_{GR-B} + PLL_{GR-S} \\ \qquad = POB \cdot c_T \cdot (1 - SM) \\ \text{with } c_T = c_{CL} + c_{GR-B} + c_{GR-S} \end{cases} \quad (3)$$

The safety metric *SM* can then be obtained, with a weighting of the attained indices based on the relative contribution to risk from different types of accidents and calculated using the risk models from the EMSA 3 study:

$$\begin{aligned} SM = \; & 0.11 \cdot A_{CL} + \\ & + 0.17 \cdot A_{GR-B} + \\ & + 0.72 \cdot A_{GR-S} \end{aligned} \quad (4)$$

With reference to the obtained weighting coefficients in (4), and considering risk investigations performed in GOALDS and EMSA 3, the topic of quantification of uncertainty was discussed, but not fully explored during eSAFE. This is due to complexity of the matter combined with the limited time frame. In fact, risk models embed different sources of uncertainty. Part of the uncertainty comes from the limited size of the sample of available data, which can be efficiently estimated. However, additional uncertainty, which is more difficult to quantify, stems from the subjective expert judgement used in quantification of the underlying risk models. As a result, this topic has been left as an important topic to be addressed in future research activities.

Combined Attained Subdivision Index - A

An alternative way for the derivation of a safety metric considering all three types of accidents is through the definition of a Combined Attained Subdivision Index, using appropriate weighting factors for the three individual A-indices, based on the relative frequencies (conditional probabilities) of the corresponding accidents, as follows:

$$\begin{aligned} A = \; & Pr_{CL} \cdot A_{CL} + \\ & + Pr_{GR-B} \cdot A_{GR-B} + \\ & + Pr_{GR-S} \cdot A_{GR-S} \end{aligned} \quad (5)$$

The combined A-index, therefore, represents a measure of the probability of survival conditional to the occurrence of a flooding accident, hence not considering differences in the consequences for the different accident categories. The relative frequencies (conditional probabilities) Pr_{CL}, Pr_{GR-B} and Pr_{GR-S} were determined from the analysis of historical data. The accidents database which was used for the accidents data analysis is the same as the one developed and used within the EMSA 3 project (Konovessis et al., 2015). The sampling plan and

filtering of data was chosen in order to be relevant for the scope of the project.

It is noted that the size of available accidents sample, after the filtering, was rather limited, corresponding to 16 accidents in total. Although this is a good outcome from a safety perspective, it leads to a large uncertainty in the estimated relative fractions of different types of accidents, i.e. in the weighting coefficients of different A-indices. This is evident from the results in Table 1, where Pr_{CL}, Pr_{GR-B} and Pr_{GR-S} estimated from the available data are reported, together with corresponding 95% confidence intervals.

Table 1: Weighting factors for combined A-index.

Type of accident	Number of accidents	Pr_i (i = CL, GR-S, GR-B) with 95% confidence interval
CL	4	25% [7% , 52%]
GR-B	3	19% [4% , 46%]
GR-S	9	56% [30% , 80%]

From the analysis of data, the following Combined Attained Subdivision Index, A, was eventually derived:

$$\begin{aligned} A = \; & 0.25 \cdot A_{CL} + \\ & + 0.19 \cdot A_{GR-B} + \\ & + 0.56 \cdot A_{GR-S} \end{aligned} \qquad (6)$$

Discussion on selection and use of the safety metric

Two safety metrics have been defined which share the characteristic that they can both be determined as weighted combinations of individual A-indices corresponding to different types of accidents.

Both options for a combined measure of survivability after a flooding event have been thoroughly discussed during the eSAFE project, and it was concluded that the risk-based approach is to be the preferred one.

The risk-based safety metric SM (see (4)) is a risk-based approach directly related to societal risk (*PLL*) from collision, bottom grounding and side grounding/contact damages. It is based on the EMSA 3 risk models for collision and grounding/contact accidents relevant to cruise ships, which were developed in the EMSA 3 project and the applied methodology has been evaluated by the IMO FSA Experts Group (IMO, 2015). Weighting coefficients in the risk-based safety metric represent the relative contribution to societal risk stemming from different types of accidents, on the basis of the assumed risk models, in a hypothetical condition where the attained index is the same for all types of accidents.

The combined attained subdivision index A (see (6)), represents a measure of the probability of survival conditional to the occurrence of a flooding accident. The weighting coefficients of the combined A-index are obtained from the direct analysis of accidents data, and the weighting coefficients correspond to the relative frequencies of different types of accidents. If the objective of watertight subdivision and damaged stability analysis is to maximize the probability of a ship to survive an accident and remain afloat, then the combined index A appears to be the natural choice. However, it is not possible to reflect the risk-level of the vessel directly from this index, and therefore the combined A-index is not a direct risk-based safety metric.

Comparing (4) and (6), it can be seen that the weighting coefficients for the three attained indices in the two metrics are different. This is a consequence of the fact that the two metrics provide measures associated with two different quantities: societal risk on the basis of the assumed risk models in case of SM, and probability of ship survival conditional to the occurrence of a flooding accident in case of the combined A-index. Accordingly, on the one hand, the weighting coefficients in the combined A-index only accounts for relative frequencies of different types of accidents (see Table 1). On the other hand, the weighting coefficients in SM also embed the relative effect of consequences from different types of accidents, on the basis of the assumed risk models.

The estimated weighting coefficients for both metrics are affected by uncertainty due to the limited sample size coming from accidents data. In addition, the risk-based safety metric SM also embeds a certain level of uncertainty coming from the subjective expert judgement related to the structure of the underlying risk models and to the specification of probabilities of some events.

Considering the main characteristics and inherent limitations of the two alternatives, it was

agreed within eSAFE to use the risk-based safety metric SM .

However, as shown in the sensitivity analysis in EMSA 3, as well as when going into the details of the underlying accident statistics, the number of accidents in the various branches of the event tree of the risk models is small, which, as already highlighted, leads to uncertainty in the coefficients for SM .

In addition, the calculated weighting coefficients show that side grounding/contact seems to be the dominating risk for flooding. This result raised some concerns during the discussions, because it is based on past casualty reports, and it may not reflect the actual situation of cruise ships. Modern technical features and improved operational procedures may have changed the probability for grounding and contact events, respectively the consequences. Hence, the application of the safety metric SM in its current form, which to a larger degree is based on historical accident data, may not lead to the proper focus during the design of cruise ships. Thus, even if the combined evaluation of different types of damages is regarded as favourable, these aspects require further investigations.

Therefore, it has been decided to use the attained indices separately for collision, bottom grounding and side grounding/contact, for the time being.

In addition, a regular review and update of the risk models is recommended to achieve a more robust measure for the risk due to flooding. It is also worth mentioning that research&development in this respect is expected to be carried out in the framework of the forthcoming Horizon 2020 "FLooding Accident REsponse (FLARE)" project, with a review of the recent risk model for side and bottom damages.

4. SOFTWARE IMPLEMENTATION IN VIEW OF PRACTICAL APPLICATION

General

In industrially oriented projects, the implementation of scientific and technical advances into practically applicable tools is of utmost importance in order to quantify and maximize the impact and benefit of the fundamental developments. Accordingly, practical implementation was one of the drivers in eSAFE, where project partners representing different stakeholders of the cruise industry, together strived to develop, test and put into practice innovative methodologies related to ship safety. In this context, the developments related to the combined non-zonal approach for collision, bottom grounding and side grounding/contact have been implemented in a design-oriented, practically applicable, NAPA software functionality.

A testing tool implemented in NAPA

By utilizing and extending the technology and a tool developed in the EMSA 3 project (Zaraphonitis et al., 2015), a new functionality was developed for generating also collision damages, on the basis of the non-zonal approach stemming from eSAFE. This functionality was made available in a modified test version of NAPA, for evaluation use in the project.

The tool in NAPA was first extended to cover collision damages which, as described in section 2, are consistent with current SOLAS with the addition of a probabilistic model for the extent of damage below water. In addition, the tool embedded an update of the EMSA 3 approach for addressing bottom grounding and side grounding/contact damages, with the aim of harmonizing some aspects of the calculation methods among different types of damages. Similarly to the original EMSA 3 tool, the results from the calculation (A-indices) are finally listed separately for each damage type (collision, bottom grounding, side grounding/contact) and for each calculation draught.

The tool was then tested through pilot applications by the developers of the methodology and by the designers (Lindroth et al., 2017). Results from the pilot usage were eventually used to provide insight to the newly developed approach and to guide subsequent calculations within the project.

A number of systematic tests have also shown the usability and robustness of the tool, so that it can be used in daily design work.

The tool allows the application of the non-zonal approach considering three types of breaches, namely:

- Bottom grounding (B00 damages), according to EMSA 3 modelling (Zaraphonitis et al., 2015);
- Side grounding/contact (S00 damages), according to EMSA 3 modelling (Zaraphonitis et al., 2015);

- Collision (C00 damages), according to the approach developed in eSAFE, which is in line with, and extends, SOLAS (see section 2).

It is noted that in the eSAFE application, breaches for each damage type are generated separately for each calculation draught. As a result, the calculation of probabilities for each damage case is also draught dependent for each type of damage. This represents an improvement compared to the EMSA 3 approach. In fact, in the EMSA 3 non-zonal calculations for bottom grounding and side grounding/contact, damage cases and corresponding probabilities were calculated only at the deepest draught, and remained the same for the other calculation draughts (Zaraphonitis et al., 2015; Bulian et al., 2016). This approximation was introduced for reasons related to computational time. In eSAFE, instead, this limitation has been overcome.

As the ship length considered for bottom grounding and side grounding/contact is the ICLL length (IMO, 2019b), whereas the ship length for collision calculations is the SOLAS subdivision length (IMO, 2019a), the tool consequently offers separate relevant input.

A representative view of the NAPA tool interface is shown in Figure 4, where the user can control the generation and calculation parameters. Ship modelling and other needed preparation work are not addressed by this interface, as they are part of the ship model preparation for the statutory damage stability analysis in NAPA. As a result, the non-zonal calculations (Monte Carlo generation of breaches and subsequent determination of A-indices) are quick to set up and easy to perform through the dedicated interface.

Notably, as the impact on flooding by bottom or side damages is slightly different, the designer might need to use different opening definitions and compartment connections for the different damage types. The tool, therefore, offers this flexibility.

For larger calculation sets or repetitions the tool also allows the preparation and automatic execution of multiple runs in batch. In such case, the input required for the different runs is provided by the user through a dedicated table.

In addition to generating breaches and calculating A-indices using the s-factor from SOLAS, the tool also offers alternatives for the generation and for the survivability assessment. Some of these options stem from objectives and activities within the eSAFE project, while other originate from external sources, e.g., regulatory interpretations.

Additionally to the successful pilot testing of the tool performed in the eSAFE project, there is an interest in continuing to explore the potentials and benefits of the developed approach and associated tool. Therefore, implementation and further development of the tool as a new and supported NAPA feature is planned.

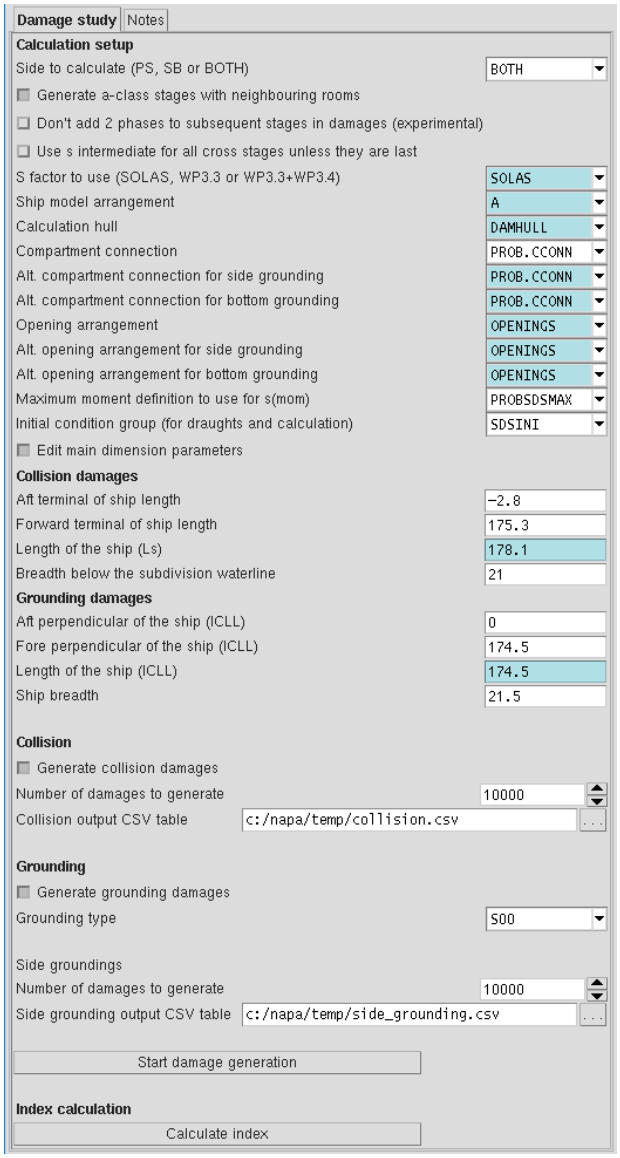

Figure 4: Representative view of the NAPA tool interface for the application of the non-zonal approach.

5. EXAMPLE OUTCOMES

The developed non-zonal approach has been extensively applied throughout the eSAFE project.

At first, a series of calculations were carried out in order to verify the correct implementation of the non-zonal approach for collision (Bulian et al., 2017; Lindroth et al., 2017). In this context, among other verification checks, an example verification was carried out for a barge (Lindroth et al., 2017) with and without double bottom, and without any additional horizontal subdivision boundary below the waterline. The barge configuration with double bottom is depicted in Figure 5. The subdivision of the configuration without double bottom is exactly the same as that shown in Figure 5, but without the inner bottom. The barge does not have any longitudinal bulkhead, and all compartments extend from side to side.

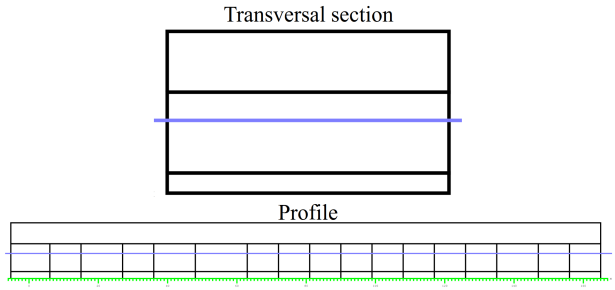

Figure 5: Barge used for testing. Configuration with double bottom.

For the case of the barge without double bottom, the SOLAS zonal approach provides exact results in terms of A-indices. Therefore, the non-zonal approach could be directly compared with SOLAS for such configuration. Instead, in case of barge with double bottom, the standard SOLAS zonal approach cannot be directly compared with the non-zonal approach due to the use of the "worst-case approach" in SOLAS/II-1/B-1/7-2/6.2 (Bulian et al., 2018). Therefore, for the barge configuration with double bottom, the outcomes from the non-zonal approach have been compared with those from the SOLAS zonal approach supplemented by the use of the "u-factor" (Bulian et al., 2018). The verification was successful in both cases, confirming the proper implementation of the non-zonal approach for collision in a way which is consistent with SOLAS. As an example, a comparison of A-indices for the barge with double bottom is shown in Figure 6. The figure reports A-indices from the non-zonal approach, from SOLAS zonal approach supplemented by "u-factor", and from standard SOLAS. In order to increase the accuracy of non-zonal calculations, a total of 12 repetitions with 10^5 breaches for each repetition were carried out, and the non-zonal data in Figure 6 correspond to the average A-indices across repetitions, together with 95% confidence interval (which are indeed so small that they are hardly visible in the graphs). The observed very small differences in Figure 6 between SOLAS+"u-factor" and non-zonal results, are associated with random sampling uncertainty. Instead, the differences with respect to standard SOLAS are due to the use of the "worst-case approach" in the standard SOLAS zonal approach.

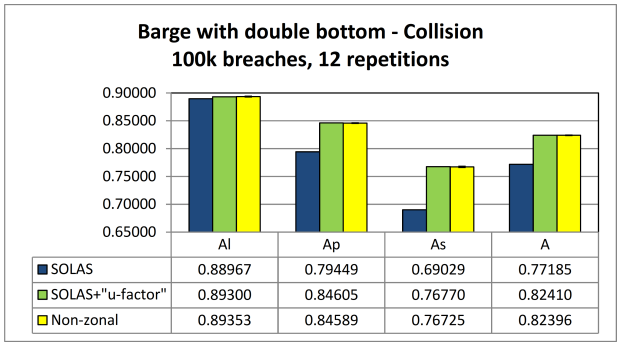

Figure 6: Barge with double bottom. Comparison between non-zonal approach (average with 95% confidence interval) and SOLAS zonal approach supplemented by u-factor.

An example practical application of the non-zonal approach for collision on a cruise ship is shown in Figure 7. The figure compares the attained subdivision indices for the considered cruise vessel, calculated according to the standard SOLAS zonal approach, the SOLAS zonal approach supplemented by the "u-factor", and the non-zonal approach for collision (average index across repetitions, with 95% confidence interval).

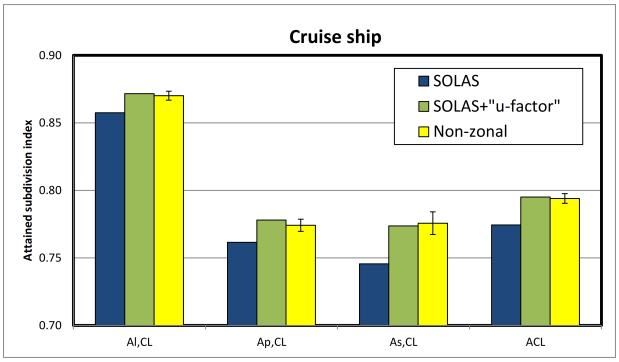

Figure 7: Example cruise ship. Comparison between SOLAS zonal approach, SOLAS zonal approach supplemented by u-factor, and non-zonal approach (average with 95% confidence interval from 5 repetitions with 10^4 breaches each).

Differently from the case of the barge in Figure 6, in case of the cruise ship in Figure 7 the zonal SOLAS+"u-factor" approach is an approximate one, because the vessel is not box-shaped and the compartments are, in general, not box-shaped as well. Therefore, in this case, results from the non-zonal approach are to be considered as the "exact" ones, bearing in mind the random sampling uncertainty which is reflected by the confidence intervals in Figure 7. It is therefore expected that results from the non-zonal approach and the SOLAS+"u-factor" approach do not perfectly match. Nevertheless, it can be seen that the zonal SOLAS+"u-factor" provides a very good approximation of the results obtained from the non-zonal approach. It can also be noticed that the introduction of a probabilistic model for the lower limit of damage below the waterline (SOLAS+"u-factor" and non-zonal approaches) provides, as expected, an increase of calculated attained subdivision indices (see Bulian et al. (2018) for more details on this topic).

Further example outcomes from practical application on the considered cruise ship are shown in Figure 8. The figure shows A-indices from the non-zonal approach for the three considered types of damages: collision (CL), bottom grounding (GR-B), side grounding/contact (GR-S). The reported indices are global ones, i.e. indices averaged for the three calculation draughts using standard SOLAS weighting factors (i.e. 0.2 for d_l, 0.4 for d_p, and 0.4 for d_s). In this respect, it is worth noting that the eSAFE project also investigated the suitability of SOLAS assumptions regarding the relative frequency of different draughts in the specific case of cruise vessels, showing that the actual operational profile of cruise vessels would call for the use of weighting factors different from the standard ones (Paterson et al, 2017, 2018).

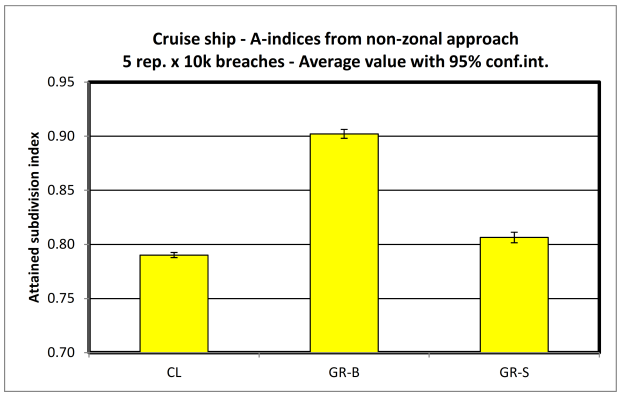

Figure 8: Example cruise ship. A-indices from non-zonal approach for collision (CL), bottom grounding (GR-B) and side grounding/contact (GR-S). Average with 95% confidence interval from 5 repetitions with 10^4 breaches each.

6. CONCLUSIONS

The paper provided an overview of some main outcomes from the eSAFE project, regarding, specifically, the development and implementation of a common framework for probabilistic damage ship stability assessment, considering collision, bottom grounding and side grounding/contact damages.

In this respect, the non-zonal approach, originally developed in the EMSA 3 project for bottom grounding and side grounding/contact has been extended in eSAFE to the case of collision.

Consistency with present SOLAS has been taken as a key objective, and it was verified during testing. Moreover, the lack of a probabilistic description for the lower limit of collision damage in present SOLAS zonal approach has also been overcome.

A software functionality has been developed in a test version of NAPA for the application of the common non-zonal methodology for collision, bottom grounding and side grounding/contact. A number of systematic tests have shown the usability and robustness of the tool, so that it can be used in daily design work.

Different alternatives have been considered for dealing with the attained subdivision indices from different types of damages: a risk-based safety metric, a combined attained subdivision index, and the separate use of attained indices from different types of damages. An extensive analysis and

discussion was carried out within eSAFE regarding the different alternatives. Eventually, it has been recommended by eSAFE to actively use the new tools and gain experience in what effects design changes might have on the survivability from collision, bottom grounding and side grounding/contact, by using the attained indices separately for collision, bottom grounding and side grounding/contact, for the time being. In addition, a regular review and update of the risk models has been recommended to achieve a more robust measure for the risk due to flooding. In this respect, it can also be added that a more complete collection of accident details, with collection of additional and higher quality data, would definitely be important to achieve the goal of improving the risk models through the review and update process.

The non-zonal approach provides now the basis for a holistic assessment of survivability after flooding considering collision, bottom grounding and side grounding/contact. The experience gained during eSAFE also shows that the approach can be of practical application in the actual design activity.

ACKNOWLEDGEMENTS

This work was carried out in the framework of the project "eSAFE – enhanced Stability After a Flooding Event – A joint industry project on Damage Stability for Cruise Ships". The funding partners of eSAFE are: Carnival Corporation Plc, DNV GL, Fincantieri, Lloyd's Register, Meyer Werft, RINA Services, Royal Caribbean Cruises Ltd. and STX France. The financial support from the eSAFE funding partners is acknowledged.

A number of the achievements from eSAFE reported in this paper build upon and extend some of the outcomes from the EMSA 3 project "Study assessing the acceptable and practicable risk level of passenger ships related to damage stability" (EMSA/OP/10/2013 - www.emsa.europa.eu/damage-stability-study.html). The original funding of EMSA 3 project from the European Maritime Safety Agency (EMSA), as well as the encouragement to continue the research&development activity in the framework of the eSAFE project, are highly acknowledged.

DISCLAIMER

The information and views as reported in this paper are those from the authors and do not necessarily reflect the views of the eSAFE Consortium.

The views as reported in this paper are those of the authors and do not necessarily reflect the views of the respective organizations.

REFERENCES

Bulian, G., Francescutto, A., 2010, "Exploratory data analysis of ship-ship collision data from the updated GOALDS database", Project GOALDS (GOAL based Damage Stability) - Grant Agreement 233876, 30 August.

Bulian, G., Lindroth, D., Ruponen, P., Zaraphonitis, G., 2016, "Probabilistic assessment of damaged ship survivability in case of grounding: development and testing of a direct non-zonal approach", *Ocean Engineering*, Vol. 120, pp. 331-338.

Bulian, G., Zaraphonitis, G., Francescutto, A., Ruponen, P., 2017, "eSAFE-D2.1.1 - Description of geometrical and probabilistic model for collision damage", Joint Industry Project "eSAFE - enhanced Stability After a Flooding Event – A joint industry project on Damage Stability for Cruise Ships", 03 May (Rev.1).

Bulian, G., Cardinale, M., Francescutto, A., Zaraphonitis, G., 2018, "Complementing SOLAS framework with a probabilistic description for the damage extent below water", Proceedings of the 13th International Conference on the Stability of Ships and Ocean Vehicles (STAB2018), 16-21 September, Kobe, Japan, pp. 638-647.

IMO, 2008, "Resolution MSC.281(85) – Explanatory Notes to the SOLAS Chapter II-1 Subdivision and Damage Stability Regulations", 4 December.

IMO, 2012, "SLF 55/INF.7 - The GOAL based Damage Stability project (GOALDS) – Derivation of updated probability distributions of collision and grounding damage characteristics for passenger ships", Submitted by Denmark and the United Kingdom, 14 December.

IMO, 2015, "SDC 3/3/4 - Report of the intersessional meeting of the Experts Group on Formal Safety Assessment (FSA)", Submitted by the Chairman of the FSA Experts Group, 12 November.

IMO, 2017, "Resolution MSC.429(98) – Revised Explanatory Notes to the SOLAS Chapter II-1 Subdivision and Damage Stability Regulations", 9 June.

IMO, 2019a, "International Convention for the Safety of Life at Sea (SOLAS)", Consolidated edition.

IMO, 2019b, “International Convention on Load Lines, 1966, as amended by the 1988 Protocol by res. MSC.143(77) in 2003”, Consolidated edition.

Konovessis, D., Hamann, R., Eliopoulou, E., Luhmann, H., Cardinale, M., Routi, A.-L., Kujanpaa, J., Bertin, R., Harper, G., Pang, E., Papanikolaou, A., 2015, “Risk Acceptance Criteria and Risk Based Damage Stability, Final Report, part 2: Formal Safety Assessment”, DNVGL Report No.: 2015-0166 Rev.3, Project EMSA/OP/10/2013, European Maritime Safety Agency, 29 June.

Lindroth, D., Bulian, G., Dafermos, G., Zaraphonitis, G., Cardinale, M., Luhmann, H., Ruponen, P., 2017, “eSAFE-D2.3.1 – Final report of ‘WP2.3 – Development of a software tool for the application of the combined methodology’ ”, Joint Industry Project “eSAFE - enhanced Stability After a Flooding Event – A joint industry project on Damage Stability for Cruise Ships”, 09 August (Rev.0).

Luhmann, H., Olufsen, O., Atzampos, G., Bulian, G., 2018a, “eSAFE-D4.3.1 – Summary report”, Joint Industry Project “eSAFE - enhanced Stability After a Flooding Event – A joint industry project on Damage Stability for Cruise Ships”, 24 October (Rev.4).

Luhmann, H., Bulian, G., Vassalos, D., Olufsen, O., Seglem, I., Pöttgen, J., 2018b, “eSAFE-D4.3.2 – Executive summary”, Joint Industry Project “eSAFE - enhanced Stability After a Flooding Event – A joint industry project on Damage Stability for Cruise Ships”, 24 October (Rev.3) – available from: https://cssf.cruising.org/projects .

Lützen, M., 2001, "Ship Collision Damages", PhD Thesis, Department of Mechanical Engineering, Technical University of Denmark, December.

Lützen, M., 2002, “Damage Distributions”, Document 2-22-D-2001-01-4, Project HARDER (Harmonisation of Rules and Design Rationale), 29 July.

Mains, C., 2010, "WP3 Database of damage characteristics - File: GOALDS-database-rev3.xls”, Project GOALDS (GOAL based Damage Stability).

Paterson, D., Atzampos, G., Vassalos, D., Boulougouris, E., 2017, “eSAFE-D1.2.1 – Analysis of onboard data with regards to probabilities of initial draughts”, Joint Industry Project “eSAFE - enhanced Stability After a Flooding Event – A joint industry project on Damage Stability for Cruise Ships”, 01 March (Rev.5).

Paterson, D., Vassalos, D., Atzampos, G., Boulougouris, E., Cichowicz, J., Luhmann, H., 2018, “Rebooting SOLAS – Impact of Drafts on Damage Survivability of Cruise Ships”, Proceedings of the 13th International Conference on the Stability of Ships and Ocean Vehicles (STAB2018), 16-21 September, Kobe, Japan, pp. 663-674.

Pawłowski, M., 2004, "Subdivision and damage stability of ships", Euro-MTEC book series, Foundation for the Promotion of Maritime Industry, Gdansk, Poland, Poland, ISBN 83-919488-6-2, 311p.

Vassalos, D., Hamann, R., Zaraphonitis, G., Luhmann, H., Kuusisto, T., Lietzen, J., 2015, “Combined assessment of cost-effectiveness of previous parts, FSA compilation and recommendations for decision making”, DNVGL Report No.: 2015-0404 Rev.1, Project EMSA/OP/10/2013, European Maritime Safety Agency, 17 July.

Zaraphonitis, G., Bulian, G., Lindroth, D., Hamann, R., Luhmann, H., Cardinale, M., Routi, A.-L., Bertin, R., Harper, G., Papanikolaou, A., Francescutto, A., Ruponen, P., 2015, “Evaluation of risk from raking damages due to grounding, Final report”, DNVGL Report No.: 2015-0168 Rev.2, Project EMSA/OP/10/2013, European Maritime Safety Agency, 17 June.

Zaraphonitis, G., Bulian, G., Hamman, R., Eliopoulou, E., Cardinale, M., Luhmann, H., 2017, “eSAFE-D2.2.1 - Description of methodology”, Joint Industry Project “eSAFE - enhanced Stability After a Flooding Event – A joint industry project on Damage Stability for Cruise Ships”, 29 March (Rev.2).

CFD in damage stability

Eivind Ruth, *DNV GL,* eivind.ruth@dnvgl.com
Odd Olufsen, *DNV GL,* odd.olufsen@dnvgl.com
Olav Rognebakke, *DNV GL,* olav.rognebakke@dnvgl.com

ABSTRACT

This paper presents some of the key learnings from CFD simulations of flooding events following a collision damage, as gained during the corresponding research and development activity carried out within the eSAFE project. The software STAR-CCM+ was used and allowed for full-scale simulations of the fully-coupled behaviour of the vessel, and of external and internal flows. All stages of the flooding process were included: i.e., transient and progressive flooding. The captured effects include the water inside the vessel propagating through corridors, ducts and other openings, dynamic response of the vessel due to water ingress, and waves influence. It was concluded that CFD simulations is generally a satisfactory tool for simulating flooding events. However, the simulation time was an issue, particularly for progressive flooding and statistical evaluations where many damage cases have to be evaluated.

Keywords: *eSAFE, Dynamic stability, CFD, simulations.*

1. INTRODUCTION

Software tools for simulation of flooding (e.g. PROTEUS3 [1], FREDYN [2][3], ROLLS [4][5], NAPA [6] and others) have been under development and put to practical use for many years. In connection with the eSAFE project [7][8] it was suggested to use CFD as a means to validate the simulation tools. It was recognised that while there are several results from model tests available for roro passenger vessels, there is very little data available for cruise ships. eSAFE used CFD to study the behaviour of a cruise ship during transient flooding in calm water and regular waves as well as progressive flooding in regular waves. The definition of the flooding stages is shown in Figure 1.

In the process of planning the extent and scope of CFD simulations, the ITTC recommendations on Numerical simulations of Capsize behaviour of damaged ships in irregular beam seas [9] was referred to.

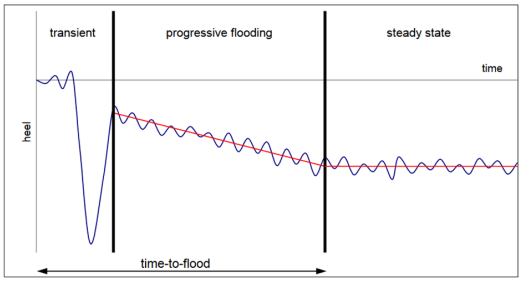

Figure 1: Phases of flooding process (from Ruponen [6]).

2. SELECTED FLOODING CASES

The main objective of the CFD work was to validate the results provided by the simulation software PROTEUS3 [1][10]. Based on initial PROTEUS3 simulations, a limited number of damage cases were selected to cover the relevant physics during flooding. Two cases where capsize could occur in the transient phase and two cases where capsize could occur in the progressive phase were selected. It should be noted that the selected damage cases were severe, affecting at least three vertical zones.

3. MODELLING

The geometry models used in the CFD calculations were taken from the NAPA model used

by the shipyard for conventional damage stability calculations. In addition, structures restricting the flow in cross ducts and air vents were included. A-class bulkheads and hypothetical subdivision in way of e.g. cabin areas were not included. The assumed damage was limited in extent vertically up to deck 4, two decks above the bulkhead deck. Damages were imposed by removing structure in the damage definition volume.

The simulations were performed with STAR-CCM+ 9.04.011. Initial simulations were performed to derive a set of reasonable simulation parameters. The work on roll damping in Kristiansen et. al. [11], validated by model tests, was used as starting point. It was found possible to coarsen both mesh and time step, and still achieve reliable results. An example of meshing in way of cross flooding ducts is shown in Figure 2. In addition, important observations were that compressibility and air vents were important, and that the viscosity model was less important.

In the progressive flooding case the mesh and time step were coarsened further to allow for a very long simulation time. Simulating 30 minutes of progressive flooding in waves still took 50 days on 200 CPUs.

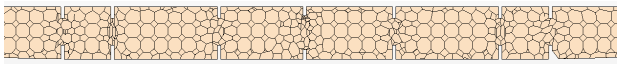

Figure 2: Example of cross-flooding duct and mesh.

4. TRANSIENT FLOODING IN CALM WATER

When a large portion of a ship, at or below the waterline is opened to the sea, a violent dynamic response due to sea water rapidly entering the ship will occur. This can result in rather extreme angles of heel during the first roll cycles that could lead to capsize. This is called transient flooding, see Figure 1, and has been subject to substantial research efforts e.g. Manderbacka [12] and Vassalos [13].

Two damage cases that by use of PROTEUS3 indicated capsize were simulated by CFD, for which one case is presented here. As a basis for comparison both results from using PROTEUS3 and NAPA for the same damage case are presented in Figure 3. Quasi-static NAPA calculations are performed with two different virtual transverse subdivisions of the machinery and cabin space. The finer division is denoted as "NAPA_1" in Figure 3, whereas the case indicated as "NAPA_2" is based on a coarser modelling. In PROTEUS3, two different properties of deck 4 were simulated. In one case the deck was completely transparent to water (denoted by "_1" in Figure 3), and in the other case completely watertight (denoted by "_2" in Figure 3). Deck 4 was barely touching the water at the maximum roll angle, but still produced a significant difference with respect to survivability. All NAPA and CFD simulations were performed with a completely watertight deck 4. The same CFD case was calculated by both LR and DNVGL giving similar results. It is worth noting that all software provided approximately the same maximum angle of heel. However, there appeared to be a difference in the dynamic behaviour after the initial transient.

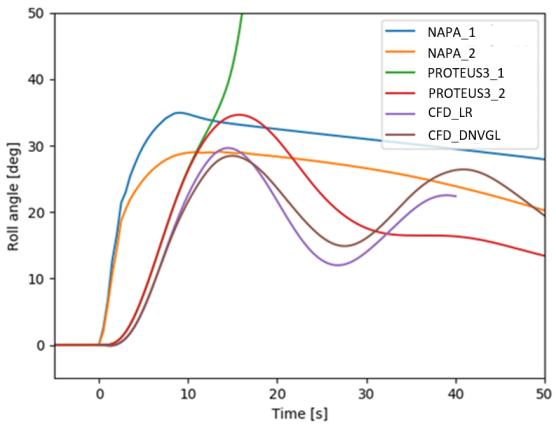

Figure 3: Transient flooding – response from various simulations.

A screenshot of the situation close to the maximum angle of heel is shown in Figure 4. The left side shows the portion of the ship opened to the sea. It was observed that the water level on the opposite side is higher due to the rolling of the vessel. This contributes to reduced transient roll angle. A significant advantage of the CFD simulations is the ability to accurately simulate and visualize the internal flow as opposed to only simulating filling levels under the assumption of a horizontal free surface.

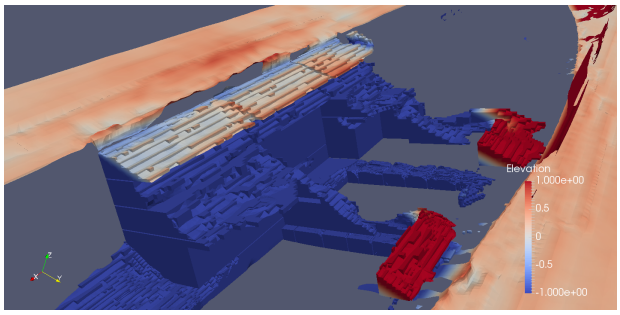

Figure 4: Screenshot - transient flooding.

5. TRANSIENT FLOODING IN WAVES

The same transient flooding damage case was simulated in regular beam sea waves to study the effect of waves in the transient phase. A wave height of 8m was found reasonable for the transient case, representing an "extreme" wave in 4m significant wave height. Steep waves are believed to be worse. Hence, the wave period was set to 7s.

The vessel was allowed to reach stationary behaviour in the waves prior to introducing the damage. The damage was imposed at four different positions (90 deg out of phase) in the wave to check the importance of phasing between wave and damage. The resulting roll time series are seen in Figure 5. Run_35 is the calm water and run 37 to 40 are the same damage introduced at different positions in the wave. It is observed that for this case the maximum roll angle shows small dependency on wave phasing or if the waves were present at all,

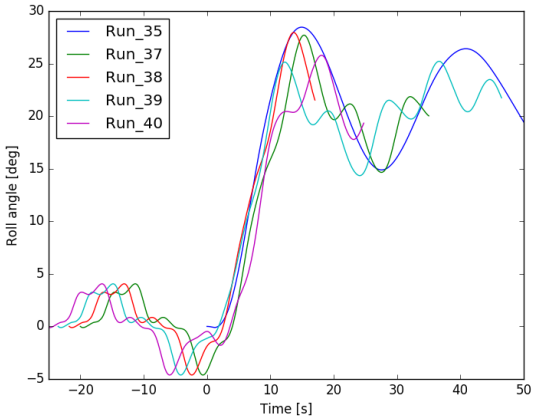

Figure 5: Opening to the sea at various phases of the waves.

6. PROGRESSIVE FLOODING IN REGULAR WAVES

The damage cases selected for validation of progressive flooding were among those where PROTEUS3 simulations resulted in capsize. The affected compartments are visualised in Figure 6. To ease comparison, regular waves were used. The wave height was set to 4 metres and the wave period to 5 seconds, to approximate a reasonable probable steep sea state lasting for an hour.

The simulation in waves was run for some time (to get realistic vessel motion) before the damage was introduced. Run 4100 shows the result in calm water. In Run_4108 the damage is introduced after 9s, and in Run_4107 after 11.5 seconds. The resulting roll angles are seen in Figure 7. Apparently, the starting point was not important for this case where the waves are relatively small, and the transient was not a problem in calm water. The initial transient is, in this case, reduced when the waves are present.

In Figure 8 and Figure 9 the progressive flooding in PROTEUS and CFD is compared. The PROTEUS3 results show that the flooding develops to an excessive angle of heel while the CFD calculations result in a steady state or slowly increasing angle of heel. The reason for the different behaviour is not clear but could be caused by different modelling assumptions.

It is believed that the resulting vessel motion from the waves is not significant for the progressive flooding phase. From the videos, it seemed like the effect from waves pushing water into the vessel was more important.

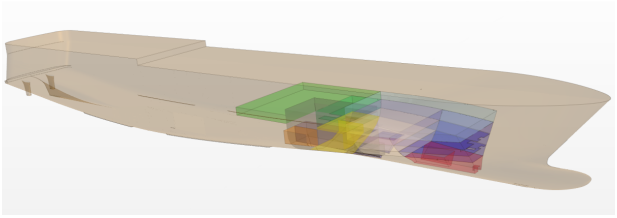

Figure 6: Illustration of ship model and flooded space.

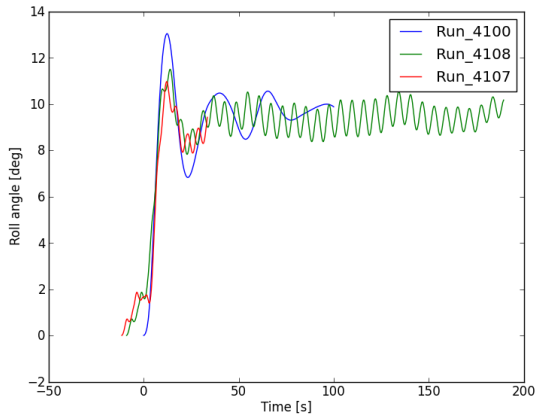

Figure 7: Introduction of damage at various time steps.

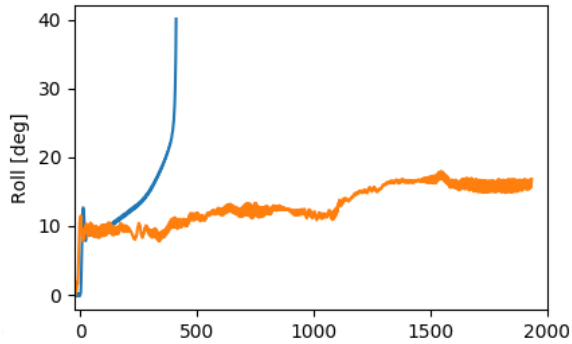

Figure 8: Comparison roll – PROTEUS3 (blue) and CFD (orange).

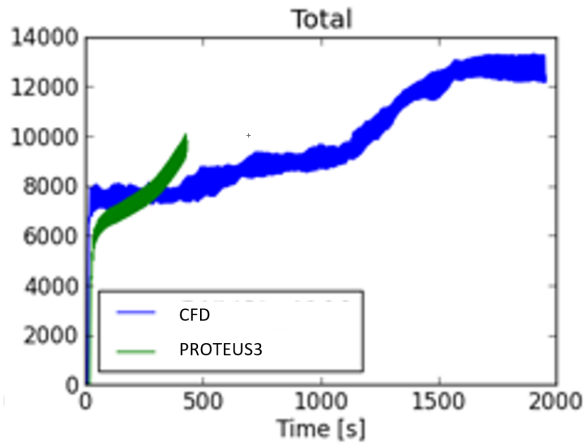

Figure 9: Comparison – flooded volume.

7. SOME THOUGHTS ON FUTURE USE OF CFD FOR DAMAGE STABILITY

In the presented work, CFD has been applied to complex damage stability cases and has given reasonable results. With respect to applicability of CFD in damage stability calculations, it is foremost the computational cost and time that are limiting.

CFD can be efficiently applied to selected parts of the damage stability assessment. For instance, CFD can be used to simulate:

- Wind forces on the superstructure
- Drag forces on the underwater hull
- Drift speed
- Wind heeling angle
- Cross flooding ducts

These kinds of simulations are significantly simpler and can be performed within a reasonable cost and time frame.

Simulating the entire problem of vessel motions, external and internal flows, is currently deemed reasonable for a limited selection of transient flooding cases. Progressive flooding in CFD is considered research scope.

Model tests may be cost efficient when performing parameter studies. Although some effects like wind are hard to model, most real physics may be accurately accounted for. The cost of preparing a vessel model with complex internal compartmenting is very high, and significant simplifications are normally required. CFD is already a preferred alternative when a low number of short duration events are studied for each damage case with specific flooded compartments.

If CFD is used for validation purposes, the damage cases selected for comparison should not be too complicated. Differences in assumptions or simplifications should be avoided when considering the basic capability of the simulation software. When relevant, CFD may be a useful tool to validate the effect of any simplification in the simulation tool.

Visualization is an important advantage of CFD. In the CFD simulation all physical quantities are known in the entire domain. This can be used to investigate and learn about detailed flow patterns or special effects.

8. CONCLUSIONS

CFD simulations of selected severe damage stability cases have successfully been performed. Both transient and progressive flooding in calm water and in waves were evaluated. For many cases PROTEUS3 compared well with CFD. However, for the progressive flooding simulation, there were significant differences. This is not necessary a

shortcoming of one of the tools, but could also be caused by modelling differences.

The main advantage of CFD is the ability to visualize and investigate detailed flow patterns and include arbitrary geometrical models. Currently, CFD can efficiently be applied to study specific details or parts of the damage stability assessment like wind forces or cross flooding ducts. The main challenge with respect to full damage stability simulations is currently simulation time and cost, however future developments in computational power might help to overcome this.

ACKNOWLEDGEMENTS

This work was carried out in the framework of the project "eSAFE – enhanced Stability After a Flooding Event – A joint industry project on Damage Stability for Cruise Ships". The funding partners of eSAFE are: Carnival Corporation Plc, DNV GL, Fincantieri, Lloyd's Register, Meyer Werft, RINA Services, Royal Caribbean Cruises Ltd. and STX France. The financial support from the eSAFE funding partners is acknowledged.

DISCLAIMER

The information and views as reported in this paper are those from the authors and do not necessarily reflect the views of the eSAFE Consortium.

The views as reported in this paper are those of the authors and do not necessarily reflect the views of the respective organizations.

REFERENCES

[1] Jasionowski, A., 2001, "An Integrated Approach to Damage Ship Survivability Assessment", PhD Thesis, University of Strathclyde, Glasgow, UK.

[2] van't Veer, R., de Kat, J.O., 2000, "Experimental and Numerical Investigation on Progressive Flooding and Sloshing in Complex Compartment Geometries", Proc. 7th International Conference on Stability of Ships and Ocean Vehicles (STAB2000), 7-11 February, Launceston, Tasmania, Australia, pp. 305-321

[3] Ypma, E., Turner, T., 2010, "An Approach to the Validation of Ship Flooding Simulation Models", Proc. 11th International Ship Stability Workshop (ISSW2010), 21-23 June, Wageningen, The Netherlands, pp. 173-184

[4] Petey, F., 1988, "Ermittlung der Kentersicherheit lecker Schiffe im Seegang aus Bewegungssimulation", Bericht Nr. 487, November, Technische Universität Hamburg-Harburg.

[5] Krüger, S., Dankowski, H., Teuscher, C., 2012, "Numerical Investigations of the Capsizing Sequence of SS HERAKLION", Proc. 11th International Conference on the Stability of Ships and Ocean Vehicles (STAB2012), 23-28 September, Athens, Greece, pp. 743-753

[6] Ruponen, P., 2007, "Progressive flooding of a damaged passenger ship", Doctoral Dissertation, Helsinki University of Technology.

[7] Luhmann, H., Olufsen, O., Atzampos, G., Bulian, G., 2018, "eSAFE-D4.3.1 – Summary report", Joint Industry Project "eSAFE - enhanced Stability After a Flooding Event – A joint industry project on Damage Stability for Cruise Ships", 24 October (Rev.4)

[8] Luhmann, H., Bulian, G., Vassalos, D., Olufsen, O., Seglem, I., Pöttgen, J., 2018, "eSAFE-D4.3.2 – Executive summary", Joint Industry Project "eSAFE - enhanced Stability After a Flooding Event – A joint industry project on Damage Stability for Cruise Ships", 24 October (Rev.3) – available from: https://cssf.cruising.org/projects .

[9] ITTC, 2017, "Recommended Procedures and Guidelines – 7.5-02-07-04.4 – Numerical Simulations of Capsize behaviour of Damages Ship in Irregular Beam Seas (Rev. 02)".

[10] Ruth, E., Caldas, A., Olufsen, O., York, A., Jenkins, J., 2017, "eSAFE-D3.2.2 – Results from Validation", Joint Industry Project "eSAFE - enhanced Stability After a Flooding Event – A joint industry project on Damage Stability for Cruise Ships", 14 December (Rev.6)

[11] Kristiansen, T., Ruth, E., Firoozkoohi, R., Borgen, H. and Berge, B. O., 2014, "Experimental and numerical investigation of ship roll damping with and without bilge keels", ASME 33rd International Conference on Ocean, Offshore and Arctic Engineering, OMAE2014, June 8-13, San Francisco, USA, OMAE2014-24585.

[12] Manderbacka, T., 2015, "Fast simulation for transient flooding of a ship", Doctoral Dissertation, Aalto University.

[13] Vassalos, D., Letizia, L., 1998, "Characterisation of Flooding Process of Damaged Ro-Ro Vessel", International Journal of Offshore and Polar Engineering, Vol. 8, No. 3, September, pp. 192-199

eSAFE - cruise ship survivability in waves

Georgios Atzampos, *Maritime Safety Research Centre*, georgios.atzampos@strath.ac.uk
Dracos Vassalos, *Maritime Safety Research Centre*, d.vassalos@strath.ac.uk
Jakub Cichowicz, *Maritime Safety Research Centre*, jakub.cichowicz@strath.ac.uk
Donald Paterson, *Maritime Safety Research Centre*, d.paterson@strath.ac.uk
Evangelos Boulougouris, *Maritime Safety Research Centre*, evangelos.boulougouris@strath.ac.uk

ABSTRACT

Recent developments in damage stability legislation have been drawn from ships with simple internal watertight architecture such as RoPax and cargo ships. However, ships with complex internal architecture, such as cruise ships, have been rather neglected. In a regulatory context, cruise ships are currently grouped with RoPax and other passenger ships and this can be misleading. Moreover, it is well known that cruise ships vary significantly in their behaviour post-flooding incidents in comparison to RoPax ships. This problem has been acknowledged by the Cruise Ship Safety Forum Steering Committee who consequently funded the Joint Industry Project eSAFE to undertake cruise ship-focused research on damage stability. This entails analysis of pertinent simplifications embedded in SOLAS, the development of a methodology to combine consequences from collision and grounding accidents, the establishment of new survival criteria for cruise ships and finally the development of guidelines to use numerical flooding simulation in seaways as an alternative approach to assessing ship damage survivability. The findings of this research are presented in this paper, based on a full set of time-domain numerical simulations along with static calculations for a number of cruise ships. A new s-factor is derived catering specifically for cruise ships that accounts more accurately for survivability in a wave environment. A number of simulations are undertaken on varying size cruise ships with the view to deriving a relationship between the critical significant wave height and the residual stability properties of such vessels. The results provide the requisite evidence for comparison between SOLAS 2009 A-Index and the ensuing damage Survivability Index.

Keywords*: eSAFE, damage stability, survivability, s-factor, safety, time domain numerical simulations, cruise ship, flooding.*

1. INTRODUCTION

Damage stability has largely developed as a subject over the past 50 years with most of the scientific advances achieved over the latter half of this period. However, the focus concerning such developments and the ensuing legislation is clearly on ships with simple internal architecture such as RoPax and Cargo ships. Ships with complex internal architecture, on the other hand, such as cruise ships, have been treated as a side line; in essence seldom the focus of scientific research on damage stability. For example, the current SOLAS for probabilistic damage stability is based on cargo ships, irrespective of the fact that RoPax have spearheaded developments over the recent past, following a number of serious accidents. In the regulatory context, cruise ships are currently grouped with RoPax and other passenger ships and this is causing serious problems. It is obvious that cruise ships have a significantly different behaviour after flooding incidents than RoPax ships. In particular, cruise ships are usually found not so vulnerable to rapid capsize as RoPax vessels. Results from numerical time-domain simulations of damage scenarios for both ship types support this fact. More specifically, comparison between results from SOLAS2009 calculations and numerical simulations display a significant difference for cruise ships (Vassalos, 2015). This problem has been acknowledged by the Cruise Ship Safety Forum, which has consequently initiated research on this subject in a Joint Industry Project, namely eSAFE. A key objective in this project is to identify and to the degree possible quantify the differences between known and/or

expected safety levels as indicated by the results from time-domain flooding simulations of cruise ships and the simplified methodology defined in SOLAS II-1 (IMO, 2009).

This paper delves in this direction through the use of available methods to defining damage stability/survivability of passenger ships, namely the Statistical (SOLAS) and Direct (numerical time-domain simulation) approaches. In this respect, a new s-factor, specifically catering for cruise ships has been devised following the statistical approach based on four cruise ships. In addition, a number of numerical simulations in pertinent sea states are performed with the view to gauging survivability in waves, linked to collision and grounding damages for two large cruise ships. On this basis, a comparison is conducted between the statistical and direct approach results leading to drawing specific conclusions.

2. STATISTICAL APPROACH TO DAMAGE STABILITY (A-INDEX)

Critical significant wave height and capsize band

The critical sea state for a specific damage extent and loading condition can be established either with the aid of model tests or by employing time-domain numerical simulations based on first principles. Traditionally, both approaches have been utilised in the past in the course of developing damage stability criteria, including comparisons between the two (HARDER, 1999-2003, GOALDS, 2009-2012). Generally, both physical and numerical experiments refer to repeated trials (usually corresponding to 30 minutes full-scale) in a specific random sea with the view to deriving capsize rate at a specific significant wave height.

In this respect, one of the main elements, which can be derived from the characteristics of the damaged ship is the capsize band. This indicates the range of sea states within which a transition from unlikely (Pc=0; Ps=1) to certain capsize (Pc=1; Ps=0) can be observed. Another concept intrinsically linked to the capsize band is the capsize rate. The capsize rate follows always a sigmoid shape distribution. The rate of observed capsizes depends on the time of observation. In this respect, in case of a limiting case of infinite exposure the capsize rate distribution will turn into a unit step function as indicated in Figure 1 for increased simulation times. Indeed, for low capsize probability, the corresponding significant wave height will remain the same (minor difference) when the time of observation is increased (GOALDS (Papanikolaou et al., 2013)). Hence, a sea state corresponding to a low capsize rate can be established on the basis of relatively short simulations and would still remain valid for longer observations.

Following previous studies, the concept of the s-factor is linked to the critical significant wave height. Originally, during the EU project HARDER (Tuzcu, 2003b) the s-factor was linked to the critical significant wave height of the sea state at which a ship exposed for half an hour (30m) to the action of waves would have a 50% chance of capsizing. However, based on subsequent observations in project GOALDS (Tsakalakis et al., 2010), it was found that when the simulation time increases, the capsize band contracts towards its lower boundary, with the capsize probability becoming a step function of Hs.

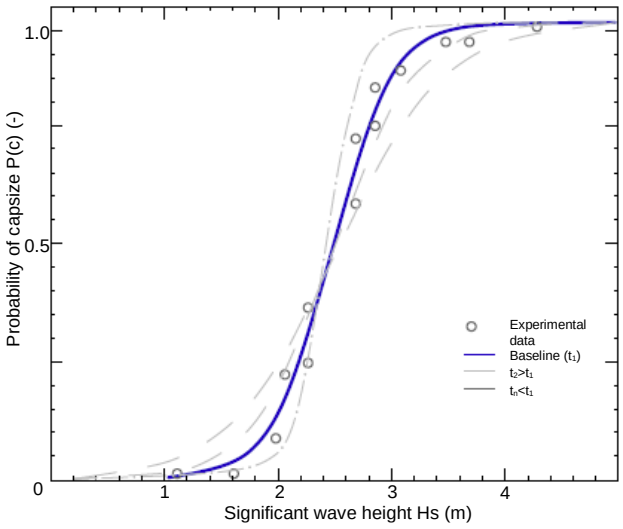

Figure 1: Indicative capsize rate transition from baseline curve with increase or decrease of observation time.

eSAFE - Cruise ship specific s-factor

In order to account for the complex internal watertight architecture and loss mechanisms of modern passenger ships, a new s-factor derivation has been developed within project eSAFE, catering specifically for cruise ships. Such internal detail can be sufficiently captured with the aid of numerical simulations. To this end, for the first time in the history of development of damage stability criteria, estimation of damage survivability is solely based on numerical time-domain simulation results for four

varying size cruise ships using the dynamic numerical time-domain code PROTEUS3 (Jasionowski, 2001).

The new s-factor, does not only account for the variations in cruise ship size but also has been proven robust for different compartment damages, namely (1, 2, 3 and 4-comparment equivalent). Based on regression of the numerical simulation results (94 points in total), a relationship has been derived between the critical significant wave height and residual stability properties, in line with previous work.

A new formula for predicting the critical significant wave height Hs_{crit} has been developed as shown by eq. (1). Based on statistical analysis of the various data sets, the most accurate regression was achieved with reference to GZ_{max} and Range properties (as in Project HARDER) but with an additional scaling factor taken into account (λ) (similar to Project GOALDS)(Cichowicz et al., 2016). The regression has been conducted with consideration of all data points, accounting for critical significant wave heights that span up to 7 meters, using global wave statistics (Paterson et al., 2017). The deviation from SOLAS of using actual wave statistics, rather than wave statistics pertaining to sea states at the time of the incident, is based on the argument that it is essential to estimate the risk of exposing ships to all operating sea states (thus, calculating pertinent risk), and not just those wave characteristics at which accidents have taken place in the past (historical risk). The multiplier in eq. (1) represents the 99th percentile of the cumulative probability.

$$Hs_{crit} = 7 \cdot \left[\frac{min(\lambda \cdot Range, TRange)}{TRange} \cdot \frac{min(\lambda \cdot GZmax, TGZmax)}{TGZmax}\right]^{1.05} \quad (1)$$

Where,

TGZ_{max}	= 30 m Target GZ_{max} value
$TRange$	= 30 degrees Target range value
λ	Scaling factor accounting for damage and ship size

The new s-factor addresses only progressive flooding and is derived on the basis of GZ_{max} and Range of the un-truncated residual stability curve. This implies that these values have not been limited to the angle in which unprotected openings are immersed but instead only the angle at which the righting lever vanishes. Such characteristics (openings) relate to local details in ship geometry that cannot be easily captured by global parameters such as properties of the residual stability curve.

In light of the derived results, a disparity was observed, which was attributed to the difference in scale in both the size of each vessel and the volume of accumulated floodwater associated with each of the respective damage cases. To account for this, it was deemed necessary to find an appropriate scaling factor. In this effort, several parameters were investigated including residual freeboard and residual volume. However, the most suitable scaling parameter was found to be the "Effective Volume Ratio"; a parameter which accounts for both the scale of the damage and that of the vessel. Therefore, the EVR is provided as follows,

$$\text{Effective Volume Ratio} = \frac{V_{residual}}{V_{flooded}} \quad (2)$$

Where, the residual volume $V_{residual}$ is provided from eq. (3) below,

$$V_{residual} = V_{WTE} - V_{Displacement} - V_{Flooded} \quad (3)$$

Where specifically,

V_{WTE}	Weathertight Envelope is the real weathertight extent and refers to the total volume of all rooms contained in the area spanning from the base line up to and including the deck at which weathertight structure spans vertically. This reflects the physical properties of the vessel.
$V_{Displacement}$	Volume displacement of a given vessel (m^3).
$V_{Flooded}$	Volume of the water in the flooded compartments at the final stage of flooding, based on static calculations.

Thus, the scaling factor (λ) is the Effective Volume Ratio of the vessel in consideration divided by 8.6 for every damage respectively. Given this, a formulation to calculate the s-factor is given by the regressed CDF of wave heights from IACS Global wave statistics. The new s-factor is provided next:

$$s\left(H_{s_{crit}}\right) = e^{-e(1.1717-0.9042\times H_S)} \quad (4)$$

Where,

Hs_{crit} critical significant wave height

[Notably, when Hs_{crit}=7m, $s\left(H_{s_{crit}}\right)$ = 1]

3. DIRECT APPROACH TO SURVIVABILITY ASSESSMENT OF CRUISE SHIPS

Background

The s-factor in SOLAS 2009 is estimated based on the assumption that the ship capsizes within half an hour exposure (Tuzcu, 2003a). This, however, is not the case with cruise ships, hence the need to ascertain the impact of time on cruise ship survivability and to account for this. The Time To Capsize (TTC), is a random variable, thus only known as a distribution determined through probabilistic methods. Moreover, survivability dependents upon a number of governing parameters (e.g. loading condition, sea state, damage extent) all of which are also stochastic in nature. In this respect, accounting only for the damage case scenarios implicit in SOLAS 2009 (typically over 1,000 for a typical passenger ship) and considering the 3 loading conditions, also implicit in these regulations, and some 10 sea states per damage case for estimating capsize rates, it becomes readily obvious that some form of simplification and reduction will be meritorious.

To this end, one of the most efficient ways, entails a process involving Monte Carlo sampling from distributions of pertinent random variables (damage extents, loading conditions, sea states, etc.) to generate damage scenarios and perform numerical time-domain simulations. The latter, accounts accurately for the physical phenomena of ship-floodwater-wave interactions as function of time providing robust indication on which of these scenarios would lead to ship capsize/sinking and the TTC. In this manner, any assumptions and approximations inherent in the probabilistic elements of SOLAS 2009 damage stability regulations are diminished/minimised.

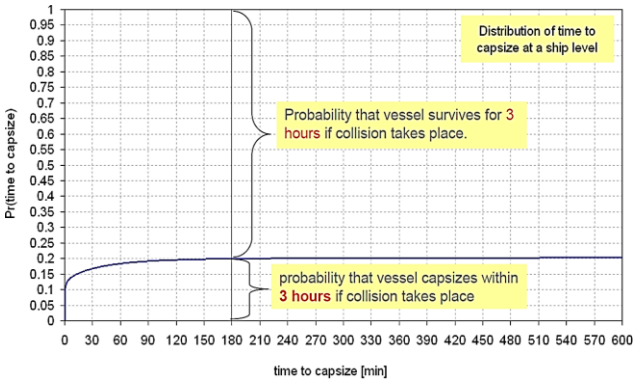

Figure 2: Cumulative marginal probability for time to capsize (Vassalos, 2015)

In the comparison of the two sets of results, it is to be noted that the Attained subdivision Index is an aggregate probability representing the average probability of survival for a set of generated damages. Hence, survivability is calculated for each damage scenario as the "expected" outcome averaged with respect to the distribution of wave heights. On the other hand, the survivability level obtained from numerical simulations (herein denoted as "Survivability Index") uses a single significant wave height sampled from pertinent wave statistics and the random outcome (survival or capsize) is then averaged across all damages and loading conditions.

$$A - I = \sum p \cdot w \cdot \bar{s} \quad (5)$$

$$S - I = \sum p \cdot w \cdot s \quad (6)$$

Monte Carlo numerical simulation methodology

Survivability can be assessed with use of time-domain simulations for a group of damages. This allows for derivation of an estimate of the expected probability of survival for a given group of damages characterised by random locations, damage extent and sea states. The Time To Capsize (TTC) can be defined through an automated process using Monte Carlo sampling (see Figure 4) and dynamic flooding simulations with the time-domain numerical simulation code PROTEUS3 (Jasionowski, 2001).

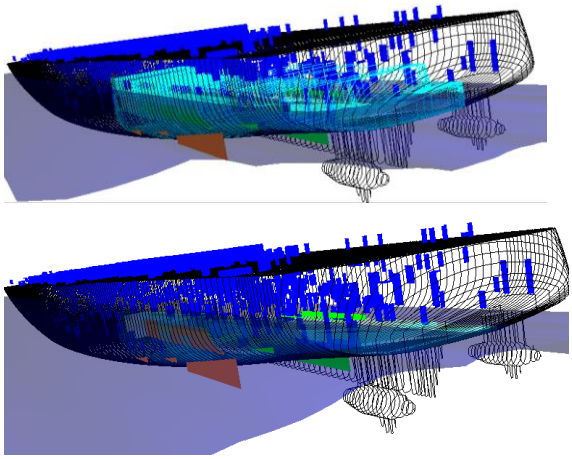

Figure 3: 3-compartment aft damage in PROTEUS3

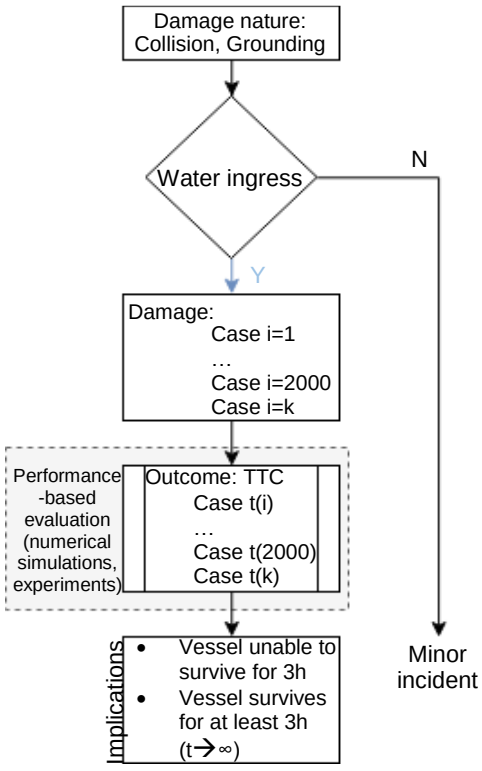

Figure 4: Monte Carlo simulation set-up

Two large cruise ships ($290 \leq L_{OA} \leq 325$) have been subjected to a number of Monte Carlo simulations for a single loading condition, namely the deepest subdivision draft. Based on previous study (Paterson et al., 2018) , cruise ships have been found to operate at the upper region of their draft distribution around the deepest subdivision draft. Significant wave heights are randomly sampled from the distribution of global wave statistics as presented in (Paterson et al., 2017), which is provided in Figure 5 below. In the case of collision scenarios, time-domain simulations were also performed in calm water, in order to ascertain the impact of waves and ship dynamics on survivability.

The total time for each simulation run is 1,820 seconds (30 minutes). The simulations are initiated after 20 seconds in order to allow for any transients to settle. This means that the damage openings are activated after 20 seconds of simulation time. Survivability is assessed not only on the basis of physical/actual capsizes (ship turns over, $\theta_{heel}>90$ deg) but also on the basis of the following three criteria:

- Capsize criteria (IITC, 2017) when the instantaneous roll angle exceeds 30 degrees or the 3-minute average heel angle exceeds 20 degrees.
- Criterion for insufficient capability of evacuation, assessing the effect of heeling angle when the angle of heel is higher or equal to 15 degrees SOLAS CH. II-1 (IMO, 2006).
- The maximum final flooding rate of mass (tons) per hour for each damage case.

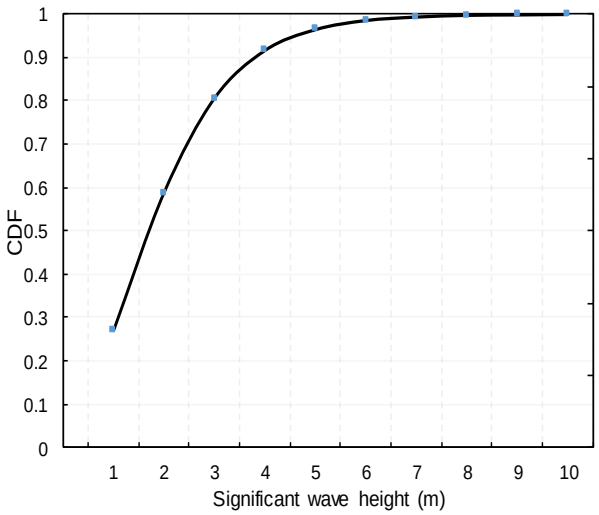

Figure 5: Cumulative distribution of the significant wave heights in the case of global wave statistics

The figures below present the damage distributions with respect to their longitudinal and transverse damage extents for each of the two vessels. The damages are sampled based on distributions, which have been derived from work presented in (Bulian et al., 2018, Zaraphonitis et al., 2013, Bulian et al., 2016). There, a probabilistic framework has been devised to account for bottom, side groundings and collisions. This overcomes the dichotomy present in SOLAS where survivability in case of collision is addressed in a probabilistic framework while the issue of grounding is addressed

in a deterministic manner. The developed approach is compatible with the SOLAS2009 conceptual framework for collision.

A total of 6,000 damages are investigated through the time domain simulations relating to 2,000 breaches for collision, side and bottom grounding, respectively for each vessel. The calm-water runs for the case of collisions were repeated for all damage case scenarios.

Numerical simulation results

The numerical simulation results are presented with indications linking these to the aforementioned failure criteria for each ship in Figure 10 below. In particular, ship A results in 72 capsizes due to collision damages, of which 19 cases are actual capsizes (26%).

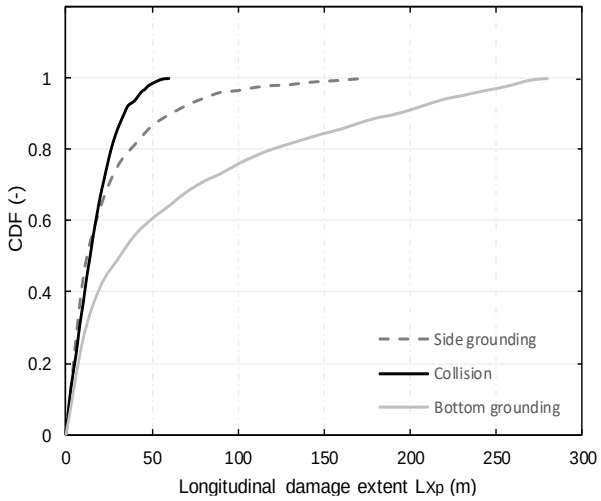

Figure 6: Cumulative distribution of the longitudinal damage extent (length) Lx,p for ship A

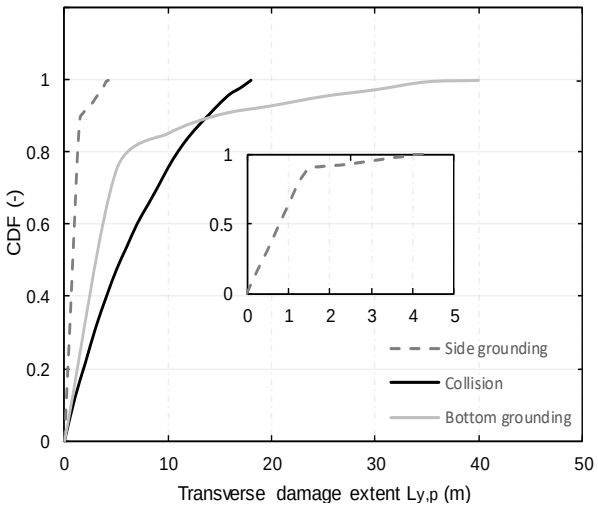

Figure 7: Cumulative distribution of the transverse damage extent (length) Ly,p for ship A

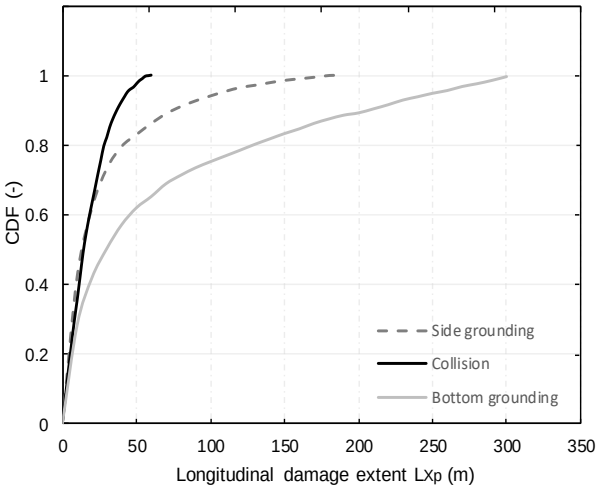

Figure 8: Cumulative distribution of the longitudinal damage extent (length) Lx,p for ship C

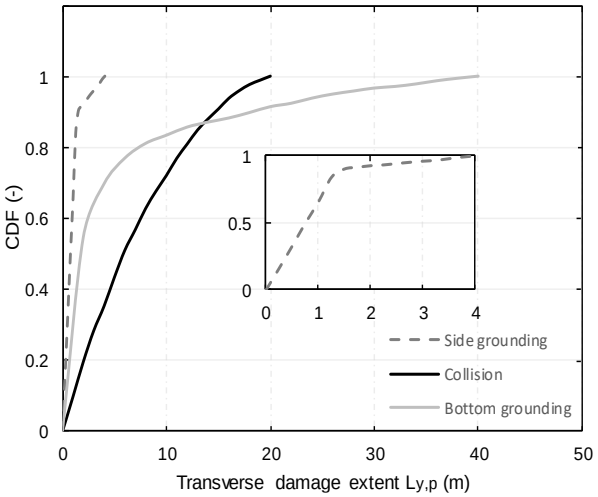

Figure 9: Cumulative distribution of the transverse damage extent (length) Ly,p for ship C

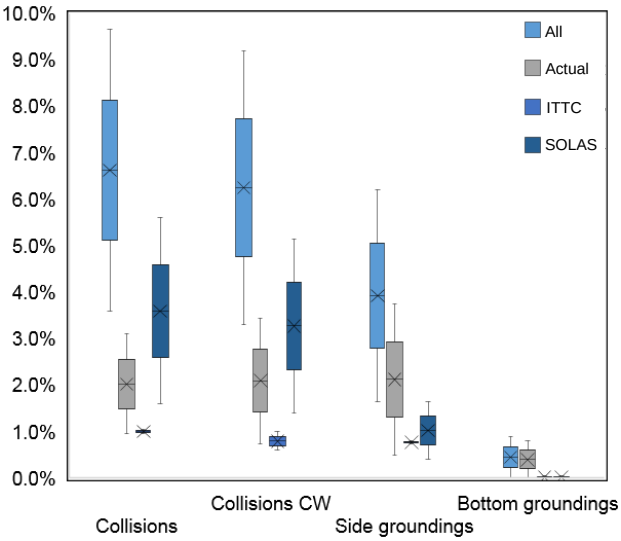

Figure 10: Quartiles of capsizes for both cruise ships for collisions in waves and Calm Water and side and bottom groundings

The cumulative distribution function for Time To Capsize in case of collision damages, based on actual capsizes, shows that the majority of capsizes occurred within the early stage of the simulations (under 5 minutes) with no cases beyond 18 minutes duration, as shown in Figure 11.

Based on these findings, the expected probability of survival as expressed by the Survivability Index lies between 0.97 and 1 with 95% confidence. However, the CDF for TTC calculated for all capsizes (i.e., actual and those violating the ITTC and SOLAS maximum heel criteria) does not stagnate, indicating that some further capsizes would be observed for longer simulation times. Nevertheless, considering the estimates based on half-an-hour runs, the average probability of surviving at least 30 minutes can be estimated to fall between 0.94 and 0.98 with 95% confidence.

The calm-water runs resulted in fewer capsizes (63 cases) when compared to collisions in waves. Specifically, three of the calm-water capsizes represent a "shift" towards more conservative failure criteria (i.e. from actual capsize to ITTC, and from ITTC to SOLAS max heel). This denotes the impact of waves on survivability assessment. In the case of side groundings, the results indicate 2% of capsize cases (33 capsizes) of which 30% represent actual capsizes. Hence, the expected probability of survival corresponds to an equivalent Attained-Index (Damage Survivability Index) of 98.3%. The simulations of Ship A for bottom groundings did not result in any capsizes or violations of the aforementioned survivability criteria. This is likely to be the result of insufficient duration of the simulations, given the slow up-flooding process. In fact, analysis of the final 3-minutes of the simulations reveals that 52 cases show significant rate of change of heel (over 2 deg/h), 2 show a rate of change of trim in excess of 1 deg/h and 39 indicate sinking at a rate of 2 m/h. Finally, in 62 cases the net floodwater inflow rate exceeded 1,000 t/h.

For the second ship, the results demonstrate that the probability of survival (1-A) for collisions corresponds to a Survivability Index of 90.35%, as indicated in Figure 13. Notably, the calm-water runs resulted in fewer capsizes (181 cases) when compared to in-waves simulations (193 cases).

Finally, the CDF of TTC for side groundings yields a Survivability Index of 93.7. In the case of bottom groundings, the simulations result in approximately 2% of capsize cases, of which 89% represent actual capsizes. In this case the cumulative probability distribution of Time To Capsize provides an Indication of Survivability Index as high as 99.1%.

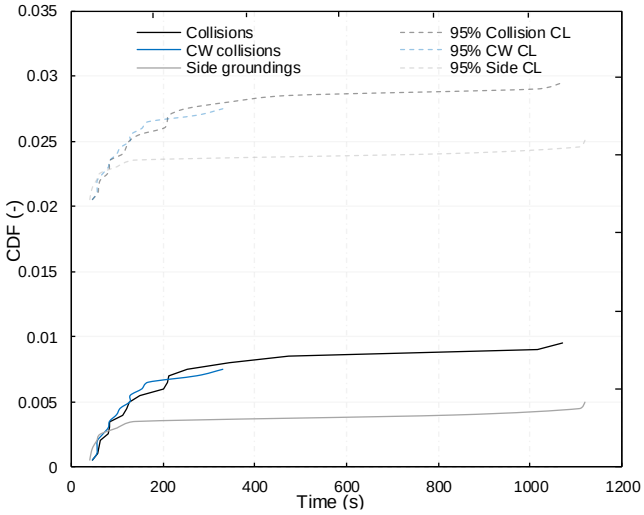

Figure 11: Cumulative probability distribution of Time To Capsize for collisions – actual capsizes (ship A).

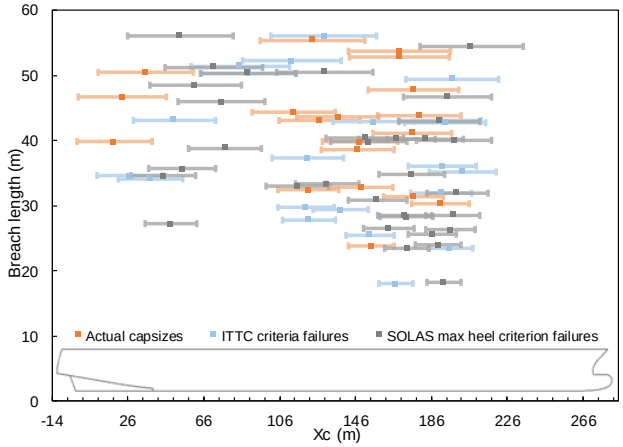

Figure 12: Distribution of critical collision damages along the length of ship A with indication of actual capsizes and cases that failed the ITTC and SOLAS criteria

The calm-water runs provide an interesting insight on the impact of waves showing that a significant number of capsizes were either missed in the calm water runs or would fail only the more conservative criteria. One of the main implications of this is that the impact of waves should be explored in more detail, which could be achieved by testing individual damages in a range of wave heights, preferably with multiple repetitions per wave height. Such approach would be an extension to the methodology employed for deriving the s-factor (based on capsize band).

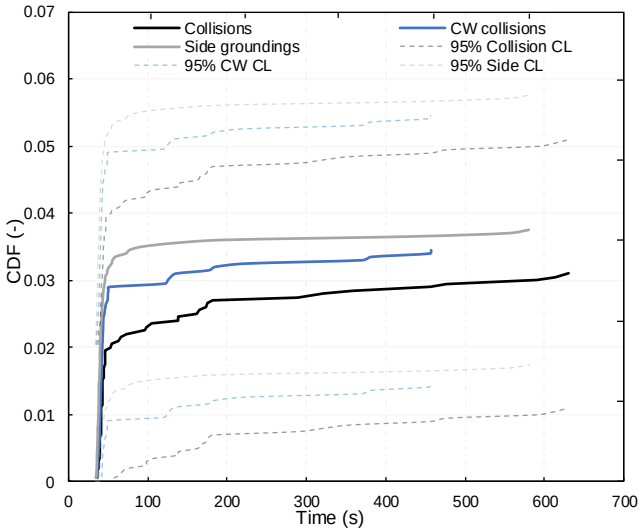

Figure 13: Cumulative distribution function of TTC – actual capsizes in collision damages (ship C)

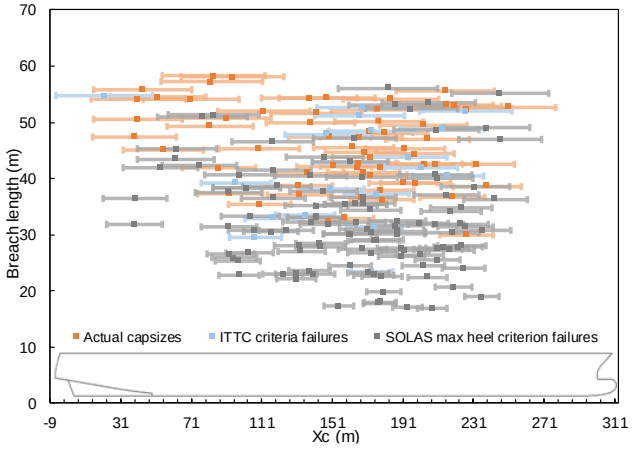

Figure 14: Distribution of critical collision damages along the length of ship C with indication of actual capsizes and cases that failed the ITTC and SOLAS criteria

Comparison between Direct and Statistical approaches

In light of the numerical results, a comparison is conducted between the static calculations linked to the statistical approach and numerical simulations as shown in Figure 15 and Figure 16, respectively, linked to the Direct Method, for both cruise vessels. Figure 15 demonstrates the impact on the Attained Subdivision Index using three different formulations namely, the current SOLAS s-factor, the non-zonal average survivability model with the current s-factor and finally the non-zonal average survivability model with the new eSAFE s-factor. In addition, Figure 16 presents the obtained survivability levels through dynamic simulations in two ways; conditionally through employing all criteria and solely actual capsizes.

On the basis of the foregoing, the newly developed survivability factor is found to underestimate survivability of cruise ships in collision damages. Cruise ships have demonstrated resistance to capsize in waves higher than 5 meters (Maximum 8m) and the prevailing s-factor does not reflect this. Numerical simulation results are consistent with the static calculations. In particular, both methods identify the same vulnerable locations along the ship. However, the numerical simulation results indicate higher survivability than the static calculations. The discrepancies in expected survivability levels are particularly large in grounding scenarios. This is likely due to relatively short simulation durations given the slowly developing up-flooding. In general, it is understood that the time-domain simulations of flooding within complex geometries require significantly longer simulation runs. Notwithstanding this, the gap between the simulation results and static calculations has been significantly reduced, in comparison to earlier results.

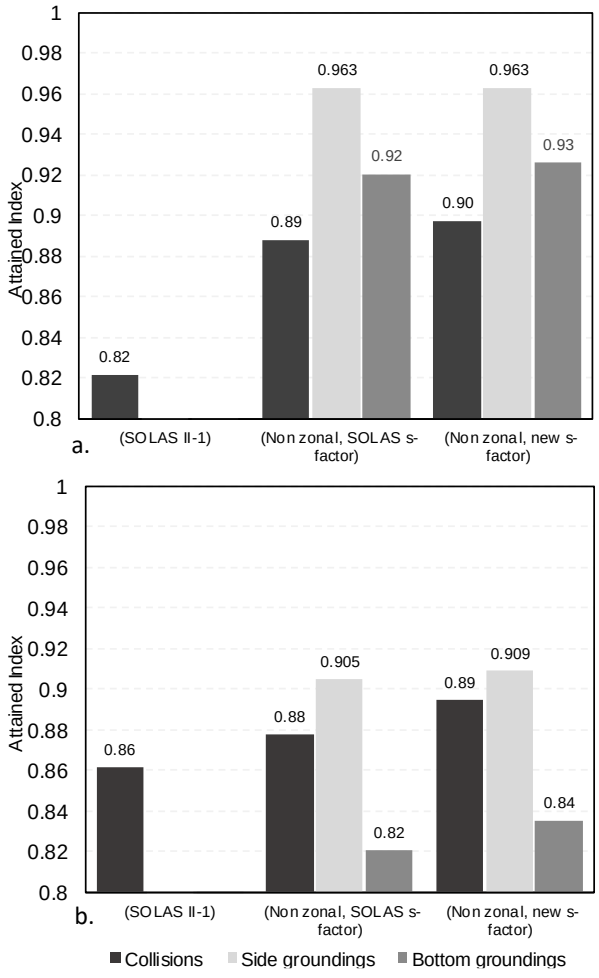

Figure 15: Comparison of survivability based on static calculations for: a.) Ship A b.) Ship C

Generally, the results represent significant steps forward in understanding flooding events, although, the differences between SOLAS Attained subdivision Index and expected survivability levels (Survivability Index), based on simulations, cannot yet be fully explained and further work is needed in this direction.

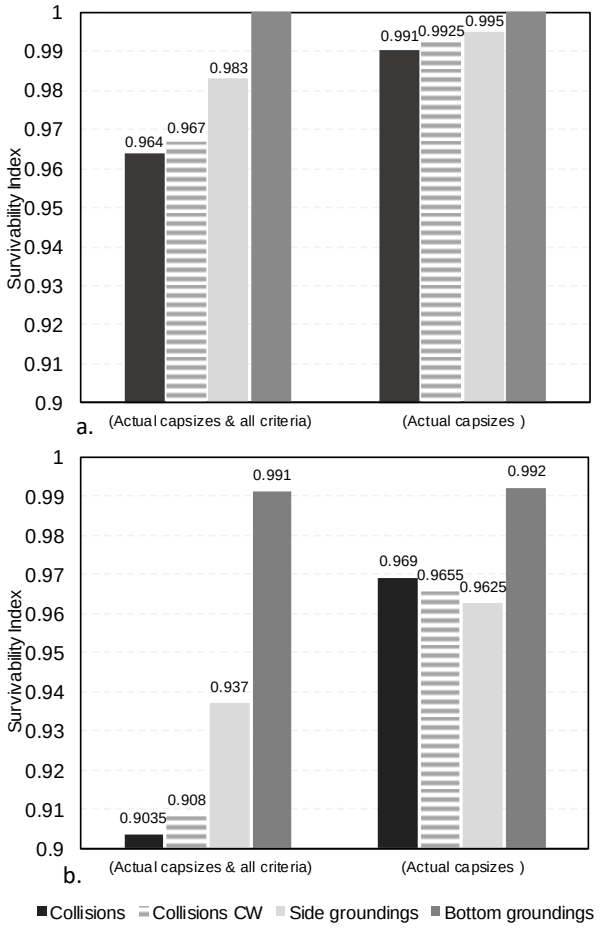

Figure 16: Comparison of survivability based on simulations for ship for: a.) Ship A b.) Ship C

4. CONCLUDING REMARKS

On the basis of the aforementioned work, a new s-factor is being proposed specifically for cruise ships and a critical Hs formulation applicable to ships in service world-wide. In addition, a comparison has been conducted between Statistical (SOLAS) and Direct (numerical time-domain simulations) approaches on survivability through time-domain numerical simulations, on the basis of which the following conclusions can be drawn:

- The results demonstrate that survivability does depend on sea state and a relationship that is cruise-ship specific has been derived, linking Hs-critical to characteristics of the residual GZ curve, namely Range and GZ_{max}.
- Similarly to the GOALDS project, where the residual intact volume following flooding was used as a parameter within the s-factor formulation, results also indicate that ship size and amount of floodwater are linked to survivability, meaning that survivability in cruise ships is affected by scale. As such, a suitable scaling factor depending on both floodwater volume and residual volume has been derived.
- Dynamic time-domain flooding simulations provide an effective means for screening flooding scenarios, likely to lead to vessel loss. At the same time, they offer additional information to address the ensuing potential risk at a forensic level not afforded by static calculations.
- The numerical simulation results indicate higher survivability than the static calculations. The discrepancies in expected survivability levels are particularly large in grounding scenarios. This is likely due to relatively short simulation durations given the slowly developing up-flooding.
- Overall, the gap between the simulation results and static calculations has been significantly reduced. In this respect, the results obtained in the eSAFE Project represent significant steps forward in understanding flooding events.
- Through this work, it has been understood that the survivability level of cruise ships is considerably higher than that postulated by rules and there is now clearer understanding why this is the case.

5. ACKNOWLEDGEMENTS

This work was carried out in the framework of the project “eSAFE – enhanced Stability After a Flooding Event – A joint industry project on Damage Stability for Cruise Ships”. The funding partners of eSAFE are alphabetically: Carnival Corporation Plc, DNV GL, Fincantieri, Lloyd’s Register, Meyer Werft, RINA Services, Royal Caribbean Cruises Ltd. and STX France. The financial support from the eSAFE funding partners is acknowledged. The authors would like to express their gratitude to all the partners in eSAFE project for their constructive criticism and help in the undertaking of this invaluable research.

6. DISCLAIMER

The information and views as reported in this paper are those from the authors and do not necessarily reflect the views of the eSAFE Consortium.

REFERENCES

Bulian, G., Cardinale, M., Francescutto, A. & Zaraphonitis, G. Complementing SOLAS framework with a probabilistic description for the damage extent below water. Proceedings of the 13th International Conference on the Stability of Ships and Ocean Vehicles, 2018 Kobe, Japan.

Bulian, G., Lindroth, D., Ruponen, P. & Zaraphonitis, G. 2016. Probabilistic assessment of damaged ships survivability in case of grounding: development and testing of a direct non-zonal approach. Ocean Engineering, 120, 331-338.

Cichowicz, J., Tsakalakis, N., Vassalos, D. & Jasionowski, A. 2016. Damage survivability of passenger ships - Re-engineering the safety factor. Safety MDPI, 2.

GOALDS 2009-2012. Goal-based Damage Stability", Project funded by the European 13th Commission, FP7- DG Research, Grant Agreement 233876.

HARDER 1999-2003. Harmonization of Rules and Design Rational". Project funded by the European Commission, DG XII-BRITE.

IITC 2017. ITTC Quality System Manual, recommended procedures and guidelines. Procedures: Numerical simulation of capsize behaviour of damaged ships in irregular seas 7.5-02-07-04.4, Specialist committee on stability in waves of the 28th ITTC.

IMO 2006. MSC 82/24 Adoption of amendments to the international convention for the safety of life at sea, Resolution MSC 216 (82). London.

IMO 2009. SOLAS (Safety of Live at Sea) consolidated edition 2009. London.

Jasionowski, A. 2001. An integrated approach to damage ship survivability assessment. PhD Thesis, University of Strathclyde.

Papanikolaou, A., Hamann, R., Lee, B., Mains, C., Olufsen, O., Vassalos, D. & Zaraphonitis, G. 2013. GOALDS- GOAL Based damage ship stability and safety standards. Accident analysis and prevention, 60, 353-365.

Paterson, D., Atzampos, G., Vassalos, D. & Boulougouris, E. Impact of wave statistics on ship survivability. Proceeding of the 16th International Ship Stability Workshop, 2017 Belgrade, Serbia.

Paterson, D., Vassalos, D., Atzampos, G., Boulougouris, E., Cichowicz, J. & Luhmann, H. Rebooting SOLAS - Impact of drafts on damage survivability of cruise ships. Proceedings of the 13th International Conference on the Stability of Ships and Ocean Vehicles, STA2018, 2018 Kobe, Japan.

Tsakalakis, N., Cichowicz, J. & Vassalos, D. The capsize band concept revisited. Proceedings of the 11th International Ship Stability Workshop, ISSW, 2010 Wageningen, Netherlands. 262-271.

Tuzcu, C. Development of factor s: the damage survival probability. 8th International Conference on the Stability of Ships and Ocean Vehicles, STAB, 2003a Madrid.

Tuzcu, C. 2003b. A unified approach to determining the damage survival factor. PhD Thesis, University of Strathclyde.

Vassalos, D. Damage stability of cruise ships - evidence and conjecture. 12th International Conference on the Stability of Ships and Ocean Vehicles, STAB2015, 2015 Glasgow.

Zaraphonitis, G., Bulian, G., Lindroth, D., Luhmann, H., Cardinale, M., Routi, A.-l., Bertin, R. & Harper, G. 2013. Evaluation of risk form ranking damages due to grounding, EMSA/OP/10/2013 report 2015-0168. DNV-GL.

A pragmatic approach to roll damping

Jakub Cichowicz, University of Strathclyde, jakub.cichowicz@strath.ac.uk
Dracos Vassalos, University of Strathclyde, d.vassalos@strath.ac.uk

ABSTRACT

Roll damping is probably the most intriguing of the components of hydrodynamic reaction in ship dynamics. It is also a problematic one - small, nonlinear, difficult to predict or measure and key determinant of ship stability. Without question, some of the problems faced in calculating or measuring roll damping are intrinsic. It can be argued, however, that most of the difficulties do not originate from physical anomalies of energy dissipation in roll but are due to fundamental flaws in the approach to roll damping estimation or measurement. The root causes of these flaws stem from three concepts, central to analysis of hydrodynamic reaction in roll: decomposition of the hydrodynamic reaction moment to added moment of inertia and roll damping moment, the assumption of small-amplitude motions and the inevitable coupling to other modes of motion. In this paper, the authors present a pragmatic approach to these fundamental concepts and discuss the implication of wrong assumptions, pertaining to definition, measurement, calculation and use of roll damping in intact and damaged ship dynamics.

Keywords: *roll motion, damping, hydrodynamics.*

1. MOTIVATION

The motivation and content for this paper derives from some of the journal and conference articles on roll damping published in recent years. Focusing only at the STAB papers and the most recent research projects, it is apparent that roll damping, as a research topic, attracts considerable attention. The problems addressed by researchers vary from uncertainty assessment in deriving critical damping from roll decay tests, estimation of damping from roll decay or forced roll (Wasserman). Both numerical and physical experiments are often conducted to the highest of standards with the help of sophisticated hardware and the most advanced analytical techniques. Unfortunately, it appears that many of the experiments on hydrodynamics of roll motion put emphasis on technicalities rather than the actual physics of the problem. Consequently, in spite of the perfect execution, the experiments per se are ill conditioned. Hence, whilst numbers are produced with remarkable efficiency and accuracy understanding of the nature of the problem is not being advanced. In the pursuit for finding a perfect solution, the fact that that effort has been expended on solving the wrong problem has been overlooked. In this respect, it is a good opportunity to have a more pragmatic view at the problem in hand.

2. THE EXPERIMENT

The following discussion is based on the physical experiments conducted in 2009/2010 at the Kelvin Hydrodynamic Laboratory of the Department of Naval Architecture, Ocean and Marine Engineering of the University of Strathclyde. The main objective of the experiments involved determining the hydrodynamic reaction in harmonic roll motion of an unconstrained cylindrical body forced to oscillate in calm water by an internal gyroscopic apparatus. The measurements, conducted in intact and damaged conditions were reported in (Cichowicz, 2012)

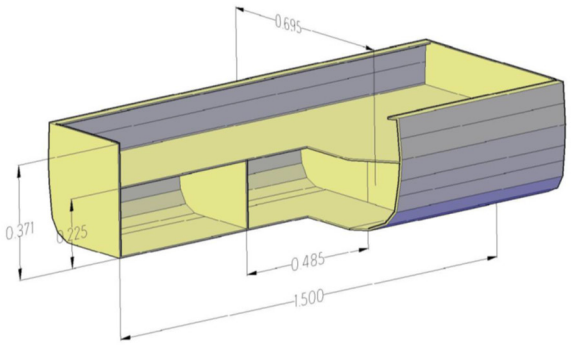

Figure 1: Main particulars of the tested cylinder

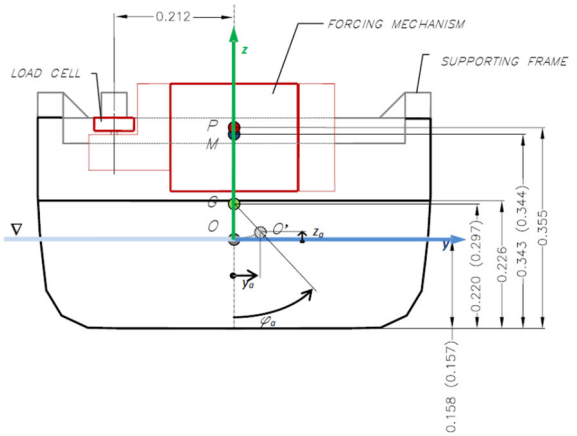

Figure 2: Schematic view of the model configuration

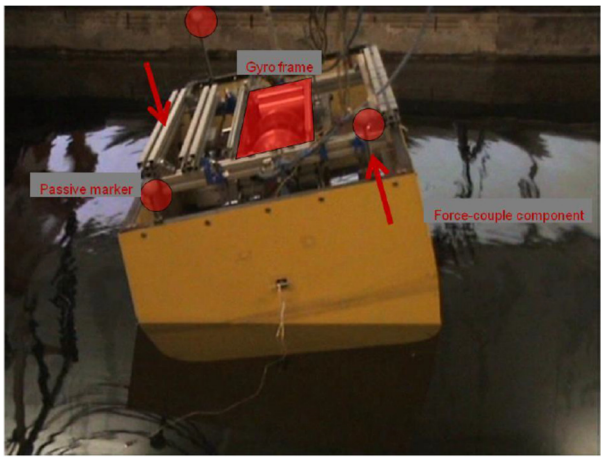

Figure 3: Photograph of the model taken during the test in intact condition

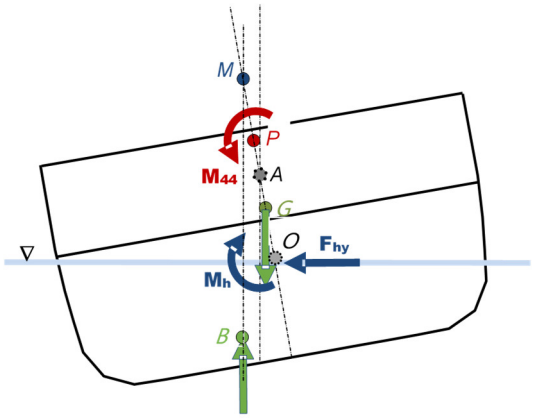

Figure 4: Free body diagram of the system under consideration

3. MATHEMATICAL MODELLING

Figure 4 shows a free-body diagram of the system under consideration. Given its cylindrical shape, the body (symmetrical with respect to centre-plane and midship-section) the system is represented as a 3DoF harmonic oscillator with the sway and heave motions resulting from coupling with roll (i.e. sway and heave are roll-induced). It is noteworthy, however, that due to the shape of the body and relatively small amplitudes of motions, the contributions from have were considered insignificant and for that reason the system could be simplified to 2DoF.

The moment to sustain motion, M_{44} ,was generated by an internal gyroscopic device pivoted about the point P. A single axis load-cell afforded the coupling between the forcing apparatus and the hull. The hydrodynamic reaction was expressed as a hydrodynamic moment, M_h and the force F_{hy} (introduced to capture the reaction due to the roll-into-sway coupled motion). The coupled motion was accounted for by the following condition

$$y_A(t) = y(t) - \overline{OA} \cdot \varphi(t) = \\ = y_a \sin(\omega t + \varepsilon_y) \\ - \overline{OA} \cdot \varphi_a \sin(\omega t + \varepsilon_\varphi) \quad (1)$$

The term $y_A(t)$ in (1) represents the lateral displacement of the instantaneous axis of rotation, $\overline{OA}$ is the elevation of the instantaneous axis of rotation above the waterplane, φ_a and y_a denote amplitudes of roll and roll-induced-sway, respectively, while ε_φ and ε_y stand for phase lags of the related motions (with respect to M_{44}), ω is circular frequency of oscillations and t, is time. It is noteworthy that the above expression would vanish if the roll and roll-induced-sway were in phase, i.e. if$\varepsilon_\varphi = \varepsilon_y$.

Given that the external moment (moment to sustain motion) was measured about the point P, it was convenient to express the equations of motion about this point as well. The system of two scalar equations of motions corresponding to the free-body diagram from Figure 4 is given below

$$a_{22}\ddot{y} + a_{24}\ddot{\varphi} + b_{22}\dot{y} + b_{24}\dot{\varphi} \\ = -m(\ddot{y} - \overline{OA} \cdot \ddot{\varphi})$$

$$a_{22}\ddot{y}\,\overline{OP} + a_{24}\ddot{\varphi}\,\overline{OP} + a_{42}\ddot{y} + a_{44}\ddot{\varphi} \\ + b_{22}\dot{y}\,\overline{OP} + b_{24}\dot{\varphi}\,\overline{OP} + b_{42}\dot{y} + b_{44}\dot{\varphi} \\ = M_{44} - (I_{44} + m\,\overline{AG}^2)\ddot{\varphi} - c_{44}\varphi \\ - \; m(\ddot{y} - \overline{OA} \cdot \ddot{\varphi})\,\overline{AP} \quad (2)$$

4. ANALYSIS

The system of equations given by (2) is constructed without any specific simplifications or assumptions (e.g., with respect to symmetry of the coefficients) and contains eight unknown hydrodynamic coefficients. Since the condition (1)

may be interpreted as kinematic constraint, Lagrange's multipliers were chosen as the method to derive the hydrodynamic coefficients from the underdetermined system of equations of motion. The results of the analysis are presented in more detail in the following paragraphs.

Phase difference between roll and roll-induced sway

The results of measurements in both intact and damaged conditions, show clearly a measurable phase difference between roll and roll-into-sway motions (i.e. difference in phase angles measured with respect to moment M_{44}). The phase difference is particularly large in case of damaged hull at the sloshing resonance frequency (around 6.5 rad/s in this experiment) where it indicates strong damping effect in the roll-into-sway coupled mode of motion (Figure 5).

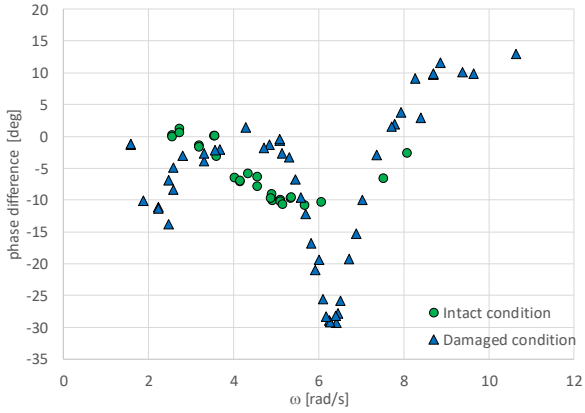

Figure 5: Phase difference between roll-into-sway and roll motion.

An immediate consequence of the relatively strong damping in roll-into-sway coupled mode of motion is that the inertia term of the sway equation in (2) does not vanish and the following paragraphs will show that this has some other, more significant, implications.

Hydrodynamic coefficients

Application of Langrange's multipliers method to the underdetermined system (2) gave rather interesting results, namely that:

- the sway coefficients a_{22} and b_{22}vanish in intact condition
- in damaged condition a_{22} and b_{22} vanish in the entire frequency range except the relatively narrow band around and beyond sloshing resonance
- the sway-into-roll coefficients a_{42} and b_{42}vanish in intact condition
- in damaged condition the coefficients a_{42} and b_{42} practically vanish outside the narrow bad around the sloshing frequency
- the roll (a_{44} and b_{44}) and roll-into-sway (a_{24} and b_{24}) coefficients are well determined across the entire frequency range

It is noteworthy that in the case of intact hull all the coefficients that vanish are those associated with the pure sway and sway-into-roll modes of motions, i.e. the motions that were not induced by the forcing device. The same holds for the damaged hull but only in the regions outside the sloshing resonance. Based on the above observations it can be concluded that the mathematical model given by (2) adequately describes motions of intact hull in the entire range of frequencies and the damaged hull outside the range of sloshing resonance. Furthermore, during the oscillations within the range of frequencies, close to sloshing resonance, the damaged ship experienced significant, constant velocity, drift. For this reason, the lateral displacement of the flooded hull was described as a linear combination of the translation in direction of the y-axis and harmonic oscillations i.e.$y(t) = v_d t + y_a \sin(\omega t + \varepsilon_y)$, where v_d stands for the constant drift velocity.

Axis of rotation

Un unconstrained body forced to roll in calm water-plane will oscillate about the so-called natural axis of rotation. This natural axis is instantaneous but herein, due to relatively small amplitudes and negligible heave motion, its eleveation is assumed constant throughout the entire cycle (at a given frequency). What is important, however, is that the elevation changes substancially across the frequency range, which is particularly well noticeable in the case of the damaged ship.

An analysis presented in (Balcer, 2004) shows that the location (i.e., elevation above the water plane) of the ship natural axis of rotation is a function of mass distribution within the oscillating system, comprising hull and the fluid domain (i.e. it is passing through the centre of mass of the entire system)

$$\overline{OA} = \frac{m\,\overline{OG} - a_{24}}{m + \delta m} \qquad (3)$$

In the original paper, sway added mass,a_{22}, was shown as parameter δm. Considering, however, that the sway added mass vanish everywhere except the range of sloshing resonance of the damage ship it was necessary to replace it with a more suitable parameter in order to balance the equation. It was achieved by taking the measured elevation $\overline{OA}$ together with the a_{24} term, determined from the measurements and solved forδm. The results of this exercise show that the mass of the hull can reasonably well approximate the parameter δm across the entire frequency range except the range of sloshing frequency of the flooded hull (Figure 7). Obviously, it can be clearly seen that neither (3) nor (4) contain all the parameters needed to describe the elevation of the axis of rotation, which must depend on other coefficients as well.

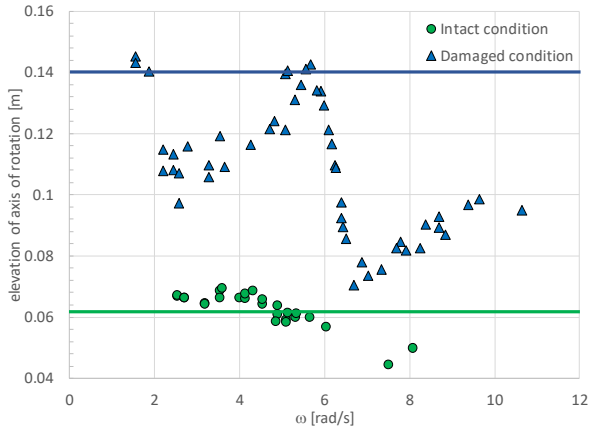

Figure 6: Elevation of axis of rotation above the calm water-plane

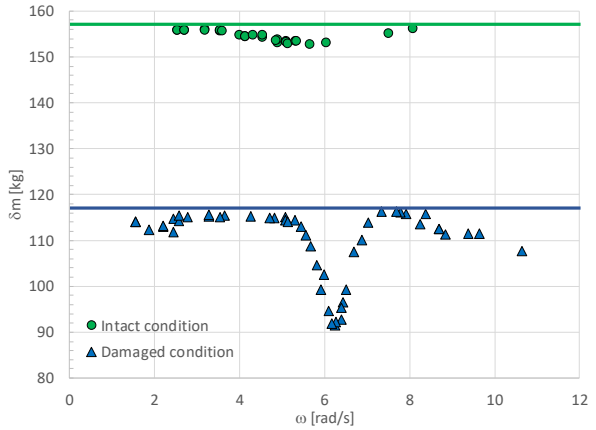

Figure 7: Comparison of the parameter δm as in (3) and the mass of the hull in intact and damaged conditions (solid lines)

Nevertheless, Figure 8 shows that outside of the sloshing resonance, the predicted elevation matches the measurements well. Hence, for the purpose of the following discussion it can be assumed that (4) describes the elevation of axis of rotation with satisfactory accuracy.

$$\overline{OA} = \frac{m\,\overline{OG} - a_{24}}{2m} \qquad (4)$$

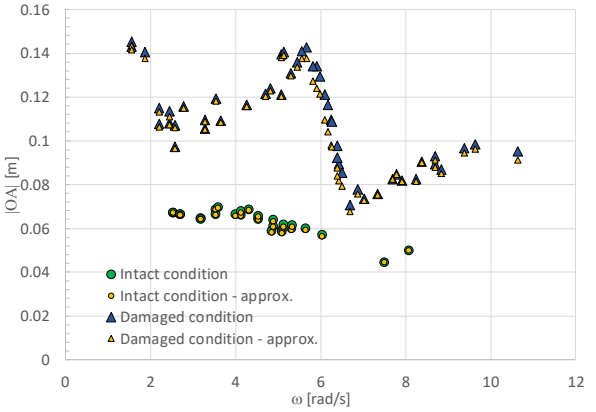

Figure 8: Comparison of measured and approximated by (4) elevation of the axis of ration.

5. SYNTHESIS

Whilst the discussion thus far has been centred about rather fragmented observations. These clearly indicated that

- Roll-induced sway is not exactly in phase with roll because of damping of in the coupling of roll-into-sway. As a result, the body is undergoing sideways motions (and the hydrodynamic reaction F_{hy} does not vanish) even if the external excitation has a form of pure moment.
- Elevation of the natural axis of rotation is determined by the mass of the body, its vertical centre of gravity and the added mass of roll-into-sway. Consequently, the elevation is a function of frequency of oscillation.
- The simple mathematical model of (2) remains valid even in the case of damaged hull, provided that the drift velocity is properly accounted for.

In order to synthesise this evidence, it is most convenient to look at the intact hull first and to subsequently attempt to extrapolate the findings for the damaged hull.

Firstly, it can be recalled that, according to Lagrange's multipliers method, all sway and sway-into-roll coefficients vanish from the intact ship equations of motions. Thus, the system (2) assumes the following, simplified form:

$$a_{24}\ddot{\varphi} + b_{24}\dot{\varphi} = -m(\ddot{y} - \overline{OA}\cdot\ddot{\varphi})$$

$$\begin{aligned} &a_{24}\ddot{\varphi}\,\overline{OP} + a_{44}\ddot{\varphi} + b_{24}\dot{\varphi}\overline{OP} + b_{44}\dot{\varphi} \\ &= M_{44} - (I_{44} + m\,\overline{AG}^2)\ddot{\varphi} - c_{44}\varphi \\ &- m(\ddot{y} - \overline{OA}\cdot\ddot{\varphi})\,\overline{AP} \end{aligned} \quad (5)$$

Taking advantage of the orthogonality, the equations can be expanded at the instant where $\omega t + \varepsilon_\varphi = 0$ and consequently $\ddot{\varphi}$ and φ vanish. At this instant it is implied that $M_{44} = M_{44a}\sin(\varepsilon_\varphi)$, $\dot{\varphi} = \varphi_a\omega$ and $\ddot{y} = -y_a\omega^2\sin(\varepsilon_y - \varepsilon_\varphi)$. Consequently, the equations of motion take the following form:

$$b_{24}\varphi_a\omega = my_a\omega^2\sin(\varepsilon_y - \varepsilon_\varphi)$$

$$\begin{aligned} &(b_{24}\overline{OP} + b_{44})\varphi_a\omega \\ &= -M_{44a}\sin(\varepsilon_\varphi) \\ &+ my_a\omega^2\sin(\varepsilon_y - \varepsilon_\varphi)\,\overline{AP} \end{aligned} \quad (6)$$

Considering that roll amplitudes are small or moderate, it is implied that $y_a = \overline{OA}\sin\varphi_a \cong \overline{OA}\varphi_a$ and the sway equation ca be expressed as:

$$b_{24} = m\,\overline{OA}\,\omega\sin(\varepsilon_y - \varepsilon_\varphi) \quad (7)$$

Following similar procedure, allows for expressing the second (moment) equation as follows:

$$\begin{aligned} &(b_{24}\overline{OP} + b_{44})\varphi_a\omega \\ &= -M_{44a}\sin(\varepsilon_\varphi) \\ &+ m\overline{OA}\varphi_a\omega^2\sin(\varepsilon_y - \varepsilon_\varphi)\,\overline{AP} \end{aligned} \quad (8)$$

However, it can be noted that the second term on the RHS of the above equation is simply $b_{24}\varphi_a\omega\overline{(AP)}$. Hence, after a simple rearrangement, the moment equation can be given as:

$$b_{44} = \frac{-M_{44a}\sin(\varepsilon_\varphi)}{\varphi_a\omega} + b_{24}(\overline{AP} - \overline{OP}) \quad (9)$$

However, since $\overline{AP} = \overline{OP} - \overline{OA}$, the above equation can be further simplified, as shown next.

$$b_{44} = \frac{-M_{44a}\sin(\varepsilon_\varphi)}{\varphi_a\omega} - b_{24}\overline{OA} \quad (10)$$

At a first glance, there is nothing particularly remarkable about this equation. However, when combined with (7), it yields

$$b_{44} = \frac{-M_{44a}\sin(\varepsilon_\varphi)}{\varphi_a\omega} - m\,\overline{OA}^2\omega\sin(\varepsilon_y - \varepsilon_\varphi) \quad (11)$$

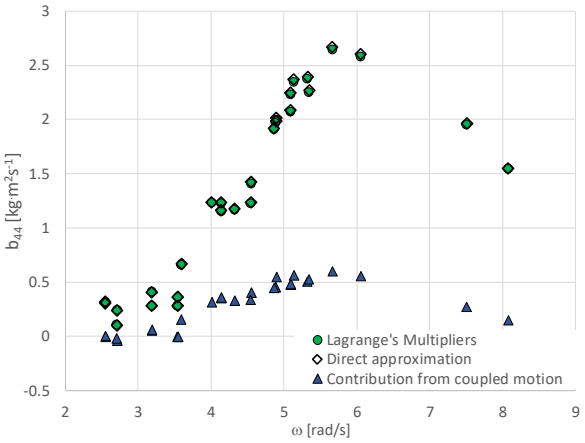

Figure 9 Comparison between b_{44} estimated by the Langrange's multipliers method as approximated by (11) for intact hull. The contribution from coupled roll-into-sway is represented by triangles.

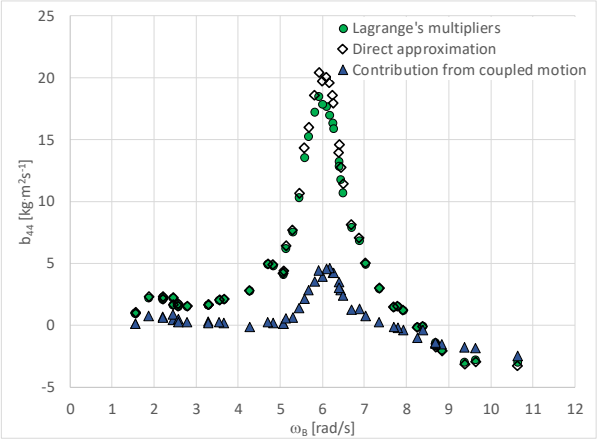

Figure 10 Comparison between b_{44} estimated by the Langrange's multipliers method and approximated by (11) for flooded hull. The contribution from coupled roll-into-sway is represented by triangles.

The results presented in Figure 9 and Figure 10 show very good agreement between the roll damping coefficient derived by Lagrange's multipliers method and approximated by (11) for both intact and flooded hull. In case of the flooded ship, direct approximation overestimates the damping in the range of flooding resonance.

6. ERRORS AND UNCERTAINTY

With roll damping being such a small quantity and of such complex composition, any inaccuracies in measurements in model experiments, particularly linked to the restoring/inertia moments will have a large impact on the value of the hydrodynamic coefficient being derived. Specifically, the uncertainty study reported in

(Cichowicz, Jasionowski, & Vassalos, 2011) and elaborated further in (Cichowicz, 2012) shows clearly that restoring coefficient, amplitude of external moment and hull inertia are dominant contributors to the uncertainty in estimates of roll added inertia (Figure 11). In the case of roll damping coefficient the key contribution comes from the phase angle between the excitation and response with some measurable impact from the magnitude of the forcing moment (Figure 12)

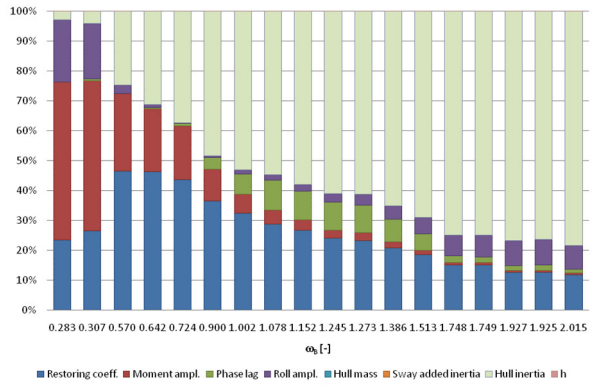

Figure 11 Relative contributions to the total error in a_{44} coefficient

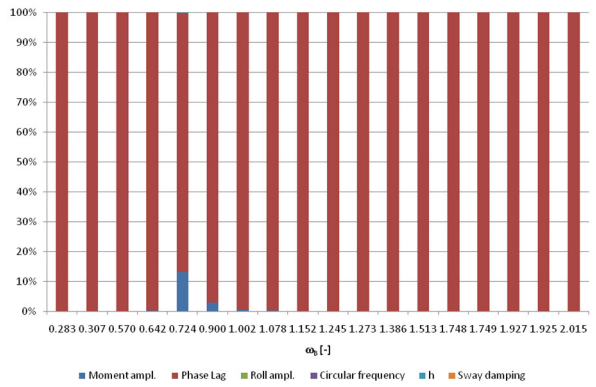

Figure 12 Relative contributions to the total error in b_{44} coefficient

7. CONCLUDING REMARKS

- Coupling of roll into sway affects roll damping through the square of the elevation of natural axis of rotation (eq. (11)).
- The elevation of axis of rotation depends on the added mass coefficient a_{24}, thus any hull fitting changing substantially the pressure distribution around the hull (i.e. added moment of inertia) such as bilge keels, will change the elevation of natural axis of rotation.
- Forcing roll motion about an arbitrary axis $\overline{OR}$, will have a strong impact on the dynamic equilibrium of the system, thus introducing additional forces necessary to maintain the constraints $\overline{OR} \neq \overline{OA}$ and $\varepsilon_y = \varepsilon_\varphi$. Since both constraints are dependent on a_{24} the forces to maintain this constraint will be affected by bilge keels, thus leading to nonlinear changes in roll damping.
- All roll and roll-into-sway coefficients can be derived from the forced-roll experiments on a floating body through (5), (7) and (11).

REFERENCES

Balcer, L. (2004). Location of ship rolling axis. *Polish Maritime Research*, 3-7.

Cichowicz, J. (2012). *Hydrodynamics of an Unconstrained Cyllinder in Forced Roll.* Glasgow: University of Strathclyde.

Cichowicz, J., Jasionowski, A., & Vassalos, D. (2011). Uncertainty Assessment in Experiments on a Floating Body in Forced Roll. *International ship Stability Workshop*. Washington DC.

Curve fit estimate of roll damping for high damping cases

Timothy Smith, *Naval Surface Warfare Center Carderock Division,* timothy.c.smith1@navy.mil

ABSTRACT

Free decay roll damping experiments at forward speed are more difficult to perform than at zero speed. The resulting roll time history often has more noise and fewer peaks to analyze to determine the roll damping. As a result, conventional roll damping analysis methods based on successive peaks produces just a few data points per run with high uncertainty. A curve fitting approach to data analysis is demonstrated for the analysis of highly damped free roll decay experiments.

Keywords: *roll damping, digital filtering.*

1. INTRODUCTION

Zero speed roll decay tests can be performed with a high degree of precision and control of initial conditions (Katayama et al., 2018; Oliva-Remoal et al., 2018; Sumislawski et al., 2018). Due to relatively low damping, often between 5-15% of critical damping, many oscillations exist to analyze and determine the roll damping. With forward speed, the roll damping increases due to hull and appendage lift. This is not necessarily a problem for forced rolling experiments where the model is excited by moving weights or gyroscopes. The roll damping analysis of forced rolling experiments does not depend on decreasing peaks. However, for free roll decay experiments, the increased damping results in fewer peaks to analyze requiring more data to define the roll damping behavior. Also, exciting the model to an initial roll angle with an external stimulus is difficult with a moving target.

Park et al. (2009, 2016, 2017) and Smith (2018) have both presented curve fitting approaches to roll decay analysis that would be appropriate for higher damping cases. Park et al. fits a decaying sine function to the entire time history to determine the roll damping coefficient and natural roll frequency. This is a linearization of the roll damping. Analysis of many time histories with varying initial conditions and model speed determines the dependency on roll angle and speed. Smith (2018) follows a similar approach but curve fits the decaying sine function to each cycle or oscillation. This produces more data points per run; the same number of points per run as peak-based analysis.

Though not often performed, pitch damping experiments are also instances of highly damped oscillations. Often only a single oscillation occurs for conventional monohulls. Figure 1 is an example of a pitch decay after a sensor polarity check. The conventional peak based analysis is not necessarily possible. A curve-fitting approach is an attractive alternative.

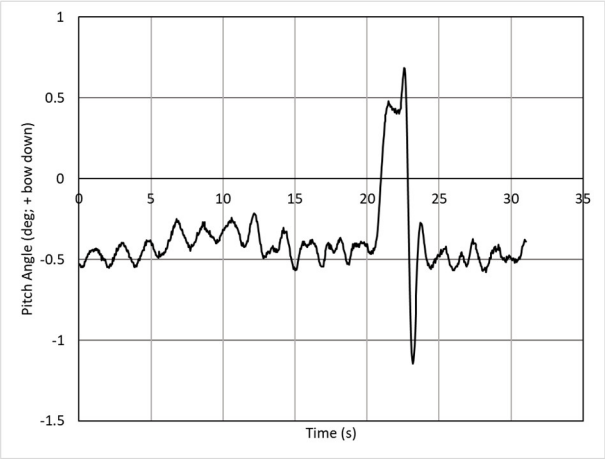

Figure 1: Example pitch decay with model held bow down and released.

A curve fitting approach will be demonstrated with simulated and actual time histories for highly damped conditions. The amount of data required for the curve fit is investigated. The use of a different curve fit function is shown for over damped cases.

2. NONLINEAR ROLL EQUATION

Synthetic data with noise was generated with a single degree-of-freedom differential equation having quadratic damping and cubic restoring (Smith, 2018; Vassilopoulos, 1971, Dalzell, 1978).

The single degree of freedom linear roll equation is a simple harmonic oscillator; Equation (1).

$$(I_{44} + A_{44})\ddot{\varphi} + B_{44\_l}\dot{\varphi} + C_{44}\varphi = 0 \quad (1)$$

$$C_{44} = GMg\Delta \quad (2)$$

where I_{44} is the roll mass moment of inertia, A_{44} is the roll added mass, B_{44_l} is linear roll damping, and C_{44} is linear hydrostatic stiffness, GM is the metacentric height, g is the acceleration due to gravity, and Δ is the ship displacement.

Re-writing Equation 1 in standard form results in Equation 3 (Karnopp, 1974)

$$\ddot{\varphi} + 2\zeta\omega_n\dot{\varphi} + \omega_n^2\varphi = 0 \quad (3)$$

$$\omega_n = \sqrt{C_{44}/(I_{44} + A_{44})} \quad (4)$$

$$\zeta = B_{44\_l}/2\sqrt{C_{44}(I_{44} + A_{44})} \quad (5)$$

where ω_n is the undamped natural frequency and ζ is the damping ratio.

The free decay solution of which is given in Equation (6):

$$\varphi = e^{-\omega_n\zeta t}\left(\frac{v_o + \omega_n\zeta x_o}{\omega_n\sqrt{1-\zeta^2}}\sin\omega_n\sqrt{1-\zeta^2}t + x_o\cos\omega_n\sqrt{1-\zeta^2}\,t\right) \quad (6)$$

where x_o and v_o are initial heel angle and roll velocity, respectively. The solution can also be written as a damped sine wave:

$$\varphi = e^{-\omega_n\zeta t}\sin\left(\omega_n\sqrt{1-\zeta^2}t + \varepsilon\right) \quad (7)$$

where ε is the phase angle set to match initial heel angle and roll rate. Equations (6) and (7) assume a zero mean heel angle. A non-zero mean heel angle. $\varphi_{OM,}$ can easily be added as seen in Equation (8).

$$\varphi = \varphi_o + e^{-\omega_n\zeta t}\,x_o\sin\left(\omega_n\sqrt{1-\zeta^2}t + \varepsilon\right) \quad (8)$$

Adding nonlinear damping and nonlinear stiffness in a single degree of freedom equation gives:

$$\ddot{\varphi} + 2\zeta\omega_n\dot{\varphi} + \beta\dot{\varphi}|\dot{\varphi}| + \omega_n^2\varphi + \gamma\varphi^3 = 0 \quad (9)$$

where the damping value is dependent on roll angle and forward speed and the stiffness values represent the righting arm curve. β is the normalized quadratic damping and γ is the normalized cubic stiffness terms. Equation 9 was solved with a fourth order Runge-Kutta method to provide roll decay data with known properties.

Experimental data from a free decay experiment will often have noise overlaid on the free decay caused by impulsive loading, steering, wave reflection, static heel, sensor error. To approximate that noise,φ_N, a sine wave (Equation (10)) was overlaid on the numerical solution to Equation (9). A sine wave was selected rather than white noise as experience indicates signal noise is due to cross-coupling from impulsive loading and steering.

$$\varphi_N = \varphi_{o_N} + \varphi_{A_N}(t_N - t)\sin(\omega_N t + \varepsilon_N)/t_N \quad (10)$$

The parameters for Equation (9) and the noise sine wave,φ_{o_N}, φ_{A_N} and ω_N, are set to nominal values as shown in Table 1. The Equation (9) parameters are typical monohull damping values with a roll period of 10.25 s. An initial roll angle of 30 degrees was selected to provide a number of peaks in a single time history. The noise sine wave parameters were selected to provide roughly 5% error that varied over the time history. The slower frequency, ω_N, represents a rudder steering or yaw influence. The parameters of the sine wave,φ_{o_N}, φ_{A_N} and ω_N, are set to nominal values as shown in Table 1. The noise ramp length, t_N, was set to the time the roll angle became small (approximately 0.2 deg). The phase, ε_N, was randomly selected.

Table 1. Coefficients for roll ordinary differential equation (Equation 9) and noise (Equation 10).

Coefficient	Units	Value
ω_n	rad/s	0.613
ζ		0.25/0.60
β		0.200
γ		0.00
x_o	deg	30.00
v^o	deg/s	0.00
φ_{o_N}	deg	0.00
φ_{A_N}	deg	3.0 (10%)
$_N$	rad/s	0.200
t_N	s	20/40

3. CURVE FITTING PROCESS

Free decay time histories can be analyzed with a number of approaches from various successive peak ratios assuming a logarithmic decrement (Handschel et al., 2015), energy loss (Handschel et al., 2015) or curve fitting techniques (Park et al., 2017). Smith (2018) demonstrated these methods produce the same results for noise free data.

The time history data were fitted with a damped sine wave (Equation (7)) over various amounts of data; half cycles, full cycles, and from each peak to the end of the run (referred to as "All"). The "All" fit damping values are associated with the initial data peak value following Park et al. (2009). Fitting the entire run linearizes the results but provides a more stable answer as more data are employed when curve fitting. Fitting smaller amounts of data captures the roll angle dependence with a potential loss of accuracy.

With curve fitting a damped sine wave, the natural frequency can be estimated as well as the damping ratio, ζ. Peak analysis of the time history will result in the damped natural frequency. This must be converted to the natural frequency by dividing the damped natural frequency by $\sqrt{1-\zeta^2}$.

The curve fitting was done with Microsoft Excel Solver function minimizing the sum of the square of the differences in time histories. Solver did not find a good answer in some instances and needed to be re-run with a better initial guess.

4. EXAMPLES

Increasing the damping reduces not only the size of the oscillation but the number of oscillations and frequency of oscillation as shown in Figure 2. Damping values above 0.5 tend to look quite similar and experimentally are nearly indistinguishable from critically and over damped cases. Bishop et al. (2005) indicates forward speed roll damping values between 0.15 – 0.25.

Two synthetic roll time histories was generated with a linear damping coefficient (0.25 and 0.60) and a quadratic damping coefficient of 0.20. A sine wave representing noise from Equation (10) was overlaid on the roll time history. The noise amplitude employed a 40 second ramp. In Figures 3 – 7, the "Theory" line is the known solution; the "Data Fit" is the fit considering all data except those obviously corrupted by noise. This was determined by looking for a change in trend or increase of scatter or non-sensical values, such as negative damping.

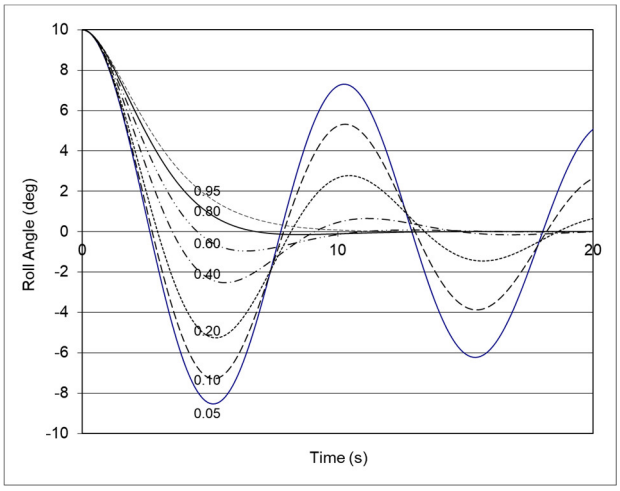

Figure 2: Roll decay curves with different linear damping coefficients ranging from 0.05 to 0.95.

Synthetic data ζ=0.25

A roll time history was generated with a linear damping coefficient of 0.25. The noise amplitude employed a 40 second ramp. The damping ratio (fraction of critical damping) for the different curve fitting approaches is shown in Figure 3.

In this case, all of the approaches, half, full, or all, would have provided a reasonable estimate of the roll damping. However, the use of data from all three approaches enables a better recognition of the damping trend with respect to roll angle. The linear regression of the data results in line nearly the same as the theoretical value.

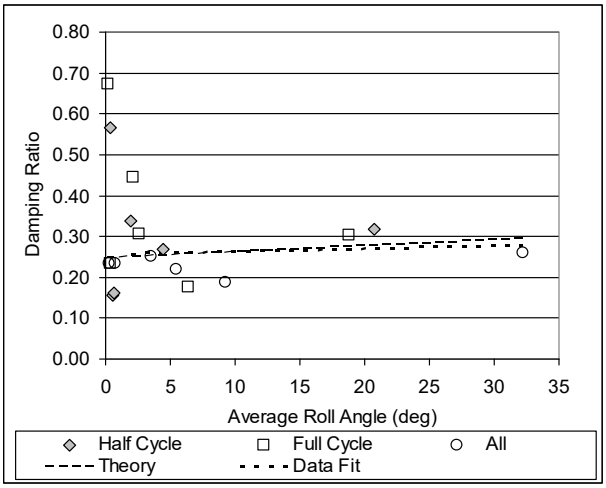

Figure 3: Roll damping ratio from time history curve fitting for synthetic data with linear damping of 0.25.

Synthetic data ζ=0.6

A roll time history was generated with a linear damping coefficient of 0.60. The noise amplitude employed a 20 second ramp. The damping ratio (fraction of critical damping) for the different curve fitting approaches is shown in Figure 4.

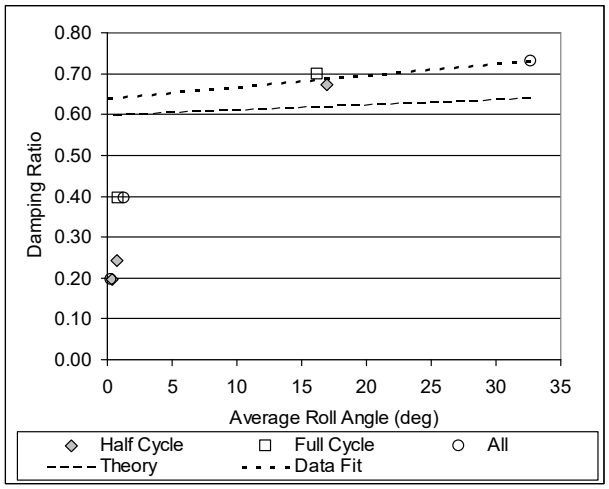

Figure 4: Roll damping ratio from time history curve fitting for synthetic data with linear damping of 0.6.

This example again shows the benefit from multiple curve fitting approaches to generate more data and identify trends. A single approach would result in either a single usable data point or an incorrect roll damping estimate with small linear damping and large quadratic damping.

Experimental data ζ=0.153

Free roll decay data from Bishop et al. (2005), Flare Topside at 25 knots (run 341) was analyzed with the curve fitting approach. This run has two impulses and decays. The decays were analyzed with a full cycle logarithmic decrement approach. The time histories were analyzed with a curve fitting method. Figure 5 is a comparison of curve fit results to reported results.

A number of curve fits did not result in acceptable results on the first attempt. Fixing the initial amplitude helped some instances but generally increased the data scatter. This type of difficulty usually indicates the presence of noise. Examination of the peaks indicated they were not monotonically decreasing. In this case, data fits with more data may have more error as more noisy cycles are included.

Bishop et al. results are very similar to the Full cycle curve fitting results. The data has the typical noise at low roll angles which are usually ignored but are included here for completeness. The trends at the highest roll angles have a notable difference between the Half cycle, Full cycle, and All data points. The "Data Fit" line employed the Half cycle points rather than All as the All values are less than both the Half and Full data. The resulting "Data Fit" line falls along Bishop et al. and Full cycle data. Inclusion of All data and not Half data resulted in a nearly horizontal "Data Fit" line. Use of only the Half cycle data would result in a slightly steeper data fit.

Whether or not curve fitting provided a significant advantage over the logarithmic decrement approach based on peaks is unclear.

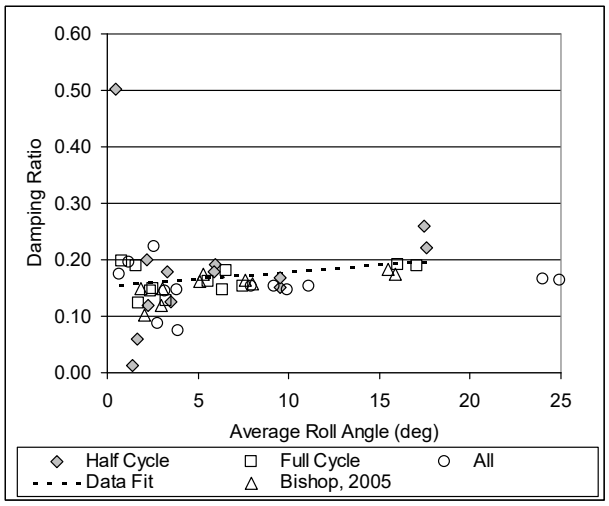

Figure 5: Roll damping ratio from ONR flare-topside time history at 25 knots (run 341).

Experimental data ζ=0.305

A more heavily damped experimental free roll decay run with a single-oscillation decay was analyzed with curve fitting. The run had two impulses and decays as shown in Figure 6. The speed was 19.2 knots full-scale. As a point of interest, pitch decay experiments have similar behavior as shown in Figure 1.

Figure 7 shows the roll damping ratio from the curve fitting analysis. Peak-based logarithmic decrement analysis had damping values from 0.53 to 0.68 with comparable data scatter. From the number of oscillations, Figure 2 indicates a damping value should be between 0.4 and 0.6. The curve fitting approach has better correlation to expected values.

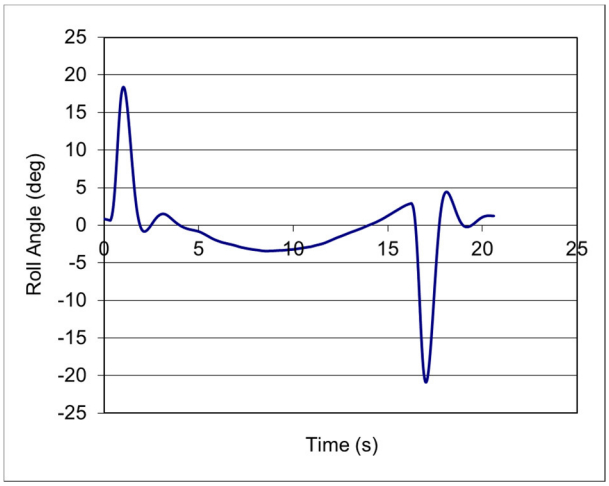

Figure 6: Time history data for single oscillation decay.

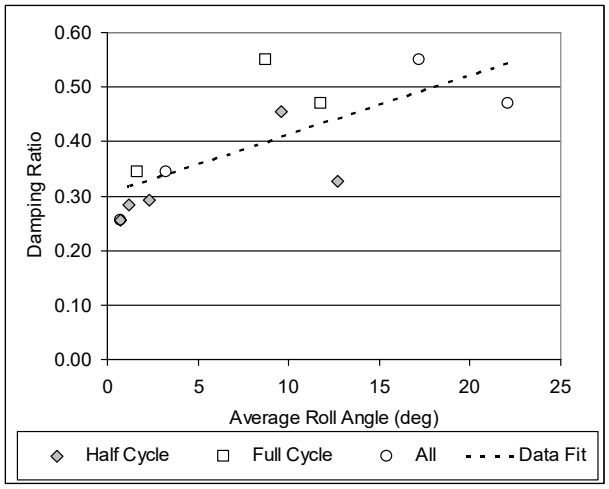

Figure 7: Roll damping ratio from experimental data with one oscillation.

Digital filtering

The noise in the roll data due to other couple motions does affect the accuracy of the estimated roll damping value. Shifting the data with an offset to correct a non-zero mean value is recommended and commonly done (Smith, 2018; Handschel et al., 2015). Further noise removal was attempted with digital filtering based on the premise that by eliminating frequencies not near the roll frequency would remove the noise allowing the data to be analyzed more accurately. This approach worked well with synthetic data where a second low frequency oscillation was added to the roll decay time history. The two peaks were easily identified after Fast Fourier Transform (FTT) and the noise peak can be removed.

With experimental data, the roll peak can be easily identified, but a noise peak may not be apparent. However, looking at ONR Flare Topside run 341 with 512-point FFT, two peaks were found as shown in Figure 8. The roll frequency from the damping analysis was 3.49 rad/s; this corresponds to the higher frequency peak. Time histories of the roll and noise signal were calculated by an inverse FFT of the spectrum filtered with a notch filter as shown in Figure 9.

Some noise is expected based on the damping analysis. The amplitude of the noise time history was larger than expected. Removal of the noise reduces the first amplitude about 40%. Roll damping values would be much different between the measured and "no noise" roll time histories. Without a benchmark value for comparison, determining if too much "noise" has been removed is difficult. Nevertheless, with more study digital filtering could possibly improve roll damping estimates.

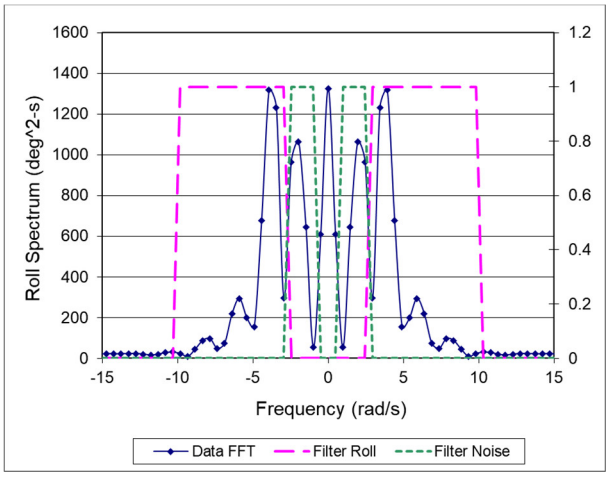

Figure 8: Roll spectrum of ONR Flare-Topside run 341 with notch filter.

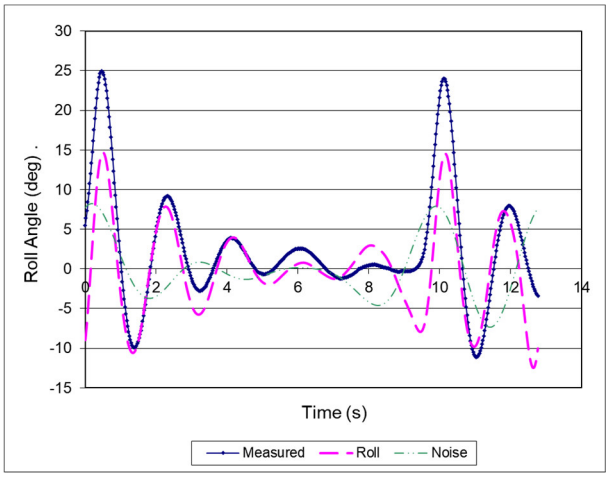

Figure 9: Time histories of ONR Flare-Topside run 341 as measured and decomposed to roll and noise signal.

5. OVERDAMPED CASES

Time histories without an oscillation by definition have damping coefficients greater than or equal to 1. In practice, time histories with damping coefficients greater than approximately 0.7 can also appear to not be oscillatory and be considered critically damped (Lloyd, 1989). However, the solution to roll motion ODE changes for critically damped and over damped cases. From Karnopp (1974), the overdamped solution is:

$$\varphi = e^{-\omega_n \zeta t}\left(\frac{v_o + \omega_n \zeta x_o}{\omega_n\sqrt{\zeta^2 - 1}}\sinh \omega_n\sqrt{\zeta^2 - 1}t + x_o \cosh \omega_n\sqrt{\zeta^2 - 1}\,t\right) \quad (11)$$

The case of critical damping has another solution. In practice, real systems are either under or over damped, rather than exactly critically damped.

Any curve fitting with a damped sine wave may not produce a result or produce an incorrect result in the over damped cases. The curve fitting process will match a portion of an oscillatory curve with the overdamped experimental data. In these cases, specifying the initial roll angle and roll rate rather than allow the curve fitting algorithm to find a match for them is necessary.

6. CONCLUSIONS

A damped sine wave was fit to roll decay data to determine the damping ratio and natural frequency. Different durations of data from Half cycle, Full cycle, and peak to end (All) were applied to the curve fit to determine the dependency on roll angle and amount of data. The use of all three was helpful to determine trends respect to roll angle. Curve fitting was especially useful for cases with very few oscillations. However, curve fitting did not necessarily produce a unique solution and multiple curve fitting attempts with different initial guess may be needed.

Digital filtering as a noise removal method shows potential. More study and benchmarking is needed to determine a robust filter.

Curve fitting of over damped cases should be possible with the solution to the over damped oscillator. Sensitivity to initial guess for the optimization algorithm may be larger than seen with the under damped cases.

7. ACKNOWLEDGEMENT

This work was supported by Dr. Woei-Min Lin of Office of Naval Research.

REFERENCES

Bassler, C. C., Reed, A. M. and Brown, A. J., 2010, "Characterization of Energy Dissipation Phenomena for Large Amplitude Ship Roll Motions", Proceedings of the 29th American Towing Tank Conference, Annapolis, MD, USA.

Bishop, R., Belknap, W. , Turner, C., Simon, B., and Kim, J. H., 2005, "Parametric Investigation on the Influence of GM, Roll damping, and Above-Water Form on the Roll Response of Model 5613", Report NSWCCD-50-TR-2005/027.

Dalzell, J. F., 1978, "A Note on the Form of Ship Roll Damping," Journal of Ship Research, Vol 22, No. 3, Sep 1978, pp. 178-185

Handschel. S., Fröhlich, M., and Abdel-Maksoud, M., 2014, "Experimental and Numerical Investigation of Ship Roll Damping by Applying the Harmonic Forced Roll Motion Technique", 30th Symposium on Naval Hydrodynamics, Hobart, Tasmania, Australia.

Handschel, S., Feder, D., and Abdel-Maksoud, M., 2015, "Estimation of Ship Roll Damping – A Comparison of the Decay and the Harmonic Excited Roll Motion Technique for a Post Panamax Container", Proc. 12th Intl. Conf. on the Stability of Ships and Ocean Vehicles, Glasgow, UK, 19-24 June, page 475-488.

Hashimoto, H., Omura, T., Matsuda, A., Yoneda, S., Stern, F., and Tahara, Y., 2018, "Some Remarks on EFD and CDF for Ship Roll Decay", Proceedings of the 10th International Conference on Stability of Ships and Ocean Vehicles, (STAB2018), Kobe, Japan, pp. 339-348

Karnopp, B., 1974, Introduction to Dynamics, Addison-Wesley, pp. 291-296.

Katayama, T., Adachi, T., Sawae, T., 2018, "Roll Damping Estimation for Small Planing Craft", Proceedings of the 10th International Conference on Stability of Ships and Ocean Vehicles, (STAB2018), Kobe, Japan, pp. 369-378.

Llyod, A. R. J. M., 1989, Seakeeping – Ship Behaviour in Rough Weather, Ellis Hornwood.

Oliva-Remola, A., Perez-Rojas, L., Diaz-Ojeda, H., 2018, "Ship Roll Damping Estimation: A Comparative Study of Different Roll Decay Tests," Proceedings of the 10th International Conference on Stability of Ships and Ocean Vehicles, (STAB2018), Kobe, Japan, pp. 312--322.

Park, J. T., Hayden, D. D., Klamo, J., and Bishop, R. C., 2009, "Analysis Methodology of Roll Decay Data for Free-Running and Captive Model Tests", Proceedings of the 18th International Conference of Ship and Shipping Research, Vol. 1, pp. 105-114, Messina, Italy.

Park, J. T., Turner, C. R., and Melendez, M. P., 2016, "Physical Properties and Roll Decay with Uncertainty Estimates for DTMB Model 5720, 23rd Scale R/V Melville", NSWCCD-80-TR-2016/018.

Park, J. T., Turner, C. R., and Melendez, M. P., 2017, "New Methodology in Analysis of Physical Properties and Roll Decay with Uncertainty Estimates for Surface-Ship Model Experiments", Proceedings 30th American Towing Tank Conference, West Bethesda, USA, 3-5 October, 2017.

Smith, T., 2018, "Determination of Roll Damping for Empirical Measurements", Proceedings of the 10th International Conference on Stability of Ships and Ocean Vehicles, (STAB2018), Kobe, Japan, pp. 301-311.

Sumislawski, P., Wassermann, S. Abdel-Maksoud, M., 2018, "Rudder Influence on Roll Damping", Proceedings of the 10th International Conference on Stability of Ships and Ocean Vehicles, (STAB2018), Kobe, Japan, pp. 360-368.

Vassilopoulos, L., 1971, "Ship Rolling at Zero Speed in Random Beam Seas with Nonlinear Damping and Restoration", Journal of Ship Research, Vol. 15, No. 4.

A step forward towards developing an uncertainty analysis procedure for roll decay tests

Adriana Oliva-Remola, *Universidad Politécnica de Madrid,* adriana.oliva@upm.es
Luis Pérez-Rojas, *Universidad Politécnica de Madrid,* luis.perezrojas@upm.es

ABSTRACT

The general approach to estimate ship roll damping is to perform roll decay tests in calm water, as they represent the easiest and approach and the most efficient in terms of time. However, how to carry out roll decays is not simple, as many parameters may affect the results. By using proper mechanical devices to initially heel the ship, the results are more reliable, however, it is deemed necessary to estimate the uncertainty associated with the determined roll damping coefficients. This paper presents an approach of developing an uncertainty analysis procedure for roll decay tests.

Keywords: *Roll damping, decay roll tests, experimental techniques, nonlinear rolling, uncertainty analysis.*

1. INTRODUCTION

Roll damping represents the energy that a body loses when rolling. It is a representative parameter to characterize a ship's seakeeping behaviour. It may be derived experimentally performing roll decay tests. Roll decay tests are based on inducing an initial heel angle to the ship model, releasing it allowing to roll freely, and recording and analysing the oscillatory roll motion.

Roll decay tests are the most common approach to estimate roll damping, because they are low time-consuming, and the infrastructures required to carry them out are less sophisticated. Nevertheless, roll decay tests present some problems. The most typical is that roll damping estimations at large rolling angles are complex and, depending on the ship type, it may not be always feasible. Another aspect is that, even testing medium roll angles, a proper mechanical device should be used (Spounge et al., 1986; Bulian et al., 2009; Irvine et al, 2013; Oliva et al., 2018). Many alternatives have been presented, some of them account also with the fluid memory effects, which represent another aspect to consider (Oliveira, 2011; Söder et al., 2012; Zhao et al., 2016; Oliva et al, 2018). Lastly, there is no standard procedure not even to carry the tests but also to analyse them, which may lead to different roll damping estimations, as pointed out by Wassermann et al., 2016.

It is important to highlight that, although roll decay tests are the primary recommended technique in current and under development stability-related international regulations (IMO 2006, 2019), some research studies have shown that they may be non-conservative and present a different trend compared to the actual roll damping of the ship under regular beam waves (Oliva, 2018).

Despite all the above-mentioned aspects, as roll decay tests constitute an experimental technique, it is necessary to know the uncertainty associated with the roll damping estimations derived from them. This paper deals with it, in view of formulating in the future a procedure suitable to be implemented in an ITTC guideline.

2. METHODOLOGY OF ANALYSIS FOR ROLL DECAYS

The scope of roll decay tests is to determine the roll damping coefficients of a floating body. They consist on initially heeling the model up to a certain angle and then releasing it, recording the decaying oscillation curve.

To specify an uncertainty analysis procedure, it is necessary to understand how the test are carried out, how to model the roll motion and how-to post-process the experimental data to estimate the roll damping coefficients. In the following, these items are explained.

Experimental set-up

There are different experimental methodologies to carry out roll decay tests. They may be categorized depending on the forced induced to the ship model as (Oliva et al, 2018):

1. Only a roll moment is applied, without changing the ship model displacement;
2. A vertical force is applied, generating a roll moment, but changing the ship model displacement;
3. Pre-exciting the ship rolling a certain number of cycles and then releasing it. The ship model displacement is maintained.

In any case, a mechanical device should be used to create the initial heel angle or to pre-excite the ship.

The physical quantity measured, at least, should be the rolling amplitude as a function of time. The sample frequency of the measurements should be fixed taking into account the (undamped) natural roll period of the body tested. Considering existing computer capabilities, the author's recommendation is to use, at least, 100Hz.

Modelling of roll motion

Generally, the motion of the ship under the roll decay tests scenario may be modelled by a 1-DOF (Degree of Freedom) roll motion equation.

The 1-DOF roll motion nonlinear differential equation in calm water, at zero forward speed, and considering non-linearities in restoring and damping terms is as follows:

$$\ddot{\phi} + d\left(\dot{\phi}\right) + \omega_0^2 \cdot r\left(\phi\right) = 0 \qquad (1)$$

where:

- ϕ [rad]: is the roll angle (dots represent derivatives with respect to time);
- $d\left(\dot{\phi}\right)$ [$1/s$]: is the normalized damping function, assumed to be dependent only on the instantaneous roll velocity ($\dot{\phi}$). The roll damping term is generally defined by the linear-quadratic-cubic damping model (ITTC, 2011):

$$d\left(\dot{\phi}\right) = 2 \cdot \mu \cdot \dot{\phi} + \beta \cdot \dot{\phi} \cdot \left|\dot{\phi}\right| + \delta \cdot \dot{\phi}^3 \qquad (2)$$

where μ [$1/s$], β [$1/rad$] and δ [s/rad^2] are the linear, quadratic and cubic damping coefficients, respectively. The δ and β coefficients may be fixed to zero, depending on the ship hull and on the presence of bilge keels, then using the so-called linear-quadratic or linear-cubic damping models;

- ω_0 [rad/s]: is the (undamped) natural roll frequency, defined as:

$$\omega_0^2 = \frac{\Delta \cdot \overline{GM}}{J_{xx}^v} \qquad (3)$$

where Δ [N] is the ship displacement, $\overline{GM}$ [m] is the metacentric height with respect to. the centre of gravity of the ship (G), considering the vessel freely floating with displacement Δ, and J_{xx}^v [$kg \cdot m^2$] is the total roll moment of inertia including the hydrodynamic added inertia;

- $r\left(\phi\right)$ [nd]: is the non-dimensional righting arm, which is equivalent to:

$$r\left(\phi\right) = \frac{\overline{GZ}\left(\phi\right)}{\overline{GM}} \qquad (4)$$

where $\overline{GZ}\left(\phi\right)$ [m] is the hydrostatic roll righting lever with respect to G.

Analysis of roll decays

Different methodologies to analyse roll decays exist, being themselves dependent on the mathematical model of the ship roll motion under the specific scenario of roll decays.

Some of them do not consider the non-linearities in the restoring and damping terms, some others only the non-linearities in one of the terms and the rest consider both.

The method used to analyse roll decays is relevant when considering an uncertainty analysis. In the present paper, the procedure considers the non-linearities in the restoring and damping terms, assuming the mathematical model described previously. The analytical procedure is described in detail in Appendix 1 of Bulian et al., 2009.

In the following, the linear-cubic damping model is considered, (see Eq. (5)) and the non-linear restoring is supposed calculated directly from the

actual GZ curve, instead of obtaining the restoring coefficients from least square fitting.

The procedure is based on the logarithmic roll-decrement curve by approximating the nonlinear model of Eq. (1) by a linear equivalent model in a limited time window:

$$\ddot{\phi} + 2 \cdot \mu_{eq}(A) \cdot \dot{\phi} + {\omega_{0,eq}}^2(A) \cdot \phi = 0 \Big|_{\left[\tilde{t} - \frac{\Delta t}{2}, \tilde{t} + \frac{\Delta t}{2}\right]} \qquad (5)$$

$$\begin{cases} \mu_{eq}(A) = \mu + \dfrac{4}{3\pi} \cdot \beta \cdot \left(\tilde{\omega}(A) \cdot A\right) + \dfrac{3}{8} \cdot \delta \cdot \left(\tilde{\omega}(A) \cdot A\right)^2 \\ \tilde{\omega}(A) = \sqrt{\omega_{0,eq}^2(A) + {\mu_{eq}}^2(A)} \approx \omega_{0,eq}(A) \\ \omega_{0,eq}(A) = \omega_0 \cdot \sqrt{\dfrac{1}{\overline{GM}} \cdot \dfrac{\int_0^{2\pi} \overline{GZ}\left(\phi = A\cos(\alpha)\right) \cdot \cos(\alpha) \cdot d\alpha}{\pi \cdot A}} \end{cases}$$

where A $[rad]$ is the rolling amplitude, $\mu_{eq}(A)$ $[1/s]$ is the equivalent linear damping coefficient and $\omega_{0,eq}(A)$ $[rad \cdot s^{-1}]$ is the equivalent (undamped) roll natural frequency.

Assuming that the (undamped) ship roll natural frequency ω_0, the metacentric height $\overline{GM}$ and the righting lever curve $\overline{GZ}(\phi)$ are known parameters, the step-by-step procedure is as follows:

1. Filter the raw measured data, if needed, and correct possible bias;
2. Determine the extremes C_i and corresponding time instants for each roll decay time history (see Fig. 1);
3. Determine the average amplitude A_i for each half cycle (also a complete cycle may be considered as well as other alternatives (Wassermann et al., 2016), however, care should be taken as there would be changes in the following equations), and calculate the equivalent linear roll damping coefficient $\mu_{eq}(A_i)$ and the equivalent linear frequency $\omega_{0,eq}(A_i)$ associated to A_i;

$$A_i \approx \frac{|C_i| + |C_{i+1}|}{2}$$

$$\mu_{eq}(A_i) = \frac{1}{t_{i+1} - t_i} \cdot \ln\left(\frac{|C_i|}{|C_{i+1}|}\right) \qquad (6)$$

$$\omega_{0,eq}(A_i) \approx \tilde{\omega}(A_i) = \frac{\pi}{t_{i+1} - t_i}$$

4. If different roll decay tests representing the same test case (same experimental set-up and initial heel angle and same ship and loading condition) have been carried out, data determined in the previous step can be aggregated. It allows a robust estimation of roll damping coefficients and a reduction of associate uncertainties when performing the step described in the following paragraph;
5. From the aggregated data, the analytical model of $\mu_{eq}(A)$, represented in Eq. 5, can be fitted through a least square fitting to determine the nonlinear roll damping coefficients (μ, β and δ). For the $\mu_{eq}(A)$ fitting, it should be considered μ_{eq} as a function of $\left(\tilde{\omega}(A) \cdot A\right)$. Moreover, as stated in Eq. 5, as for roll motion the system may be characterized as slightly damped, it may be assumed that $\tilde{\omega}(A) \approx \omega_{0,eq}(A)$. In Fig. 2 an example of experimental fitting is shown, however, in order to represent a readable X-axis, μ_{eq} is represented as a function of the roll amplitude, although in reality it has been considered as a function of $\left(\tilde{\omega}(A) \cdot A\right)$, as quoted.

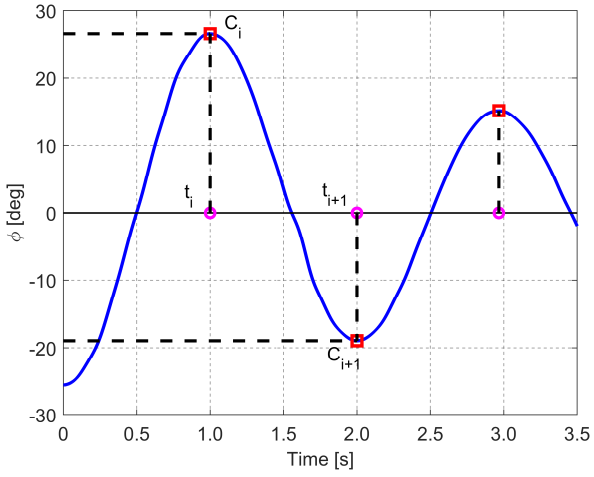

Figure 1: Example of roll decay curve.

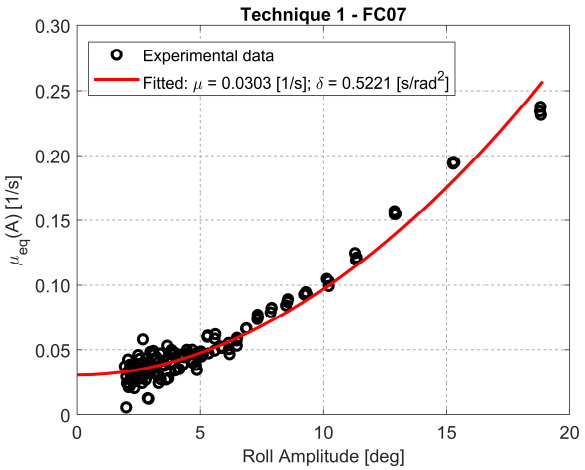

Figure 2: Example of equivalent linear roll damping fitting (quadratic damping coefficient has been fixed to zero).

The fitting of $\omega_{0,eq}(A)$ may not be required if, as assumed previously, the variables in which it depends on (see Eq. (5)) are known.

3. GENERIC UNCERTAINTY ANALYSIS BACKGROUD

Uncertainty is the level of precision of a measurement or a parameter.

According to ITTC guideline 7.5-02-01-07 (ITTCa, 2017; ITTCb, 2017), uncertainties can be classified into three categories: standard uncertainty, combined uncertainty and expanded uncertainty.

The standard uncertainty of the result of a measurement can be categorized into two types:

- Type A: uncertainty components obtained using a method based on statistical analysis of a series of observations.
- Type B: uncertainty component obtained by other means (not statistical analysis).

The standard uncertainty is delimited to a result of a measurement. For quantities not measured directly, the uncertainties propagate to obtain the combined uncertainty.

The relationship between combined and individual uncertainties is given by the law of propagation. For uncorrelated and independent measurements, this law is as follows:

$$u_c^2(y) = \sum_{i=1}^{N} \left(\frac{\partial y}{\partial x_i} \right)^2 \cdot u^2(x_i) \tag{7}$$

where u is the standard uncertainty and the derivatives $(\partial y / \partial x_i)$ are the sensitivity coefficients, which represent the functional relationship of the measurement variables with the quantity.

The expanded uncertainty appears when the confidence limit is considered. The expanded uncertainty is related with the combined (or standard) uncertainty by a coverage factor κ such as:

$$U = \kappa \cdot u_c(y) \tag{8}$$

The coverage factor equals to 2 assuming a Gaussian distribution and a confidence limit of 95%. However, for small number of samples, the coverage factor may be replaced by the inverse *Student t* at 95% confidence level.

As a result, the quantity of interest Y (measured or derived from measurements and other parameters) is represented as:

$$Y = y \pm U \tag{9}$$

4. UNCERTAINTY ANALYSIS APPLIED TO ROLL DECAYS

Uncertainty analyses have been considered in most of the engineering fields and, to the naval field and towing tank experiments, they have been implemented in the main experimental techniques such as resistance towing tank tests or propulsion tests. In fact, there are many ITTC procedures or guidelines that deal with this topic and with how to implement uncertainty analysis in different tests.

However, uncertainty analysis applied in roll damping estimations is still not addressed by ITTC, as well as how to experimentally determine ship roll damping. The later aspect is being addressed currently by the ITTC Stability in Waves Committee (ITTCc, 2017), which has to update the recommended procedure of "Numerical Estimation of Roll Damping" (ITTC, 2011) to account also for experimental techniques to estimate roll damping, therefore, re-calling it as "Estimation of Roll Damping". The former one, may be addressed as well when updating the recommended procedure, although it may need more development.

In the following, the process to perform uncertainty in roll decay tests is briefly introduced in

order to gain some feedback from interested researchers or experimentalist to address the uncertainty issue of roll damping in conjunction with the ITTC.

Some related studies regarding this topic may be found in Irvine et al., 2013 and Park et al., 2016. According to Park et al., 2016, the sources of uncertainty in roll decay tests are:

- Curve fitting;
- Time measurement;
- Angle measurement.

In the following, the logarithmic decrement technique to analyse roll decays and the linear-quadratic-cubic damping model are considered.

As a result, the method produces an uncertainty for each rolling amplitude (A) and, furthermore, the determined rolling amplitude has also an uncertainty associated with its value.

The uncertainties of the equivalent linear roll damping coefficient $\mu_{eq}(A_i)$ and the equivalent linear frequency $\omega_{0,eq}(A_i)$ are shown in Eq. 10 and 11, considering Eq. (6). Also, the uncertainty associated with the amplitude of rolling A_i is reported in Eq. 12.

$$\begin{aligned}
&\mu_{eq}(A_i) = \mu_{eq,\det} \pm k \cdot u_{c,\mu_{eq}} \\
&u^2_{c,\mu_{eq}} = \left(\frac{\partial \mu_{eq}}{\partial t_{i+1}} \cdot u(t)\right)^2 + \left(\frac{\partial \mu_{eq}}{\partial t_i} \cdot u(t)\right)^2 + \\
&+ \left(\frac{\partial \mu_{eq}}{\partial |C_i|} \cdot u(C)\right)^2 + \left(\frac{\partial \mu_{eq}}{\partial |C_{i+1}|} \cdot u(C)\right)^2 = \\
&= 2 \cdot \left(\frac{1}{(t_{i+1} - t_i)^2} \cdot \ln\left(\frac{|C_i|}{|C_{i+1}|}\right) \cdot u(t)\right)^2 + \\
&+ \left(\left(\frac{1}{C_i}\right)^2 + \left(\frac{-1}{C_{i+1}}\right)^2\right) \cdot \left(\frac{1}{(t_{i+1} - t_i)} \cdot u(C)\right)^2
\end{aligned} \tag{10}$$

$$\begin{aligned}
&\omega_{0,eq}(A_i) = \omega_{0,eq,\det} \pm k \cdot u_{c,\omega_{0,eq}} \\
&u^2_{c,\omega_{0,eq}} = \left(\frac{\partial \omega_{0,eq}}{\partial t_{i+1}} \cdot u(t)\right)^2 + \left(\frac{\partial \omega_{0,eq}}{\partial t_i} \cdot u(t)\right)^2 = \\
&= 2 \cdot \left(\frac{\pi}{(t_{i+1} - t_i)^2} \cdot u(t)\right)^2
\end{aligned} \tag{11}$$

$$\begin{aligned}
&A_i = A_{i,\det} \pm k \cdot u_{c,A_i} \\
&u^2_{c,A_i} = \left(\frac{\partial A_i}{\partial C_{i+1}} \cdot u(C)\right)^2 + \left(\frac{\partial A_i}{\partial C_i} \cdot u(C)\right)^2 = \\
&= \frac{1}{2} \cdot u(C)^2
\end{aligned} \tag{12}$$

In Eq. 10 and 11, $u(t)$ is the standard uncertainty of the measured time, which may be determined from the sample frequency $f[Hz]$ as:

$$u(t) = \frac{1}{f} \tag{13}$$

and $u(C)$ is the standard uncertainty of the angle measurement. If the calibration of the instrument used to measure the rolling amplitudes is not available by the specifications of the system, this value should be obtained performing a calibration of the device, taking as a basis the ITTC procedure for the instrument calibration (ITTCd, 2017).

The uncertainty associated with the nonlinear damping coefficients should be determined considering Eq. (5), specifically the relationship between the equivalent linear roll damping coefficient and the nonlinear damping components, in which the mean amplitude and the equivalent linear frequency also appear. A simplified approach to derive the uncertainties may be considered. It is based on considering only the uncertainties coming from the curve fitting. In this situation, the confidence intervals $k \cdot u_{c,\mu}$, $k \cdot u_{c,\beta}$ and $k \cdot u_{c,\delta}$ may be derived, assuming a confidence level of 95% and that $k \cdot u_{c,\mu_{eq}}$ present a Gaussian distribution, thus, neglecting the fact that uncertainties at smaller rolling amplitudes are larger. This approach was firstly presented by Bulian et al. 2009 and used by the authors in Oliva et al, 2018 and Oliva, 2018.

5. PRACTICAL CASE

In the following, a practical application of the uncertainty analysis procedure for roll decays is given. It will be based on previous experimental data, whose detailed information may be found in Oliva et al, 2018 and Oliva, 2018. From these references, the decay test case selected for the present work is the FC07 and Technique 1, which corresponded to an initial heeling angle of 25.88 *deg* and the experimental set-up based on applying a roll moment, without changing the ship model displacement.

The standard uncertainty of the measured time corresponds to:

$$u(t) = \frac{1}{f} = \frac{1}{120} = 0.0083\ [s] \tag{14}$$

The standard uncertainty of the angle measurement will be estimated, because the actual value is not known due to the usage of an optical trackable system. It will be estimated to be 0.1 *deg*, therefore:

$$u(C) = 0.0017\ [\text{rad}] \tag{15}$$

The uncertainty associated with the amplitude of rolling is, consequently:

$$u(A_i) = \sqrt{\frac{1}{2}\cdot u(C)^2} = 0.0012\ [rad] \tag{16}$$

The uncertainties of the equivalent linear roll damping coefficient $\mu_{eq}(A)$ and the equivalent linear frequency $\omega_{0,eq}(A)$ are represented in Fig. 3 and 4, respectively.

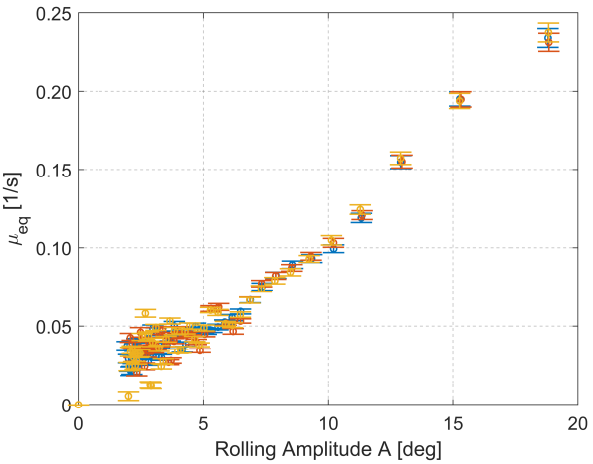

Figure 3: Uncertainty analysis of the equivalent linear roll damping coefficient.

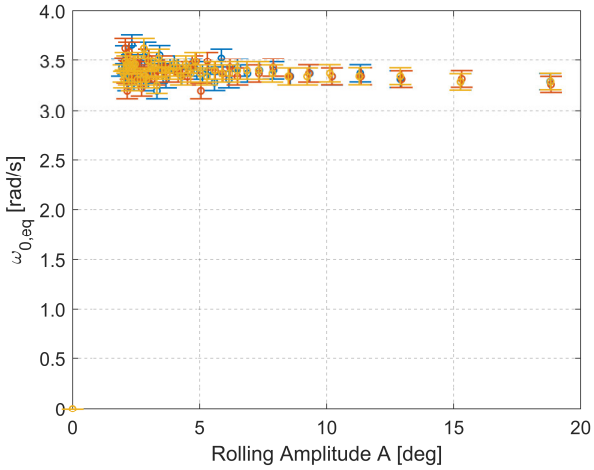

Figure 4: Uncertainty analysis of the equivalent undamped roll natural frequency.

In Fig. 5 and 6, the percentual difference of the uncertainties of $\mu_{eq}(A)$ and $\omega_{0,eq}(A)$ are represented, which have been calculated following Eq. 17:

$$diff[\%] = \frac{\kappa \cdot u(y)}{y} \tag{17}$$

From these results, it may be seen that the uncertainties at smaller rolling amplitudes are larger than uncertainties at medium and large rolling amplitudes, which is coherent, because the angle measurement precision is constant throughout the whole tests and at smaller amplitudes, the difference between the measured value and the amplitude measurement uncertainty is smaller, therefore, the relative difference is much larger.

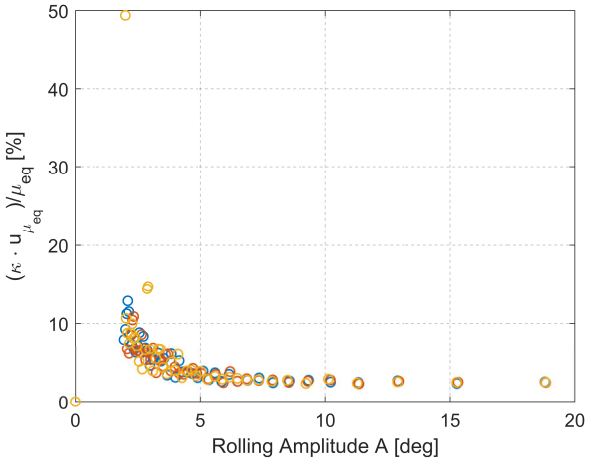

Figure 5: Percentual uncertainty of the equivalent linear roll damping coefficient.

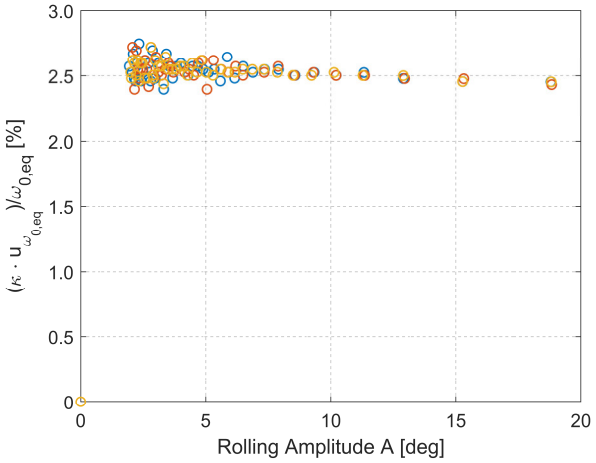

Figure 6: Percentual uncertainty of the equivalent undamped roll natural frequency.

Lastly, the uncertainties associated with the nonlinear roll damping coefficients, only considering uncertainties coming from the curve fitting, are equal to:

$$u(\mu) = 0.00095\ [1/s]$$
$$u(\delta) = 0.00950\ [s/rad^2] \quad (18)$$

In this practical case, the linear-cubic damping model has been considered, because the linear-quadratic-cubic damping model gave negative nonlinear coefficients. The values reported in Eq. 18 constitute a percentual uncertainty of the linear damping coefficient (μ) of 6.3% and a percentual uncertainty of the cubic damping coefficient (δ) of 3.7%, calculating the percentages following Eq. 17.

These last results also present the expected outcomes. The linear damping coefficient presents a larger percentual uncertainty because it is mostly related to small rolling amplitudes, which as reported in Fig. 5 and 6 present the largest experimental uncertainties. Despite of the posted results, it should be emphasized that, for the linear and cubic damping coefficients, uncertainties associated with the equivalent roll damping, the equivalent undamped rolling frequency and the rolling amplitude have not been considered. If considered, the uncertainties of nonlinear damping coefficients would be larger.

6. CONCLUSIONS

Uncertainty analysis when determining roll damping parameters should be performed, due to the importance of roll damping in the seakeeping behaviour of a ship or platform but also because it is informally accepted the existence of large uncertainties associated with this parameter and it could be interesting to demonstrate if this common assumption is true (or not).

In the paper, the procedure to determine the uncertainties associated with the equivalent linear roll damping and the equivalent undamped roll frequency uncertainties are presented. Both of them require to know the uncertainty associated with the time measurement, which may be easily determined from the sample frequency, and the uncertainty associated with the angle measurement, which, depending on the device used, may be easy to determined or may be more complex, such as when using optical trackable systems. Also, a simplified approach to determine uncertainties associated with the nonlinear damping coefficients is presented. This approach consists on only considering the uncertainties coming from the curve fitting procedure, which may represent a significant simplification.

This paper represents a first step forward towards developing an uncertainty analysis procedure for roll decay tests. However, further work needs to be carried out to improve the uncertainty assessment and to consider all the uncertainties when determining the nonlinear damping coefficients uncertainties.

7. ARISING QUESTIONS

During the development of the present work, some questions have emerged:

- Nowadays, how important is the roll damping uncertainty analysis.? How often uncertainty analyses are included when determining roll damping experimentally? When carrying out CFD validations, are experimental values including uncertainties used?
- How can we determine the standard uncertainty of the angle measurement when using an optical trackable system to measure it?
- Is it necessary to use a more complex approach to determine the uncertainties of the nonlinear roll damping coefficients?

ORCID

Adriana Oliva-Remola:
https://orcid.org/0000-0002-0491-1456

Luis Pérez-Rojas:
https://orcid.org/0000-0001-9027-8046

REFERENCES

Bulian, G., Francescutto, A., Fucile, F., 2009, Project HYD-III-CEH-5: Determination of relevant parameters for the alternative assessment of Intact Stability Weather Criterion on experimental basis – Appendix 1", Technical Report, HYDROLAB PROGRAMS, pp. 95 – 102, November 2009.

IMO 2006, "MSC. 1/Circ. 1200. Interim Guidelines for Alternative Assessment of the Weather Criterion", May 2006, London, United Kingdom.

IMO 2019, "SDC6/WP.6 – Finalization of the Second Generation Intact Stability Criteria. Report of the Expert's Group on Intact Stability", pp. 1-62, February 2019, London, United Kingdom.

Irvine, M., Longo, J., Stern, F., 2013, "Forward Speed Calm Water Roll Decay for Surface Combatant 5415: Global and Local Flow Measurements", Journal of Ship Research 54(2), pp. 202-219, DOI: 10.5957/JOSR.57.4.110043.

ITTCa, 2017, "Guide to the Expression of Uncertainty in Experimental Hydrodynamics. Procedure 7.5-02-01-01".

ITTCb, 2017, "Guideline to Practical Implementation of Uncertainty Analysis. Guideline 7.5-02-01-07".

ITTCc, 2017, "Tasks and structure of the 29th ITTC technical committees and groups (Conference changes implemented)".

ITTCd, 2017, "Uncertainty Analysis, Instrument Calibration. Procedure 7.5-01-03-01".

ITTC, 2011, "Numerical Estimation of Roll Damping. Recommended Procedure 7.5-02-07-04.5".

Oliva, A., 2018, "On Ship Roll Damping: Analysis and Contributions on Experimental Techniques", PhD Thesis, Universidad Politécnica de Madrid, DOI: 10.20868/UPM.thesis.54006.

Oliva, A., Pérez-Rojas, L., Díaz-Ojeda, H., 2018, "Ship Roll Damping Estimation: A Comparative Study of Different Roll Decay Tests", Proceedings of the 13th International Conference on Stability of Ships and Ocean Vehicles (STAB2018), September 16-21, Kobe, Japan, pp. 312-322.

Oliveira, A., 2011, "Novas abordagens para a análise do amortecimento não linear do balanço transversal de FPSOS", PhD Thesis, Universidade Federal do Rio de Janeiro.

Park, J.T., Turner, C.R., Melendez, M.P., 2016, "Physical Properties and Roll Decay with Uncertainty Estimates for DTMB Model 5720, 23rd Scale R/V Melville", Technical Report NSWCCD-80-TR-2016/018, Naval Surface Warfare Center, Carderock Division.

Söder, C.-J., Rosén, A., Werner, S., Huss, M., Kuttenkeuler, J., 2012, "Assessment of Ship Roll Damping through Full-Scale and Model-Scale Experiments and Semi-Empirical Methods", Proceedings of the 11th International Conference on Stability of Ships and Ocean Vehicles (STAB2012), September 23-28, Athens, Greece, pp. 877-886.

Spounge, J., Ireland, N., Collins, J., 1986, "Large amplitude rolling experiment techniques", Proceedings of the 3rd International Conference on Stability of Ships and Ocean Vehicles (STAB1986), September 22-26, Gdansk, Poland, pp. 95-102.

Wassermann, S., Feder, D., Abdel-Maksoud, M., 2016, "Estimation of ship roll damping: a comparison of the decay and the harmonic excited roll motion technique for a post panama container ship", Ocean Engineering 120, pp. 371-382, DOI: 10.1016/j.oceaneng.2016.02.009.

Zhao, W., Effhymiou, M., McPhail, F., Wille, S., 2016, "Nonlinear roll damping of a barge with and without liquid cargo in spherical tanks", Journal of Ocean Engineering and Science 1, pp. 84-91, DOI: 10.1016/j.joes.2015.12.002.

Analyse on several crucial factors for CFD simulation of roll damping

Min Gu, *China Ship Scientific Research Center, Wuxi, China* gumin702@163.com
Shuxia Bu, *China Ship Scientific Research Center, Wuxi, China* bushuxia8@163.com
Ke Zeng, *China Ship Scientific Research Center, Wuxi, China* 398638829@qq.com

ABSTRACT

Ship roll damping is one of key factors for the large amplitude roll motions, and the accurate prediction of a ship roll damping is very difficult. CFD method is one of important methods for the accurate prediction of roll damping. In this paper, several crucial factors for CFD simulations, such as boundary condition, wall function, mesh quantity and quality are analysed based on one ship model. Secondly, the influences of bilge keels on roll damping are also studied. Finally, several questions related to the CFD simulation of roll damping are discussed and the suggestions for the simulation are also proposed.

Keywords: *roll damping, crucial factors, CFD simulation.*

1. INTRODUCTION

The roll damping is a critical hydrodynamic factor to accurately predict large amplitude roll motion, such as synchronous roll or parametric rolling phenomena. At present, the simulation of roll damping is dominated by empirical formulations, experiment or CFD method.

In general, the most common empirical method is Ikeda's simplified method. The method decomposed ship roll damping into seven parts and combined them linearly to calculate roll damping for wall-sided hull forms at small angles, with and without forward speed (Himeno, 1981). Currently, vulnerability criteria for parametric roll and dead ship conditions are suggested to use the Ikeda`s simplified method. The simplified method can be used quite well for most traditional ships. However, if the ships are outside the application range of Ikeda' method, or the large amplitude roll motion in moderate or extreme wave, the accuracy of the damping coefficient is low. The experience or semi-experience formulas can`t cover all characteristics for unconventional ships, which limits the application of empirical formulations.

As the development of the second generation of intact stability criteria, the correspondence group on Intact Stability also proposed that the roll damping could be calculated by roll decay/forced roll model test or CFD simulation (United States & Japan, 2014). Although the model tests can give the reliable results, and the PIV measurement promote the analysis of detailed flow characteristics for roll damping recent years, but high cost and complexity in local flow measurement still hold back its application. Particularly, it is difficult for the large-scale model test (Haddara & Bass, 1988).

In the last decade, the numerical methods of Computational Fluid Dynamic (CFD) keep a rapid development. Direct CFD simulations are becoming feasible for calculating the roll damping of ships due to the viscous effects are important. In terms of high-performance computing systems become faster and more efficient, the simulation based on CFD methods is adopted by more and more researchers. Forced roll method and free decay method are two main methods for calculation of the roll damping by CFD, but the experience and principle of the modelling of this phenomenon are still in developing.

Over recent years, numerous researchers conducted CFD simulations to estimate damping coefficients with experiment data to improve accuracy of CFD technology. For instance, Chen et al. (2001), simulated with RANS method using overset mesh in conjunction with 6 Degree-of-Freedom (DoF) motion for time domain simulation of barge roll decay. Yang et al. (2013) performed numerical simulations of free decay for DTMB 5512 bare hull model at Fr=0.138 and 0.280 and

using Fluent with a dynamic mesh technique. The paper found that the natural period is overestimated by 1.3% for the low speed case and under-estimated at higher speed by 2.50%. Begovic et al. (2015) and Simon et al. (2018) presented the roll decay simulations for DTMB 5415 by Star CCM + at zero speed. The authors investigated the accuracy and efficiency of the numerical approach with different meshes, time steps and turbulence models. Handschel et al. (2012a, 2012b) used sliding interface mesh to calculate roll damping coefficients of a Post-Panamax container ship Duisburg Test Case in model scale at two forward speeds by free roll decay and forced roll motion. The decay simulations are free in 3 DOF, heave, sway and roll. The authors concluded that the simulation of the forced roll case is more stable and results in less computational time, especially for large roll amplitudes. And then, considering roll amplitude, ship speed, and vertical position of the roll axis on roll damping, the authors applied RANS numerical setup to calculate roll damping coefficients of a Ro-Pax ferry at full scale.

In our previous studies (Gu Min, et al, 2015), the forced roll motions of one 2D ship section based on the methods of orthogonal design and variance analysis were carried out, in which different calculation parameters for the roll damping was analyzed. Then the feasibility of CFD for the prediction of the roll damping was validated by taking one pure car carrier and one standard model 2792 as examples, in which two methods were used during numerical simulations: one is sliding interface method and another is dynamic overset grid method (Gu Min, et al, 2016). We (Gu Min, et al, 2018) also conducted the free roll decay motions under different scale factors of the three-dimensional ship and two-dimensional ship section.

In this paper, according to the previous studies, firstly we discuss several crucial factors for better CFD simulations, such as boundary condition, wall function, mesh quantity and quality et al. Secondly, the effects of bilge keels on roll damping are also studied. Finally, several other questions related to the CFD simulation of roll damping are discussed and the suggestions for the simulation are also proposed. The aim of the paper is to give some proposers to improve the accuracy for CFD simulation and discuss some factors that effects the simulation of roll damping.

2. COMPUTATION METHOD AND NUMERICAL SET UP

Mathematic model

The numerical simulations for the roll damping conducted based on RANS model. The free surface is modelled with the two phase VOF approach with a High-Resolution Interface Capturing (HRIC) scheme based on the Compressive Interface Capturing Scheme for Arbitrary Meshes. The pressure-correction algorithm of SIMPLE type is used for the pressure-velocity coupling. An Algebraic Multi-Grid (AMG) solver to accelerate the convergence of the solution. A segregated flow solver approach is used for all simulations.

The wall function approach was used for the near wall treatment, the approach is formulated to assure reasonable answers for meshes of intermediate resolution considered to capture the boundary layer flow with acceptable accuracy. The mesh quality (y+) has the most important effect on the roll damping, according to our study, the values of wall y + ≈ 1 is appropriate.

The non-dimensional roll damping coefficients can be got by formula (1).

$$B_{44} = \frac{M_R}{\omega \phi_0} \Rightarrow \hat{B}_{44} = \frac{B_{44}}{\rho \nabla B^2} \sqrt{\frac{B}{2g}} \qquad (1)$$

Where ϕ_0 is the initial roll amplitude, ω is the frequency of rolling, B is the width of model, ∇ is the volume for the model, M_R is the instant roll moment at the maximum rolling angular velocity.

Boundary Condition, Mesh Model and Time Step

Boundary conditions have effects on the simulation results, but the effects are not obvious. For the forced roll motions of 2D ship section, all wall boundary conditions are appropriate. For the free roll decay of 3D ships, the boundary of the computational domain is composed of inlet boundary, outlet boundary, wall boundary (hull surface). All of the outer domain boundary is velocity-inlet, except the outlet boundary is the pressure-outlet.

The mesh is the critical factor for CFD simulation. Based on our previous studies, a dynamic overset grid method and sliding method could perform the roll damping simulation with a pure car carrier and CEHIPAR 2792. The roll periods calculated by the overset gird method agree

with the experimental data better than the sliding mesh method, but the roll amplitudes calculated by the sliding mesh method have higher precision. We choose a RoPax to conduct further validation, the main particulars of the RoPax are given in Table 1, the hull geometry is shown in figure 1.

We can see from figure 2 that the roll amplitude caculated by the overset mesh agree well with the experimental data. We can also find in table 2 that the roll periods calculated by the overset gird method are within 1% error comparing with experiment results. In the table 3, we can obtain the same conclusion with our previous study, but the error is a little bigger than the experiment at small initial heel.

According to the ITTC Procedures and Guidelines (2011) recommendation for periodic phenomena (e.g. roll decay, vortex, shedding, incoming waves etc.) use at least 100 time steps per period. From the previous work, the convergence is obtained with 500 to 1000 time steps per period.

Especially for the dynamic overset mesh, the numerical stability of donor and acceptor cells scheme needs very short time step. The setting of time steps should guarantee the convective courant number less than 5.

Table 1: Principal particulars of the RoPax.

Items	Model
Mean draught: T	0.145m
GM:	0.064 m
KG:	0.195m

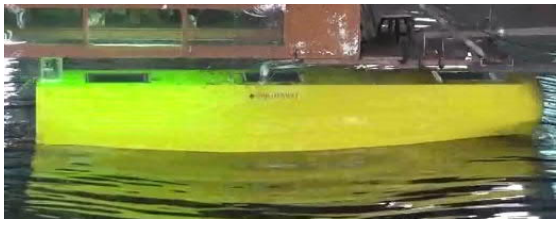

Figure 1: Hull geometry of the RoPax.

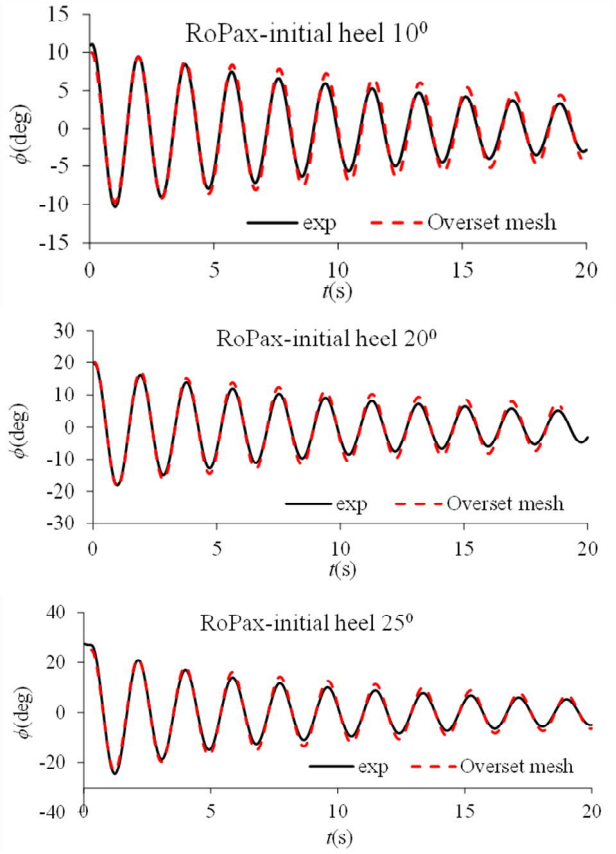

Figure 2: Free decay curves for a RoPax with initial heel 10°、20° and 25°.

Table 2: Roll periods with overset mesh.

Initial heel	Exp	Overset mesh	
	Value	Value	Error
10	14.85	14.74	0.74%
20	14.78	14.80	0.17%
25	14.77	14.74	0.19%

Table 3: Results of 2α calculated by different methods.

Initial heel	Exp	Overset mesh		sliding mesh		Ikeda	
	Value	Value	Error	Value	Error	Value	Error
10	0.0082	0.0050	39.02%	0.0060	26.83%	0.0046	43.90%
20	0.0103	0.0082	20.39%	0.0089	13.59%	0.0072	30.10%
25	0.0119	0.0092	22.69%	0.0100	15.97%	0.0085	28.57%

3. EFFECT OF BILGE KEEL

Even at small roll amplitudes, the bilge keel damping components have a large portion to the total damping and these contributions increase with both roll amplitude and roll frequency. In Ikeda's method, the bilge keel-hull interaction component is assumed not to depend on forward speed (Bassler et al, 2009).

The bilge keel provides a vortex generation around the ship which increases the viscous effect. The generated vortices by bilge keels suppress the roll motion by transferring energy from the ship to the surrounding fluid. Particularly, the exit of bilge keel leads to the flow separation, which increases the difficulty for CFD simulation.

To study the effect of the bilge keel on CFD simulation, we calculated the section of Series 60 non-dimensional roll damping coefficients with and without bilge keel by forced roll motion, as experimental tests on its forced roll have been conducted by Ikeda (Ikeda et al. 1977). During the calculation, the roll centre is located in the intersection between waterline and mid-perpendicular. The non-dimensional frequency ($\hat{\omega}$) is equal to 0.861, and the initial roll amplitudes are 0.1rad, 0.13rad, 0.15rad, 0.2rad respectively. The results are shown in figure 2.

We can see that non-dimensional roll damping from CFD simulation are in good accordance with the experimental results, while the damping with bilge keel is significantly larger than bare section. As the increasing of roll amplitude, the roll damping almost increases linearly. It indicated that the bilge keel damping is important for the roll damping accuracy in CFD simulation.

To further study the effect of the bilge keel on roll damping directly, we show the vorticity contours around the hull section at 1/4, 1/2, 3/4 and 1 period in forced roll motion.

The vorticity around the ship model section with bilge keel is obviously stronger than the bare ship model. The vorticity generation from the bilge keel changes the bilge keel force and the roll damping. The vortex shedding is the main physical phenomena involved in the viscous damping of the roll motion and it affects the flow velocity around the body that may lead to pressure change.

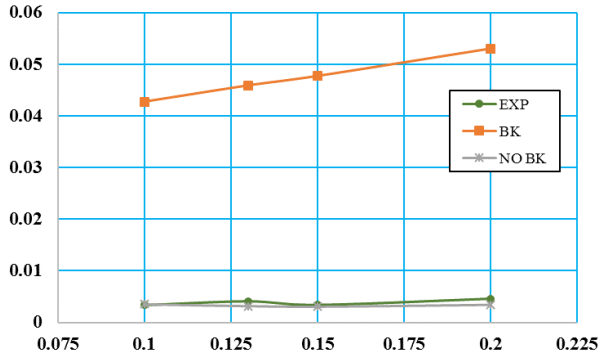

Figure 3: The non-dimensional damping coefficients for different roll amplitudes. (the Series 60 section S.S.5)

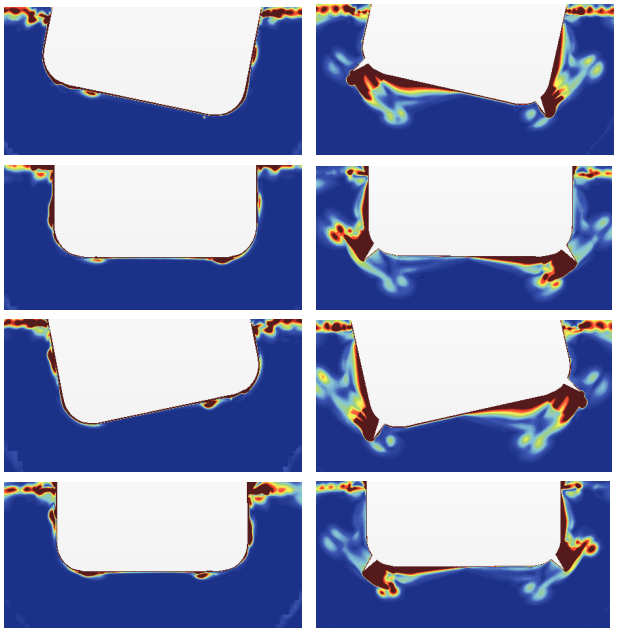

Figure 4: Vorticity contours around the hull section at 1/4, 1/2, 3/4 and 1 period (roll amplitude 0.2rad)

At this point roll direction changes, vortex starts to occur from the tip of the bilge keels and rolls up gradually with increasing strength. The vortex always follows the bilge keel, we can find vorticity generation around the bilge keel root at roll direction.

4. OTHER FACTORS

Scale effect

The large roll damping is strongly nonlinear, which has relationships with fluid viscosity and flow characteristics, such as the flow separation and vortex shedding. The scale effect could be important to simulate the roll damping. Nowadays, the model to full-scale is based on the Froude law of similarity. The Reynolds number are different

between model-scale and full-scale, which affect the boundary layer of hull and flow separation.

Since the difference between different scales is mainly in the difference of Re, which lead to the different thickness of the first gird layer. To obtain the sufficient accuracy, the value of y+ should guarantee to be located near 1.

According to the research, for the 2D ship section with bilge keels, the scale effects on roll damping coefficients are obvious, especially for the large initial roll amplitude. However, for the ship without bilge keels, the scale effects can be ignored. The reason may be that the bilge keels roll damping possesses an important part of the total roll damping, and the formation and shedding of the vortices around bilge keels are obvious. The example results are shown in figure 5 and 6.

Influence of degree of freedom

The effect of degrees of freedom is investigated with the pure car carrier, the simulations are performed with 3-DoF – roll, sway, and heave, 2-DoF – roll and heave.

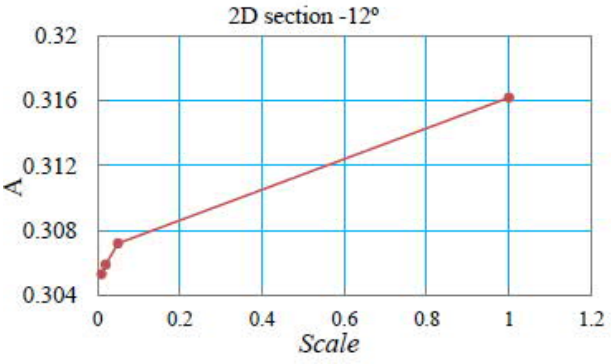

Figure 5: Comparisons of linear roll damping coefficients with different scale factors for a 2D ship section.

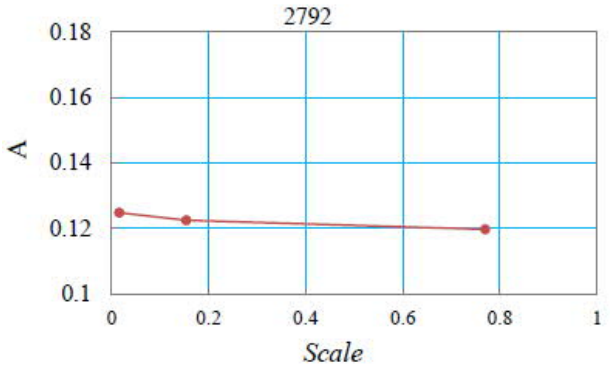

Figure 6: Comparisons of linear roll damping coefficients with different scale factors for CEHIPAR 2792.

It can be noted from figure 7 that the differences in roll amplitude with sway and without sway are negligible. It can be seen from figure 8 that coupling with sway can decrease the heave amplitude. In the simulation, as shown in figure 9, we find that the model drifts along one side, this phenomenon may cause from the pressure difference at the initial time. However, the model was constrained with spring at the horizontal position, the drift motion was not observed in the model test. The difference between the CFD simulation and model test for the drift motion needs further research.

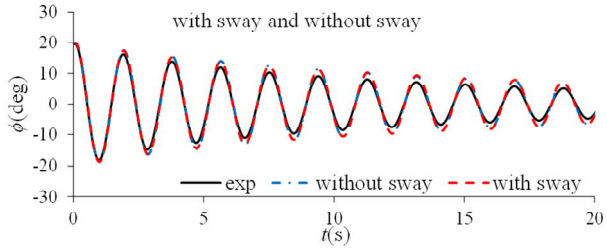

Figure 7: Comparisons of roll decay curve with sway and without sway for pure car carrier.

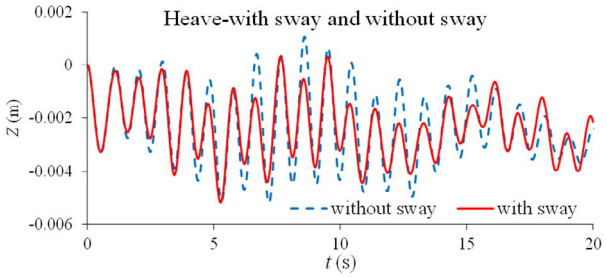

Figure 8: Heave amplitude with sway and without sway for pure car carrier.

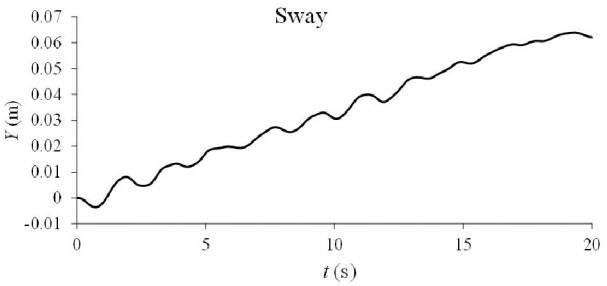

Figure 9: sway motion in CFD simulation.

5. DISCUSSIONS

In this paper, we summarize some crucial factors for CFD simulation of roll damping. In general, roll damping can be estimated using semi empirical methods, computational fluid dynamics (CFD) calculations, model tests or full-scale tests. None of these methods may be sufficient to capture

all roll damping behaviour of a given ship in any given condition separately.

The method based on RANS numerical solver has been used for the estimation of the roll damping successfully. The unsteady flow around a forced rolling and free roll decay is computed. The numerical results have a good agreement with experimental data in some conditions. Considering different dynamic mesh method, the time step may be a key factor, it usually should be less than 1/500 period for the roll damping simulation.

The flow around the hull with bilge keels is visualized and the generation of vortices is shown, it is observed that the strength of the vortex, to simulate the roll damping of ship model with bilge keel, the mesh around the bilge keel should be refine to capture the vortex variations.

Scale effects on roll damping coefficients are very obvious, especially for the large initial roll amplitude with bilge keel. The influence of viscosity around bilge keels may be the main reason for the scale effects of roll damping. The full-scale model test needs to be conducted to validate the scale effects with CFD simulation.

The simulation of roll damping is still a topic in developing. More works need to be made in future to improve accuracy of roll damping. Considering the speed effects on the roll damping simulation, comparing with the forced roll model test may be a promising. The uncertainly of the experimental and numerical simulations are both important works needed to be done.

6. ACKNOWLEDMENTS

This research is supported by Ministry of Industry and Information Technology of China (No. [2017] 614). The authors sincerely thank the above organization.

REFERENCES

Begovic, E., Day, A.H., Incecik, A., Mancini, S., Pizzirusso, D., 2015. Roll damping assessment of intact and damaged ship by CFD and EFD methods. In: Proceedings of 12th International Conference on Stability of Ships and Ocean Vehicles. Glasgow, 2015, ISBN-13: 978-1-909522-13-8.

Bassler C C, Reed A M. 2009.An analysis of the bilge keel roll damping component model[C]//Proc. 10th Intl. Conf. Stability of Ships and Ocean Vehicles.

Chen, H.C., Liu, T., Huang, E.T., 2001. Time domain simulation of large ship roll motions by a chimera RANS method. In: Proceedings of 11th ISOPE Conference, ISBN 1-880653-51-6.

Gu, M., Jiang Lu, Shuxia Bu, Chengsheng Wu, GengyaoQiu, 2015, Numerical Simulation of the Ship Roll Damping, 12th STAB, Glasgow UK, pp:341-348.

Gu, M., Bu, S., Qiu, G., Zeng, K., Wu, C., Lu, J., 2016. Validation of CFD simulation for ship roll damping using one pure car Carrier and one standard model. In: Proceedings of the 15th International Ship Stability Workshop, 13-15 June 2016, Pp. 165–172, Stockholm, Sweden.

Gu, M., Bu, S., Lu Jiang, 2018, Numerical Simulation of the Ship Roll Damping, 13th STAB, Japan, pp:323-330.

Himeno, Y., 1981, Prediction of Ship Roll Damping-State of the Art, Dept. of Naval Architecture and Marine Engineering, Univ. of Michigan, Report 239.

Handschel, S., Köllisch, N., Soproni, J.P., Abdel-Maksoud, M., 2012a. A numerical method for estimation of ship roll damping for large amplitudes. In: 29th Symposium on Naval Hydrodynamics Gothenburg, Sweden, pp. 26–31 August 2012.

Handschel, S., Kollisch, N., Abdel-Maksoud, M., 2012b. Roll damping of twin-screw vessels: comparison of RANSE with established methods. In: Proceedings of the 11th International Conference on the Stability of Ships and Ocean Vehicles, Athens, Greece, pp. 887–897.

ITTC Procedures and Guidelines, 2011. Practical Guidelines for Ship CFD Applications.7.5-03-02-03.

Ikeda, Y., Himeno, Y., & Tanaka, N., 1977a, “On Eddy Making Component of Roll Damping Force on Naked Hull”, Journal of the society of Naval Architects of Japan. Vol. 162, pp. 59-69.

Simon, Begovic, E., Day, A. H., & Incecik, A. 2018. Verification and validation of numerical modelling of DTMB 5415 roll decay. Ocean Engineering, 162, 209-223.

United States and Japan, 2014, “Draft Guidelines of Direct Stability Assessment Procedures as a Part of the Second Generation Intact Stability Criteria, IMO SDC1/INF.8, Annex 27.

Haddara, M.R. BASS, D.W., 1988, “Non-linear Models of Ship Roll Damping”, International Shipbuilding Progress, 35/401, pp. 5-24.

Yang, C.L., Zhu, R.C., Miao, G.P., Fan, J., 2013. Numerical simulation of rolling for 3-D ship with forward speed and nonlinear damping analysis. J. Hydrodyn. 25 (1), 148–155.

Study on short-term prediction of roll in beam sea

Toru Katayama, *Osaka Prefecture University*, katayama@marine.osakafu-u.ac.jp
Mai Kankaku, Student, *Osaka Prefecture University*, szb03054@edu.osakafu-u.ac.jp
Atsuo Maki, *Osaka University,* maki@naoe.eng.osaka-u.ac.jp
Kei Sugimoto, *ClassNK,* sugimoto@classnk.or.jp
Yusuke Fukumoto, *ClassNK*, y-fukumoto@classnk.or.jp

ABSTRACT

The formula to determine the roll angle for structural strength assessment in ClassNK's Technical Rule and Guidance gives an value based upon maximum roll amplitude at probability Q=10^{-8} on long-term prediction of roll amplitude. The long-term prediction is obtained from combining short-term prediction of roll amplitude and a probability of occurrence of short-term irregular sea in long term. In the current rule, non-linearity of roll is included as some correction coefficients obtained from model experiments and empirical knowledge at the time of development. However, the type of vessels has increased after the time of development, and the coefficients are not always suitable for the newest vessels. However, the type of vessels has increased after the time of development, and the coefficients are not always suitable for the newest vessels. The purpose of this study is to propose a rational short-term prediction method considering nonlinearity of roll. In this paper, applicability of a non-Gaussian PDF (Probability Density Function) for PDF of roll angle is investigated.

Keywords: *Short-term Prediction, Roll, Non-Gaussian Distribution.*

1. INTRODUCTION

The current formula to determine the roll angle for structural strength assessment in ClassNK's Technical Rule and Guidance gives an value based upon maximum roll amplitude at probability Q=10^{-8} on long term prediction of roll amplitude. The probability Q is defined as the number of encounter waves, which is roughly corresponding to 25year of designed life of a ship divided by 10s of average encounter wave period. The long-term prediction is obtained from combining short-term prediction of roll amplitude and a probability of occurrence of short-term irregular sea in long term. And the short-term prediction is the energy spectrum method based on the principle of linear superposition, which uses roll response function at small wave height and wave spectrum of short-term irregular waves. Additionally, non-linearity of roll is included as some correction coefficients obtained from model experiments and empirical knowledge at the time of development. However, the type of vessels has increased after the time of development, and the coefficients are not always suitable for the newest vessels.

Therefore, the fundamental revision is required, which is not only revision of correction coefficients to apply the present formula to all type vessels in recent years, but also proposal of rational new method to be able to apply to the vessel which will be further diversified in the future.

The purpose of this study is to propose a rational short-term prediction method including non-linearity of roll. In this paper, it is considered to apply a non-Gaussian PDF (: Probability Density Function) to PDF of roll angle. Roll measurement tests in irregular beam waves for scale models of PCC and LNG carrier are carried out to obtain probability density of roll, and the measured results are compared with Gaussian PDF and a non-Gaussian PDF to investigate its applicability.

2. PROBABILITY DENSITY FUNCTION OF ROLL

Gaussian distribution

Gaussian PDF is given as:

$$p_1(\phi) = \frac{1}{2\pi\sigma}\exp\left\{-\frac{\phi^2}{2\sigma^2}\right\} \tag{1}$$

where ϕ is roll angle (: time history data) [rad] and σ is standard deviation of roll angle. The standard deviation of roll angle σ is obtained from time history data of roll angle in irregular wave. If roll is linear, standard deviation can be obtained using Eq. (2) according to energy spectrum method[1)] based on the assumption of linear superposition.

$$\sigma^2 = \int_0^\infty [f(\omega)]^2 [A(\omega)]^2 d\omega \tag{2}$$

where f (ω) is wave spectrum and A (ω) is frequency response function of roll for small wave height.

Non-Gaussian distribution

If roll can be expressed by a one degree of freedom motion equation, a non-linear roll equation can be given as

$$\ddot{\phi} + \alpha\dot{\phi} + \beta\dot{\phi}\left|\dot{\phi}\right| + \frac{W}{I_{xx}}GZ(\phi) = M_{wave}(t)$$
$$GZ(\phi) = GM\phi + GZ_2\phi^2 + GZ_3\phi^3 + GZ_4\phi^4 + GZ_5\phi^5 \tag{3}$$

where t is time, a is linear damping coefficient, β is quadratic damping coefficient, W is ship weight, I_{xx} is moment of inertia of roll (including added component), GM is metacentric height, GZ_i is ith component of GZ polynomial fit and M_{wave} (t) is time history of wave excitation moment.

Maki (2016) and Maki et al. (2018) apply the method which is proposed by Sakata et al. (1979 and 1980) and Kimura et al. (1980, 1995, 1998 and 2000) to roll motion problem in irregular waves. In this frame work, solution of FPK (: Fokker-Planck-Kolmogorov) equation for external force as white-noise is approximately utilized. Kimura et al.(1995) reports that the form of PDF is strongly affected by the potential of the system for the case of non-white excitation. Therefore, they approximate the actual PDF for colored noise by the PDF for white noise. The non-Gaussian PDF of roll angle and roll angular velocity is described as:

$$p_2(\phi,\dot{\phi}) = C\exp\left[-d\left\{\alpha H(\phi,\dot{\phi}) + \frac{8\beta}{9\pi}\left(2H(\phi,\dot{\phi})\right)^{\frac{3}{2}}\right\}\right] \tag{4}.$$

The coefficients C and d in Eq.(4) are determined by Eqs.(5)-(6). Eq.(5) means the normalization condition of the PDF whereas Eq.(6) does the condition for variance.

$$\int_{-\infty}^{\infty} d\dot{\phi} \int_{\phi_{VN}}^{\phi_{VP}} p_2(\phi,\dot{\phi};d)d\phi = 1.0 \tag{5}$$

$$\int_{-\infty}^{\infty} d\dot{\phi} \int_{\phi_{VN}}^{\phi_{VP}} \phi^2 p_2(\phi,\dot{\phi};d)d\phi = E[\phi^2] \tag{6}$$

$$H(\phi,\dot{\phi}) = \frac{1}{2}\dot{\phi}^2 + \frac{{\omega_0}^2}{GM}\int_0^{\phi} GZ(\phi)d\phi \tag{7}$$

where ϕ_{VP} and ϕ_{VN} indicate two vanishing angles of roll restoring moment. H in Eq.(7) is dynamic energy at certain roll angle and roll angular velocity. In this research, integrations described by Eqs.(5)-(6) are conducted by using double exponential formula.

In order to obtain the PDF of Eq.(4), variance of roll angle, damping coefficients and restoring coefficients are necessary. In this study, the following three approaches are considered, however, and only first one of them is adopted. First one is that variance of roll angle and damping coefficients are obtained from model tests, and restoring coefficients are calculated. Second one is that coefficients of roll motion equation Eq. (3) are obtained theoretically (e.g. a strip method, Ikeda's roll damping prediction method and restoring calculation of) and variance of roll angle is obtained from solving Eq. (4) with Monte-Carlo Simulation. Third one is that all coefficients of Eq.(4) are obtained from the least square fit for measured probability density of roll angle.

3. SUBJECT SHIPS

Principal particulars of model ships

Subject ships are typical large PCC and LNG carrier in recent years. Figure 1 shows the body plans of the ships, and Table 1 shows their principle particulars of the subject ships. Height of the center of gravity KG and natural roll period T_n are obtained from an inclining test and a free roll decay test, respectively.

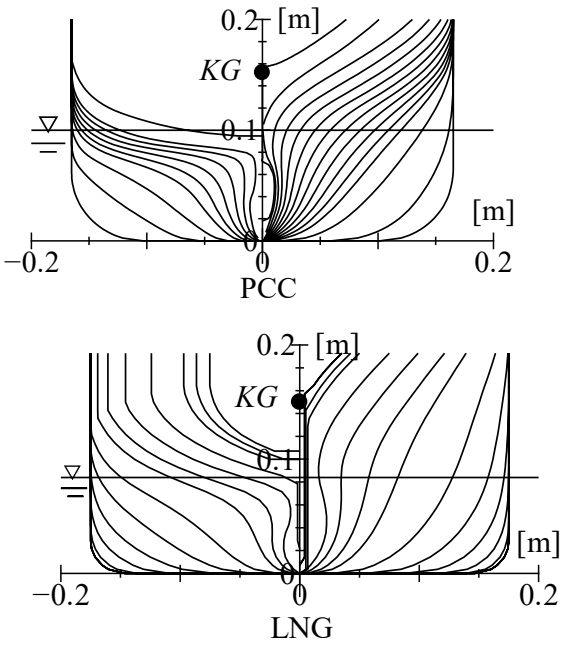

Figure 1: Body plan of models of PCC and LNG carrier.

Table 1: Principal particulars of the models.

name of ship	PCC	LNG
scale	1/97.5	1/140
overall length: L_{OA} [m]	2.054	2.095
breadth: B [m]	0.330	0.35
depth: D [m]	0.351	0.193
draught: d [m]	0.100	0.084
ship weight: W [kgf]	36.68	41.22
height of the center of gravity: KG [m]	0.152	0.150
metacentric height GM [m]	0.0126	0.0118
natural roll period: T_n [s]	1.96	2.19
position of bilge keels	s.s.3.4 - s.s.5.6.	s.s.3.65- s.s.6.45
initial trim [m]: $d_a - d_f$	0	0
LCG [m] from midship (+ aft)	0.0615	- 0.0193

Characteristics of roll restoring

Figure 2 shows calculated GZ-curves of the models. In the calculation, GZ is obtained under the equilibrium condition of vertical force and trim moment for each heel angle. This figure also shows the linear restoring lever GM of the GZ-curve. This figure shows that GZ-curve of PCC is linear up to 22 degree of heel angle and GZ-curve of LNG career is linear up to 10 degree of heel angle.

Eq. (8) and Eq. (9) show the fifth order polynomials for GZ-curves ($-30 < \varphi < 30$) of PCC and LNG carrier whose coefficients are decided by the least squares method.

$$GZ(\phi) = 0.0126\phi + 0.00310\phi^3 + 0.00727\phi^5 \quad (8)$$

$$GZ(\phi) = 0.0118\phi + 0.04099\phi^3 - 0.06807\phi^5 \quad (9)$$

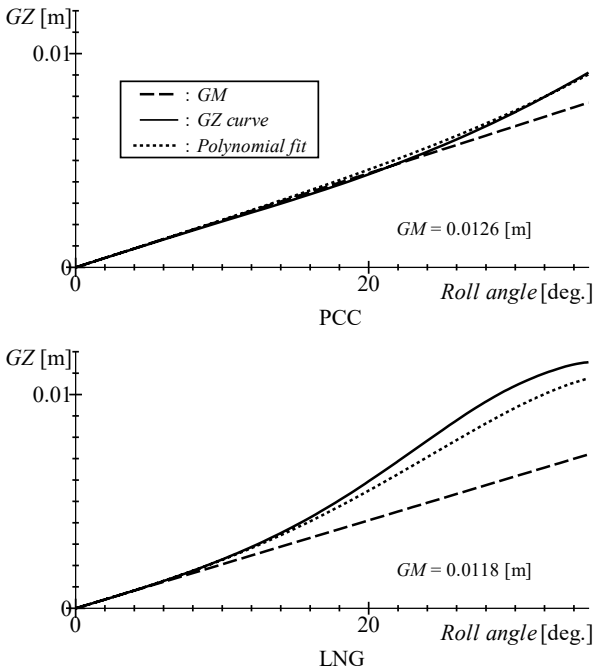

Figure 2: Calculated GZ-curve of these models.

Characteristics of roll damping

In order to obtain roll damping coefficients, free decay test is conducted. Roll, heave, pitch and sway of model are free. Measurement device is shown in Figure 5. By constraining the roll axis of the measurement devise, four initial heel angles (5, 10, 15 and 20deg.) are given. After releasing the constrain instantly, roll decay motion is measured with a potentiometer.

Using the measured results, the figure whose vertical and horizontal axis are roll peak angle φ_n and its occurrence time t_n is obtained as shown in Figure 3. And the curve in Figure 3 is fitted by a polynomial by the least squares method. From the polynomial, φ_n at t_n is re-obtained, and $\Delta\varphi_n$ and φ'_n of extinction curves shown Fig.4 are obtained by Eq. (10).

$$\varphi'_n = \frac{\varphi_n + \varphi_{n+1}}{2}, \quad \Delta\varphi = \varphi_n - \varphi_{n+1} \quad (10)$$

where sign of φ is degree. In order to obtain roll damping coefficients of Eq. (3), extinction curve is express as the Froude's expression of Eq. (11).

$$\Delta\varphi = a\,\varphi'_n + b\,\varphi'^2_n \quad (11)$$

The relation between extinction coefficients and roll damping coefficients is Eq. (12).

$$\alpha = \frac{4a}{T_\phi}, \quad \beta = \frac{3b}{4} \cdot \frac{180}{\pi} \tag{12}$$

where, T_ϕ is natural roll period.

Roll damping coefficients of PCC and LNG carrier are obtained from Fig.4 as α=0.254, β=0.486 for PCC and α=0.281, β=0.374 for LNG carrier.

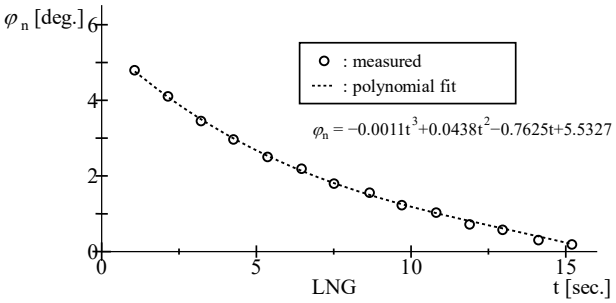

Figure 3: Peak angle of roll obtained by free decay test measured by potentiometer with 4 degree of free model (□0 = 5 deg.).

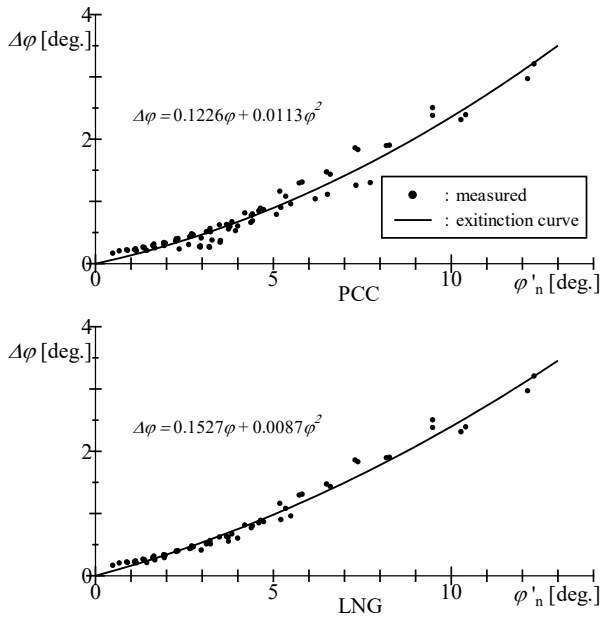

Figure 4: Extinction curves obtained by the data on Fig. 3.

4. ROLL MEASURMENT IN BEAM WAVES

Measuring device and coordinate system

Figure 5 shows a schematic view of experiment and its coordinate system. In this model experiment, surge and yaw are fixed whereas roll, sway (and drift), heave and pitch are free. Wave height is measured with a servo type wave height meter attached to model basin. Data is collected with 100Hz of sampling frequency. The carriage is pushed according to the drifting speed in order to avoid the sub-carriage hit both ends.

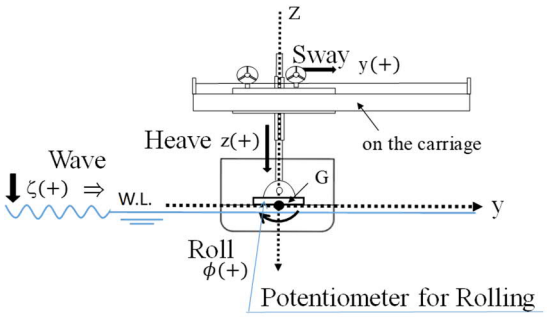

Figure 5: Schematic view of the motion measurement with fixed surge and yaw from the behind of hull.

Roll measurement in irregular beam waves

The wave spectrum of the long wavelength irregular wave of IACSRec.34 (: ISSC spectrum) shown as Eq.(13) is used.

$$S(\omega) = \frac{H_{1/3}^2}{4\pi}\left(\frac{2\pi}{T_Z}\right)\omega^{-5}\exp\left[-\frac{1}{\pi}\left(\frac{2\pi}{T_Z}\right)^4\omega^{-4}\right] \tag{13}$$

where $H_{1/3}$ is significant wave height and T_z is average zero up-crossing wave period. In this paper, it is adopted that peak period of the wave spectrum T_p is natural roll period T_n to cause large roll amplitude. The relation between peak period T_p and T_z is given as Eq. (14).

$$T_Z = T_p\left(\frac{4}{5\pi}\right)^{0.25} \tag{14}$$

Therefore, T_z of PCC and LNG carrier are 1.392s and 1.561s, respectively.

The formulas of significant wave height for strength assessment in ClassNK's Technical Rule and Guidance is given as

$$H_{1/3} = 0.85 \times \left\{10.75 - \left(\frac{300-L}{100}\right)^{1.5}\right\} \times \sqrt{\frac{L+\lambda-25}{L}} \tag{15}$$

where L is overall length of ship and λ is wavelength obtained by using natural roll period. From Eq.(15), the measuring conditions of the significant wave height of PCC and LNG carrier are 16.089 cm and 13.996 cm. The number of encounter waves is at least 700 waves each case.

Results

Fig.7 shows the PDF of roll angle. In this figure, measured result, Gaussian PDF of Eq.(1) and non-Gaussian PDF of Eq.(4) are shown. It is noted that non-Gaussian PDF shows the integral value of Eq.(4) for roll angular velocity.

Comparing these results, it is clear that the difference of them is negligible up to about ϕ=10deg regardless type of ship. On the other hands, in the range over ϕ=10deg, non-Gaussian PDF is smaller than Gaussian PDF and the measured results is similar to Gaussian PDF, however, the measured results for PCC shows asymmetry and the measured results for LNG carrier become lager than Gaussian PDF around ϕ=20deg.

Non-Gaussian PDF includes the non-linearity of roll damping and roll restoring, therefore, non-Gaussian PDF becomes smaller than Gaussian PDF at larger roll angle. However, non-Gaussian PDF include the effects of asymmetry of time average value of roll angle, it is difficult to see the effects on the results. On the other hand, non-Gaussian PDF include the effects of asymmetry of time average value of roll angle, however, it is difficult to see the effects on the results.

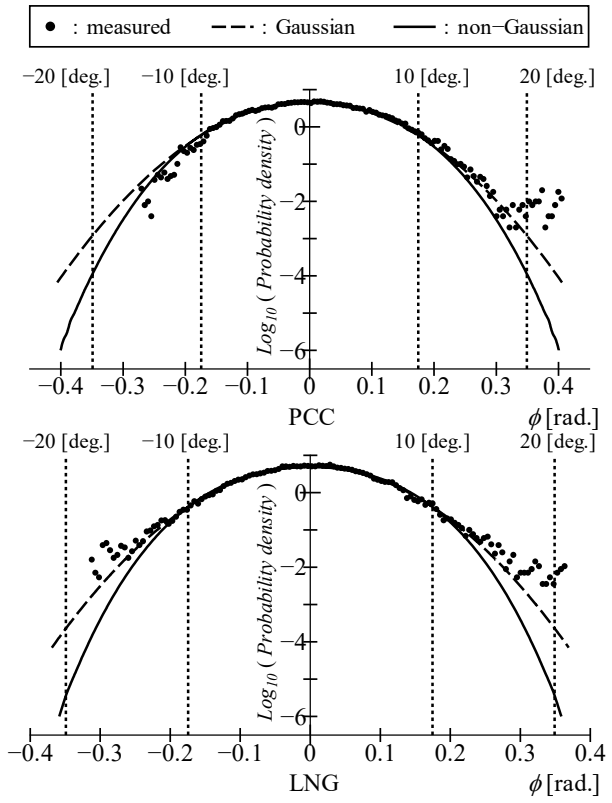

Figure 7: Probability density of roll angle.

In this paper, it is assumed that roll can be expressed by a one degree of freedom motion equation, non-Gaussian PDF is obtained. In order to make the reasons of discrepancies clear, the coupling motion effects on roll in irregular waves may need to be investigated.

5. CONCLUTIONS

In order to propose a rational short-term prediction method including non-linearity of roll, a non-Gaussian PDF is investigated and compared with measured results and Gaussian PDF, and the following conclusions are obtained.

1. The non-Gaussian joint PDF of roll angle and roll rate is utilized for the analysis. Here, this PDF is for the one degree of freedom roll equation with non-liner damping and restoring.
2. It is confirmed that the non-Gaussian PDF indicates the non-linear effects of roll equation by comparing with the Gaussian PDF.
3. The non-Gaussian PDF is compared with measured results, however, there is difference between them.

One of the reasons of the difference may be that the actual roll cannot be represented by the one degree of freedom equation due to coupling effects from sway to roll. In the near future, it will be investigated what equation is suitable for roll motion analysis.

ACKNOWLEDGMENT

Part of this research was supported by ClassNK.

REFERENCES

Kimura, K. and Sakata, M., 1980, “Non-Stationary Responses of a Non-Symmetric Non-Linear System Subjected to a Wide Class of Random Excitation”, Journal of Sound and Vibration, Vol.76, No.2, pp.261-272.

Kimura, K., 1995, “Non-Gaussian Equivalent Linearization for Estimation of Stochastic Response Distribution of Nonlinear Systems (in Japanese)”, Transactions of the Japan Society of Mechanical Engineers Series C, Vol.61, No.583, pp.831-835.

Kimura, K. and Morimoto, T., 1998, “Estimation of Non-Gaussian Response Distribution of a Nonlinear System Subjected to Random Excitation (Application to Nonwhite Excitation with Nonrational Spectrum (In Japanese)”, Journal of the Japan Society of Mechanical Engineers, Vol.64, No.617, pp.1-6.

Kimura, K., Takahara, K. and Yamamoto, S., 2000, “Estimation

of Non-Gaussian Response Distribution of a System with Nonlinear Damping (in Japanese)", Dynamics and Design Conference.

Maki A, 2017, "Estimation method of the capsizing probability in irregular beam seas using non-Gaussian probability density function". Journal of Marine Science and Technology, Vol. 22, No. 2, pp.351–360.

Maki, A, Sakai, M. and Umeda, N., 2018, "Estimating a non-Gaussian probability density of the rolling motion in irregular beam seas", Journal of Marine Science and Technology, doi.org/10.1007/s00773-018-0606-7 (First Online).

Sakata, K. and Kimura, K., 1979, "The Use of Moment Equations for Calculating the Mean Square Response of a Linear System to Non-Stationary Random Excitation", Journal of Sound and Vibration, Vol.67, No.3, pp.383-393.

Sakata, K. and Kimura, K., 1980, "Calculation of the Non-Stationary Mean Square Response of a Non-Linear System Subjected to Non-White Excitation", Journal of Sound and Vibration, Vol.73, No.3, pp.333-343.

Dunwoody A.B., 1989, "Roll of a Ship in Astern Seas – Response to GM Fluctuations", *Journal of Ship Research* 33(4), pp. 284-290.

IMO 2006, "MSC.1/Circ.1200 - Interim Guidelines for Alternative Assessment of the Weather Criterion", 24 May.

Kawahara, Y., Maekawa, K., Ikeda, Y., 2009, "A Simple Prediction Formula of Roll Damping of Conventional Cargo Ships on the Basis of Ikeda's Method and Its Limitation", Proceedings of the 10th International Conference on Stability of Ships and Ocean Vehicles, (STAB2009), St. Petersburg, Russia, pp. 387-398.

Interpretation of results of numerical simulation

Arthur M. Reed, *David Taylor Model Basin, Carderock Division, Naval Surface Warfare Center*

ABSTRACT

Running a numerical simulation of motions in waves is in and of itself of little significance. The results of the simulation—the motion time histories must be processed to produce statistical quantities if they are to be of any practical use. Techniques for dealing with time histories of non-rare and rare events are presented. In the realm of nonrare statistics, the techniques are further divided into statistics for the linear and nonlinear motion regimes. The focus is on non-rare events, but predicting rare event statistics is discussed.

1. INTRODUCTION

The raw output from a time-domain simulation of motions in random seas is of little use, unless the simulation is lucky enough to encounter a rare event—a stability failure that results in the termination of the run. Thus, the simulations must be planned based on the expected outcomes from the simulations. This planning needs to establish objectives as to what will be achieved by performing the simulations.

Without belaboring the planning process, which is worthy of a paper of its own, it is assumed that the interest is in knowing the "aver-age" motion amplitudes, the maximum motions that a vessel would be expected to experience, whether a vessel will have exceeded a particular motion threshold in given operational period in a given sea state or if it could be expected to suffer a stability failure over its lifetime. These are different questions, which are approached using different statistical techniques. This paper will discuss the methods by which answers to both the non-rare and rare problems of seakeeping and ship stability are de-rived from the results of a time-domain simulation of motions in a random seaway. For the most part, the problem of setting of objectives and further planning will not be discussed. whether a vessel will have exceeded a particular motion threshold in given operational period in a given sea state or if it could be expected to suffer a stability failure over its lifetime. These are different questions, which are approached using different statistical techniques.

The first of these questions requires statistical analysis to determine the single significant amplitude (SSA) motion amplitude and the confidence intervals on the SSA motion—the non-rare problem. The other questions, relating to maximum motions and rare problem, will require either an extremely long computer simulation resulting, with a bit of luck in a stability failure, or reliance on statistical extrapolation.

This paper will discuss the methods by which answers to both the non-rare and rare problems of seakeeping and ship stability are de-rived from the results of a time-domain simulation of motions in a random seaway. The problem of setting of objectives and further planning will not be discussed.

2. THE NON-RARE PROBLEM

I n the case of simulations associated with a non-rare problem, either the "average" motions that a vessel will experience under a certain operational condition (loading condition, speed and heading) in a given sea state are computed, or the maximum motions that a vessel will experience in a given loading and operational condition in a specific sea state are determined. Either way, it is necessary to determine the "average" motions—the single significant amplitude (SSA) motions, so that further decisions can be made regarding the statistical approaches that will be employed.

The characterization of a vessels expected maximum motions in a given sea state and condition takes further statistical analysis relatively simple of quite complex, depending on whether the motions are in the linear or nonlinear regime.

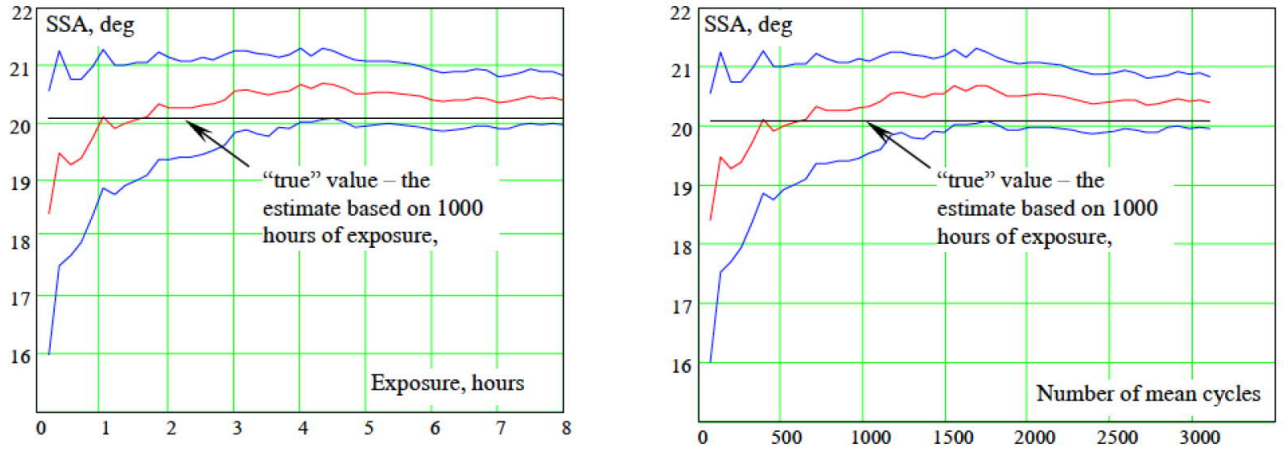

Figure 1: SSA Convergence of predicted roll motion as a function of run length based on synthetic data generated by LS3DoF; left-hand figure as function of time, right-hand figure as a function of cycles. (Courtesy of Vadim Belenky)

The process begins with the computation of the vessels motions for a minimal period of time, typically 3 h[1]. The length of time necessary to characterize the motions with a reasonable certainty is discussed in Reed (2019). Reed (2019) shows that at least 1000–1200 motion responses are necessary — many more responses than recommended in some other references that state that as few as 50 wave encounters are adequate.

For a seaway with a modal period of around 10 s, 1000 wave encounters requires around 3 h of data. However, it should be noted that a vessel does not respond to every wave encounter in every mode of motion, so that in fact it could require 25–30-percent longer than the 3 h to achieve the ideal 1000–1200 responses. Figure 1 shows the convergence of the SSA for roll as both a function of time and number of wave encounters, using synthetic data generated using LS6DoF (K. M. Weems and Belenky 2015). Based on this data, it might even be concluded that 6 h of data and 2500 wave encounters are required for convergence.

The motion computations can be a single run of 3 hs duration, or could be an ensemble of several shorter runs totaling 3 h, say 9 20 min runs. If a single run is employed, then care must be taken to ensure that the autocovariance function of the incident wave train remains well behaved throughout the entire length of the simulation, without any repeats—this requires a great number of Fourier series terms if the seaway is represented by a series with random phases, which is the most common way of generating a seaway for simulations. On the other hand, if a number of shorter runs is used, to ensure that the runs are statistically independent, unique wave seeds must be used to initialize seaway for each run.

To compute the SSA motions and confidence intervals for the motions of interest, the variance and variance of the variance of the motion time histories are computed (Belenky, Pipiras, and K. Weems 2015; ITTC 2017; Pipiras et al. 2018). Given the variance and the variance of the variance, the standard deviations of the motions are calculated as the square root of the variance and the SSA is twice the standard deviation. The confidence intervals follow in a similar manner, based on the confidence intervals of the variance.

If the only requirement is to predict the "average" motions, the SSA of the motions, that a vessel will experience while operating at a condition in a given sea state, this completes the process. This process must be repeated for every speed, heading to the seas, loading condition and seaway—significant wave height and modal period.

When it is necessary to predict the maxi-mum motions that a vessel will experience in a given condition in a particular seaway or to determine whether a vessel will exceed a particular motion limit or criteria, then additional statistical analysis is required. Computationally and statistically both of these questions are answered in a similar manner. Assuring, with a reasonable confidence, that the vessel does not exceed an operational limit only

[1] Unless otherwise noted, all times will be full-scale durations.

requires comparing the expected maximum motions against the requirement to see if that limit will be exceeded.

The statistics used to predict the maximum expected motions depend on the magnitude of the motions that are expected and the vessels hull form. The magnitude of the motions and the hull form determines whether the statistics are being analyzed in the linear motion regime or the nonlinear motions regime, and thus the statistical models that are required.

The process in the linear regime

If the motions are in the linear region then the problem is simple, while if the motions are in the nonlinear regime, then statistical extrapolation must be employed. Significantly greater simulated time is required for predictions in the nonlinear regime. For roll, the motion which this paper will focus on, linearity depends on the GZ curve, linearity applies as long as the initial range of the GZ curve relatively constant slope—for virtually all vessels, it can be reason-ably assumed that the motions are linear through 25º or 30º. This is where the expected motion amplitude comes into play, if the vessels motions will not exceed the linear response regime then it should not be necessary to simulate more than the 3 h of motions used to determine the SSA motions.

For motions in the linear regime the maximum expected motions ae purely a function of the standard deviation (σ) of the motions, and the only decision is whether to use σ or to be conservative and use a "σ" based on the upper confidence limit for the motions. The key here is that ship motions are assumed to be Gaussian and for narrow banded seas, the motions are equally or even more narrow banded due to the ship being a well-tuned filter for those modes of motion for which there is a restoring force. Thus the extremes of the process are Rayleigh, and for linear statistics the extremes of the Rayleigh distribution are directly related to the standard deviation of the motions (Ochi and Motter 1973; Ochi 1998).

For a given number of responses, there are available tables that give the expected extreme motions with a 95-percent confidence limit, i.e., 95-percent of the responses will be less than this limit (SNAME 1989, p. 91). The 95-percent non-exceedance maximum amplitudes, $\hat{y}_n$, are:

$$n = 100 \quad \hat{y}_n = 3.90\sqrt{m_0}$$
$$n = 1000 \quad \hat{y}_n = 4.45\sqrt{m_0}$$

where n is the number of cycles over which the limit is to apply and m_0 is the variance of the motions ($\sqrt{m_0}$ is the standard deviation). For motion limits, n = 1000 is a good choice, as most storms only last about 3 h, which corresponds to approximately 1000 wave encounters. SNAME (1989) provides no source for the above $\hat{y}_n$ limits, but equation (6.19) of Ochi (1998) provides a generalized formula for computing the limit:

$$\hat{y}_n = \sqrt{2\ln(n/\alpha)}\sqrt{m_0} \tag{1}$$

where α if the fraction of cycles that are to exceed the limit, and m_0 is as before. In the table above α is 0.05 (= 1 − 0.95).

Equation (1) is sufficient to assess the expected motions of a vessel based on its motion time history. However, it can also be used to determine whether the vessel meets a limiting criteria, and to determine the acceptable SSA motions for a vessel to satisfy a criteria.

As a *totally fictitious* example, if there were a requirement that a cruise ship not exceed 25º of roll in a storm, the formula $\hat{y}_n = 4.45\sqrt{m_0}$ could be inverted to determine that the SSA based on the computed motions should not exceed 11.2º (11.2º = 25º/2.225, where 2.225 = 4.45/2).

Based on the above, it obvious that it is easy to assess the interpret the results of a simulation when the motions are in the linear regime. How-ever, when the motions are extreme, and thus outside the linear regime the interpretation be-comes more complex and requires the simulation of longer time histories.

The process in the nonlinear regime

In the event of needing to characterize non-rare motions in the nonlinear regime, requires the development of the statistical distribution of the motions that have been predicted so that tail of the distribution can be evaluated to determine the probability of a certain motion level being exceeded. This is accomplished by fitting an appropriate statistical distribution to a histogram of the predicted motions, which in turn requires sufficient data for the histogram to represent the tail with sufficient fidelity.

There is not a good definition of what is enough data. The American Petroleum Institute (API) (API 2005) in their guidance for model testing states that to characterize ship motions, 3 h of data should be collected, and that to characterize extremes that at least five times more data is required. Extending the API guidance for model testing to simulations and assuming that motions in the nonlinear regime are extreme motions, that would say that a minimum of 15 h of motion data is required. K. M. Weems, Belenky, and K. J. Spyrou (2018) have used 50 h of data for their studies on statistical extrapolation (obtained as 100 1/2 h data sets). However, they have not performed any convergence studies to determine minimum data requirement—they obtain satisfactory results with 50 h of data for their cases. So it appears that somewhere between 15 and 50 h of motions must be simulated for statistical extrapolation, *for each condition that includes nonlinear motions*. Yet other researchers have used 100 h of data (Glotzer et al. 2017)

As stated above, the statistical extrapolation process requires fitting a statistical distribution to a histogram of the time-history data from the simulation. Knowledge of the appropriate statistical distribution affects the amount of date required, as it influences the number of parameters that need to be determined to define the distribution for extrapolation. If the motions are in the linear range, then the normal distribution is appropriate and only one parameter needs to be determined, the standard deviation (as has been described above, statistical extrapolation is not required if the data is Gaussian). Figure 2 shows a histogram with a distribution fit and illustrates statistical extrapolation.

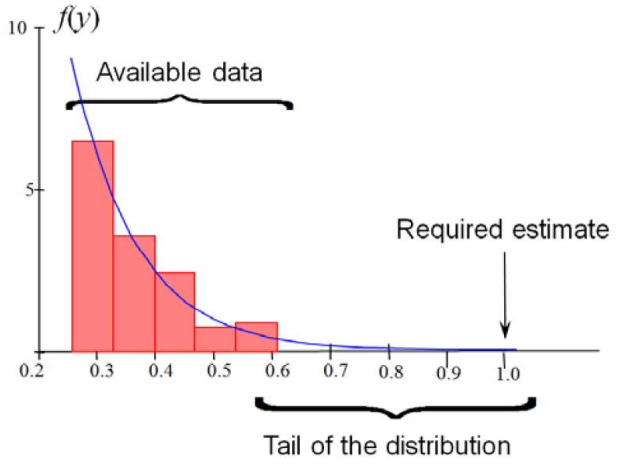

Figure 2: Tail of histogram fit with a GPD, showing extrapolation. (Campbell et al. 2014)

When the motions data is from the non-linear range, then usually the most general of distributions, the generalize Pareto distribution (GPD) (Pickands 1975; R. L. Smith 1987) must be employed. The probability density function (*pdf*) of the GPD is defined as:

$$f_{(\xi,\mu,\sigma)}(x) = \frac{1}{\sigma}\left(1+\frac{\xi(x-\mu)}{\sigma}\right)^{\left(-\frac{1}{\xi}-1\right)}$$

for $x \geq \mu$ when $\xi \geq 0$, and $\mu \leq x \leq \mu - \sigma/\xi$ when $\xi < 0$; where ξ is the shape, μ is the threshold (also called the location in the literature) where GPD starts to be applicable and σ is the scale. For $\xi = 0$ the GPD is the exponential distribution. If the tail of the distribution is above the exponential distribution the distribution has a "heavy tail; $\xi > 0$ and is defined for all $z \geq 0$. However, if the tail of the distribution lies below the exponential distribution the distribution has a "light tail; $\xi < 0$ and $0 \leq z \leq -1/\xi$. Figure 3 illustrates heavy and light tails relative to the exponential distribution.

The threshold is more of a parameter for the GPD, than a value describing the character of the distribution. The GPD is used in particular to fit the tail of distribution and is not appropriate for approximating an entire distribution over its whole range of support. Therefore, the choice of the threshold is not particularly critical to the fit of the distribution. If the threshold is chosen too small, portions of the underling distribution that are inappropriate to the describing the tail of the distribution will be included, and if too large a threshold is chosen, useful data for defining the tail will be excluded. Thus, several choices for the threshold should be used and the smallest one that does not appear to affect the details of the tail chosen, as it should minimize uncertainty.

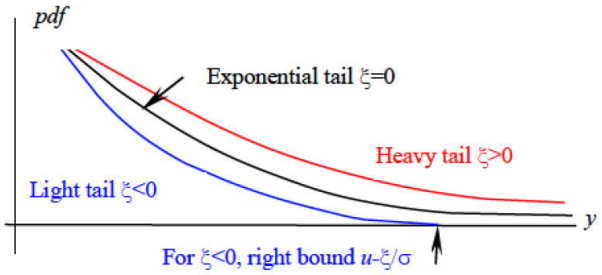

Figure 3: Heavy and light tails of a distribution relative to an exponential distribution. (Belenky, K. Weems, Pipiras, et al. 2018)

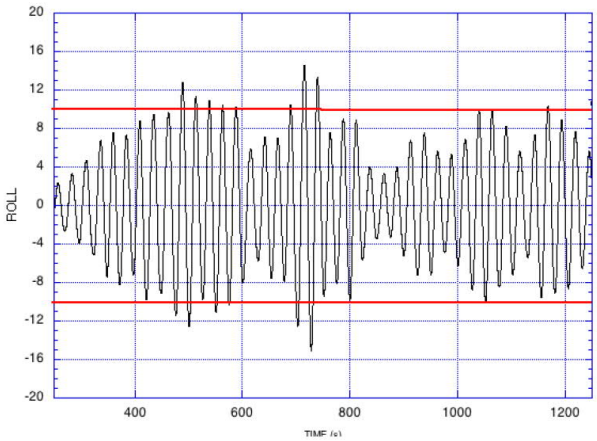

Figure 4: Peaks over threshold (POT) for a Roll Time History, heavy horizontal lines are the threshold.

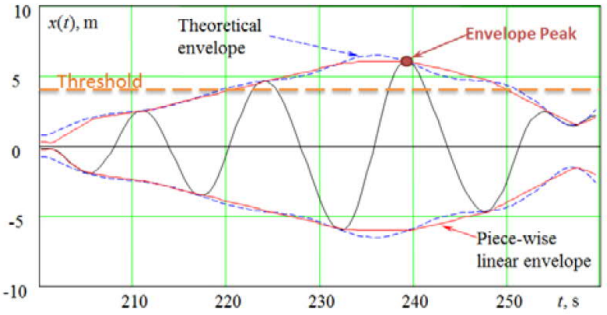

Figure 5: Envelope peaks over threshold (EPOT) for a Heave Time History (Campbell et al. 2014)

The scale and shape parameters are the ones that need to be fitted to define the tail of the GPD distribution. The need to accurately deter-mine these parameters will have a significant influence on the length of the simulation that must be run—the amount of data required to fit these parameters with reasonable accuracy.

There are a number of papers that describe fitting a GPD to ship motions time history data. As it is necessary to only fit the tail of the histogram, these papers apply either one of two methods to exclude the majority of the data, the data that makes up the peak of the histogram. These methods are peaks over threshold (POT) and envelop peaks over threshold (EPOT)[2]. In the EPOT approach, an envelope is constructed connecting the peaks and reflected troughs motion time history. The envelope can be deter-mined by taking the Hilbert transform of the time history (), or by brute force connecting the peaks and reflected troughts with straight lines—either is satisfactory for the purpose of determining the peaks above the threshold. Figure 4 shows an example of a POT using ±10º as the threshold, and Figure 5 shows an EPOT, for a different roll time history, again using a 10◦ threshold. Either the POT or EPOT approach is acceptable, though one must use a statistically independent set of peaks, so the clustering that results from the POT is less ideal than the EPOT approach, as one must eliminate clustered (adjacent) peaks, selecting only the maximum from the cluster, when using the POT approach. All the papers mentioned in the following discussion use EPOT.

The earliest of the papers fitting a GPD to the data is Campbell et al. (2014). T. C. Smith and Zuzick (2015) (and T. C. Smith 2019) per-form a formal validation of statistical extrapolation methods for predicting the tail of the distributions for roll, pitch and vertical and lateral acceleration. They employ two methods to determine the confidence intervals of their fit distribution, one that assumes a normal distribution for the distribution of the scale and shape parameters, and the other follows the method used by Campbell et al. (2014), except that they use the logarithm of the scale parameter to ensure that it remains positive. More recently Belenky, Glozter, et al. (2016) have used the GPD to study the nature of the tail of the extreme roll distribution.

As the tail of the roll distribution is fat (Belenky, K. Weems, Vladas Pipiras, et al. 2018), it is possible to make use of that fact to simplify the statistical extrapolation of roll by using a power law—Pareto distribution (PD) to fit the tail rather than the GPD. The *pdf* of the PD is defined as:

$$f_{(x_m,\alpha)}(x) = \frac{\alpha x_m^{\alpha})}{x^{1+\alpha}}$$

for $x \geq x_m$, where x_m is the threshold and α is the exponent (equivalent to $1/\xi$ in the GPD). The threshold of the PD serves the same function as the threshold of the GPD, so the PD only has one parameter, the exponent, that defines the tail, reducing the length of record (amount of data) needed to define the distribution, and rigor-ous methods for determining the exponent (Beir-lant et al. 2004; Dupuis and Victoria-Feser 2006; Mager 2015).

[2] Note that this threshold in not the same threshold that is used in the definition of the GPD.

Glotzer et al. (2017) have evaluated a number of methods for fitting the confidence interval (particularly the upper bound) for the exceedance probability in the GPD framework: the normal method, the lognormal method, the boundary method, the bootstrap method, the profile (likelihood) method, and the quantile method. Glotzer, et al. use the maxim likelihood method for estimators ξ and σ, employing both direct and quantile methods. They conclude that the quantile method based on profile likelihood works best, and the bootstrap method the poor-est. They also find that the normal and lognormal methods are slightly anticonservative.

In an effort to reduce uncertainty, Glotzer et al. (2017) examine using knowledge of the expected motion responses to further refine the fit. In particular, they take advantage of the fact that if the roll exceeds a certain limit, that capsize will result, and the fact that pitch is typically limited to 12º–15º, based on the shape of the longitudinal GZ curve. These limit dictate that the shape parameter of the GPD will be negative, and determine its value. Resulting in the need to fit only a single parameter, the scale parameter, σ.

3. THE RARE PROBLEM

It should be recognized that the simulation of a single stability failure is of little statistical significance—what if the vessel were to experience the 1-in-100,000 wave in the first few minutes of the simulation? And, in the case of predicting stability failures such as capsize in the dead-ship condition, one is seldom lucky enough to predict a failure in a reasonable length simulation. Proving that this is a truly rare stability failure in a random seaway, would require the simulation of many thousands of additional hours of motion histories. Therefore, another approach to predicting the occurrence of actual rare events.

The split-time method appears to be the most feasible way of assessing stability failure. However, it must be noted that the split-time method does not rely on a single time history of motions, but rather relies on repeated perturbations of a motion time history to identify up-crossings at high enough rates so as to result in a stability failure. This requires a custom modification of a motion simulation code and thus is in reality beyond the scope of the effort defined by the title of this paper—interpretation of the results of a numerical simulation.

The split-time method was first reported in Belenky, K. M. Weems, and Lin (2007) and Belenky, K. M. Weems, and Lin (2008), where roll at zero speed in beam seas was analyzed. The essential idea behind the split-time method is that of breaking the motion responses into nonrare and a rare portions. The motions are predicted in the usual manner until the predicted motion amplitude exceeds a pre-established threshold. At the point the simulation is halted and the state recorded. Then the motion predictions are continued for a a few cycles to oscillating about its upright equilibrium position or proceeds to a stability failure. The motion predictions are then repeated from the state where the threshold was exceeded with the roll rate at the moment of exceedance perturbed upward or downward to identify the critical roll rate at up-crossing that defines the boundary between stable motion equilibrium and stability failure. Figure 6 illustrates this process.

A series of the "distances" of the roll rate from that dividing rate is used as a metric to de-fine the exceedance rate, accumulated over an extended period of time—50 to 100 h, is fitted with a GPD to determine the exceedance rate. This process must be repeated multiple times to assure that the results are statistically consistent.

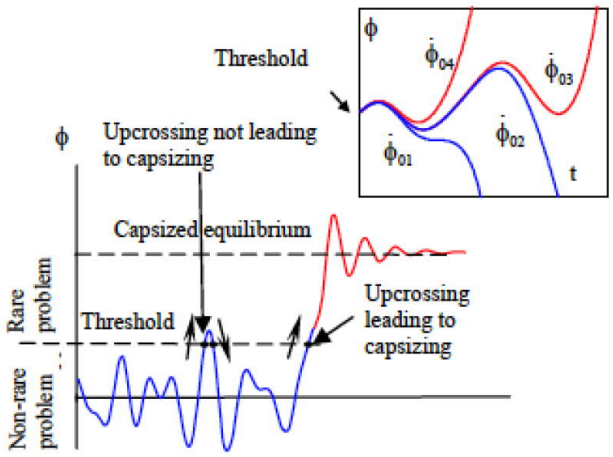

Figure 6: Split-time method at zero speed in beam seas, showing extrapolations with different roll rates at the threshold—threshold is constant. (Belenky, K. Spyrou, et al. 2012)

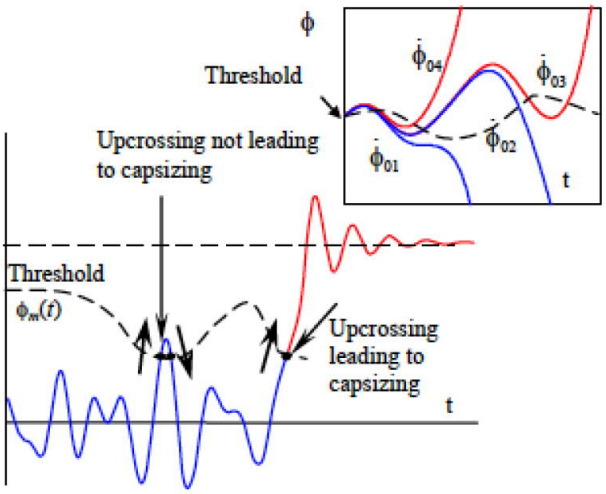

Figure 7: Split-time method at speed in bow quartering seas, showing extrapolations with different roll rates at the threshold—threshold varies with time (as a function of attitude on waves). (Belenky, K. Spyrou, et al. 2012)

The problem described above is idealized, in that the righting-arm curve of a vessel in beam seas is essentially constant—like that of a vessel in calm water. In bow or stern quartering seas, the righting-arm curve becomes time varying, complicating the problem even further. The extension of the split-time method to an unsteady righting arm curve is illustrated in Figure 7.

Belenky, K. M. Weems, Lin, and K. Spyrou (2010) extended their split-time method model to forward speed in bow quartering seas to deal with this more complicated problem, of a time varying righting-arm curve and began to discuss the application of the split-time method to surf riding and broaching, Belenky, K. Spyrou, et al. (2012) further extended their bow quartering seas and surf-riding analyses. Belenky, Pipiras, and K. M. Weems (2013) extended split-time method to pure loss of stability in waves, which requires a rigorous assessment of the instantaneous roll restoring force in waves. All of the above work is summarized in Belenky, K. Weems, and Lin (2016).

K. M. Weems and Belenky (2018) and K. M. Weems, Belenky, and K. J. Spyrou (2018) present a validation of the split-time method using a simplified model for predicting the motions, this simplified model allows the simulation of hundreds of thousands to millions of full-scale hours of motions in extreme seas in a few days. Each of these extended runs produces a few hundred stability failures, allowing the calculation of exceedance rates against which the results of the split-time method exceedance rates can be compared. Belenky, K. Weems, Pipiras, et al. (2018) use this data to study the tail of the distributions of the metric used to determine the critical roll rate.

4. SUMMARY

The characterization of ship motions in the linear and nonlinear regimes is described. In the linear regime, the extremes can be easily characterized using the standard deviation of the motions. In the nonlinear regime, an extended simulation length is required for a reasonable pre-diction of the tail of the statistical distribution to be determined—this tail in turn can be evaluated to provide estimates of the probability of extreme motions. The Generalized Pareto Distribution and Pareto Distribution are used for these fits. To facilitate the fitting of the tail to a histogram of the motion data a peaks over threshold (POT) or preferably an envelope peaks over threshold (EPOT) technique is employed to eliminate the smaller motions from the histogram.

It is not reasonable to directly observe stability failures using a time domain ship motion simulation tool. Therefore advanced techniques such as the split-time method must be utilized. A high-level over view of the split-time method is provided with many references to the implementation of the method. Even with the use of the split-time method, the prediction of exceedance rates for stability failures is not trivial.

REFERENCES

API (2005). Design and Analysis of Stationkeeping Systems for Floating Structures. Upstream Segment. Recommended Practice RP 2SK. Version Third Edition. Washington, DC: American Petroleum Institute. vii+181.

Beirlant, J., Y. Goegebeur, J. Segers, and J. L. Teugels (2004). Statistics of Extremes: Theory and Applications. Contributions by Daniel De Waal and Chris Ferro. New York: Wiley Interscience. xi+520.

Belenky, V., D. Glozter, V. Pipiras, and T. P. Sapsis (2016). "On the Tail of Nonlinear Roll Motions". In: Proceedings 15th International Ship Stability Workshop. (Stockholm, Sweden). STAB International Organizing Committee. Chalmers University of Technology and KTH Royal Institute of Technology. Chap. 4, pp. 109–114.

Belenky, V., V. Pipiras, and K. M. Weems (2013). "Split-time Method for Calculation of Probability of Capsizing Due to Pure Loss of Stability". In: Proceedings 13th International Ship Stability Workshop. Brest, France, p. 9.

Belenky, V., V. Pipiras, and K. Weems (2015). "Statistical Uncertainty of Ship Motion Data". In: Proceedings 12th International Conference on the Stability of Ships and Ocean Vehicles (STAB'15). Ed. by STAB2015 Secretariat. Glasgow, UK, p. 12.

Belenky, V., K. Spyrou, K. M. Weems, and W.-M. Lin (2012). "Split Time Method for the Probabalistic Characterization of Stability Failures in Quartering Seas". In: Proceedings 29th Symposium on Naval Hydrodynamics. Gothenburg, Sweden, p. 20.

Belenky, V., K. M. Weems, and W.-M. Lin (2008). "Numerical Procedure for Evaluation of Capsizing Probability with Split Time Method". In: Proceedings 27th Symposium on Naval Hydrodynamics. Seoul, South Korea, p. 25.

Belenky, V., K. M. Weems, W.-M. Lin, and K. Spyrou (2010). "Numerical Evaluation of Capsizing Probability in Quartering Seas with Split Time Method". In: Proceedings 28th Symposium on Naval Hydrodynamics. Pasadena, CA, p. 17.

Belenky, V., K. Weems, and W.-M. Lin (2016). "Split-time method for estimation of probability of capsizing caused by pure loss of stability". In: Ocean Engineering 122, pp. 333–343.

Belenky, V., K. Weems, V. Pipiras, D. Glotzer, and T. Sapsis (2018). "Tail Structure of Roll and Metric of Capsizing in Irregular Waves". In: Proceedings 32nd Symposium on Naval Hydrodynamics. (Hamburg, Germany). Ed. by K.-H. Kim and M. Abdel-Maksoud. Arlington, VA and Hamburg, Germany: Office of Naval Research nd the Hamburg University of Technology, p. 18.

Belenky, V., K. M. Weems, and W.-M. Lin (2007). A Probabilistic Procedure for Evaluating the Dynamic Stability and Capsizing of Naval Vessels, Phase 1: Technology Demonstration. SAIC Technical Report ASTD 08-017. Science Applications International, Corp. 211 pp.

Campbell, B. L., V. Belenky, and V. Pipiras (2014). "On the Application of the Generalized Pareto Distribution for Statistical Extrapolation in the Assessment of Dynamic Stability in Irregular Waves". In: Proceedings 14th International Ship Stability Workshop. (Kuala Lumpur, Malaysia), p. 8.

Dupuis, D. J. and M.-P. Victoria-Feser (2006). "A Robust Prediction Error Criterion for Pareto Modelling of Upper Tails". In: The Canadian Journal of Statistics 34.4, pp. 639–658.

Glotzer, D., V. Pipiras, V. Belenky, B. Campbell, and T. Smith (2017). "Confidence Intervals for Exceedance Probabilities with Application to Extreme Ship Motions". In: REVSTAT— Statistical Journal 15.4, pp. 537–563.

ITTC (2017). Single Significant Amplitude and Confidence Intervals for Stochastic Processes. Recommended Procedures and Guidelines 7.5-02-01-08. Procedure. Version 1. International Towing Tank Conference. 28 pp.

Mager, J. (2015). "Automatic Threshold Selection of the Peaks Over Threshold Method". Master's Thesis. Munich, Germany: Technische Universit¨at M¨unchen. viii+106.

Ochi, M. K. (1998). Ocean Waves: The Stochastic Approach. Ed. by I. Dyer, R. Eatock Taylor, J. N. Newman, and W. G. Price. Cambridge Ocean Technology Series 6. Cambridge, UK: Cambridge University Press. xii+319.

Ochi, M. K. and L. Motter (1973). "Prediction of slamming characteristics and hull responses for ship design". In: Transactions of SNAME. Vol. 81, pp. 144–173.

Pickands III, J. (1975). "Statistical Inference Using Extreme Order Statistics". In: The Annals of Statistics 3.1, pp. 119–131.

Pipiras, V., D. Glotzer, V. Belenky, M. Levine, and K. Weems (2018). "On Confidence Intervals of Mean and Variance Estimates of Ship Motions". In: Proceedings 13th International Conference on the Stability of Ships and Ocean Vehicles (STAB'18). (Kobe, Japan). Ed. by N. Umeda, T. Katayama, and A. Maki, pp. 575–586.

Reed, A. M. (2019). "Practical Aspects of Validating a Six-Degrees-of-Freedom Maneuvering in Irregular Waves Code for Extreme Conditions". In: Probabilistic Engineering mechanics. Ed. by P. D. Spanos. Submitted for publication.

Smith, R. L. (1987). "Estimating Tails of Probability Distributions". In: The Annals of Statistics 15.3, pp. 1174–1207.

Smith, T. C. (2019). "Validation Approach for Statistical Extrapolation". In: Contemporary Ideas on Ship stability and Capsizing in Waves, 2018. Ed. by V. L. Belenky, K. J. Spyrou, F. van Walree, M. A. Santos Neves, and N. Umeda. Cham, Switzerland: Springer Nature Switzerland AG. Chap. 49, pp. 573–589.

Smith, T. C. and A. Zuzick (2015). "Approaches to Ship Motion Simulation Acceptance Criteria". In: Proceedings 12th International Conference on the Stability of Ships and Ocean Vehicles (STAB'15). (Glasgow, UK). Ed. by STAB2015 Secretariat, pp. 1157–1170.

SNAME (1989). "Motions in Waves". In: Principles of Naval Architecture. Volume III. Motions in Waves and Controllability. Ed. by E. V. Lewis. Vol. 2. 3 vols. Jersey City, NJ: Society of Naval Architects and Marine Engineers. Chap. 8, pp. 1–190.

Weems, K. M. and V. Belenky (2015). "Rapid Ship Motion Simulations for Investigating Rare Stability Failures in Irregular Seas". In: Proceedings 12th International Conference on the Stability of Ships and Ocean Vehicles (STAB'15). Ed. by STAB2015 Secretariat. Vol. 2. 2 vols. Glasgow, UK: STAB2015 Secretariat, Department of Naval Architecture and Marine Engineering, University of Strathclyde, pp. 911–921.

Weems, K. M. and V. Belenky (2018). "Extended Fast Ship Motion Simulations for Stability Failures in Irregular Seas". In: Proceedings 13th International Conference on the Stability of Ships and Ocean Vehicles (STAB'18). (Kobe, Japan). Ed. by N. Umeda, T. Katayama, and A. Maki, pp. 587–597.

Weems, K. M., V. Belenky, and K. J. Spyrou (2018). "Numerical Simulations for Validating Models of Extreme Ship Motions in Irregular Waves". In: Proceedings 32nd Symposium on Naval Hydrodynamics. (Hamburg, Germany). Ed. by K.-H. Kim and M. Abdel-Maksoud. Arlington, VA and Hamburg, Germany: Office of Naval Research and the Hamburg University of Technology, p. 14.

Verification of damage ship survivability with computational fluid dynamics

Athanasios Niotis, *MSRC,* NAOME, Glasgow, athanasios.niotis@strath.ac.uk
Dracos Vassalos, *MSRC,* NAOME, Glasgow, d.vassalos@strath.ac.uk
Evangelos Boulougouris, *MSRC,* NAOME, Glasgow, evangelos.boulougouris@strath.ac.uk
Jakub Cichowicz, *MSRC,* NAOME, Glasgow, jakub.cichowicz@strath.ac.uk
Georgios Atzampos, *MSRC,* NAOME, Glasgow, georgios.atzampos@strath.ac.uk
Donald Paterson, *MSRC,* NAOME, Glasgow, donald.paterson@strath.ac.uk

ABSTRACT

In the new era of direct stability assessment (DSA) for ship survivability in intact and damaged conditions, direct and accurate evaluation of the safety level achieved by the design plays a vital role. Two are the most popular methods for DSA namely, time domain numerical simulation (TDNS) and Computational Fluid Dynamics (CFD). Both can be used for the evaluation of the safety level of a ship post casualties, following collision or a grounding incidents. It is common practice for the TDNS methods to have as a core a hydraulic model for capturing the propagation of the floodwater and its dynamics in order to reduce the computational cost. However, more recently, CFD methods have matured enough to provide a credible alternative, particularly concerning the investigation of complex fluid dynamics problems. The catch, however, is higher computation costs and this is where ingenuity helps. This paper proposes and demonstrates the feasibility of using high fidelity computational fluid dynamics tools for direct damage stability assessment of ships.

Keywords: *damaged ship, numerical tank, survivability verification, CFD, OpenFOAM.*

1. INTRODUCTION

The survivability of a ship after damage has been in the forefront of interest of the maritime community for almost six decades. Accidents of the past with devastating consequences in terms of human loses, environmental damage and financial cost have raised the alarm in the area of maritime safety. Engineers and scientist have been trying to investigate this complex hydrodynamic challenge using as main tools model experiments and numerical simulations.

Until the 1980s, the primary way to investigate the behaviour of a ship after damage was by model testing. However, limitations such as facility availability, cost, time, and physical constraints (e.g., scale effects and dynamic similarity) encouraged the development of mathematical models and numerical tools, which capture the physics accurately and to study allow to study the problem by means of numerical simulations.

Time domain simulation of flooding after damage is a very intriguing theoretical and engineering challenge, which started being investigating numerically since the 1980s at the University of Strathclyde in Glasgow. The main difficulty in this inquiry stems from the coupled non-linear dynamics between ship and floodwater, with complex interactions between ship, floodwater and environmental conditions.

The first time-domain simulation model was introduced by Spouge, 1985, for the investigation of the European Getaway accident. The ship motion was calculated by a quasi-static approach and the floodwater ingress with a hydraulic model. Vredeveldt & Journee in 1991 used hydraulic flow assumption coupled with one degree of freedom (DoF) dynamic roll motion model, which later expanded to a non-linear six DoF model (Journee, Vermee, & Vredeveldt, 1997). In their work Vassalos & Turan, 1994, developed a 3DoF dynamic model for the simulation of the behaviour of roro passenger vessels in irregular waves. One year later, the first 6 DoF model for the dynamics of a ship after flooding was introduced by the work of Letizia & Vassalos, 1995 & Vassalos D. , 2000. Papanikolaou

and Spanos introduced a lumped-mass model for the simulation of the floodwater dynamics inside the damaged compartment (Zaraphonitis, Papanikolaou, & Spanos, 1997; Spanos & Papanikolaou, 2001; Papanikolaou & Spanos, 2002). Santos & Soares, in 2006 used shallow water equations for the modelling of the floodwater behaviour. Ruponen, in 2007, developed a pressure correction technique based on the hydraulic model assumptions for the floodwater propagation in the internal spaces of the ship, which is represented as a hydraulic network.

The majority of the methods, which have been proposed are based on coupling hydraulic models for the floodwater propagation with quasi-static or dynamic models. Furthermore, the equations of ship motions are often linearized and based on the impulse response technique for transforming the results of the potential flow frequency domain to the time domain (Cummins, 1962). The fundamental assumptions of these models and the complexity of the phenomenon in question still leave some uncertainties regarding the capturing of its crucial characteristics, especially in the transient phase of flooding, which can profoundly influence the survivability of ships after damage (Vassalos, et al, 2003).

On the other hand, the astonishing theoretical and technological advancements in the field of CFD allowed researchers to use grid based RANS solvers or mesh free CFD techniques for the simulation of flooding of a ship after damage (van't Veer & de Kat, 2000; Strasser, Jasinowski, & Vassalos, 2009; Sadat-Hosseini, et al., 2012; Gao, Vassalos, & Gao, 2010; Shen & Vassalos, 2011; Skaar & Vassalos, 2006). However, their complexity and computational cost rendered the systematic use in a more systematic manner infeasible.

This work attempts to demonstrate the utilisation of CFD techniques for direct damage stability assessment and the survivability of ships after damage. Furthermore, it discusses challenges, limitations and opportunities in the direct comparison between high fidelity numerical fluid dynamic algorithms and time-domain simulation tools in the problem at hand.

2. TIME-DOMAIN SIMULATION

The time-domain simulation software, which has been used in this work is PROTEUS3 (Jasionowski, 2001).

The three main elements in the time-domain simulation of the motion of a ship after damage are the mathematical description of ship motion, the floodwater ingress and dynamics, and the environmental conditions, which influence the behaviour of both ship and floodwater.

Ship Dynamics

The mathematical description of ship motions is based on six degree of freedom rigid body motion equations, which derive from the conservation of linear and angular momentum.

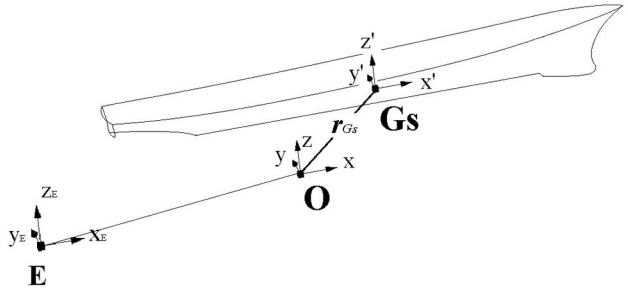

Figure 1: The coordinate systems used in the analysis.

The modelling of rigid body dynamics, involves three coordinate systems. An earth-fixed inertial frame of reference is assumed in point E with axes $x_E y_E z_E$. The second, inertial reference system has its origin at point O (usually placed at the intersection of the midship section, with the centre line plane and the waterline plane of the intact vessel at calm sea), local axis xyz and it moves with the average velocity of the hull.

The equations of motion of the ship are solved based on a third reference system $G_S x'y'z'$ attached to the centre of gravity of the intact vessel.

The motions of the ship are described by two vector equations, derived from the conservation of linear and angular momentum respectively (Jasionowski, 2001).

$$\frac{D}{Dt}\boldsymbol{P} = \boldsymbol{F} \tag{1}$$

$$\frac{D}{Dt}\boldsymbol{K_O} = \boldsymbol{M_O} \tag{2}$$

Where, $\boldsymbol{F}$ and $\boldsymbol{M_O}$ are the external forces and moments acting on the body in respect to the Oxyz frame of reference. The linear momentum of the translating body $\boldsymbol{P}$ and the angular momentum $\boldsymbol{K}_O$ relative to the same coordinate system are

$$\boldsymbol{P} = \sum m_i \cdot \boldsymbol{v_i} \tag{3}$$

$$\boldsymbol{K_O} = \sum \boldsymbol{r_O} \times m_i \cdot \boldsymbol{v_i} \quad (4)$$

Where m_i is the finite mass of the rigid body, $\boldsymbol{v_i}$ its velocity and $\boldsymbol{r_O}$ its position vector with respect to the $Oxyz$.

The total mass of the vessel in each time instant is the sum of the intact ship mass M_S and the total floodwater mass M_w, which is equal with the addition of the floodwater mass in each individual compartment j , $\sum_j m_j$.

$$M = M_S + M_w = M_S + \sum_j m_j \quad (5)$$

Assuming that the floodwater mass m_j in each compartment is concentrated to its centre of gravity the equations (3) and (4) are equal with

$$\boldsymbol{P} = M_S \cdot \boldsymbol{v_S} + \sum m_j \cdot \boldsymbol{v_j} \quad (6)$$

$$\boldsymbol{K_O} = \boldsymbol{r_{Gs}} \times M_S \cdot \boldsymbol{v_S} + \sum \boldsymbol{r_j} \times m_j \cdot \boldsymbol{v_j} \quad (7)$$

where, $\boldsymbol{r_{Gs}}$, $\boldsymbol{v_S}$ the position and velocity vectors of the centre of gravity of the intact ship mass with respect to the $Oxyz$ coordinate system, and $\boldsymbol{r_j}, \boldsymbol{v_j}$ the position and velocity vectors of the centre of gravity of each floodwater mass in respect to the same coordinate system.

The final equations of linear and angular momentum equations as derived form the (6) , (7) after the trnasformation of the frame of reference form the $Oxyz$ to the $G_Sx'y'z'$ are (Jasionowski, 2001),

$$\begin{aligned} & M_w \cdot \left[\frac{d}{dt}\boldsymbol{v'_{GsGw}} + 2 \cdot \boldsymbol{\omega'} \times \boldsymbol{v'_{GsGw}}\right] \\ & + M_w \cdot \left[\frac{d}{dt}\boldsymbol{\omega'} \times \boldsymbol{r'_{GsGw}} + \boldsymbol{\omega'} \times (\boldsymbol{\omega'} \times \boldsymbol{r'_{GsGw}})\right] \\ & + \frac{d}{dt} M_w \cdot (\boldsymbol{v'_{GsGw}} + \boldsymbol{\omega'} \times \boldsymbol{r'_{GsGw}}) \\ & + (M_s + M_w) \cdot \frac{d}{dt}\boldsymbol{v'_{Gs}} + \frac{d}{dt} M_w \cdot \boldsymbol{v'_{Gs}} + \boldsymbol{\omega'} \times (M_s + M_w) \cdot \boldsymbol{v'_{Gs}} = \boldsymbol{F'} \end{aligned} \quad (8)$$

$$\begin{aligned} & (I'_s + I'_w) \cdot \frac{d}{dt}\boldsymbol{\omega'} + M_w \cdot \left[\boldsymbol{r'_w} \times \left[\frac{d}{dt}\boldsymbol{v'_{Gs}}\right]\right] \\ & + M_w \cdot [(\boldsymbol{\omega'} \times \boldsymbol{r'_w}) \times \boldsymbol{v'_w}] + \left(\frac{d}{dt} I'_w\right) \cdot \boldsymbol{\omega'} \\ & + M_w \cdot \left[\boldsymbol{r'_w} \times \left[\frac{d}{dt}\boldsymbol{v'_w} + \boldsymbol{\omega'} \times (\boldsymbol{v'_{Gs}} + \boldsymbol{v'_w})\right]\right] \\ & + \frac{d}{dt} M_w \cdot [\boldsymbol{r'_w} \times (\boldsymbol{v'_{Gs}} + \boldsymbol{v'_w})] \\ & + \boldsymbol{\omega'} \times \left[\left((I'_s + I'_w) \cdot \boldsymbol{\omega'}\right)\right] = \boldsymbol{M'_{Gs}} \end{aligned} \quad (9)$$

In the equations (8) and (6) the force $\boldsymbol{F'}$ and the momentum $\boldsymbol{M'_{Gs}}$ and are calculated in the body fixed reference system $G_Sx'y'z'$.

The external forces and moments are determined based on the supposition of the following hydrostatic and hydrodynamic entities: Froude-Krylov forces calculated with body exact formulation; radiation and diffraction forces calculated in the frequency domain using linear potential theory and then transferred to time domain with the incorporation of convolution and spectral techniques (Vassalos D. , 2014). These forces pre – calculated for a range of loading conditions, speed and headings; and the values are stored in a hydrodynamic database. During the time-domain simulations the instantaneous values interpolated from the database.

Floodwater ingress

The floodwater ingress and propagation use hydraulic models. The volumetric flow rate Q is calculated, based on the Bernoulli equations as a function of the difference of the hydrostatic heads dh between sea and damaged compartment (Vassalos, Turan, & Pawlowski, 1997).

$$Q = K \cdot A \cdot \int_t^{t+dt} \sqrt{2 \cdot g \cdot dh} \cdot dt \quad (10)$$

Where, K is a pressure loss coefficient, A the effective area of the opening and g the accelleration of gravity.

3. CFD FOR FLOODING SIMULATION

A step change in the investigation of survivability of a ship after damage comes from the application of CFD techniques for the analysis of this problem. However, despite impressive developments in the field of numerical fluid mechanics, the computational cost remains significant. For this reason, high fidelity CFD algorithms are used selectively, for the treatment of

specific issues that simplified time-domain simulation models cannot capture.

The flooding process after collision or grounding can be divided into three stages: transient, progressive flooding, and stationary-state (Vassalos, Jasionowski, & Guarin, 2006; Jasionowski, Vassalos, & Guarian, 2004). The peculiarity of this problem is that each stage requires a different level of detail in its physical modelling.

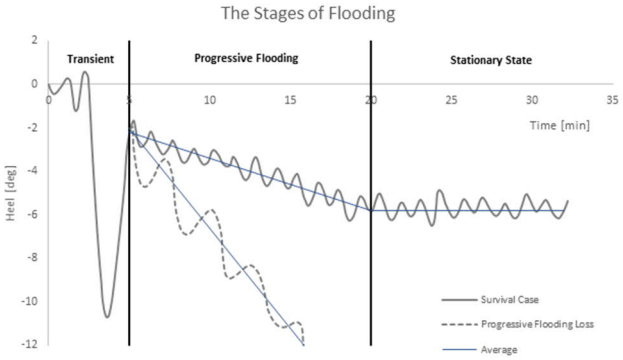

Figure 2: Flooding stages of a ship after damage.

CFD for transient flooding

When a ship or floating structure suffers from a breach on her hull, the very first moment of the incident is characterised by the complex hydrodynamics equilibrium. The pressure gradient in the vicinity of the damage opening prompts the generation of a high momentum fluid jet. The accurate capturing of the impact of the jet is vital for the assessment of the survivability of the vessel in transient response. The momentum of the jet is influenced by the hydrodynamic pressure at the opening, the geometry of the damage and the internal arrangement that receives the impacting jet. High fidelity CFD tools can provide critical insight into the complex hydrodynamics of this stage that simplified hydraulic models cannot capture.

CFD for progressive flooding

The next stage of the flooding process is the propagation of the floodwater in the vicinity of the damaged compartments through internal openings. The course of this stage is highly influenced by the watertight and non-watertight subdivision of the vessel as well as the sea condition. The problem can be closer to a hydraulic network routing in case of ships with a complex arrangement such as cruise ships or a hydrodynamic nature in the case of ships with large undivided spaces, such as the car deck of RoPax vessels. A key element for the accurate prediction of the survivability of the ship, during this stage, is her response to waves. In the final stages of the progressive flooding and before the stationary state condition the fast, simplified models have an advantage as the nature of the problem is driven largely by hydraulic energy rather than the hydrodynamic momentum. Still, CFD models can give a better insight into the impact of various design details, which influence the outcome of the incident. Examples include the collapse of watertight doors, the influence of the arrangement of the openings, and a better prediction of the motions of the vessel under various environmental conditions.

4. LIFE-CYCLE FLOODING RISK ASSESSMENT FRAMEWORK

The Life-Cycle Flooding Risk Assessment Framework introduces a coherent decision-making rationale for the evaluation of the safety level of a ship against flooding. This approach entails the survivability assessment of the ship after flooding during the design phase, the operational phase and the emergency response phase, each of them having deferent safety objectives and employs different tools (Vassalos, et al., 2018).

A primary characteristic of this approach is that it evolves as the design and the operation of the vessel unfolds. The initial stage of the design starts with static vulnerability assessment and as the design process unfolds and becomes more detailed the assessment changes in nature and becomes dynamic with the use of time-domain simulation tools. The assessment finally is verified with the incorporation of CFD tools, which are used for vulnerability assessment and verification in critical scenarios.

Static Vulnerability Screening (SVS)

The static vulnerability screening stage includes the probabilistic damage calculations based on the current SOLAS accident statistics. The output from this stage is the most critical scenarios which pass to the next stage of the dynamic vulnerability screening. The demarcation of the critical cases is based on the hydrostatic properties at the equilibrium position as it judged by the SOLAS regulations.

Dynamic Vulnerability Screening (DVS)

After the identification of critical scenarios, the time domain simulation tool Proteus3 is employed for the dynamic survivability assessment of the ship in waves. The investigation will be performed for

various operating and environmental conditions. The identified vulnerabilities can be either limited by design solutions or watertight door management and damage control options.

Verification & Approval (V&A)

This stage incorporates the use of a numerical wave tank based on high fidelity CFD tools for the verification of the survivability of the ship in critical damage scenarios. The process includes:

1) Identification of critical cases from DVS
2) Numerical wave tank set up
3) Execution of simulations
4) Uncertainty analysis of the results
5) Submission to the authorities for approval.

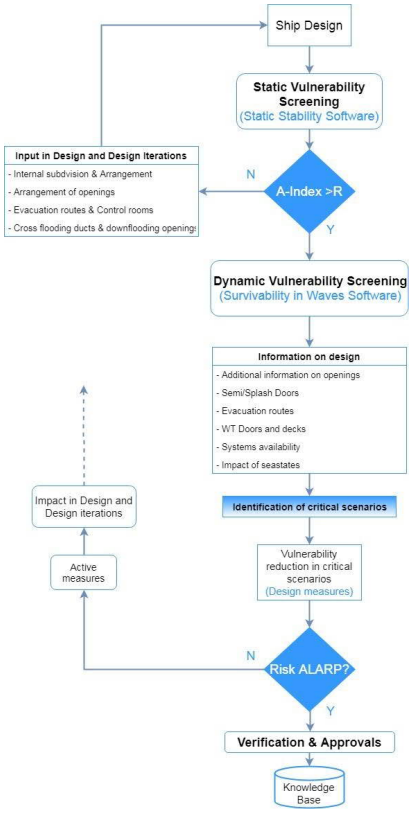

Figure 3: Survivability assessments of a ship after flooding during the design phase (Vassalos, et al., 2018).

5. VERIFICATION OF TIME-DOMAIN SIMULATION WITH CFD

Governing equations

For the development of a numerical tank for the verification of survivability of ships after damage with high fidelity CFD tools the OpenFOAM, an open source CFD toolbox, is used.

The governing equations for unsteady, incompressible, isothermal, viscus two-phase flow are given by the Navier – Stokes equation (Ferziger & Peric, 2002; Moukalled, Mangani, & Darwish, 2016).

$$\nabla \cdot \boldsymbol{u} = 0 \tag{11}$$

$$\frac{\partial(\rho \boldsymbol{u})}{\partial t} + \nabla \cdot (\rho \boldsymbol{u}\boldsymbol{u}) = -\nabla p + \nabla \cdot \boldsymbol{T} + \rho \boldsymbol{g} + \boldsymbol{f_\sigma} \tag{12}$$

Where, ρ is the density of the fluid, $\boldsymbol{u}$ the velocity vector, p the pressure, $\boldsymbol{T}$ the stress tensor, $\boldsymbol{g}$ the gravitational acceleration, and $\boldsymbol{f_\sigma}$ the force due to surface tension which in the specific engineering problem can be assumed negligible. As the flow is assumed incompressible, the density is constant so the momentum equation is transformed into:

$$\frac{\partial \boldsymbol{u}}{\partial t} + \nabla \cdot (\boldsymbol{u}\boldsymbol{u}) = -\frac{\nabla p_{rgh}}{\rho} + \nabla \cdot \left(v_{ef} (\nabla \boldsymbol{u} + (\nabla \boldsymbol{u})^T) \right) \tag{13}$$

Where, $p_{rgh} = p + \rho \boldsymbol{g} h$ the total pressure and $v_{ef} = v + v_{turbulence}$ the effective viscosity which takes into account the turbulence model. For more details please see references (Damian; Foundation, 2014) and the source code.

For the determination of the interface between water and air, the volume of fluid model (VoF) is implemented (Jasak H. , 2017). With the assumption of one continuum medium in the problem domain the VoF includes one more unknown scalar a which is defined as the volume of fraction between the air and the water. Assuming that the volume of fraction defined as

$$0 \leq a \leq 1 \tag{14}$$

Where, $a = 0$ refers to the air, $a = 1$ refers to water and $0 < a < 1$ refers to the transitional region between the two fluids. The volume of fluid method introduces one more governing equation which is the scalar transport equation of the volume fraction a, defined as,

$$\frac{\partial \alpha}{\partial t} + \nabla \cdot (\boldsymbol{u} a) + \nabla \cdot \boldsymbol{u_c} a(1-a) = 0 \tag{15}$$

Where, $\nabla \cdot \boldsymbol{u_c} a(1-a)$ is an anti – diffusion term used to sharpen the interface in the parts of the domain where there is a transition between the two phases (So, Hu, & Adams, 2009). The velocity $\boldsymbol{u_c}$ is difined as the relative velocity between water and air.

The VoF model introduces the assumption of one medium in the field with density and viscosity equal with,

$$\rho = a\rho_1 + (1-a)\rho_2 \quad (16)$$

$$\mu = a\mu_1 + (1-a)\mu_2 \quad (17)$$

where, ρ_i and μ_i the value of the density and viscosity of the fluid i.

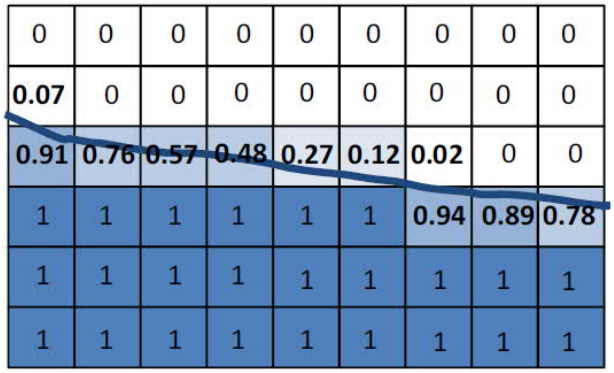

Figure 4: Volume of fluid interface capturing method (Davidson, Cathelain, Guillemet, Huec, & Ringwood, 2015)

Finite Volume Method

The governing equations of the motion of fluid should be discretized in time and space for the numerical solution of the flow variables. Finite Volume Method (FVM) is the preferable discretisation technique as it is a well-established method in the field of computational fluid dynamics (Moukalled, Mangani, & Darwish, 2016).

The significant advantage of the FVM is the use of integral representation of the governing equations which fulfil easier the conservation laws of fundamental physics (Moukalled, Mangani, & Darwish, 2016). For this reason, this discretisation technique is popular for engineering application which encompasses complex geometries and complex fluid dynamics. After the discretisation of the problem domain in a computational grid of finite volumes, the method uses the Gauss Theorem to transform the volume integral into surface integrals. Introducing a new scalar variable φ as the volumetric flux through the surface of the cells the flow is described for the following equation

$$\frac{\partial(\rho\varphi)}{\partial t} + \nabla\cdot(\rho\boldsymbol{u}\varphi) = \nabla\cdot(\Gamma^{\varphi}\nabla\varphi) + Q^{\varphi} \quad (18)$$

Which, are solved numerically with the incorporation of techniques which will be presented in the next section.

Discretisation for Flooding Simulation

One of the biggest challenges in the grid-based computational fluid dynamic techniques is the generation a proper gird representation of the domain under investigation (Jasak H. , 1996). The space discretisation approach is a vital pre-processing step, as the mesh should have the appropriate level of detail to capture the geometry of the domain and, the underlying physical phenomena. Generally there is not rule of thumb, and the investigators should choose a discretization technique based on the balance between computational cost and desired accuracy (Foundation, 2014).

In the problem of flooding of a ship after damage the following parts of the domain need specific attention:

Region of Damage and Internal Openings

The damage openings and the compartment openings in the case of ship flooding simulation introduce a geometrical constraint in the meshing process. The cell size should be small enough in order to capture the geometrical details reassuring the accurate representation of the engineering problem.

In addition to geometry definition the discretisation in the vicinity of the openings should have adequate volumetric extent, as in this area high velocity and pressure gradients especially in the transient and the progressive flooding stage of the simulation are expected. The level of refinement in these areas influences the total number of mesh elements, the computational time and the accuracy of the solution.

Hull Region

In case of the simulation of the motion of a ship in intact or damage condition, the current geometrical representation of the hull under investigation has crucial importance for the fidelity of the numerical solution. The mesh element size on the surface of the hull is influenced geometrically from the curvature and the complexity of the surface. Form the physics point of view the element size should be chosen based on $y+$ value as it is defined by the law of the wall for turbulent flow (Moukalled, Mangani, & Darwish, 2016). The $y+$ is defined in the wall boundaries as,

$$y^+ = \frac{du_t}{v} \quad (19)$$

Where, d the normal distance to the wall, v is the kinematic viscosity and u_t is the friction velocity in terms of the wall sheer stress.

Free Surface Region

In marine CFD simulations, researchers usually have to deal with the free surface between water and air. For the case of the flooding simulation of a ship after damage in calm water, a low level of mesh refinement is adequate to capture the deformation of the free surface in the vicinity of the hull and the underlying velocity gradients. Thought, the volumetric discretisation of the region of the free surface is more critical in the case of the investigation of the motions of the ship in waves. In the case in which the wave propagation is solved with the Navier-Stokes equations incorporating the VoF method for interface capturing, the refinement of the free surface cells should be increased otherwise deformation of the wave characteristics may occur (ITTC, 2011). On the other hand, if the number of cells is increased too much, the computational penalty could significantly high. For the avoidance of these effects, it is advisable to use 80 up 160 cells per wave length with an aspect ratio adjusted to the wave steepness (Peric, 2018).

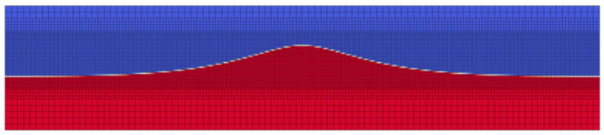

Figure 5: Mesh discretization for the simulation of wave propagation (Roenby, Larsen, Bredmose, & Jasak, 2017).

Pimple Algorithm in OpenFOAM

The challenge in the solution of Navier-Stokes equations is the coupled pressure momentum system. The selection of the solution algorithm has high influence to the computational time of the simulation, and it should be chosen based on the nature of the problem under investigation.

As the simulation of flooding of the damaged ship is a time-marching problem and time discretisation is introduced the choice of an appropriate time step. The time discretisation is restricted by the Courant-Friendrichs-Lewy number defined as (Ferziger & Peric, 2002),

$$CFL = \frac{U\Delta t}{\Delta x} \quad (20)$$

Where, U is the magnitude of the velocity, Δt is the time step and Δx is the length internval which represents the length of the cell.

The solution algorithms which are under investigation for the time domain simulation of a ship after damage are PISO (Pressure Implicit with Splitting of Operator) and PIMPLE (Implicit Pressure Method for Pressure-Linked Equations). Both the algorithms are iterative solvers for transient simulations. PISO algorithm is suitable for CFL number below one. On the other hand, the PIMPLE algorithm is a combination of SIMPLE (Semi-Implicit Method for Pressure-Linked Equations) used for steady state problems and PISO (Moukalled, Mangani, & Darwish, 2016). PIMPLE algorithm is more flexible as it can be stable for CFL numbers bigger than one. Furthermore, it provides the opportunity for adjustment of the iterative procedure between convergence (speed) and stability (Holzmann, 2018; Foundation, 2014).

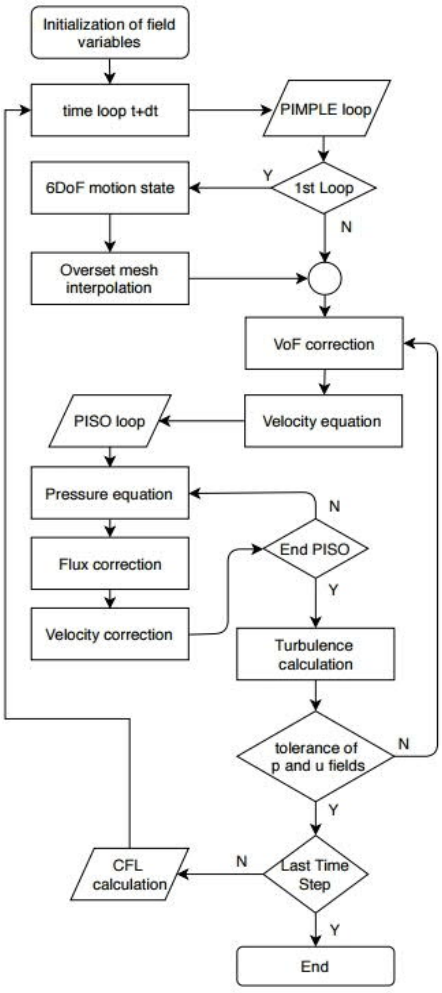

Figure 6: PIMPLE solution algorithm implemented in OpenFOAM (Aguerre, Damian, Gimenez, & Nigro, 2013).

6. BENCHMARKING

A benchmark case is presented in the following section. The vessel in consideration is examined with time-domain simulation of flooding for a range of KG values. Following this, flooding simulation with CFD is performed.

The ship under investigation is a combat vessel with general particulars as presented in the following table. The damage condition under investigation is a four-compartment damage with the opening in the starboard side of the ship. The compartments R1, R2 are extended from port to starboard, and the two double bottom compartments from the centre line symmetry plane to starboard side. For demonstration purposes, the investigation is performed for four hypothetical KG values, 5.8 m, 6.71 m, 7.13 m , and 8.0 m respectively.

Table 1: Main Particulars of the vessel.

Main Particulars – Full scale					
L_{BP}	141.8	m	**Δ_{mld}**	8684	t
B_{mld}	20.6	m	**LCG[1]**	-0.65	m
T_{mld}	7.49	m	**KG_{mld}**	7.84	m
Volumes of the Compartments					
DB1	143.4	m^3	**R1**	1,266.3	m^3
DB2	165.9	m^3	**R2**	1,650.9	m^3

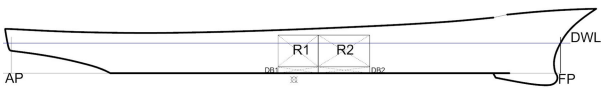

Figure 7: Profile view of the hull.

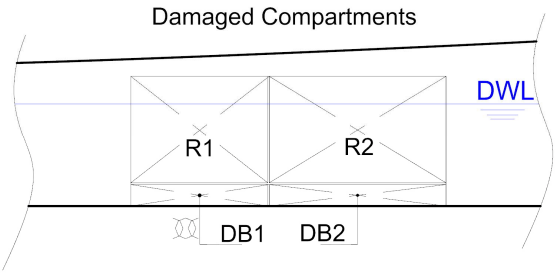

Figure 8: The four damaged compartments of the case under investigation.

[1] The Longitudinal reference point is located amidships.

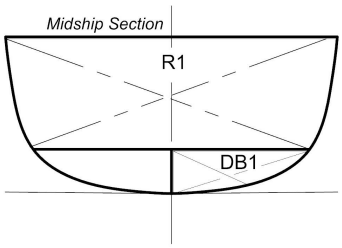

Figure 9: Midship section presenting the DB1, R1 compartments.

Static Stability

The first step in the stability assessment for the specific damage case is the calculation of the curve of static stability, GZ. For the calculation of the righting arm the method of lost buoyancy has been used.

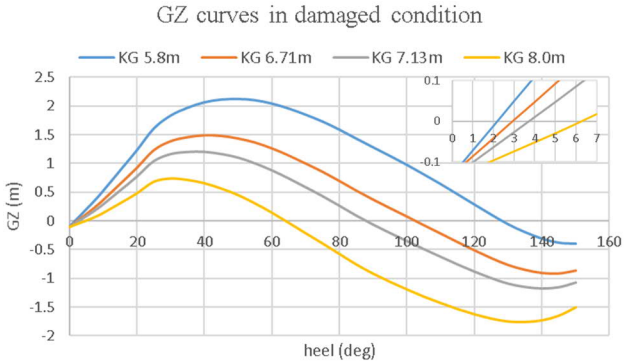

Figure 10: Curves of static stability for the four KG values.

Time-Domain Simulations

For the four cases under investigation time-domain simulation of flooding after damage has been performed. The tool, which has been used is PROTEUS3 and the results are presenting in the following graphs.

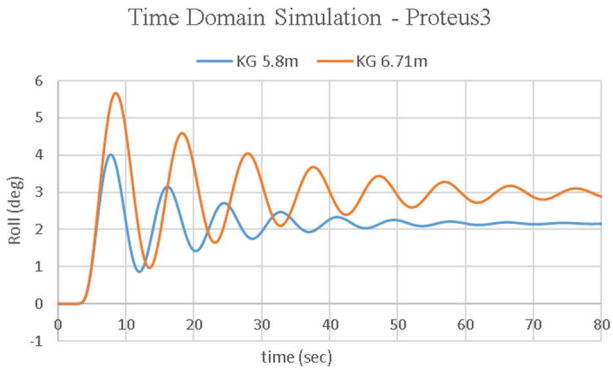

Figure 11: Roll response of the vessel for KG 5.8 m & 6.71 m.

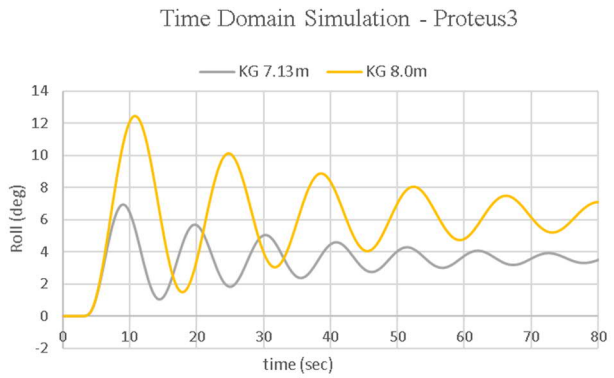

Figure 12: Roll response of the vessel for KG 7.13 m & 8.0 m.

The roll response follows the same pattern for all the cases. As the KG value increases the impact of flooding in the transient response of the vessel increases.

Verification with CFD

For CFD analysis, the OpenFOAM v1812 is used. The overInterDyMFoam solver is used for two incompressible, isothermal fluids with VOF interface capturing approach, incorporating optional overset mesh motion (Foundation, 2014). The forces and the moments on the hull are calculated with the coupling of sixDoFRigidBodyMotion library, which is provided with the package.

The CFD simulations have been performed in the Archie – WeSt High Performance Computing Facilities located at the University of Strathclyde. For each simulation 20 cores of Intel Xeon Gold 6138 have been used with frequency 2.0 GHz and 4.8 GB RAM per core.

Pre-Processing

The pre-processing steps involve the preparation of the geometrical model and the generation of the grids, which will be used. The problem domain incorporates two main regions. The first is a cylinder with radius 2B, which includes the fluid domain in the vicinity of the hull and the four internal compartments of the ship. The second domain represents the earth-fixed environment in which the ship is moving and is used for the interpolation of the fluid variables from and to the overset region.

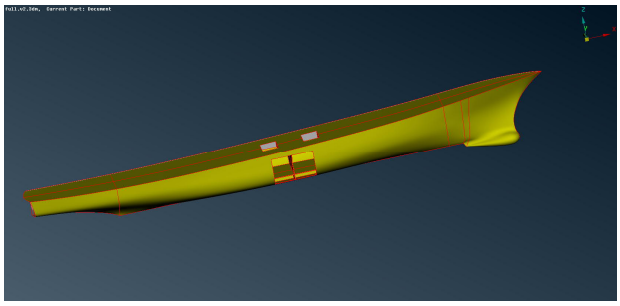

Figure 13: 3D representation of the hull.

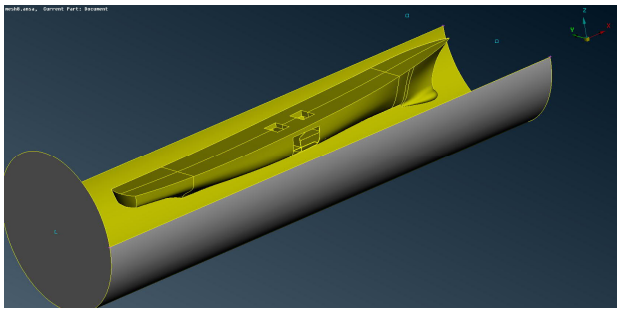

Figure 14: The overset region which encompass the hall and the internal arrangement.

For grid generation, the ANSA v19.0.1 software has been used, developed by the BETA CAE. For the cylindrical volume of the overset region, the grid elements, which have been chosen are tetrahedral for two main reasons. The first is their ability to capture easier the geometry of the hull, and the edges inside the ship arrangement. Furthermore, unstructured tetrahedral elements provide the advantage of a smoother transition between the areas and volumes with different cell size. The smooth transition of the volumetric regions are crucial for the accurate velocity and pressure gradients and the stability of the solver.

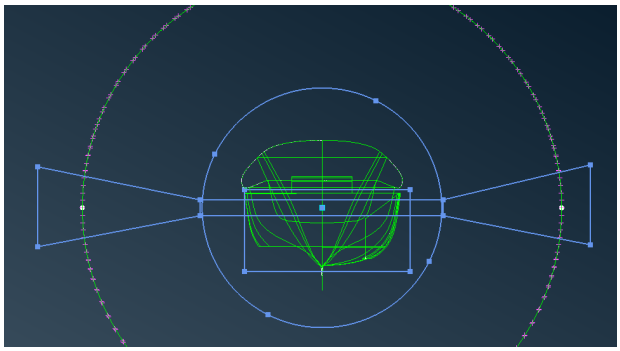

Figure 15: Transverse view of free surface, hull, and internal refinement regions.

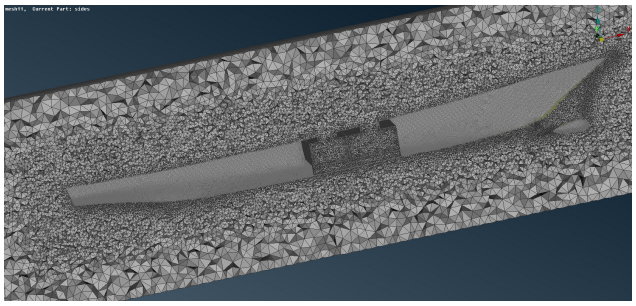

Figure 16: The grid of the overset region.

The total number of cells of the overset region are presented in the following table.

Table 2: Mesh sizes.

	Regions	
Mesh	Overset	Background
Coarse	1,158,782	623,563
Medium	1,881,975	173,911
Fine	4,338,449	623,563

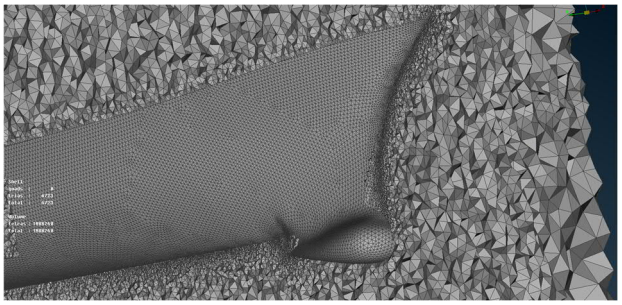

Figure 17: Fine mesh discretization close to the bulbous bow.

The background domain is a rectangular region developed only with hexahedral elements locally refined close to the free surface and the overset region where the interpolation of the fluid variables is performed.

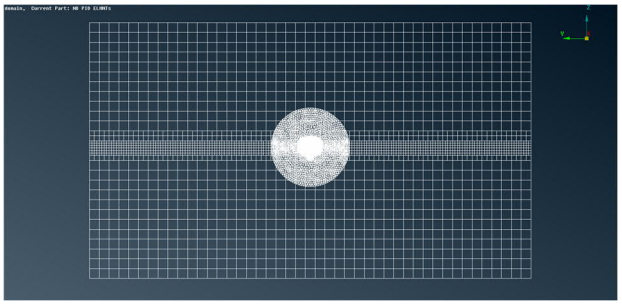

Figure 18: The problem domain with the background and the overset mesh regions.

Simulation Set-Up

The set-up of the simulation has been chosen based on the demand of adequate accuracy and reasonable computational cost. For this reason the numerical tank uses the PIMPLE algorithm, which allows large time steps without jeopardizing the stability of the calculation (Holzmann, 2018; Foundation, 2014). In the simulations, the time step control is based on the maximum CFL number in the domain and in the free-surface interface. Courant numbers have been chosen as

$$CFL < 25 \ \& \text{ free surface } CFL < 5 \qquad (22)$$

For the control of PIMPLE the tolerance of the velocity and pressure fields have been set to the values of 10^{-5} and 10^{-4}, respectively. This is a conservative option as the aim was the stability of the simulation.

A very interesting and important topic in the CFD field is the selection of the appropriate turbulence model for the engineering problem under investigation. For this study, the kOmegaSST model has been chosen as it is the safest option for this kind of hydrodynamic problems (ITTC, 2011). For the capturing of the viscosity near the wall boundaries, the default wall faction which in provided for the CFD toolkit is implemented.

The results for the simulation of medium mesh in comparison with the results of the time-domain simulation for KG =7.13m are presented in the following figures.

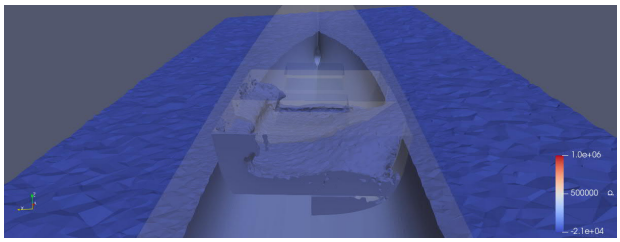

Figure 4: A screenshot of the flooding at 4.0 sec.

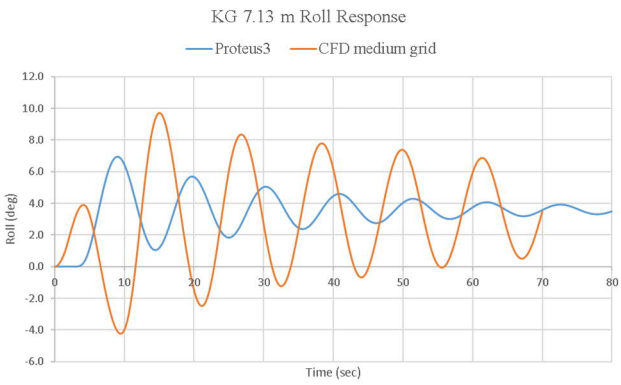

Figure 20: Comparison between time-domain simulation and CFD.

The results obtained demonstrate the impact of floodwater dynamics in the roll response of the vessel. Initially, from 0.0 up to 4.0 seconds the ship rolls to the side of the damage with a maximum roll angle approximately 4 degrees, two degrees below the roll angle that the time domain simulation predicts. This phase is characterised by the motion of floodwater water front, resembling a dam-break phenomenon. From 4.5 sec, the roll angle starts to decrease and at 10 sec the vessel rolls to the port side with a maximum angle approximately -4.0 degrees. This stage is defined by the large hydrodynamic impact induced by the momentum of the floodwater to the port side of the hull. After the first 10 sec the synchronisation of the sloshing of the water inside the compartments and the motion of the hull produces a roll angle close to 10 degrees, the worst of the flooding scenario. After the initial transient stage the roll oscillation is decreased smoothly due to the damping of the motion of the hull. A very interesting outcome of the stationary stage is the smooth roll decade of the damaged hull.

In the figure, the roll response of the vessel as it has been calculated by CFD is presented. The agreement of the medium (2 m cells) and fine (4 m cells) mesh is notable. Furthermore, the coarse mesh calculates a maximum roll angle lower by approximately 3.5 degrees. The difference should be occurred due to the coarse background mesh and its impact in the interpolation of the flow variables with the overset region.

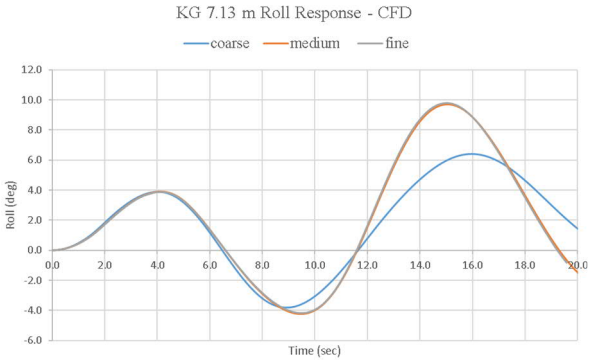

Figure 21: Mesh convergence analysis.

In terms of computational cost it has been noticed that the most important factor is the time step in each stage of the simulation. In the transient stage where the bigger CFL number is the waterfront of the floodwater the time step has a value close to 0.001. After the dam break phenomenon when the water touches the port side wall and up to the moment where the water reaches the maximum level inside the compartment the maximum time step is approximately 0.005. In the steady stationary state, with maximum CFL limit 25, the time step increases to a value of 0.015. The optimized choice of time and space discretization is most vital factor for the reduction of the computational cost of the simulations.

7. CONCLUTIONS

This work presented the utilisation of CFD for the assessment of the survivability of a ship after damage. Despite the big computational cost related with high fidelity numerical simulations, it is proven that they can be an important tool in naval architect's arsenal for the investigation of flooding of ship after damage. Time-domain simulation based on CFD can capture important phenomena that fast time-domain tools, based on hydraulic assumptions cannot, in a level of detail that sometimes is important. The discrepancies that have been between DTNS and CFD are under investigation. Furthermore, the selection of the time and space discretization is a key factor and it needs more research.

8. ACKNOWLEDGMENTS

The authors of this paper would like to express their gratitude to the sponsors of the Maritime Safety Research Centre, Royal Caribbean International & DNV – GL for their courtesy to support the research endeavours of the centre. Results were obtained using the ARCHIE-WeSt High Performance Computer (www.archie-west.ac.uk) based at the University of Strathclyde. Spacial thanks to the BETA CAE Systems (www.beta-cae.com) which supported this research work with for the provision of the advance pre - processing platform ANSA v19.0.1.

REFERENCES

Aguerre, H. J., Damian, S. M., Gimenez, J. M., & Nigro, N. M. (2013). Modelling of Compressible Fluid Problems with OpenFOAM Using Dynamic Mesh Technology. Asociación Argentina de Mecánica Computacional.

Cummins, W. E. (1962). The Impulse Response Function and Ship Motions. Hydromechanics Laboratory Research and Development Report MIT.

Damian, S. M. (n.d.). Description and Utilization of interFoam Multiphase Solver. Final Work - Computatioanl Fluid Dynamics.

Davidson, J., Cathelain, M., Guillemet, L., Huec, T. L., &

Ringwood, J. V. (2015). Implementation of an OpenFOAM Numerical Wave Tank for Energy Experiments. Proceedings of the 11th European Wave and Tidal Energy Conference. Nantes, France.

Ferziger, J. H., & Peric, M. (2002). Computational Methods for Fluid Dynamics (3rd ed.). Germany: Springer.

Foundation, O. (2014). OpenFOAM The OpenSource CFD Toolbox User Gide Version 2.3.0.

Gao, Z., Vassalos, D., & Gao, Q. (2010). Modelling water flooding into a damaged vessel by the VOF method. Journal of Ocean Engineering, 1428-1442.

Holzmann, T. (2018). Mathematics, Numerics, Derivations and OpenFOAM(R). Holzmann CFD. doi:10.13140/RG.2.2.27193.36960

ITTC. (2011). ITTC - Recommended Procedures and Guidelines. Practical Guidelines for Ship CFD Applications. International Towing Tank Conference.

Jasak, H. (1996). Error Analysis and Estimation in the Finite Volume Method with Applications to Fluid Flows. University of London: Ph.D thesis Imperial College.

Jasak, H. (2017). CFD Analysis in Subsea and Marine Technology. First Conference of Computational Methods in Offshore Technology. IOP Publishing.

Jasionowski, A. (2001). An Integrated Approach to Damage Ship Survivability Assessment. PhD thesis University of Strathclyde , Glasgow.

Jasionowski, A., Vassalos, D., & Guarian, L. (2004). Theoretical Developments on Survival Time Post - Damage. Proceedings of hte 7th Int Ship Stability Workshop. Shanghai.

Journee, J. M., Vermee, H., & Vredeveldt, A. W. (1997). Systematic Model Experiments on Flooding of Two RoRo Vessels. 6th International Conference on stability of Ships and Ocean Vehicles, (pp. 81-98). Varna, Bulgaria.

Letizia, L., & Vassalos, D. (1995). Formulatiion of a Non - Linear Mathematical Model for a Damaged Ship with Progressive Flooding. International Symposium on Ship safery in a Seaway, (p. 20pp). Kaliningrand, Russia.

MARIN. (2003). Large Passenger Ship Safety. Time-to-flood simulations for a large passenger ship - initial study. IMO, Sub-Committee on Stability and Load Line and on SIshing Vessels Safety, 46th session, Agenda item 8.

Moukalled, F., Mangani, L., & Darwish, M. (2016). The Finite Volume Method in Computational Fluid Dynamics. An Advanced Introduction with OpenFOAM(R) and Matlab(R). Springer International Publishing Switzerland.

Papanikolaou, A. D. (2007). Review of damage stability of ships recent developments and trends. Proceedings 10th Int. Symposium on Practical Design of Ships and Other Floating Structures. Houston.

Papanikolaou, A., & Spanos, D. (2002). On the Modelling of Floodwater Dynamics and its Effects on Ship Motion. 6th International Ship Stability Workshop. New York: Webb Institute.

Peric, M. (2018). Best practices for wave flow simulations. The Naval Architect International Journal of the Royal Institute of Naval Architects (RINA).

Roenby, J., Larsen, B. E., Bredmose, H., & Jasak, H. (2017). A new volume-of-fluid method in OpenFOAM. VII International Conference on Computational Methods in Marine Egineering MARINE.

Ruponen, P. (2007). Progressive Flooding of a Damaged Passenger Ship Docoral Dissertation. Esploo, FInland: Helsinki University of Technology.

Sadat-Hosseini, H., Kim, D. H., Lee, S. K., Rhee, S. H., Carrica, P., Stern, F., & Rhee, K.-P. (2012). CFD and EFD Study of Damaged Ship Stability in Calm Water and Regular Waves. Proceeding of the 11th International Conference on the Stability of Ships and Ocean Vehicles, (pp. 425-452). Athens, Greece.

Santos, A., & Soares, G. (2006). Study of the Dyanamics of a Damaged RoRo Passenger Ship. 9th International Conference on Stability of Ships and Ocean Vehicles. Rio de Janeiro, Brazil.

Shen, L., & Vassalos, D. (2011). Application of 3D Parallel SPH to Ship Sloshing and Flooding. In Contemporary Ideas on Ship Stability and Capsizing in Waves (pp. 709-721). Springer.

Skaar, D., & Vassalos, D. (2006). The Use of a Mesh-less CFD Method to Model the Progressive Flooding of a Damaged Ship. 9th International Conference on the Stability of Ships and Ocean Vehicles. Rio de Janeiro, Brazil.

So, K. K., Hu, X. Y., & Adams, N. A. (2009). Anti - diffusion method for interface steeping in two - phase incompressible flow.

Spanos, D., & Papanikolaou, A. (2001). Numerical Study of the Damage Stability of Ships in Intermediate Stages of Flooding. 5th International Workshop of Stability and Operational Safety od Ships. Trieste: University of Trieste.

Spouge, J. R. (1985). The technical investigation of the sinking of the Ro Ro Ferry European Getaway. Transactions of RINA, 49-72.

Strasser, C., Jasinowski, A., & Vassalos, D. (2009). Calculation of the Time to Flood of a Box - Shaped Barge Using CFD.

Proc. 10th International Conference of Stability of Ships & Ocean Vehicles, (pp. 733-740). St. Petersburg, Russia.

van't Veer, R., & de Kat, O. (2000). Experimental adn Numerical Investigation on Progressive Flooding in Complex Compartment Geometries. Proceedings of the 7th International Conference on Stability of Ships and Ocean Vehicles, (pp. 305-321). Lainceston, Tasmania, Australia.

Vassalos, D. (2000). The Water on Deck Problem of Damaged Ro-Ro Ferries. Contemporary Ideas on Ship Stability , Elsevier, 163-185.

Vassalos, D. (2009). Risk - Based Ship Design Methods, Tools and Applications. (A. Papanikolaou, Ed.) Veerlag Berlin Heidelberg: Springer.

Vassalos, D. (2014). Damage Stability and Survivability - 'nailing' passenger ship safety problems. Ship and Offshore Structures, 9(3), 237-256.

Vassalos, D., & Turan, O. (1994). A Realistic Approach to Assessing the Damage Survivability of Passenger Ships. Transactions of Society of Naval Architects and Marine Engineers,SNAME, Vol 102, 367-394.

Vassalos, D., Atzampos, G., Cichowicz, J., Karolius, K. B., Boulougouris, E., Svensen, T., . . . Luhmann, H. (2018). Life-Cycle flooding risk management of passenger ships. 13th International Conference of Stability of Ships and Ocean Vehicles , (pp. 648-662). Kobe, Japan.

Vassalos, D., Jasionowski, A., & Guarin, L. (2006). Passenger Ships Safety - Science Paving the Way. Journal of Marine Science and Technology, 63-71.

Vassalos, D., Turan, O., & Pawlowski, M. (1997). Dynamic stability assessment of damaged passenger/Ro-Ro ships and proposal of rational survival critiria. Marine Technology, 34(4), 241-266.

Vredeveldt, A. W., & Journee, J. M. (1991). Roll motions of ships due to sudden water ingress, calculations and experiments. RINA International Conference on Ro Ro Safety and Vulnerability the Way Ahead. London, UK: RINA.

Zaraphonitis, G., Papanikolaou, A., & Spanos, D. (1997). On a 3-D mathematical model of the damage stability of ships in waves. 6th International Conference on Stability of Ships and Ocean Vehicles, (pp. 233-244). Varna, Bulgaria.

Intact stability of passenger ships: safety issue or design concern? Neither!

Dracos Vassalos, *Maritime Safety Research Centre*, d.vassalos@strath.ac.uk
Georgios Atzampos, *Maritime Safety Research Centre*, georgios.atzampos@strath.ac.uk
Donald Paterson, *Maritime Safety Research Centre*, d.paterson@strath.ac.uk
Jakub Cichowicz, *Maritime Safety Research Centre*, jakub.cichowicz@strath.ac.uk
Kristian B. Karolius, *Maritime Safety Research Centre,* kristian.karolius@strath.ac.uk
Evangelos Boulougouris, *Maritime Safety Research Centre*, evangelos.boulougouris@strath.ac.uk
Dimitrios Konovessis, *Singapore Institute of Technology,* Dimitrios.Konovessis@SingaporeTech.edu.sg

ABSTRACT

Stability has been a primary focus of the maritime industry and of immense interest to the IMO from the outset. Despite several attempts to resolve stability-related issues, the problem of stability remains one that has yet to be resolved. Reasons for this, range from the complexity of the problem itself to misconceptions in its very nature, particularly concerning intact or compromised conditions of the ship in question. Emphasis in this paper is placed on the latter. More specifically, whilst intact stability of ships is an extremely interesting scientific problem, to what extent is it a determining factor in the design and operation of passenger ships? Currently, intact stability and damage stability share the same stage from a regulatory perspective and, consequently, they have equal impact on design and operation-related decisions, an example of which is the use of combined intact and damage stability GM limit curves (e.g. IACS Rec 110 Rev1). However, in line with goal-based regulations and standards, design and operational decisions should be risk-informed in which case, matters relating to damage stability are of higher concern, simply by virtue of the fact that damage stability is by far the greater risk contributor. In fact, for passenger ships (>500GT), the level of risk associated with intact stability is indiscernible in contrast to that of damage stability. More importantly, in the operational loading conditions of such vessels, damage stability is a more dominant constraint. Hence, such ships can be designed on the basis of damage stability considerations alone. This paper delves in this direction by drawing on the current regulation-making process for risk estimation as adopted by IMO as well as current design and operational practice. Findings from European research and related studies are provided in order to substantiate the argument that intact stability for passenger ships is neither a safety issue nor a design concern.

Keywords: *Intact stability, FSA, ship safety/risk, ship design and operation*

1. INTRODUCTION

From a basic Naval Architecture perspective, concerning the design of a ship, the most fundamental objective is for the ship to remain afloat and upright, in normal operations and in emergencies, particularly flooding casualties. The relevant terms are “displacement”, relating to overall capacity at the design draft and “freeboard”, relating to the residual capacity, measured from the design draught to the freeboard deck (IMO ILLC’66). The second fundamental goal is that the ship will remain upright in the presence of external forces, even following serious loss of internal buoyancy (potentially with a list in this case). Both concepts emerged together with Naval Architecture and are as ancient as Archimedes, circa 250 BC. The topic of stability of ships (and more generally of floating bodies) has fascinated eminent scientists throughout the centuries and despite unrelenting efforts institutionally and at world scale, research remains relevant and of high focus. Stability combines deep scientific understanding with practical and ethical

concerns stemming from a continually changing industry and society and, as such, it represents a prime driver for naval architects. It is not a coincidence that the form and consequences of stability regulations are at the forefront of interest at the IMO (e.g., Maritime Safety Committee and Sub-Committee on Ship Design and Construction). Many ship stability problems remain "unsolved" and the subject will remain a key focus for as long as there is human activity at sea.

From a wider perspective, maritime safety permeates all physical and temporal boundaries and, as such, is one of the most influential goals in ship design and operation. All human activity in a "risky" environment, such as the sea, is fraught with wide-ranging problems that tend to undermine safety. This is particularly true for knowledge-intensive and safety-critical ships, such as passenger ships, where the need for innovation creates unprecedented safety challenges. The Design for Safety philosophy and the ensuing formalised methodology, Risk-Based Design, was introduced in the maritime industry as late as in the mid-nineties as a design paradigm to help bestow safety as a design objective and a life-cycle imperative (Vassalos and Fan, 2016). This was meant to ensure that rendering safety a design driver would incentivise the maritime industry to seek cost-effective safety solutions, in response to rising societal expectations. In this respect, the adoption of a goal-based approach to address safety has had a profound effect, the full impact of which is yet to be delivered (IMO GBS-SLA). As a result, the subject of ship safety is one of the fastest changing topics, absorbing all forms of knowledge in the strife to respond to unrelenting societal pressure for higher safety standards and do so cost-effectively. Stability is a key focus in this quest.

However, with the focus clearly on passenger ships, certain fundamental principles have been overlooked, as a result of which all matters of stability are being pursued in the same vein, irrespective of the fact that safety implications between intact and damage stability are strikingly different. Put it differently, whilst damage stability for passenger ships constitutes the most severe safety problem, responsible for over 90% of loss of life at sea, intact stability-related loss of life, is miniscule. In fact, it is orders of magnitude lower, apart from small ships where these can be overpowered by waves, cargo shift and other excessive moments leading to capsize and potential loss of life. Usually, such ships are not involved in international trade.

Using this notion as a platform, this paper will demonstrate that loss of life (the risk) attributed to intact stability is too small to be measured for practical use. The basis for this is the IMO-established methodology for risk estimation of a given hazard in support of the regulation-making process i.e., the Formal Safety Assessment (FSA). In this respect, evidence will be presented to substantiate this claim in support of the argument that intact stability is not a safety issue for passenger ships. Industry has realised this many years ago and took action by: (a) increasing GM 3-fold to avoid dynamic stability problems (e.g., parametric roll, dead-ship condition) and (b) installing sophisticated motion stabilisers to ensure reduced motions and accelerations as well as provide maximum comfort in all operating conditions.

Having said this, with focus on damage stability considerations, innovative solutions will be identified, which with time, could potentially render damage stability an equitable risk contributor to intact stability (Vassalos, et al, 2019). Risk balance will then become a key design concern in which case both intact and damage stability will be deserve due attention.

Intact stability is not a design concern! This sounds even more precarious than intact stability not being a safety issue. However, evidence presented in the paper demonstrates that within the operational range of passenger ships (cruise ships and RoPax), ship design and operation are governed by damage stability considerations. This is unsurprising, as it is the case for other safety-critical ship types such as surface combatants.

Realising this, will not change current design practice substantially (in terms of substituting one limiting curve with another or continue using the 2nd Generation Intact Stability criteria as guidelines, currently under consideration at IMO (SDC 6/5, 2019), but will help the profession to focus, identify and resolve damage stability issues as primary concern, thus investing cost-effectively to improve maritime safety. In addition, operational data for these ships will be used to show that, in the range of drafts where passenger ships normally operate,

stability requirements are dictated by damage stability considerations. Stemming from the above, specific conclusions are drawn.

2. FORMAL SAFETY ASSESSMENT

With the advent of goal-based standards, risk-based approaches and regulations have been introduced in the maritime industry to guide ship design and operation. However, whilst such approaches address by definition the life cycle of the ship, the focus of the regulations remains design-biased.

Risk-based ship design introduces risk analysis and evaluation into the traditional design process with the ultimate aim of meeting safety objectives cost-effectively. Risk, in this respect, is a metric for quantifying safety performance. With safety treated as a measurable objective, design optimisation can effectively be expanded and the new objective to minimise risk can be addressed alongside other traditional design objectives relating to earning potential, speed, cargo carrying capacity, etc., (Sames, 2007). One of the main outputs relates to "balanced" decision-making concerning risk, cost and performance on the basis of risk evaluation thresholds.

The vehicle for this in the maritime industry is IMO, concerning regulatory developments and amendments. One instrument that is fundamentally risk-centric is the Formal Safety Assessment (FSA) process, which was introduced by the IMO as a direct response to the explosion of the Piper Alpha offshore platform in the North Sea, where 167 people lost their lives. The first integration of FSA in the regulation-making process took place in 2002, by the approval of relevant guidelines laid out in MSC/Circ. 1023 - MEPC/Circ. 392 (IMO, 2002). Recently, the FSA guidelines have been revised twice by MSC/Circ.1180 - MEPC/Circ.474 (IMO, 2005) superseded by MSC-MEPC.2/Circ.5. (IMO, 2018). The FSA is a rational, holistic and systematic process for assessing risks relating to maritime safety, the protection of the marine environment, and for evaluating costs and benefits of various options to reduce these risks (IMO, 2015). Notably, the use of FSA is consistent with, and will provide support to, the IMO decision-making process, leading to international legislation for rendering pertinent risks As Low As Reasonably Practicable (ALARP). The FSA includes a number of generic, logically arranged steps as indicated in Figure 1, which reflect different stages of resolving a safety issue.

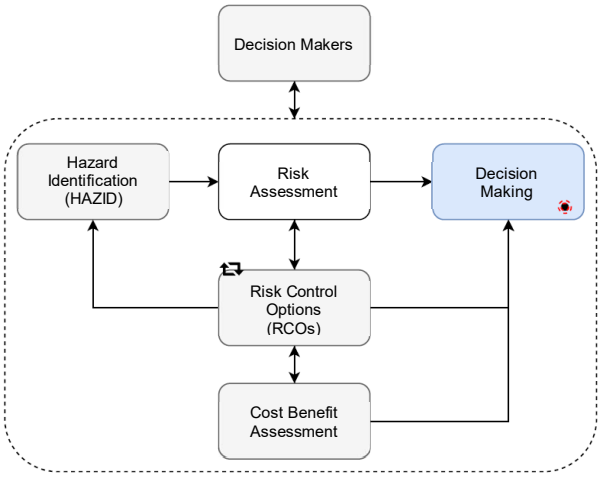

Figure 1: Process of Formal Safety Assessment (FSA)

In the era in which the maritime community changes direction from a reactive to a proactive safety approach, the Formal Safety Assessment provides the right vehicle for risk-informed legislation and general decision making.

Relating to the problem at hand, the European project (SAFEDOR, 2005-2009) performed Formal Safety Assessments for both RoPax and Cruise Ships with the view to quantifying related risks during the life-cycle. Table 1 next, summarises the results of the FSAs.

As one could readily observe, intact stability is absent from the potential risk contributors, not because it was omitted from the analysis but because the contribution to risk from intact stability concerns is negligible. Despite the fact that loss includes consequences of heavy seas and tropical rain, large ship motions and impact of water ingress into the cargo hold, the risk remains negligible.

In the case of RoPax ships, the FSA includes accidents from 1994 to 2004 (IMO, 2008b) and for cruise ships from 1990 to 2004 (IMO, 2008a). Even though, the risk for collisions, grounding and contact/impact is very high, water ingress due to damage has been investigated separately for the case of RoPax vessels. The results indicate a PLL (Potential Loss of Life) due to flooding as high as 1.12E-1 per ship-year.

Table 1: FSA findings for Passenger ships derived from project SAFEDOR. Indication of frequency and Potential Loss of Life per ship year.

	Type	Frequency (per ship year)	PLL (per ship year)
RoPax	Collision	1.25E-02	2.34E-02
	Grounding	9.57E-03	2.57E-02
	Impact	1.25E-02	1.39E-03
	Flooding	2.39E-03	1.12E-01
	Fire	8.28E-03	5.95E-02
	Total	**4.52E-02**	**2.22E-01**
Cruise Ships	Collision	4.60E-03	2.40E-01
	Contact	1.20E-03	9.20E-03
	Grounding	9.80E-03	1.50E-01
	Fire/Explosion	8.90E-03	1.50E-02
	Others	2.00E-02	6.40E-03
	Total	**4.45E-02**	**4.21E-01**

3. SAFEDOR CASE STUDY

In the European project (SAFEDOR, 2005-2009), (Themelis et al., 2007) presented a novel method of probabilistic assessment for intact stability, applicable to different ship types. One of the ship types considered is a RoPax ferry, which aided in identifying the fraction of risk for different problems related to intact stability.

The approach was tailored for a specific ship, assessing three failure modes, namely: beam-sea resonance, parametric rolling and pure loss of stability for specific routes in Mediterranean Sea. The methodology entailed identification of critical wave groups that give rise to dynamic responses exceeding a threshold, which is established based on the probability of encountering pertinent critical wave groups for the areas under consideration. The assessment of the intact stability-related failure modes or else "instability" is based on the development of wave environment thresholds. The developed failure norms address distinctively the safety of the ship. For the RoPax vessel, this norm is expressed through a critical angle of roll.

The results of the study are provided in Table 2. In particular, the findings of the analysis indicate very low probability of instability when mean seasonal values (even for winter) are considered. This is the case for the marginal probabilities of Hs and Tz, accordingly. From an operational perspective, in order to account for actual cases, the joint probability of encountering Hs and Tz is considered (Themelis and Spyrou, 2007), as shown in the table below, in which the values refer to the entire voyage time.

Table 2: Probabilities for ROPAX (Themelis and Spyrou, 2007)

	Total probability	Critical time ratio
Beam-sea resonance Ship (φ>35°)	1.88E-16	2.74E-16
Parametric rolling Ship (φ>35°)	4.99E-28	9.64E-28
Pure loss of stability Ship (φ>35°)	6.49E-19	1.86E-19

In simple terms, indicative values for intact-stability-related risk are miniscule on the basis of such low frequencies of encountering critical wave conditions, even assuming conservatively that such encounters will lead to life loss.

According to the authors (Themelis and Spyrou, 2007): "These probabilities represent the number of critical waves over the total number of encountered waves. With this in mind, considering a ship lifetime of 25 years, half of which at sea and a mean wave period of 8 seconds, for a year of continuous vessel operation (60 x 60 x 24 x 365/8), 25 years of the ship lifetime produces 10^8 waves per ship". This means that a fleet of 5E20 needs to operate continuously for 25 years in order to have 1 parametric roll according to the low probabilities shown in Table 2. However, it will be of interest to undertake a complete study aimed at clarifying this issue as a general concern.

4. LIMITING GM CURVES

Design Condition

Currently, intact and damage stability considerations and ensuing requirements are expressed in the form of limiting GM curves for intact and damage stability, both presented without any due consideration of the risk associated with each condition. This leads to the same emphasis being placed for intact and damage stability requirements and this, in turn, may lead to sub-optimal designs. More specifically, for passenger ships, the risk due to damage stability is orders of magnitude higher than that pertaining to intact stability and this information is not being reflected

through the limiting curves, thus not being properly accounted for in the design process and during operation.

Damage stability is assessed for thousands of damage cases and potential scenarios, in three loading conditions (dl, dp, ds), using the Attained Index as a means of statutory compliance. On this basis, the Limiting GM curves are derived following compliance of each draft with the inequality A≥0.9R for passenger ships. This way, risk (for example, Potential Loss of Life – PLL) is calculable and reflects all requisite knowledge. For intact stability, on the other hand, to date, the limiting curve is derived following compliance with the severe wind and rolling criterion for different KGs, indicating the ability of a vessel to withstand the combined effects of beam wind and rolling in a scenario that bears little or no relation to reality. Second generation intact stability criteria address more realistically intact-stability related concerns, including potential problems but risk estimation remains characteristically absent. This being the case, the ensuing results lack risk content and information. Therefore, from a risk-based perspective, any deduction on risk pertaining to intact and damage stability and comparison between the two, could be misleading. In the face of this, ships may be sub-optimally designed.

On the other hand, the limiting GM curve linked to intact stability provides implicit information on the payload as a function of draft and KG. This, in turn, allows designers at the early stages of design to make decisions concerning global ship parameters and loading conditions. Accounting for this, it will be of interest to examine if passenger ships could be designed from damage stability considerations alone.

Pertaining to the above, Figure 2 and Figure 3 below indicate the limiting GM curves for intact and intact stability relating to medium/large passenger ships (cruise ship and RoPax). Three points are noteworthy:

(a) ships are designed with a large GM margin for better life-cycle stability management
(b) the damage stability limiting GM is dominant, particularly at the design draft (5.35m for RoPax and 8.75m for the cruise ship)
(c) The gap between intact and damage stability requirements widens with increasing drafts.

Related to this, previous studies from (Paterson et al., 2018) have demonstrated that passenger ships operate at the upper region of their draft distribution when actual operational profiles are considered. More specifically, almost 75% of the loading conditions operate at drafts higher than the SOLAS damage stability partial draft.

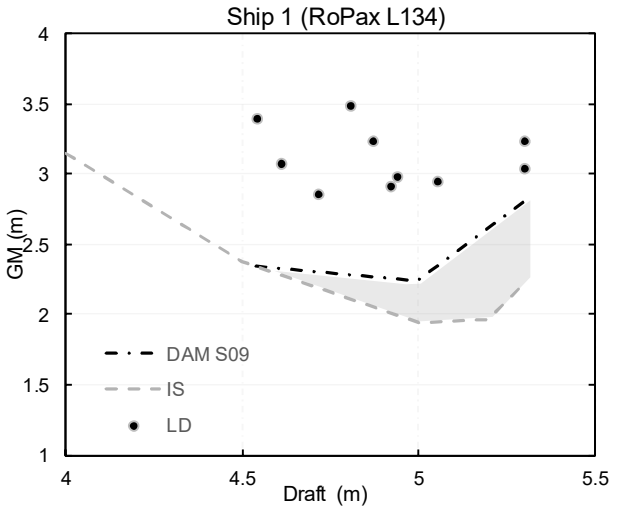

Figure 2: Intact and damage limiting GM curves along with design loading conditions for a medium size RoPax

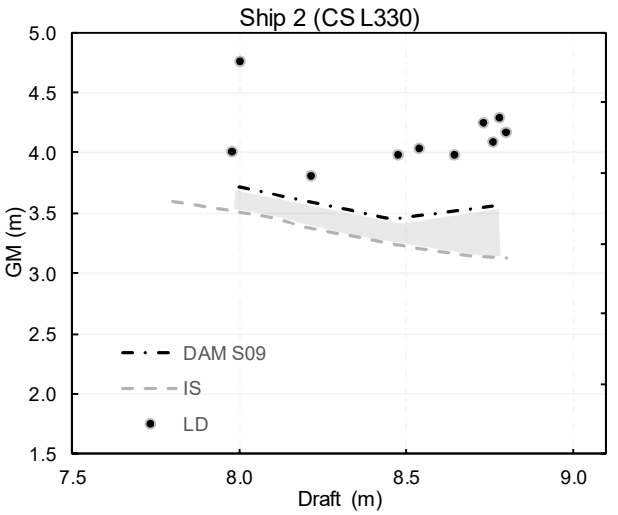

Figure 3: Intact and damage limiting GM curves along with design loading conditions for a large cruise ship

These limits, as described above, are meant to provide for safe operation and, as such, there is a link to risk. Attempting to calculate this for both intact and damage stability is not straightforward and hence a heuristic approach is utilised herewith, based on frequency estimation of pertinent events. This is used as a metric for Potential Loss of Life (fatalities)

as a function of the People On Board (POB). This is shown in Figure 4 for the RoPax and cruise ship referred to earlier.

This way, for intact stability, incident-specific frequency per ship year is used incorporating all three potential modes of loss as provided in Table 2. For damage stability, pertinent results for this ship are given in the EMSA III Project (EMSA, 2013).

Figure 4 shows the difference between intact and damage stability-related risk (PLL), which spans orders of magnitude. The difference between RoPax and Cruise ship stems merely from the difference in size and passenger capacity. Following this process of assigning risk content in the intact stability limiting curve, leads to uncharacteristically low intact stability limiting GMs. As a result, it would not be sensible to consider intact and damage stability limits together, a point made frequently in the past.

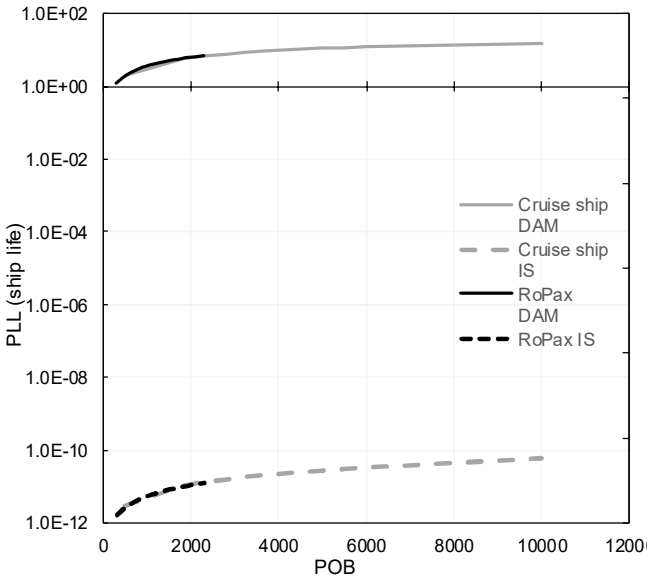

Figure 4: Potential Loss of Life per ship life for one cruise ships and one RoPax for intact and damage stability respectively

Operational condition

In the operational stage of the life-cycle of passenger ships, vessels tend to operate at the upper envelope between the partial and deepest damage stability drafts, as mentioned in the foregoing. This is demonstrated in Figure 5 and Figure 6 for RoPax and Cruise ship, respectively. The graphs show that all operational conditions are governed by damage stability requirements for the related operational range.

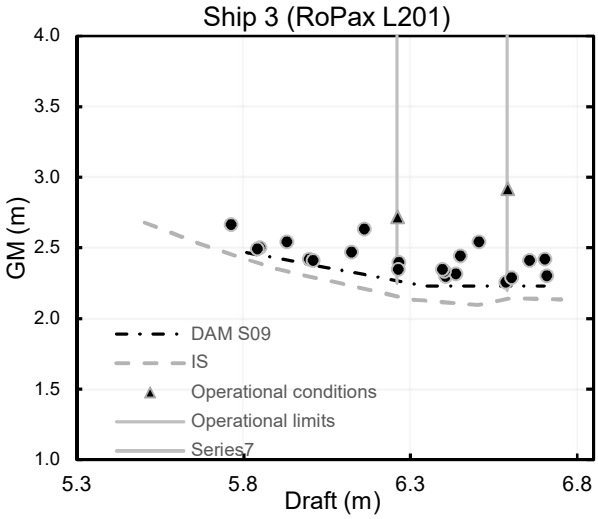

Figure 5: Operational and design conditions along with damage and intact damage limiting GM curves for a large RoPax

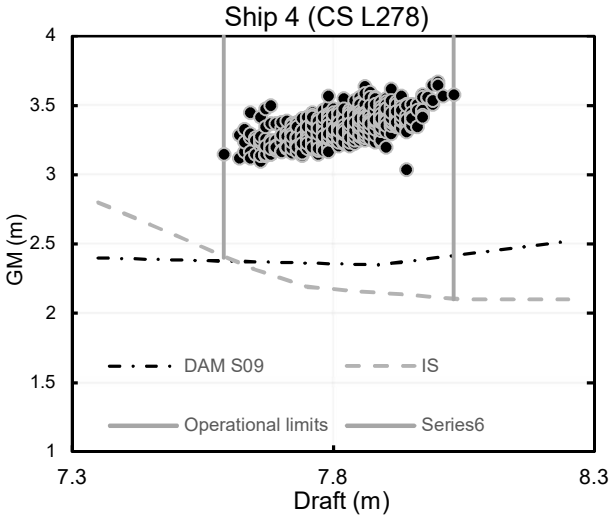

Figure 6: Operational conditions, damage and intact damage limiting GM curves for a large cruise ship

5. CONCLUSIONS

Based on the information and arguments presented in the foregoing, the following conclusions nay be drawn:

- For passenger ships (>500GT), the level of risk associated with intact stability is indiscernible in contrast to that of damage stability.

- Given that design and operational decisions should be risk informed, matters relating to damage stability should be given priority. In this respect, recently agreed 2nd Generation Intact

Stability Recommendations will serve a useful purpose.

- However, given that in the operational draft range of passenger ships damage stability considerations are dominant, ships could be designed on the basis of damage stability considerations alone, in that this indirectly caters for intact stability requirements.

6. REFERENCES

IMO 2008a. MSC 85/17/1 Formal Safety Assessment (FSA) cruise ships. London.

IMO 2008b. MSC 85/17/2, Formal Safety Assessment (FSA) RoPax ships. London.

IMO 2015. Revised Guidelines for Formal Safety Assessment (FSA) for Use in The IMO Rule - Making Process. In: IMO (ed.). London.

Vassalos, D, Patterson, D. & Boulougouris, E. Flooding Containment System, MT Journal, 2019.

Paterson, D., Vassalos, D., Atzampos, G., Boulougouris, E., Cichowicz, J. & Luhmann, H. Rebooting SOLAS - Impact of drafts on damage survivability of cruise ships. Proceedings of the 13th International Conference on the Stability of Ships and Ocean Vehicles, STA2018, 2018 Kobe, Japan.

SAFEDOR 2005-2009. Design, Operation and Regulation for Safety, EU project, FP6-516278.

Sames, P. Risk-Based Frameworks for ship designa and approval. 10th Int. Symposium on Practical Design of Ships and other Floating Structures, PRADS, 2007 Houston.

Themelis, N. & Spyrou, K. Probabilistic assessmemt of ship stability. Transactions - Society of Naval Architects and Marine Engineers, 2007 SNAME. 181-206.

Themelis, N., Spyrou, K. & Niotis, S. 2007. SAFEDOR-D-2.3.6-2007-06-15-NTUA–rev-1, Implementation and application of probabilistic procedures In: NTUA (ed.). Athens.

Vassalos, D., Atzampos, G., Cichowicz, J., Paterson, D., Karolius, K., Boulougouris, E., Svensen, T., Douglas, K. & Luhmann, H. Life-cycle flooding risk management of passenger ships. Proceedings of the 13th International conference on the stability of ships amd ocean vehicles, STAB, 2018 Kobe, Japan.

Vassalos, D. & Fan, M. Risk-Based design - Realising the triple-a navy. 13th International Naval Engineering Conference and Exhibition (INEC 2016), 2016 Bristol.

EMSA, 2013. Risk acceptance criteria and risk based damage stability, Final report, part 2: Formal Safety Assessment (EMSA/OP/10/2013).

Proceedings of the 17th International Ship Stability Workshop (ISSW 2019)